SEISMIC PERFORMANCE ASSESSMENT OF QUASI-ISOLATED HIGHWAY BRIDGES WITH SEAT-TYPE ABUTMENTS

BY

JIE LUO

DISSERTATION

Submitted in partial fulfillment of the requirements
for the degree of Doctor of Philosophy in Civil Engineering
in the Graduate College of the
University of Illinois at Urbana-Champaign, 2016

Urbana, Illinois

Doctoral Committee:

Professor James M. LaFave, Chair, Director of Research
Associate Professor Larry A. Fahnestock, Co-Chair, Co-Director of Research
Assistant Professor Ahmed E. Elbanna
Associate Professor Scott M. Olson

ABSTRACT

Seismic isolation is one of the most popular strategies to protect civil engineering structures against earthquake hazards. For highway bridges, isolation physically decouples a bridge superstructure from its substructures resting on a shaking ground, leading to a significant reduction in the seismic forces transmitted from the superstructure to the substructures and foundations. The isolation technique has conventionally been employed in protecting highway bridges in high-seismic zones and the decoupling is typically realized by interposing specially designed isolators between bridge superstructures and substructures.

In recent years, bridge engineers of the Illinois Department of Transportation developed an innovative "quasi-isolation" strategy to improve bridge seismic resilience in geographical regions with low-to-moderate seismicity, such as the Midwestern United States. Different from conventionally isolated bridges, non-seismically designed commonplace bearing components are employed as sacrificial connections between superstructures and substructures of quasi-isolated bridges. During a major earthquake, fusing actions of the sacrificial connections as well as subsequent bearing deformation and sliding are intended to reduce seismic demands on bridge substructures and foundations. In conjunction with the sacrificial connections, conservatively designed bearing seat widths at substructures are relied upon to accommodate displacement demands of bridge superstructures and eventually prevent span loss.

The objectives of this study are to assess the seismic performance of prototype quasi-isolated highway bridges with seat-type abutments, validate the current design strategy, and provide recommendations for improving the bridge seismic performance. To encompass common configurations of quasi-isolated highway bridges, a suite of prototype bridges with variations in the span arrangement, girder type, skew angle, pier column height, and foundation soil condition were computationally studied. Detailed yet efficient three-dimensional nonlinear finite-element models

were developed for the bridges, incorporating various critical structural components and geotechnical mechanisms. Multi-mode adaptive pushover analyses were conducted to investigate bridge response characteristics in terms of force distribution among substructures, sequence of limit state occurrences, fusing of sacrificial connections, and vulnerability of critical bridge components. Additionally, eigenvalue modal analyses were performed in the elastic and inelastic bridge deformation states to reveal modal response characteristics of the bridges.

The study culminated in a comprehensive and extensive seismic performance assessment of prototype quasi-isolated bridges, for which thousands of nonlinear dynamic time-history analyses were carried out using a supercomputer. The bridges were subjected to a suite of site-specific earthquake ground motions, taking into account the site condition and regional seismicity of Cairo, Illinois. The assessment results validated that the current quasi-isolation bridge design strategy is generally effective and the majority of the studied prototype bridges are unlikely to fail in global collapse when subjected to horizontal earthquake ground motions with a 1,000-year return period in the Midwestern United States. Although many of the prototype bridges exhibited satisfactory seismic performance, the response of a small number of bridges demonstrated a high risk of bearing unseating and severe pier column damage. Aiming at improving the seismic performance of these bridges, preliminary recommendations for calibrating the current design strategy were proposed and their efficacy was demonstrated by comparative studies.

To my parents, for their supports, encouragements, and sacrifices.

ACKNOWLEDGMENTS

I would like to express my sincere gratitude to my research advisors Dr. James LaFave and Dr. Larry Fahnestock for giving me the opportunity to work on this project and the invaluable guidance and support they have given me. Without their guidance and support, my research work could not have been accomplished.

I am also very grateful to Dr. Scott Olson and Dr. Ahmed Elbanna for serving on my doctoral committee. Their insightful and critical guidance on my research work is greatly appreciated.

I can never fully express my appreciation for the unconditional supports and encouragements of my parents. I benefited greatly from their teaching me surviving and thriving through tough times. I also owe great thanks to Jiaqi for supporting and encouraging me.

I am also grateful for the excellent work of former graduate research assistants Dr. Josh Steelman, Evgueni Filipov, and Jessica Revell working on the first phase of the research project. Their work laid a solid foundation for the research of the second phase. I would also like to thank my research project teammate Derek Kozak for his support.

I would like to thank the IDOT Technical Review Panel, chaired by Mr. Mark Shaffer, for their important input on designing the prototype bridges and other aspects of the research.

The Illinois Center for Transportation provided support for a part of my doctoral study. University of Illinois at Urbana-Champaign provided support for my dissertation work through the Dissertation Completion Fellowship. The funding support from these sources is gratefully acknowledged.

The dissertation research is part of the research project ICT R27-133, “Calibration and Refinement of Illinois’ Earthquake Resisting System Bridge Design Methodology: Phase II”. ICT R27-133 was conducted in cooperation with the Illinois Center for Transportation (ICT), the Illinois Department of Transportation (IDOT), and the U.S. Department of Transportation, Federal

Highway Administration (FHWA). The contents do not necessarily reflect the official views or policies of the ICT, IDOT, or FHWA.

TABLE OF CONTENTS

LIST OF TABLES

LIST OF FIGURES

CHAPTER 1

INTRODUCTION

1.1 Quasi-Isolation Strategy for Earthquake Resisting System (ERS) Highway Bridges in Illinois

In early 2008, the American Association of State Highway and Transportation Officials (AASHTO) published revised standards for the design of earthquake-resistant highway bridges, namely the AASHTO Load and Resistance Factor Design (LRFD) Bridge Design Specifications (AASHTO 2008a) and AASHTO Guide Specifications for LRFD Seismic Bridge Design (AASHTO 2008b). In the revised standards, return period of the design earthquake was increased from 500 years to 1,000 years for the first time. The longer return period represents a significantly increased design accelerations for highway bridges in the West Coast with high seismicity and some regions in the Midwest and East Coast, such as the southern Illinois area, where high-magnitude low-probability seismic hazards have also been a primary concern for the safety of transportation infrastructures.

In response to the increased demand on seismic design and construction of highway bridges, bridge engineers of the Illinois Department of Transportation (IDOT) developed an innovative framework for design, construction, and retrofit of earthquake resisting system (ERS) highway bridges in the state of Illinois (Tobias et al. 2008; IDOT 2012a). Conventional bridge isolation strategies using seismically designed isolators, restrainers, and dampers are typically employed in regions with high seismicities, such as the Western United States. Figures 1.1a and 1.1b illustrate the configuration of a friction pendulum bearing (Dao et al. 2013) and a lead-rubber bearing (Robinson 1982), which are typically used for conventionally isolated structures. In contrast, the quasi-isolated bridge system features a simplified and economical design and construction process, yet it is expected to protect the highway bridges in regions with moderate seismicities, such as the Midwestern United States, from excessive seismic damage and collapse.

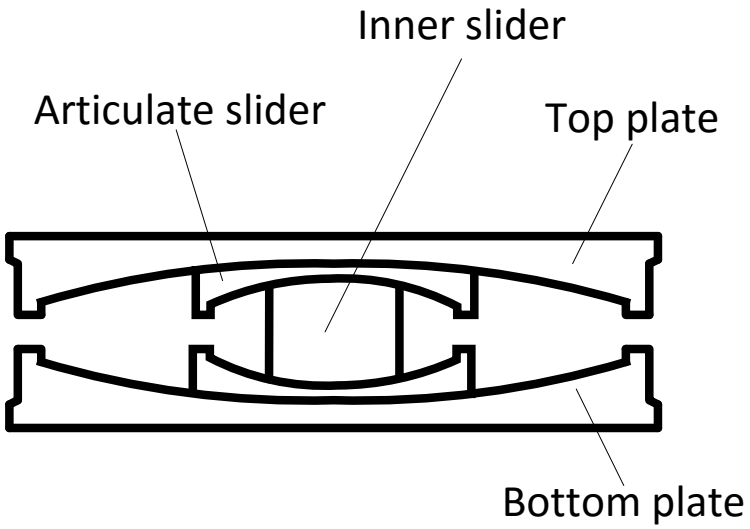

(a) Friction pendulum bearing

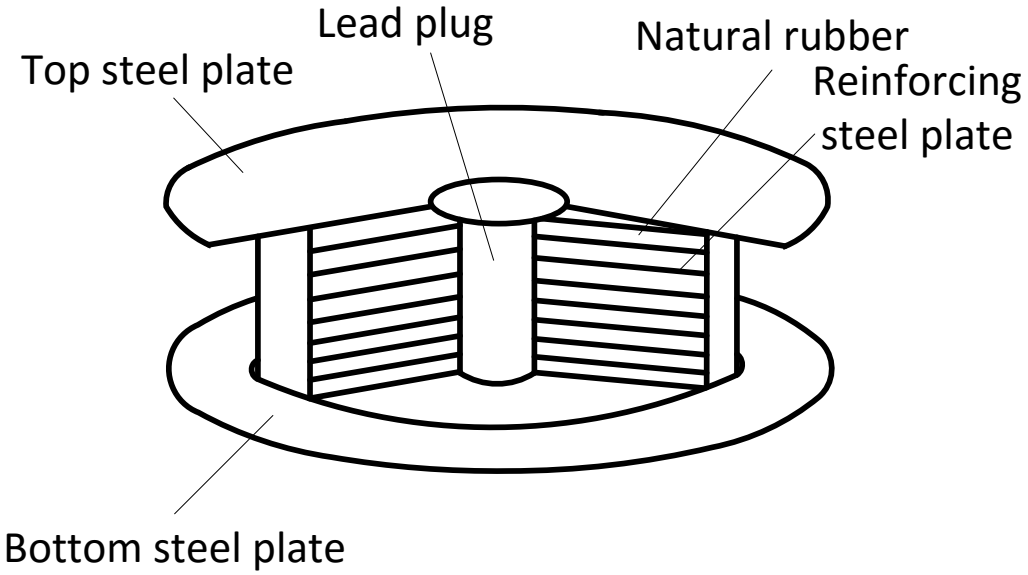

(b) Lead rubber bearing

Figure 1.1: Seismically designed isolators for conventionally isolated structures

The quasi-isolation strategy employs non-seismically designed sacrificial connections between bridge superstructures and substructures in conjunction with conservatively designed bearing seat widths at substructures. During a major earthquake, damage and failure of these fuse-like connections are expected to limit superstructure inertia forces transferred down to substructures and foundations, dissipate seismic energy, and elongate structural periods, thereby protecting bridge substructures and foundations from severe seismic damage. After fusing of the sacrificial connections during a major earthquake, bridge superstructures may slide on substructures with only weak restraints comprised mainly of frictions at bearing-substructure interfaces. Sliding and displacement response of superstructures and bearings is accommodated by conservatively designed bearing seat width at substructures. As the primary objective of IDOT's ERS bridge design strategy, the conservative seat width is relied upon to prevent loss of bridge span (IDOT 2012a), which can directly result in disruption of transportation lifelines and cause loss of life.

In the quasi-isolation bridge design strategy of Illinois, three tiers of seismic structural redundancy are strategically employed to prevent excessive seismic damage and span loss during major earthquakes (Tobias et al. 2008). The first tier consists of sacrificial superstructure-substructure connections, such as elastomeric expansion bearings, bearing transverse retainers, low-profile steel fixed bearings, and steel dowel connections. Figures 1.2a and 1.2b illustrate the configuration of IDOT Type I elastomeric expansion bearing and low-profile steel fixed bearing, respectively. The Type I bearing consists of a block of steel-reinforced, laminated elastomer vulcanized to a steel plate on its top. The steel plate is connected to the bottom flange of a bridge girder via welded studs. The bottom of the elastomer is directly placed on top of a concrete substructure. When the bearing is subjected to horizontal forces, the elastomer experiences shear deformation. Additionally, the bottom of the elastomer is subjected to initial static or kinetic sliding friction at the elastomer-concrete interface. In the transverse bridge direction, a pair of L-shaped steel retainer brackets are anchored to concrete substructures on both sides of an elastomeric bearing. The steel fixed bearing consists of a curved top steel plate and a flat bottom steel plate anchored to the concrete substructure. The top and bottom steel plates mate via two steel pintles. An elastomeric leveling pad is secured between the bottom steel plate and the concrete surface of the substructure. Concrete shear keys are rarely included in the quasi-isolated bridge system, although they are widely used in other types of highway bridges. These connections are designed as the weakest

fuses with relatively small fusing capacities in the entire bridge system. The second tier is the conservatively designed bearing seat width at substructures. This tier is intended to prevent bridge span loss by accommodating large superstructure and bearing displacements after fusing of the first tier. As the last tier of seismic structural redundancy, limited yielding and damage of substructure and foundation components, such as reinforced-concrete (RC) pier columns, foundation piles, and backfill/embankment soil, is allowed to occur. Preferably, the capacity of these components should be larger than that of the sacrificial superstructure-substructure connections in the first tier.

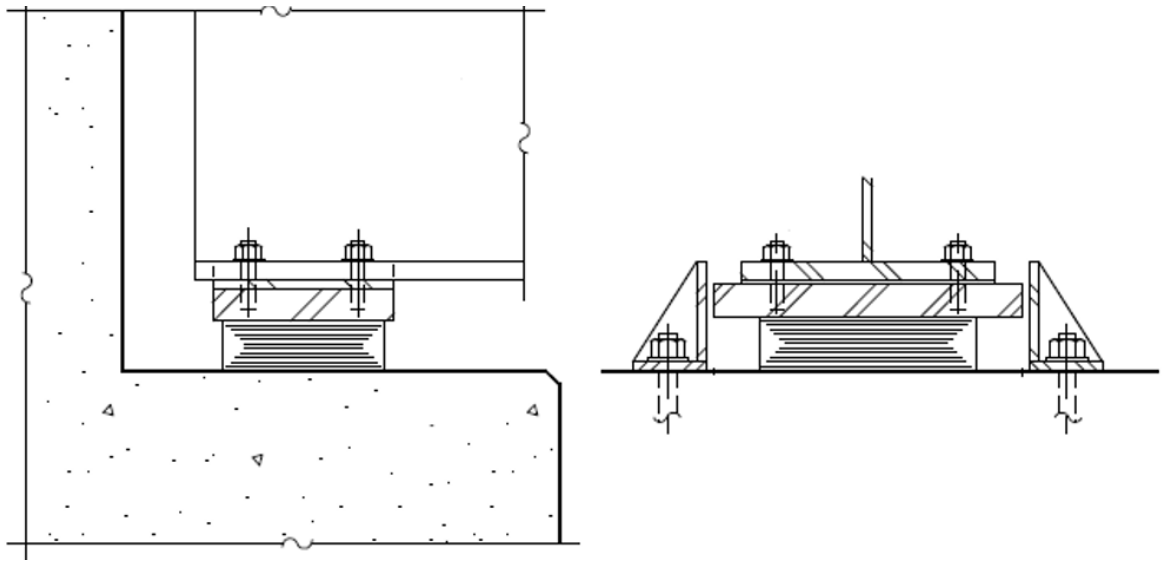

(a) Type I elastomeric expansion bearing with transverse bearing retainers

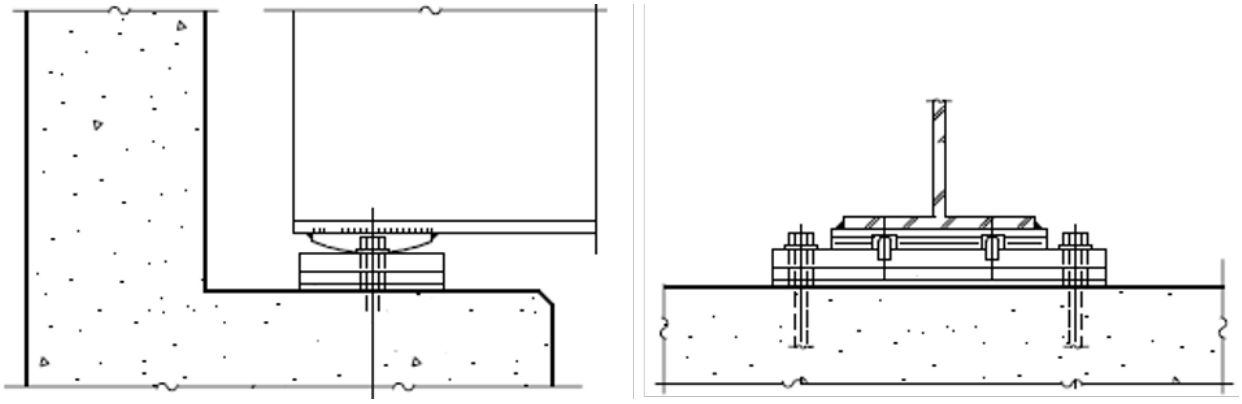

(b) Low-profile steel fixed bearing

Figure 1.2: Type I elastomeric bearing with transverse bearing retainers and low-profile steel fixed bearing employed by quasi-isolated highway bridges in Illinois (after IDOT 2012a)

1.2 Objectives and Scope of Research

The dissertation research is a primary part of the research project, "Calibration and Refinement of Illinois' Earthquake Resisting System Bridge Design Methodology: Phase II" , sponsored by the Illinois Department of Transportation (IDOT) and the Illinois Center for Transportation (ICT). The objectives of the dissertation research are to assess seismic performance of prototype quasi-isolated highway bridges with seat-type abutments, reveal seismic response characteristics of bridges with various permutations of typical configurations, identify deficient performance and potential risks of severe damage to critical components and global bridge collapse, and recommend practical strategies for seismic performance improvement.

To accomplish these objectives, extensive and comprehensive computational investigations were performed on a suite of prototype quasi-isolated bridges. The suite encompasses three-span and four-span bridges with steel-plate and prestressed-precast-concrete (PPC) girders, which are categorized into four major types of bridges based on the span number and girder type. The bridges are supported by non-skew and skew seat-type abutments in conjunction with RC multi-column intermediate piers. These substructures are supported by steel H pile foundations. Figure 1.3 shows an example of the bridges studied in the dissertation. Integral-abutment bridges are being studied as another primary part of the research project and is out of the scope of the presented research. In order to cover common bridge configuration variations in the assessment, the suite of prototype bridges includes five bridge skew angles, two pier column heights, and two foundation soil conditions for each of the four major types of bridges, which results in 80 bridge variants in total.

For each of the 80 bridge variants, a three-dimensional nonlinear finite-element model was created. Especially, a detailed yet efficient nonlinear finite-element model was developed for seat-type bridge abutments, considering seismic superstructure-abutment-foundation interactions. Multi-mode adaptive pushover and eigenvalue modal analyses were performed on these bridge models, as the first step of the seismic assessment program. Various bridge pushover and modal responses were investigated. As the most important part of the research, a comprehensive and extensive assessment of seismic performance for the quasi-isolated bridge variants, in which thousands of nonlinear dynamic time-history analyses were conducted using a suite of site-specific earthquake

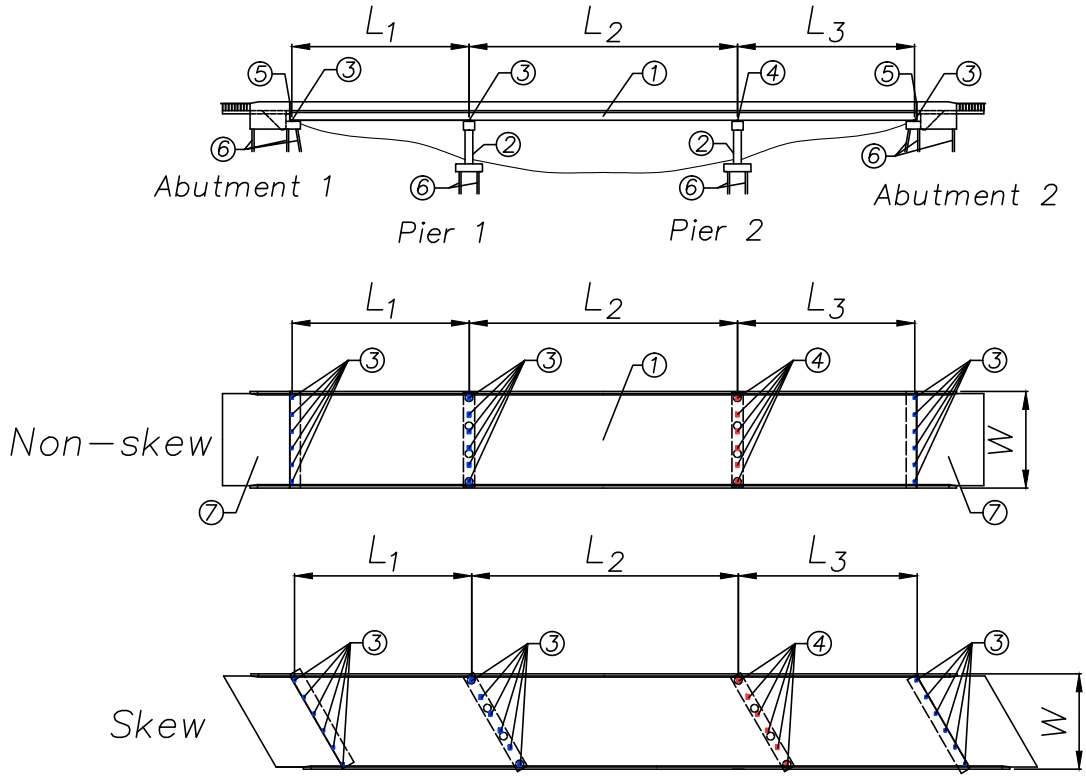

Figure 1.3: A prototype quasi-isolated seat-type abutment highway bridge in Illinois

ground motions taking into account the regional seismicity and geotechnical condition of southern Illinois. Bridge seismic response characteristics including bearing unseating, fusing of sacrificial superstructure-substructure connections, and critical component damaging at substructures and foundations were revealed. The research culminated in preliminary recommendations for improving bridge seismic performance and reduce risks of excessive critical component damage and global bridge collapse. The efficacy of the recommendations were demonstrated by comparative studies.

1.3 Organization of Dissertation

The chapters of the dissertation are organized in the following order:

- Chapter 1 introduces the background and core concepts of the quasi-isolation earthquake-resistant highway bridge design strategy, and provides objectives and scope of the dissertation research.

- Chapter 2 presents a review of previous research on the quasi-isolation seismic bridge design strategy, computational modeling of seat-type abutments for seismic highway bridge analysis, and seismic response analysis of highway bridges.

- Chapter 3 presents a detailed description of the prototype quasi-isolated highway bridge variants that are computationally modeled and studied in the dissertation. The computational modeling approaches for bridge superstructures, multi-column substructures, and pile foundations are discussed.

- Chapter 4 presents a detailed computational model of seat-type bridge abutments, which takes into account seismic superstructure-abutment-foundation interactions.

- Chapter 5 discusses response characteristics of quasi-isolated bridge variants observed in static pushover and eigenvalue modal analyses.

- Chapter 6 presents a comprehensive and extensive seismic performance assessment of prototype bridge variants via nonlinear dynamic time-history analyses using a suite of site-specific

earthquake ground motions. The seismic performance of the prototype bridge variants is statistically summarized. Deficiencies of the bridge seismic performance are revealed. Strategies for improving the seismic performance are proposed and the efficacy is demonstrated through comparative studies.

- Chapter 7 summarizes the presented research, presents important conclusions drawn from the various bridge analyses, and recommends future research directions.

CHAPTER 2

LITERATURE REVIEW

The literature review presented in this chapter begins with a brief introduction to the methodology and achievements of prior research on quasi-isolated highway bridges in Illinois. Various investigations on the stiffness and capacity properties of seat-type bridge abutments in passive conditions is then reviewed. Finally, a number of representative computational and analytical studies on seismic response analysis of seat-type abutment highway bridges are introduced, as the methodologies or conclusions of these studies are relevant to the present research.

2.1 Prior Research on Quasi-Isolated Highway Bridges in Illinois

In order to calibrate and refine the earthquake resisting system (ERS) bridge design methodology, the Illinois Department of Transportation (IDOT) and the Illinois Center for Transportation (ICT) sponsored a research project with the University of Illinois at Urbana-Champaign. During its first phase (Project No. ICT-R27-070) that was completed in 2013, experimental and computational investigations were carried out primarily in the following research areas:

1. Laboratory experimental tests on full-scale specimens of typical bearing components for quasi-isolation;

2. Computational modeling of bearing components validated and calibrated using full-scale experimental results;

3. Computational modeling of complete bridge systems;

4. Parametric studies employing complete bridge models and synthetic ground motions to explore system-level seismic performance for a suite of prototype Illinois bridges;

5. Recommendations for improving seismic design of quasi-isolated ERS bridges based on experimental and computational results.

Detailed results of these investigations have been documented in published technical reports (LaFave et al. 2013a,b) and journal articles (Steelman et al. 2013, 2014, 2016; Filipov et al. 2013a,b). Summarized approaches and important findings and conclusions are reviewed in the following subsections.

2.1.1 Laboratory experimental tests on full-scale specimens of typical bearing components for quasi-isolation

Experimental testing program on full-scale specimens of typical bridge bearing components in Illinois was conducted in the Newmark Civil Engineering Laboratory at the University of Illinois at Urbana-Champaign (LaFave et al. 2013a; Steelman 2013). The experimental setup is shown in Figure 2.1, which was designed to simulate real seismic loading conditions for the bearing components installed in bridges. A pair of actuators with a 445-kN (100-kip) force capacity was used to apply approximately constant vertical loading during a test on the bearing specimen, in order to simulate gravity loads of bridge superstructures imposed on the bearing. Additionally, another actuator with a 980-kN (220-kip) force capacity and 762 mm (30 in.) stroke was used to apply horizontal forces and displacements on the specimen, simulating lateral seismic demands on the bearing specimen.

Full-scale specimens of three types of non-seismically designed bridge bearings were tested, namely steel-reinforced laminated elastomeric expansion bearings (IDOT Type I bearings), bearings comprised of a steel-reinforced laminated elastomer and a stainless steel-on-Teflon sliding surface (IDOT Type II bearings), and low-profile steel fixed bearings. Configurations of the Type I bearing and low-profile steel fixed bearing are shown in Figure 1.2, while configuration of the Type II bearing is shown in Figure 2.2. For the Type II bearing, the elastomer is vulcanized between a pair of steel plates on its top and bottom, denoted as bottom and middle plate of the bearing. The bottom plate is anchored to concrete substructures. A thin layer of PTFE material is firmly attached to the top surface of the bearing middle plate. A stainless-steel sheet is installed on the bottom surface of the bearing top plate as the mating surface of the PTFE material. Sliding of

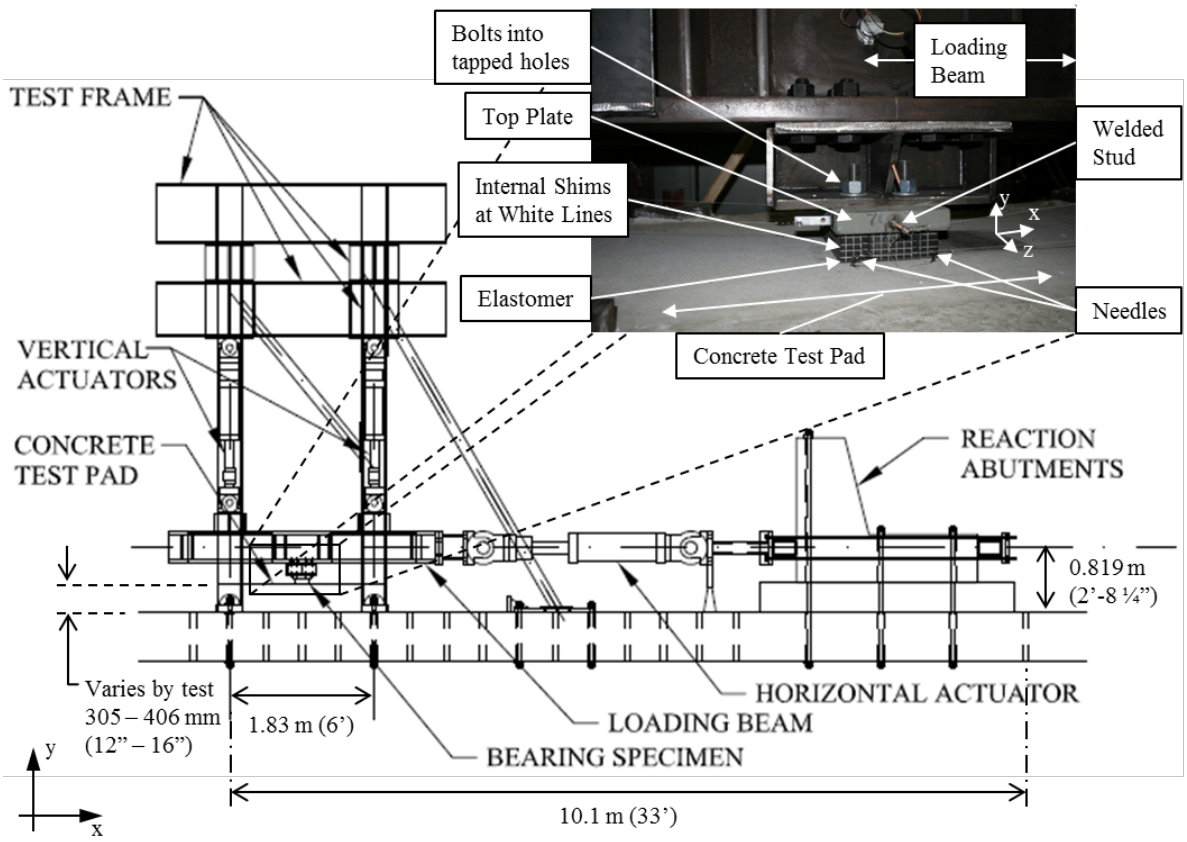

Figure 2.1: Experimental setup for full-scale bearing tests (after LaFave et al. 2013a; Steelman 2013)

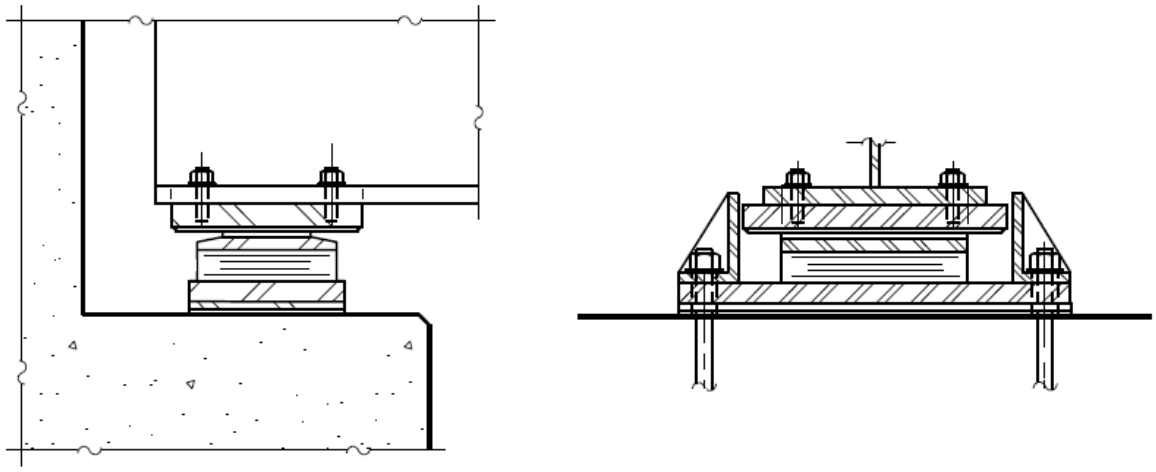

Figure 2.2: Type II elastomeric bearing with transverse bearing retainers employed by quasi-isolated highway bridges in Illinois (after IDOT 2012a)

Type II bearings occurs at this PTFE-stainless steel interface between the middle and top steel plates. These bearing components were tested under various monotonic and cyclic, quasi-static and dynamic displacement protocols in the longitudinal and transverse bridge directions.

For Type I elastomeric bearings, Steelman et al. (2013) indicated that the tested bearing specimens exhibited an approximately linear elastic response before sliding. The initial coefficient of friction is in the range of 0.25 to 0.50 at a shear strain between 125% to 250%, varying with the contact surface roughness, loading velocity, and axial load on the bearing. Under cyclic displacement protocols, noticeable deterioration of slip resistance under constant vertical load was found, as roughness of the concrete surface was reduced by the abraded elastomer fragments. Additionally, coefficients of friction observed during the tests was significantly affected by the varying vertical load. These two parameters followed an inversely proportioned nonlinear trend. The AASHTO specification (AASHTO 2010) recommends a coefficient of friction for elastomer to concrete interface of 0.20, which was found to be a conservative lower bound of the observed coefficient of friction during the tests under different vertical loads. In the quasi-static tests, the coefficient of friction for elastomer sliding on concrete ranged from about 0.20 to 0.55.

For Type II elastomeric bearings, Steelman et al. (2016) indicated that large bearing sliding displacements would cause delamination and progressive removal of the PTFE material from the bearing middle plate, but the bearing slided well with up to 20% of the Teflon exposed during a test. The coefficient of friction at the PTFE to stainless steel interface varied with vertical loads and sliding rates, and was found to range from about 0.12 to 0.18.

Two possible failure mechanisms of low-profile steel fixed bearings were examined by Steelman et al. (2014): weak anchors securing the bottom steel plate to the concrete substructure, and weak pintles mating the top and bottom steel plates. It was found that the weak anchor design option is preferred to the weak pintle option, as the weak anchor design exhibited a clear shear failure of the anchor bolts with limited damage to the surrounding concrete and also insensitive bearing behavior to loading orientations. Fusing capacity of one anchor bolt, R_u, can be reliably predicted using Equation (2.1)

$$R_u = \phi(0.6)(0.8)F_u A_g \tag{2.1}$$

where ϕ is the strength reduction factor ($\phi = 1.0$ for nominal capacity), F_u is the ultimate tensile

strength of the anchor bolt material, and A_g is the gross cross-sectional area of the anchor bolt. The coefficient of friction for the post-fusing sliding of the elastomeric leveling pad on concrete substructures is around 0.30.

Width of the bearing side retainer in the transverse bridge direction was found to have significant influence on its interaction with the concrete to which it is anchored. Per the IDOT Bridge Manual (IDOT 2012a), anchorage of the bearing retainer is intended to be fused by a lateral load equal to 20% of the superstructure dead load on the bearing, but retainer specimens exhibited much higher fusing capacity in the experimental tests. Representative failure process starts with elasto-plastic deformation of the retainer anchor bolt. Subsequent crushing of surrounding concrete near the anchor and retainer toe was clearly observed. The process ended with shear-tension rupture of the anchor bolt. Fusing capacity of one retainer anchor bolt, R_u, can be reliably predicted using Equation (2.2)

$$R_u = \phi(0.8)F_u A_g \tag{2.2}$$

where ϕ is the strength reduction factor ($\phi = 1.0$ for nominal capacity), F_u is the ultimate tensile strength of the anchor bolt material, and A_g is the gross cross-sectional area of the anchor bolt.

2.1.2 Computational models of typical bearing components in quasi-isolated highway bridges

Filipov et al. (2013a) developed a coupled bi-directional nonlinear element to capture the shear and sliding behavior of Type I and II elastomeric bearings using experimentally tested bearing response data. The model captures a number of distinct phases of bearing shear and sliding behavior by using multiple coefficients of friction, namely an initial static coefficient of friction μ_{SI}, a kinetic coefficient of friction, μ_{K}, and a stick-slip coefficient of friction μ_{SP}. Figure 2.3 shows the schematic of shear and sliding behavior of the bearing element. The model has been validated and calibrated using results of experimental tests on full-scale bearing specimens. In numerical simulations on complete bridge models, μ_{SI}, μ_{K}, and μ_{SP} specified for Type I bearings are 0.60, 0.45, 0.50, respectively; for Type II bearings, the values are 0.16, 0.15 and 0.15, respectively. 85 psi was used as shear modulus of the elastomer.

A coupled bi-directional nonlinear element was developed to capture the elasto-plastic behavior

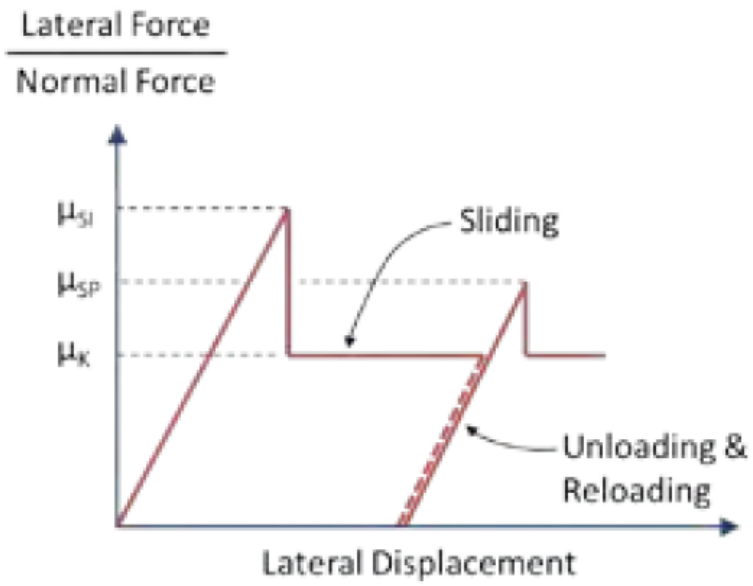

Figure 2.3: Schematic of computational model for stick-slip shear and friction behavior of elastomeric bearings (after LaFave et al. 2013b; Filipov et al. 2013a)

of the steel anchor bolts securing low-profile steel fixed bearing into concrete when subjected to horizontal shear demands (LaFave et al. 2013b; Filipov et al. 2013b). Figure 2.4 schematically illustrates the force-displacement relation of the model. Additionally, the model for sliding behavior of elastomer on concrete is superimposed to the steel anchor model, in order to simulate the post-fusing sliding at the elastomeric pad-concrete interface. This combination of two different types of model was also validated against experimental results.

Yielding and rupture of the retainer anchor bolt under lateral forces was modeled using a unidirectional elasto-plastic computational model (LaFave et al. 2013b; Filipov et al. 2013b). Figure 2.5 schematically illustrates the force-displacement relation of the model.

2.1.3 Parametric studies employing complete bridge models and synthetic seismic ground motions

In the computational parametric study conducted in the first phase of the research project, a suite of 48 quasi-isolated highway bridges with three-span continuous superstructures, non-seismically designed bearing components, and non-skew seat-type abutments were developed (LaFave et al. 2013b; Filipov et al. 2013b). Parametric variations of these bridges are shown in Figure 2.6.

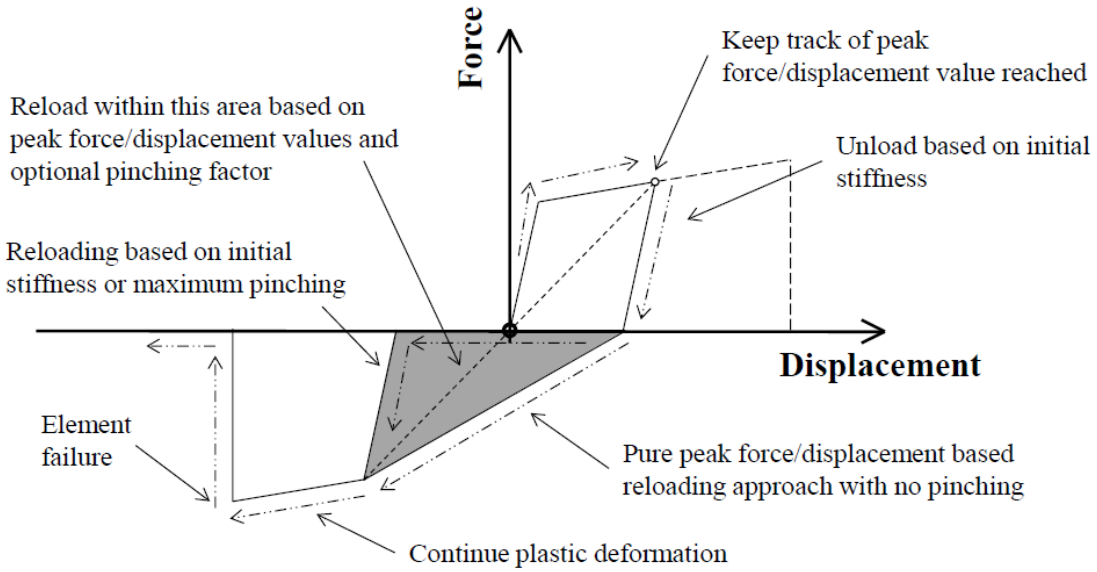

Figure 2.4: Schematic of computation model for elasto-plastic shear behavior of steel fixed bearing anchors (after LaFave et al. 2013a; Filipov et al. 2013b)

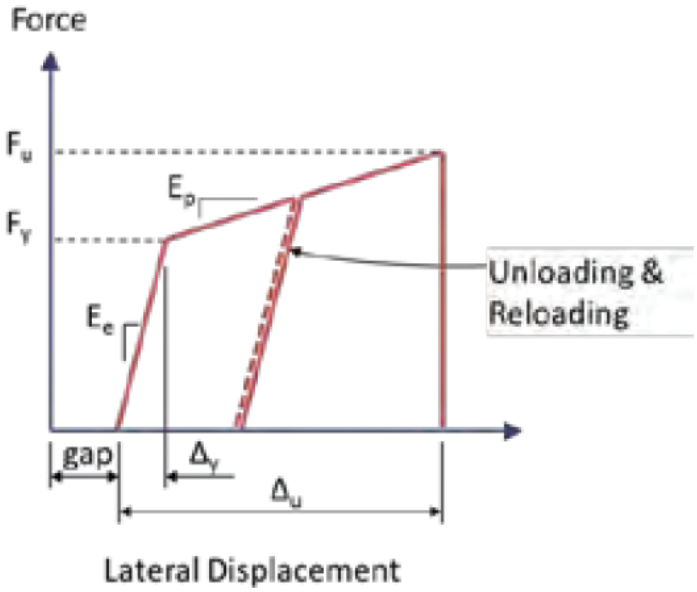

Figure 2.5: Schematic of computational model for elasto-plastic shear behavior of bearing retainer anchors (after LaFave et al. 2013b; Filipov et al. 2013a)

Among the 80 bridges that are studied in the present research, only 2 bridges have very similar

		Bridge Type 1 Steel - Short				Bridge Type 2 Steel - Long				Bridge Type 3 Concrete - Short				Variations
Parameter	**Alternatives**	1	2	3	4	5	6	7	8	9	10	11	12	
Span Length & Bridge Type (ft)	50' - 50' - 50'	*	*	*	*									3
	60' - 60' - 60'									*	*	*	*	
	80' - 120' - 80'					*	*	*	*					
Intermediate Sub-Structure	Continuous Wall	*	*			*	*			*	*			2
	Multi Column Pier			*	*			*	*			*	*	
Intermediate Sub-Structure Height	Short - 15'	*		*		*		*		*		*		2
	Tall - 40'		*		*		*		*		*		*	
Movement Bearings	Type I Elastomeric	All (12) of the above bridges are modeled with Elastomeric Type I and Type II Bearings												2
	Type II Elastomeric													
Foundations	Fixed Foundation	All (24) of the above bridges are modeled with Fixed and Flexible Foundations												2
	Flexible Foundation													

Figure 2.6: Bridge variants studied in prior research (after LaFave et al. 2013b; Filipov 2012)

configurations to two bridges studied in the prior research, while the other 78 bridges were not studied in the prior phase of the research project. Nonlinear finite-element models were developed for these 48 bridges. A suite of 20 synthetic ground motions developed by (Fernandez and Rix 2008) with an approximately 1,000-year return period were employed in nonlinear dynamic bridge analyses. A number of important observations were made from the nonlinear dynamic bridge analysis results and are briefly summarized as follows:

- Most of the bridges did not experience bearing unseating under design-level earthquake excitations.

- Bridges equipped with Type I elastomeric bearings demonstrated reliable behavior in preventing bridge span loss. For bridges equipped with Type I bearings, unseating was not observed when the bridges were subjected to longitudinal earthquake ground motions, but was observed when the bridges were subjected to MCE-level transverse earthquake ground motions.

- Bridges equipped with Type II elastomeric bearings were shown to be more prone to unseating than those with Type I bearings.

- Displacement response of bridges with tall piers and Type II bearings was significantly larger than the other bridges.
- Response of a few bridges under bi-directional seismic excitation was found to be smaller than their response under uni-axial ground motions.

Based on the dynamic analysis results, a few recommendations were made for improving the quasi-isolation strategy:

- Use of Type II elastomeric bearings should be limited to regions of low or moderate seismicity due to its high risk of unseating.
- Type I bearings are appropriate for use in regions with all seismic hazard levels.
- Contribution of abutment backwall to limiting bridge longitudinal response should be considered in bridge seismic design.

2.2 Computational Modeling of Seat-Type Bridge Abutments for Seismic Analysis of Highway Bridges

Seat-type abutments are commonly used for highway bridges in many regions of the United States. The structural components of a typical seat-type abutment may include a backwall, two wingwalls, a stem wall (pile cap) and piles, an approach slab, and bearing components. A primary feature that distinguishes seat-type bridge abutments from integral and semi-integral abutments is that an expansion joint is set between the abutment backwall and adjacent superstructure end to accommodate thermally induced bridge deformation by separating the superstructure from abutments.

The abutment backwall and wingwalls are traditionally designed to withstand active pressure of backfill soil and maintain integrity of the abutment. Design of abutment for service conditions is relatively straightforward, which typically ensures that the reinforced concrete walls, foundation, and connections can withstand gravity load of bridge superstructure and traveling vehicles, as well as active pressure of backfill soil, but complications arise when seismic demands are considered. Seat-type abutments and their foundations provide considerable resistance to the longitudinal seismic displacements of bridge superstructures and, in return, are subjected to large seismic force

demands brought by the superstructures. A number of post-earthquake reconnaissance reports have indicated seismic bridge damage and failures caused by superstructure-abutment-foundation interactions under moderate to strong earthquakes, including unseating of superstructures at abutments (Buckle 1994; Elnashai et al. 2010; Kawashima et al. 2011; Lee and Loh 2000; Yen et al. 2011), overturning and large residual displacements of abutment foundations (Jennings 1971; Sardo et al. 2006), local pounding damage and global failure of concrete backwall (Lee and Loh 2000; Sardo et al. 2006; Yen et al. 2011), excessive deformation of backfill and embankment soil (Lee and Loh 2000), as well as shear key failure (Shamsabadi 2007; Kawashima et al. 2011; Yen et al. 2011).

In view of these seismic damage and failures of bridge abutments, researchers have conducted various investigations for better understanding and proper modeling of abutment response characteristics and superstructure-abutment-foundation interactions under seismic demands. In recent years, a number of large-scale field experimental tests on the capacity and stiffness properties of seat-type abutments in passive conditions were carried out (e.g. Stewart et al. 2007; Bozorgzadeh et al. 2008; Wilson and Elgamal 2010).

Stewart et al. (2007) and Lemnitzer et al. (2009) experimentally tested a 4.6-m wide, 1.67-m tall full-scale concrete backwall that was pushed by static loading into silty sand backfill. The backwall was not vertically restrained. The failure surface exhibited a nearly logarithmic-spiral shape. The length of failure soil wedge was approximately three times the backwall height. The measured force-displacement backbone curve can be well represented by a hyperbolic shape until an ultimate capacity was reached at a wall top displacement equal to 3% of wall height. The wall-soil interface friction angle was in the range of 13° to 20°. The initial loading stiffness was found to be smaller than the measured reloading stiffness.

Bozorgzadeh et al. (2008) performed a series of large-scale field tests on bridge abutments to study the stiffness and capacity of the abutment in the longitudinal bridge direction. In the first phase of the test program, diaphragm abutment specimens were tested. In the second phase, the backwall of a seat-type abutment was tested. The backwall of the seat-type abutment was assumed to be already sheared off from the stemwall and wingwall. Test results demonstrated that the bridge abutment response in the longitudinal direction is nonlinear, and the major resistance to abutment displacement is the backfill passive resistance. It was found that the abutment capacity and stiffness

depend on a number of factors such as the soil properties, vertical wall movement, height and area of backwall. The passive backfill resistance was found to be significantly affected by the soil shear strength and soil-wall friction angle.

Wilson and Elgamal (2010) conducted large-scale passive soil load-displacement tests. A concrete backwall was placed in a 6.7-m long, 2.9-m wide soil container. Densely compacted sand with 7% silt was placed behind the backwall. The backwall was buried in the soil with a depth of 1.68 m. The backwall was monotonically pushed against the soil. It was found that the ultimate backfill capacity was reached at a displacement of 3% of the wall height. The passive failure soil wedge was found to fully developed near the peak load. After the ultimate capacity, the passive resistance dropped to a residual level of around 60% the ultimate capacity. The experimentally measured load-displacement relation up to the ultimate capacity can be approximated by a hyperbolic curve.

In addition to these experimental tests, analytical studies (Wilson 1988; Shamsabadi et al. 2005, 2007) were also conducted to estimate the stiffness and capacity characteristics of bridge abutments for seismic performance-based bridge design and analysis.

Wilson (1988) developed a simple analytical model to describe the stiffness of non-skew monolithic bridge abutments. The model employs three translational and three rotational linear elastic springs to account for the equivalent stiffness of the abutment walls, piles, and soil in six degrees-of-freedom. The nonlinear inelastic response of the abutment piles and soil was not considered.

Shamsabadi et al. (2005, 2007) proposed an analytical limit-equilibrium method for estimating passive nonlinear force-deformation response of abutment backfill with different soil properties. The method employs logarithmic-spiral failure surfaces coupled with a modified hyperbolic soil stress-strain behavior. The method can estimate the passive force-deformation response of abutment backfill up to the ultimate capacity and has been validated against a number of field experiments conducted on backfill soil with various properties. Using this method to estimate the passive force-deformation response of abutment backfill is recommended by Caltrans (2013).

Besides these experimental and analytical investigations, numerical simulations (Crouse et al. 1987; Martin et al. 1997; Rollins et al. 2010b) and system identifications (Werner et al. 1987; Wilson and Tan 1990; Goel and Chopra 1997) were also conducted to investigate the stiffness and capacity characteristics of bridge abutments during earthquakes and the implications for seismic

bridge response.

Article 5.2.3.3 of the AASHTO Guide Specifications for LRFD Seismic Bridge Design (AASHTO 2011) specifies an idealized bilinear model for estimating longitudinal force-deformation relation of seat-type bridge abutments, as shown in Figure 2.7. Per AASHTO (2011), the backfill

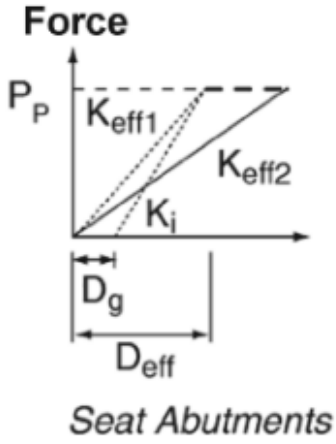

Figure 2.7: Characterization of abutment capacity and stiffness (after AASHTO 2011)

passive capacity, P_{p} may be determined as

$$P_{\mathrm{p}} = p_{\mathrm{p}} H_{\mathrm{w}} W_{\mathrm{w}} \tag{2.3}$$

where p_p is the passive lateral earth pressure behind backwall, H_w is the height of backwall, and W_w is the width of backwall. The value of p_p for different types of backfill soil is also recommended by AASHTO (2011). The initial estimate of the effective secant stiffness for seat-type abutments is specified as

$$K_{\mathrm{eff}} = \frac{P_{\mathrm{p}}}{F_{\mathrm{w}} H_{\mathrm{w}} + D_{\mathrm{g}}} \tag{2.4}$$

where F_{w} is a factor taken as between 0.01 to 0.05 for different backfill soils and D_{g} is the width of gap between backwall and superstructure. The effective stiffness K_{eff} should then be iteratively determined to achieve a consistency between K_{eff} and the abutment displacement D_{eff}.

Article 7.8.1 of the Caltrans Seismic Design Criteria (Caltrans 2013) specifies that a bilinear approximation of the force-deformation relationship may be used for abutment longitudinal response analysis, which is shown in Figure 2.8. The nonlinear force-deformation relationship proposed

by Shamsabadi (2007) may be used as an alternative to the bilinear approximation. The ultimate

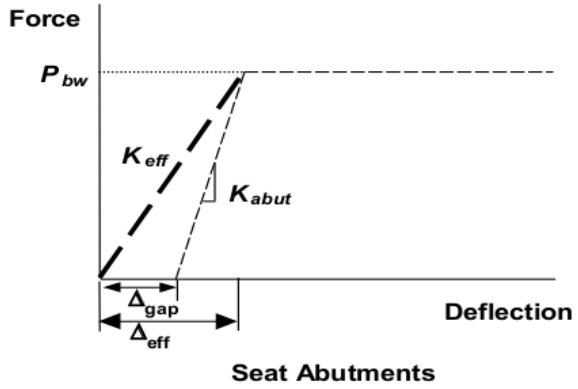

Figure 2.8: Abutment capacity and stiffness (after Caltrans 2013)

passive resistance, P_{bw}, is calculated according to the following equation

$$P_{\text{bw}} = A_{\text{e}} \times 5.0 \text{ ksf} \times \left(\frac{h_{\text{bw}}}{5.5}\right) \quad \text{(ft, kip)} \tag{2.5}$$

where h_{bw} is the backwall height and A_{e} is the effective backwall area. The abutment stiffness, K_{abut}, is determined according to Equation (2.6).

$$K_{\text{abut}} = K_{\text{i}} \times w \times \left(\frac{h_{\text{bw}}}{5.5 \text{ ft}}\right) \tag{2.6}$$

where $K_{\text{i}} \approx \frac{50 \text{ kips / in.}}{\text{ft}}$ is the initial stiffness of the embankment fill material.

2.3 Seismic Response Analysis of Highway Bridges with Seat-Type Abutments

Seismic response of seat-type abutment highway bridges has been extensively studied by many researchers over the past several decades using various analytical, numerical, and experimental approaches. A number of representative computational and analytical studies published in the 21st century are reviewed herein. Among all the studies on seismic response analysis of highway bridges, these studies are most relevant to the present research, in terms of the methodology or conclusion.

Meng et al. (2001) proposed a simplified analytical model for skew highway bridges. In this model, the bridge deck was assumed to be rigid, the abutments only provide vertical constraints to the deck, and the mass of pier columns is small compared to that of the deck. Formulas for estimating earthquake response of these bridges were also proposed. A number of parameters that affects the dynamic behavior of skew bridges were identified through a parametric study, which includes the deck aspect ratio, the stiffness eccentricity ratio, the skew angles, the natural frequencies, and the rotational to translational frequency ratio.

Zhang and Makris (2002) employed a stick-spring bridge model and a more sophisticated finite element model to compute seismic response of two instrumented highway bridges in California, taking into account the soil-structure interaction at bridge embankments. The dynamic stiffness of bridge embankments and pile group foundations were approximated by springs an dashpots. Bridge seismic response estimated by the proposed bridge models was validated against measured seismic response. It was concluded that the seismic bridge response can be reliably estimated with the stick-spring bridge model under certain conditions.

Nielson and DesRoches (2007) conducted seismic evaluations for a multi-span simply supported and a multi-span continuous girder bridge with typical configurations in the Central and Southeastern United States. Three-dimensional bridge models were developed and ground motions with a probability of exceedance of 2% in 50 years were employed in the seismic bridge analysis. It was found that using concrete continuity diaphragms between precast girders to make a continuous superstructure may result in high seismic demands to pier columns and abutments. It was concluded that the response of multi-span continuous-girder bridges was found to be dominated in the longitudinal direction and a 2-D longitudinal model may be used for assessing the seismic risk of this type of bridges. The multi-span simply-supported bridge was found to sustained similar degree of bearing deformations in the longitudinal and transverse directions.

Kalantari and Amjadian (2010) developed an analytical method for dynamic analysis of skewed highway bridges with continuous rigid deck. The deck was assumed to be rigid in its plane and vertically restrained. The translational and rotational stiffness of the substructures and shear stiffness of the bearings are modeled with linear springs. The bridge natural frequencies, mode shapes, and internal forces can be determined by simplified formulas of this method. The accuracy of the method was validated by a finite-element bridge model subjected to earthquake excitation. It was

claimed by the authors that this method can be used by bridge engineers for preliminary seismic design of skew bridges.

Mitoulis (2012) performed a comparative study on the seismic response of three real seat-type abutment bridges with various total length, expansion joint opening width, and backfill models. Nonlinear dynamic time-history analyses were performed on these bridges using moderate-to-strong earthquake ground motions. The analysis results demonstrated that the seat-type abutments can effective reduce the longitudinal seismic superstructure displacements and bending moments of pier columns. It was found that small expansion joints result in more effective reductions in bridge seismic demands. The author claimed that the seismic participation of seat-type abutment and backfill soil can lead to cost-effective bridge design as the participation of seat-type abutment can reduce the member size of pier columns, bearings, and foundations or be utilized as a second line of defense against seismic demands.

Kaviani et al. (2012) conducted extensive seismic analyses on reinforced concrete highway bridges with skew-angled seat-type abutments. A number of bridge variants were developed from three real highway bridges with seat-type abutments in the state of California by varying the abutment skew angles, column heights, and span arrangements. The bridge models were subjected to forty earthquake ground motions that are representative of the types of expected seismic excitation in California. The analysis results indicated that seismic response of skew bridges, such as deck rotation and column drift, was higher than the equivalent non-skew bridges under the same seismic excitation, and skew bridges are more prone to collapse then non-skew ones. It was also found that the seismic response of skew bridges was large affected by the bridge skew and column height, but appeared to be insensitive to the span arrangement.

Kwon and Jeong (2013) studied one- and two-span skew highway bridges supported by elastomeric bearings. Analytical and numerical simulations were performed to investigate the seismic displacement demands of these bridges. The effects of vertical ground motions, skew angles, aspect ratios, and ground motion characteristics on bridge displacement demands were studied. It was concluded that the vertical ground motions do not largely affect the maximum bridge lateral displacement demand. The skew angle was found to increase the rotational demand of bridge superstructures when subjected to near-fault ground motions but does not significantly increase the maximum abutment-parallel displacement. The bridge skew was found to have important effects

on deck end displacements in the abutment-normal direction. It was also concluded that the minimum seat width specified by AASHTO may not be conservative for preventing deck unseating of bridges when subjected to near-fault ground motions.

Through reviewing the existing studies, it was learned that the computational bridge model should at least incorporate reasonably developed nonlinear models for bearing components, pier columns, and abutments. Especially, the superstructure-abutment interaction effect needs to be sufficiently accounted by the abutment model, so that the dynamic pounding forces between abutments and deck ends, unseating of deck ends at abutments, rotation of skew bridge decks, and other critical seismic response of seat-type abutment bridges can be captured. In contrast, the bridge superstructure is typically modeled using linear elastic beam or shell elements to save computational cost, as it is not expected to sustain excessive seismic damage. The bridge foundation can be modeled using either lumped springs or explicit piles with distributed soil springs. The ground motions used in the existing studies are typically accelerograms recorded from major historical earthquakes.

CHAPTER 3

COMPUTATIONAL MODELING OF PROTOTYPE QUASI-ISOLATED HIGHWAY BRIDGES

To comprehensively investigate the seismic response characteristics of quasi-isolated seat-type abutment highway bridges in Illinois, a suite of prototype bridges were computationally modeled for subsequent studies. The suite encompasses three-span and four-span bridges with steel-plate and prestressed-precast-concrete (PPC) girders, which are categorized into four major types of bridges based on the span arrangement and girder type. For each of the four major bridge types, 20 bridge variants that differ in the skew angle, pier column height, and foundation soil condition were included, in order to investigate the effect of these parameters on bridge seismic response. The 80 bridge variants in total were intended to represent both common existing quasi-isolated bridges and design trends for future bridges in the state of Illinois.

The nonlinear finite-element package Open System for Earthquake Engineering Simulation (*OpenSees*) was employed to computationally model the bridges. Detailed three-dimensional (3-D) finite-element models were created for all the 80 prototype bridge variants. The finite-element bridge model includes various nonlinear materials and elements for modeling critical structural components and geotechnical mechanisms of the bridges, which will be introduced in detail in Chapters 3 and 4.

3.1 Prototype Quasi-Isolated Highway Bridges

The prototype bridges studied in the present research have either three or four spans, steel-plate girders or precast-prestressed-concrete (PPC) girders, concrete deck, sacrificial superstructure-substructure connections, as well as seat-type abutments and reinforced-concrete (RC) multi-column piers that are supported by steel pile foundations. The four major types of these bridges will hereafter be designated by "**3S**" bridges (**3**-span **S**teel-plate-girder bridges), "**4S**" bridges (**4**-

span **S**teel-plate-girder bridges), "**3C**" bridges (**3**-span precast-prestressed-**C**oncrete-girder bridges), and "**4C**" bridges (**4**-span precast-prestressed-**C**oncrete-girder bridges). The configurations and dimensions of these types of bridges were determined based on a survey of existing bridges in Illinois using a bridge inventory database (IDOT n.d.) and internal discussions with IDOT bridge engineers. These bridges were proportioned according to the IDOT Bridge Manual (IDOT 2012a) and intended to represent both common existing quasi-isolated bridges and design trends for future bridges in the state of Illinois.

Figures 3.1 to 3.8 present the non-skew and skew prototype bridges. In addition to these figures, Table 3.1 lists detailed design parameters of critical structural components for each major bridge type. Some of the components and their computational models will be introduced in more detail in later sections. From each major bridge type, a number of bridge variants were generated. These variants constitute a bridge suite for the subsequent static and dynamic analyses that are discussed in detail in later chapters. Specifically, five skew angles ($0°, 15°, 30°, 45°,$ and $60°$), two pier column clear heights [4.57 m (15 ft) and 12.19 m (40 ft)], and two foundation soil conditions (hard and soft) were considered, thereby 20 variants were generated from each major bridge type and 80 in total were included in the bridge suite, as indicated in Table 3.2. In this study, the bridges are exclusively "left" skewed. The skew direction and angles are shown in Figures 3.1, 3.3, 3.5, and 3.7.

In the present study, the deck width was an invariant for all the prototype bridges. The out-to-out deck width, 43 ft - 2 in. (13.2 m), is a typical width for two-lane highway bridges with roadways and shoulders. On the basis of post-earthquake reconnaissance after the 2010 Chile earthquake, Kawashima et al. (2011) studied a number of skew bridges with different aspect ratios (deck width divided by length) and indicated that the aspect ratio of skew bridge decks plays an important role in affecting in-plane rotational response of skew bridges during an earthquake. The effect of deck width in affecting seismic response of quasi-isolated bridges, especially skew ones, can be investigated in future research.

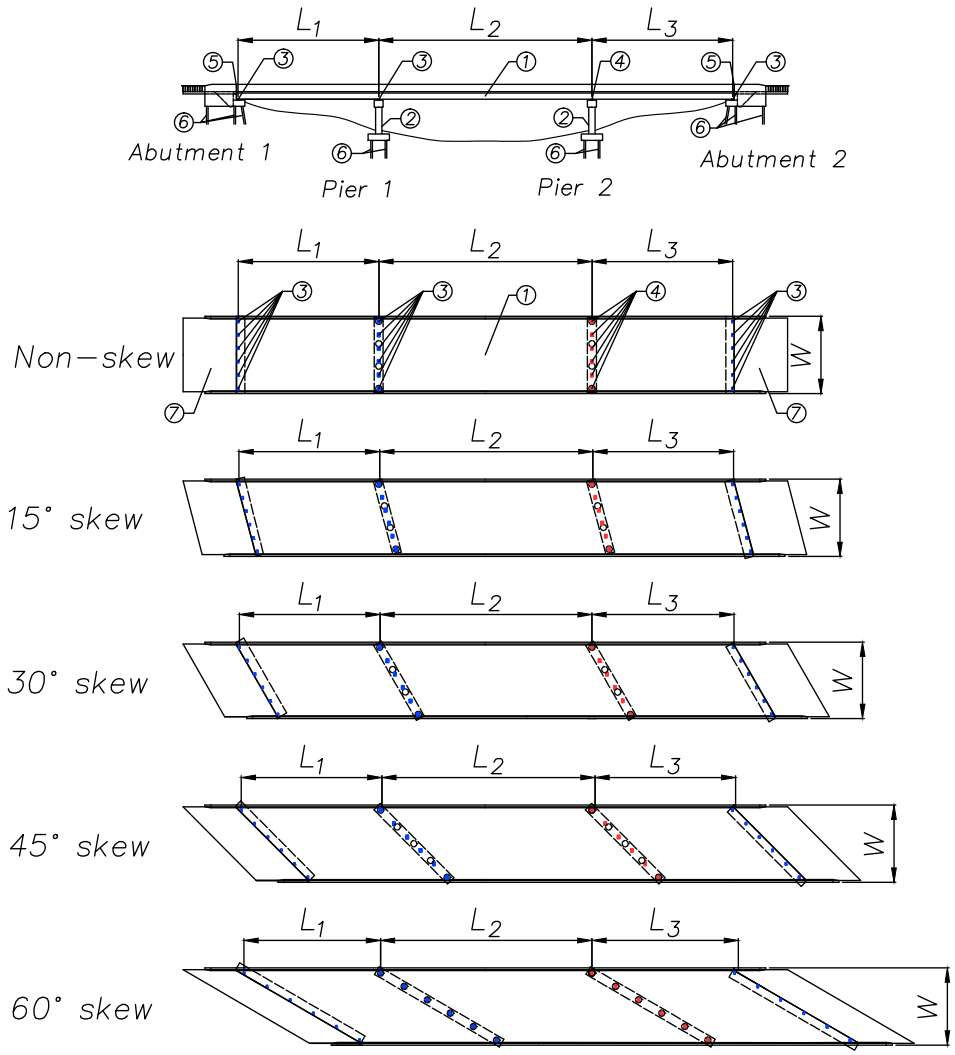

① Steel plate girders with composite concrete deck
② Multi−column reinforced concrete pier
③ IDOT Type I elastomeric expansion bearing with side retainers
④ IDOT low−profile steel fixed bearing
⑤ Thermal expansion joint between deck end and abutment backwall
⑥ Steel H pile
⑦ Concrete approach slab

W = 13.16 m (43'−2")
L_1 =24.38 m (80')
L_2 =36.58 m (120')
L_3 =24.38 m (80')

Note: Superstructure consists of six girders. Each girder is supported by one bearing at substructures.

Figure 3.1: Prototype three-span steel-plate-girder (3S) quasi-isolated seat-type abutment bridges

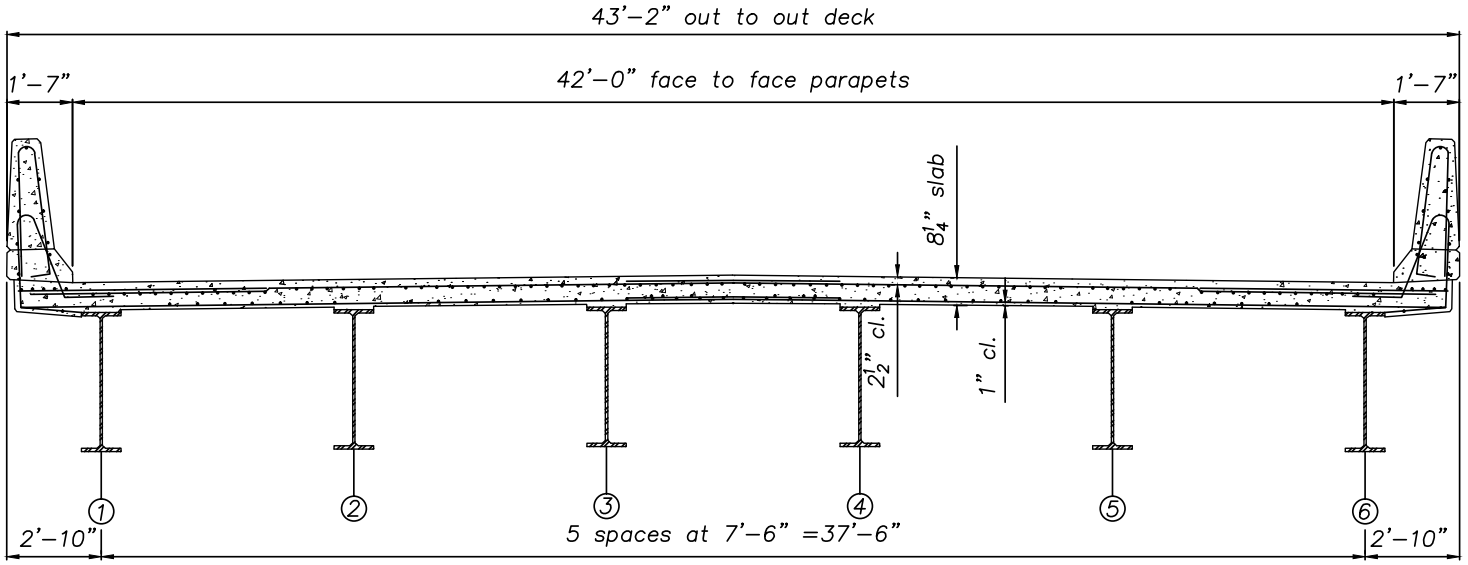

Figure 3.2: Cross-section of a 3S bridge superstructure

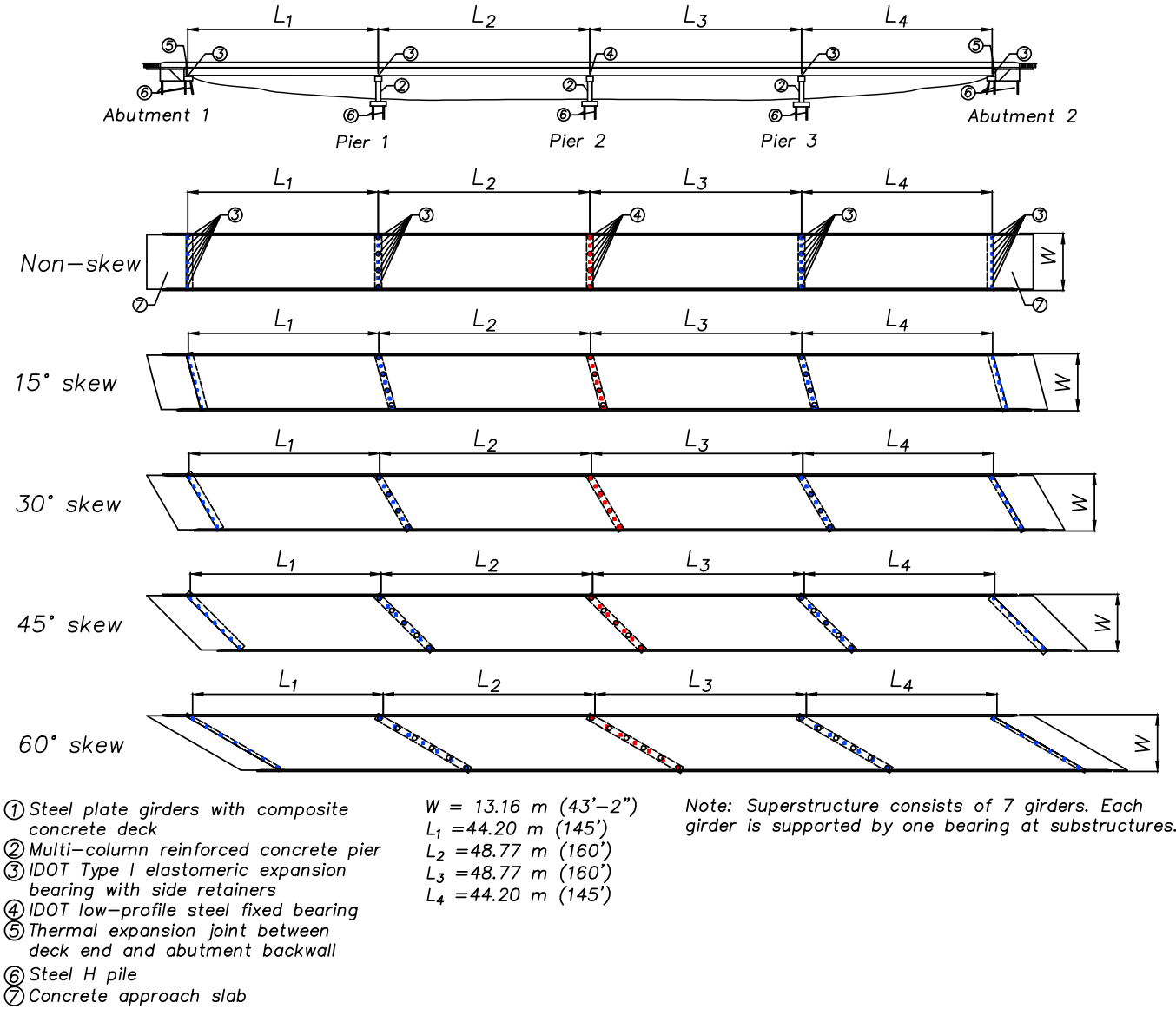

Figure 3.3: Prototype four-span steel-plate-girder (4S) quasi-isolated seat-type abutment bridges

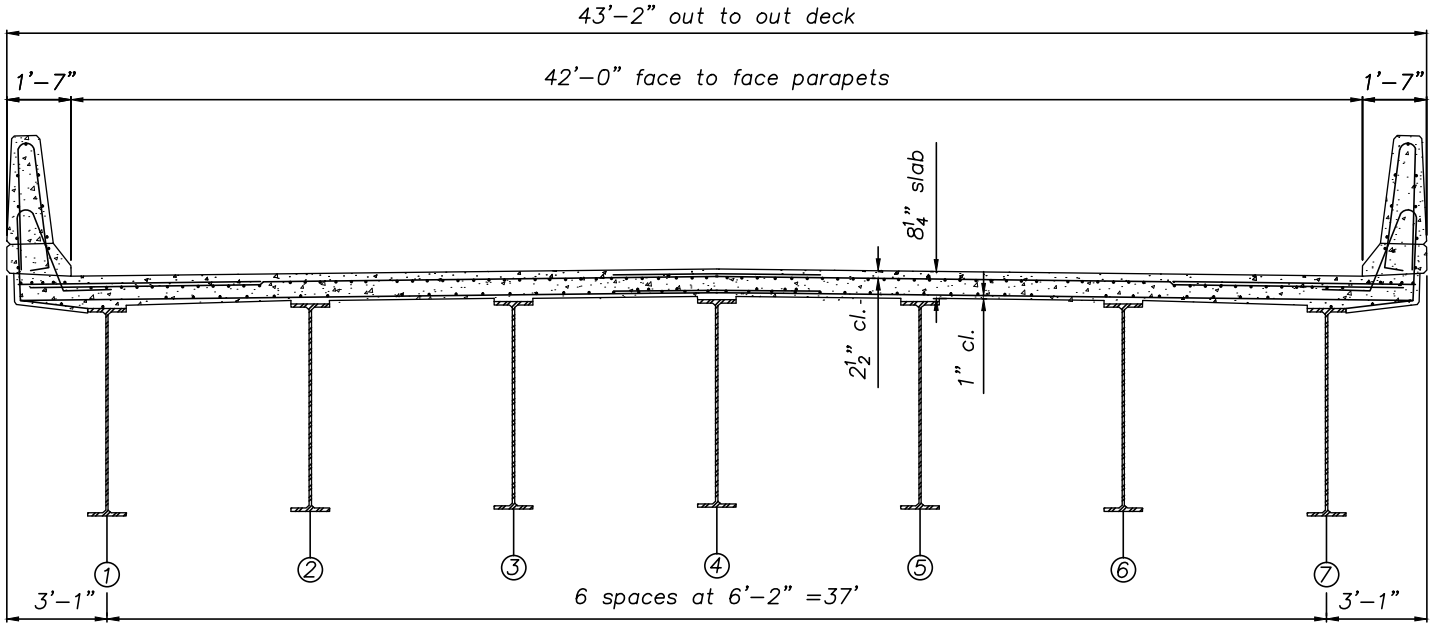

Figure 3.4: Cross-section of a 4S bridge superstructure

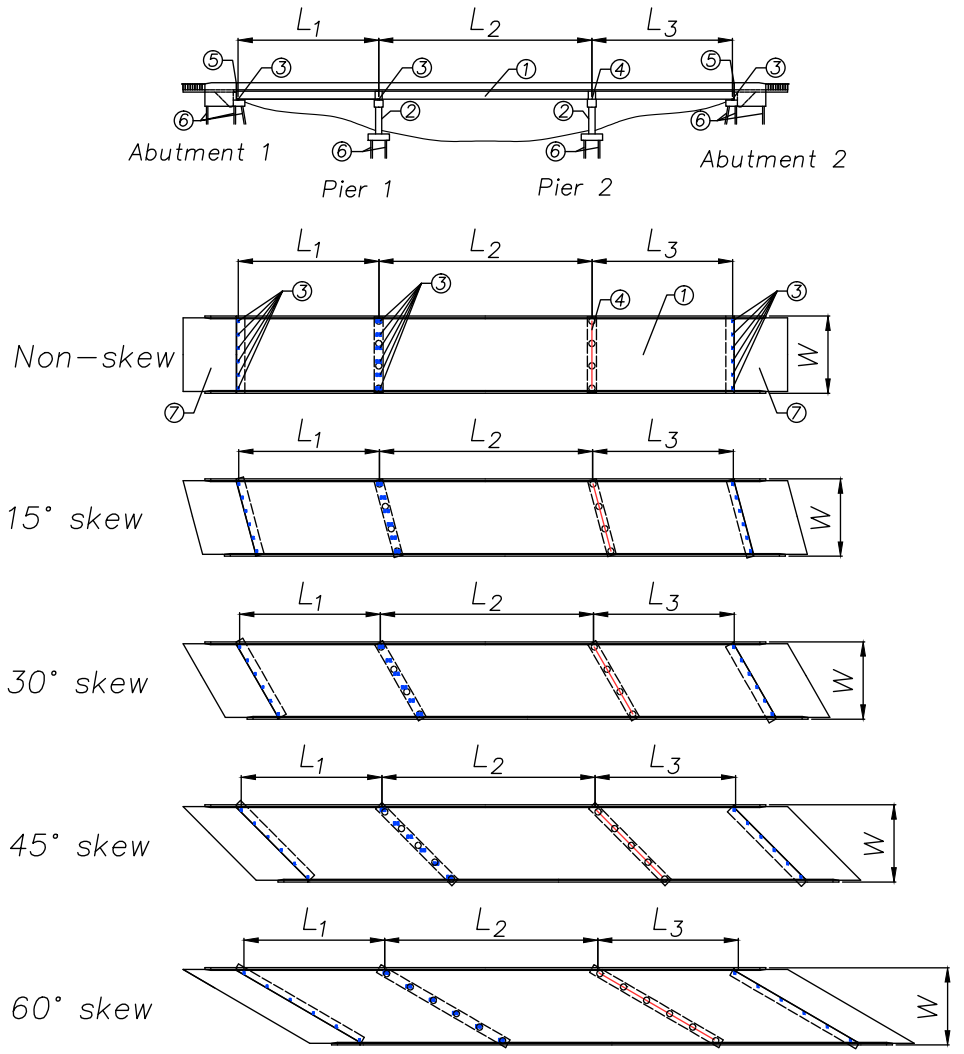

① PPC girders with composite concrete deck
② Multi−column reinforced concrete pier
③ IDOT Type I elastomeric expansion bearing with side retainers
④ #8 (U.S.) steel dowel connection
⑤ Thermal expansion joint between deck end and abutment backwall
⑥ Steel H pile
⑦ Concrete approach slab

W = 13.16 m (43'−2")
L_1 =24.38 m (80')
L_2 =36.58 m (120')
L_3 =24.38 m (80')

Note: Superstructure consists of 6 girders. Each girder is supported by two bearings at Pier 1 but supported by only one bearing at the other substructures.

Figure 3.5: Prototype three-span prestressed-precast-concrete-girder (3C) quasi-isolated seat-type abutment bridges

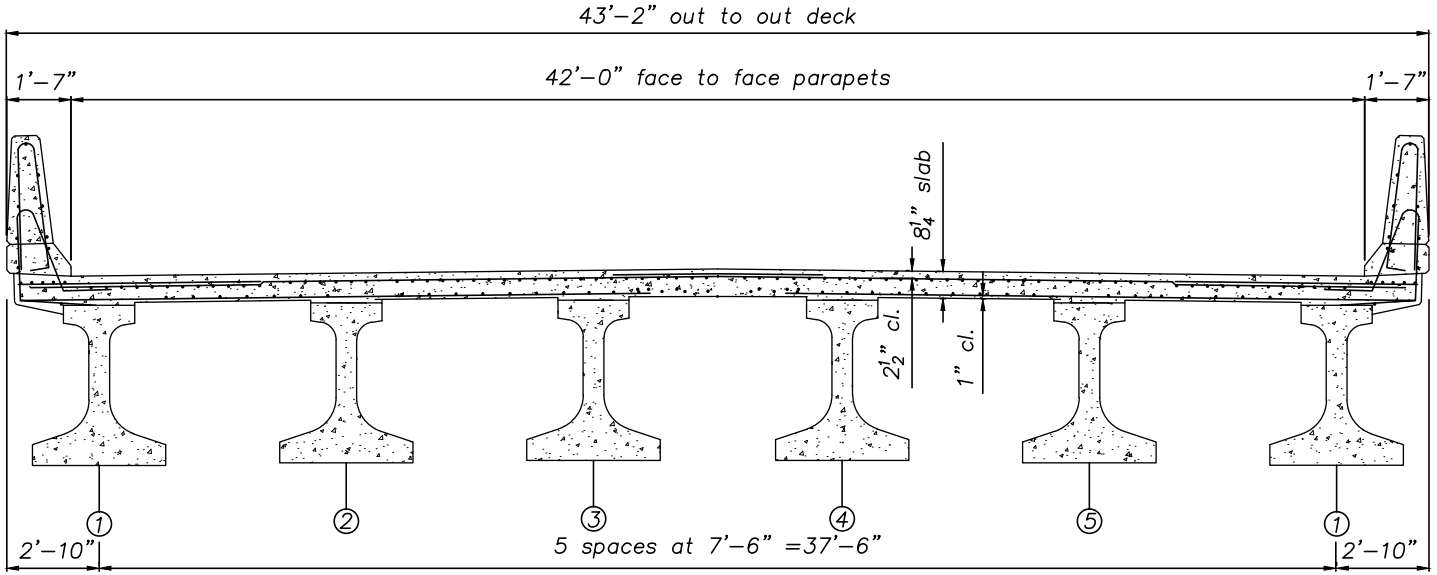

Figure 3.6: Cross-section of a 3C bridge superstructure

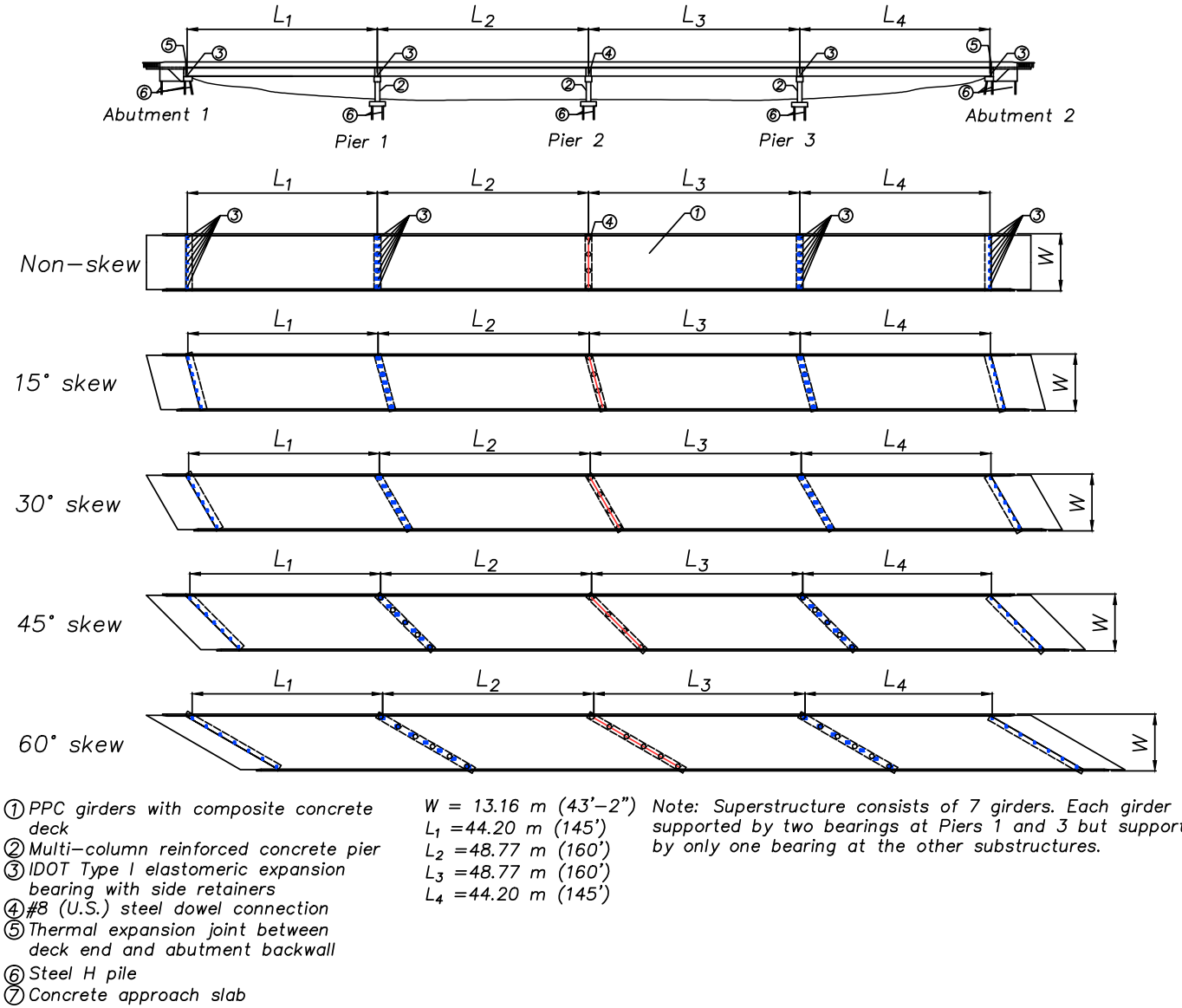

Figure 3.7: Prototype four-span prestressed-precast-concrete-girder (4C) quasi-isolated seat-type abutment bridges

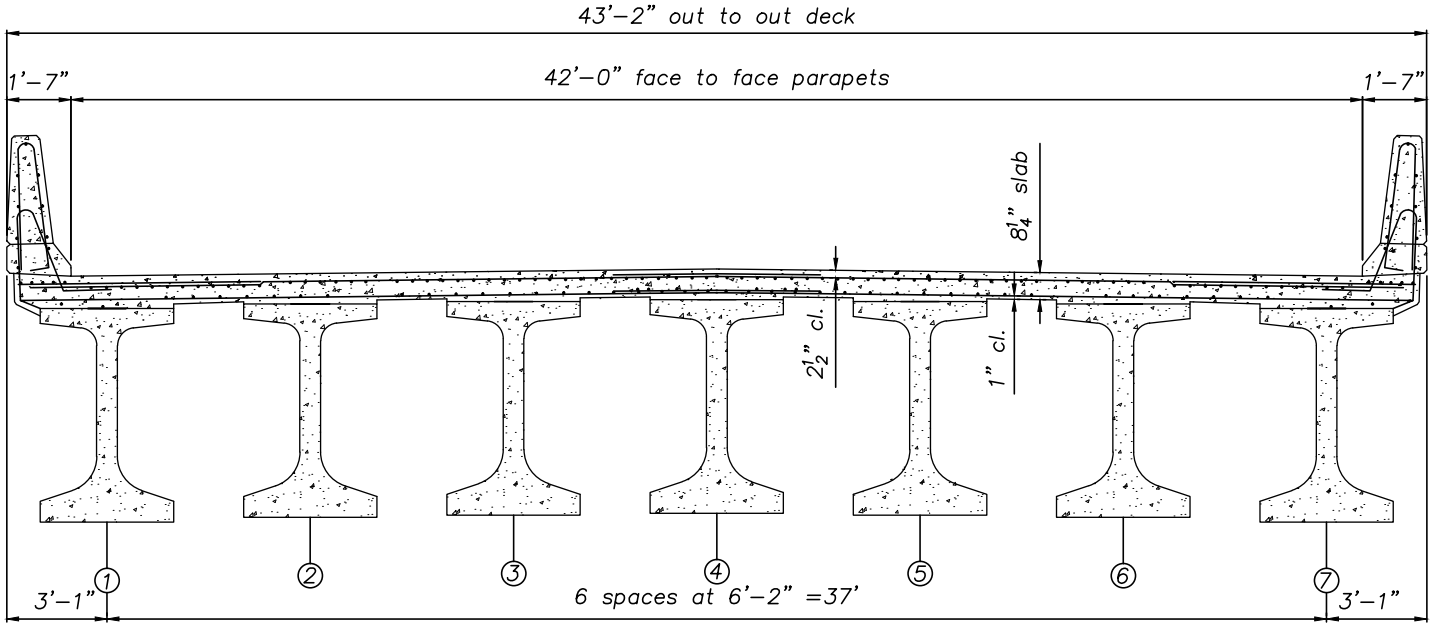

Figure 3.8: Cross-section of a 4C bridge superstructure

Table 3.1: Design parameters of critical structural components of prototype quasi-isolated bridges

Bridge type	**3-span steel-girder (3S) bridges**	**4-span steel-girder (4S) bridges**	**3-span concrete-girder (3C) bridges**	**4-span concrete-girder (4C) bridges**
Span length [m (ft)]	24.4-36.6-24.4 (80-120-80)	44.2-48.8-48.8-44.2 (145-160-160-145)	24.4-36.6-24.4 (80-120-80)	44.2-48.8-48.8-44.2 (145-160-160-145)
Skew angle	0°, 15°, 30°, 45°, 60°	0°, 15°, 30°, 45°, 60°	0°, 15°, 30°, 45°, 60°	0°, 15°, 30°, 45°, 60°
Superstructure				
No. of girders	6	7	6	7
Girder depth [mm (in.)]	1,067 (42)	1,676 (66)	1,372 (54)	1,829 (72)
Girder spacing [m (ft)]	2.29 m (7.5)	1.88 m (6.2)	2.29 m (7.5)	1.88 m (6.17)
Deck width [m (ft)]	13.15 (43.2)	13.15 (43.2)	13.15 (43.2)	13.15 (43.2)
Deck thickness [mm (in.)]	210 (8.25)	210 (8.25)	210 (8.25)	210 (8.25)
Bearing components				
Bearings at abutments	Type I, 11-d	Type I, 15-e	Type I, 12-e	Type I, 15-e
Elastomer planar dimensions [mm (in.)]	280×406 (11×16)	381×610 (15×24)	305×457 (12×18)	381×610 (15×24)
Elastomer thickness [mm (in.)]	89 (3.50)	133 (5.25)	100 (3.94)	133 (5.25)
No. of anchor per retainer	1	1	1	1
Retainer anchor dia. [mm (in.)]	25.4 (1.0)	31.8 (1.25)	31.8 (1.25)	38.1 (1.5)
Retainer anchor steel	A36	A36	A36	A36
Bearings at expansion pier(s)	Type I, 18-a	Type I, 20-a	Type I, 13-b (two rows)	Type I, 15-b (two rows)
Elastomer planar dimensions [mm (in.)]	457×610 (18×24)	508×610 (20×24)	330×508 (13×20)	381×610 (15×24)
Elastomer thickness [mm (in.)]	76 (3.0)	83 (3.25)	64 (2.5)	76 (3.0)
No. of anchor per retainer	1	1	1	1
Retainer anchor dia. [mm (in.)]	38.1 (1.5)	50.8 (2)	31.8 (1.25)	38.1 (1.5)
Retainer anchor steel	A36	A36	A36	A36
Sacrificial connections at fixed pier	Steel fixed bearing	Steel fixed bearing	#8 (U.S.) steel dowel bars	#8 (U.S.) steel dowel bars
Anchor diameter [mm (in.)]	38.1 (1.5)	31.8 (1.25)	25.4 (1.0)	25.4 (1.0)
No. of anchor per girder line	2	4	3 bars at an exterior girder 6 bars at an interior girder	3 bars at an exterior girder 6 bars at an interior girder
Anchor steel grade	A36	A36	A36	A36
Multi-column pier				
Column clear height [mm (ft)]	4.57 (15) / 12.19 (40)	4.57 (15) / 12.19 (40)	4.57 (15) / 12.19 (40)	4.57(15) / 12.19 (40)
Column diameter [m (ft)] (4.57-m- / 12.19-m-tall columns)	1.07 (3.5) / 1.22 (4.0)	1.07 (3.5) / 1.22 (4.0)	1.07 (3.5) / 1.22 (4.0)	1.07 (3.5) / 1.22 (4.0)

Table 3.1 (cont.)

Bridge type	**3-span steel-girder (3S) bridges**	**4-span steel-girder (4S) bridges**	**3-span concrete-girder (3C) bridges**	**4-span concrete-girder (4C) bridges**
No. of columns for different skews	4 (0°, 15°, 30°) 5 (45°) 6 (60°)	4 (0°, 15°, 30°) 5 (45°) 6 (60°)	4 (0°, 15°, 30°) 5 (45°) 6 (60°)	4 (0°, 15°, 30°) 5 (45°) 6 (60°)
Concrete nominal strength [MPa (ksi)]	24 (3.5)	24 (3.5)	24 (3.5)	24 (3.5)
Reinforcement ratio	2 %	2 %	2 %	2 %
Reinforcement yield strength [MPa (ksi)]	414 (60)	414 (60)	414 (60)	414 (60)
Pier cap cross-sectional width and height [m (ft)]	1.52 × 1.22 (5 × 4)	1.52 × 1.22 (5 × 4)	1.52 × 1.22 (5 × 4)	1.52 × 1.22 (5 × 4)
Pile cap cross-sectional width and height [m (ft)]	3.66 × 1.07 (12 × 3.5)	3.66 × 1.07 (12 × 3.5)	3.66 × 1.07 (12 × 3.5)	3.66 × 1.07 (12 × 3.5)
Steel pile	HP12 × 84 (U.S.)	HP12 × 84 (U.S.)	HP12 × 84 (U.S.)	HP12 × 84 (U.S.)
No. of piles at a pier for different skews	14 (0°, 15°) 16 (30°) 18 (45°) 22 (60°)	16 (0°, 15°, 30°) 18 (45°) 22 (60°)	14 (0°, 15°) 16 (30°) 18 (45°) 22 (60°)	20 (0°, 15°, 30°, 45°) 22 (60°)
Seat-type abutment				
Expansion joint width for different skews (normal to joint edge) [mm (in.)]	44.5 (1.75) (0°, 15°, 30°) 38.1 (1.5) (45°) 31.8 (1.25) (60°)	57.2 (2.25) (0°, 15°) 50.8 (2.0) (30°) 44.4 (1.75) (45°) 38.1 (1.5) (60°)	44.5 (1.75) (0°, 15°, 30°) 38.1 (1.5) (45°) 31.8 (1.25)	57.2 (2.25) (0°, 15°) 50.8 (2.0) (30°) 44.4 (1.75) (45°) 38.1 (1.5) (60°)
Backwall cross-section [m (in.)]	1.14 × 0.61 (45 × 24)	1.81 × 0.61 (71 × 24)	1.42 × 0.61 (56 × 24)	1.91 × 0.61 (75 × 24)
Pile cap cross-section [m (in.)]	1.98 × 1.07 (78 × 42)	1.98 × 1.07 (78 × 42)	1.98 × 1.07 (78 × 42)	1.98 × 1.07 (78 × 42)
Steel pile	HP12 × 84 (U.S.)	HP12 × 84 (U.S.)	HP12 × 84 (U.S.)	HP12 × 84 (U.S.)
No. of piles at an abutment for different skews	9 (0°, 15°, 30°) 11 (45°) 13 (60°)	9 (0°, 15°, 30°) 11 (45°) 13 (60°)	9 (0°, 15°, 30°) 11 (45°) 13 (60°)	11 (0°, 15°, 30°, 45°) 13 (60°)
Approach slab length × width × thickness [m (ft)]	9.14 × 12.19 × 0.38 (30 × 40 × 1.25)	9.14 × 12.19 × 0.38 (30 × 40 × 1.25)	9.14 × 12.19 × 0.38 (30 × 40 × 1.25)	9.14 × 12.19 × 0.38 (30 × 40 × 1.25)

Table 3.2: Prototype quasi-isolated bridge variants for computational studies

Component	Alternatives	3-span steel (3S)				4-span steel (4S)				3-span concrete (3C)				4-span concrete (4C)				Variants
		1	2	3	4	5	6	7	8	9	10	11	12	13	14	15	16	
Span length [m (ft)]	24.4-36.6-24.4 (80-120-80)	✓	✓	✓	✓					◊	◊	◊	◊					4
	44.2-48.8-48.8-44.2 (145-160-160-145)					○	○	○	○					□	□	□	□	
Pier column height [m (ft)]	4.57 (15)	✓		✓		○		○		□		□		◊		◊		2
	12.19 (40)		✓		✓		○		○		□		□		◊		◊	
Foundation soil condition	Hard	✓	✓			○	○			□	□			◊	◊			2
	Soft			✓	✓			○	○			□	□			◊	◊	
Skew angle	0°, 15°, 30°, 45°, 60°	5 skew angles are considered for each of the above 16 combinations.																5
Total number of bridge variants		**80**																

Each of the 80 bridge variants shown in Table 3.2 is uniquely referred to by a nomenclature string comprised of 8 characters, as illustrated in Figure 3.9. For instance, **"3S45P15H"** indicates the three-span steel-plate-girder bridge (**3S**) with a left skew of 45° (**45**), pier columns with a clear height of 15-ft (4.57-m) (**P15**) and the hard foundation soil (**H**).

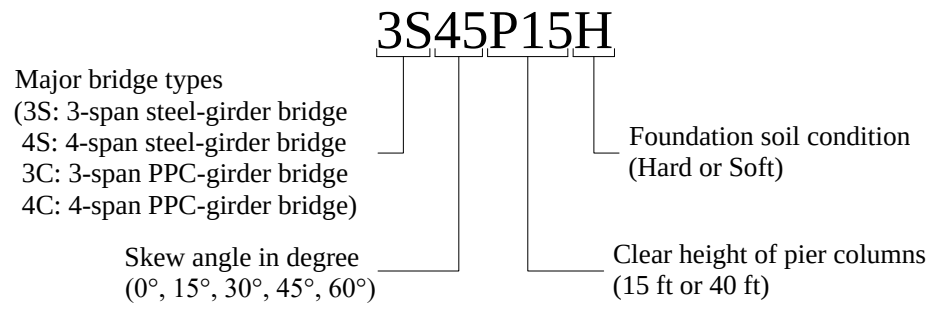

Figure 3.9: Nomenclature for prototype bridge variants

Table 3.3 lists the component and total mass of a few prototype bridges. The superstructure mass does not change much in the non-skew and skew bridge variants of a same type. The 4C bridges have the heaviest superstructures of all the prototype bridges, while the 3S bridges have the lightest superstructures. The superstructure mass is directly related to the seismic force demand on the bridge.

Table 3.3: Component and total mass of prototype bridges (units: 10^3 kg)

Bridge	3S00P15H	4S00P15H	3C00P15H	4C00P15H
Superstructure	1197	2758	1680	3949
Abutments				
Backwall	48	72	58	76
Pile cap	128	128	128	128
Wingwall	54	78	62	81
Approach slab	206	206	206	206
Pile body (6.1 m)	12	14	14	18
Piers				
Pier cap	117	176	117	176
Pier column	79	117	79	117
Pile cap	240	360	240	386
Pile body (6.1 m)	19	38	21	48
Total mass	2289	4227	2798	5532

Figures 3.10 to 3.13 illustrate the 3-D finite-element models of a few bridges. The computational

models of bridge superstructures, piers, foundations, sacrificial connections, and abutments will be introduced in detail in later sections of this chapter and Chapter 4.

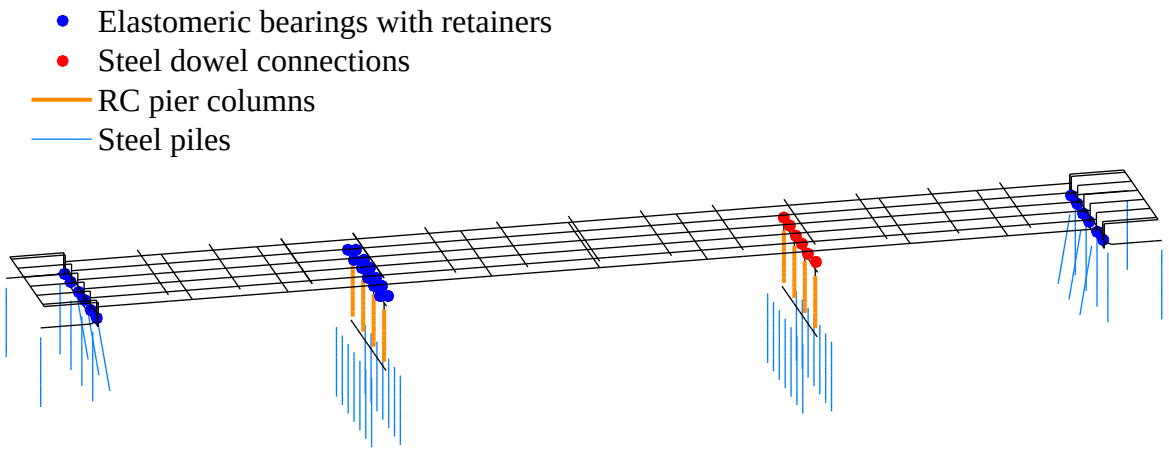

Figure 3.10: 3-D finite-element model of 3C00P15H bridge

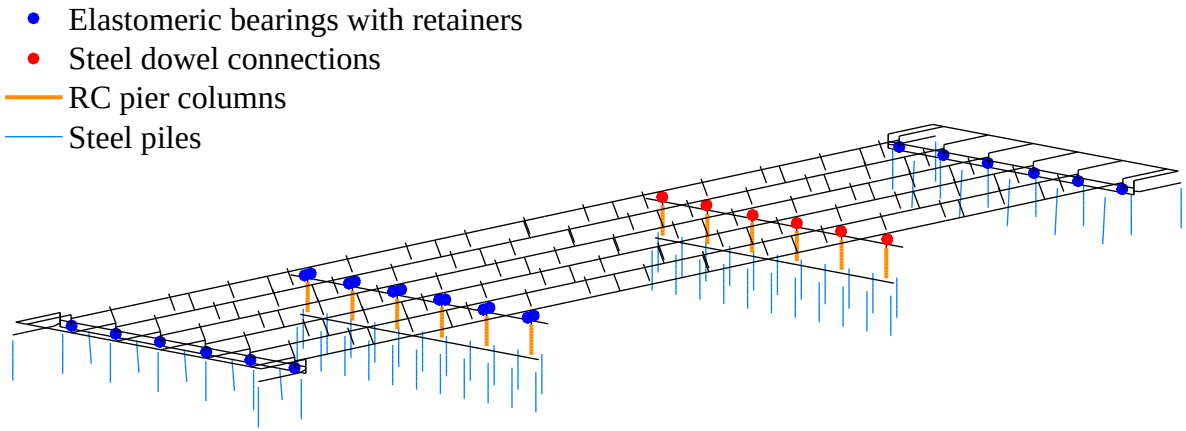

Figure 3.11: 3-D finite-element model of 3C60P15H bridge

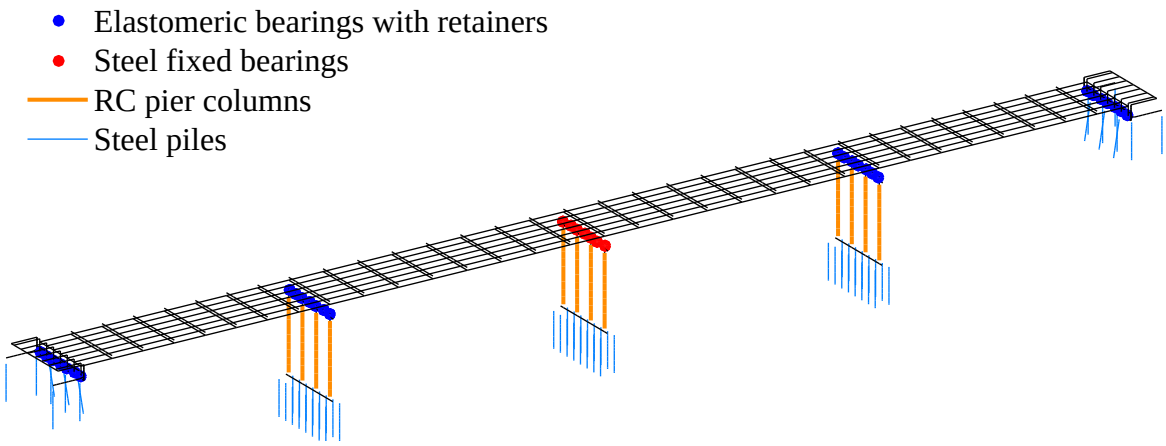

Figure 3.12: 3-D finite-element model of 4S00P40 bridge

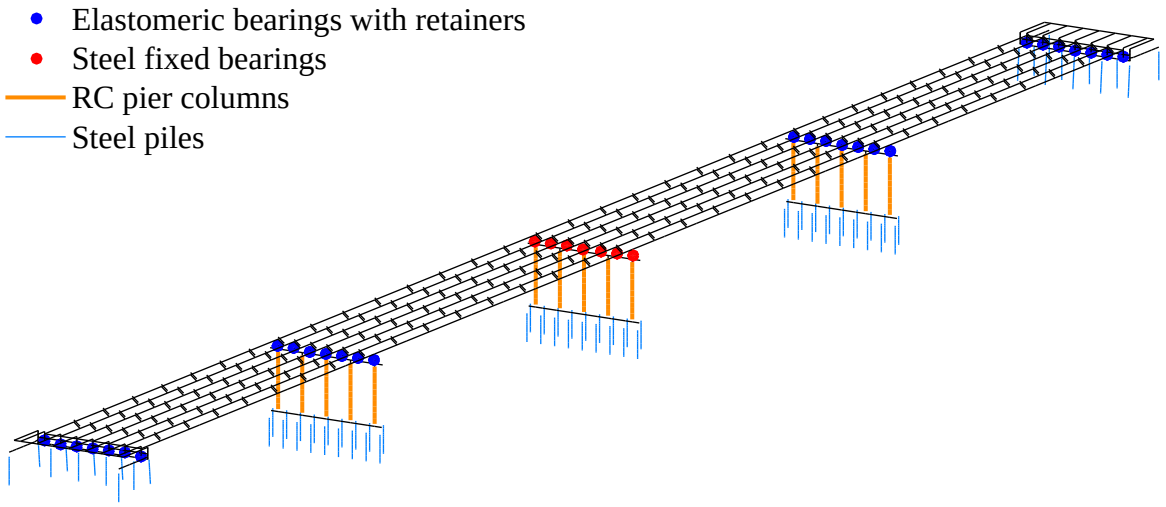

Figure 3.13: 3-D finite-element model of 4S45P40 bridge

3.2 Bridge Superstructure Model

The superstructure configuration of the prototype bridges is shown in Figures 3.2, 3.4, 3.6, 3.8, and Table 3.1. The bridge superstructure was modeled using a grillage modeling approach (O'Brien et al. 2015). Figure 3.14 shows the schematic of a portion of the entire grillage superstructure model that consists of longitudinal and transverse elastic beam elements. The elastic beam elements were laid out in a grid pattern and the members were rigidly connected to each other at the nodes. The longitudinal beam elements were used to model the composite behavior of girders with associated concrete slabs connected to the girder top flanges, which are depicted by the red lines in Figure 3.14. The transverse beam elements were used to model the concrete slab and diaphragms (cross-frames) between girders, which are depicted by the orange and blue lines in Figure 3.14, respectively.

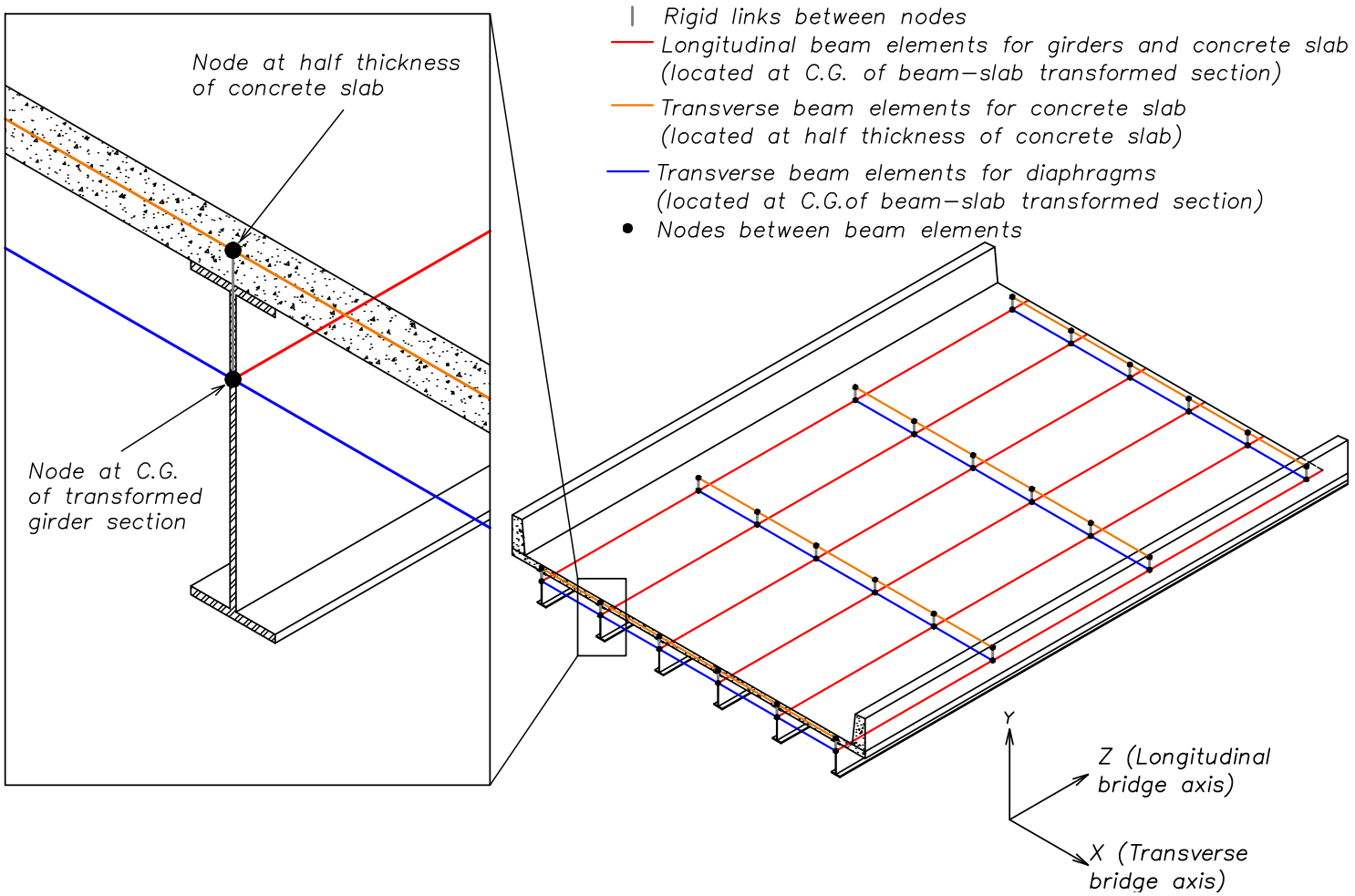

Figure 3.14: Schematic of grillage superstructure model

The properties of the longitudinal beam elements were determined using composite sectional properties of girders with associate concrete slab. Per Article 4.6.2.6 of the AASHTO LRFD Bridge Design Specification (AASHTO 2010), the slab effective flange width, b_{eff}, of the interior girders is taken as the tributary width perpendicular to the axis of the girder. As shown in Figures 3.2 to 3.8, the multiple girders in a superstructure have equal spacings between each other. Thus, b_{eff} of interior girders is equal to the girder spacing. For the exterior girders with deck overhang and concrete parapets, b_{eff} includes half of the girder spacing, the full overhang width that is further extended to take into account the concrete parapet, per the same article of the AASHTO specification (AASHTO 2010). After determining b_{eff}, the concrete slab within b_{eff} was transformed into an extended portion of the girder section, on the basis of the elastic modular ratio between the girder steel and slab concrete materials ($n_{\text{E}} = \frac{E_{\text{s, girder}}}{E_{\text{c,slab}}}$), or between the concrete materials of the PPC girder and slab ($n_{\text{E}} = \frac{E_{\text{c, girder}}}{E_{\text{c, slab}}}$). Figure 3.15 illustrates the transformed section of a steel plate girder with concrete slab. The strength and elastic modulus of the superstructure materials are listed as follows

- Concrete of slab: $f'_{\text{c, slab}} = 27.6$ MPa (4 ksi), $E_{\text{c, slab}} = 24.9$ GPa $(3,605$ ksi)
- Concrete of PPC girder: $f'_{\text{c, girder}} = 48.3$ MPa (7 ksi), $E_{\text{c, girder}} = 32.9$ GPa $(4,769$ ksi)
- Steel of plate girder: $f_{\text{y, girder}} = 345$ MPa (50 ksi), $E_{\text{s, girder}} = 200$ GPa $(29,000$ ksi)

The properties of the transformed sections were calculated and listed in Table 3.15. Then, these properties were assigned to the longitudinal beam elements in the grillage model. In the finite-element grillage model shown in Figure 3.14, the longitudinal beam elements are located at the center of gravity of the transformed girder sections.

Table 3.4: Sectional properties of longitudinal beam elements in superstructure models ($x - x$ and $y - y$ axes are defined in Figure 3.15)

Major bridge type		3S[1]	4S[1]	3C[2]	4C[2]
Girder type		Steel plate girder	Steel plate girder	PPC girder (IL54-2438)	PPC girder (IL72-3838)
Girder depth [cm (in.)]		116.8 (46)	174 (68.5)	137.2 (54)	182.9 (72)
Flange width [cm (in.)]		30.5 (12)	55.9 (22)	Top: 61.0 (24) Bottom: 96.5 (38)	96.5 (38)
Flange thickness [cm (in.)]		5.1 (2)	3.2 (1.25)	Top: 15.4 (6.1) ~ 31.8 (12.5) Bottom: 17.8 (7) ~ 55.9 (22)	Top: 12.7 (5) ~ 31.8 (12.5) Bottom: 17.8 (7) ~ 55.9 (22)
Web depth [cm (in.)]		106.7 (42)	167.6 (66)	49.5 (19.5)	95.3 (37.5)
Web thickness [mm (in.)]		1.1 (0.44)	1.3 (0.5)	17.8 (7)	17.8 (7)
Concrete slab thickness [mm (in.)]		21.0 (8.25)	21.0 (8.25)	21.0 (8.25)	21.0 (8.25)
Properties of transformed interior girder section	Area [cm^2 ($in.^2$)]	1024 (158.7)	1057 (163.9)	9131 (1415)	9797 (1519)
	Moment of inertia about x-x axis [cm^4 ($in.^4$)]	2.27×10^6 (5.43×10^4)	5.51×10^6 (1.32×10^5)	3.11×10^7 (7.46×10^5)	5.67×10^7 (1.36×10^6)
	Moment of inertia about y-y axis [cm^4 ($in.^4$)]	2.58×10^6 (6.18×10^4)	1.44×10^6 (3.46×10^4)	1.79×10^7 (4.30×10^5)	1.18×10^7 (2.83×10^5)
	Torsional consant [cm^4 ($in.^4$)]	8.57×10^4 (2059)	6.88×10^4 (1653)	1.85×10^6 (4.44×10^4)	1.90×10^6 (4.56×10^4)
Properties of transformed exterior girder section	Area [cm^2 ($in.^2$)]	1138 (176)	1245 (192.9)	9828 (1523)	1.09×10^4 (1695)
	Moment of inertia about x-x axis [cm^4 ($in.^4$)]	2.37×10^6 (5.70×10^4)	5.96×10^6 (1.43×10^5)	3.32×10^7 (7.98×10^5)	4.73×10^7 (1.51×10^6)
	Moment of inertia about y-y axis [cm^4 ($in.^4$)]	4.96×10^6 (1.19×10^5)	3.66×10^6 (8.79×10^4)	2.94×10^7 (7.06×10^5)	2.60×10^7 (6.24×10^5)
	Torsional consant [cm^4 ($in.^4$)]	1.03×10^5 (2467)	9.66×10^4 (2321)	1.95×10^6 (4.68×10^4)	2.06×10^6 (4.96×10^4)

1. Sectional properties are calculated based on the elastic modulus of plate girder steel ($E_{s,\,steel} = 200$ GPa).

2. Sectional properties are calculated based on the elastic modulus of PPC girder concrete ($E_{c,\,girder} = 32.9$ GPa).

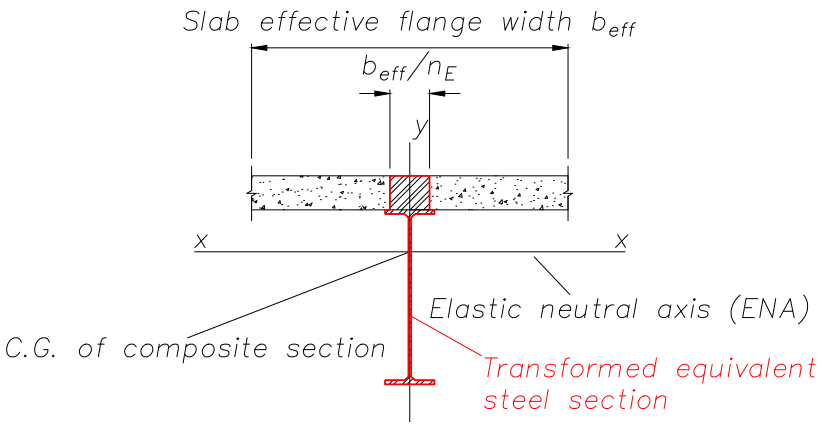

Figure 3.15: Transformed section of a steel plate girder with concrete slab

In the transverse direction, elastic beam elements were used to model the concrete slab and diaphragms between the girders, which are depicted by the orange and blue lines in Figure 3.14, respectively. The sectional properties of the beam elements modeling the concrete slab were determined based on the tributary slab area, the slab thickness [21.0 cm (8.25 in.)] and elastic modulus of the concrete material. The member size, longitudinal spacing, and configuration of the diaphragm (cross-frame) members are shown in Table 3.5 and Figure 3.16. In the 3S, 3C, and 4C bridges, a single C- or MC-shaped structural steel is used to connect the webs of adjacent girders at bracing locations along the span, while cross-frames are used in the 4S bridges (IDOT 2012a, 2015a).

Table 3.5: Configuration of diaphragms (cross-frames) between girders

Major bridge type	3S	4S	3C	4C
Member size	C15×50	Top chord: WT7×21.5 Diagnoal members: L8×8×1 Bottom chord: L8×8×1	MC12×31	MC18×42.7
Longitudinal spacing [m (ft)]	6.10 (20)	6.10 (20)	Spans up to 90 ft shall be braced at 0.33L and 0.67L ; Spans over 90 ft shall be braced at 0.25L , 0.5L , and 0.75L ; where L is the span length (IDOT 2012). Concrete panel diaphragms are used to connect girders between spans.	

The diaphragm using C- or MC-shaped structural steel was modeled using a transverse beam element whose elastic stiffness was determined based on the sectional properties of the corresponding steel shape. Stiffness properties of the cross-frame in 4S bridges were determined using

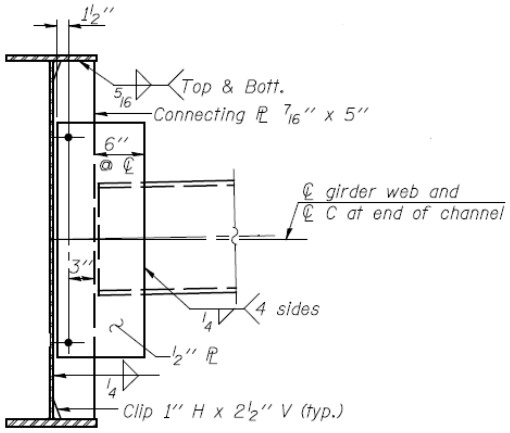

(a) Diaphragm of 3S bridges (C15 × 50 structural steel)

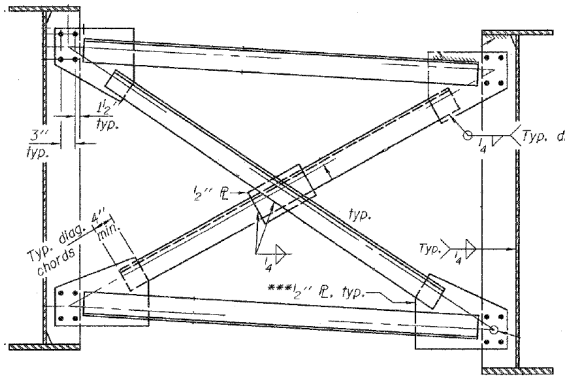

(b) Cross-frame of 4S bridges (WT7 × 21.5 for the top chord, L8 × 8 × 1 steel for the other members)

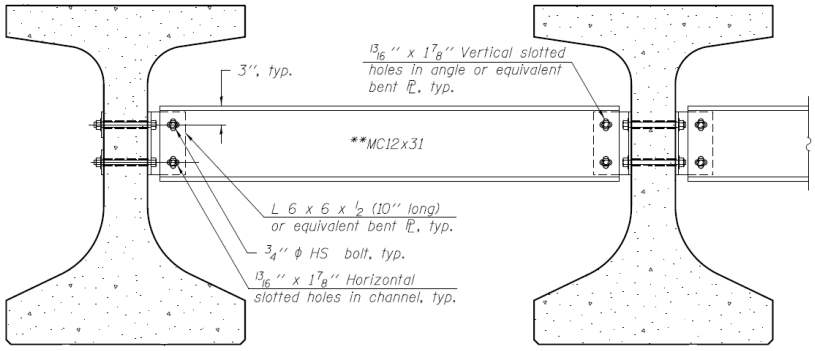

(c) Diaphragm of 3C bridges (MC12 × 31)

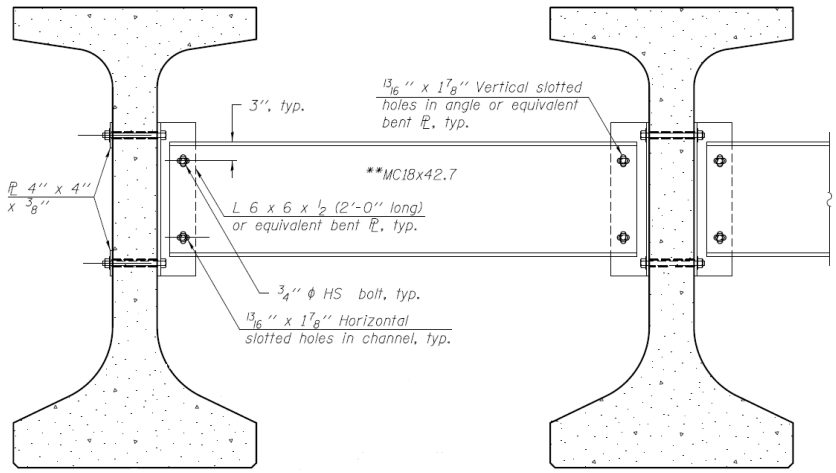

(d) Cross-frame of 4C bridges (MC18 × 42.7)

Figure 3.16: Configurations of diaphragms and cross-frames in prototype bridges (after IDOT 2012a)

an equivalent beam approach introduced by AASHTO/NSBA Steel Bridge Collaboration (2014). In this approach, the cross-frame is simplified into an equivalent Euler-Bernoulli beam, as shown in Figure 3.17. The in-plane deflection, Δ_t and Δ_b, of the cross-frame under a force couple, Pd, were calculated by a truss analysis and used to determine the equivalent end rotation, $\theta = \frac{\Delta_t + \Delta_b}{d}$. θ was then used to calculate the flexural stiffness of the equivalent beam, $EI = \frac{PdL}{4\theta}$. EI is the approximate in-plane flexural stiffness of the transverse beam element modeling the cross-frame in the grillage model. The other stiffness properties of the cross-frame, such as the axial stiffness, out-of-plane flexural stiffness, and torsional stiffness were determined using similar equivalent beam approaches.

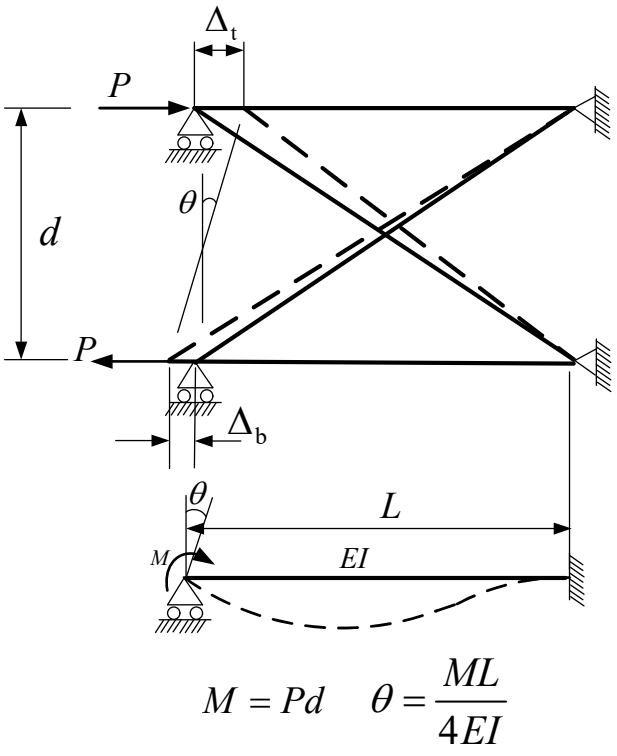

Figure 3.17: Equivalent beam analogy for modeling cross-frames in a grillage superstructure model (AASHTO/NSBA Steel Bridge Collaboration 2014)

Article 6.7.4.2 of the AASHTO LRFD Bridge Design Specifications (AASHTO 2010) specifies that "where support lines are not skewed more than 20 degrees from normal, intermediate diaphragms or cross-frames may be placed in contiguous skewed lines parallel to the skewed supports; where support lines are skewed more then 20 degrees from normal, intermediate diaphragms

or cross-frames shall be normal to the girders and may be placed in contiguous or discontinuous lines. In the superstructure models, diaphragms were placed according to these requirements. Diaphragm spacing in the longitudinal bridge direction indicated in Table 3.5 was determined in accordance with AASHTO and IDOT specifications (AASHTO 2010; IDOT 2012a). Figures 3.18 and 3.19 illustrate the superstructure diaphragm patterns of 4S and 4C bridge variants with different skews, respectively. The diaphragm patterns of 3S and 3C bridge variants are similar to the equivalent four-span bridges.

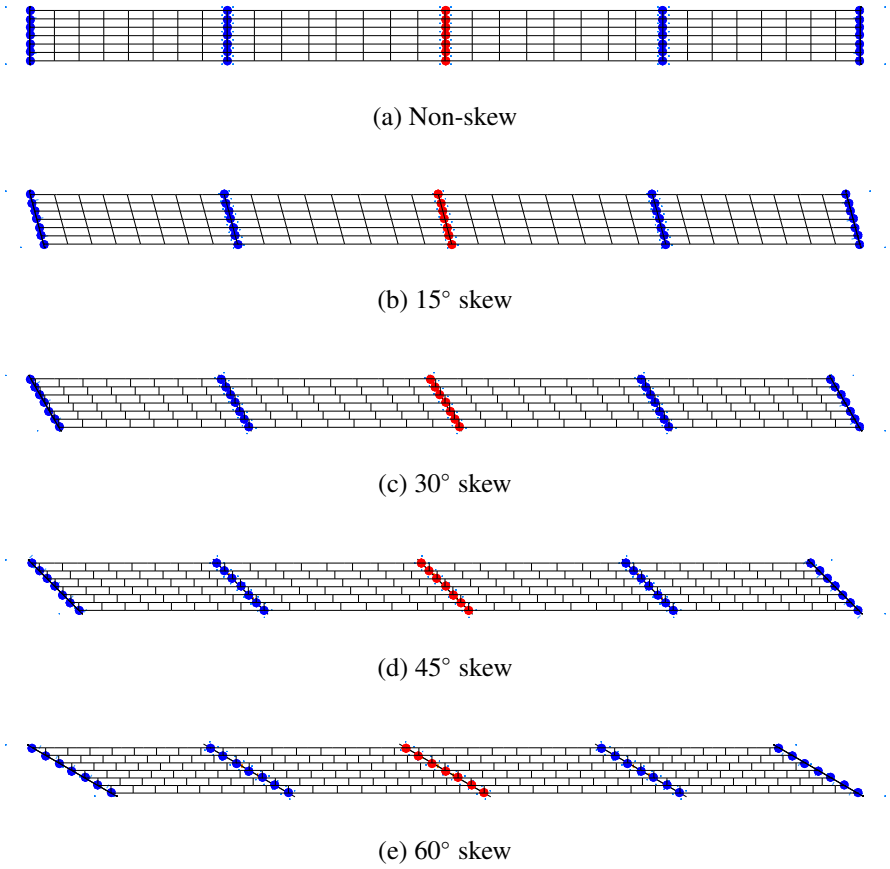

(a) Non-skew

(b) 15° skew

(c) 30° skew

(d) 45° skew

(e) 60° skew

Figure 3.18: Superstructure diaphragm pattern of 4S bridge variants with different skews

Alternatively, the grillage superstructure model employed in this study can be simplified by a so-called "spine" model to save computational costs. In such a model, only one line of elastic beam elements are used to model the behavior of multiple girders with a composite deck on the top (Makris and Zhang 2004). These beam elements possess the composite sectional properties of the bridge superstructure. Due to the largely reduced number of beam elements, the spine su-

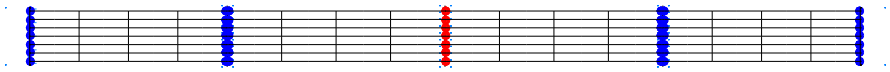

(a) Non-skew

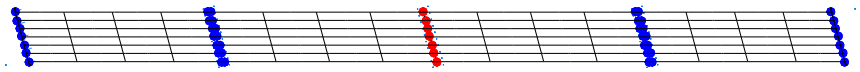

(b) 15° skew

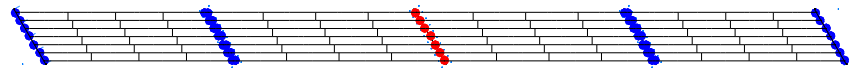

(c) 30° skew

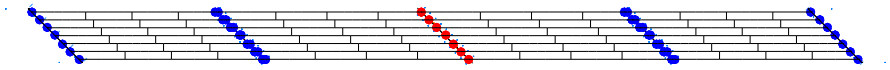

(d) 45° skew

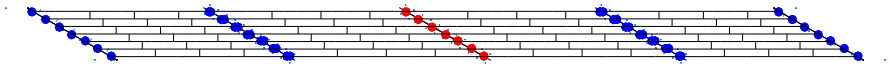

(e) 60° skew

Figure 3.19: Superstructure diaphragm pattern of 4C bridge variants with different skews

perstructure model can reduce the number of degrees of freedom of the global bridge model and reduce the computational cost. The spine model is typically employed when the bridge superstructure essentially behaves elastically and is not expected to sustain significant inelastic deformation and damage.

3.3 Bridge Substructure Model

The bridge superstructure is supported by RC multi-column intermediate piers in conjunction with seat-type abutments. For bridge variants with different skews, the pier consists of four to six circular pier columns, a pier cap, a pile cap, and multiple steel H-piles. The two or three piers of a bridge variant have the same column clear height, either 4.57 m (15 ft) or 12.19 m (40 ft). Figure 3.20 depicts such a pier and its finite-element model. As shown in Figures 3.1, 3.3, 3.5, and 3.7, the pier length increases with bridge skew and more pier columns are needed to meet a standard practice of column spacing that requires the center-to-center column spacing to be smaller than 5 times the column diameter. Therefore, bridge variants with different skews vary in the number and spacing of pier columns. Table 3.6 lists the number, diameter, and spacing of pier columns for bridge variants with different skews.

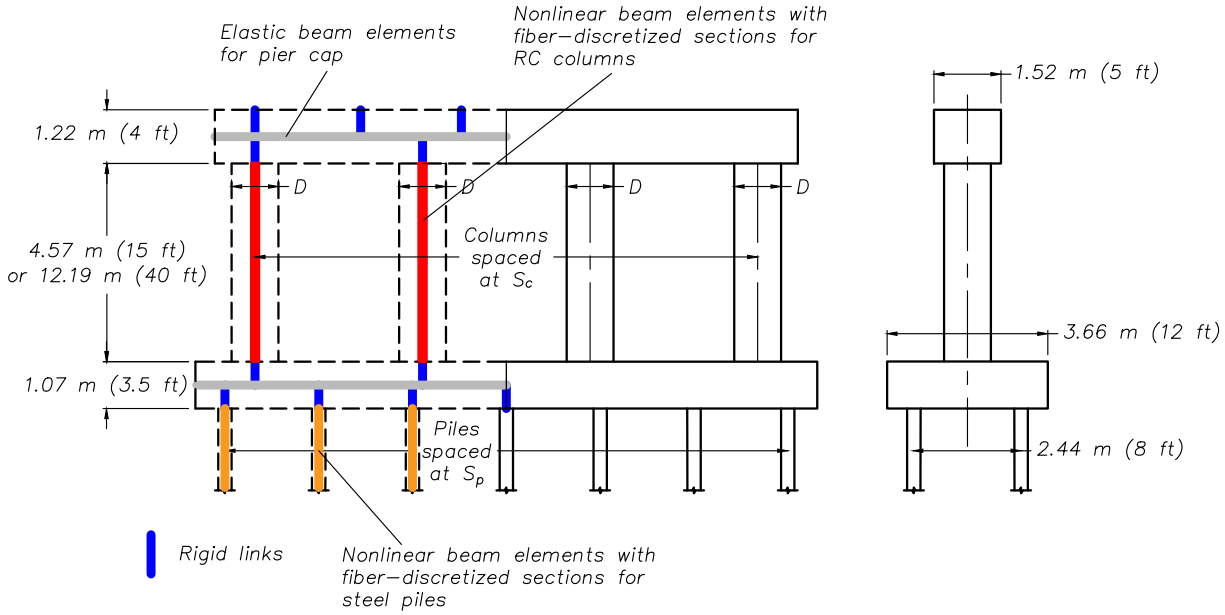

Figure 3.20: Multi-column intermediate pier substructure and schematic of its finite-element model

In the finite-element pier model shown in Figure 3.20, linear elastic beam elements were used to model the pier cap and pile cap. The pier columns and piles were modeled using nonlinear beam elements with distributed plasticity (Neuenhofer and Filippou 1997). Each pier column was discretized into ten such nonlinear beam elements of equal length and each element had three integration points for Legendre-Gauss quadrature. At each integration point, a fiber-discretized RC

Table 3.6: Number, diameter, and spacing of columns at an intermediate pier

Bridge skew (°)	0	15	30	45	60
Column number per pier	4	4	4	5	6
Diameter of 4.57-m-tall columns [m (ft)]	1.07 (3.5)	1.07 (3.5)	1.07 (3.5)	1.07 (3.5)	1.07 (3.5)
Diameter of 12.19-m-tall columns [m (ft)]	1.22 (4.0)	1.22 (4.0)	1.22 (4.0)	1.22 (4.0)	1.22 (4.0)
Center-to-center column spacing [m (ft)]	3.81 (12.5)	3.94 (12.94)	4.4 (14.43)	4.04 (13.26)	4.57 (14.99)
Spacing normalized to diameter (4.57-m-tall columns)	3.56	3.68	4.11	3.78	4.27
Spacing normalized to diameter (12.19-m-tall columns)	3.12	3.22	3.61	3.31	3.75

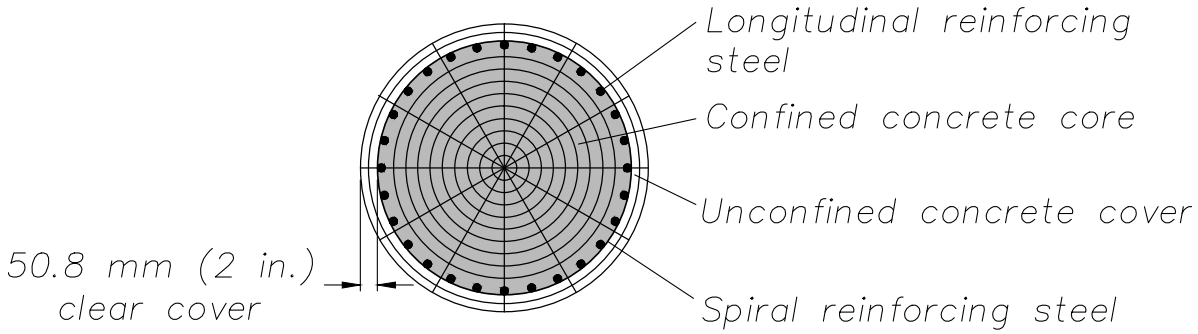

Figure 3.21: Fiber-discretized section of RC pier columns

section was utilized to determine the element stiffness matrix, considering the nonlinear constitutive relation of concrete and steel materials under combined axial and flexural loads. Figure 3.21 shows the fiber mesh of the column cross-section. Fibers of three types of materials were included in the section for modeling the unconfined concrete cover, confined concrete core, and the vertical reinforcing steel. Table 3.7 summarizes the properties of the concrete and reinforcing steel. Constitutive properties of the confined concrete core was determined using the model proposed by Mander et al. (1988), per Article 8.8.4 of the AASHTO Guide Specifications for LRFD Seismic Bridge Design (AASHTO 2011). The material properties were assigned to the Concrete02 (Mohd Yassin 1994) and Steel02 (Menegotto and Pinto 1973) materials in *OpenSees*. Figure 3.22 illustrates the constitutive models of these two materials in *OpenSees*. While the axial and flexural stiffnesses of the column were captured by the fiber-discretized sections, shear stiffness of the column section was determined as $0.8G_cA_g$, where G_c is the shear modulus of concrete and A_g is the gross cross-sectional area of the column, per Article 8.6.2 of the AASHTO Guide Specifications for LRFD Seismic Bridge Design (AASHTO 2011). Per Article 5.6.5 of the same specification (AASHTO 2011), the effective torsional moment of inertia of the column cross-section was determined as $0.2J_g$, where J_g is the gross torsional moment of inertia of the column cross-section.

In the finite-element model shown in Figure 3.20, the pier columns, as well as the pier and pile caps were all modeled at their axis locations, which resulted in offsets between the column ends and the pier and pile caps. Thus, rigid links were used to overcome the offsets and connect the column ends to the pier and pile caps. Similarly, rigid links were also used to connect the pier cap to the bearings and the pile cap to the steel piles.

In order to validate the pier column model, experimentally measured cyclic responses of circular RC pier columns (Kunnath et al. 1997; Lehman and Moehle 1998) were compared with responses computed using the finite-element column model. The properties of the two experimentally tested pier columns are listed in Table 3.8. Consistent with the experimental setup, a cantilever column with a fixed base was modeled for each of the two columns, which was assigned with the properties listed in Table 3.8. The column model was comprised of 10 nonlinear beam elements with fiber-discretized sections. The top of the column model was then laterally loaded using the cyclic displacement protocol recorded in the experiment. In addition to the cyclic horizontal load, the column top was subjected to a constant axial compressive force that was also applied in the exper-

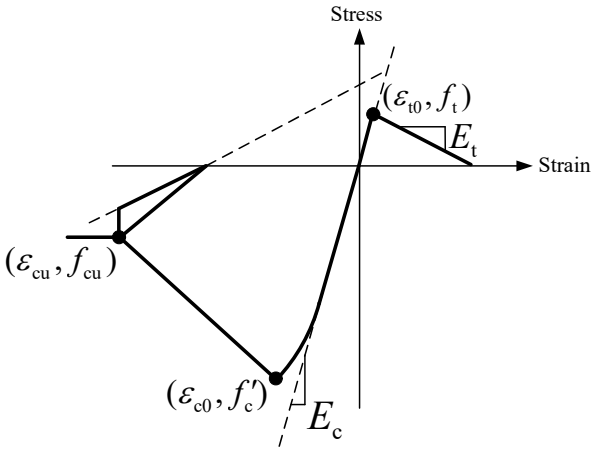

(a) Concrete02

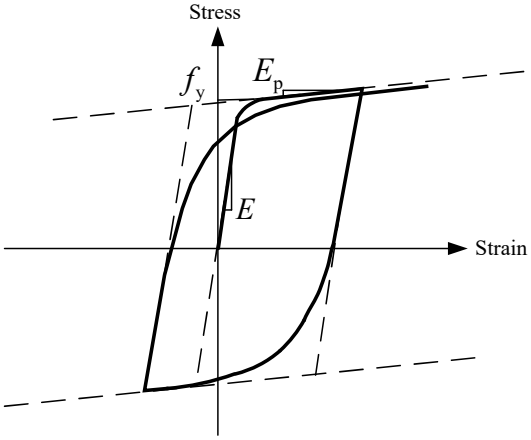

(b) Steel02

Figure 3.22: Nonlinear constitutive models of Concrete02 and Steel02 materials in *OpenSees* (Mohd Yassin 1994; Menegotto and Pinto 1973)

Table 3.7: Material properties of pier column

	Column property	4.57-m-tall pier columns	12.19-m-tall pier columns
Concrete	Clear cover thickness [mm (in.)]	50.8 (2.0)	50.8 (2.0)
	Compressive strength [MPa (ksi)]	24.1 (3.5)	24.1 (3.5)
Vertical reinforcement	Bar diameter [mm (in.)]	28.7 (1.128)	28.7 (1.128)
	No. of bars	28	36
	Yield strength [MPa (ksi)]	414 (60)	414 (60)
	Reinforcement ratio	2%	2%
Transverse reinforcement	Spiral diameter [mm (in.)]	12.7 (0.5)	12.7 (0.5)
	Spiral hoop spacing [mm (in.)]	76.2 (3.0)	76.2 (3.0)
	Yield strength (MPa)	414 (60)	414 (60)

iment, in order to simulate the superstructure gravity load. The computed cyclic response in terms of column top deflection and horizontal force is shown in Figure 3.23. A good correlation between the experimental and computed responses can be observed.

Table 3.8: Properties of experimentally tested circular RC pier columns (Kunnath et al. 1997; Lehman and Moehle 1998)

Column property		Column 415 (Lehman and Moehle 1998)	Column A2 (Kunnath et al. 1997)
Column height (m)		2.44	1.37
Column diameter (m)		0.61	0.31
Test configuration		Cantilever	Cantilever
Axial compression (kN)		654	200
Concrete	Clear cover thickness (mm)	22.2	14.5
	Compressive strength (MPa)	31	29
Vertical reinforcement	Bar diameter (mm)	15.9	9.5
	No. of bars	22	21
	Yield strength (MPa)	462	448
	Reinforcement ratio	0.015	0.02
Transverse reinforcement	Spiral diameter (mm)	6.4	4
	Spiral hoop spacing (mm)	31.8	19
	Yield strength (MPa)	607	434

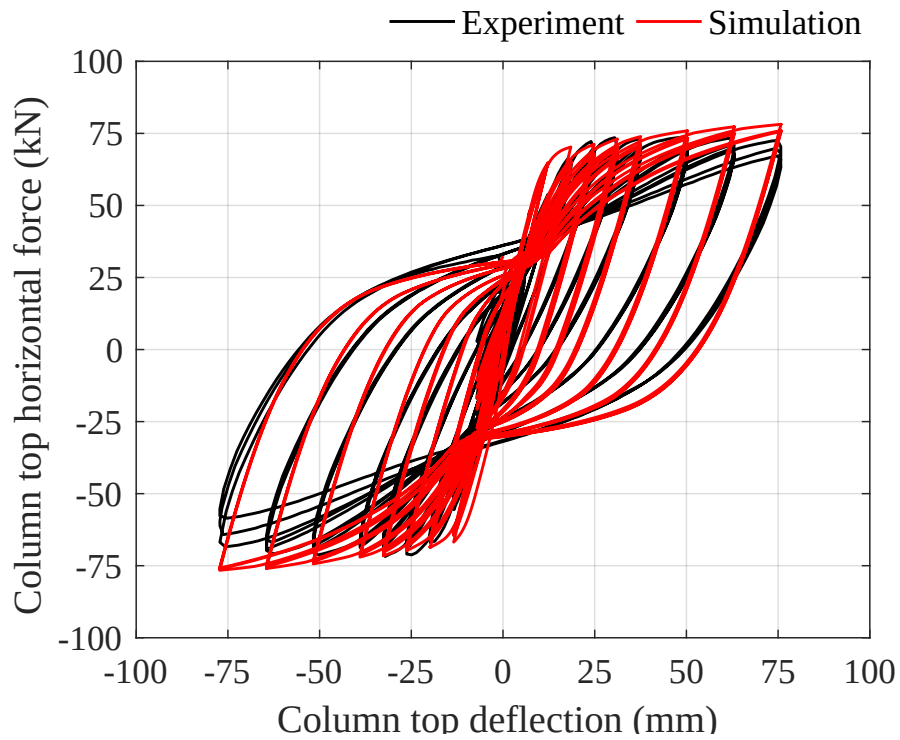

(a) Column A2 (Kunnath et al. 1997)

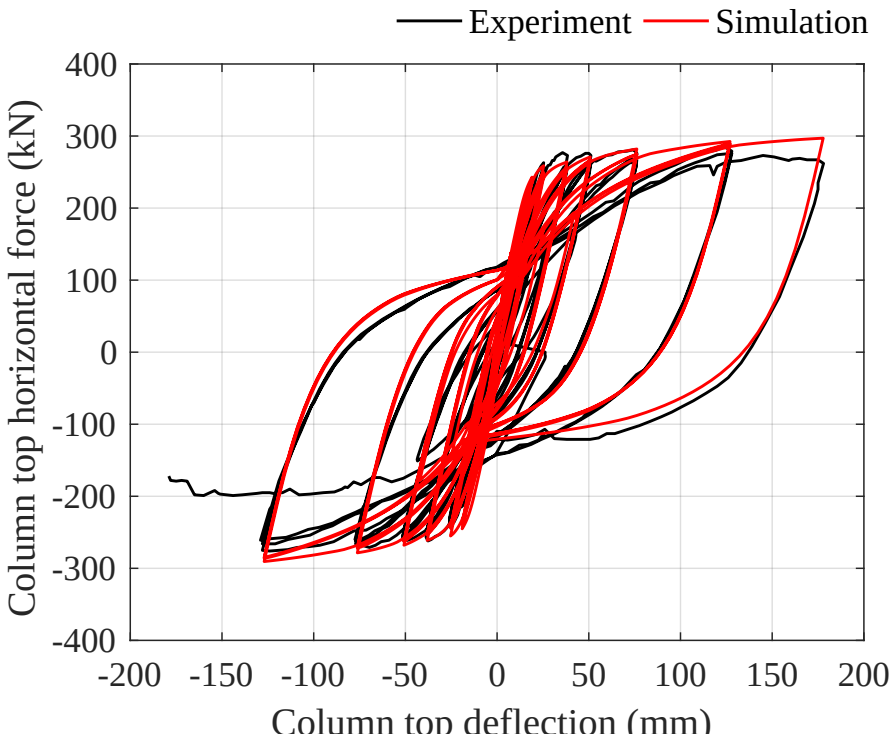

(b) Column 415 (Lehman and Moehle 1998): experimental response plotted until -179 mm top deflection

Figure 3.23: Comparison between experimental and computed response of cantilever RC pier columns subjected to constant axial and cyclic lateral loads

3.4 Bridge Foundation Model

In order to represent very soft and very hard foundation soil conditions for the prototype bridges, two real soil profiles were selected from 20 sets of geotechnical boring logs for bridge construction projects in the southernmost 10 counties in Illinois, which possess the highest seismicity of the entire state. In the two selected soil profiles, the portion between the ground surface and a depth of 14.6 m (48 ft) were considered, as it was assumed that the steel H piles of the prototype bridges were driven to the bedrock at this depth. Driving bridge foundation piles into the bedrock is a common practice in Illinois. The soft and hard soil profiles were illustrated in Figure 3.24. These two soil profiles will be referred to as the "soft foundation soil condition" and "hard foundation soil condition" in later chapters.

For the clayey strata in the profiles shown in Figure 3.24, the undrained shear strength s_u was determined as a half of the unconfined compressive strength q_u that was recorded in the boring logs (Terzaghi et al. 1996). For the sandy strata in the profiles, the relative density D_r was estimated using Equation (3.1)

$$D_r = \sqrt{\frac{(N_1)_{60}}{40}} \tag{3.1}$$

proposed by Kulhawy and Mayne (1990), based on the SPT blow counts $(N_1)_{60}$. Then, the internal friction angle ϕ was determined using Equation (3.2)

$$\phi = 16D_r^2 + 0.17D_r + 28.4 \tag{3.2}$$

given by API (1987), which was also employed by Rollins et al. (2005) to estimate the friction angle of sand.

Figure 3.25 shows the layout of piles at an intermediate pier foundation. For all the bridge variants, two rows of HP12 × 84 steel piles were used to support an intermediate pier. The number of piles in one row (N_p) and the center-to-center pile spacing (S_p) may vary in different bridge variants. The number of piles supporting the pier was primarily determined based on the dead and live gravity loads applied to the foundation and also to ensure that the maximum pile spacing should not exceed 2.44 m (8 ft), which is required by Article 3.10.1.11 of the IDOT Bridge Manual (IDOT 2012a). In conjunction with Figure 3.25, Table 3.9 lists the pile number (N_p) and spacing

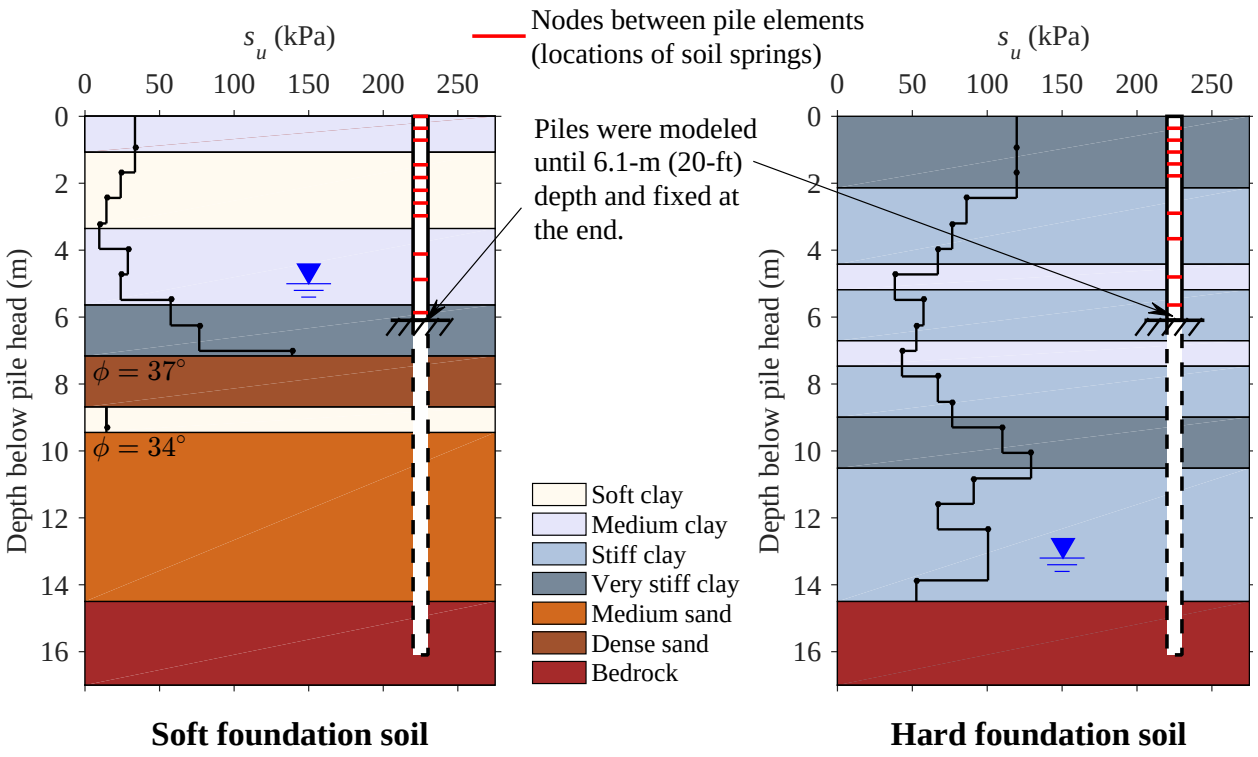

Figure 3.24: Soft and hard foundation soil profiles for modeling bridge pile foundations

(S_p) in one row for different bridge variants.

Similar to the RC pier column model, the steel H piles supporting the intermediate piers and abutments were modeled using the nonlinear beam elements with distributed plasticity (Neuenhofer and Filippou 1997), in order to take into account the nonlinear material behavior of steel. Each pile was meshed into a number of elements. The number and size of the elements were determined to have at least five elements for the top pile portion of ten diameters and at least five elements for the rest of the pile, as recommended by Kornkasem et al. (2001). The pile meshes in the soft and hard profiles are illustrated in Figure 3.24. The short red lines in the figure represent the nodes between pile elements. Each element of the pile had three integration points for Legendre-Gauss quadrature. Figure 3.26 shows the fiber-discretized pile section at each integration point of the nonlinear beam element. Through static analyses performed on the pier and abutment pile foundations, it was found that even if a large lateral deflection occurred at the pile cap level, the pile deflection at the depth of 6.1 m (20 ft) was nearly zero. Therefore, to reduce the number of pile elements included in the model and save computational costs, the pile bodies were cut off

Table 3.9: Pile number and spacing at an intermediate pier (N_p and S_p are defined in Figure 3.25)

Major bridge type	Skew (°)	Pile member size	Pile number in one row N_p	Center-to-center Pile spacing S_p [m (ft)]	Spacing normalized to pile width S_p / b_p
3S	0	HP 12×84	7	2.13 (7)	6.8
	15		7	2.13 (7)	6.8
	30		8	2.13 (7)	6.8
	45		9	2.29 (7.5)	7.3
	60		11	2.44 (8)	7.8
4S	0	HP 12×84	8	1.83 (6)	5.9
	15		8	1.83 (6)	5.9
	30		8	2.13 (7)	6.8
	45		9	2.29 (7.5)	7.3
	60		11	2.44 (8)	7.8
3C	0	HP 12×84	7	2.13 (7)	6.8
	15		7	2.13 (7)	6.8
	30		8	2.13 (7)	6.8
	45		9	2.29 (7.5)	7.3
	60		11	2.44 (8)	7.8
4C	0	HP 12×84	10	1.52 (5)	4.9
	15		10	1.52 (5)	4.9
	30		10	1.68 (5.5)	5.4
	45		10	1.83 (6)	5.9
	60		11	2.44 (8)	7.8

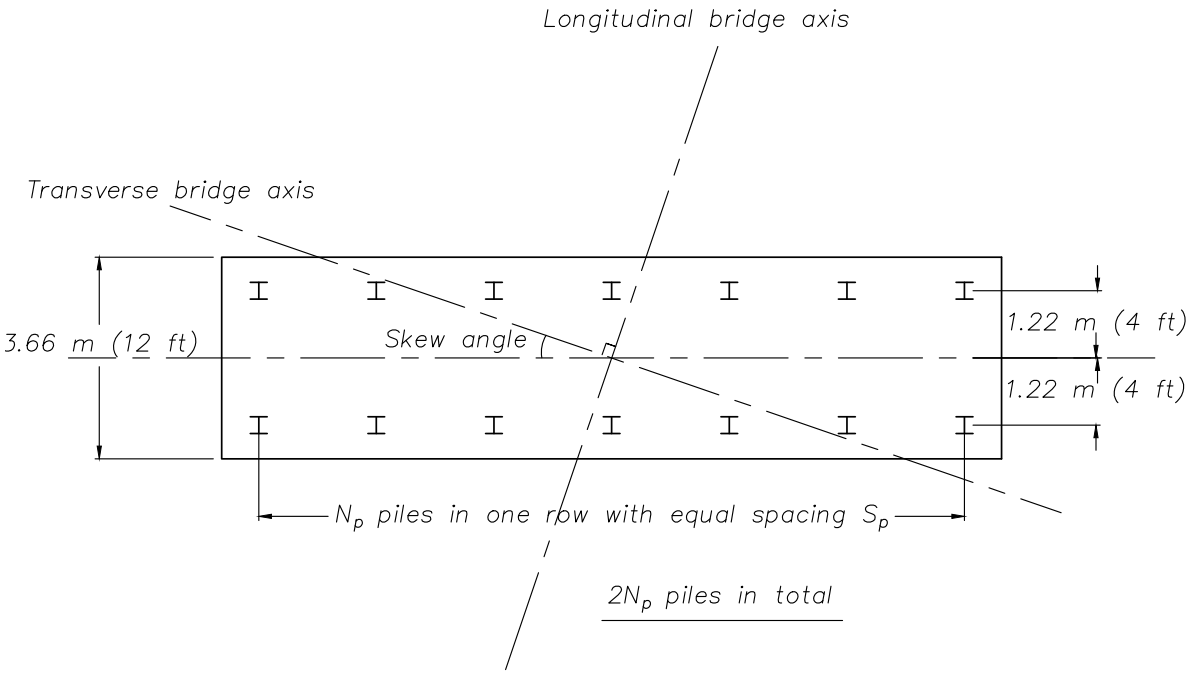

Figure 3.25: Layout of piles at intermediate pier foundations

at the fixity depth of 6.1 m (20 ft) and a fixed boundary condition was imposed at this depth. The pile bodies beyond this fixity depth were neglected in the foundation model.

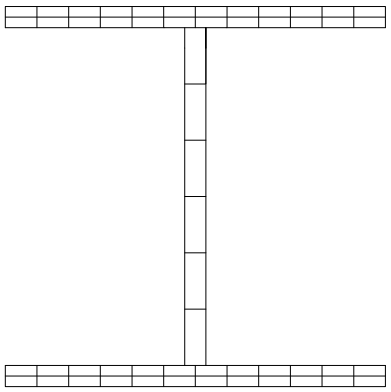

Figure 3.26: Fiber discretized section of foundation piles

Interactions between the pile body and surrounding soil were modeled using the beam on a nonlinear Winkler foundation method that is a widely used modeling strategy for pile foundation under axial and lateral loads (Matlock et al. 1978; Novak and Sheta 1980; Nogami et al. 1992). At each node between two pile elements, a nonlinear $p - y$ spring and a nonlinear $t - z$ spring

developed by Boulanger et al. (1999) for use in *OpenSees* were employed to simulate the lateral soil resistance to the pile and the vertical skin friction between the pile and surrounding soil, respectively. A schematic of the pile model with nonlinear springs is shown in Figure 3.27. The backbone curves of the $p - y$ springs for soft clay and sand approximate the analytical models proposed by Matlock (1970) and API (1987), respectively. For stiff clay, the $p-y$ spring developed by Boulanger et al. (1999) was modified to approximate the analytical backbone curve proposed by Reese and Van Impe (2011). These three analytical models are reviewed later in this section. Figure 3.28 demonstrates the validation of the backbone $p - y$ spring curves against the analytical models for soft clay, sand, and stiff clay. In Figure 3.28, p_{ult} denotes the ultimate capacity of the $p - y$ spring while y_{50} is the deformation corresponding to 50% of the p_{ult}. p_{ult} and y_{50} are two critical parameters that need to be specified for implementing the $p - y$ springs in the *OpenSees* pile foundation model. The determination of p_{ult} and y_{50} for different soils is introduced later in this section. The cyclic behavior of the $p - y$ and $t - z$ springs can be found in the technical paper of Boulanger et al. (1999).

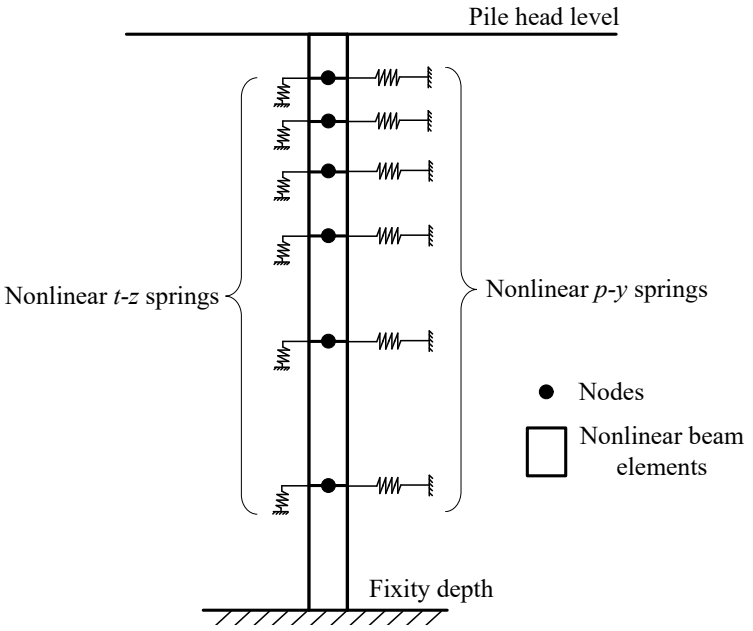

Figure 3.27: Schematic of pile model with $p - y$ and $t - z$ springs

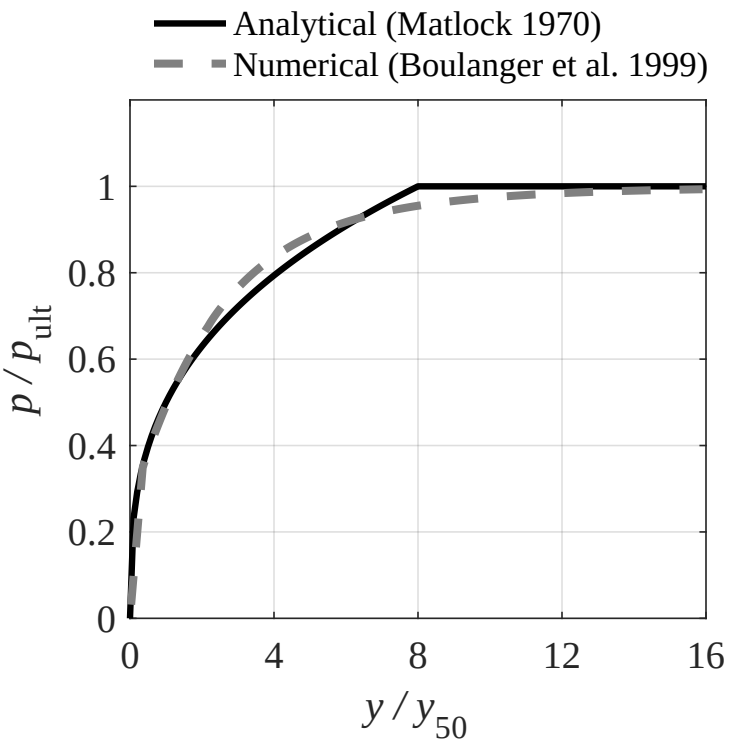

(a) Soft clay

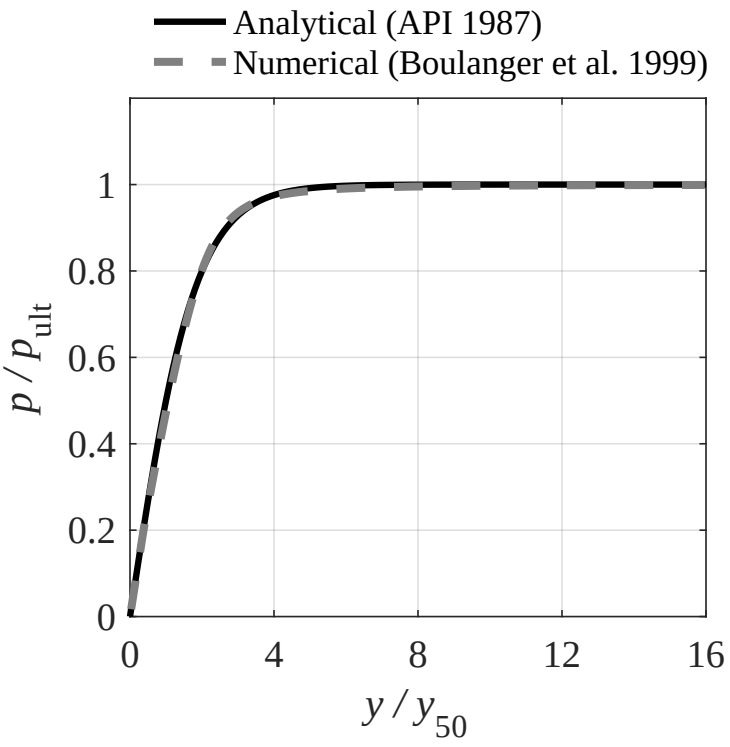

(b) Sand

Figure 3.28: Validation of numerical $p - y$ curves against analytical models

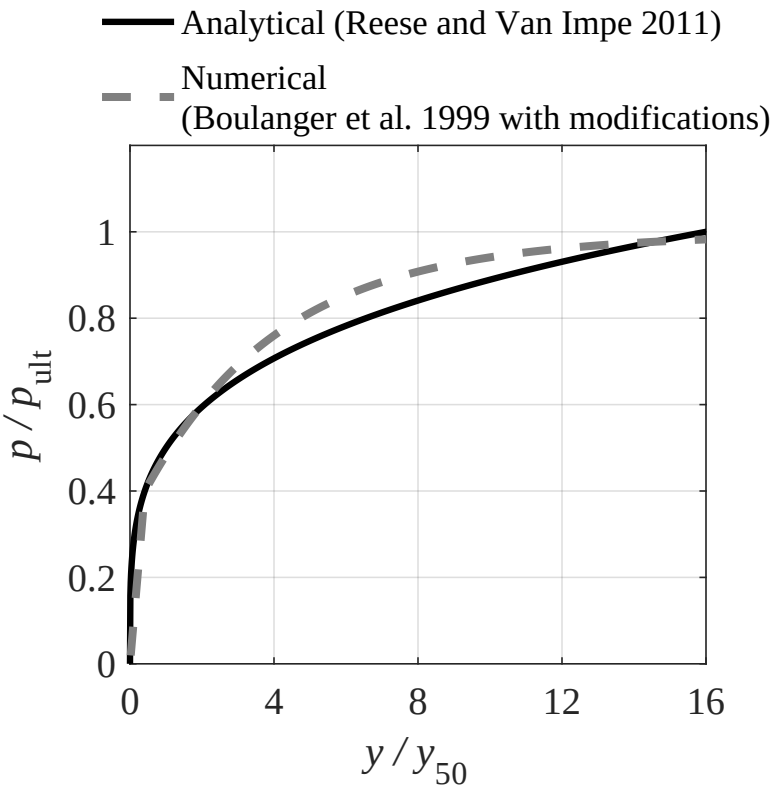

(c) Stiff clay

Figure 3.28 (cont.)

The procedure for developing $p - y$ curves of soft clay as well as determining p_{ult} and y_{50} (Matlock 1970) is summarized as follows:

Step 1: compute ultimate lateral bearing capacity per unit length of pile, denoted as p_{ult}, using the smaller of the values given by Equations (3.3) and (3.4)

$$p_{\text{ult}} = \left(3 + \frac{\gamma\prime}{s_u}z + \frac{J}{D}z\right)s_u D \tag{3.3}$$

$$p_{\text{ult}} = 9s_u D \tag{3.4}$$

where

z = depth,

s_u = undrained shear strength at depth z,

$\gamma\prime$ = effective soil unit weight,

D = pile diameter,

J = 0.5 for soft clay and 0.25 for medium clay.

For use in *OpenSees*, the p_{ult} needs to be multiplied by the tributary pile length.

Step 2: compute the deformation at 50% of p_{ult}, denoted as y_{50}, using the following equation

$$y_{50} = 2.5\epsilon_{50}D \tag{3.5}$$

where typical values of ϵ_{50} for clay with different undrained shear strength were recommended by Reese and Van Impe (2011).

Step 3: the $p - y$ relation is determined as

$$p(y) = 0.5p_{\text{ult}}\left(\frac{y}{y_{50}}\right)^{\frac{1}{3}} \quad \text{for} \quad y \leq 8y_{50} \tag{3.6}$$

$$p(y) = p_{\text{ult}} \quad \text{for} \quad y > 8y_{50} \tag{3.7}$$

The procedure for developing $p-y$ curves of sand as well as determining p_{ult} and y_{50} (API 1987) is summarized as follows:

Step 1: compute ultimate lateral bearing capacity per unit length of pile for sand at shallow and deep depths using the following equations

$$p_{us} = (C_1 z + C_2 D)\gamma' z \tag{3.8}$$

$$p_{ud} = C_3 D \gamma' z \tag{3.9}$$

where

C_1, C_2, C_3 = coefficients determined from design charts,

z = depth,

γ' = effective soil unit weight,

D = pile diameter.

Step 2: the theoretical ultimate soil resistance p_s is determined as the smaller of p_{us} and p_{ud} given by Equations 3.8 and 3.9.

Step 3: determine the factor to account for cyclic or static loading condition, which is evaluated by

$A = 0.9$ for cyclic loading,

$A = (3.0 - 0.8\frac{z}{D}) \geq 0.9$ for static loading.

$A = 0.9$ is used in this study to account for cyclic loading.

Step 4: the ultimate lateral bearing capacity per unit length of pile, denoted as p_{ult}, is determined as

$$p_{\text{ult}} = A p_s \tag{3.10}$$

For use in *OpenSees*, the p_{ult} needs to be multiplied by the tributary pile length.

Step 5: the $p - y$ relation is determined as

$$p(y) = p_{\text{ult}} \tanh\left(\frac{kz}{p_{\text{ult}}} y\right) \tag{3.11}$$

where k is the initial modulus of subgrade reaction determined from design charts.

Step 6: the deformation at 50% of p_{ult}, denoted as y_{50}, is determined as

$$y_{50} = \frac{\text{atanh}(0.5) p_{\text{ult}}}{kz} \tag{3.12}$$

The procedure for developing $p-y$ curves of stiff clay as well as determining p_{ult} and y_{50} (Reese and Van Impe 2011) is summarized as follows:

Step 1: compute the ultimate lateral bearing capacity per unit length of pile, p_{ult}, using the smaller of the values given by Equations 3.3 and 3.4, with $J = 0.5$. For use in *OpenSees*, the p_{ult} needs to be multiplied by the tributary pile length.

Step 2: compute the deformation, y_{50}, at 50% of p_{ult} using Equation 3.5.

Step 3: the $p - y$ relation is determined as

$$p(y) = 0.5 p_{\text{ult}} \left(\frac{y}{y_{50}} \right)^{\frac{1}{4}} \quad \text{for} \quad y \leq 16 y_{50} \tag{3.13}$$

$$p(y) = p_{\text{ult}} \quad \text{for} \quad y > 16 y_{50} \tag{3.14}$$

The backbone curve of the $t - z$ spring (Boulanger et al. 1999) for clay approximates the curve proposed by O'Neil and Reese (1999), while the backbone curve for sand approximates the analytical model proposed by Mosher (1984). Figure 3.29 demonstrates the validation of the backbone $t - z$ spring curves. Similar to the $p - y$ springs, t_{ult} and z_{50} are two critical parameters that need to be specified for implementing the $t - z$ springs in OpenSees.

The procedure for determining t_{ult} and z_{50} of the $t-z$ spring in clay per API (2000) is summarized as follows:

Step 1: compute Ψ using the following equation

$$\Psi = \frac{c}{p'_o} \tag{3.15}$$

where c is the undrained shear strength of the soil at the point in question and p'_o is the effective overburden pressure at the point in question.

Step 2: compute α using the following equations

$$\alpha = 0.5 \Psi^{-0.5} \quad \text{for } \Psi \leq 1.0 \tag{3.16}$$

$$\alpha = 0.5 \Psi^{-0.25} \quad \text{for } \Psi > 1.0 \tag{3.17}$$

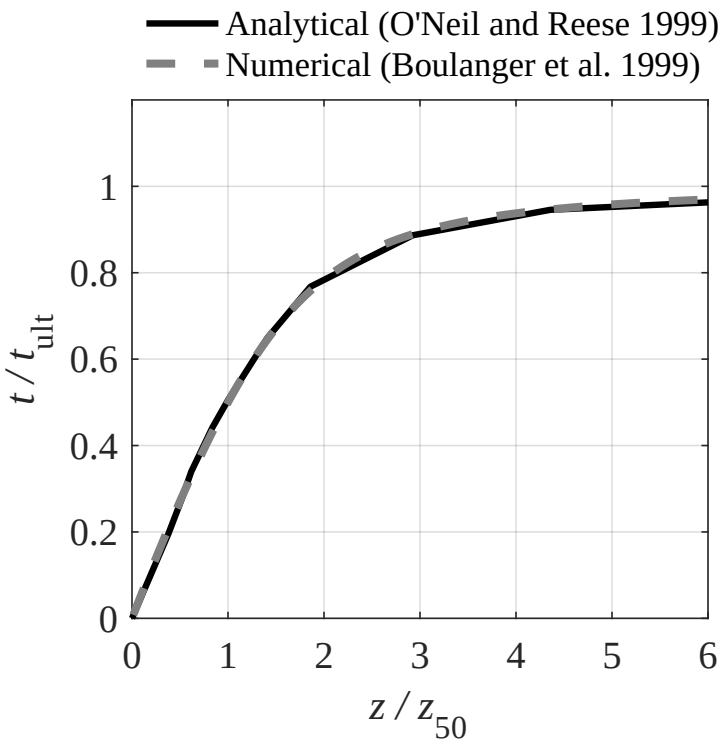

(a) Clay

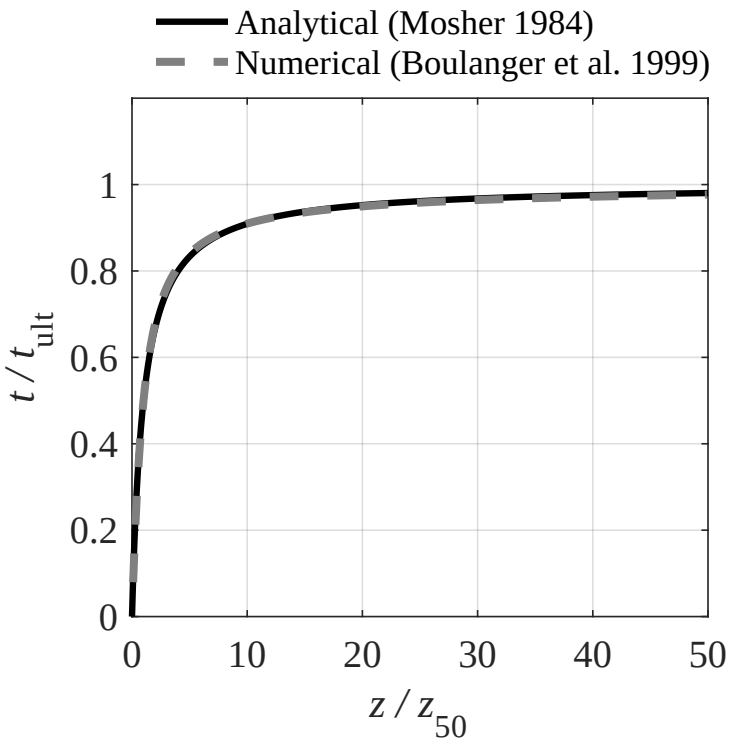

(b) Sand

Figure 3.29: Validation of numerical $t - z$ curves

Step 3: compute t_{ult} using c and α

$$t_{ult} = \alpha c \tag{3.18}$$

For use in *OpenSees*, the t_{ult} needs to be multiplied by the tributary pile length.

Step 4: compute z_{50} using the following equation

$$z_{50} = 0.0031D \tag{3.19}$$

where D is the pile diameter.

The procedure for determining t_{ult} and z_{50} of the $t - z$ spring in sand per Mosher (1984) is summarized as follows:

Step 1: determine t_{ult} using the chart shown in Figure 3.30a. For use in *OpenSees*, the t_{ult} needs to be multiplied by the tributary pile length.

Step 2: determine k_f using the table shown in Figure 3.30b.

Step 3: determine z_{50} using the following equation

$$z_{50} = \frac{t_{ult}}{k_f} \tag{3.20}$$

It can be seen in Table 3.9 that the piles of the prototype bridges are typically widely spaced. The center-to-center spacings of adjacent piles are all greater than 4.0 times of the pile width. As indicated by Wang and Reese (1986) and Reese and Wang (1996), for such pile spacings, the pile group effect is insignificant and the efficiency of the pile group is quite close to 1.0. Therefore, the $p - y$ and $t - z$ curves for single piles were not modified in the prototype bridge models.

As concluded by Castilla et al. (1984), when the ratio of embedded length to pile width is greater than two, the rotation of the pile head reaches a constant value independent of the ratio of embedded length to pile width, which indicates the fixed end condition is achieved. Article 3.15.5.5 of the IDOT Bridge Manual (IDOT 2012a) requires that "piles at abutments, pier footings, and pier cap beams should typically be embedded a minimum of 2 ft-0 in. to ensure a fixed boundary condition." For the HP12×84 piles supporting the prototype bridges, this required 2-ft embedded length is nearly twice of the pile width, and sufficient to develop a fixed end condition per Castilla et al. (1984). Thus, it was assumed that the piles are rigidly connected to the pile cap

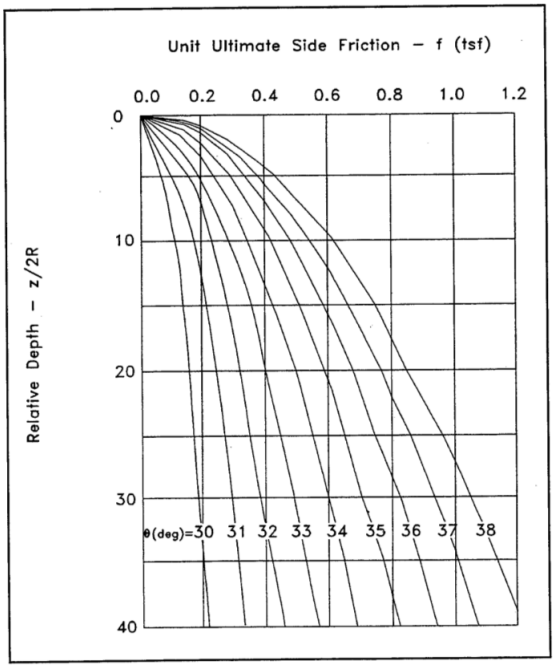

(a)

Table 1
k_f (psf/in.) as Function of Angle of Internal Friction of Sand for Method SSF1

Angle of Internal Friction (degrees)[1]	k_f (psf/in.)
28 - 31	6,000 - 10,000
32 - 34	10,000 - 14,000
35 - 38	14,000 - 18,000

[1] A table of factors for converting non-SI units of measurement to SI (metric) units is presented on page x.

(b)

Figure 3.30: Ultimate side friction for piles in sand (after Mosher 1984)

in the prototype bridge models.

In addition to the piles, passive soil resistance to the pile cap of intermediate piers in both the longitudinal and transverse directions was also modeled using nonlinear compression-only springs. These springs were also used to model the passive soil resistance to the backwall and pile cap, which will be introduced in Chapter 4. It was assumed that the pile cap was embedded and 2-ft-deep soil was placed on top of the pile cap.

In the bridge models, piles supporting both the abutments and piers are assigned with the same soil condition, either the “hard soil” or the “soft soil" illustrated in Figure 3.24. Additionally, a "mixed" soil condition in which the abutment piles are embedded in the hard soil while the pier piles are embedded in the soft soil was studied to account for a different geological condition. The lateral response of a prototype bridge with this soil condition was compared to that of the same bridge with the soft soil condition. It was found that the bridge lateral response was quite similar in these two soil conditions. Therefore, the mixed soil condition was not considered in the subsequent bridge analysis.

3.5 Bridge Superstructure-Substructure Connection Model

As introduced in Chapter 1, non-seismically designed elastomeric expansion bearings, transverse bearing retainers, low-profile steel fixed bearings, and steel dowel connections are employed in the quasi-isolated bridges as sacrificial superstructure-substructure connections. In the last phase of the research project, numerical models for these components were developed on the basis of experimentally measured response characteristics. The configurations, experimental behaviors, and computational models of these components are briefly reviewed in the following sub-sections and more details can be found elsewhere (Filipov et al. 2013a,b; LaFave et al. 2013a,b; Steelman et al. 2013, 2014, 2016).

3.5.1 Elastomeric expansion bearings

Figure 3.31a shows the configuration of IDOT Type I elastomeric expansion bearings (IDOT 2012a) placed at the abutments and expansion piers of quasi-isolated bridges. Figure 3.31b illus-

trates the computational model for shear and sliding behavior of the steel shim reinforced bearing elastomer. The bearing elastomer is directly placed on top of the concrete substructure. When the bridge is subjected to seismic demands, the bearing elastomer may experience shear deformation and subsequent sliding on the substructure. Shear and stick-slip sliding behavior of the elastomer was simulated using a coupled bi-directional stick-slip friction model (Filipov et al. 2013a). In this model, the initial static coefficient of friction of $\mu_I = 0.6$ and the kinematic coefficient of friction of $\mu_K = 0.45$ were used to model the initial static and kinematic friction between the elastomer and concrete substructure. The coefficients of friction were determined through experimental tests on full-scale bearing specimens (Steelman et al. 2013). The shear stiffness of the elastomer (the slope in Figure 3.31b) was estimated as the material shear modulus multiplied by the plan area of the elastomer and then divided by the thickness of the elastomer (Filipov et al. 2013a). A shear modulus of 586 kPa (85 psi) was determined by experimental testes (Steelman et al. 2013).

3.5.2 Transverse retainers of elastomeric expansion bearings

While shear and sliding of the elastomeric bearing in the longitudinal bridge direction is only restrained by elastomer-concrete interface friction, a pair of bearing retainers is placed on the two transverse sides of each elastomeric expansion bearing to restrain its shear deformation and sliding in the transverse bridge direction, in conjunction with the elastomer-concrete friction at the bearing bottom. Figure 3.32a shows the configuration of the bearing retainers. A steel anchor bolt secures each single retainer into the concrete substructure.

The IDOT Bridge Manual (IDOT 2012a) provides a method for nominally proportioning the anchor bolts of bearing retainers. In line with this method, when one anchor bolt is used for each single retainer, the required anchor bolt diameter, d_ra, is determined as

$$d_{ra} = \sqrt{\frac{4C_{il}(DL)}{\pi\phi(0.48)F_u}} \tag{3.21}$$

where $\phi = 0.75$ is the specified strength reduction factor, F_u is the ultimate tensile strength of the anchor bolt material, DL is the superstructure dead load at the given bearing under consideration, C_{il} is a coefficient of 0.2, leading to a nominal anchor fusing capacity equal to 20% of the

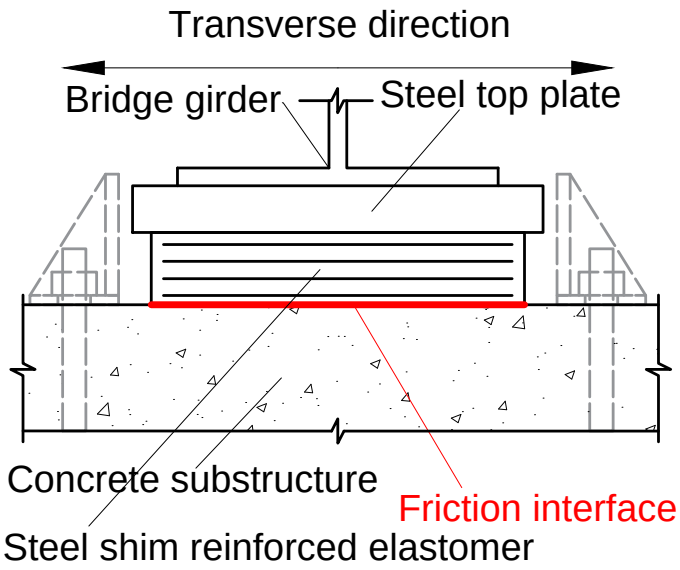

(a) Configuration

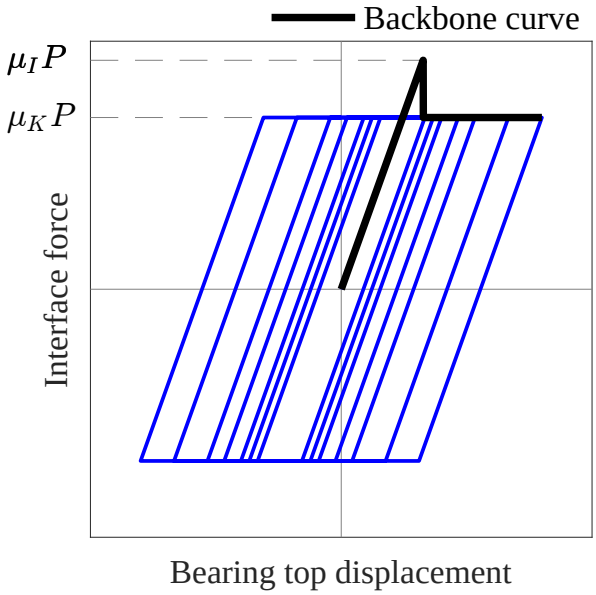

1. Axial compression P
2. Initial static coeff. of friction$\mu_I = 0.60$
3. Kinematic coeff. of friction $\mu_K = 0.45$

(Coeff. of friction obtained from experimental results)

(b) Computational model for elastomer shear and sliding (without transverse retainers)

Figure 3.31: Configuration and computational model of IDOT Type I elastomeric expansion bearings employed in quasi-isolated bridges (IDOT 2012a; Filipov et al. 2013a; LaFave et al. 2013b; Steelman et al. 2013)

superstructure dead load at the given bearing. The retainer anchors of the prototype bridges were proportioned on the basis of Equation 3.21. The IDOT Bridge Manual also provides a number of available options for the anchor diameter (0.625 in., 0.75 in., 1.0 in., 1.25 in., 1.5 in., 2 in., and 2.5 in.). The computed d_r was rounded up to the nearest available diameter. The number, size, and material grade of the retainer anchors proportioned for different prototype bridges are listed in Table 3.1.

The experimentally measured retainer anchor behavior when subjected to seismic demands was simulated using a uni-directional elasto-plastic computational model that considers the initial gap, yielding, strain hardening, and ultimate rupture responses (Filipov et al. 2013a). Figure 3.32b schematically illustrates the computational model. In this model, the expected ultimate and yielding capacities of a single retainer anchor bolt, R_u and R_y, were determined using Equations (3.22) and (3.23) (Filipov et al. 2013b; LaFave et al. 2013b).

$$R_u = \phi 0.8 A_b F_u \tag{3.22}$$

$$R_y = R_u / 1.8 \tag{3.23}$$

where A_b is the nominal cross-sectional area of the anchor bolt, F_u is the ultimate tensile strength of the anchor bolt material, and ϕ is the strength reduction factor ($\phi = 1.0$ for unreduced capacity). The equations were calibrated against experimentally measured retainer anchor response data (Filipov et al. 2013b; LaFave et al. 2013a,b).

3.5.3 Low-profile steel fixed bearings

For the quasi-isolated bridges with steel-plate girders, IDOT low-profile steel fixed bearings (IDOT 2012a) are typically installed on one intermediate pier (the so-called "fixed pier") to compensate the flexibility of the elastomeric expansion bearings and resist superstructure motions caused by vehicle braking forces. Figure 3.33a shows the configuration of the low-profile steel fixed bearing. The bottom steel plate of the bearing is secured into the supporting concrete substructure by anchor bolts. An elastomeric neoprene leveling pad is placed between the bearing bottom plate and top surface of the concrete substructure. The top steel plate is mated to the bottom plate via two steel

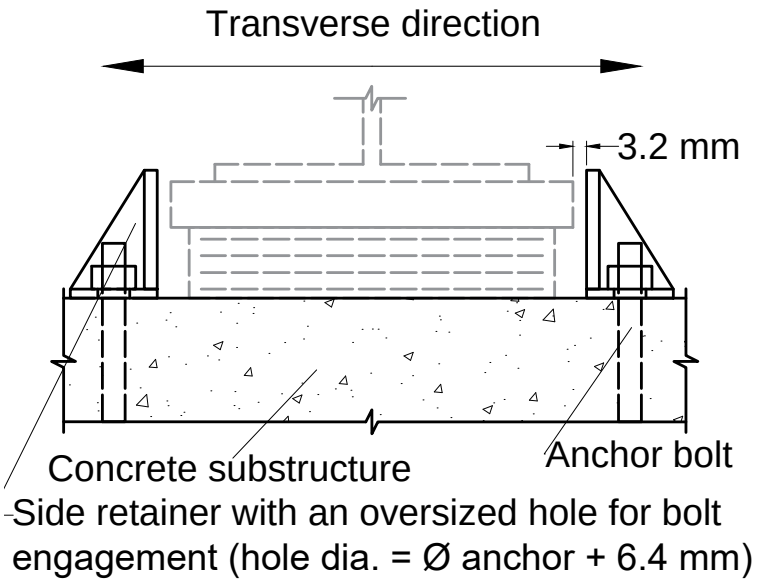

(a) Configuration

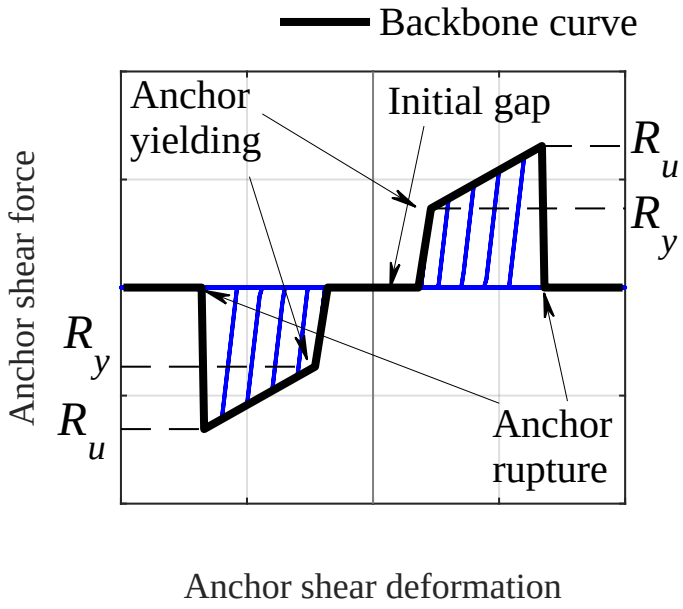

(b) Computational model of retainer anchor (without elastomeric bearing)

Figure 3.32: Configuration and computational model of transverse bearing retainers employed in quasi-isolated bridges (IDOT 2012a; Filipov et al. 2013a; LaFave et al. 2013b; Steelman et al. 2013)

pintles.

The IDOT Bridge Manual (IDOT 2012a) provides a method for nominally proportioning the anchor bolts of steel fixed bearings, considering anchor shear as the only failure mode. In this method, the number of anchor bolts required along each beam line, N, is given by Equations (3.24) and (3.25).

$$N = \frac{C_{il}(DL)}{F} \tag{3.24}$$

$$F = \phi(0.48)A_b F_u \tag{3.25}$$

where DL is the superstructure dead load at the given bearing under consideration, C_{il} is a coefficient of 0.2, leading to a nominal anchor fusing capacity equal to 20% of the superstructure dead load at the given bearing, $\phi = 0.75$ is the specified strength reduction factor, F_u is the ultimate tensile strength of the anchor bolt material.

By inspection of the plans of many recently constructed quasi-isolated highway bridges in Illinois, it was found that the specified nominal fusing capacity of low-profile steel fixed bearing anchors, namely 20% of the superstructure dead load on the bearing, is typically over-designed. A primary potential reason for this design trend in practice may be that bridge designers tend to regard the specified fusing capacity as a minimum requirement and use larger or more anchor bolts for conservatism. A secondary potential reason is that a fusing capacity in the close vicinity of 20% of the dead load on the bearing is not always available in actual design due to the limited options for anchor diameters. In this situation, bridge designers may round the anchor diameter up to the nearest available size and result in over-designed nominal fusing capacity. In the prototype bridges, this trend of over-designed fixed bearing anchors has been considered. The number, size, and material grade of the fixed bearing anchors in the prototype bridges are listed in Table 3.1.

Through full-scale experimental studies, it was found that a properly proportioned steel fixed bearing can achieve predictable and reliable behavior of anchor rupture and subsequent sliding, when subjected to seismic demands (Steelman et al. 2014). Shear behavior of the anchor bolts was simulated using a coupled bi-directional model possessing a similar elasto-plastic behavior to the model for retainer anchors (Filipov et al. 2013b; LaFave et al. 2013b), as shown in Figure 3.33b. The expected ultimate and yielding capacities of a single anchor bolt, R_u and R_y, were determined

using Equations (3.26) and (3.27) (LaFave et al. 2013b).

$$R_u = \phi(0.8A_b)(0.6F_u) \tag{3.26}$$

$$R_y = \phi(0.8A_b)(0.6F_y) \tag{3.27}$$

where $0.8A_b$ is the nominal cross-sectional area of the anchor bolt at the threaded portion, $0.6F_u$ and $0.6F_y$ are the ultimate and yielding shear strength of the anchor bolt material, respectively, ϕ is the strength reduction factor ($\phi = 1.0$ for unreduced capacity). The equation was validated by experimentally measured steel-fixed bearing response data (Filipov et al. 2013b; Steelman et al. 2014). Additionally, the interface friction between the bearing bottom plate and elastomeric leveling pad was simulated using the same model as the elastomeric expansion bearings, but with different coefficients of friction ($\mu_I = \mu_K = 0.30$).

3.5.4 Steel dowel connections of PPC-girder bridges

Different from the steel-plate-girder bridges, the prototype PPC-girder bridges employ steel dowel connections between superstructures and fixed piers. Figures 3.34a and 3.35b show the configuration of such superstructure-to-fixed-pier connections. #8 (U.S.) steel dowel bars with a nominal diameter of 25.4 mm (1.0 in.) are used to connect the pier cap to the diaphragm and PPC girder bottom flanges. As shown in Figure 3.35b, on each face of the pier between two adjacent girders, the minimum required number of dowel bars, denoted by N, is given by the following equation

$$N = \frac{1}{2}\left[\frac{0.2DL}{28.3(S)} - 2\right] \geq 2 \tag{3.28}$$

where DL is the sum of all superstructure dead loads at the given pier under consideration in kips; S is the number of beam spaces. Except the N dowel bars on each face between two adjacent girders, additional dowels are placed at each girder line to connect the girder bottom flange to the pier cap (one bar for each exterior girder and two bars for each interior girder). In additional to the dowels, a 12.5-mm(0.5-in.)-thick layer of preformed joint filler is placed between the PPC girder bottom and concrete pier cap.

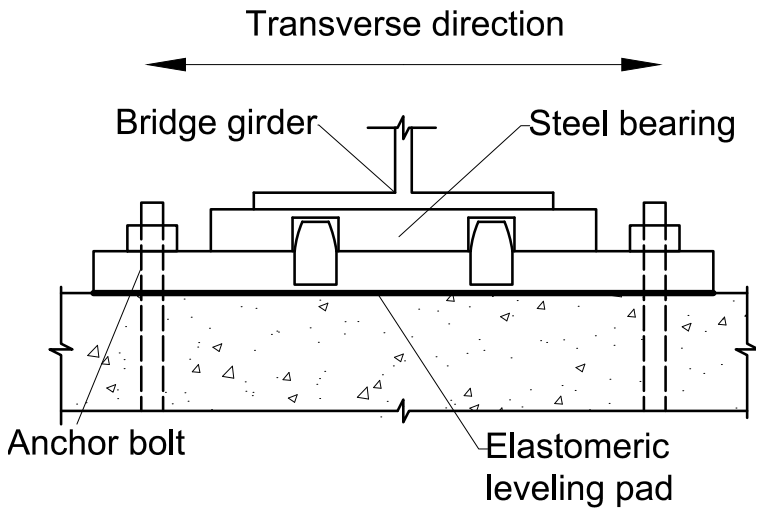

(a) Configuration

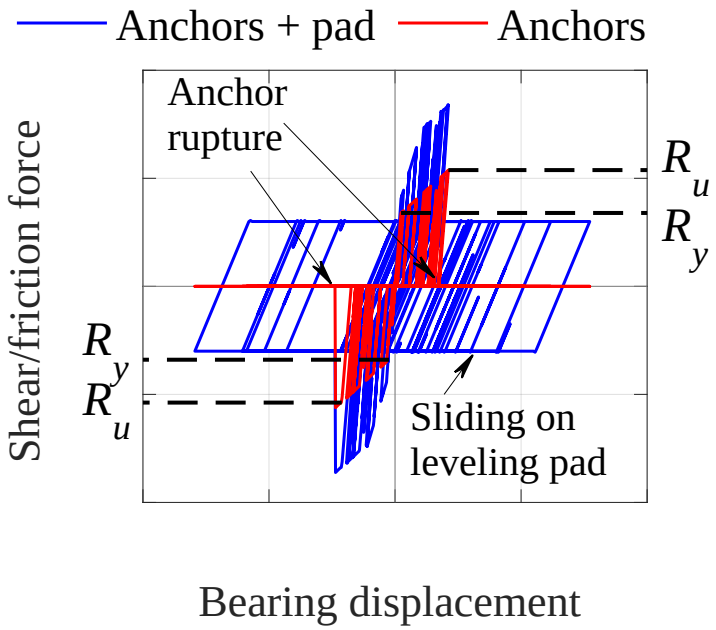

(b) Computational model of fixed bearing anchor shear and level pad friction

Figure 3.33: Configuration and computational model of low-profile steel fixed bearings employed in quasi-isolated bridges (IDOT 2012a; Filipov et al. 2013b; LaFave et al. 2013b; Steelman et al. 2014)

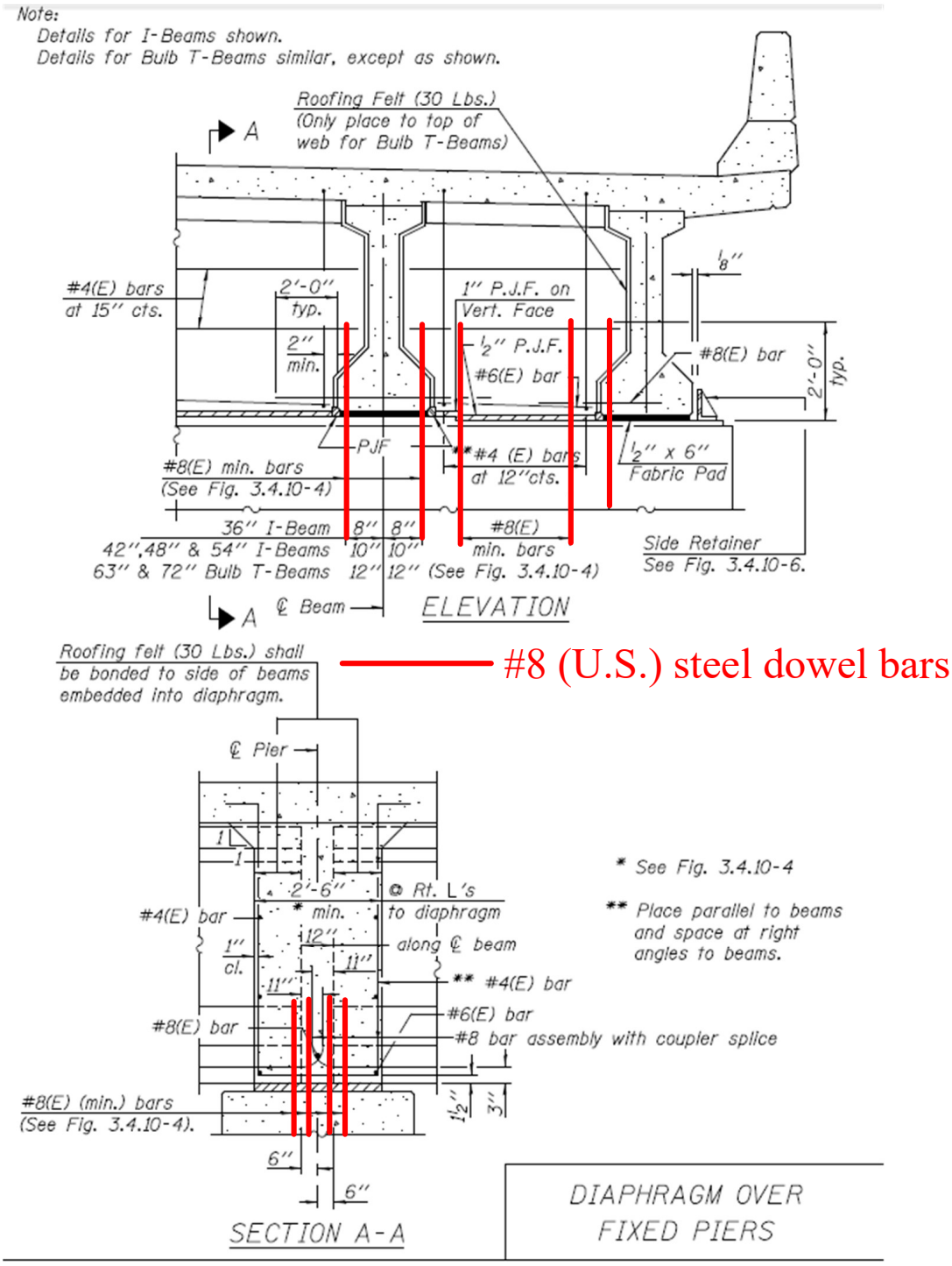

(a) Elevation view

Figure 3.34: Details of superstructure-to-fixed-pier connections in PPC girder bridges (after IDOT 2012a)

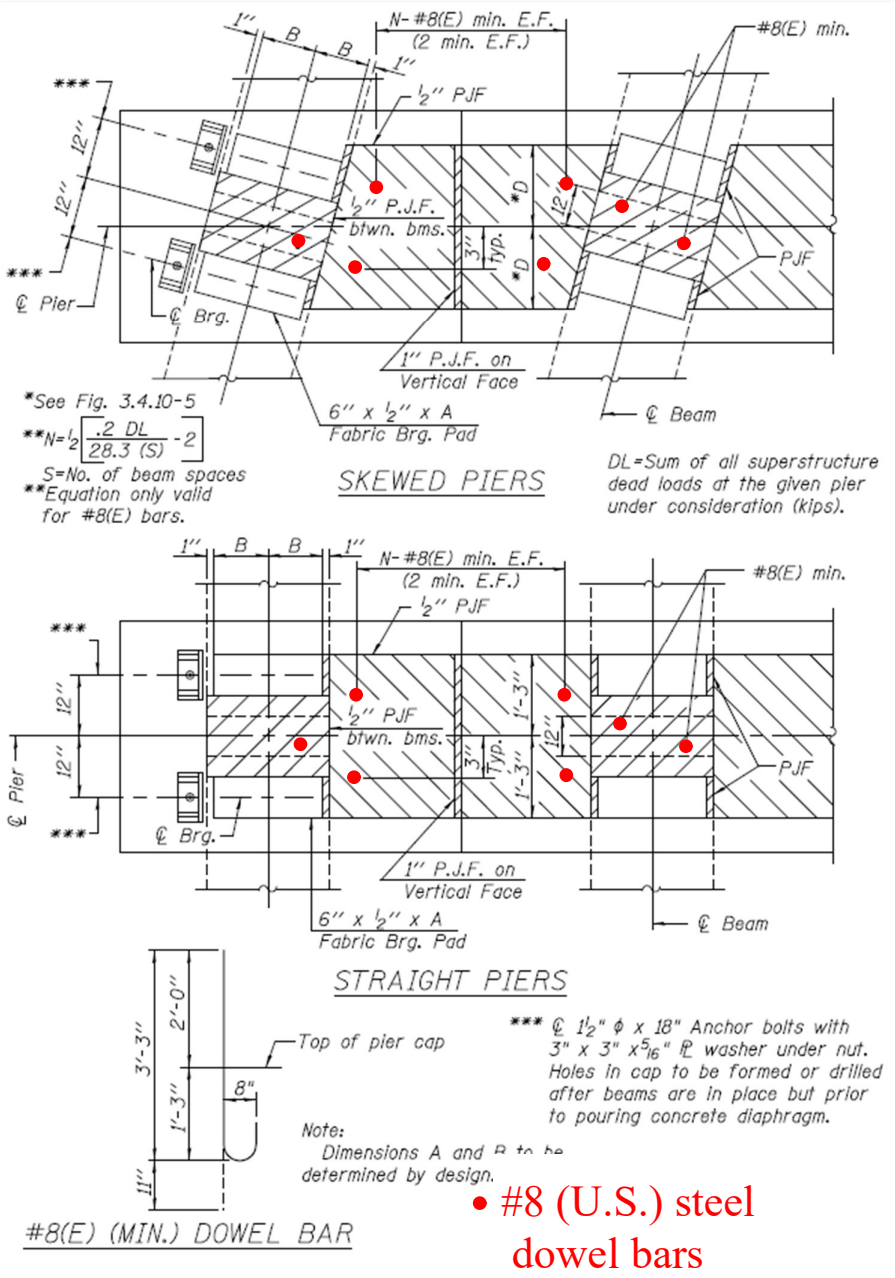

(b) Top view

Figure 3.34 (cont.)

Similar to the steel fixed bearing anchors, the steel dowel bars embedded in concrete tend to be subjected to shear forces during seismic events and friction tends to develop between the preformed joint filler and concrete. Due to these similarities and a lack of experimental data on these steel dowel connections, they were simulated using the same computational models as the low-profile steel fixed bearings, but with different parameters to account for the number and size of steel dowels.

CHAPTER 4

DETAILED MODELING OF SEAT-TYPE BRIDGE ABUTMENTS CONSIDERING SEISMIC SUPERSTRUCTURE-ABUTMENT-FOUNDATION INTERACTIONS

4.1 Overview of Seat-Type Bridge Abutment Model

In many regions of the United States, seat-type abutments, also known as stub abutments, are employed to support highway bridges. Abutments of this type are also commonly used in quasi-isolated highway bridges in the state of Illinois, besides integral abutments and semi-integral abutments. Figure 4.1 depicts the sectional view of a typical non-skew seat-type bridge abutment in Illinois. Skew seat-type abutments have similar configurations to the non-skew one, except that the approach slab is skewed, and the two pieces of wingwalls are not perpendicular to the backwall and pile cap.

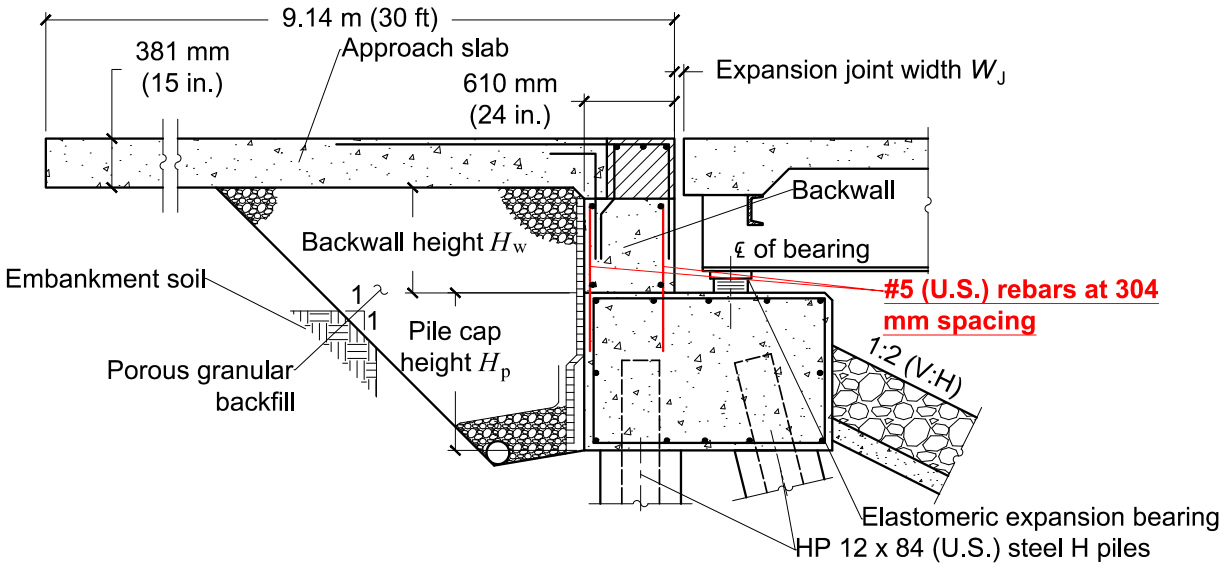

Figure 4.1: A typical seat-type bridge abutment for quasi-isolated highway bridges in Illinois (IDOT 2012a)

In service conditions, seat-type bridge abutments withstand gravity loads of superstructures and traveling vehicles, provide traffic transitions between a bridge and its approach embankments, and retain backfill and embankment soil. In the vertical load-transfer path of highway bridges, seat-type bridge abutments act as end supports for bridge superstructures by transferring tributary gravity loads of superstructures and vehicles down to embankments and the ground below through their foundations. A primary feature that distinguishes seat-type bridge abutments from integral and semi-integral abutments is that an expansion joint is set between the abutment backwall and adjacent superstructure end to accommodate thermally induced bridge deformation by separating the superstructure from abutments.

During major earthquakes, a critical response characteristic of quasi-isolated bridges with seat-type abutments is the sliding of superstructures on supporting substructures after sufficient fusing of the sacrificial superstructure-substructure connections. In this situation, bridge superstructures may act somewhat as "floating bridges" with only limited frictional resistance at the superstructure-substructure interface (Steelman et al. 2014). The superstructure sliding that is only weakly restrained by the friction may result in significant dynamic interactions between deck ends and seat-type abutments. Displacements of bridge superstructures are limited by the abutments to varying degrees, while the abutments are in turn subjected to impact forces from superstructures. The impact of superstructure ends will cause force and deformation demands on the abutment and its foundation buried in the embankment. In order to reasonably model bridge seismic response, the superstructure-abutment-foundation interaction (SAFI) needs to be taken into account in the computational bridge model.

In this chapter, a detailed yet computationally efficient nonlinear finite-element model for typical seat-type bridge abutments in Illinois is discussed. As a subassembly of the *OpenSees* full bridge model introduced in Chapter 3, the abutment model incorporates a number of structural components and geotechnical mechanisms that are critical to capture the seismic SAFIs. Figure 4.2 illustrates the nonlinear finite-element model of the typical seat-type abutment shown in Figure 4.1. A number of critical structural connections and geotechnical mechanisms were modeled using nonlinear springs. In addition, elastic beam elements were used to model some reinforced concrete members, including the pier cap, backwall body, wingwalls, and approach slab. For these massive concrete members, seismic damage is most likely to occur only at their joints and connections,

rather than anywhere else along their length. Thus, for the sake of saving computational cost, elastic beam elements were used to model these members, in lieu of nonlinear beam elements. In order to capture the nonlinear material response of steel piles, nonlinear beam elements with fiber-discretized sections were employed. The following sections introduce the modeling approaches for the pile foundation, expansion joint, backwall, backwall-wingwall connection, backfill passive resistance, wingwall, and pile cap.

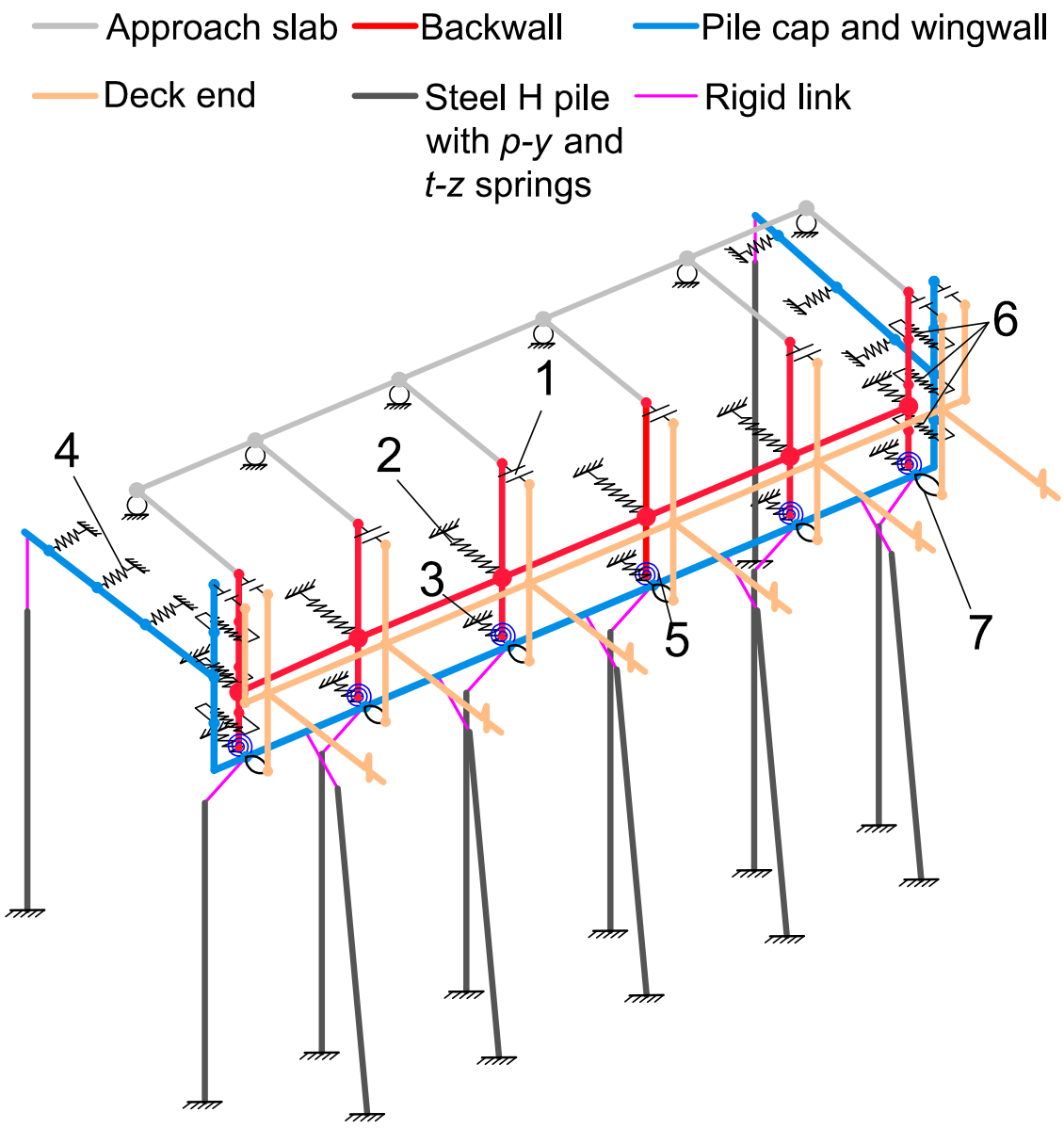

Figure 4.2: A 3-D finite-element model for the typical seat-type bridge abutment shown in Figure 4.1

4.2 Abutment Pile Foundation Model

The abutments of different bridge variants differ in the layout of foundation piles, due to different dead and live gravity loads from superstructures, as well as different pile cap length of bridges with various skews. For bridges with a skew angle of α, the length of the abutment pile cap is increased by a factor of $\frac{1}{\cos\alpha}$ as compared to non-skew bridges, as illustrated in Figure 4.3. In this situation, to meet the maximum pile spacing of 2.43 m (8.0 ft) specified by IDOT (2012a), more piles may be needed for skew abutments than for non-skew abutments.

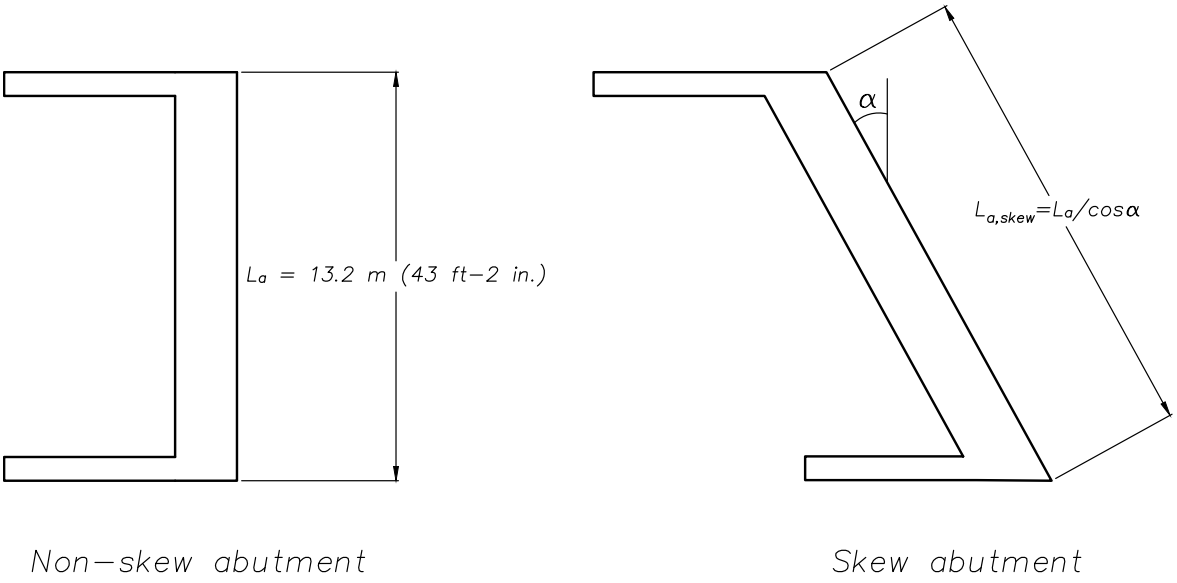

Figure 4.3: Pile cap length of non-skew and skew abutments

Figure 4.4 shows the pile layout at an abutment. As indicated in the figure, N_{ab} batter piles with a slope of 152.4 mm (6 in.) of vertical rise for every 25.4 mm (1 in.) of horizontal run are placed in the front row (the row near the deck end). The angle of batter (the angle made by the batter pile with the vertical) is 9.5°. The direction of batter is to the deck end. N_{av} vertical piles are placed in the back row (the row near the embankment). In addition to these two rows, a single pile supports the end of each piece of wingwall. In conjunction with Figure 4.4, Table 4.1 indicates the pile number and spacing at the abutments of various prototype bridges. Similar to the pile layout at intermediate piers, the abutment piles are also widely spaced (spacing is greater than four times of pile width). Thus, pile group effect was not taken into account in the model. The soil profile and modeling approach for vertical abutment piles are the same as those for the pier piles, which were

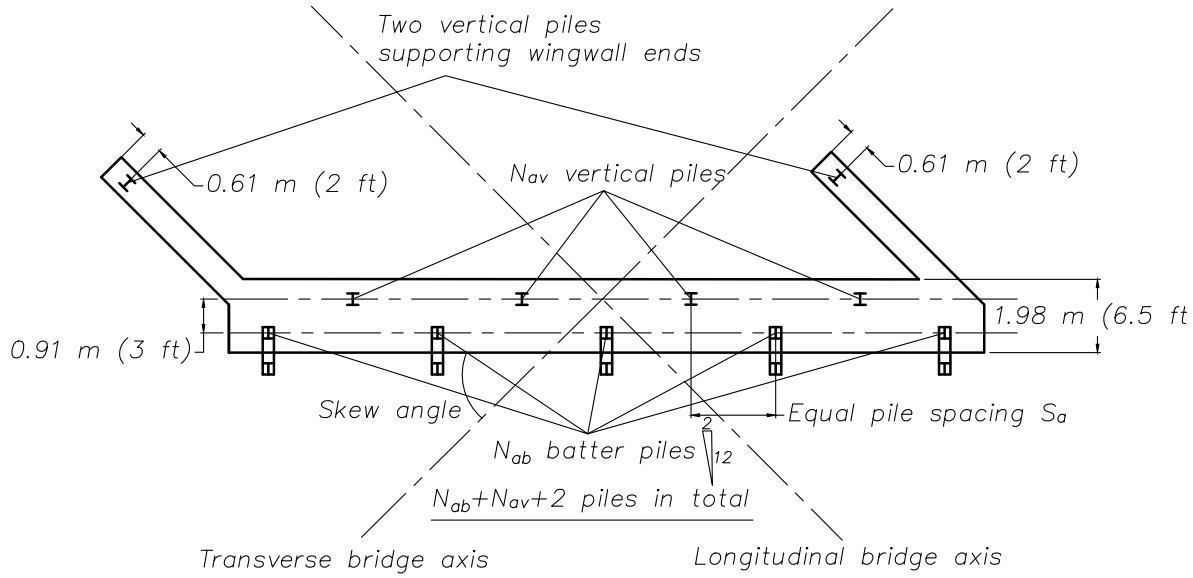

Figure 4.4: Pile layout at an abutment

introduced in Section 3.4.

Table 4.1: Pile number and spacing at an abutment (N_{av} and N_{ab} are defined in Figure 4.4)

Major bridge type	Skew (°)	Pile member size	No. of batter pile N_{ab}	No. of vertical pile N_{av}	Center-to-center Pile spacing S_a [m (ft)]	Spacing normalized to pile width S_a / b_p
3S, 4S, 3C	0	HP 12×84	3	4	1.98 (6.5)	6.3
	15		3	4	2.13 (7)	6.8
	30		3	4	2.43 (8)	7.8
	45		5	4	2.26 (7.5)	7.3
	60		5	6	2.43 (8)	7.8
4C	0	HP 12×84	5	4	1.52 (5)	4.9
	15		5	4	1.52 (5)	4.9
	30		5	4	1.83 (6)	5.9
	45		5	4	2.29 (7.5)	7.3
	60		5	6	2.43 (8)	7.8

The convention for “in-batter” and “out-batter” piles is defined in Figure 4.5 (Reese and Van Impe 2011). Under seismic excitations, the abutment batter piles may act as both in-batter and out-batter piles, due to the cyclic seismic forces. However, the dominant longitudinal seismic force demand on the abutment piles results from the impact of superstructure ends on the abutments. In this loading scenario, the abutment batter piles behave as in-batter piles. Studies for the behavior of batter piles under lateral loads have been sparse in literature. Kubo (1964) proposed values of

p-multipliers for modifying the $p - y$ curves of piles with various batter angles, on the basis of experimental results. For the in-batter abutment piles in this study ($\theta = -9.5°$), a p-multiplier of 1.2 was proposed by Kubo (1964). However, the experimental results of Awoshika and Reese (1971) demonstrated that there is little difference between the behavior of a vertical pile and an in-batter pile under later loads, which means a p-multiplier of unity. Considering both studies, a p-multiplier of 1.1 was employed to modify the $p - y$ springs of abutment batter piles. In the abutment model, the ultimate lateral resisting force of the $p-y$ springs connected to the batter piles was multiplied by 1.1. Except this p-multiplier, the abutment batter piles were modeled using the same approach as the pier piles, which were introduced in Section 3.4. As an example, Figure 4.6 illustrates the vertical and batter abutment piles in the finite-element bridge model.

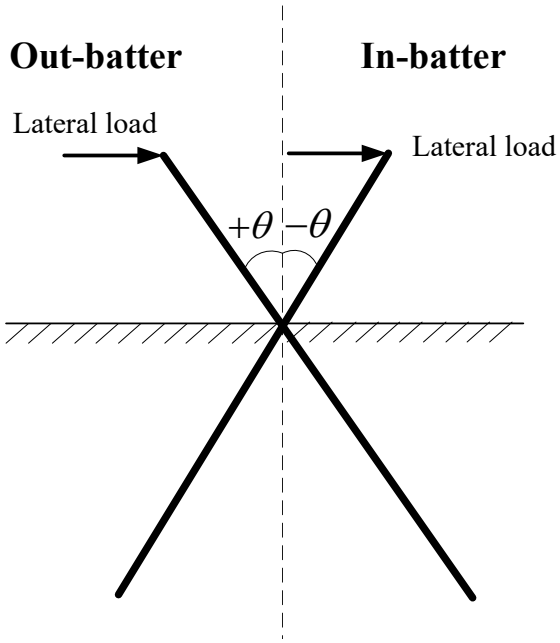

Figure 4.5: Convention for in- and out-batter piles

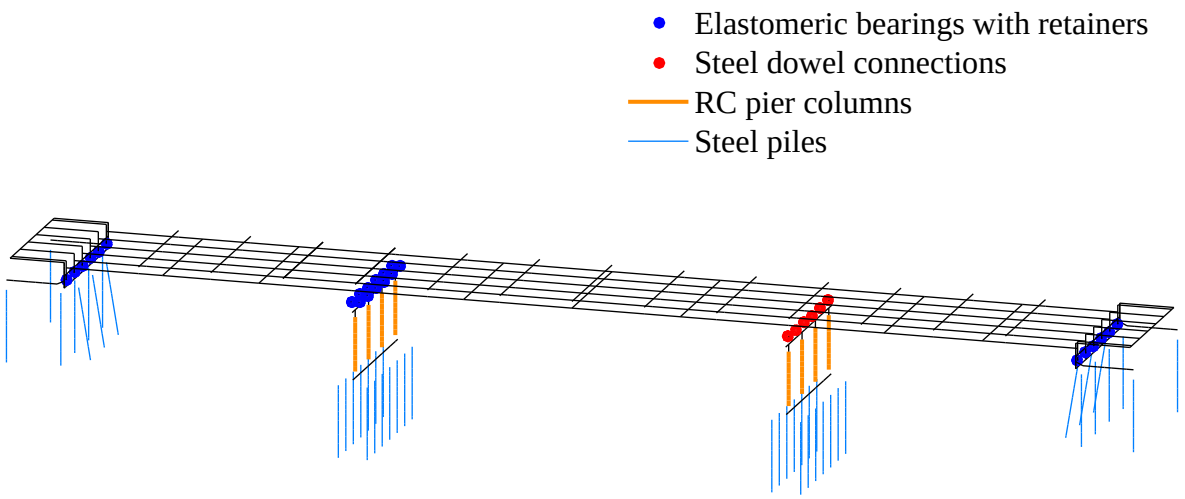

Figure 4.6: Vertical and batter abutment piles in the finite-element bridge model

4.3 Expansion Joint Model

In the typical seat-type bridge abutment, an expansion joint is configured between the backwall and adjacent superstructure end to accommodate thermally induced bridge deformation by separating the superstructure and abutment and allowing relative displacements between the two. The joint opening width normal to the joint edge, W, is illustrated in Figure 4.7. The IDOT Bridge Manual (IDOT 2012a) specifies the design value of W at 50°F by the following equation

$$W(\text{in.}) = [L\,(\text{ft.}) \times 80\,(^{\circ}\text{F}) \times 12(\text{in./ft}) \times 0.0000065/^{\circ}\text{F}] \cos\alpha + 0.5(\text{in.}) \qquad (4.1)$$

where L is the contributing expansion length of the superstructure in feet and α is the skew angle.

In the abutment model, a number of gap-spring elements were employed to simulate the instantaneous gap opening/closing, contact and release at each step of a static or dynamic analysis. These elements are labeled as component No. 1 in Figure 4.2. The force-deformation relation of the gap-spring element is shown in Figure 4.8. When the element is subjected to tension or compressive deformation smaller than the joint opening width W, the element does not provide any resisting force and has a zero stiffness. When the compressive deformation exceeds the joint opening width W, the element becomes very stiff to simulate the hard contact between the deck end and abutment backwall. In the abutment model that is illustrated in Figure 4.2, the gap-spring

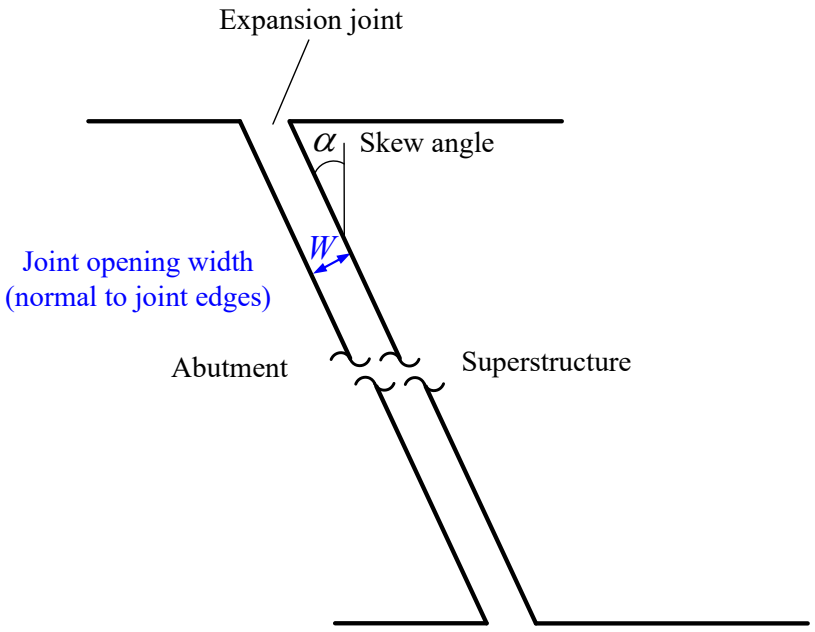

Figure 4.7: Expansion joint opening between abutment and superstructure

elements were placed at the girder line and parapet locations. The elements were oriented normal to the edge of the expansion joint.

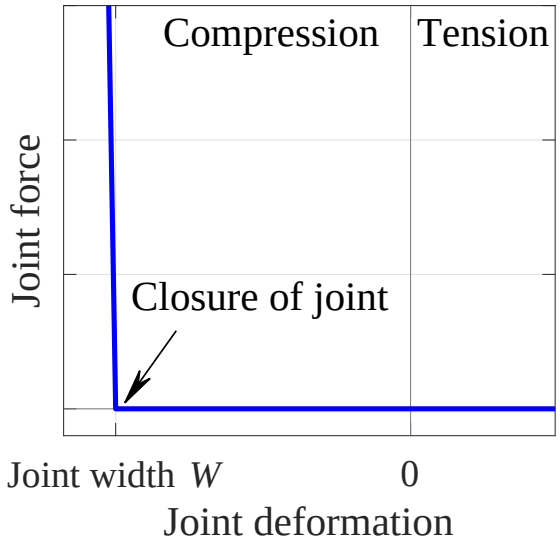

Figure 4.8: Force-deformation relation of gap-spring elements modeling expansion joints

4.3.1 Abutment backwall model

The RC backwall is connected to the pile cap by two rows of #5 (U.S.) reinforcing steel (15.8-mm diameter) with a 0.3-m (1-ft) spacing along the wall. The reinforcing steel is provided as the shrinkage and temperature reinforcement in concrete walls specified by AASHTO (2010). As shown in Figure 4.1, the thickness of the backwall is 0.61 m (2 ft), which is a standard practice in the state of Illinois (IDOT 2012a).

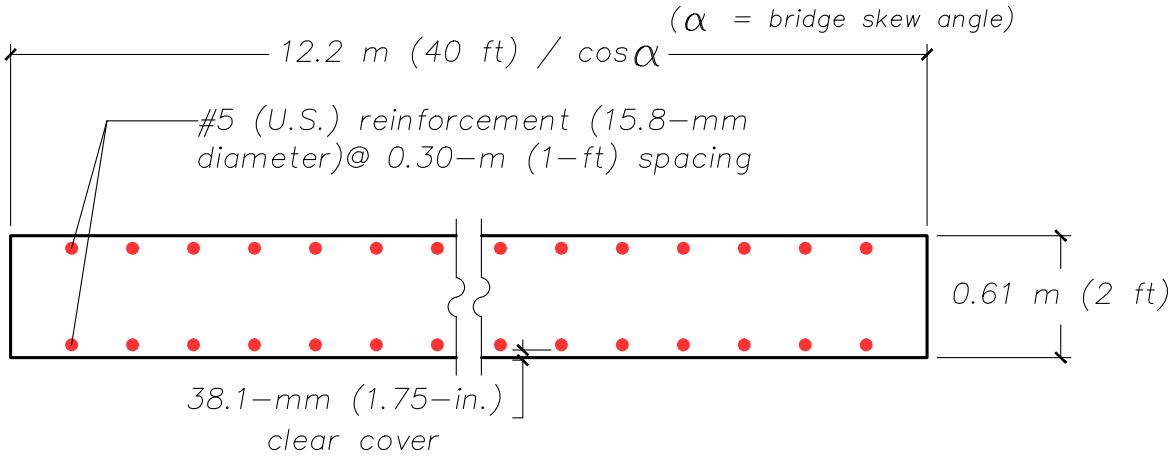

Figure 4.9: Cross-section of abutment backwall

When the bridge is subjected to longitudinal seismic demands, the backwall that is engaged by

the bridge superstructure is subjected to out-of-plane forces. In the abutment model, the backwall was modeled as a cantilever wall whose bottom is connected to the pile cap through an elasto-plastic hinge. To obtain the moment-curvature relation of the backwall section shown in Figure 4.9, a sectional analysis was conducted using *SAP2000*. On the basis of the obtained moment-curvature relation, an equivalent plastic hinge method proposed by Abo-Shadi et al. (2000) for modeling out-of-plane bending behavior of RC walls was employed to determine the moment-rotation relation of backwall bottom. For the non-skew prototype bridges, the computed moment-rotation relation of backwall bottom is shown in Figure 4.10. For skew prototype bridges, as shown in Figure 4.9, the abutment backwall is elongated by a factor of $\frac{1}{\cos\alpha}$, where α is the bridge skew angle. Thus, for a skew prototype bridge, the moment-rotation relation of the backwall bottom hinge was obtained through multiplying the hinge moment of the equivalent non-skew bridge shown in Figure 4.10 by a factor of $\frac{1}{\cos\alpha}$. In the finite-element abutment model, the moment-rotation relation shown in Figure 4.10 was distributed into a number of rotational nonlinear springs at the backwall bottom, one the basis of tributary wall width of each spring. These springs are labeled as component No. 5 in the finite-element abutment model shown in Figure 4.2. The backwall body was modeled using elastic beam elements. The estimated shear capacity of the concrete backwall body is higher than the shear demand that is required to cause flexural failure of the wall-bottom hinge. Thus, shear failure of the backwall body was not explicitly modeled.

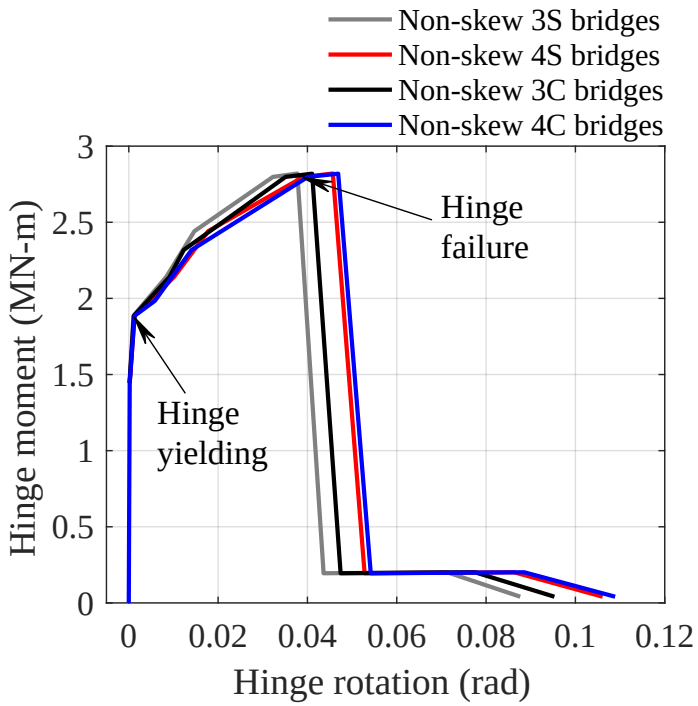

Figure 4.10: Moment-rotation relation of backwall bottom

4.4 Backwall-Wingwall Connection Model

In the typical seat-type bridge abutment, pairs of bent steel dowel bars are typically embedded in the concrete at the junction between a backwall and a wingwall, crossing the construction joint between the two (IDOT 2012a). The configuration of these steel dowel bars can be found in Luo et al. (2016). The purpose of these connections is to strengthen the construction joint between the backwall and wingwall, and maintain integrity of the abutment. During earthquake events, the backwall-wingwall connections help resist out-of-plane bending response of the abutment backwall, in conjunction with the backwall-to-pile-cap connections at the wall bottom, which was introduced in Section 4.3.1. In return, the backwall-wingwall connections will be subjected to shear demands from the superstructure-abutment interactions. The shear force-deformation relation of each pair of steel dowel bars was estimated using an analytical model proposed by Vintzeleou and Tassios (1986). Calibrated by full-scale experimental results, the analytical model was proposed for predicting the shear force-deformation behavior of steel dowel bars embedded in concrete when subjected to interface shear. The idealized shear force-deformation relation of one pair of steel dowel bars is shown in Figure 4.11. In the abutment model shown in Figure 4.2, a nonlinear

spring was used to simulate each pair of dowel bars connecting the backwall and wingwall, labeled as component No.6. The shear force-deformation relation shown in Figure 4.11 was assigned to each nonlinear spring.

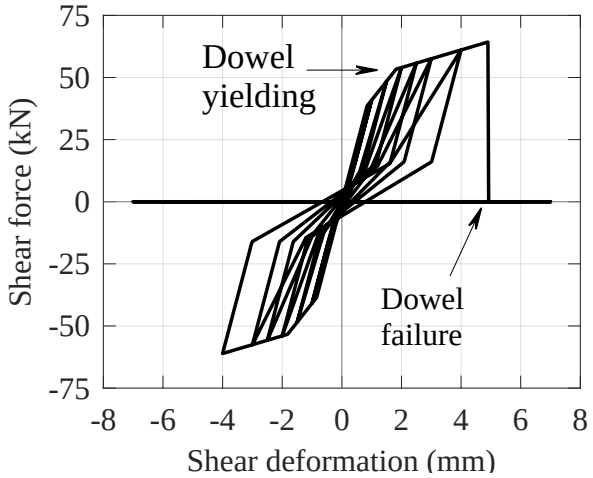

Figure 4.11: Idealized shear force-deformation relation of one pair of steel dowel bars connecting the abutment backwall and wingwall (Vintzeleou and Tassios 1986)

4.5 Backfill Passive Resistance Model

When the bridge is subjected to seismic demands, sufficiently large superstructure displacement in the longitudinal direction can cause close of the expansion joint and engagement between the superstructure and abutment backwall. In this situation, the backwall is pushed against the backfill and embankment soil by the superstructure. As a result, passive resistance from the backfill and embankment soil is mobilized and acts as a major resistance to the displacement of the abutment and superstructure, in addition to the resistance of abutment foundation.

The force-displacement relation of the passive soil resistance behind the backwall was determined using an experimentally validated model proposed by Shamsabadi et al. (2005, 2007). This model was developed on the basis of the limit-equilibrium logarithmic-spiral surface, method of slices, and hyperbolic stress-strain behavior of soils (Terzaghi et al. 1996; Shields and Tolunay 1973). As claimed by Shamsabadi et al. (2005, 2007), the passive force-displacement response of cohesive and cohesionless backfill soils predicted by this model is in good agreement with small- and full-scale experimental test results.

For the prototype bridges, as shown in Figures 4.1 and 4.12, a nearly isosceles right triangular region of porous granular material is placed adjacent to the abutment backwall and pile cap. Figure 4.12 illustrates a typical logarithmic-spiral soil failure surface in passive conditions (Terzaghi et al. 1996). Stewart et al. (2007) and Bozorgzadeh et al. (2008) performed large-scale experimental tests on passive response of bridge abutment backfill and found that the length of the passive soil failure wedge, labeled as L_{wedge} in Figure 4.12, was usually greater than twice the height of the soil wedge, H_{wedge} labeled in Figure 4.12. For the prototype bridge abutment, this wedge shape means that the soil failure surface tends to develop in the embankment soil outside the porous granular material, as shown in Figure 4.12. The embankment soil was assumed to be compacted clean sand, as compaction of road embankment soil is required by the Standard Specifications for Road and Bridge Construction of IDOT (2012b). The soil properties listed in Table 4.2 (Rollins et al. 2010a; Shamsabadi et al. 2007) for compacted clean sand were used in determining the backwall passive resistance.

In addition to the soil properties, the other critical factor for determining backfill passive resistance is the backwall and pile cap height. The backwall height, labeled as H_{w} in Figure 4.12, is the

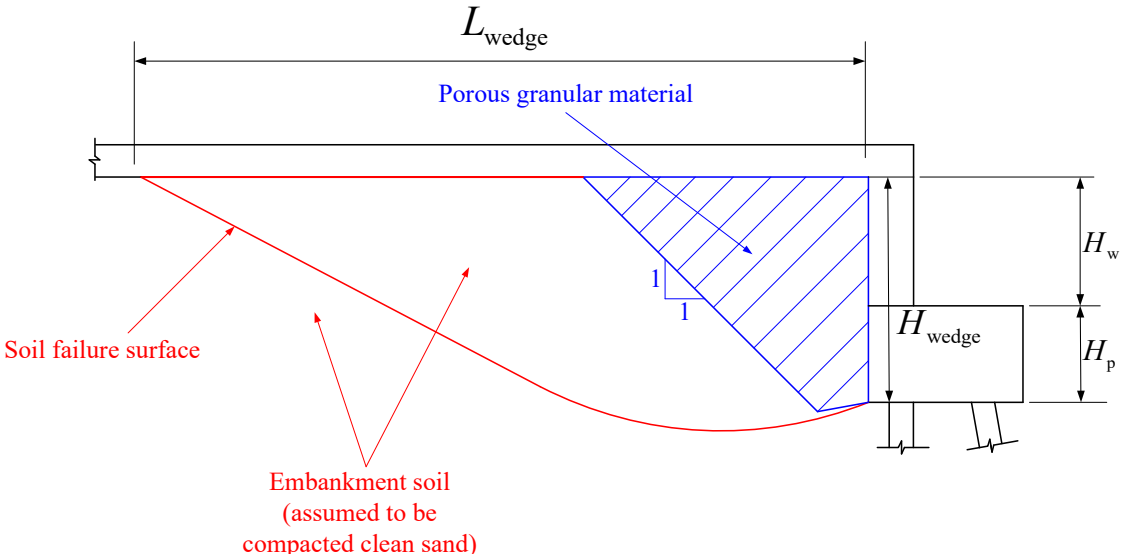

Figure 4.12: Logarithmic-spiral soil failure surface in passive conditions (Terzaghi et al. 1996)

Table 4.2: Soil properties for determining backfill passive resistance (Rollins et al. 2010a; Shamsabadi et al. 2007)

Assumed backfill soil	Unit weight γ [kN/m^3]	Angle of internal friction φ'(°)	Cohesion intercept c [kPa]	Angle of wall friction δ (°)	Poisson's ratio v	Strain at 50% strength ε_{50}	Failure ratio R_f
Compacted clean sand	16.5	37.3	0	25	0.3	0.0035	0.97

summation of the girder depth and bearing height, and varies in different major bridge types. The abutment pile cap height, labeled as H_p in Figure 4.12, remains the same for bridges of different major types. Table 4.3 summarizes H_w and H_p for the four major bridge types. The summation of H_w and H_p was regarded as the height of the passive soil wedge, H_{wedge}, for computing the backfill passive resistance.

Table 4.3: Height of abutment backwall and pile cap defined in Figures 4.1 and 4.12

Major bridge type	3S	4S	3C	4C
Backwall height H_w [m (ft)]	1.14 (3.75)	1.81 (5.94)	1.42 (4.66)	1.91 (6.27)
Pile cap height H_p [m (ft)]	1.07 (3.5)	1.07 (3.5)	1.07 (3.5)	1.07 (3.5)
Total height $H_w + H_p$ [m (ft)]	2.21 (7.25)	2.88 (9.44)	2.49 (8.16)	2.98 (9.77)

For the non-skew prototype bridges, the computed force P versus backwall top displacement D of backfill passive resistance is shown in Figure 4.13. The ascending branch of the backbone curves exhibits a hyperbolic shape and is flattened after the ultimate passive capacity is reached. The unloading/reloading response was assumed to be linear based on the experimental results of Stewart et al. (2007). The force-displacement relation, $P(D)$, shown in Figure 4.13 was then distributed to the backwall and pile cap based on a triangular soil pressure distribution and a trapezoidal one (Terzaghi et al. 1996), as schematically shown in Figure 4.14. The resistance on the backwall, P_{BW}, and that on the pile cap, P_{PC}, were further distributed into a number of nonlinear springs in the abutment model, on the basis of tributary backwall width of each spring. These springs were located at the centroids of the triangle and trapezoid shown in Figure 4.14. The springs for P_{BW} and P_{PC} are labeled as components No. 2 and 3 in Figure 4.2.

As shown in Figure 4.15, the backfill passive resistance normal to the backwall of a skew abutment, P_{skew}, was computed using the backfill resistance P of a counterpart non-skew abutment with the same width W_a. Marsh (2013) investigated backfill passive resistance of skew abutments through large-scale experimental tests, and proposed the following equations

$$P_{skew} = R(\theta)P \tag{4.2}$$

$$R(\theta) = 8 \times 10^{-5}\theta^2 - 0.0181\theta + 1 \tag{4.3}$$

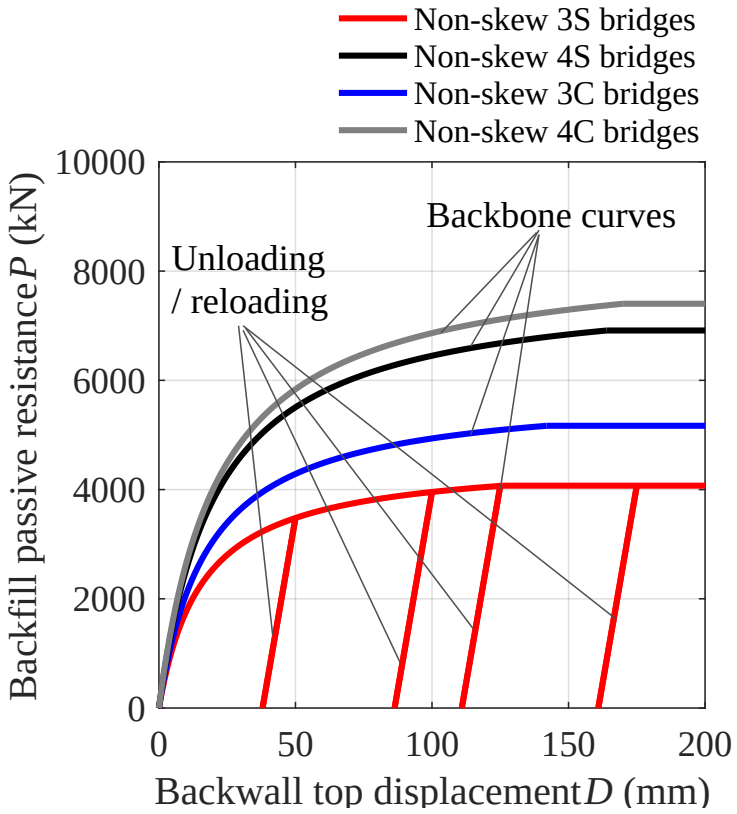

Figure 4.13: Passive resistance of abutment backfill of non-skew prototype bridges

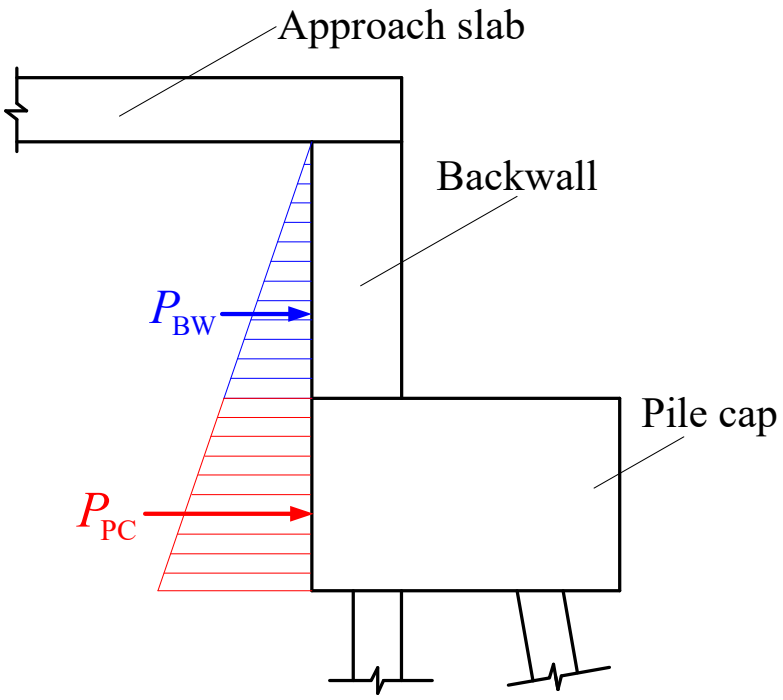

Backfill passive resistance on backwall P_{BW}

Backfill passive resistance on pile cap P_{PC}

Total backfill passive resistance $P = P_{PC} + P_{BW}$

Figure 4.14: Distribution of backfill passive resistance between backwall and pile cap

where P_{skew} and P are the ultimate passive resistance of skew and non-skew abutments, and θ is the bridge skew angle in degree. The R factor defined in Equation (4.3) is plotted in Figure 4.16. It can be seen that the R factor of skew bridges is always smaller than unity, which means that the ultimate backfill passive resistance of a skew abutment is smaller than that of the counterpart non-skew abutment. For the prototype skew bridges, the passive resistance P of non-skew bridges shown in Figure 4.13 was multiplied by the R factor defined in Equation 4.3. Additionally, in the finite-element model of skew abutments, the nonlinear springs for backfill passive resistance (components No. 2 and 3 in Figure 4.2) were oriented normal to the abutment backwall and pile cap.

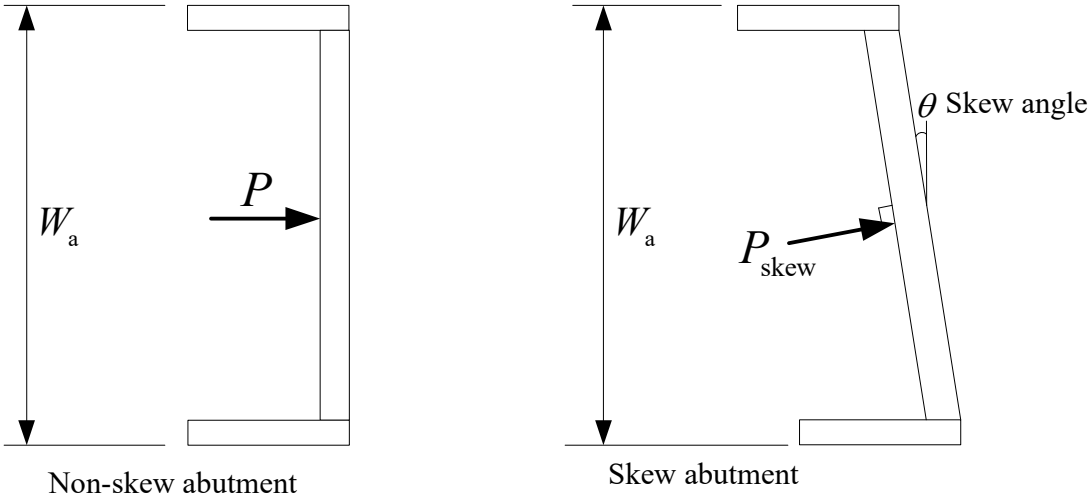

Figure 4.15: Backfill passive resistance of non-skew and skew abutments

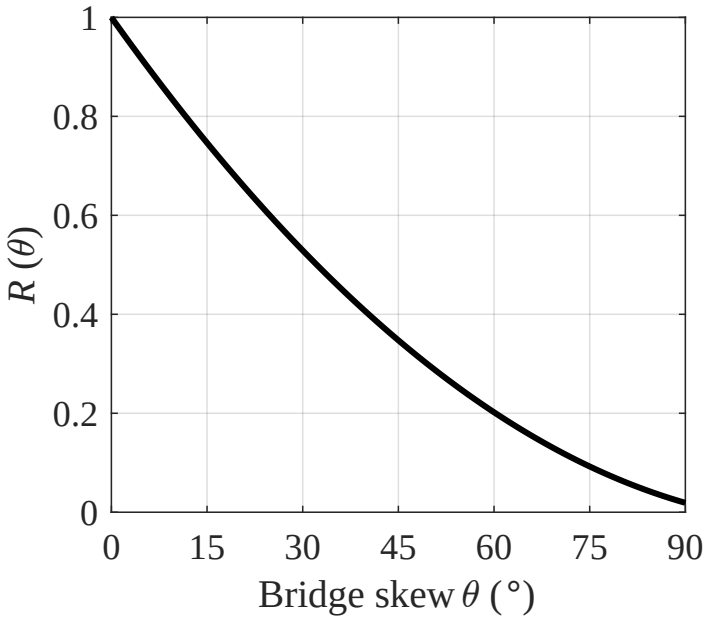

Figure 4.16: Reduction factor *R* for backfill passive resistance of skew abutments (Marsh 2013)

4.6 Wingwall Model

The backfill/embankment passive resistance applied to the abutment wingwalls was modeled using the same approach as that applied to the backwall. The nonlinear springs for passive soil resistance on wingwalls are labeled as component No. 4 in the abutment model shown in Figure 4.2. For many bridge embankments in Illinois, the top width of the embankment is close to the abutment width and there is not sufficient soil outside the two wingwalls for developing a passive soil failure wedge. Thus, the passive resistance from the soil enclosed by the abutment was considered, but that from the soil outside the wingwalls was neglected. This means that the nonlinear springs for passive soil resistance to wingwalls, labeled as component No. 4 in Figure 4.2, can only subjected to compression.

4.7 Approach Slab Model

As shown in Figure 4.1, a concrete approach slab is connected to the top of abutment backwall. In the prototype bridges, the length of the approach slab is typically 9.14 m (30 ft), the width is 12.19

m (40 ft), and the thickness is 0.38 m (1.25 ft). The weight of an approach slab is around 1,000 kN (225 kips). In order not to neglect this large amount of mass in the bridge seismic analysis, the approach slab was included in the abutment model. As shown in Figure 4.2, the slab body is modeled using a grid of elastic beam elements. The total slab mass was distributed into a number of nodal masses lumped to the boundary nodes of the beam elements.

4.8 Global Validation of Bridge Model

So far, large-scale shake-table tests on the seismic performance of full quasi-isolated bridges have not been conducted. A global validation of the finite-element bridge model could only be available after large- to full-scale shake-table tests are performed on quasi-isolated bridges. Although large-scale shake-table tests on other types of highway bridges have been very sparsely reported in the literature (e.g. Cruz-Noguez and Saiidi 2010), these test results cannot provide a reliable and comprehensive validation of the quasi-isolated bridge model, due to the inherent differences between the different types of bridges.

Alternatively, seismic response data collected from field-instrumented quasi-isolated bridges during real earthquakes would also be used for global validation of the quasi-isolated bridge model. However, such data have not been collected in the current stage. Although seismic response data have been collected for a few instrumented bridges during historical earthquakes (e.g. Zhang and Makris 2002), the ability of these data to validate the quasi-isolated bridge model is very limited, due to the inherent differences between the instrumented bridges and quasi-isolated bridges.

Although a global model validation is not available in the current state due to the lack of shake-table and field test data on quasi-isolated bridges, numerical models of many of the critical bridge components have been validated either by the author or the developer of the component models that were employed in the global bridge model, as introduced in Chapters 3 and 4.

CHAPTER 5

STATIC PUSHOVER AND MODAL ANALYSES OF PROTOTYPE QUASI-ISOLATED BRIDGES

In this chapter, static pushover analyses were performed on a number of prototype quasi-isolated bridges in the longitudinal and transverse directions, for the purpose of investigating bridge response characteristics including lateral force distribution among substructures, sequence of component limit states, fusing of sacrificial superstructure-substructure connections, and vulnerability of critical components. A multi-mode adaptive pushover procedure that is a variant of the algorithms proposed by Antoniou and Pinho (2004) and Abbasnia et al. (2013) was employed to overcome limitations of the conventional pushover procedure, by means of taking into account the varying bridge stiffness and modal properties and also the contribution of multiple vibration modes. In each pushover analysis, multiple eigenvalue modal analyses were conducted at different bridge deformation states and the instantaneous periods and mode shapes were recorded. These modal responses were also studied in order to provide insight into modal response characteristics of the prototype quasi-isolated bridges.

Historically, nonlinear static pushover procedures have been employed to estimate dynamic response of structures, in order to avoid running the computationally expensive nonlinear dynamic time-history analysis. A representative of such procedures is the Capacity Spectrum Method (Freeman 1978). It compares the structural capacity curve obtained from a static pushover analysis with the seismic response spectrum that represents the seismic demand on the structure and estimates the peak structural displacement response through such a comparison. As indicated by Gencturk and Elnashai (2008), although the Capacity Spectrum Method was widely used due to its ability to estimate structural dynamic response with relatively low computational cost, it has many inherent limitations such as non-convergence issues, incomparability between capacity and demand diagrams, and high overestimation of displacement demand. In this dissertation, since the much more accurate and reliable nonlinear dynamic time-history analyses were extensively per-

formed, the nonlinear static analysis was not used to estimate the dynamic response of the bridges. The static analysis results in the dissertation are mainly used to provide insight into the bridge response characteristics under lateral loads. Besides the prototype quasi-isolated bridges in this study, the pushover procedure outlined in this chapter can be also employed in other quasi-isolated bridges and even some bridges with different seismic-resistant strategies to investigate the limit state hierarchy and damage sequence under lateral loads.

5.1 Multi-Mode Adaptive Pushover Procedure

In the conventional pushover analysis procedure, a predefined force pattern is applied to the structural model. Since the pushover analysis is typically utilized as an alternative to dynamic time history analysis, the predefined force pattern is typically determined based on the predominant mode shape in the elastic structural state. Then, at each step of the analysis, the amplitudes of all the individual forces applied to different locations of the structure are scaled by a same load factor. The load factor is determined for achieving a equilibrium between the externally applied forces and the internal resistance of the deformed structure. Although the force amplitude may be adjusted stepwise by the load factor, the force pattern is an invariant during the entire analysis. In other words, the direction of each individual force and the amplitude ratio between different forces remain unchanged in the analysis. The analysis is terminated when the controlled location has displaced to a predefined displacement target.

Although the conventional pushover procedure is sufficient for analyzing linear elastic structural models whose response is typically dominated by a few invariant modes, its applicability to nonlinear inelastic structural models can be limited (Lawson et al. 1994; Krawinkler and Seneviratna 1998). As the structural model experiences inelastic deformation, damage, and failure, the structure is globally softened and its periods and mode shapes can vary significantly due to the stiffness degradation and component failure. In this situation, the initial force pattern determined in accordance with the initial elastic state may not be appropriate anymore for capturing the varied stiffness and modal properties and, eventually, may result in an unrealistically deformed structural shape that is largely different from that occurs in the dynamic analysis. Additionally, for many

civil engineering structures, multiple structural modes may possess close modal contributions and, thus, these modes should be taken into account when determining the pushover force pattern. In view of these limitations of the conventional procedure, a variety of advanced pushover procedures have been proposed by researchers (Bracci et al. 1997; Gupta and Kunnath 2000; Elnashai 2001; Chopra and Goel 2002; Antoniou and Pinho 2004; Abbasnia et al. 2013), which, at least, conceptually and theoretically overcome such limitations of the conventional procedure.

As introduced in Chapters 3 and 4, the bridge models in this study incorporate highly nonlinear components, and its global stiffness may experience significant changes due to responses such as closure and reopening of the expansion joints, fusing of the sacrificial superstructure-substructure connections, as well as yielding of the pier columns and foundation piles. For such highly nonlinear models, a modified multi-mode adaptive pushover procedure that is a variant of the algorithms proposed by Antoniou and Pinho (2004) and Abbasnia et al. (2013) was employed. The major steps of the procedure are shown in Figure 5.1. A computer program for the procedure was developed in *OpenSees* and *MATLAB* environment.

In Steps 1 and 2, the finite-element bridge model is created and a load-controlled gravity analysis is conducted in *OpenSees*, during which gravity forces are gradually applied to the bridge components in proportion to their nodal masses. The full gravity load is kept unchanged during the subsequent pushover analysis.

In Step 3, the displacement of the centroid of the bridge superstructure is controlled and a displacement increment for this controlled location at each analysis step is selected and denoted as Δd. In the pushover analyses discussed in this chapter, $\Delta d = 1$ mm is selected as the step size, which is small enough to capture detailed structural responses during the analysis.

In Step 4, an eigenvalue analysis is performed in *OpenSees* on the basis of the instantaneous tangential stiffness properties of the full bridge model. Equation (5.1) defines the generalized eigenvalue problem

$$\left[\mathbf{K}^{(i)} - \mathbf{K}_G^{(i)}\right]\mathbf{\Phi}^{(i)} = \mathbf{M}\mathbf{\Phi}^{(i)}\mathbf{\Omega}^{(i)} \tag{5.1}$$

where $\mathbf{K}^{(i)}$ is the tangential global stiffness matrix , $\mathbf{K}_G^{(i)}$ is the geometric stiffness matrix, $\mathbf{\Phi}^{(i)}$ is the mode shape matrix, $\mathbf{\Omega}^{(i)}$ is a diagonal matrix containing the frequencies of different modes, and $\mathbf{M}$ is the mass matrix of the bridge model. Except the invariant mass matrix $\mathbf{M}$, all of these quantities

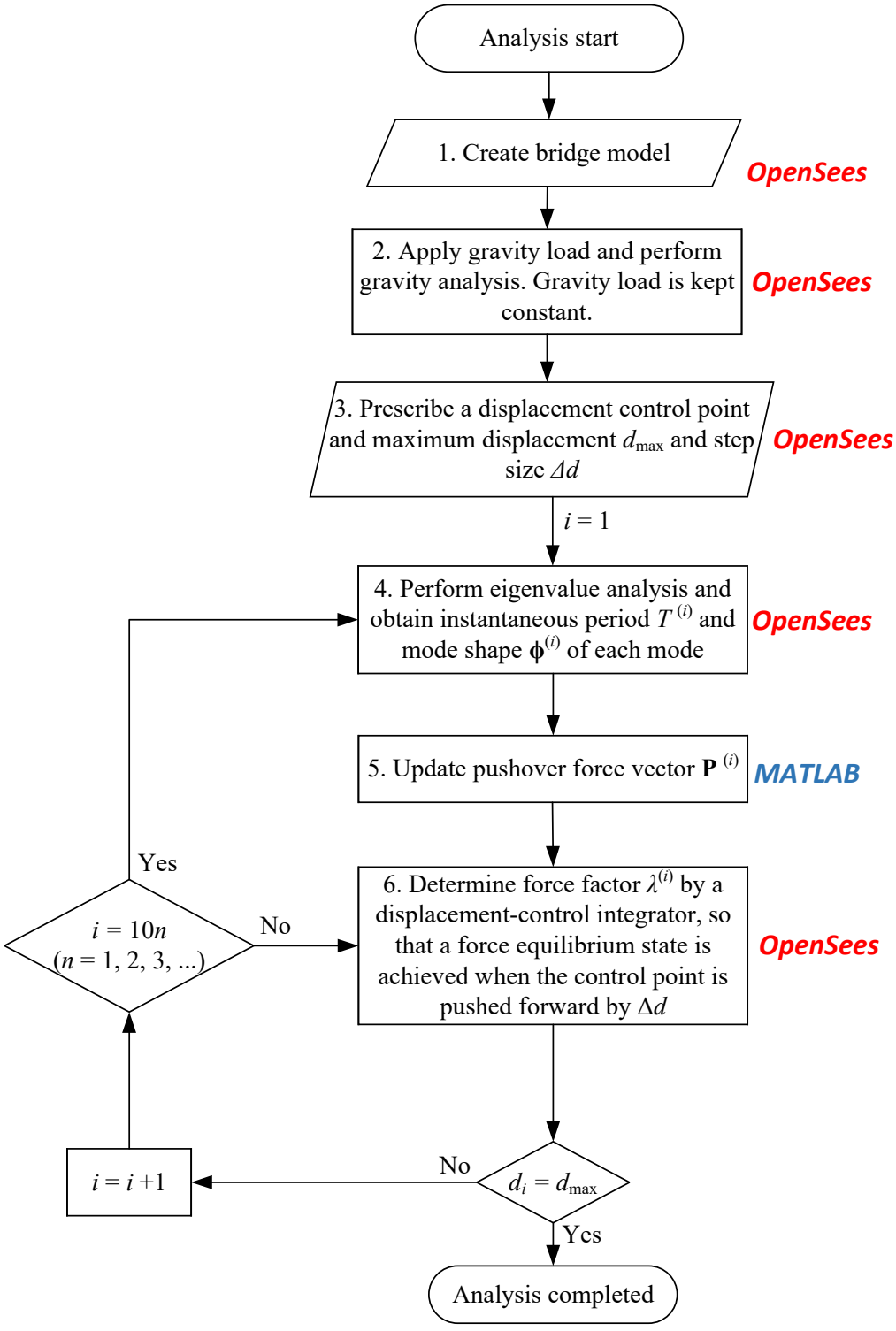

Figure 5.1: Flowchart of the employed multi-mode adaptive static analysis procedure (Antoniou and Pinho 2004; Abbasnia et al. 2013)

are evaluated at the i-th analysis step, as indicated by the superscript (i).

Step 5 is the critical step of the entire procedure and it is conducted in *MATLAB*. After finishing the eigenvalue analysis in Step 4, the instantaneous mode shapes ($\boldsymbol{\phi}_1^{(i)}, \boldsymbol{\phi}_2^{(i)}, \boldsymbol{\phi}_3^{(i)}, \ldots$) at the i-th analysis step are obtained. Subsequently, the instantaneous modal mass participation factor (Clough and Penzien 1975) of the r-th mode in the pushover direction (either the longitudinal or transverse direction) is determined as

$$\Gamma_r^{(i)} = \frac{\boldsymbol{\phi}_r^{(i),T}\mathbf{M}\boldsymbol{\gamma}}{\boldsymbol{\phi}_r^{(i),T}\mathbf{M}\boldsymbol{\phi}_r^{(i)}} \tag{5.2}$$

where $\boldsymbol{\phi}_r^{(i)}$ is the mass-normalized mode shape vector of the r-th mode at the i-th analysis step. $\boldsymbol{\gamma}$ is the invariant load distribution vector for horizontal earthquake ground motions. In addition to the modal participation factor, the instantaneous effective modal mass ratio (ATC 1996) of the r-th mode is defined as follows

$$\alpha_{\mathbf{M},r}^{(i)} = \frac{\left[\boldsymbol{\phi}_r^{(i),T}\mathbf{M}\boldsymbol{\gamma}\right]^2}{\left[\boldsymbol{\phi}_r^{(i),T}\mathbf{M}\boldsymbol{\phi}_r^{(i)}\right] M_{\text{Total}}} \tag{5.3}$$

where M_{Total} is the total mass of the bridge model. The effective modal mass ratio is a unitless scalar and the summation of the ratios of all the modes equals to one. It is employed to evaluate the modal contribution of different modes to the bridge response. In this chapter, "the predominant mode" refers to the mode with the largest effective modal mass ratio.

At the same analysis step, the modal force vector of the r-th mode applied to the bridge model is determined as

$$\mathbf{f}_r^{(i)} = \Gamma_r^{(i)}\,\mathbf{M}\boldsymbol{\phi}_r^{(i)}\,S_a\left(\zeta_r^{(i)}, T_r^{(i)}\right) \tag{5.4}$$

where $S_a\left(\zeta_r^{(i)}, T_r^{(i)}\right)$ is the pseudo-spectral acceleration of selected site-specific ground motions to which the bridge is expected to be subjected, evaluated on the basis of the instantaneous period $T_r^{(i)}$ and damping ratio $\zeta_r^{(i)}$ of the r-th mode. This term is introduced to the pushover force pattern for taking into account the spectral amplification effect of site-specific ground motions (Mwafy and Elnashai 2000). The suite of ground motions in this study will be introduced in Section 1 of Chapter 6.

Subsequently, the modal force vectors of multiple modes are combined after weighted by their

respective effective modal mass ratios, as shown in Equation (5.5)

$$\mathbf{F}^{(i)} = \sum_{r=1}^{n} \left[\alpha_{\mathbf{M},r}^{(i)} \mathbf{f}_r^{(i)} \right] = \sum_{r=1}^{n} \left[\alpha_{\mathbf{M},r}^{(i)} \Gamma_r^{(i)} \, \mathbf{M}\boldsymbol{\phi}_r^{(i)} \, S_a\left(\zeta_r^{(i)}, T_r^{(i)}\right) \right] \tag{5.5}$$

where $\mathbf{F}^{(i)}$ is the force pattern vector at the i-th step of the analysis and n is the total number of modes considered. For the bridge variants in this study, the effective modal mass of the first 20 modes is typically sufficient to incorporate, at least, the bridge superstructure mass that is over 50% of the total mass of the bridge system.

When the force pattern vector $\mathbf{F}^{(i)}$ is obtained, the pushover force vector $\mathbf{P}^{(i)}$ applied to the bridge model at the i-th step is determined using a modified version of the incremental updating technique proposed by Antoniou and Pinho (2004), as shown in Equation (5.6).

$$\mathbf{P}^{(i)} = \mathbf{P}^{(i-s)} + \left[\lambda^{(i-1)} - \lambda^{(i-1-s)} \right] \mathbf{F}^{(i)} \tag{5.6}$$

where $\mathbf{P}^{(i-s)}$ is the pushover force vector for the $(i-s)$-th step, $\lambda^{(i-1)}$ and $\lambda^{(i-1-s)}$ are the force factors at the $(i-1)$-th and $(i-1-s)$-th steps, respectively; and s is the number of steps for each force updating. Since the selected pushover step size, 1 mm, is quite small, the bridge structure is not likely to experience significant changes of stiffness and modal properties at each pushover step with such a small displacement increment. Considering the large computational cost of eigenvalue analysis and force updating on the detailed 3-D bridge model, the frequency for the eigenvalue analysis and force updating is reduced from every step to every 10 steps (every 10-mm deck center displacement) in this study. In other words, the same force pattern vector $\mathbf{P}^{(i)}$ is used from the (i)-th to the $(i+9)$-th steps and, then, it is updated at the $(i+10)$-th step. Through trial analyses, it was found that more frequent force updating (smaller s) did not significantly affect the pushover results. Thus, in order to reduce the computational cost to an affordable amount, $s = 10$ is used in this study.

In Step 6 of Figure 5.1, after updating the pushover force vector $\mathbf{P}^{(i)}$ at the i-th step, the displacement-controlled integrator of the pushover analysis iterates on the force factor $\lambda^{(i)}$ until a force equilibrium state is achieved between the external pushover forces, $\lambda^{(i)}\mathbf{P}^{(i)}$, and the internal forces of the deformed bridge after the controlled location of the bridge is pushed forward by a displacement

increment Δd (Δd = 1 mm in this study). These steps will continue until the displacement at the controlled location reaches the predefined $d_{\max}$.

The multi-mode adaptive procedure is employed to perform pushover analyses on the prototype bridges. For each basic bridge type, pushover analyses were performed on a number of representative variants, in both the longitudinal and transverse directions.

5.2 Identification of Component Limit State Occurrence

For each pushover or dynamic analysis, the time series or envelope values of various structural responses were recorded into output data files. In the pushover analysis, the displacement of the controlled location is regarded as the pseudo-time, which is equivalent to the time in the dynamic analysis. The data files were post-processed to identify the occurrence of a variety of component fusing and damaging limit states that are listed in Table 5.1. In addition to the pushover analyses in this chapter, these limit states are also the focus of the nonlinear dynamic time-history analyses that will be discussed in Chapter 6. The fusing limit states are generally preferred for the quasi-isolation bridge system, such as rupture of steel fixed bearing anchors and sliding of elastomeric bearings. The unacceptable damaging limit states, namely unseating of bearings at substructures, are very likely to cause extensive damage to bridge superstructures and even span loss. Therefore, it is intended to be eliminated by calibrating the quasi-isolation design methodology. The other damaging limit states, such as yielding of reinforcing steel and crushing of concrete cover at pier columns, as well as yielding of piles, are accepted as long as the extent of damage is not severe enough to cause global bridge failure. The criteria for identifying the occurrence of these limit states from the recorded structural response data are explained as follows

Closure of expansion joint (CEJ)

As introduced in Chapter 4, at a bridge abutment, the response characteristics of the expansion joint is distributed into a number of nonlinear springs along the width of the backwall. As long as one of the springs experiences compressive deformation that exceeds the joint opening width at a certain time step during an analysis, closure of this expansion joint is identified in this analysis.

Mobilization of backfill ultimate capacity (MBU)

Table 5.1: Fusing and damaging limit states of critical bridge components

	Limit states	Abbreviation	Category
Abutments (A1 and A2)	Closure of expansion joint	CEJ@A1 and/or A2	Preferred
	Mobilization of backfill ultimate capacity	MBU@A1 and/or A2	Damaging, acceptable
	Failure of backwall-to-pile-cap connection	FBP@A1 and/or A2	Fusing, acceptable
	Rupture of retainer anchor	RRA@A1 and/or A2	Fusing, preferred
	Sliding of elastomeric bearing	SEB@A1 and/or A2	Fusing, preferred
	Unseating of elastomeric bearing at acute deck corner	UBA@A1 and/or A2	Damaging, unacceptable
	Unseating of elastomeric bearing at obtuse deck corner	UBO@A1 and/or A2	Damaging, unacceptable
	Yielding of pile supporting wingwall	YPW@A1 and/or A2	Damaging, acceptable
	Yielding of pile supporting backwall	YPB@A1 and/or A2	Damaging, acceptable
Expansion piers (P1 and P3)	Rupture of retainer anchor	RRA@P1 and/or P3	Fusing, preferred
	Sliding of elastomeric bearing	SEB@P1 and/or P3	Fusing, preferred
	Unseating of elastomeric bearing	UEB@P1 and/or P3	Damaging, unacceptable
	Yielding of vertical reinforcing steel at column base	YRS@P1 and/or P3	Damaging, acceptable
	Crushing of concrete cover at column base	CCC@P1 and/or P3	Damaging, acceptable
	Yielding of pile at pier	YPP@P1 and/or P3	Damaging, acceptable
Fixed pier (P2)	Rupture of retainer anchor (only for 3C and 4C bridges)	RRA@P2	Fusing, preferred
	Rupture of steel dowel connection (only for 3C and 4C bridges)	RSD@P2	Fusing, preferred
	Rupture of steel fixed bearing anchor (only for 3S and 4S bridges)	RFA@P2	Fusing, preferred
	Unseating of steel fixed bearing	USB@P2	Damaging, unacceptable
	Yielding of vertical reinforcing steel at column base	YRS@P2	Damaging, acceptable
	Crushing of concrete cover at column base	CCC@P2	Damaging, acceptable
	Yielding of pile at pier	YPP@P2	Damaging, acceptable

As introduced in Chapter 4, at a bridge abutment, the overall passive resistance of the backfill soil is distributed into a number of uni-axial compression-only nonlinear springs along the width of the backwall. At any time step during an analysis, if the summation of the spring forces exceeds 95% of the backfill ultimate capacity, mobilization of backfill ultimate capacity at this abutment is identified.

Failure of backwall-pile cap connection (FBP)

As introduced in Chapter 4, the backwall-pile-cap connection at a bridge abutment is distributed into a number of rotational springs along the width of the backwall. At any time step during an analysis, if the rotation of all the springs exceeds the ultimate rotational capacity of the connection, failure of this backwall-pile-cap connection is identified.

Rupture of retainer anchor (RRA)

As introduced in Chapter 3, retainer anchor rupture is explicitly simulated by the component model. The maximum shear deformation (absolute value) of each pair of retainer anchors at an abutment or a pier is recorded in the analysis. By observing the analysis results, it was found that in most analyses, the maximum deformation and fusing state of different pairs of retainer anchors are similar to each other. In other words, if one pair of retainer anchors was ruptured during an analysis, the other retainer anchors at the same substructure typically were also ruptured in this analysis, because there is little difference in the superstructure transverse displacements at different girder locations on a substructure. Therefore, the maximum deformations of these pairs of anchors are averaged into a single deformation value. If this averaged deformation value exceeds the ultimate shear deformation of a retainer anchor, retainer anchor rupture at this substructure is identified.

Sliding of elastomeric bearing (SEB)

As introduced in Chapter 3, the computational bearing model accounts for both the shear deformation and sliding behaviors of the elastomer. At any time step during an analysis, if the instantaneous shear deformation of an elastomer exceeds its shear deformation limit in either the longitudinal or transverse bridge axis, sliding of this bearing occurs. If any of the several bearings at an abutment or a pier slides, sliding of elastomeric bearings at this substructure is identified.

Unseating of elastomeric bearing at acute or obtuse corner of deck end (UBA@A1 and/or A2, UBO@A1 and/or A2)

In this study, bearing unseating is not explicitly simulated in analysis, but is identified by comparing the maximum bearing sliding distance with the minimum seat width at substructures. Figure 5.2 schematically illustrates the critical sliding direction and distance of the elastomeric bearing supporting the acute and obtuse deck corners of a skew bridge, which can potentially result in unseating of the bearing from the abutment pile cap. The minimum seat width for a 1000-year seismic event, in inches, is designated as N and calculated using Equation (5.7) (IDOT 2012a)

$$N = 3.94 + 0.0204L + 0.084H + 1.087\sqrt{H\left[1 + \left(\frac{2B}{L}\right)^2\right]}\frac{1 + 1.25F_vS_1}{\cos\alpha} \tag{5.7}$$

where

L = Typically the length between expansion joints (ft)

H = Height of tallest substructure unit between expansion joints, including units at the joints (ft)

B = Out-to-out width of superstructure (ft)

α = skew angle (°)

F_vS_1 = One second period spectral response coefficient modified for site class

B/L = Not to be taken greater than 3/8.

According to the IDOT Bridge Manual (IDOT 2012a), N is measured along the beam from the edges of piers or abutments to the end of the beam in the longitudinal direction; in the transverse direction, N is measured from the edges of piers or abutments to the centerline of the fascia beam. The calculated minimum seat width N at the substructures of different basic bridge types is listed in Table 5.2.

Table 5.2: Minimum required seat width N at substructures of prototype bridges (units: mm)

	3S bridges	3C bridges	4S bridges	4C bridges
4.57-m columns	772 / cos α	772 / cos α	1085 / cos α	1085 / cos α
12.19-m columns	996 / cos α	996 / cos α	1303 / cos α	1303 / cos α

α is the skew angle, measured as the acute angle between a line perpendicular to the bridge longitudinal axis and the pier centerline

As illustrated in Figure 5.2, using the seat width N, skew angle α, as well as the width W_e and length L_e of the bearing elastomer, the sliding limit in the abutment-parallel and abutment-normal directions, designates as d_p and d_n, can be calculated using Equations (5.8) and (5.9).

For the acute deck corner shown in Figure 5.2(a),

$$d_p = N\cos\alpha + \left(d_e - \frac{W_e}{2}\right)\sin\alpha - \frac{L_e}{2}\cos\alpha \tag{5.8a}$$

$$d_n = \cos\alpha\left(N - d_e - \frac{W_e}{2}\right) - \frac{L_e}{2}\sin\alpha \tag{5.8b}$$

For the obtuse deck corner shown in Figure 5.2(b),

$$d_p = N\cos\alpha - \left(d_e + \frac{W_e}{2}\right)\sin\alpha - \frac{L_e}{2}\cos\alpha \tag{5.9a}$$

$$d_n = \cos\alpha\left(N - d_e - \frac{W_e}{2}\right) - \frac{L_e}{2}\sin\alpha \tag{5.9b}$$

Finally, d_p and d_n are compared with maximum bearing sliding distances in the corresponding directions recorded in the analysis. If the maximum sliding distance exceeds d_p or d_n, bearing unseating is identified.

Yielding of pile supporting wingwall (YPW)

As introduced in Chapter 4, each single pile in the bridge model is discretized into a number of nonlinear beam-column elements along its length. For each beam-column element of a single pile, the peak normal strain (absolute value) at the four exterior flange corners of the H-shape section at the uppermost integration point is recorded. Then, the maximum of these peak strains of all the elements is regarded as the "maximum pile strain". Since there are two piles supporting the two pieces of wingwall at an abutment, the maximum pile strains of these two piles are averaged. If this averaged maximum pile strain exceeds the yield strain of the pile material (A572 Gr. 50 steel), 0.0017, occurrence of this limit state is identified.

Yielding of pile supporting backwall (YPB)

Similar to the last limit state, the maximum pile strains of the several piles supporting the backwall at an abutment are averaged and if this averaged maximum pile strain exceeds the yield strain

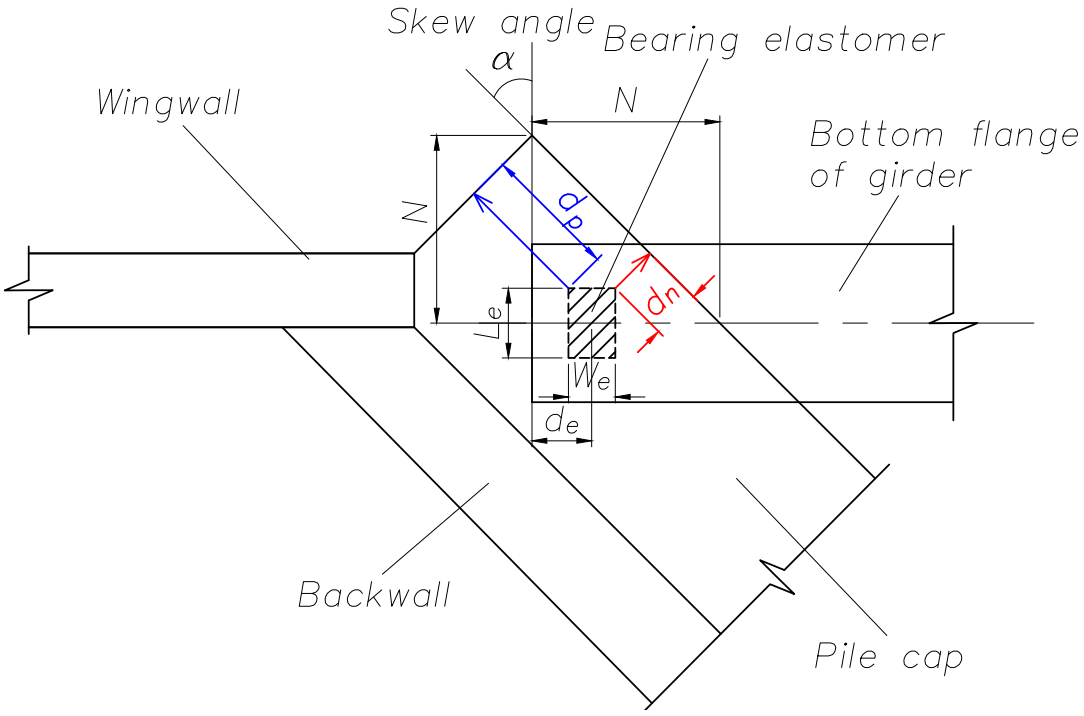

(a) Unseating of elastomeric bearing at acute deck corner

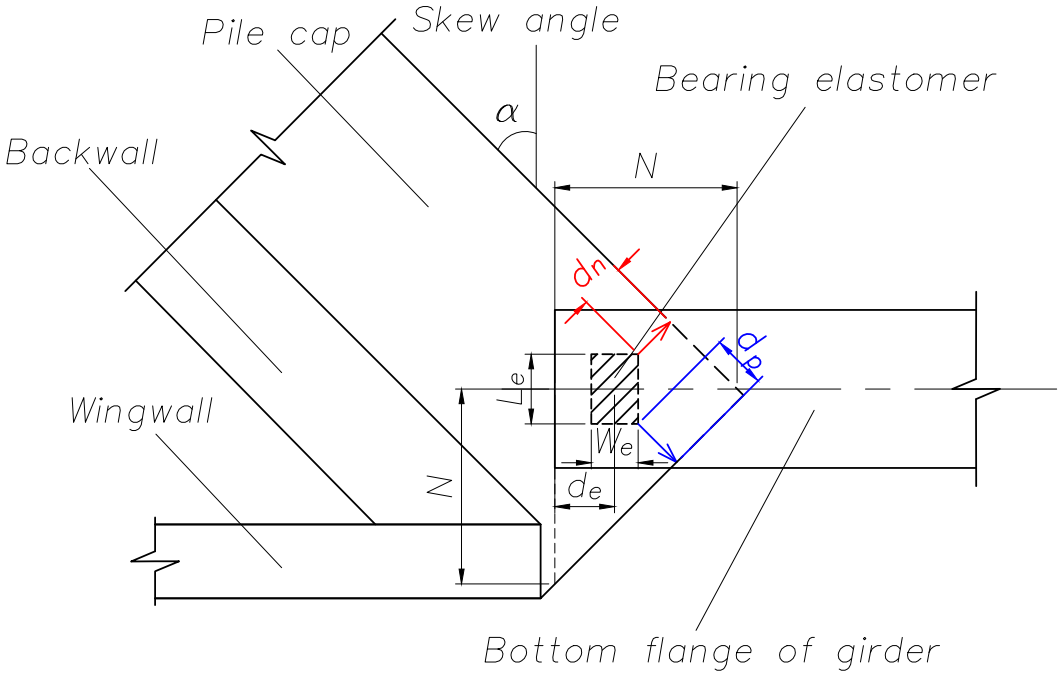

(b) Unseating of elastomeric bearing at obtuse deck corner

Figure 5.2: Unseating of elastomeric bearings at deck corners: (a) acute deck corner; (b) obtuse deck corner

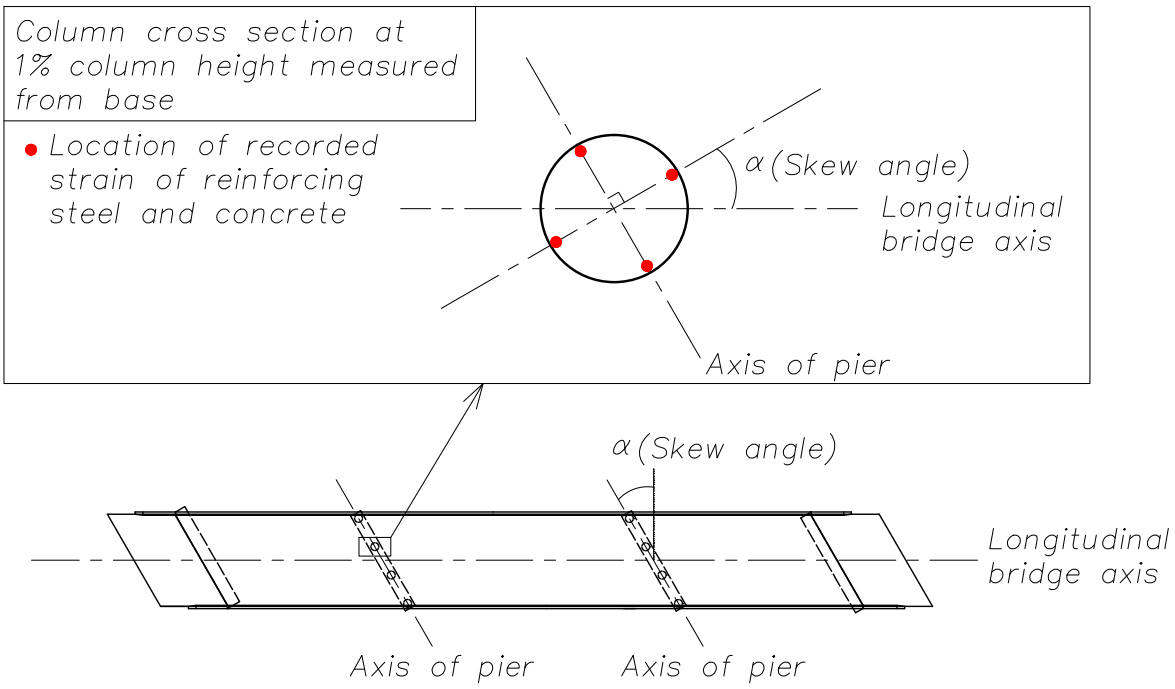

Figure 5.3: Monitored locations for strain of reinforcing steel and concrete cover at each column base

of the pile material (A572 Gr. 50 steel), 0.0017, occurrence of this limit state is identified.

Unseating of elastomeric bearing (UEB@P1 and/or P3)

Unseating of the two exterior elastomeric bearings at the expansion pier is identified using the same approach as that at the abutment, with the same minimum required seat width N indicated in Table 5.2. The dimensions (length and width) of the bearing elastomer at the expansion pier are used instead of those of the elastomer at the abutment.

Yielding of vertical reinforcing steel at column base (YRS)

As introduced in Chapter 4, each pier column in the bridge model was discretized into a number of nonlinear beam-column elements along its length and each element has three integration points. For the bottommost element of each column at a pier, the peak tensile strains of the reinforcing steel were monitored at four locations along the perimeter of the circular column section at the bottommost integration point (about 1% column height measured from the base), as illustrated in Figure 5.3. If the maximum peak tensile strain of all the monitored locations at a pier exceeds the yield strain of the reinforcing steel, this limit state is identified.

Crushing of concrete cover at column base (CCC)

The identification of this limit state is similar to that of YRS, except that the peak compressive strain of concrete was recorded at the four locations of a column base illustrated in Figure 5.3, instead of the tension strain of reinforcing steel.

Yielding of pile at pier (YPP)

The identification of this limit state is similar to YPW and YPB, except that the piles at an intermediate pier are the focus.

Rupture of steel dowel connection (RSD)

The identification of this limit state is similar to RRA, except that the steel dowel bars are the focus.

Rupture of steel fixed bearing anchor (RFA)

The identification of this limit state is similar to RRA, except that the anchors of the steel fixed bearings are the focus.

Unseating of steel fixed bearings (USB@P2)

Unseating of the two exterior steel fixed bearings at the fixed pier after failure of their anchors is identified using the same approach as that at the abutment, with the same minimum required seat width N indicated in Table 5.2. The dimensions (length and width) of the steel fixed bearing at the fixed pier are used instead of those of the elastomer at the abutment. Shear deformation of elastomer is not considered for the steel fixed bearings.

5.3 Pushover Analysis Results

5.3.1 Three-span steel-plate-girder (3S) bridges

3S00P15H Bridge

Figures 5.4a and 5.4b illustrate the longitudinal and transverse pushover responses of 3S00P15H bridge variant, respectively. In these two and the following figures illustrating pushover responses of different bridge variants, the resisting force from each substructure and their summation are plotted against the deck center displacement that is regarded as the pseudo time of pushover analyses. Additionally, the damaging and fusing limit states occurred in the analysis are labeled on the

curves and their abbreviations are arranged in order of occurrence in the figure legend, indicating the sequence of fusing and damaging limit states.

In the longitudinal analysis shown in Figure 5.4a, closure of the expansion joint in the pushing direction (CEJ@A2) substantially increased the lateral stiffness of the bridge system, as the abutment that was pushed by the superstructure (Abutment 2) started to provide large resistance to the displaced superstructure after the joint closure. Before the joint closure, the fixed pier (Pier 2) sustained the majority of the pushover force, but Abutment 2 took over the major resisting substructure after the joint closure. The piles of Abutment 2 yielded (YPW & YPB@A2) shortly after closure of the expansion joint. At the fixed pier, yielding of the reinforcing steel (YRS@P2) and crushing of the concrete cover (CCC@P2) at the column bottom preceded fusing of the steel fixed bearings (RFA@P2), which did not occur after pushing the superstructure for 200 mm. The two pier damaging limit states resulted in global yielding of Pier 2, indicated by the flat curve with a nearly zero slope. This sequence of damage is undesired by the quasi-isolation design strategy, as the substructure sustained extensive damage and global yielding before the fusing of its sacrificial connections. Due to the effect of isolation provided by the elastomeric bearings, Abutment 1 and the expansion pier (Pier 1) experienced much smaller forces than the other substructures. Figure 5.5f depicts the deformed bridge shape at the state of 150-mm deck center displacement shown in Figure 5.4a. Deflection of the piles at Abutment 2 can be clearly observed. Additionally, the columns of Pier 2 sustained larger deflection than that of the columns of Pier 1, due to the high stiffness of the unfused steel fixed bearings.

In the transverse analysis shown in Figure 5.4b, the first fusing limit state encountered is the rupture of transverse bearing retainer anchors at Abutment 1 (RRA@A1). Subsequently, the bearing retainers at the expansion pier (Pier 1) and the steel fixed bearings at the fixed pier (Pier 2) were also fused (RRA@P1 & RFA@P2). After each of these fusing limit states, the force demand on the corresponding substructure was reduced, which is intended by the quasi-isolation design strategy. The two piers experienced larger forces than did the abutments, which is opposite to the distribution of substructure forces in the longitudinal analysis shown in Figure 5.4a. Figure 5.6 depicts the deformed bridge shape at the end of the response shown in Figure 5.4b. Due to the early fusing of retainers at Abutment 1, the superstructure rotated about the fixed pier and experienced the largest transverse displacement at Abutment 1.

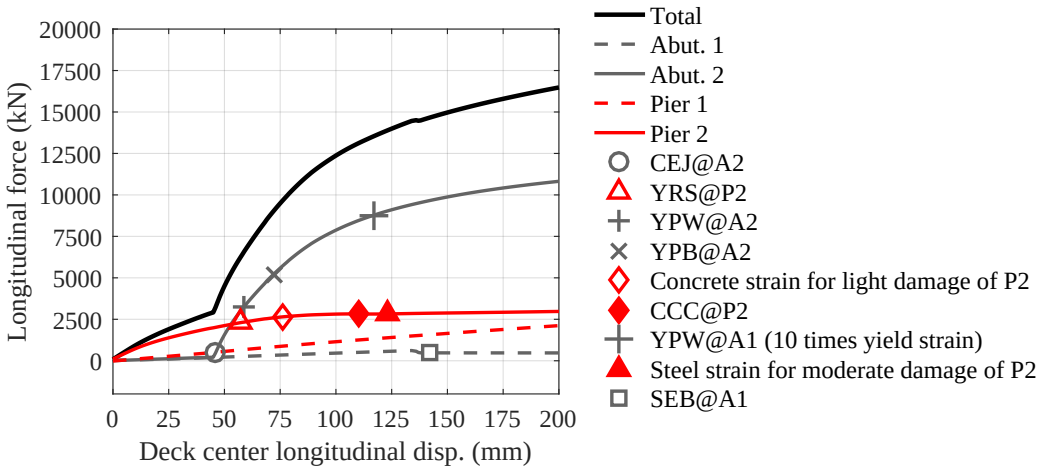

(a) Longitudinal analysis

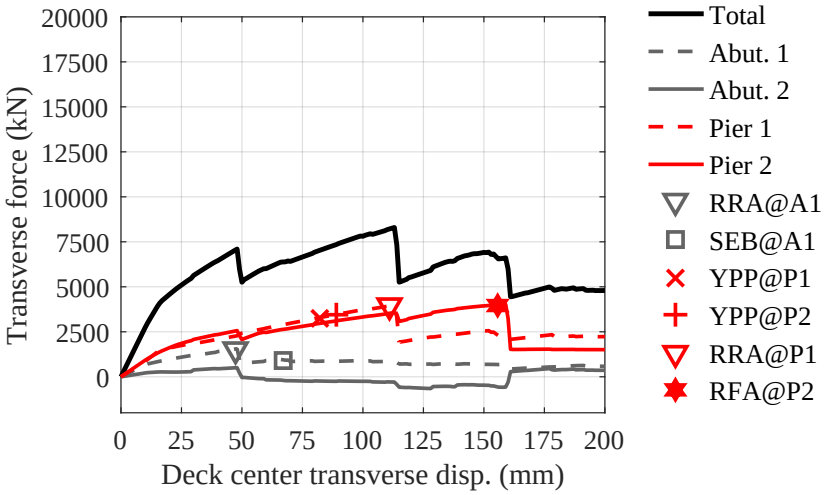

(b) Transverse analysis

Figure 5.4: Pushover response of 3S00P15H bridge variant: (a). longitudinal analysis; (b). transverse analysis

As introduced in Section 5.1, the adaptive pushover algorithm was employed in order for the bridge to deform in accordance with its instantaneous modal properties. This is achieved through performing multiple eigenvalue analyses through out the pushover analysis and updating the force pattern on the basis of the instantaneous modal properties. To demonstrate this procedure, Figure 5.5 compares the predominant mode shape, pushover force pattern, and deformed bridge shape at two different bridge deformation states in the analysis shown in Figure 5.4a, namely the states of 20-mm and 150-mm deck center displacements.

Figure 5.5a depicts the predominant mode shape at the state of 20-mm deck center displacement. At this state, the expansion joint at Abutment 2 was not closed and in the predominant mode shape, the response concentrates on the superstructure and pier columns, but not on Abutment 2. Because of the high stiffness of the unfused steel fixed bearings at Pier 2, the Pier 2 columns deflect much more than those of Pier 1.

Figure 5.5c depicts the pushover force pattern at the state of 20-mm deck center displacement. In this figure, the bridge deformation is utilized to visualize the force pattern. In order to make a clear comparison between the predominant mode shape and pushover force pattern, the amplification effect of nodal masses on the force pattern is excluded from Figure 5.5c. The depicted force pattern is expressed by Equation (5.10), which is derived from Equation (5.5) by excluding the mass matrix $\mathbf{M}$.

$$\mathbf{F}'^{(i)} = \sum_{r=1}^{n} \left[\alpha_{\mathbf{M},r}^{(i)} \Gamma_r^{(i)} \boldsymbol{\phi}_r^{(i)} S_a \left(\zeta_r^{(i)}, T_r^{(i)} \right) \right] \tag{5.10}$$

The bridge locations with large deformations are subjected to large components of the force pattern defined in Equation 5.10, and vice versa. Due to the adaptiveness of the pushover procedure, the force pattern at this state is consistent with the predominant mode shape shown in Figure 5.5a and, thus, the forces were concentrated on the superstructure while little force was applied to Abutment 2, as shown in Figure 5.5c.

Figure 5.5e depicts the deformed bridge shape. It can be seen that except the vertical deck deflection due to the gravity load, the laterally deformed shape is quite consistent with the predominant mode shape at the same state, which is intended by this adaptive pushover procedure.

Figure 5.5b depicts the predominant mode shape at the state of 150-mm deck center displacement. At this state, the expansion joint at Abutment 2 was already closed and in the predominant

(a) The predominant mode shape (20-mm deck center disp.)

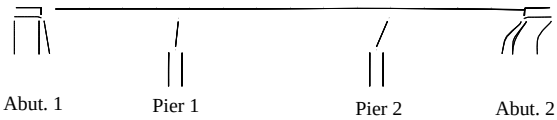

(b) The predominant mode shape (150-mm deck center disp.)

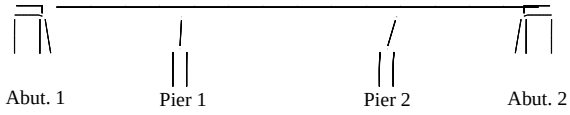

(c) Pushover force pattern (20-mm deck center disp.)

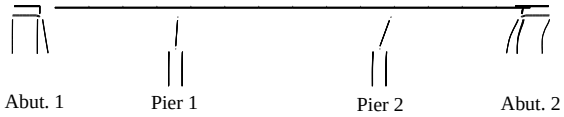

(d) Pushover force pattern (150-mm deck center disp.)

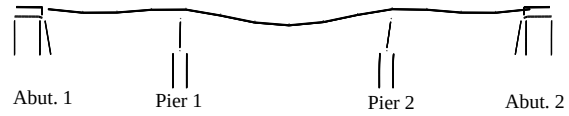

(e) Deformed shape (20-mm deck center disp.; magnified by 60 times)

(f) Deformed shape (150-mm deck center disp.; magnified by 20 times)

Figure 5.5: Mode shape, pushover force pattern, and deformed shape of 3S00P15H bridge in the longitudinal pushover analysis shown in Figure 5.4a

mode shape, the response concentrates on the superstructure, pier columns, and also Abutment 2.

Figure 5.5d depicts the pushover force pattern at the state of 150-mm deck center displacement. The force pattern was adaptively evolved on the basis of the most shape shown in Figure 5.5b, and, in this new pattern, forces have been applied to Abutment 2, which is different from the force pattern shown in Figure 5.5c. The consistency between the deformed bridge shape shown in Figure 5.5f and the mode shape shown in Figure 5.5b demonstrates again that the adaptive algorithm can effectively capture the varying modal properties of the bridge and enable the bridge to deform accordingly.

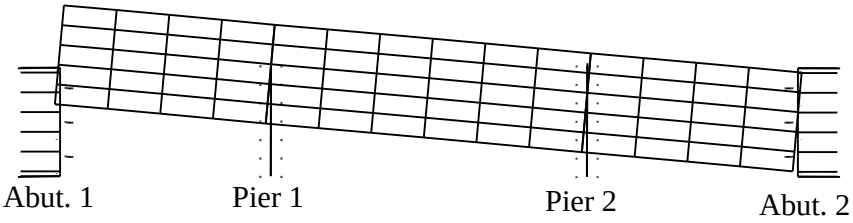

Figure 5.6: Deformed shape of 3S00P15H bridge in the transverse pushover analysis (200-mm deck center disp.; magnified by 20 times)

3S45P15H Bridge

Figure 5.7a illustrates the longitudinal pushover response of 3S45P15H bridge, which is representative of skew 3S bridges. A major difference of the longitudinal pushover response between the skew and non-skew bridges shown in Figures 5.4a and 5.7a is that the skew abutment pushed by the superstructure provided much smaller longitudinal force than the non-skew abutment. This observation is consistent with the finding reported by Bignell et al. (2005), who conducted nonlinear pushover analyses on wall pier supported highway bridges in Illinois and indicated that the longitudinal ultimate load capacity was significantly reduced when skew was introduced to the bridge. The other major difference is that the skew bridge (3S45P15H) sustained coupled longitudinal and transverse displacements at the deck end supported by Abutment 2 and resulted in rupture of transverse bearing retainer anchors at Abutment 2.

Reconnaissance of the 1971 San Fernando earthquake and the 2010 Chile earthquake indicates that skew bridges experienced in-plane deck rotation and their acute deck corners tended to drop off the abutment under strong earthquake ground motions (Priestley et al. 1996; Kawashima et al. 2011; Mitchell et al. 2013). This observed behavior of skew bridges is generally consistent with the pushover response in this study. For instance, Figure 5.8c depicts the deformed shape of the 3S45P15H bridge at the end of the response shown in Figure 5.7a. As highlighted, the deck end at Abutment 2 experienced coupled longitudinal and transverse displacements and the acute deck corner tended to drop off Abutment 2; a clockwise rotation of the entire deck can be observed in the figure. In addition, Figure 5.8d shows the trace of the right deck end center in the pushover analysis. Before the expansion joint is closed, the deck end basically translates in the longitudinal direction. However, after the joint is closed, the right deck end experienced coupled longitudinal

and transverse displacement and tended to drop off the abutment at the acute deck corner, which is consistent with the deformed shape shown in Figure 5.8c. Additionally, Figures 5.8a and 5.8a show the shape of the predominant mode in the longitudinal direction and the distribution of pushover forces at the end of the analysis. The deformed bridge shape and the distribution of pushover forces is quite close to the shape of the predominant mode at the same bridge state, which means the bridge was properly pushed in the analysis in accordance with its modal properties.

It has been concluded that the oblique impact between the skew deck end and abutment after closure of the expansion joint is a major cause of the rotational response of the bridge superstructure (Maragakis and Jennings 1987; Kawashima et al. 2011; Dimitrakopoulos 2011). Figure 5.9 shows a schematic of the in-plane deck rotation of a skew bridge during a longitudinal pushover analysis. As the right deck end engages with Abutment 2 after closure of the expansion joint, the oblique abutment resistance to the deck end results in an in-plane moment on the bridge superstructure and the superstructure tends to rotate clockwise under this moment.

In the transverse bridge response shown in Figure 5.7b, fusing of the steel fixed bearings at Pier 2 (RFA@P2) and the bearing retainers at the two abutments (RRA@A1 & A2) occurred at almost the same deck center displacement. Fusing of the bearing retainers at Pier 1 (RRA@P1) occurred at a much larger deck displacement. The deformed shape with a 200-mm deck center displacement is depicted in Figure 5.10. The deck sustained in-plane rotation in the clockwise direction. The acute deck corner at Abutment 1 experienced a large abutment-normal displacement and tended to drop off the abutment. This response characteristic is also consistent with the large displacements at the acute deck corners of skew bridges observed in the aforementioned post-earthquake reconnaissance.

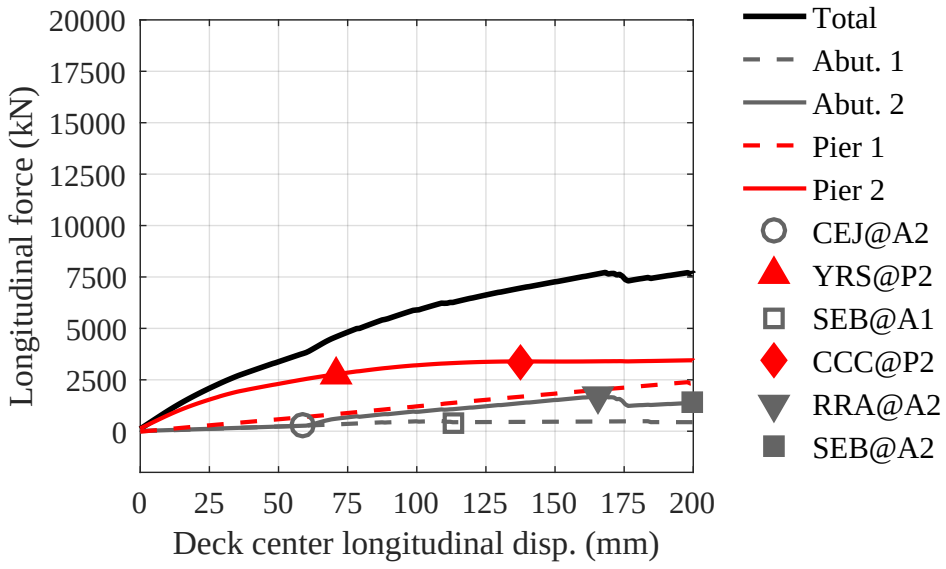

(a) Longitudinal analysis

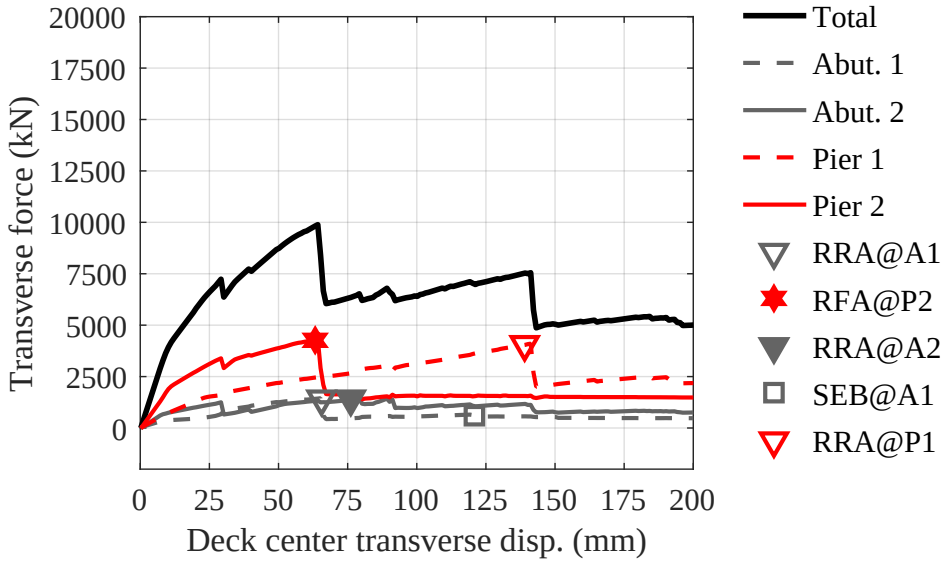

(b) Transverse analysis

Figure 5.7: Pushover response of 3S45P15H bridge variant: (a). longitudinal analysis; (b). transverse analysis

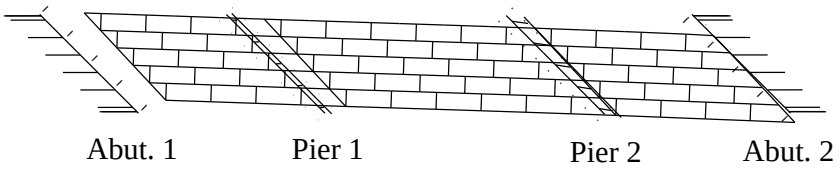

(a) The predominant mode shape (Mode 1)

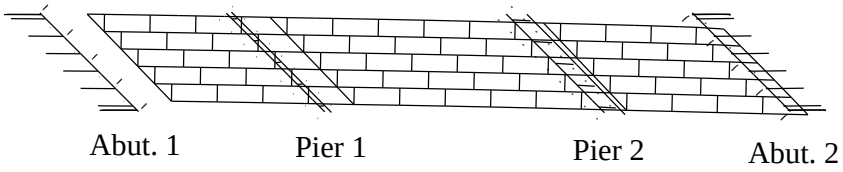

(b) Pushover force pattern

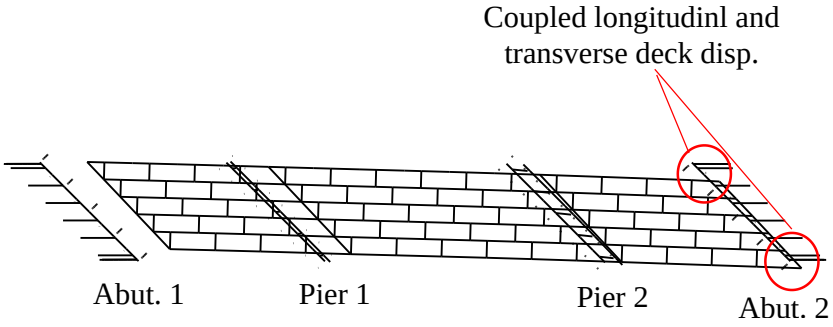

(c) Deformed shape (magnified by 20 times)

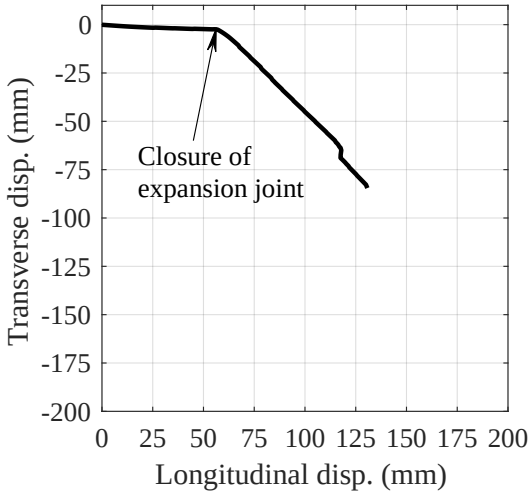

(d) Trace of right deck end center in the longitudinal analysis shown in Figure 5.7a

Figure 5.8: Mode shape, pushover force pattern, deformed shape, and deck end trace of 3S45P15H bridge in the longitudinal pushover analysis (the first three items are at the end of the analysis)

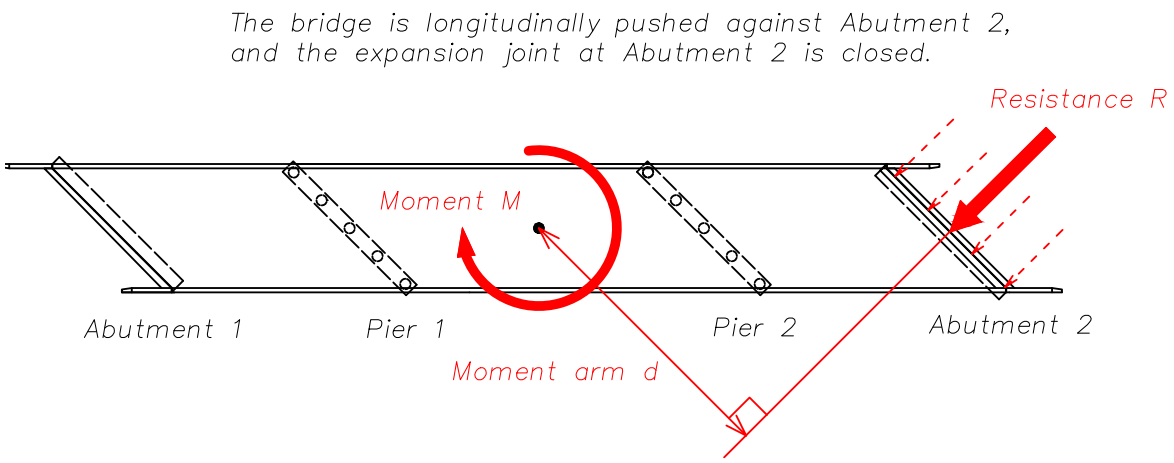

Figure 5.9: In-plane deck rotation of skew bridges due to superstructure-abutment interaction

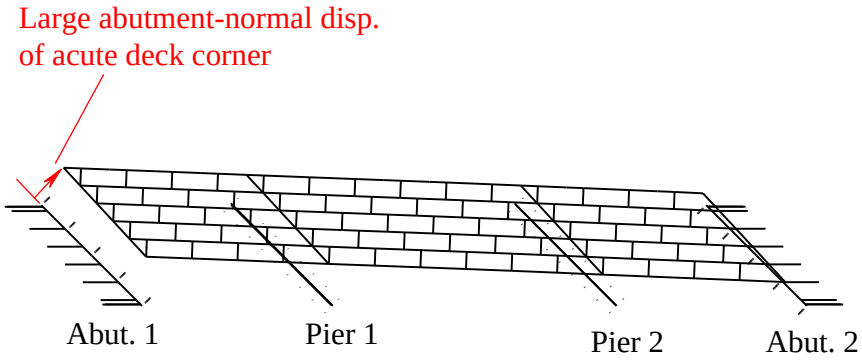

Figure 5.10: Deformed shape of 3S45P15H bridge variant in transverse pushover analysis (200-mm deck center disp.; magnified by 20 times)

3S00P40H Bridge

Figures 5.11a and 5.11b illustrate the longitudinal and transverse pushover responses of 3S00P40H bridge variant, respectively.

The general longitudinal response is similar to that of the short-pier equivalent bridge (3S00P15H bridge). The major difference lies in the force of the two intermediate piers. The tall expansion and fixed piers sustained much lower longitudinal forces than the short piers at the same deck displacement. This difference is expected as the tall pier has much lower lateral stiffness than the short ones. Although the columns of the high pier have a little larger diameter (1.22 m) than those of the short pier (1.07 m), the much larger column clear height (12.2 m v.s. 4.6 m) outweighs the slightly larger diameter and results in much lower lateral stiffness of the tall piers. Additionally, the lateral forces sustained by the expansion and fixed piers are quite close, which is different from the response of the short-pier 3S00P15H bridge. The deformed bridge shape at the end of the analysis is shown in Figure 5.12a. It can be seen that the two piers also sustained similar lateral deflection. A potential explanation to the similar behavior of the two piers is that the lateral stiffness of the bearing-column assembly is analogous to that of two springs in series. If the two springs significantly differ in stiffness, the total stiffness is quite close to the smaller component stiffness. In the tall-pier bridge, the total stiffness of either the six elastomeric bearings or the six steel fixed ones is much larger than that of the four pier columns. Thus, the expansion and fixed piers exhibit similar lateral stiffness that is close to the total stiffness of the four pier columns.

In the transverse analysis, different from the response of 3S00P15H bridge, the tall-pier bridge did not experience fusing of the steel fixed bearings at Pier 2 (RFA@P2) or the retainer anchors at Pier 1 (RRA@P1). This is directly influenced by the tall pier columns. Fusing of the sacrificial connections prefers a laterally stiff and strong substructure that is capable of providing sufficient reaction for rupturing the anchors without experiencing large displacement or even yielding itself. On the contrary, if a substructure is very flexible, it may not be able to provide the reaction for rupturing the anchors on its top without experiencing large displacements or yielding itself. The unfused bearing retainers and steel fixed bearings resulted in increasing force demands on Piers 1 and 2, and eventually caused yielding of the reinforcing steel at the pier column bases (YRS@P1 & P2). The deformed bridge shape at the end of the analysis is shown in Figure 5.12b. The transverse superstructure displacement at Abutment 1 and deflection of pier columns can be observed.

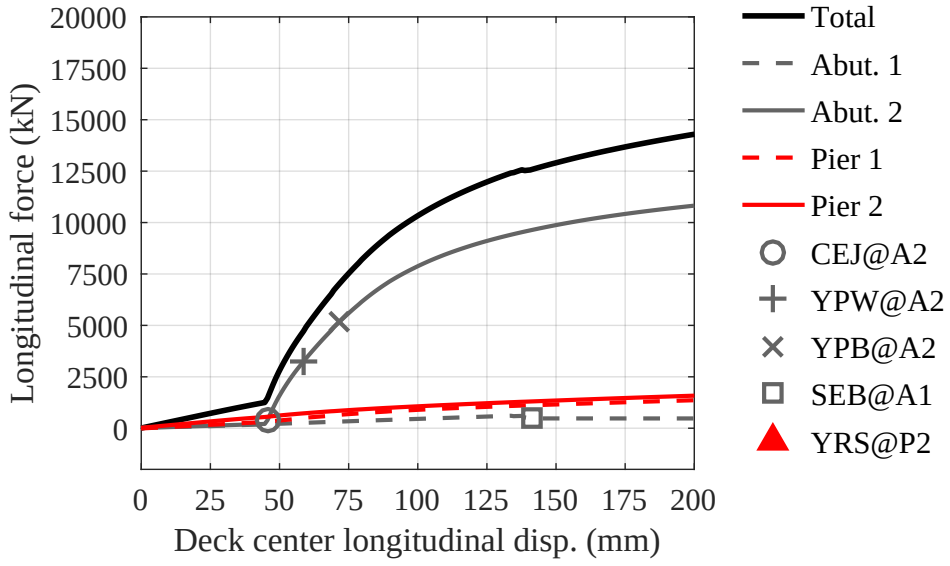

(a) Longitudinal analysis

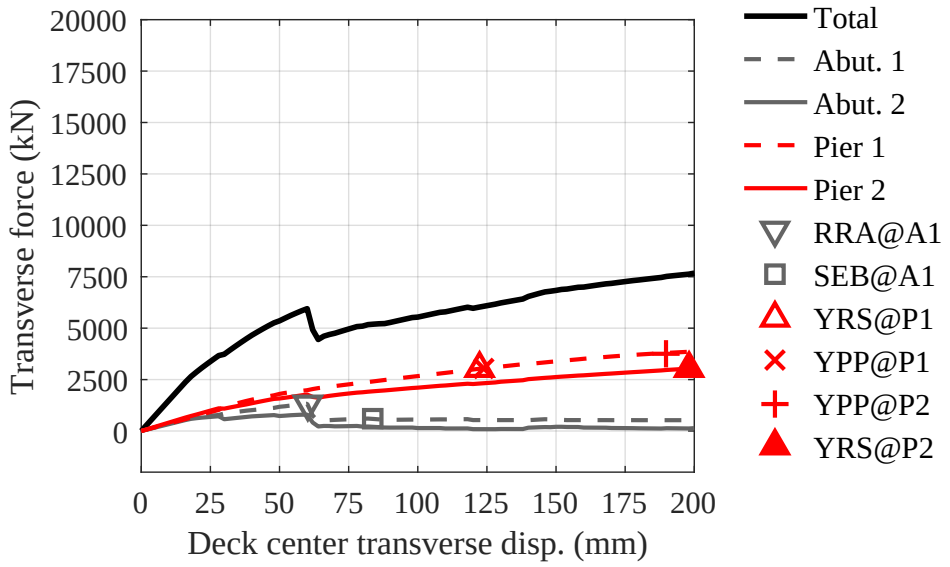

(b) Transverse analysis

Figure 5.11: Pushover response of 3S00P40H bridge variant: (a). longitudinal analysis; (b). transverse analysis

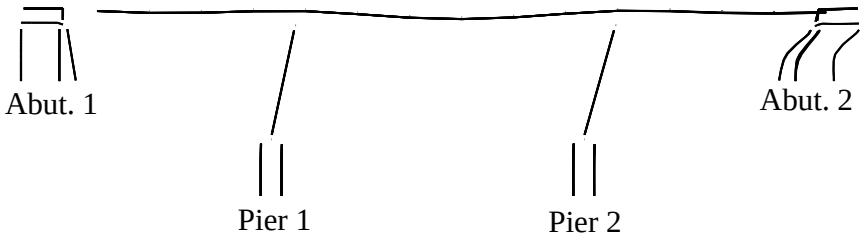

(a) Deformed shape of 3S00P40H bridge in longitudinal pushover analysis (deformation corresponds to the response state with a 200-mm deck center displacement in Figure 5.11a and is magnified by 20 times)

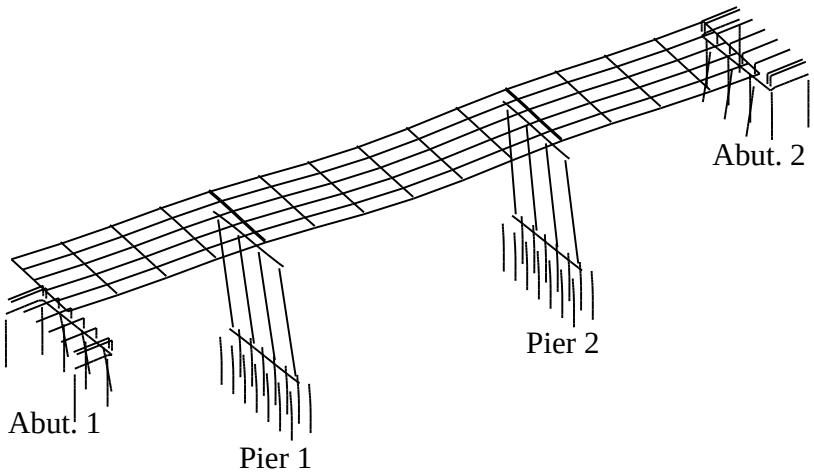

(b) Deformed shape of 3S00P40H bridge in transverse pushover analysis (deformation corresponds to the response state with a 200-mm deck center displacement in Figure 5.11b and is magnified by 20 times)

Figure 5.12: Deformed shape of 3S00P40H bridge in pushover analyses

3S00P15S Bridge

The foundation soil condition was found to have an important influence on the fusing performance of sacrificial connections. For instance, Figure 5.13b illustrates the transverse pushover response of 3S00P15S bridge, which is a soft-soil equivalent of the 3S00P15H bridge. Comparison between the response of these two bridges shown in Figures 5.4b and 5.13b indicates that a larger superstructure displacement is required to fuse the retainer anchors at Abutment 1 (RRA@A1) in the presence of the soft foundation soil and rupture of the steel fixed bearing anchors (RFA@P2) did not occur in the presence of the soft soil. Similar to the response of the tall-pier 3S00P40H bridge, the soft foundation soil reduces the lateral stiffness of substructures and necessitates larger bridge displacements to fuse the connections. Due to the lower soil stiffness, the pier piles in the soft soil yielded (YPP@P1 & P2) at a smaller superstructure displacement than in the case with the hard soil. Yielding of abutment piles (YPW and YPB@A1) occurred in the presence of the soft soil but not in the case with the stiff soil. The deformed bridge shape at the end of the transverse analysis is shown in Figure 5.14. The transverse displacement of the superstructure at Abutment 1 and deflection of the pier piles can be observed, which are consistent with the response shown in Figure 5.13b.

Comparison between Figures 5.4a and 5.13a demonstrates that due to the lower soil stiffness, the soft foundation soil resulted in smaller substructure forces and total force than the hard soil at the same deck displacement.

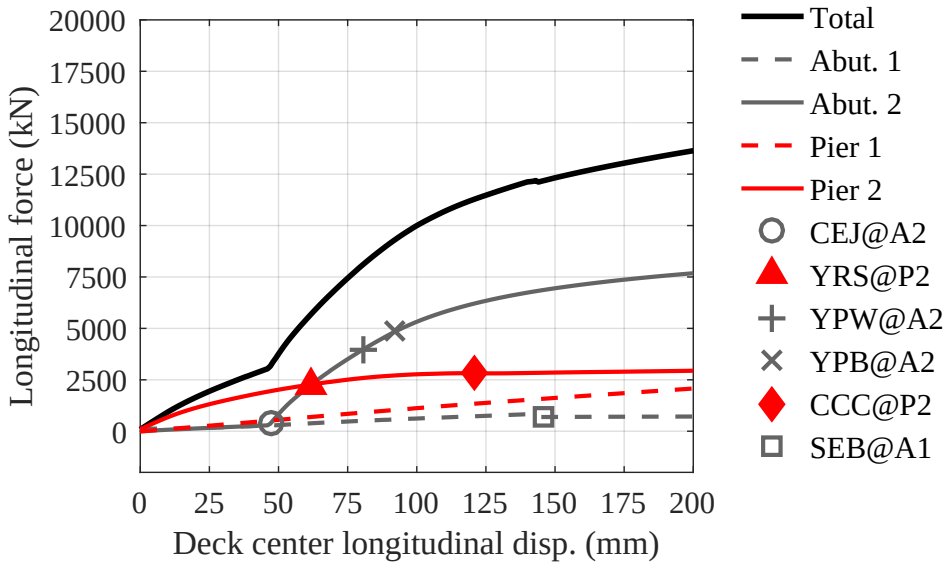

(a) Longitudinal analysis

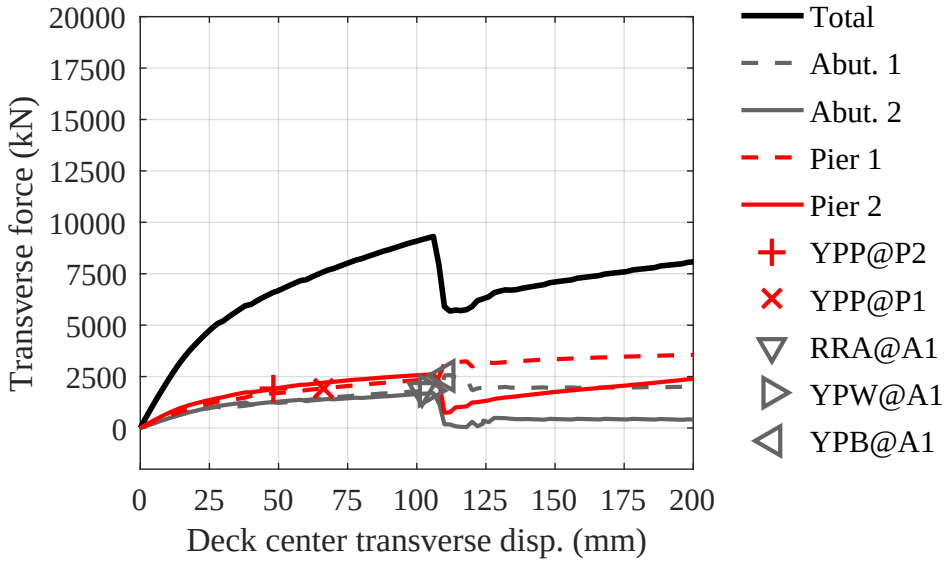

(b) Transverse analysis

Figure 5.13: Pushover response of 3S00P15S bridge variant: (a). longitudinal analysis; (b). transverse analysis

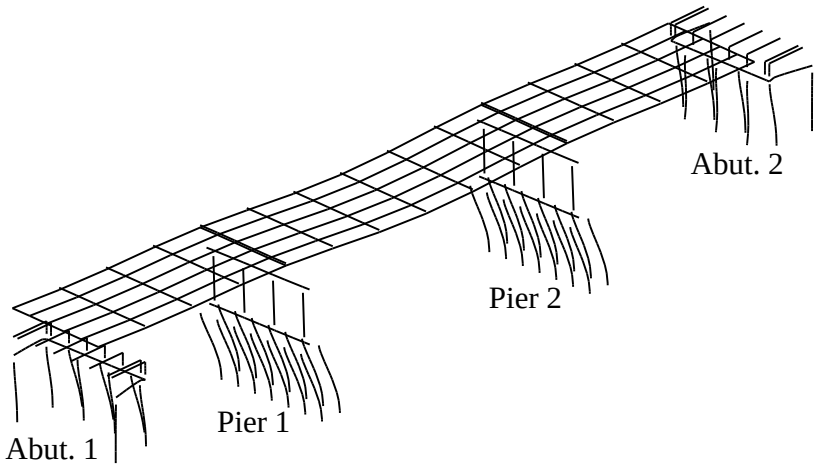

Figure 5.14: Deformed shape of 3S00P15S bridge in transverse pushover analyses (corresponding to the response state with a 150-mm deck center displacement in Figure 5.13b; deformation is magnified by 20 times)

5.3.2 Four-span steel-plate-girder (4S) bridges

4S00P15H Bridge

Figures 5.15a and 5.15b illustrate the longitudinal and transverse pushover responses of 4S00P15H bridge variant, respectively.

The longitudinal response is generally similar to that of the 3S equivalent bridge (3S00P15H bridge). Yielding of reinforcing steel (YRS) and crushing of concrete cover (CCC) were observed at all the three intermediate piers, but the fixed pier (Pier 2) columns were damaged at a much smaller deck center displacement than the expansion pier (Piers 1 & 3) columns. The abutment that was pushed by the superstructure was the major source of resistance, compared with the other substructures. The deformed shape at the end of the analysis is shown in Figure 5.16a. It can be seen that the fixed pier deflected more than the expansion piers and the piles at Abutment 2 largely deflected.

The transverse response is quite different from that of the 3S00P15H bridge. Rupture of the fixed bearing anchors at Pier 2 (RFA@P2) was the only fusing limit state observed, after which the total pushover force dramatically decreased. Rupture of the retainer anchors at the two abut-

ments (RRA@A1 and A2) or the expansion piers (RRA@P1 and P3) did not occur in the analysis that was terminated at a 300-mm deck center displacement. This sequence of fusing limit states is significantly different from that of the equivalent 3S bridge, in which fusing of the retainer anchors at one abutment was encountered first. This difference lies in the configurations of four-span and three-span non-skew bridges. In the transverse pushover analysis, the stiffness center of the three-span bridge is eccentric because the fixed and expansion piers have different transverse stiffness, but the mass center is basically located at the midspan. The eccentricity between the mass and stiffness centers caused the rotational response of 3S00P15H bridge and rupture of retainer anchors occurred first at the deck end supported by Abutment 1 (RRA@A1). Different from the asymmetric 3S bridge, the 4S00P15H bridge has a symmetric configuration about the midspan. Figure 5.16b illustrates the deformed bridge shape with a 200-mm deck center displacement in the transverse pushover analysis. The deformed shape is symmetric about the midspan and the maximum transverse superstructure displacement occurred at the midspan. As shown in Figure 5.15b, due to the early fusing of steel fixed bearings (RFA@P2), the columns at Pier 2 were isolated and did not sustain increasing forces. Differently, due to the unfused transverse bearing retainers at the abutments and expansion piers, the forces on these two piers kept increasing in the analysis. The expansion piers experienced larger forces than the abutments.

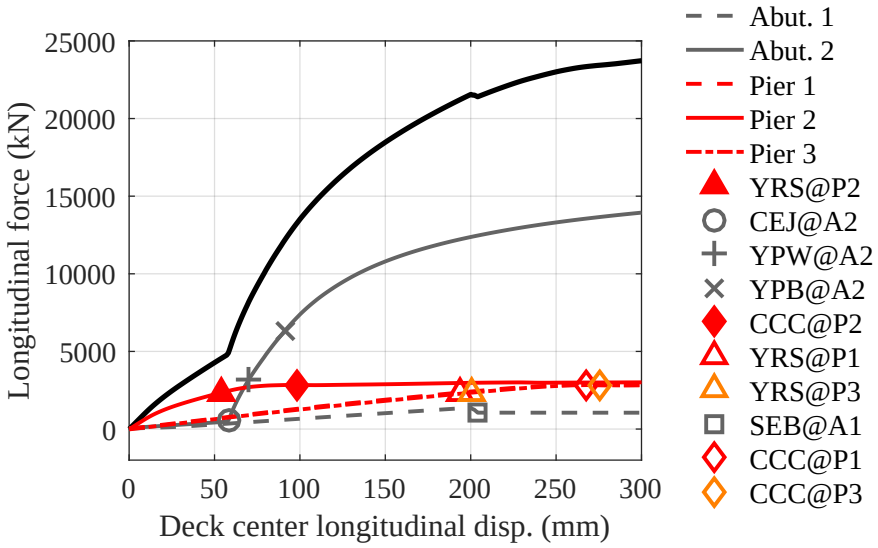

(a) Longitudinal analysis

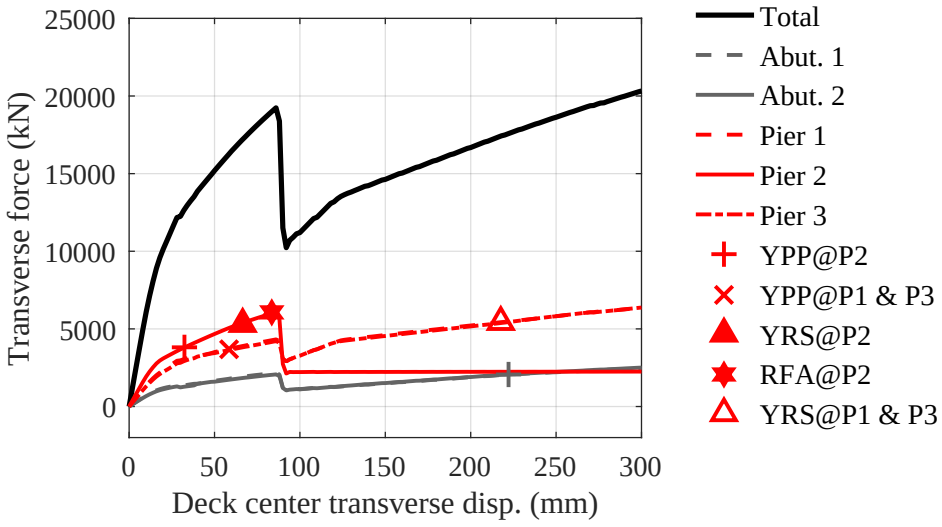

(b) Transverse analysis

Figure 5.15: Pushover response of 4S00P15H bridge variant: (a). longitudinal analysis; (b). transverse analysis

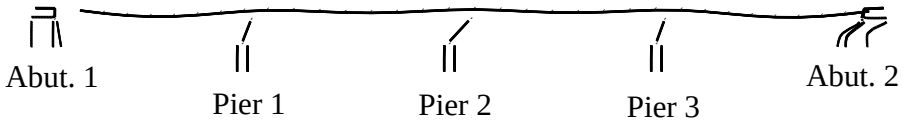

(a) Deformed shape of 4S00P15H bridge in longitudinal pushover analysis (deformation corresponds to the response state with a 300-mm deck center displacement in Figure 5.15a)

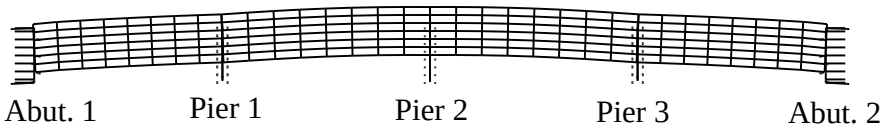

(b) Deformed shape of 4S00P15H bridge in transverse pushover analysis (deformation corresponds to the response state with a 200-mm deck center displacement in Figure 5.15b)

Figure 5.16: Deformed shape of 4S00P15H bridge in pushover analyses (deformation is magnified by 20 times)

4S45P15H Bridge

Figures 5.17a and 5.17b illustrate the longitudinal and transverse pushover responses of 4S45P15H bridge variant, respectively.

Similar to the response characteristics of the equivalent 3S bridge (3S45P15H bridge), the longitudinal force capacity of the skew 4S bridge (4S45P15H) is lower than that of the equivalent non-skew bridge (4S00P15H) at the same deck center displacement, due to the oblique contact between the skew deck end and abutment. The fixed pier (Pier 2) was globally yielded and the retainers at Abutment 2 was fused (RRA@A2) due to the transverse displacement of the skew deck end at Abutment 2. Figure 5.18a depicts the deformed shape at the end of the longitudinal analysis. Similar to the deformed shape of 3S45P15H bridge shown in Figure 5.8c, the skew deck end at Abutment 2 experienced coupled longitudinal and transverse displacements.

In the transverse analysis, the first fusing limit state is rupture of the steel fixed bearing anchors at Pier 2 (RFA@P2), similar to the response of the non-skew equivalent bridge (4S00P15H bridge). After this limit state, rupture of the retainer anchors at the abutments and Pier 1 occurred in turn (RRA@A1, A2, and P1). Pile yielding was observed at all the three intermediate piers (YPP@P1, P2, and P3). Figure 5.18b depicts the deformed shape at the end of the transverse analysis. In addition to transverse displacements, the superstructure was also subjected to in-plane rotation abut Pier 3, at which the retainers were not fused. Similar to the response of the 3S45P15H bridge, the acute deck corner at Abutment 1 sustained large abutment-normal displacement and tended to drop off the abutment.

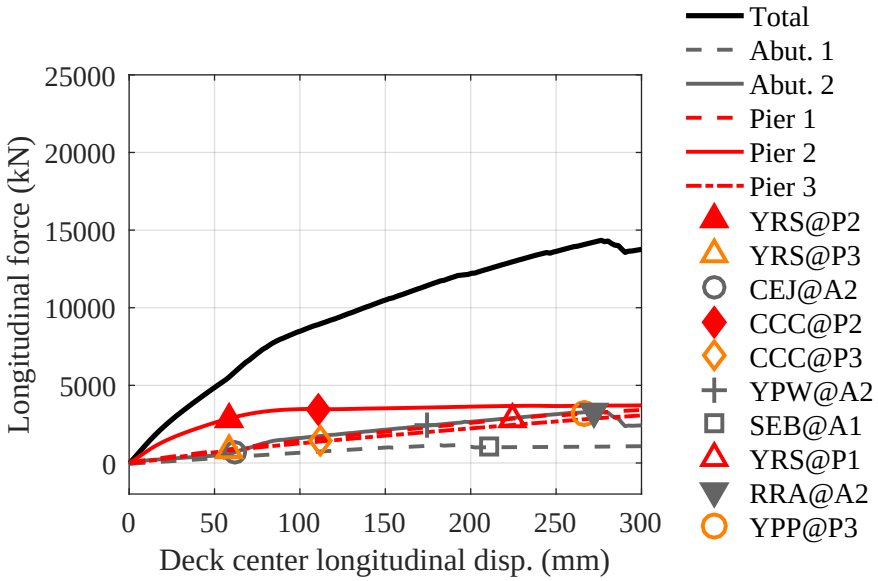

(a) Longitudinal analysis

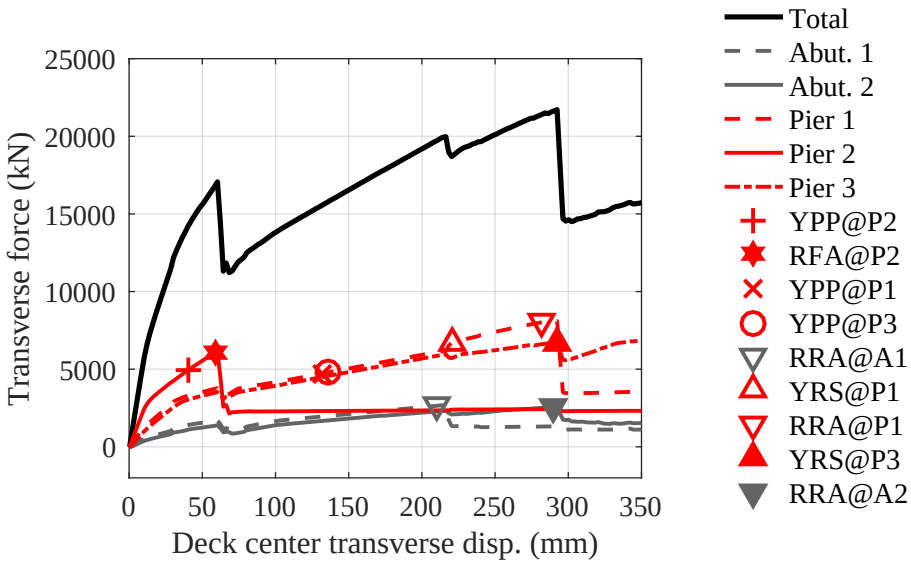

(b) Transverse analysis

Figure 5.17: Pushover response of 4S45P15H bridge variant: (a). longitudinal analysis; (b). transverse analysis

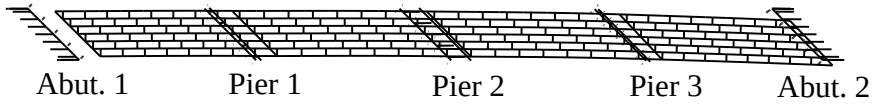

(a) Deformed shape of 4S45P15H bridge in longitudinal pushover analysis (deformation corresponds to the response state with a 300-mm deck center displacement in Figure 5.17a)

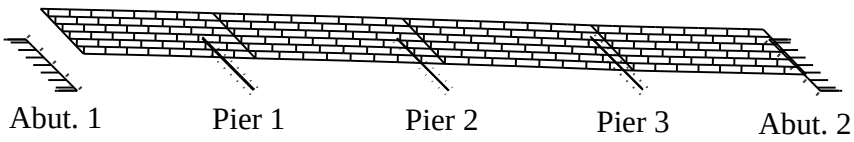

(b) Deformed shape of 4S45P15H bridge in transverse pushover analysis (deformation corresponds to the response state with a 300-mm deck center displacement in Figure 5.17b)

Figure 5.18: Deformed shape of 4S45P15H bridge in pushover analyses (deformation is magnified by 20 times)

4S00P40H Bridge

Figures 5.19a and 5.19b illustrate the longitudinal and transverse pushover responses of 4S00P40H bridge variant, respectively.

In the longitudinal analysis, the abutment that was pushed by the superstructure (Abutment 2) provided the majority of the resisting force after closure of the expansion joint (CEJ@A2). In comparison with Abutment 2, the three tall piers provided much smaller resisting forces and essentially deflected in an elastic state. At about a 290-mm deck center displacement, the ultimate backfill capacity at Abutment 2 was mobilized (MBU@A2) and the slope of total force became much smaller than that at the moment of joint closure. The piles of Abutment 2 yielded shortly after closure of the expansion joint. Figure 5.20a depicts the deformed shape of 4S00P40H bridge at the end of the longitudinal analysis with a 300-mm deck center displacement. It can be seen that the piles of Abutment 2 experienced significant deflection. As discussed on the 3S00P40H bridge, the longitudinal responses of the tall expansion and fixed piers are generally similar, although different bearings are installed on top of them. The reason is that the lateral stiffness of the bearing-column assembly is dominated by the flexible tall pier columns, which are the same for both types of piers.

In the transverse analysis, fusing action of any sacrificial connection was not observed in the analysis. As yielding of pier column reinforcing steel (YRS@P1, P2, & P3) and substructure piles (YPP@P1, P2, & P3; YPW@A1 & A2) occurred, the bridge system was gradually softened in the transverse direction. The fixed pier (Pier 2) experienced global yielding after crushing of the concrete cover at its column bottoms (CCC@P2), but the expansion piers were not completely yielded when the analysis was terminated at a 300-mm deck center displacement. Figure 5.20b depicts the deformed shape of 4S00P40H bridge at the end of the transverse analysis with a 300-mm deck center displacement. The deformed superstructure exhibited a parabolic shape. The largest superstructure displacement occurred at the midspan, while the displacements at the two abutments and expansion piers are smaller.

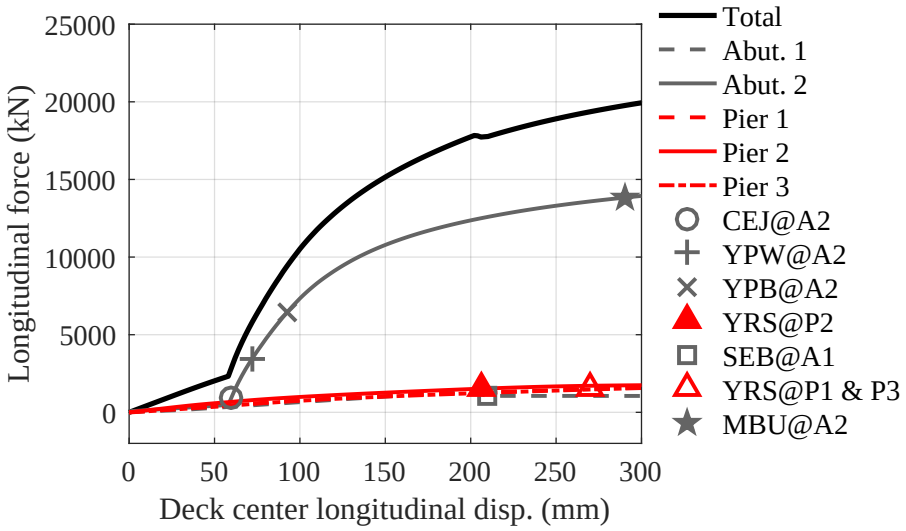

(a) Longitudinal analysis

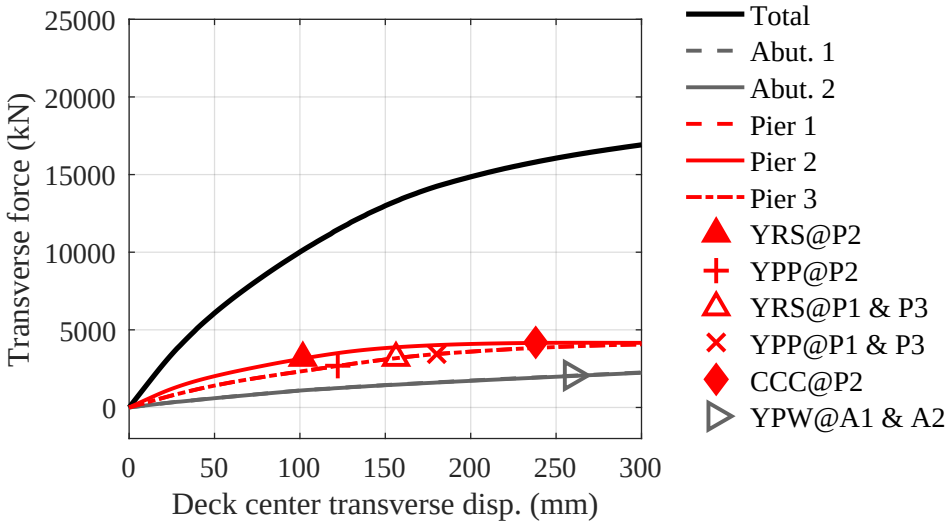

(b) Transverse analysis

Figure 5.19: Pushover response of 4S00P40H bridge variant: (a). longitudinal analysis; (b). transverse analysis

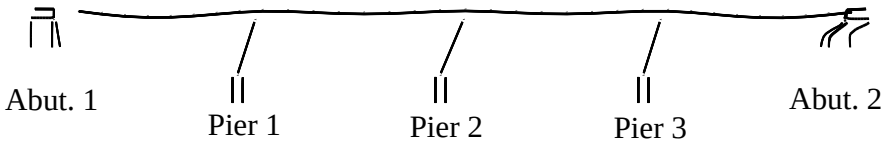

(a) Deformed shape of 4S00P40H bridge in longitudinal pushover analysis (deformation corresponds to the response state with a 300-mm deck center displacement in Figure 5.19a)

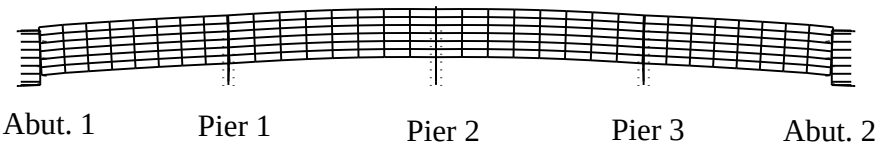

(b) Deformed shape of 4S00P40H bridge in transverse pushover analysis (deformation corresponds to the response state with a 300-mm deck center displacement in Figure 5.19b)

Figure 5.20: Deformed shape of 4S00P40H bridge in pushover analyses (deformation is magnified by 20 times)

4S00P15S Bridge

Figures 5.21a and 5.21b illustrate the longitudinal and transverse pushover responses of 4S00P15S bridge variant, respectively.

Comparison between the responses of 4S00P15S bridge shown in Figure 5.21a and 4S00P15H bridge shown in Figure 5.15a indicates that the foundation soil condition did not significantly affect the general longitudinal bridge response. Except the total force is lower in the presence of the soft foundation soil, the ultimate passive capacity of backfill soil was mobilized (MBU@A2), which did not occur in the bridge with the hard foundation soil (4S00P15H bridge). This difference is reasonable because when the foundation soil is soft and provides relatively low resistance to the displaced superstructure, a larger pushover force needs to be shared by the backfill soil than the force in the case with the hard foundation soil. All the three intermediate piers were globally yielded. The piles of Abutment 2 were yielded shortly after closure of the expansion joint. The deformed bridge shape at the end of the analysis is similar to that shown in Figure 5.20a.

In the transverse analysis, the only observed fusing limit state is the rupture of retainer anchors at the two abutments (RRA@A1 & A2). This response is different from that of the equivalent bridge in the hard foundation soil (4S00P15H bridge), which is shown in Figure 5.21b. For the 4S00P15H bridge, the observed limit state is fusing of the steel fixed bearings at Pier 2 (RFA@P2). Due to the relatively low resistance of the soft soil, pile yielding occurred at all the substructures early in the analysis (YPW & YPB@A1 & A2; YPP@P1, P2, & P3), but damages to the pier columns (yielding of reinforcing steel and crushing of concrete cover) were not observed. The global bridge system was gradually softened.

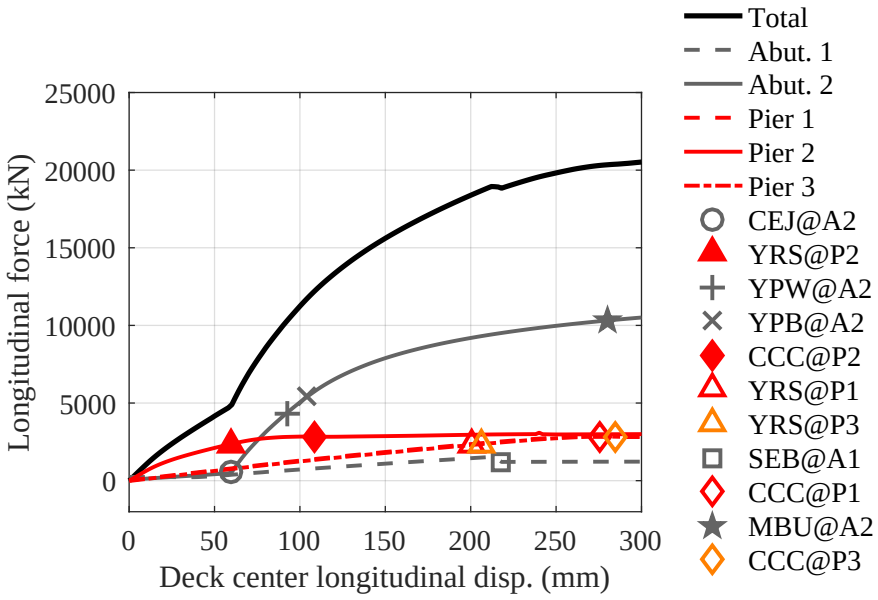

(a) Longitudinal analysis

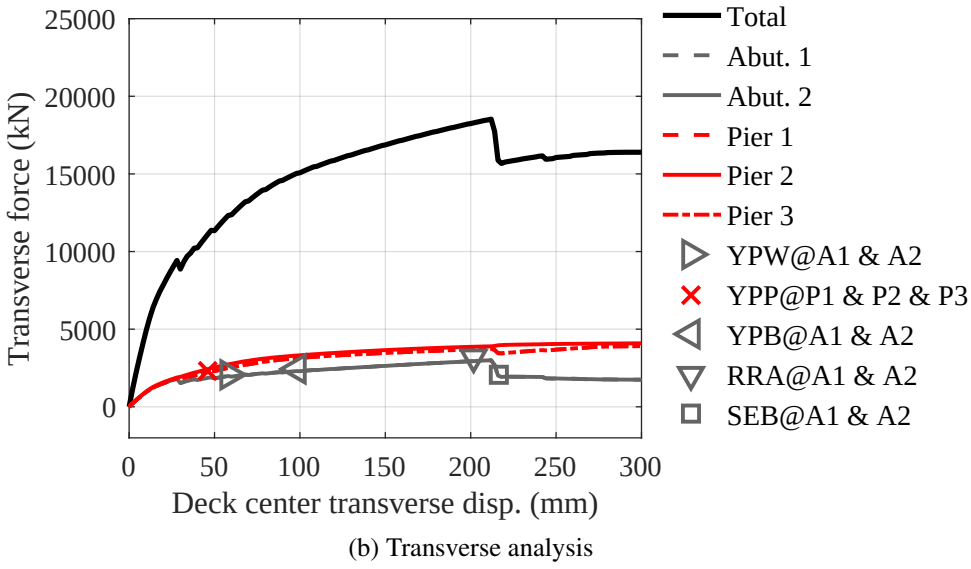

(b) Transverse analysis

Figure 5.21: Pushover response of 4S00P15S bridge variant: (a). longitudinal analysis; (b). transverse analysis

5.3.3 Three-span prestressed-precast-concrete-girder (3C) bridges

3C00P15H Bridge

Figures 5.22a and 5.22b illustrate the longitudinal and transverse pushover responses of 3C00P15H bridge variant, respectively.

In the longitudinal analysis, the steel dowel connection between the superstructure and fixed pier (Pier 2) appeared to be too strong to be fused before globally yielding the pier columns, which is the same as the behavior of 3S00P15H bridge shown in Figure 5.4a. Pile yielding at the abutment that was pushed by the superstructure (YPW@A2 & YPB@A2) occurred shortly after closure of the expansion joint. The deformed bridge shape at the end of the analysis is similar to that shown in Figure 5.5f.

In the transverse analysis, the observed sequence of fusing limit states was the same as that of the 3S00P15H bridge shown in Figure 5.4b, but the limit states occurred at different deck center displacements. Rupture of the retainer anchors at Abutment 1 (RRA@A1) preceded fusing of the sacrificial connections at Piers 1 and 2 (RRA@P1 & RSD@P2). Pile yielding at the piers (YPP@P1 & P2) was observed early in the analysis. The deformed shape of the bridge is similar to that shown in Figure 5.6.

At the same deck center displacement, the longitudinal and transverse force capacities of the 3C00P15H bridge are slightly higher than those of the equivalent 3S bridge (3S00P15H bridge).

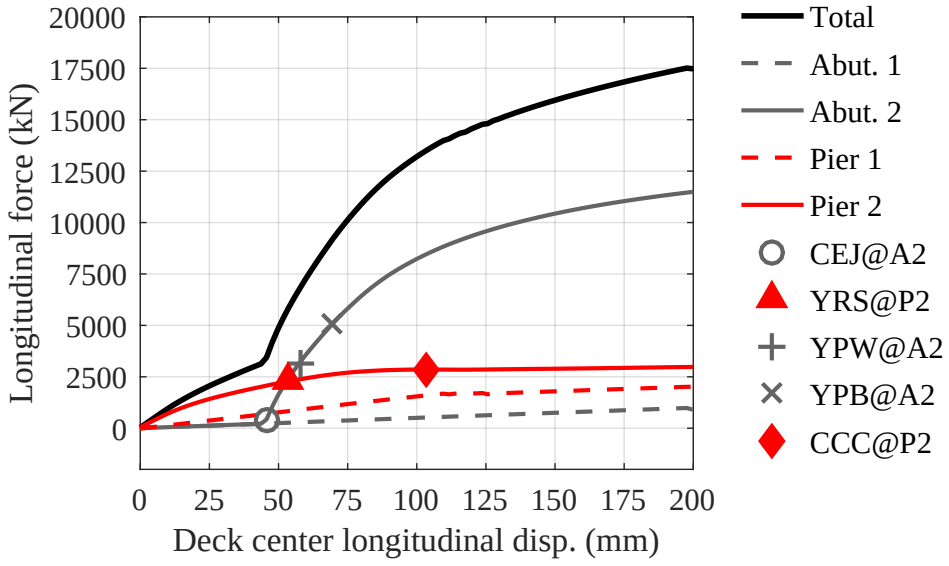

(a) Longitudinal analysis

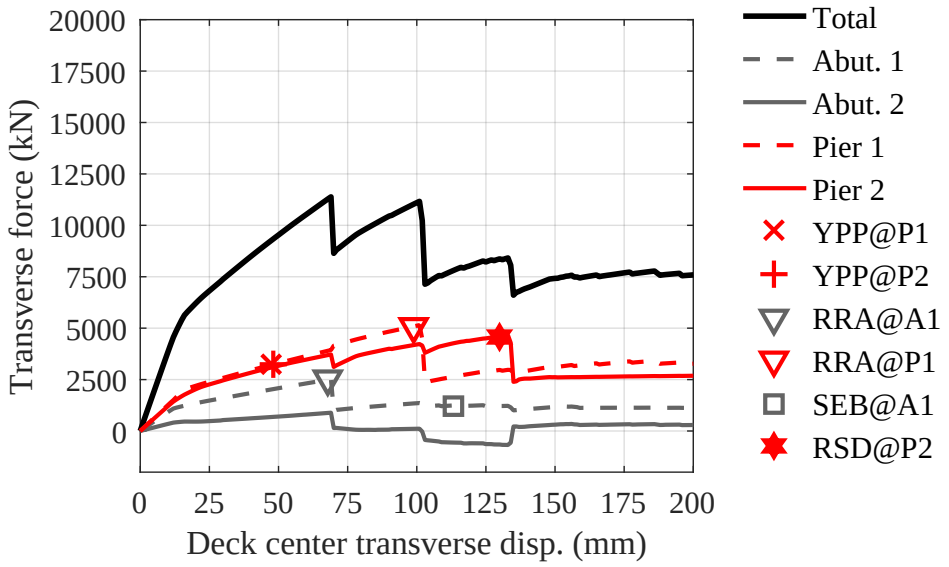

(b) Transverse analysis

Figure 5.22: Pushover response of 3C00P15H bridge variant: (a). longitudinal analysis; (b). transverse analysis

3C45P15H Bridge

Figures 5.23a and 5.23b illustrate the longitudinal and transverse pushover responses of 3C45P15H bridge variant, respectively.

In the longitudinal analysis, the fixed pier (Pier 2) sustained a larger longitudinal force demand than the other substructures. At the fixed pier, yielding of the reinforcing steel (YRS@P2) and crushing of the concrete cover (CCC@P2) preceded rupture of the steel dowel connections (RSD@P2). This undesired sequence of damage resulted in global yielding of Pier 2. Interactions between the skew deck end and abutment caused coupled longitudinal and transverse displacements of the deck end at Abutment 2. Yielding of the two piles supporting the wingwalls of Abutment 2 (YPW@A2) occurred after closure of the expansion joint (CEJ@A2). The general response of this bridge is similar to that of the equivalent 3S bridge (3S45P15H), except the occurrence of a few fusing limit states. Compared with the 3C00P15H bridge, the global force capacity at the same deck center displacement is reduced due to the oblique contact between the skewed deck end and abutment. The deformed bridge shape at the end of the analysis is similar to that of the 3S45P15H bridge shown in Figure 5.8c.

In the transverse analysis, the first major fusing limit state was the rupture of steel dowel connections at Pier 2 (RSD@P2). Following this limit state, fusing of the retainer anchors at Abutment 1 (RRA@A1), Pier 1 (RRA@P1), and Abutment 2 (RRA@A2) occurred in turn. This sequence of fusing is different from that of the equivalent 3S bridge (3S45P15H). In addition to these fusing limit states, yielding of the piles supporting the two piers (YPP@P1 & P2) was also observed, which was not observed in the equivalent 3S bridge. Figure 5.24 depicts the deformed shape of the bridge at the end of the transverse pushover analysis. Similar to the response of the 3S and 4S bridges, the deck sustained in-plane rotation. The acute deck corner at Abutment 1 experienced large abutment-normal displacement and tended to drop off the abutment.

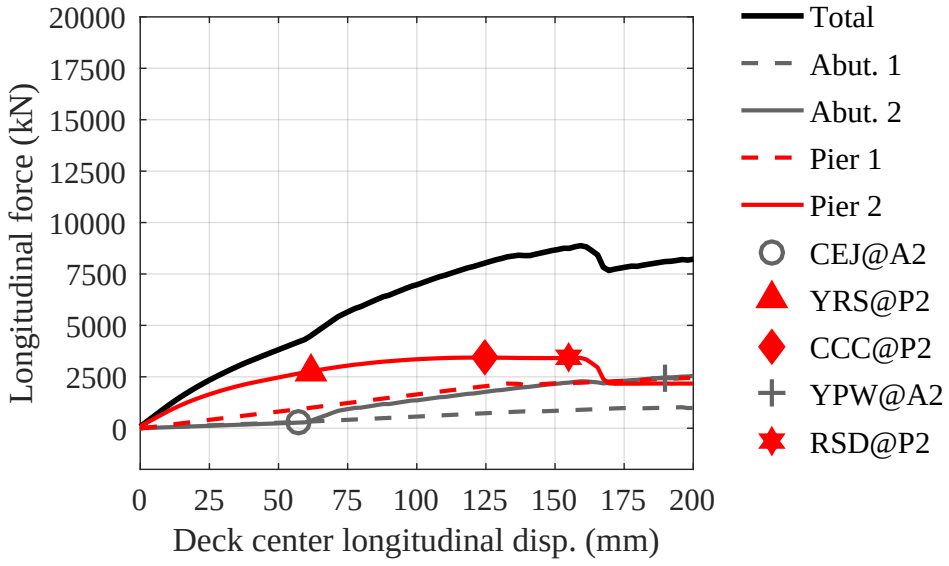

(a) Longitudinal analysis

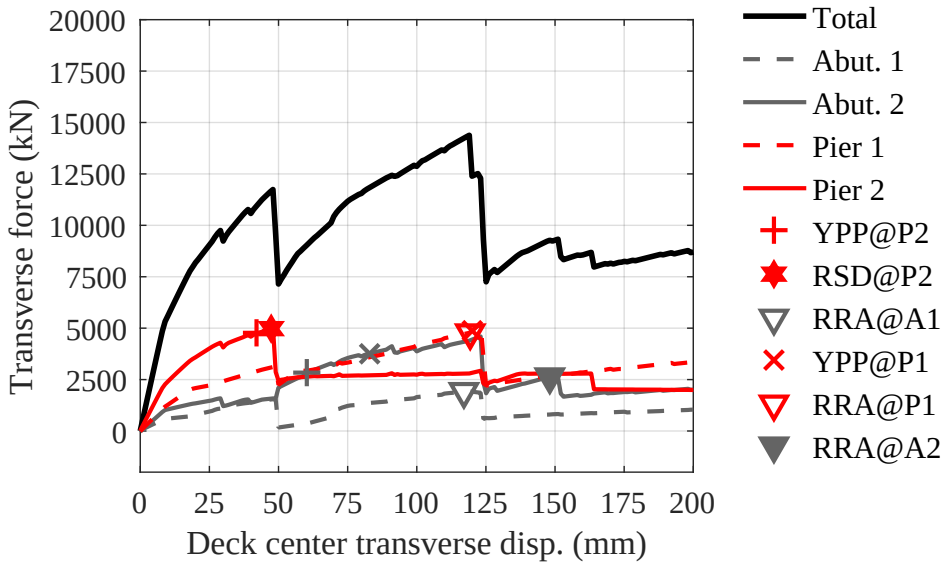

(b) Transverse analysis

Figure 5.23: Pushover response of 3C45P15H bridge variant: (a). longitudinal analysis; (b). transverse analysis

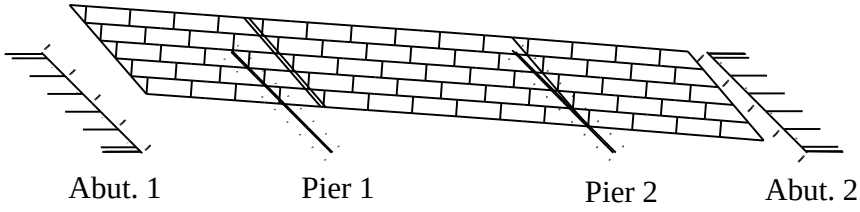

Figure 5.24: Deformed shape of 3C45P15H bridge in transverse pushover analyses (deformation corresponds to the response state with a 200-mm deck center displacement in Figure 5.23b; deformation is magnified by 20 times)

3C00P40H Bridge

Figures 5.25a and 5.25b illustrate the longitudinal and transverse pushover responses of 3C00P40H bridge variant, respectively.

In the longitudinal analysis, Abutment 2 was the major source of resistance to the superstructure, after closure of the expansion joint (CEJ@A2). The two tall piers elastically deflected and provided much smaller forces than Abutment 2. Yielding of the piles at Abutment 2 (YPW & YPB@A2) occurred shortly after the joint closure. The steel dowel connections at Pier 2 were not fused in the analysis. The global force capacity is slightly lower than that of the 3C00P15H bridge at the same deck center displacement, due to the flexible tall piers.

In the transverse analysis, different from the response of the short-pier equivalent bridge (3C00P15H bridge), the only fusing limit state observed is the rupture of retainer anchors at Abutment 1 (RRA@A1). As discussed on the 3S00P40H bridge, the flexible tall piers are unfavorable to the fusing action of the sacrificial superstructure-substructure connections. As a result, neither the steel fixed bearings at Pier 2 nor the bearing retainers at Pier 1 were fused in the analysis. Close to the occurrence of this limit state, pile yielding was observed at three substructures (YPW@A1; YPP@P1 & P2). Additionally, yielding of column reinforcing steel was observed at both piers (YRS@P1 & P2). The entire bridge system was gradually softened. Figure 5.26 depicts the deformed bridge shape at the end of the analysis. Due to the unfused sacrificial connections at the two piers, the pier columns experienced significant transverse deflections, which can be clearly observed in the deformed bridge shape.

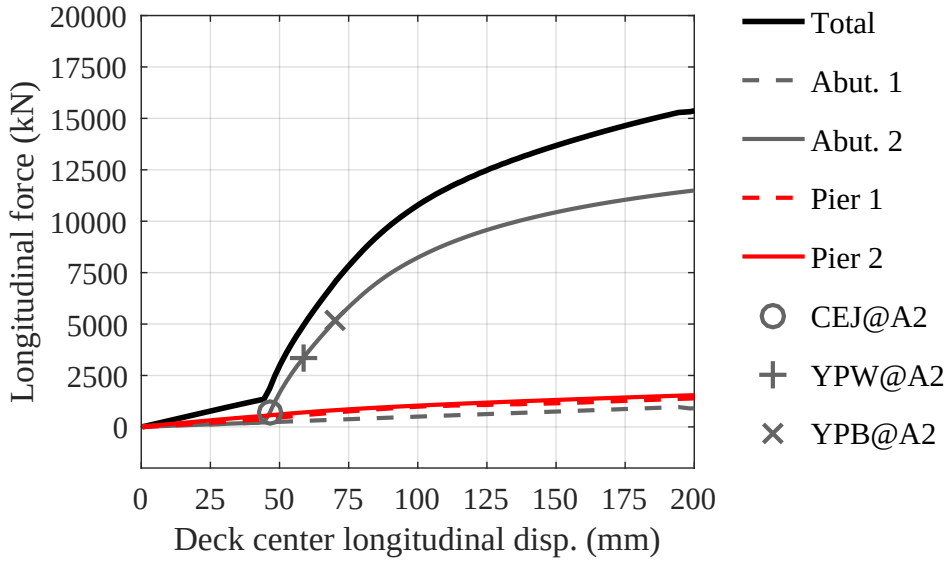

(a) Longitudinal analysis

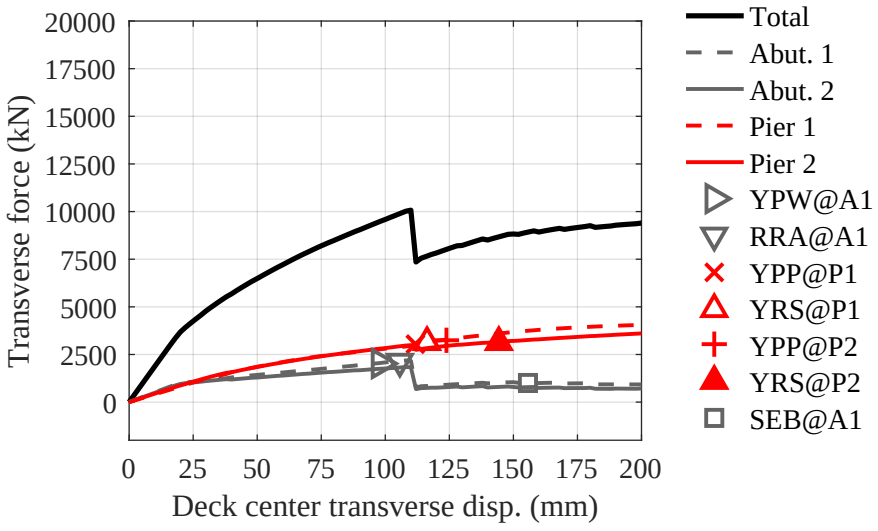

(b) Transverse analysis

Figure 5.25: Pushover response of 3C00P40H bridge variant: (a). longitudinal analysis; (b). transverse analysis

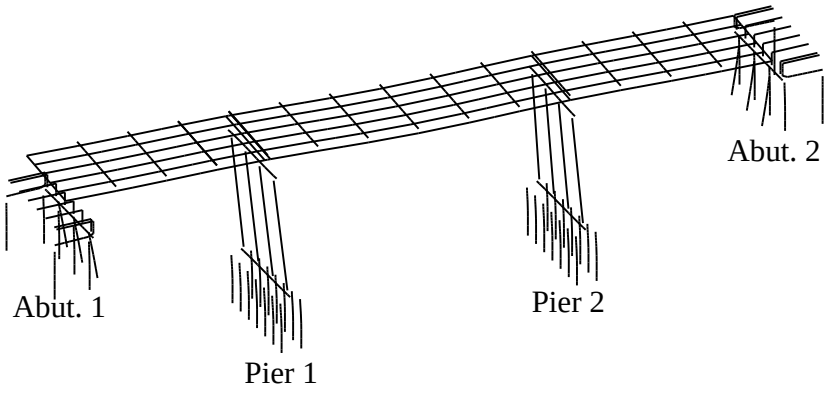

Figure 5.26: Deformed shape of 3C00P40H bridge in transverse pushover analyses (deformation corresponds to the response state with a 200-mm deck center displacement in Figure 5.25b; deformation is magnified by 20 times)

3C00P15S Bridge

Figures 5.27a and 5.27b illustrate the longitudinal and transverse pushover responses of 3C00P15S bridge variant, respectively.

The global longitudinal response is similar to that of the equivalent bridge in the hard foundation soil (3C00P15H bridge). The steel dowel connections at the fixed pier (Pier 2) were not fused in the analysis. As a result, the fixed pier globally yielded after the occurrence of the two damaging limit states of its columns (YRS@P2 and CCC@P2). The expansion pier (Pier 1) was not damaged in the analysis. Due to the soft foundation soil, the overall force capacity of the bridge is lower than that of the equivalent bridge in the hard foundation soil at the same deck center displacement.

As discussed on the 3S00P15S bridge, the soft foundation soil is unfavorable to the fusing action of the sacrificial connections. As a result, the only observed fusing limit state is rupture of the retainer anchors at Abutment 2 (RRA@A2), which is quite different from the connection fusing performance of the 3S00P15H bridge. Pile yielding was observed at three substructures (YPP@P1 & P2; YPW & YPB@A2). The entire bridge system was gradually softened and at the end of the analysis, the bridge system has basically yielded in the transverse direction. The deformed shape at the end of the analysis is depicted in Figure 5.28. Due to the soft foundation soil and unfused sacrificial connections at the piers, the piles largely deflected in the transverse direction.

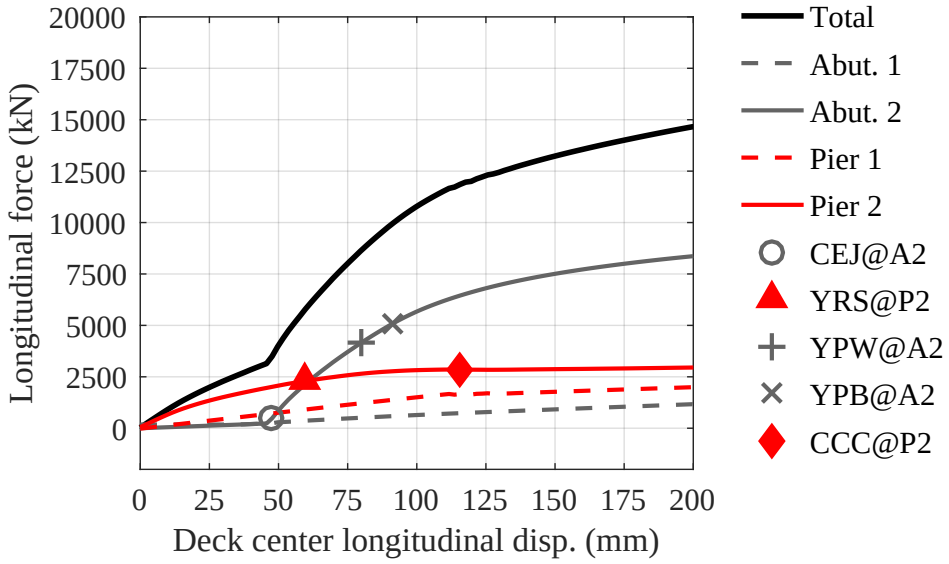

(a) Longitudinal analysis

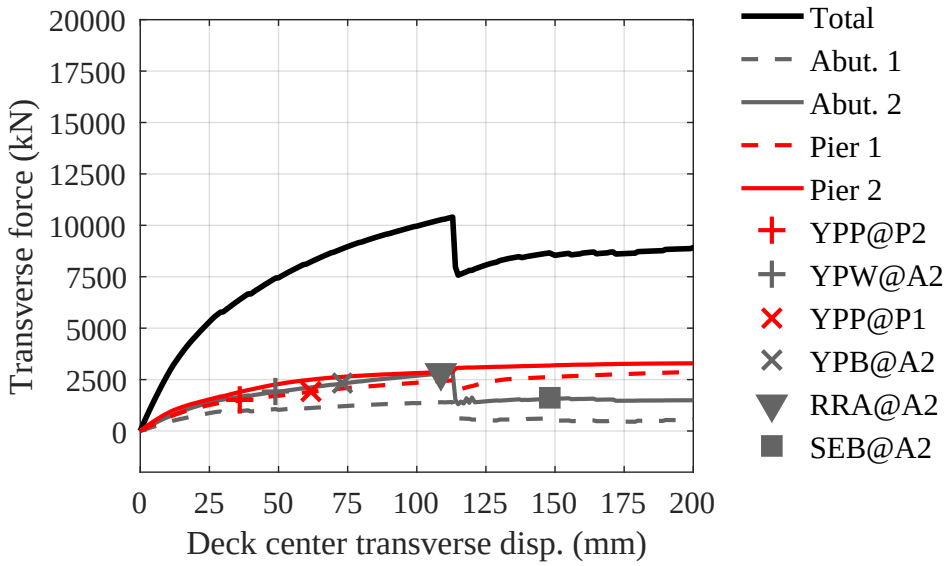

(b) Transverse analysis

Figure 5.27: Pushover response of 3C00P15S bridge variant: (a). longitudinal analysis; (b). transverse analysis

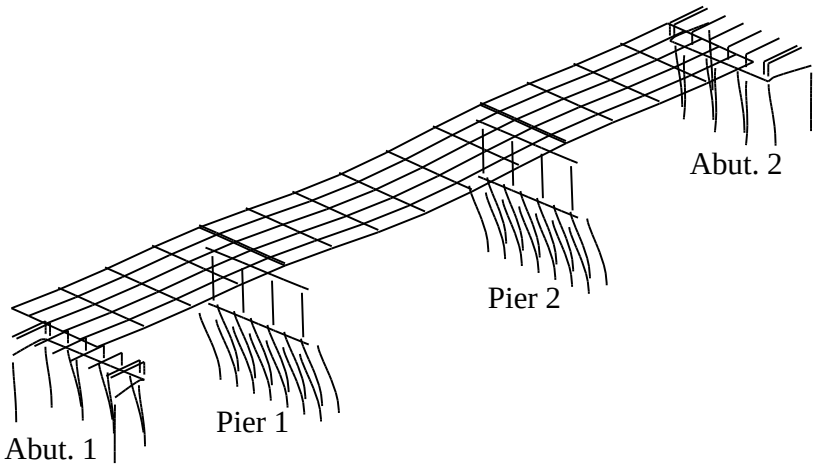

Figure 5.28: Deformed shape of 3C00P15S bridge in transverse pushover analyses (deformation corresponds to the response state with a 200-mm deck center displacement in Figure 5.27b; deformation is magnified by 20 times)

5.3.4 Four-span prestressed-precast concrete-girder (4C) bridges

4C00P15H Bridge

Figures 5.29a and 5.29b illustrate the longitudinal and transverse pushover responses of 4C00P15H bridge variant, respectively.

In the longitudinal analysis, the steel dowel connections between the fixed pier (Pier 2) and superstructure appeared to be too strong to be fused before global yielding of the fixed pier. The two expansion piers (Piers 1 & 3) sustained smaller forces than the fixed pier. Abutment 2 experienced the largest force among all the substructures and its piles yielded (YPW & YPB@A2) immediately after closure of the expansion joint (CEJ@A2). The deformed shape at the end of the analysis is similar to that shown in Figure 5.16a.

In the transverse analysis, primarily due to the symmetric configuration, the first fusing limit state was the rupture of steel dowel connections at Pier 2 (RSD@P2), followed by rupture of the retainer anchors at the same pier (RRA@P2). Fusing actions of the sacrificial connections at the expansion piers and abutments were not observed in the analysis. Pile yielding occurred at all the five substructures (YPP@P1, P2, & P3; YPW & YPB@A1 & A2). Due to fusing of the steel dowel connections and retainer anchors at Pier 2, the columns of Pier 2 was effectively protected from the

damaging limit states (yielding of reinforcing steel or crushing of concrete cover). In contrast, due to the unfused retainer anchors at the expansion piers, their columns were subjected to reinforcing steel yielding (YRS@P1 & P3) and concrete crushing (CCC@P1 & P3), and globally yielded at the end of the analysis. The piers were subjected to larger forces than the abutments in the analysis. The deformed shape at the end of the analysis is similar to that shown in Figure 5.16b.

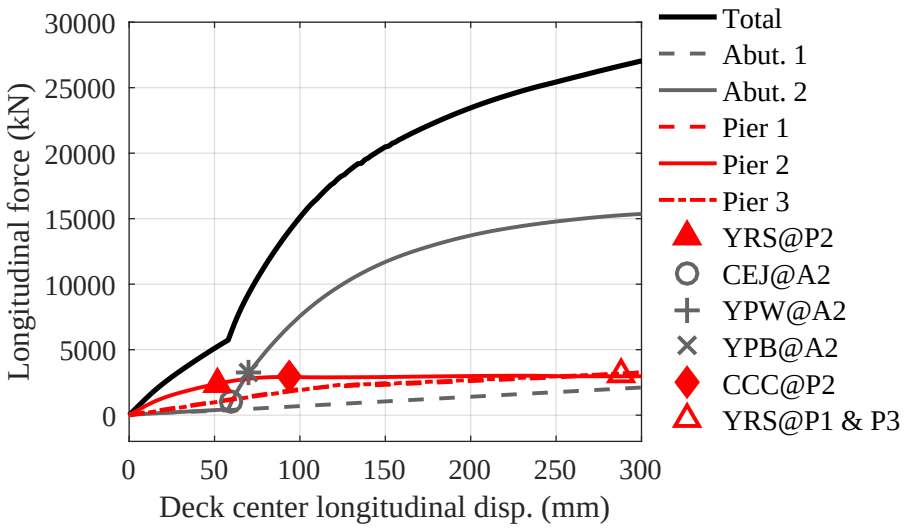

(a) Longitudinal analysis

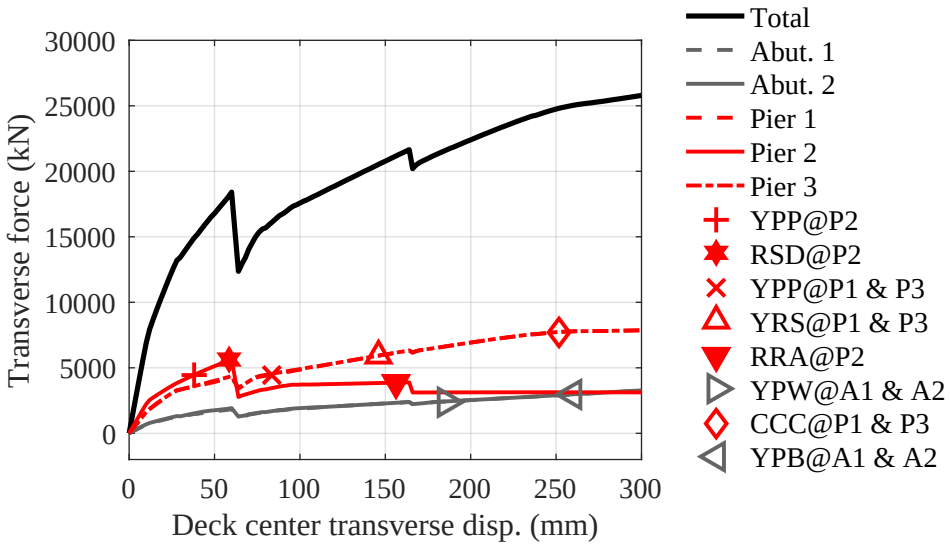

(b) Transverse analysis

Figure 5.29: Pushover response of 4C00P15H bridge variant: (a). longitudinal analysis; (b). transverse analysis

4C45P15H Bridge

Figures 5.30a and 5.30b illustrate the longitudinal and transverse pushover responses of 4C45P15H bridge variant, respectively.

In the longitudinal response shown in Figure 5.30a, fusing limit states were not observed, similar to the response of the non-skew equivalent bridge (4C00P15H bridge). The fixed pier was globally yielded after yielding of the reinforcing steel (YRS@P2) and crushing of the concrete cover (CCC@P2) at its column bases. Pile yielding occurred at Abutment 2 and Pier 3. The total longitudinal force is smaller than that of 4C00P15H bridge at the same deck displacement, due to the oblique contact between the skew deck end and abutment. The deformed bridge shape at the end of the analysis is similar to that shown in Figure 5.18a.

In the transverse analysis, the first fusing limit state was rupture of the steel dowel connections at Pier 2 (RSD@P2), similar to the response of the equivalent non-skew bridge (4C00P15H). Following this limit state, fusing of the retainer anchors at Pier 2 (RRA@P2), Abutment 1 (RRA@A1), Pier 1 (RRA@P1), Pier 3 (RRA@P3), and Abutment 2 (RRA@A2) occurred in turn. Due to the fusing limit states, the pier columns were effectively protected, especially for the fixed pier that did not sustain yielding of reinforcing steel or crushing of concrete cover. The expansion piers sustained yielding of reinforcing steel (YRS@P1 & P3) but not crushing of concrete cover at pier column bases. The two expansion piers experienced larger forces than the other substructures. Pile yielding occurred at all the five substructures. The deformed bridge shape at the end of the analysis is similar to that shown in Figure 5.18b.

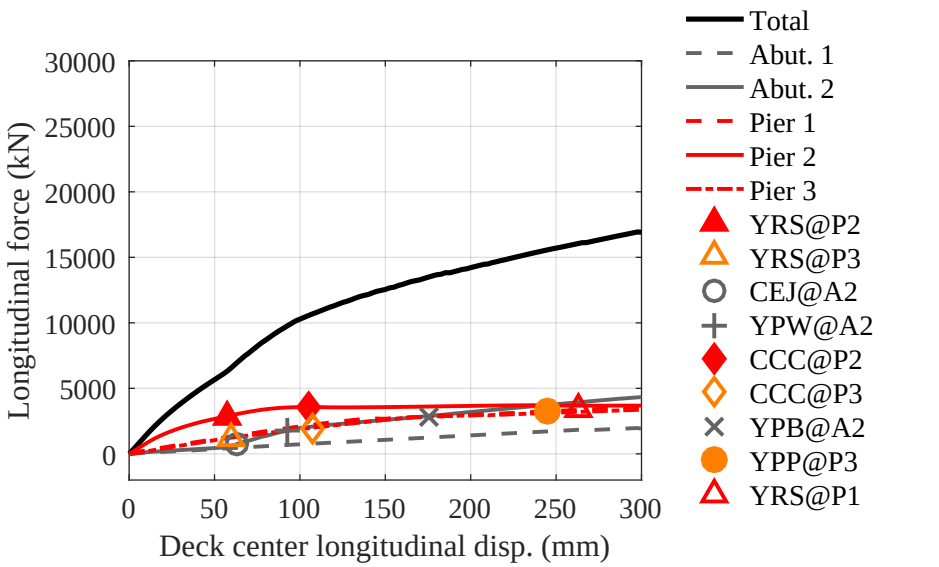

(a) Longitudinal analysis

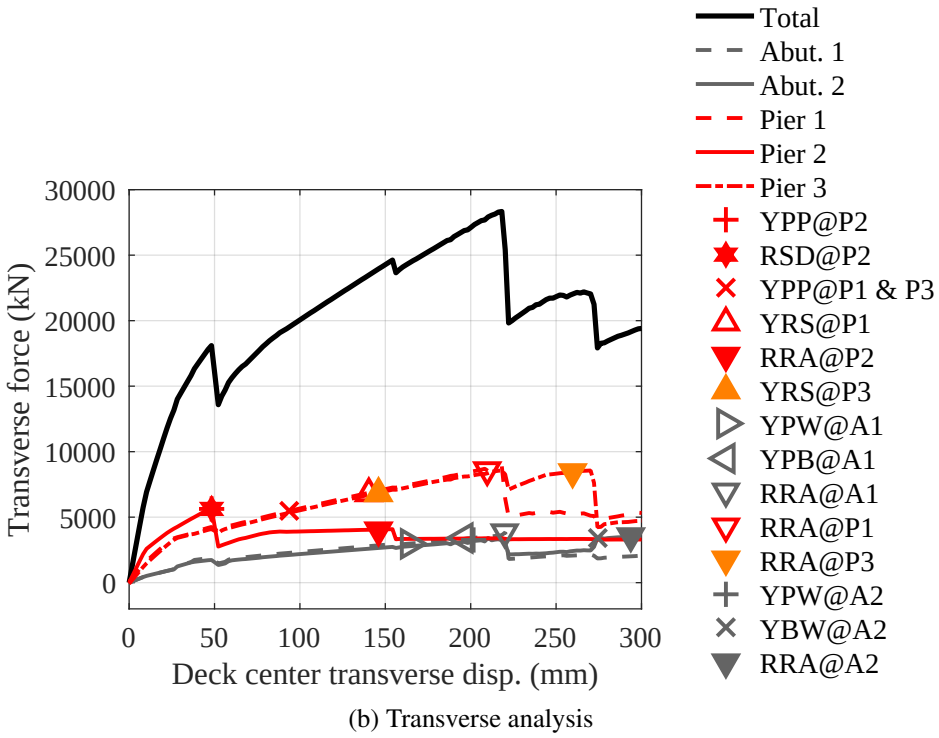

(b) Transverse analysis

Figure 5.30: Pushover response of 4C45P15H bridge variant: (a). longitudinal analysis; (b). transverse analysis

4C00P40H Bridge

Figures 5.31a and 5.31b illustrate the longitudinal and transverse pushover responses of 4C00P40H bridge variant, respectively.

In the longitudinal analysis, Abutment 2 resisted the majority of the pushover force and sustained pile yielding (YPW & YPB@A2) shortly after closure of the expansion joint (CEJ@A2). The three tall piers elastically deflected. Fusing of the sacrificial connections was not observed in the analysis, as the flexible tall pier columns are unfavorable to the fusing action of the sacrificial connections.

In the transverse analysis, similar to the response of the short-pier equivalent 4S bridge (4S00P40H bridge), fusing limit states did not occur in the analysis. Yielding of steel piles was observed at all the substructures (YPP@P1, P2, & P3; YPW & YPB@A1 & A2). Pier 2 was globally yielded after yielding of the reinforcing steel (YRS@P2) and crushing of the concrete cover (CCC@P2) at column bases. Yielding of column reinforcing steel at the expansion piers (YRS@P1 & P3) was also observed. The global bridge system was gradually softened in the transverse direction.

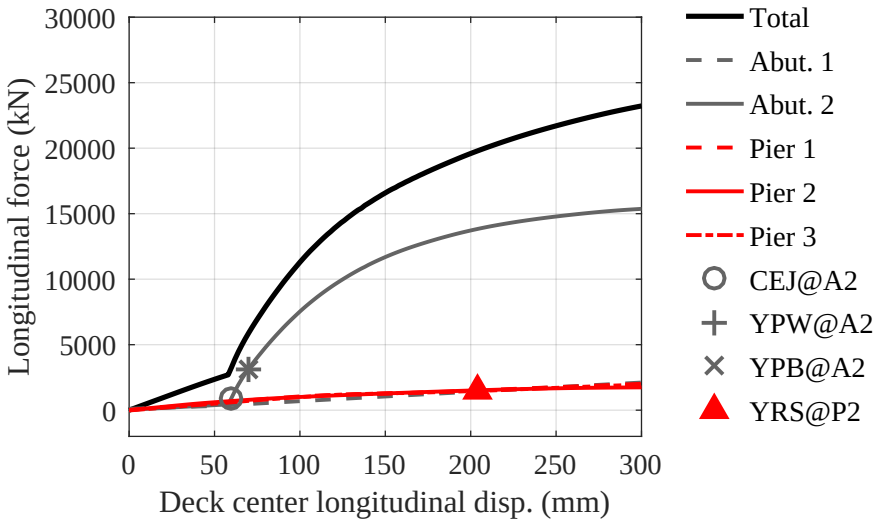

(a) Longitudinal analysis

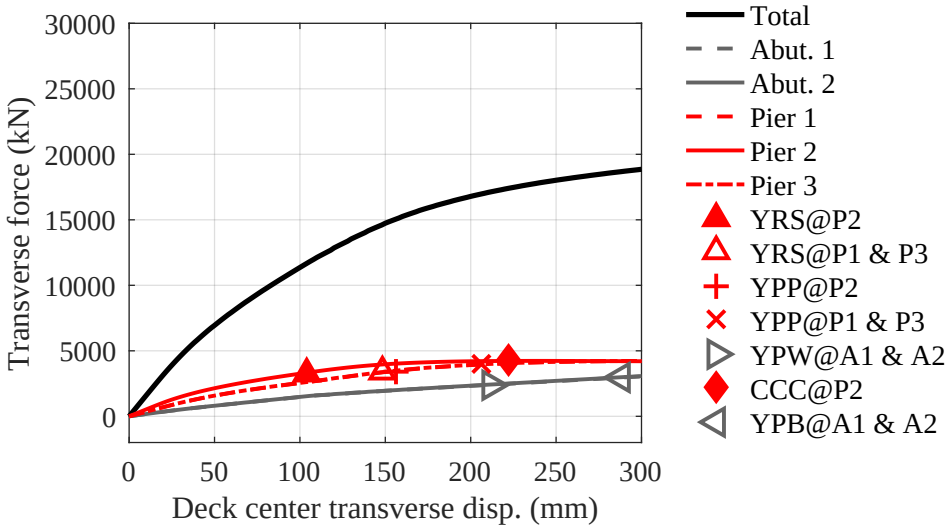

(b) Transverse analysis

Figure 5.31: Pushover response of 4C00P40H bridge variant: (a). longitudinal analysis; (b). transverse analysis

4C00P15S Bridge

Figures 5.32a and 5.32b illustrate the longitudinal and transverse pushover responses of 4C00P15S bridge variant, respectively.

The general longitudinal response was similar to that of the equivalent bridge in the hard soil (4C00P15H bridge), except the ultimate backfill passive resistance was mobilized (MBU@A2) at the end of the analysis. Because the soft foundation soil at Abutment 2 provided relatively low resistance to the displaced superstructure, a larger force was shared by the backfill soil than in the case of 4C00P15H bridge. Fusing limit states were not observed in the analysis.

The transverse analysis result was quite different from that of the 4C00P15H bridge. As discussed on the 3S00P15S bridge, the soft soil is unfavorable to fusing of the sacrificial connections. In this analysis, neither fusing of sacrificial connections nor pier column damaging limit states occurred in the analysis. The unfused connections transferred the pushover force down to the substructure foundations and caused yielding of the piles in the soft soil at all the substructures (YPP@P1, P2, & P3; YPW & YPB@A1 & A2). Figure 5.33 depicts the deformed bridge shape at the end of the analysis. It can be seen that the piles, especially those supporting the piers, sustained significant deflection in the transverse direction, which is consistent with the response shown in Figure 5.32b.

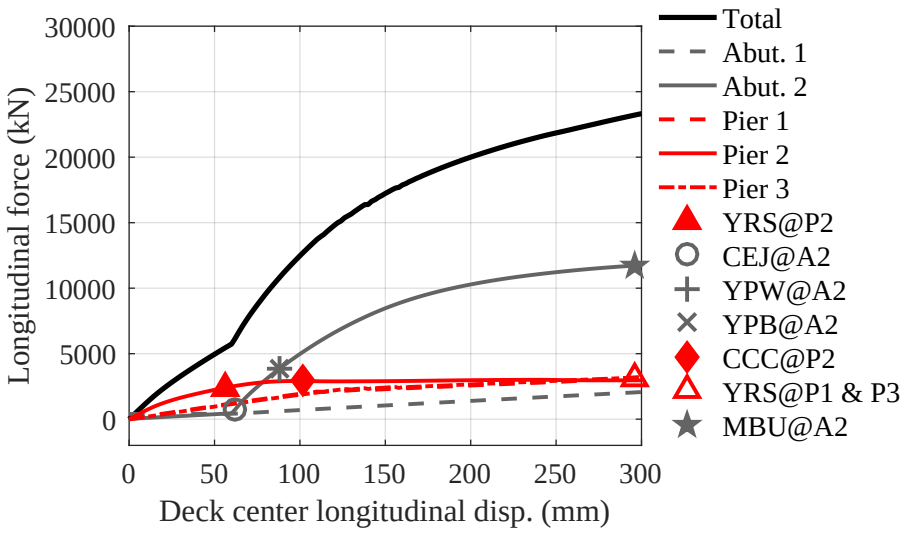

(a) Longitudinal analysis

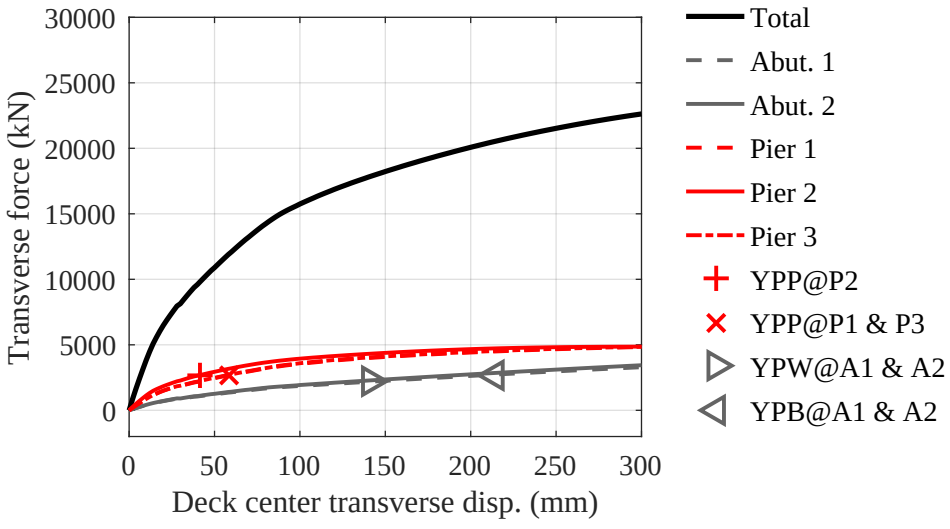

(b) Transverse analysis

Figure 5.32: Pushover response of 4C00P15S bridge variant: (a). longitudinal analysis; (b). transverse analysis

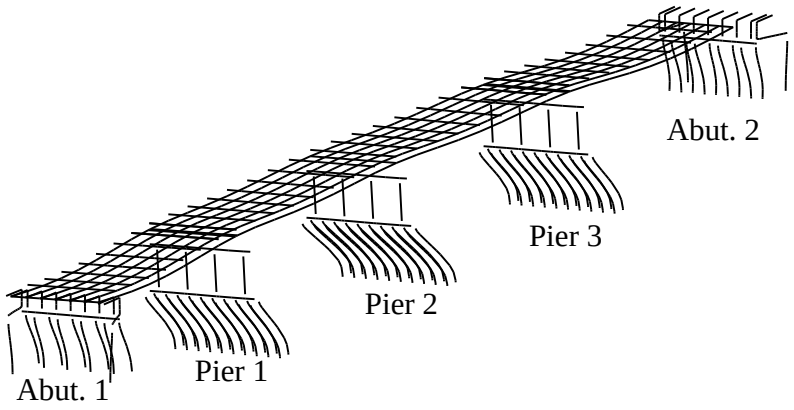

Figure 5.33: Deformed shape of 4C00P15S bridge in transverse pushover analyses (deformation corresponds to the response state with a 300-mm deck center displacement in Figure 5.32b; deformation is magnified by 20 times)

5.4 Modal Analysis Results

As introduced in Section 5.1, in the adaptive pushover analysis, the instantaneous mode shapes and periods of the bridge were recorded at multiple steps. By analyzing the recorded mode shapes and periods of different bridge variants, several important modal response characteristics of all the four basic bridge types are found and summarized as follows:

First, the predominant mode in the longitudinal or transverse direction is typically the first or the second vibration mode, regardless of the deformation state of the bridge variant. As introduced in Section 5.1, "the predominant mode" refers to the mode with the largest effective modal mass ratio that is defined in Equation (5.5). This means that the prototype quasi-isolated bridges are common civil engineering structures whose dynamic responses are usually dominated by the low-frequency modes.

Second, the period of the predominant mode is globally softened as the bridge pushover displacement increases, although there can be some local stiffening effect along the way. This is expected as many bridge components as well as the backfill and foundation soil resistance possess strain-softening constitutive behaviors.

Lastly, in the longitudinal direction, the effective modal mass (effective modal mass ratio mul-

tiplied by the total mass of the bridge) of only the predominant mode is typically sufficient to incorporate, at least, the mass of the bridge superstructure, which made up around 50% to 75% of the total bridge mass, depending on the basic bridge type. For the prototype bridges, the superstructure is the most massive subassembly in the entire bridge system. The rest of the total mass includes the mass of the piers, abutments, and foundations. The superstructure is also more flexible than the abutments and piers that are directly connected to pile foundations. Due to these two features, the superstructure can be regarded as the most active bridge subassembly during seismic events. In the transverse direction, depending on the bridge deformation state, the effective modal mass of the predominant one or two modes are needed to incorporate the superstructure mass. This characteristic means that the dynamic response of the prototype quasi-isolated bridges basically depends on one or two predominant modes, while the contribution of other modes will very likely to be insignificant.

As examples, Figures 5.34 to 5.37 illustrate the modal response of four different bridge variants in either longitudinal or transverse pushover analyses. Figures 5.34a, 5.35a, 5.36a, and 5.37a show the varying period of the predominant mode in the pushover analysis. Due to the occurrence of some limit states, such as closure of the expansion joint, the period can be temporarily shortened because the bridge system was stiffened immediately after the limit state occurrence. However, in the global trend, the period is elongated as the bridge system experiences inelastic damaging and deformation. Additionally, it can be found that in all the four examples, the predominant mode at most of the pushover steps is either the first or the second mode of the bridge variant. Figures 5.34b, 5.35b, 5.36b, and 5.37b demonstrate that the effective modal mass of the predominant one or two modes is sufficient to incorporate the mass of the bridge superstructure. Additionally, Figures 5.34 to 5.37 also depict the predominant one or two mode shapes along with the deformed bridge shape. The similarity between the deformed bridge shape and the mode shape can be observed.

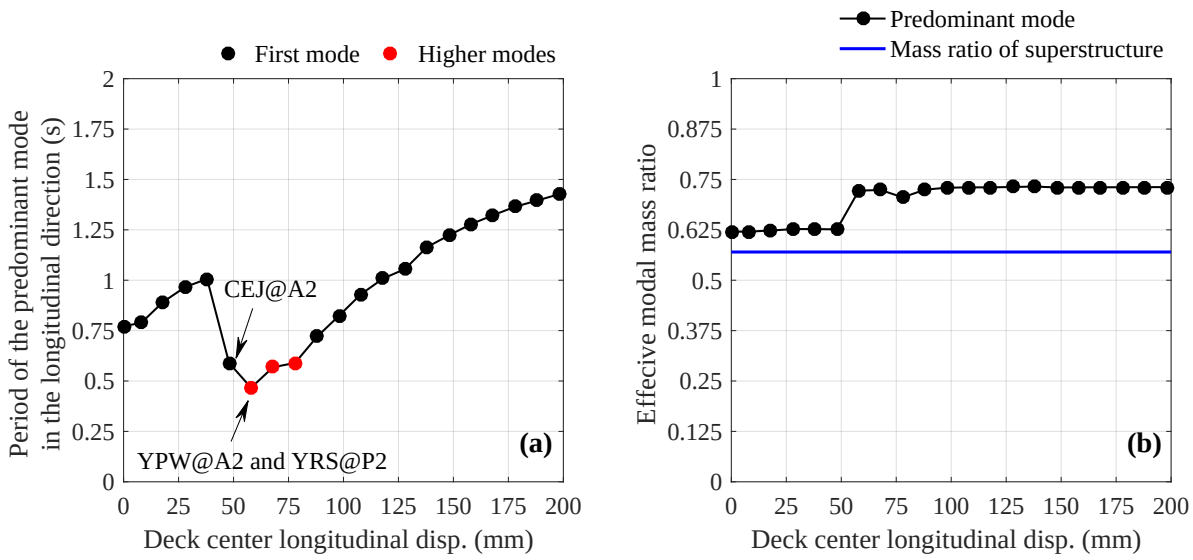

(c) The predominant mode shape (Mode 1) in the longitudinal direction at the state with a 100-mm deck center displacement

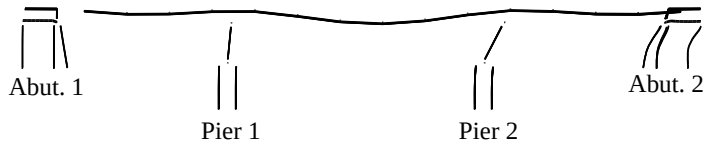

(d) Deformed bridge shape at the state with a 100-mm deck center displacement (deformation is magnified by 40 times)

Figure 5.34: Modal response of 3S00P15H bridge in longitudinal pushover analysis

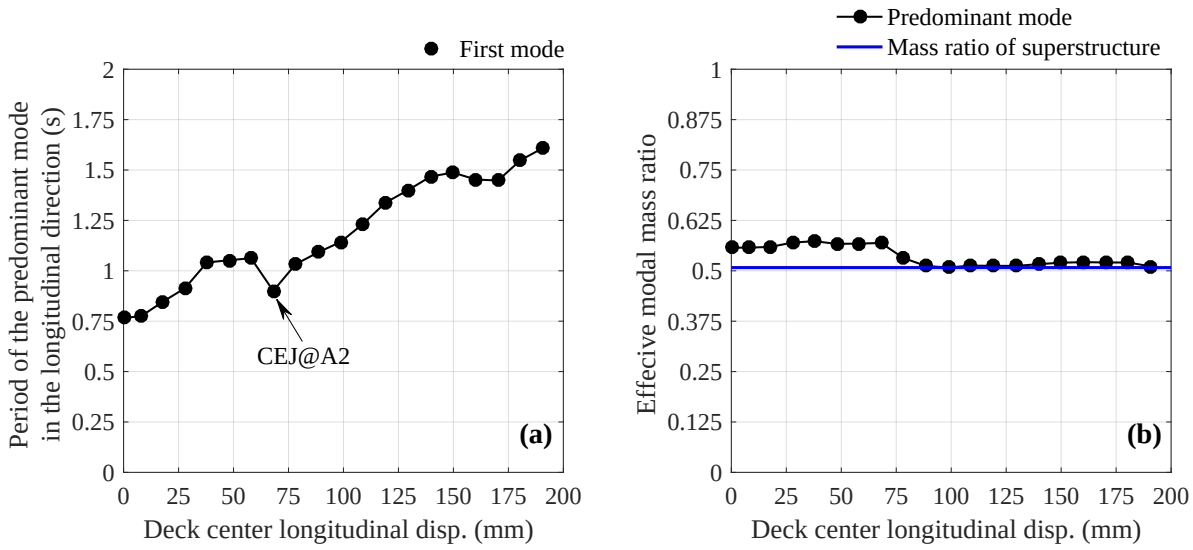

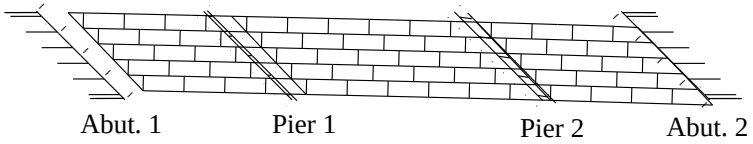

(c) The predominant mode shape (Mode 1) in the longitudinal direction at the state with a 175-mm deck center displacement

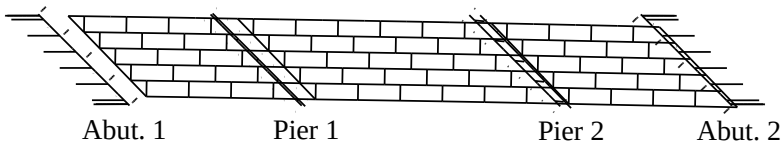

(d) Deformed bridge shape at the state with a 175-mm deck center displacement (deformation is magnified by 15 times)

Figure 5.35: Modal response of 3S45P15H bridge in longitudinal pushover analysis

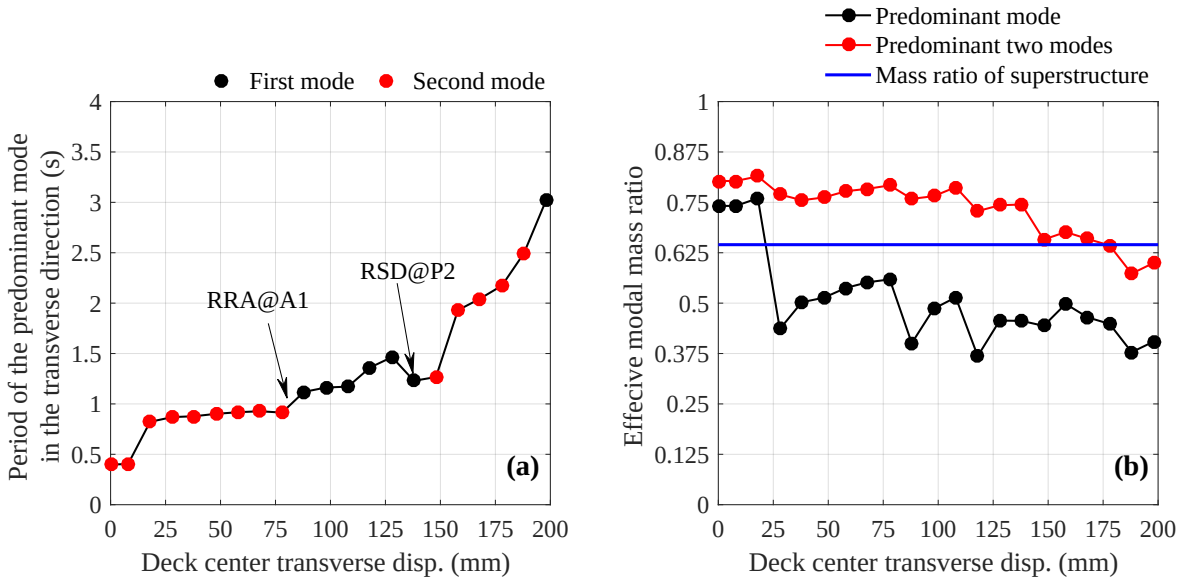

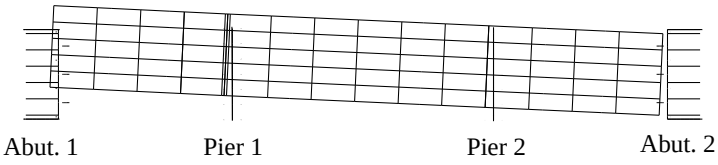

(c) The predominant mode shape (Mode 1) in the transverse direction at the state with a 200-mm deck center displacement

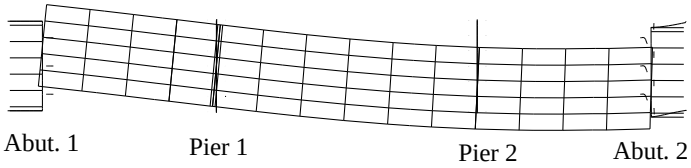

(d) The second predominant mode shape (Mode 3) in the transverse direction at the state with a 200-mm deck center displacement

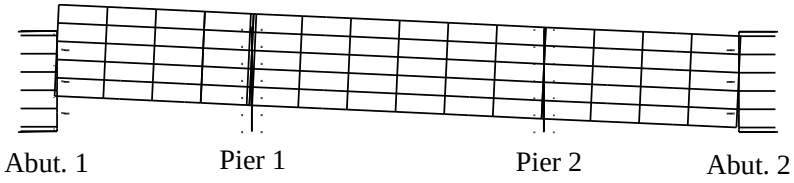

(e) Deformed bridge shape at the state with a 200-mm deck center displacement (deformation is magnified by 10 times)

Figure 5.36: Modal response of 3C00P15H bridge in transverse pushover analysis

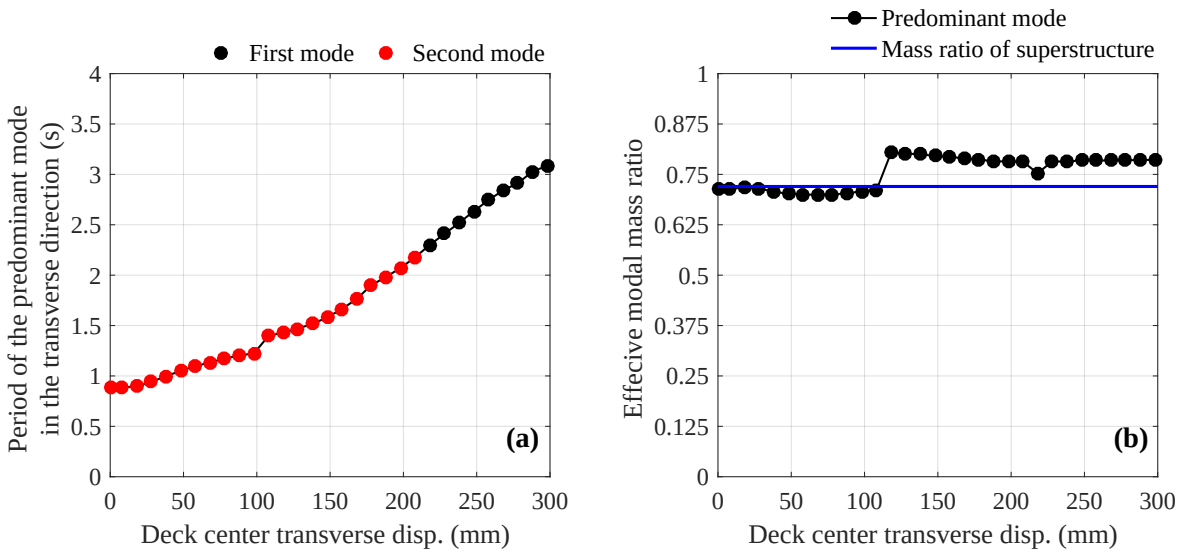

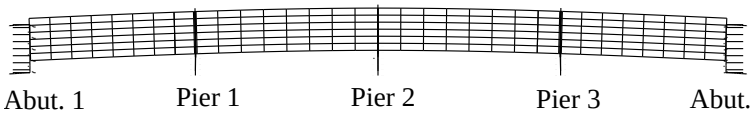

(c) The predominant mode shape (Mode 1) in the transverse direction at the state with a 300-mm deck center displacement

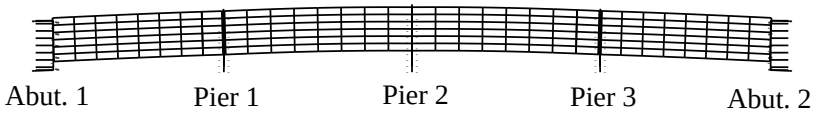

(d) Deformed bridge shape at the state with a 300-mm deck center displacement (deformation is magnified by 15 times)

Figure 5.37: Modal response of 4C00P40H bridge in transverse pushover analysis

5.5 Summary and Conclusions of Pushover and Modal Analyses

A series of multi-mode adaptive pushover analyses were conducted on the three-dimensional non-linear finite-element models of various prototype quasi-isolated bridge variants. The response characteristics of the quasi-isolated bridges, including force distribution among substructures, sequence of limit state occurrences, fusing performance of sacrificial superstructure-substructure connections, and vulnerability of critical bridge components, were investigated. In addition to the pushover analysis, multiple eigenvalue analyses were performed at different bridge deformation states in each pushover analysis. Through analyzing the bridge periods and mode shapes, several important modal response characteristics of the quasi-isolated bridges were highlighted.

5.5.1 Longitudinal pushover analyses

The following conclusions may be drawn from the pushover analyses performed in the longitudinal bridge direction:

- Closure of the expansion joint is a critical limit state that triggers significant redistribution of lateral forces among substructures. Before this limit state, the intermediate piers sustained most of the lateral force. After closure of the joint, the abutment that was pushed by the superstructure experienced much larger lateral force than the piers and the other abutment. The piles of this abutment typically yielded shortly after closure of the joint.

- For non-skew bridges, the abutment that was pushed by the superstructure provided much larger longitudinal resistance than the other substructures. For highly skewed bridges, due to the oblique contact between the deck end and abutment, the abutment resistance was smaller than that in the non-skew case and the fixed pier provided the largest resistance of all the substructures.

- For non-skew bridges, fusing of the sacrificial connections between the superstructure and fixed pier was not observed in any analysis. This undesired fusing performance typically resulted in global yielding of the short fixed pier columns. Due to the higher deflection capacity, the tall fixed pier columns elastically deflected, although their connections to

the superstructure were not fused, either. For some highly skewed bridges, fusing of the superstructure-fixed-pier connections was observed, but typically occurred after global yielding of the fixed pier columns. The expansion piers typically sustained less deflection and damage than the fixed piers.

- For highly skewed bridges, the deck end in the pushing direction sustained coupled longitudinal and transverse displacements due to the oblique contact with the abutment. The acute deck corner tended to drop off the abutment.
- The overall longitudinal stiffness of the four-span bridges is much larger than that of the counterpart three-span bridges. When pushed to a same superstructure displacement, larger forces were generally needed for the four-span bridges.
- The overall longitudinal stiffness of the PPC-girder bridge is slightly larger than that of the counterpart steel-plate-girder bridge.

5.5.2 Transverse pushover analyses

The following conclusions may be drawn from the pushover analyses performed in the transverse bridge direction:

- After fusing of the abutment bearing retainers, the acute deck corner of highly skewed bridges sustained large abutment-normal displacement and tended to drop off the abutment.
- Different from the bridge response in the longitudinal analyses, the piers typically withstood larger forces than the abutments in the transverse analyses.
- For the bridges with the hard foundation soil and short piers, fusing actions of the sacrificial connections occurred more in the transverse pushover analysis than in the longitudinal ones, primarily because of the lack of abutment resistance and the higher transverse stiffness of the intermediate piers.
- The soft foundation soil was unfavorable to the fusing action of sacrificial superstructure-substructure connections at both the piers and abutments. The tall pier columns were unfavorable to the fusing of sacrificial connections at the piers.

- Yielding of the substructure piles was commonly observed in the transverse pushover analyses. The substructure piles in the soft foundation soil typically yielded at a smaller superstructure pushover displacement than those in the hard soil.

- The three-span bridges are asymmetric about the midspan, and their retainer anchors at an abutment were typically fused first due to rotation of the bridge superstructure. In contrast, the four-span bridges are symmetric about the midspan, and their first fusing limit state occurred at the central fixed piers.

- Similar to the observation from longitudinal pushover analyses, the overall transverse stiffness of the four-span bridge is much larger than that of the counterpart three-span bridge. The overall transverse stiffness of the PPC-girder bridge is slightly larger than that of the counterpart steel-plate-girder bridge.

5.5.3 Modal analyses

The following conclusions regarding the modal characteristics of the quasi-isolated bridges may be drawn from the modal analyses conducted at elastic and inelastic bridge deformation states during the pushover analyses:

- The predominant mode (the mode with the largest effective modal mass) in the longitudinal or transverse direction was typically the first or second mode, regardless of the bridge deformation state. Consistently, the earthquake-resisting system design strategy is generally intended for common bridge types whose first mode of vibration dominates the seismic response (Tobias et al. 2008; IDOT 2012a).

- The period of the predominant mode was globally elongated as the pushover displacement increases, although there can be some local shortening effect along the way.

- In the longitudinal direction, the effective modal mass (effective modal mass ratio multiplied by the total mass of the bridge) of only the predominant mode is typically sufficient to incorporate, at least, the bridge superstructure mass. In the transverse direction, the effective modal mass of the predominant one or two modes can incorporate the superstructure mass.

CHAPTER 6

SEISMIC PERFORMANCE ASSESSMENT OF PROTOTYPE QUASI-ISOLATED BRIDGES VIA NONLINEAR DYNAMIC ANALYSES

6.1 Earthquake Ground Motion Time Histories

The earthquake ground motion time histories employed in this study were developed by modifying existing bedrock ground motions recorded from other geographic regions to match the site-specific hazard at Cairo, Illinois, which possesses the largest seismic hazard of the entire state (USGS 2015). The modification takes into account the regional seismicity and site condition of Cairo. The procedure for developing these ground motion time histories has been reported by Kozak et al. (2016) and is briefly reviewed herein.

Initially, 138 historical earthquake ground motions recorded at the bedrock were obtained from the NUREG/CR-6728 report (McGuire et al. 2001) and used as the source motions for modification. Subsequently, five conditional mean spectra (CMS) (Baker 2011) with different conditional periods (0.2, 0.3, 0.5, 1.0, and 2.0 seconds) were created for Cairo, Illinois with a selected seismic hazard level of 5% probability of exceedance in 50 years (1,000-year return period). This hazard level is consistent with the design earthquake with a 1,000-year return period that has been adopted by (AASHTO 2008b) since 2008. Four of the 138 source motions having the most similar spectral shapes with the CMS were selected and each of these four source motions was spectrally matched to the five CMS using a time-domain spectral matching program *RspMatch09* (Al Atik and Abrahamson 2010), thereby generating 20 modified ground motions. To account for the site condition, a shear wave velocity profile was developed from the boring logs of completed bridge construction projects at Cairo. Finally, one-dimensional ground response analyses were performed on the 20 modified ground motions using the nonlinear site response analysis platform *DEEPSOIL* (Hashash *et al.* 2015) and the shear wave velocity profile. As introduced in Section 3.4, a fixity depth of 6.1 m (20 ft) was used in the substructure foundation model. Therefore, the ground accel-

eration time histories at this fixity depth were generated by *DEEPSOIL* for the nonlinear dynamic bridge analyses in this study. The final output from *DEEPSOIL* were 20 ground acceleration time histories at a depth of 6.10 m (20 ft) from the ground surface, taking into account the regional seismic hazard and site condition at Cairo, Illinois. The 20 ground acceleration time histories are hereafter designated as Cro01, Cro02, ..., Cro20.

The 5%-damping elastic pseudo-acceleration response spectra of the 20 time histories were shown in Figure 6.1. Additionally, the peak ground acceleration (PGA), peak ground velocity (PGV), peak ground displacement (PGD), Arias Intensity, and predominant period of these ground motions are listed in Table 6.1. It can be found that the PGA of these ground motions is in the range of 30% to 40% of the gravitational acceleration (g, 9.81m/s^2). More information about the ground motions can be found in Appendix B.

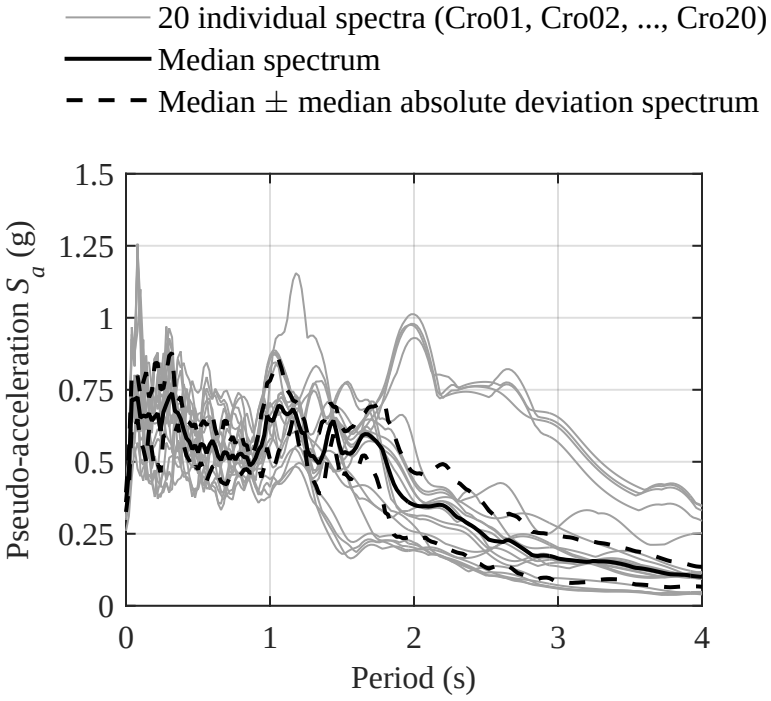

Figure 6.1: 5%-damping elastic pseudo-acceleration response spectra of seismic ground motions employed for nonlinear dynamic time-history analyses

In the subsequent nonlinear dynamic bridge analyses, the suite of 20 ground acceleration time histories was applied to each prototype bridge in four horizontal incident directions, namely the pure longitudinal (0°) and transverse (90°), 45°, and 135° directions. The four incident angles are measured from the longitudinal bridge axis, as illustrated in Figure 6.2. By acting on the nodal

Table 6.1: Parameters of earthquake ground motions employed for nonlinear dynamic bridge analyses

Individual ground motion	PGA (g)	PGV (m/s)	PGD (m)	Arias Intensity (m/s)	Predominant period (s)
Cro01	0.36	1.00	0.63	6.44	0.08
Cro02	0.40	0.45	0.25	5.69	0.22
Cro03	0.30	0.70	0.34	4.65	1.18
Cro04	0.31	0.47	0.12	2.26	0.30
Cro05	0.38	1.06	0.69	6.45	0.08
Cro06	0.39	0.44	0.26	5.02	0.32
Cro07	0.36	0.46	0.30	2.36	1.32
Cro08	0.31	0.32	0.12	2.34	0.30
Cro09	0.33	0.31	0.12	2.42	0.30
Cro10	0.26	0.45	0.31	2.18	1.36
Cro11	0.40	0.50	0.29	5.33	0.22
Cro12	0.38	1.10	0.72	6.40	0.08
Cro13	0.30	0.31	0.11	2.64	0.30
Cro14	0.35	0.44	0.20	4.30	0.12
Cro15	0.40	0.47	0.27	4.76	0.22
Cro16	0.38	1.06	0.70	6.38	0.08
Cro17	0.35	0.35	0.14	2.96	0.28
Cro18	0.35	0.45	0.20	4.37	0.12
Cro19	0.40	0.51	0.28	4.87	0.22
Cro20	0.39	0.71	0.36	6.21	0.10

masses of the finite-element bridge model, the ground motion time histories pose seismic inertia forces to bridge superstructures, substructures, and foundation piles.

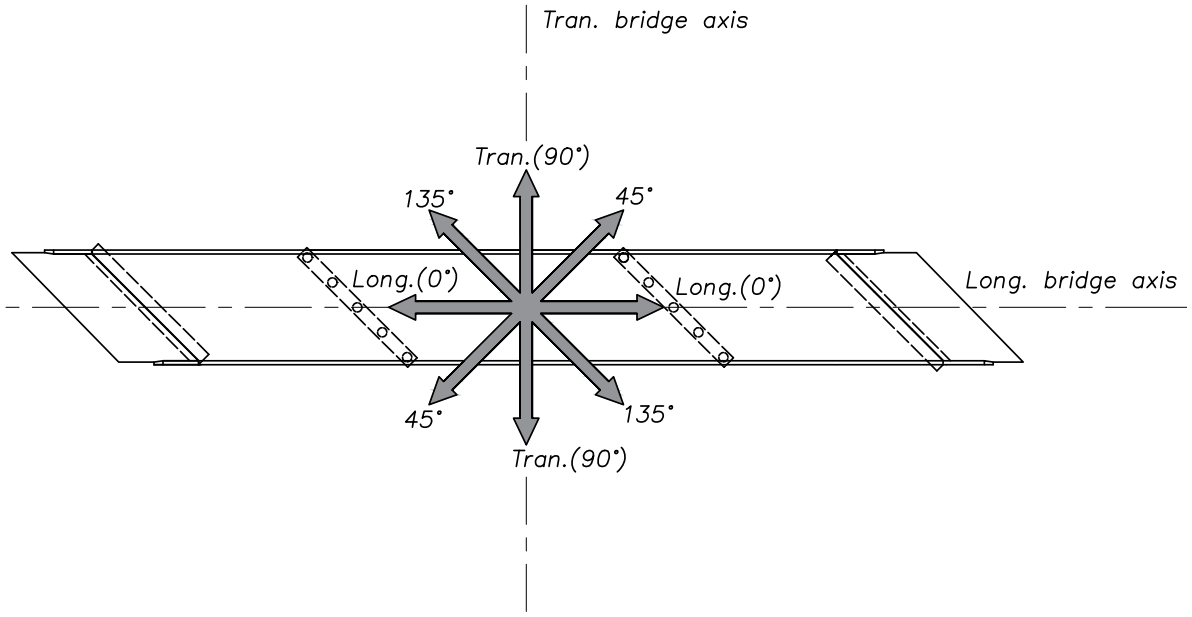

Figure 6.2: Four horizontal incident directions (0°, 45°, 90°, and 135°) of earthquake ground motion time histories for nonlinear dynamic bridge analyses

Effects of vertical ground acceleration are not included in the current study. As indicated by Zandieh and Pezeshk (2011), the observed average horizontal-to-vertical component spectral ratios suggest site amplification between 2 to 4 in the low-frequency range for the earthquakes in the New Madrid Seismic Zone. Furthermore, as indicated by Filipov et al. (2013b), the southern Illinois area is roughly 200 × 400 km north to the New Madrid Seismic Zone and the vertical ground acceleration attenuates quickly over this distance and is expected to have relatively small effect to the bridges in Southern Illinois.

6.2 Seismic Performance Assessment via Nonlinear Dynamic Analyses

6.2.1 Introduction

To provide a comprehensive and extensive assessment of seismic performance of the prototype quasi-isolated bridges, each of the 80 bridge variants was subjected to the suite of 20 earthquake ground motion time histories applied in the four horizontal incident directions, leading to 1,600 nonlinear dynamic analyses for each of the four major bridge types and 6,400 analyses in total for all the bridges.

In the nonlinear dynamic analyses, stiffness-proportional viscous damping was employed. At each step of a dynamic analysis, the viscous damping matrix is constructed using the tangential global stiffness matrix multiplied by a constant coefficient that was determined using a targeted viscous damping ratio for the fundamental mode and the initial elastic fundamental period of the bridge, according to Equation (6.1)

$$a = \frac{\zeta T_1^{(0)}}{\pi} \tag{6.1a}$$

$$\mathbf{C}^{(i)} = a\mathbf{K}^{(i)} \tag{6.1b}$$

where ζ is the targeted viscous damping ratio for the fundamental mode and $\zeta = 5\%$ was adopted in this study (AASHTO 2011); $T_1^{(0)}$ is the initial elastic fundamental period of the bridge; $\mathbf{C}^{(i)}$ and $\mathbf{K}^{(i)}$ are the viscous damping matrix and global stiffness matrix at the i-th step of the analysis, respectively. Pant et al. (2013) studied a number of schemes for constructing Rayleigh-type damping matrix by comparing the experimental and computed seismic response of a base-isolated RC building excited by a shake table. It was concluded that the stiffness-proportional damping with a constant coefficient determined using the frequency of the entire base-isolated building rather than the superstructure alone provides a reasonable estimate of the peak structural response. Use of tangential-stiffness-proportioned damping in nonlinear dynamic structural analyses was also recommended by Petrini et al. (2008) and Charney (2008), and, thus, it was adopted in this study.

In the nonlinear dynamic analyses, the equations of motion were solved by the Trapezoidal Rule

with the second-order Backward Difference Formula (TRBDF2) integration scheme proposed by Bathe (2007). It is a direct implicit time-integration scheme with second-order accuracy and unconditional stability. Different from the Newmark-β and HHT-α schemes, this scheme has no parameter to choose or adjust by the analyst. A five-millisecond default time step size was used in the analyses. At each time step, the Krylov Subspace accelerated Newton algorithm proposed by (Scott and Fenves 2010) was employed as the default iterative algorithm for solving the nonlinear system of equations. It was claimed by the developers that the algorithm has a larger radius of convergence and requires fewer matrix factorizations than the standard Newton's method. Consistent with these claimed advantages, it was observed that the algorithm typically outperformed the standard Newton's method in terms of computing speed and convergence performance in the dynamic bridge analyses. Whenever convergence difficulties were encountered at a time step, alternative iterative algorithms (e.g., the Newton's method with line search) and a smaller step size were relied upon to achieve convergence at this step. After the convergence was achieved, the default iterative algorithm and time step size were resumed in the next step.

Considering the large number of nonlinear dynamic analyses to perform, the supercomputer "Stampede" at the Texas Advanced Computing Center (TACC), the University of Texas at Austin, was utilized to process the computational jobs in parallel. The multi-processor interpreter of *OpenSees*, *OpenSeesMP* (McKenna and Fenves 2008), was complied and configured on Stampede for running analyses. Each standard computing node of Stampede is equipped with 16 CPU cores that can process 16 analyses in parallel without affecting the computing speed. Furthermore, multiple computing nodes can be requested for one multi-threaded job. In this study, each bridge variant was subjected to the suite of 20 ground motions applied in the four incident directions. Therefore, five computing nodes with 80 CPU cores in total were requested for one multi-threaded job in which all the 80 dynamic analyses of one bridge variant were included.

6.3 Statistical Summary of Bridge Seismic Response

The component limit states introduced in Section 5.2 were identified for each of the 6,400 nonlinear dynamic analyses and occurrences of these limit states were statistically studied. In addition to

the limit states, the peak values of some critical structural responses were also recorded in each analysis, such as the tensile strain of reinforcing steel and compressive strain of concrete cover at pier column bases as well as the displacement and rotation of bridge superstructures. For a specific structural response, the median of the 20 peak values excited by the 20 ground motions applied in the same incident direction was employed to statistically measure the response amplitude, as shown in Equation (6.2a)

$$\text{median}\,(u) = \underset{GM\,=\,\text{Cro01, ..., Cro20}}{\text{median}} \left(\max_{t} |u\,(t; GM)| \right) \tag{6.2a}$$

$$\text{MAD}\,(u) = \underset{GM\,=\,\text{Cro01, ..., Cro20}}{\text{median}} \left(\left| \max_{t} |u\,(t; GM)| - \text{median}\,(u) \right| \right) \tag{6.2b}$$

where $u\,(t; GM)$ denotes the time series of a specific structural response, $u(t)$, excited by a ground motion GM. The statistic measure determined by Equation (6.2a) is hereafter referred to as "median peak response". Because the bridge model is highly nonlinear and may sustain many damaging and rupture events in an analysis, some of the peak responses in a data set can be significantly distanced away from the other observations and are viewed as outliers. Therefore, the median was preferred over the mean in this study because the median is generally more robust against outliers than is the mean (Ryan 2006).

To measure the statistical dispersion of the response data, the median absolute deviation (MAD) was employed. As a robust statistic, the MAD is generally less sensitive to outliers than is the standard deviation (Sheskin 2011). For the standard deviation, the large deviations of outliers are heavily weighted and the more distanced the outliers are from the mean, the more the standard deviation is influenced. In contrast, for the MAD, deviations of a few outliers may not be influential at all because the median of deviation scores is used. The MAD of the peak values of a structural response u was calculated using Equation (6.2b).

Seismic response of the four major types of prototype bridges will be discussed in the rest of this section.

6.3.1 Three-span steel-plate-girder (3S) bridges

Superstructures of 3S bridges

Table 6.2 indicates the medians and median absolute deviations of the peak deck center displacements of 3S bridges excited by the 20 seismic ground motions applied in different incident directions. For skew 3S bridges, even though the ground motions were applied along one bridge axis, either longitudinally (0°) or transversely (90°), the deck center displacements were always excited along both bridge axes. This response characteristic is consistent with the observations from the pushover analyses. In general, the bi-axial deck displacement behavior of highly skewed 3S bridges are more significant than the those with smaller skews.

Table 6.2: Peak deck center displacements (units: mm) of 3S bridges (longitudinal and transverse displacements are placed on the left and right sides of the commas, respectively; numbers outside the parentheses are medians while those inside are median absolute deviations; for each bridge, the largest median peak displacement caused by the ground motions in the four incident directions is highlighted by bold numbers)

Foundation soil condition			Hard				Soft			
Pier column height (m)			4.57		12.19		4.57		12.19	
Longitudinal (0º) ground motions	Bridge skew (º)	0	**79** (4) , 0 (0)		**113** (14) , 0 (0)		**95** (8) , 0 (0)		**160** (29) , 0 (0)	
		15	**82** (6) , 17 (1)		**119** (14) , 24 (4)		**103** (9) , 15 (1)		**158** (22) , 32 (5)	
		30	**84** (6) , 27 (2)		**123** (15) , 57 (10)		**117** (10) , 20 (1)		**161** (20) , 57 (12)	
		45	**82** (6) , 28 (1)		**113** (19) , 78 (15)		**103** (9) , 24 (4)		**157** (23) , 71 (19)	
		60	**80** (11) , 22 (1)		**131** (22) , 91 (13)		**119** (16) , 26 (5)		**164** (31) , 44 (4)	
45º ground motions	Bridge skew (º)	0	68 (5) , 32 (4)		88 (7) , 58 (5)		76 (4) , 44 (5)		118 (8) , 76 (8)	
		15	70 (4) , 33 (3)		93 (11) , 68 (6)		77 (6) , 43 (3)		122 (15) , 83 (6)	
		30	73 (6) , 38 (4)		102 (13) , 90 (6)		87 (9) , 50 (4)		128 (17) , 99 (16)	
		45	65 (3) , 45 (5)		97 (13) , 111 (21)		66 (5) , 50 (6)		120 (23) , 115 (20)	
		60	61 (5) , 49 (7)		87 (24) , 126 (27)		55 (3) , 51 (8)		108 (21) , 128 (39)	
Transverse (90º) ground motions	Bridge skew (º)	0	1 (1) , **46** (6)		1 (0) , **110** (24)		1 (1) , **67** (8)		1 (0) , **132** (35)	
		15	22 (3) , **49** (8)		52 (5) , **118** (17)		20 (3) , **65** (8)		48 (4) , **140** (24)	
		30	33 (2) , **53** (10)		70 (6) , **129** (20)		23 (3) , **64** (9)		68 (6) , **145** (24)	
		45	38 (5) , **57** (10)		70 (10) , **121** (19)		21 (4) , **63** (8)		71 (16) , **138** (29)	
		60	30 (3) , **58** (8)		62 (6) , **131** (29)		15 (4) , **67** (11)		70 (15) , **148** (30)	
135º ground motions	Bridge skew (º)	0	67 (6) , 32 (4)		87 (7) , 56 (5)		77 (4) , 44 (5)		118 (9) , 75 (7)	
		15	66 (4) , 38 (5)		103 (7) , 70 (11)		91 (8) , 48 (6)		121 (9) , 86 (16)	
		30	65 (7) , 45 (6)		105 (19) , 109 (16)		103 (9) , 50 (5)		129 (23) , 109 (19)	
		45	53 (6) , 52 (7)		106 (16) , 94 (15)		96 (15) , 58 (7)		127 (28) , 108 (19)	
		60	48 (6) , 44 (7)		120 (12) , 90 (10)		81 (12) , 55 (7)		118 (26) , 109 (20)	

The longitudinal and transverse median peak displacements excited by the bi-axial (45° and 135°) ground motions were always quite comparable to each other, but either component was smaller than that excited by the uni-axial ground motions. In other words, uni-axial ground motions

were more critical for exciting large deck displacements along the two bridge axes than the bi-axial ones, as highlighted in Table 6.2. This response characteristic was also observed in the prior phase of the research project (LaFave et al. 2013b; Filipov et al. 2013b). The smaller displacements excited by the bi-axial ground motions can be largely attributed to the fact that the bi-axial motions caused 29% (1-cos 45°) smaller seismic force along either bridge axis than the uni-axial motions.

It can be noted in Table 6.2 that 3S bridges supported by tall pier columns experienced much larger peak deck displacements than their short-pier equivalents, regardless of the ground motion direction. In general, 3S bridges in the soft foundation soil experienced larger peak deck displacements than those in the hard soil.

In addition to the deck displacements, the peak in-plane deck rotations of 3S bridges were studied and their medians and median absolute deviations are listed in Table 6.3. The "counter-clockwise" direction referred to in the table and accompanying text is illustrated in Figure 6.3. It can be found that in all of the tabulated cases, the median peak rotations in either direction were smaller than 1°. Another important observation is that for each left-skewed 3S bridge (the skew direction in this study is solely to the left), the peak clockwise deck rotation was always larger than the counterclockwise. This characteristic is consistent with the in-plane rotational response and predominant mode shape of skew bridges discussed in Chapter 5. It can be seen in Table 6.3 that the clockwise rotations of highly skewed (45° and 60°) 3S bridges were generally larger than those of 3S bridges with smaller skews. However, the counterclockwise rotations might increase, stay the same or even decreases as bridge skew increased, depending on the particular combination of bridge variant and ground motion direction in the table.

Figure 6.3 explains the reason why the clockwise deck rotation is more significant than the counterclockwise rotation. As shown in Figure 6.3a, when the bridge is subjected to a longitudinal seismic force to the right, the deck tends to contact with the right abutment after closure of the expansion joint. In this situation, the resultant force R of the normal contact force R_n and tangential friction R_t between the right deck end and abutment backwall tends to cause the acute corner of the right deck end to move away from the abutment and may result in a clockwise deck rotation. This trend can also be explained by an analogy of a skew mass block sliding on a slope under the gravity load, as shown in Figure 6.3a. If the frictional resistance is larger enough, the skew block may stay on the slope; if the friction is insufficient, the skew block will slide down the slope.

Table 6.3: Peak deck rotations (units: 0.01°) of 3S bridges (data for clockwise and counterclockwise rotations are placed on the left and right sides of the commas, respectively; numbers outside the parentheses are medians while those inside are median absolute deviations; for each bridge, the largest median peak rotation caused by the ground motions in the four incident directions is highlighted by bold numbers)

Foundation soil condition			Hard				Soft			
Pier column height (m)			4.57		12.19		4.57		12.19	
Longitudinal (0º) ground motions	Bridge skew (º)	0	0 (0) , 0 (0)		0 (0) , 0 (0)		0 (0) , 0 (0)		0 (0) , 0 (0)	
		15	4 (0) , 4 (0)		7 (1) , 4 (0)		4 (0) , 3 (0)		9 (1) , 5 (1)	
		30	6 (1) , 5 (1)		19 (5) , 6 (1)		7 (1) , 3 (0)		15 (5) , 5 (1)	
		45	7 (1) , 4 (1)		28 (14) , 8 (1)		7 (1) , 3 (0)		22 (8) , 5 (1)	
		60	6 (1) , 3 (0)		28 (11) , 7 (2)		4 (1) , 2 (0)		13 (2) , 4 (1)	
45º ground motions	Bridge skew (º)	0	7 (1) , 7 (2)		8 (1) , 8 (1)		6 (1) , 6 (1)		8 (1) , 8 (0)	
		15	7 (1) , 7 (1)		10 (1) , 8 (1)		7 (1) , 6 (1)		10 (1) , 7 (1)	
		30	8 (1) , 6 (1)		20 (3) , 7 (1)		7 (0) , 6 (1)		23 (6) , 8 (1)	
		45	8 (1) , 6 (1)		31 (9) , 5 (1)		7 (1) , 5 (1)		34 (9) , 4 (1)	
		60	8 (1) , 5 (1)		38 (13) , 5 (1)		7 (1) , 5 (1)		41 (10) , 4 (0)	
Transverse (90º) ground motions	Bridge skew (º)	0	**13** (5) , **13** (4)		**30** (5) , **33** (9)		**10** (2) , **10** (2)		**29** (16) , **27** (14)	
		15	**15** (4) , **15** (4)		**31** (4) , **29** (4)		**10** (2) , **10** (3)		**32** (10) , **21** (6)	
		30	**15** (3) , **15** (3)		**32** (5) , **22** (3)		**11** (2) , **11** (2)		**34** (7) , **19** (4)	
		45	**14** (3) , **13** (2)		**34** (4) , 15 (2)		**13** (2) , **11** (1)		**33** (7) , 11 (1)	
		60	**13** (2) , **9** (1)		**40** (10) , 9 (1)		**15** (3) , **10** (1)		**40** (7) , 8 (0)	
135º ground motions	Bridge skew (º)	0	7 (1) , 8 (1)		9 (1) , 9 (2)		6 (1) , 5 (1)		8 (1) , 8 (1)	
		15	9 (2) , 9 (1)		18 (4) , 15 (4)		7 (1) , 6 (1)		12 (2) , 9 (1)	
		30	11 (2) , 10 (2)		31 (5) , 20 (1)		6 (1) , 5 (1)		25 (8) , 18 (5)	
		45	13 (3) , 11 (1)		26 (4) , **15** (1)		7 (1) , 6 (1)		26 (6) , **14** (2)	
		60	12 (2) , 9 (1)		25 (3) , **12** (0)		8 (2) , 6 (1)		26 (5) , **10** (2)	

However, no matter how much is the friction on the slope, the block will not slide upward on the slope. Similarly, if the friction between the right deck end and abutment backwall as well as the bearing retainer resistance is large enough, the right deck end is restrained from moving away from the abutment; if the resistance is insufficient, the acute deck corner tends to move away from the abutment and the deck tends to rotate clockwisely. However, as long as the bridge is subjected to a pure longitudinal seismic force and the expansion joint is closed, the bridge deck is unlikely to rotate in the counterclockwise direction. Figure 6.3b illustrates the situation in which the deck is subjected to a seismic force to the left. The deck also tends to rotate clockwisely.

Additionally, Figure 6.4 illustrates the rotational behavior of bridges subjected to transverse seismic forces. As shown in Figure 6.4a, when the bridge is subjected to an upward seismic force, the expansion joint at the right abutment tends to be closed. At this joint, in addition to the resistance of bearing retainers, the contact between the deck end and backwall restrains the upward displacement of the deck end through the resultant R of the normal contact force R_n and the tangential friction R_t. In contrast, at the left abutment, the expansion joint tends to stay open and become wider, and the abutment backwall does not restrain the upward displacement of the left deck end. At this joint, the only major restraint for the deck is from the bearing retainers. Therefore, the trend of clockwise deck rotation is more significant than the counterclockwise rotation. Figure 6.4b illustrates a similar trend for the bridge subjected to a downward seismic force.

Consistent with the above analysis, field reconnaissance of the 2010 Chile earthquake indicates that all of the four left skew bridges (the skew direction in this study) that was observed during the reconnaissance experienced clockwise deck rotation and their acute deck corners tended to drop off the abutment (Yen et al. 2011). As an example for this behavior, Fig. 6.5 shows the collapse of a 40°-left-skew bridge during the 2010 Chile earthquake. The failure pattern of the two curtain walls at one abutment demonstrated that the acute deck corner knocked off the curtain wall adjacent to it and dropped off from the abutment, which caused the entire superstructure unseating and global collapse of the bridge, while the curtain wall adjacent to the obtuse deck corner was intact. This observed seismic behavior of skew bridges is generally consistent with the rotational bridge response in this study.

Similar to its effect on the deck displacements, the pier column height is also a critical factor affecting the deck rotations. As can be seen in Table 6.3, tall-pier 3S bridges rotated more than

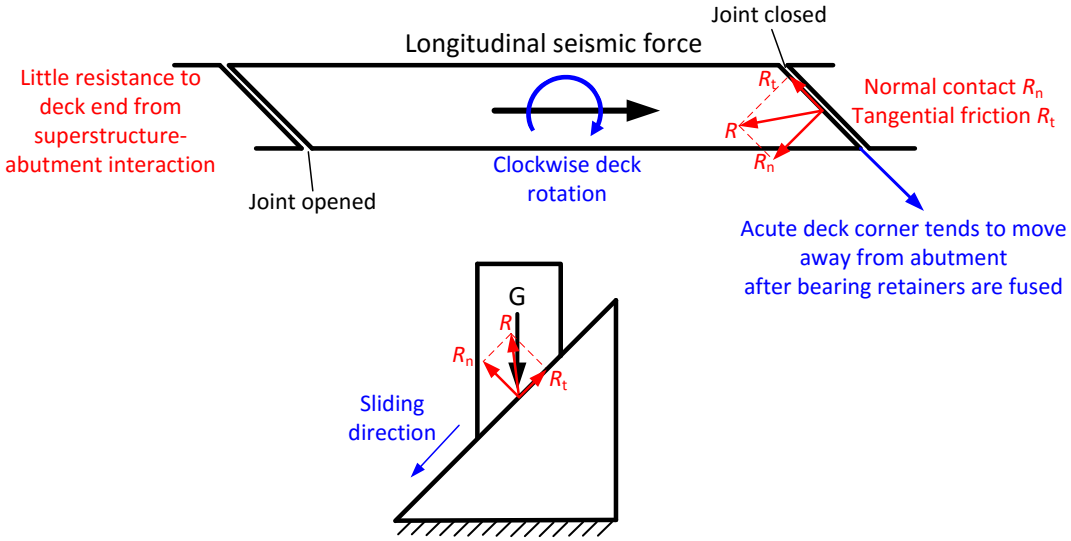

(a) Right seismic force

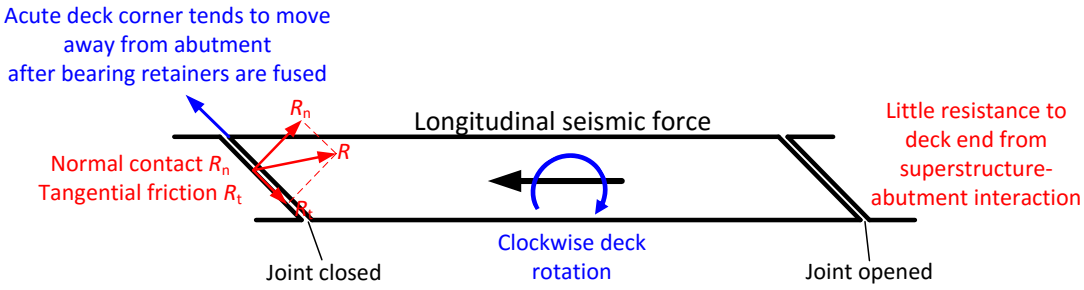

(b) Left seismic force

Figure 6.3: Rotation of bridge superstructure subjected to longitudinal seismic forces

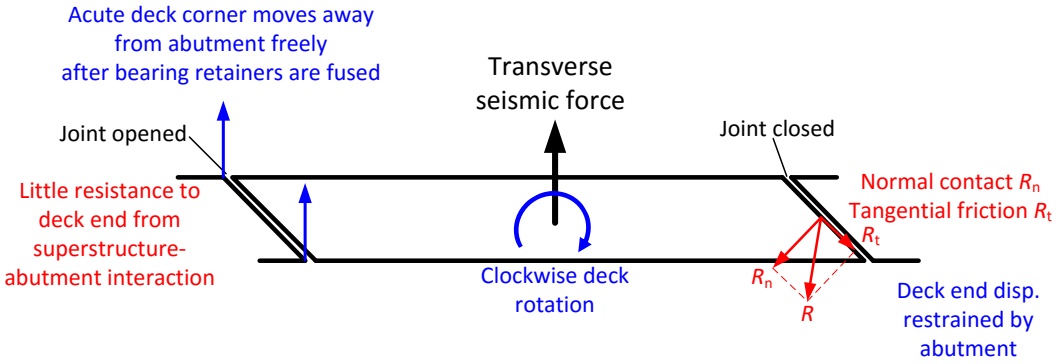

(a) Upward seismic force

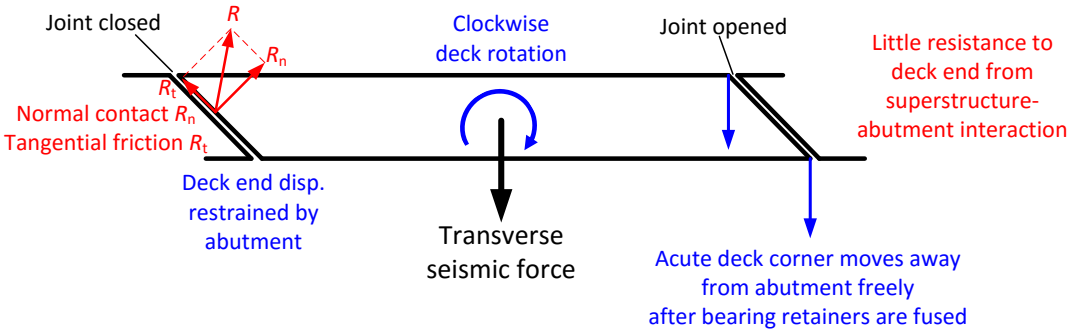

(b) Downward seismic force

Figure 6.4: Rotation of bridge superstructure subjected to transverse seismic forces

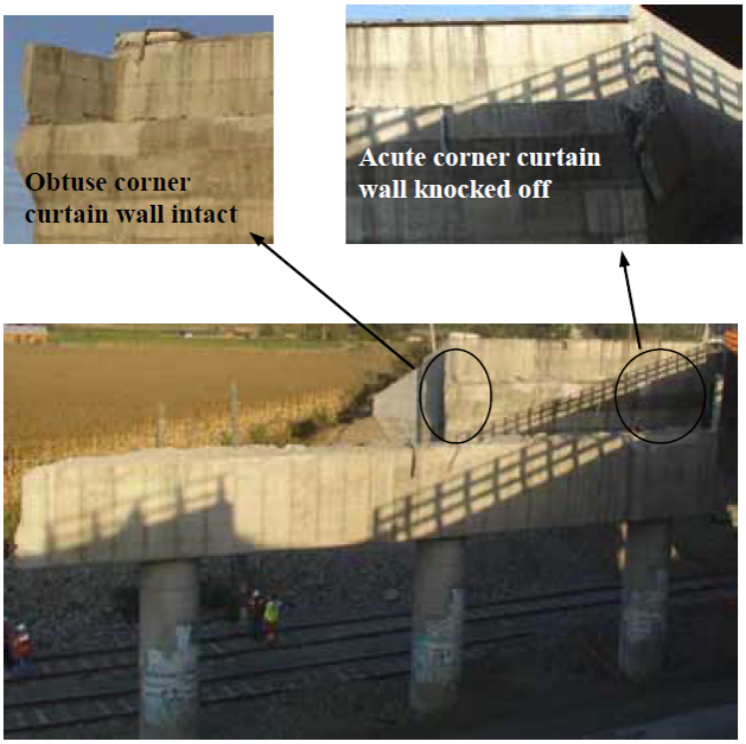

Figure 6.5: Collapse of Route 5 overcrossing at Hospital during the 2010 Chile earthquake (after Yen et al. 2011)

their short-pier equivalents in both the clockwise and counterclockwise directions. The largest clockwise rotations for different ground motion directions were always experienced by 60°-skew, tall-pier 3S bridge variants. As highlighted in the table, for most 3S bridges, the maximum median peak rotation was typically caused by the transverse ground motions as compared to those in the other directions, except that the 135° ground motions caused the maximum median peak rotation of a few highly skewed bridges supported by tall piers. The influence of foundation soil condition on the deck rotations appeared to be insignificant for 3S bridges.

Full data of limit state occurrences for 3S bridges

Table 6.4 lists the full data of component limit state occurrences for each of the 20 3S bridge variants, when subjected to the suite of 20 seismic ground motions applied in the four different incident directions. Each percentage in the table indicates the number of analyses with occurrences of a limit state out of the 20 analyses with the 20 ground motions applied to a bridge variant in one incident direction. For example, the percentage of occurrence of CEJ (closure of expansion joint) at Abutment 1 of the 3S00P15H bridge variant when subjected to the pure longitudinal ground motions (0°) is 100%, as shown in Table 6.4. This percentage means that closure of the expansion joint at Abutment 1 was observed in all of the 20 analyses performed on the 3S00P15H bridge with the longitudinal ground motions. Three gradient color scales, blue, yellow, and red, were used in conjunction with the percentages in Table 6.4 to highlight the occurrences of the preferred, acceptable, and unacceptable limit states defined in Table 5.1.

The data listed in Table 6.4 were subsequently grouped by bridge substructures, namely the two abutments, one expansion pier, and one fixed pier. For the substructure groups, the data in Table 6.4 were further analyzed and their statistical summaries are presented in Tables 6.5, 6.7, and 6.11.

Table 6.4: Limit state occurrences of each 3S bridge variant under 0° and 45° ground motions (each percentage indicates the number of analyses with occurrences of a limit state out of the 20 analyses with the ground motions applied to a bridge variant in an incident direction)

Ground motion direction	Bridge variant	Critical limit states																												
		Abutment 1 (A1)									Pier 1 (P1, expansion pier)						Pier 2 (P2, fixed pier)					Abutment 2 (A2)								
		CEJ	MBU	FBP	RRA	SEB	UBA	UBO	YPW	YPB	RRA	SEB	UEB	YRS	CCC	YPP	RFA	USB	YRS	CCC	YPP	CEJ	MBU	FBP	RRA	SEB	UBO	UBA	YPW	YPB
0°	3S00P15H	100%	0	0	0	0	0	0	100%	95%	0	0	0	0	0	0	0	0	100%	0	0	100%	0	0	0	0	0	0	100%	70%
	3S15P15H	100%	0	0	0	0	0	0	100%	95%	0	0	0	0	0	0	0	0	100%	0	0	100%	0	0	0	0	0	0	100%	100%
	3S30P15H	100%	0	0	0	0	0	0	100%	95%	0	0	0	0	0	0	0	0	100%	5%	0	100%	0	0	0	0	0	0	100%	100%
	3S45P15H	100%	0	0	0	0	0	0	100%	45%	0	0	0	0	0	0	60%	0	100%	0	45%	100%	0	0	0	0	0	0	100%	90%
	3S60P15H	100%	0	0	0	0	0	0	10%	0	0	0	0	0	0	0	100%	0	10%	0	75%	100%	0	0	0	0	0	0	35%	0
	3S00P40H	100%	0	0	0	35%	0	0	100%	95%	0	0	0	5%	0	0	0	0	0	0	0	100%	0	0	0	30%	0	0	100%	95%
	3S15P40H	100%	0	0	0	50%	0	0	100%	100%	0	0	0	5%	0	0	0	0	0	0	0	100%	0	0	0	40%	0	0	100%	100%
	3S30P40H	100%	0	0	65%	45%	0	0	100%	100%	0	0	0	5%	0	0	0	0	25%	0	0	100%	0	0	65%	60%	0	0	100%	100%
	3S45P40H	100%	0	0	75%	60%	0	0	100%	80%	0	0	0	0	0	0	0	0	35%	0	0	100%	0	0	75%	70%	0	0	100%	90%
	3S60P40H	100%	0	0	90%	65%	0	0	100%	40%	0	0	0	5%	0	0	10%	0	60%	0	40%	100%	0	0	80%	75%	0	0	100%	75%
	3S00P15S	100%	0	0	0	0	0	0	75%	75%	0	0	0	0	0	0	0	0	100%	0	0	100%	0	0	0	0	0	0	80%	60%
	3S15P15S	100%	0	0	0	0	0	0	85%	95%	0	0	0	0	0	0	0	0	100%	0	15%	100%	0	0	0	0	0	0	95%	100%
	3S30P15S	100%	0	0	0	0	0	0	90%	90%	0	0	0	0	0	0	0	0	100%	15%	90%	100%	0	0	0	0	0	0	95%	100%
	3S45P15S	100%	0	0	0	0	0	0	65%	80%	0	0	0	0	0	0	0	0	80%	0	100%	100%	0	0	0	0	0	0	70%	95%
	3S60P15S	100%	0	0	0	5%	0	0	30%	30%	0	0	0	0	0	0	30%	0	0	0	100%	100%	0	0	5%	10%	0	0	25%	35%
	3S00P40S	100%	25%	0	0	70%	0	0	100%	100%	0	0	0	25%	0	0	0	0	35%	0	0	100%	15%	0	0	75%	0	0	100%	100%
	3S15P40S	100%	25%	0	0	80%	0	0	100%	100%	0	0	0	15%	0	0	0	0	40%	0	0	100%	15%	0	0	80%	0	0	100%	100%
	3S30P40S	100%	0	0	20%	80%	0	0	100%	100%	0	0	0	0	0	0	0	0	55%	0	5%	100%	5%	0	35%	100%	0	0	100%	100%
	3S45P40S	100%	0	0	45%	70%	0	0	100%	100%	0	0	0	0	0	0	0	0	40%	0	80%	100%	0	0	65%	80%	0	0	100%	100%
	3S60P40S	100%	0	0	0	60%	0	0	90%	100%	0	0	0	0	0	30%	0	0	20%	0	100%	100%	0	0	0	80%	0	0	95%	95%
45°	3S00P15H	100%	0	0	0	0	0	0	95%	70%	0	0	0	0	0	0	0	0	100%	0	0	100%	0	0	0	0	0	0	100%	30%
	3S15P15H	100%	0	0	0	0	0	0	100%	80%	0	0	0	0	0	0	0	0	100%	0	0	100%	0	0	0	0	0	0	100%	75%
	3S30P15H	100%	0	0	0	0	0	0	100%	85%	0	0	0	0	0	0	0	0	100%	0	0	100%	0	0	0	0	0	0	100%	85%
	3S45P15H	100%	0	0	0	0	0	0	100%	65%	0	0	0	0	0	0	0	0	100%	0	0	100%	0	0	20%	0	0	0	100%	80%
	3S60P15H	100%	0	0	0	0	0	0	60%	5%	0	0	0	0	0	0	30%	0	80%	0	0	100%	0	0	0	0	0	0	70%	30%
	3S00P40H	100%	0	0	15%	0	0	0	100%	95%	0	0	0	0	0	0	0	0	0	0	0	100%	0	0	0	0	0	0	100%	100%
	3S15P40H	100%	0	0	45%	5%	0	0	100%	100%	0	0	0	5%	0	0	0	0	0	0	0	100%	0	0	35%	0	0	0	100%	100%
	3S30P40H	100%	0	0	80%	35%	0	0	100%	100%	0	0	0	5%	0	0	0	0	10%	0	0	100%	0	0	85%	50%	0	0	100%	100%
	3S45P40H	100%	0	0	90%	75%	0	0	100%	95%	0	0	0	20%	0	0	0	0	40%	0	0	100%	0	0	95%	80%	0	0	100%	85%
	3S60P40H	100%	0	0	75%	75%	0	0	100%	80%	0	0	0	50%	0	0	0	0	75%	0	0	100%	0	0	90%	80%	0	0	100%	75%
	3S00P15S	100%	0	0	0	0	0	0	10%	70%	0	0	0	0	0	10%	0	0	100%	0	75%	100%	0	0	0	0	0	0	25%	50%
	3S15P15S	100%	0	0	0	0	0	0	40%	60%	0	0	0	0	0	0	0	0	100%	0	5%	100%	0	0	0	0	0	0	45%	40%
	3S30P15S	100%	0	0	0	0	0	0	65%	65%	0	0	0	0	0	0	0	0	100%	0	0	100%	0	0	0	0	0	0	70%	75%
	3S45P15S	100%	0	0	5%	0	0	0	30%	55%	0	0	0	0	0	0	0	0	95%	0	5%	100%	0	0	0	0	0	0	25%	40%
	3S60P15S	100%	0	0	10%	0	0	0	0	10%	0	0	0	0	0	0	0	0	40%	0	0	100%	0	0	0	0	0	0	5%	15%
	3S00P40S	100%	0	0	0	5%	0	0	100%	100%	0	0	0	5%	0	65%	0	0	5%	0	15%	100%	0	0	0	10%	0	0	100%	100%
	3S15P40S	100%	0	0	20%	40%	0	0	100%	100%	0	0	0	5%	0	10%	0	0	10%	0	5%	100%	0.05	0	5%	40%	0	0	100%	100%
	3S30P40S	100%	5%	0	70%	70%	0	0	100%	100%	0	0	0	10%	0	0	0	0	35%	0	0	100%	0	0	55%	55%	0	0	100%	100%
	3S45P40S	100%	0	0	85%	75%	0	0	100%	100%	0	0	0	30%	0	0	0	0	60%	0	0	100%	0	0	90%	80%	0	0	100%	100%
	3S60P40S	100%	0	0	75%	75%	0	0	90%	100%	0	0	0	35%	0	0	0	0	75%	0	0	100%	0	0	80%	80%	0	0	75%	90%

Preferred limit states:	0	20%	40%	60%	80%	100%
Acceptable limit states:	0	20%	40%	60%	80%	100%
Unacceptable limit states:	0	20%	40%	60%	80%	100%

Table 6.4 Continued: limit state occurrences of each 3S bridge variant under 90° and 135° ground motions

Ground motion direction	Bridge variant	Critical limit states																												
		Abutment 1 (A1)									Pier 1 (P1, expansion pier)						Pier 2 (P2, fixed pier)					Abutment 2 (A2)								
		CEJ	MBU	FBP	RRA	SEB	UBA	UBO	YPW	YPB	RRA	SEB	UEB	YRS	CCC	YPP	RFA	USB	YRS	CCC	YPP	CEJ	MBU	FBP	RRA	SEB	UBO	UBA	YPW	YPB
90°	3S00P15H	0	0	0	50%	5%	0	0	0	5%	0	0	0	0	0	0	0	0	0	0	15%	0	0	0	0	0	0	0	0	0
	3S15P15H	60%	0	0	65%	10%	0	0	0	15%	0	0	0	0	0	5%	0	0	0	0	20%	5%	0	0	0	0	0	0	0	0
	3S30P15H	95%	0	0	80%	15%	0	0	35%	40%	0	0	0	0	0	0	0	0	5%	0	15%	25%	0	0	5%	0	0	0	0	0
	3S45P15H	100%	0	0	70%	15%	0	0	35%	15%	0	0	0	5%	0	0	0	0	0	0	10%	90%	0	0	5%	0	0	0	0	0
	3S60P15H	100%	0	0	55%	10%	0	0	40%	5%	0	0	0	5%	0	0	0	0	10%	0	0	95%	0	0	0	0	0	0	0	0
	3S00P40H	0	0	0	100%	85%	0	0	0	0	0	0	0	65%	0	65%	0	0	15%	0	10%	0	0	0	55%	10%	0	0	0	5%
	3S15P40H	100%	0	0	100%	100%	0	0	70%	55%	0	0	0	70%	0	60%	0	0	20%	0	5%	100%	0	0	60%	10%	0	0	5%	5%
	3S30P40H	100%	0	0	100%	100%	0	0	100%	95%	0	0	0	60%	0	10%	0	0	50%	0	5%	100%	0	0	90%	40%	0	0	75%	50%
	3S45P40H	100%	0	0	100%	100%	0	0	100%	90%	0	0	0	25%	0	0	0	0	15%	0	0	100%	0	0	90%	35%	0	0	95%	40%
	3S60P40H	100%	0	0	100%	80%	0	0	95%	80%	0	0	0	60%	0	0	0	0	35%	0	0	100%	0	0	80%	75%	0	0	75%	45%
	3S00P15S	0	0	0	25%	5%	0	0	0	15%	0	0	0	0	0	95%	0	0	0	0	100%	0	0	0	0	0	0	0	0	0
	3S15P15S	10%	0	0	35%	5%	0	0	0	20%	0	0	0	0	0	95%	0	0	0	0	95%	5%	0	0	0	0	0	0	0	0
	3S30P15S	60%	0	0	40%	0	0	0	0	20%	0	0	0	0	0	70%	0	0	0	0	45%	10%	0	0	0	0	0	0	0	0
	3S45P15S	100%	0	0	65%	15%	0	0	0	20%	0	0	0	0	0	10%	0	0	0	0	25%	40%	0	0	5%	0	0	0	0	0
	3S60P15S	100%	0	0	70%	20%	0	0	0	15%	0	0	0	10%	0	0	0	0	0	0	0	95%	0	0	20%	0	0	0	0	0
	3S00P40S	0	0	0	90%	65%	0	0	0	60%	0	0	0	35%	0	90%	0	0	10%	0	85%	0	0	0	30%	10%	0	0	0	60%
	3S15P40S	95%	0	0	90%	80%	0	0	0	75%	0	0	0	40%	0	95%	0	0	10%	0	95%	90%	0	0	40%	25%	0	0	0	65%
	3S30P40S	100%	0	0	95%	85%	0	0	35%	90%	0	0	0	60%	0	90%	0	0	25%	0	85%	100%	0	0	70%	35%	0	0	0	80%
	3S45P40S	100%	0	0	100%	100%	0	0	65%	100%	0	0	0	15%	0	55%	0	0	10%	0	75%	100%	0	0	85%	50%	0	0	35%	60%
	3S60P40S	100%	0	0	100%	90%	0	0	65%	95%	0	0	0	50%	0	0	0	0	45%	0	35%	100%	0	0	85%	75%	0	0	55%	70%
135°	3S00P15H	100%	0	0	0	0	0	0	100%	55%	0	0	0	0	0	0	0	0	100%	0	0	100%	0	0	0	0	0	0	90%	45%
	3S15P15H	100%	0	0	15%	5%	0	0	65%	30%	0	0	0	0	0	0	0	0	100%	0	10%	100%	0	0	0	0	0	0	80%	20%
	3S30P15H	100%	0	0	30%	5%	0	0	20%	5%	0	0	0	0	0	0	0	0	90%	0	40%	100%	0	0	5%	0	0	0	40%	0
	3S45P15H	90%	0	0	45%	5%	0	0	0	5%	0	0	0	0	0	0	20%	0	5%	0	65%	100%	0	0	5%	0	0	0	5%	0
	3S60P15H	90%	0	0	35%	5%	0	0	0	0	0	0	0	0	0	0	45%	0	0	0	25%	100%	0	0	0	0	0	0	0	0
	3S00P40H	100%	0	0	25%	0	0	0	100%	100%	0	0	0	0	0	0	0	0	0	0	0	100%	0	0	0	0	0	0	100%	95%
	3S15P40H	100%	0	0	85%	40%	0	0	100%	100%	0	0	0	20%	0	10%	0	0	5%	0	0	100%	0	0	15%	5%	0	0	100%	100%
	3S30P40H	100%	0	0	100%	95%	0	0	80%	35%	0	0	0	60%	0	25%	0	0	70%	0	5%	100%	0	0	100%	45%	0	0	95%	80%
	3S45P40H	100%	0	0	100%	95%	0	0	15%	15%	0	0	0	20%	0	15%	0	0	75%	0	55%	100%	0	0	85%	30%	0	0	75%	55%
	3S60P40H	100%	0	0	100%	80%	0	0	10%	35%	0	0	0	10%	0	0	60%	0	75%	0	65%	100%	0	0	40%	20%	0	0	20%	0
	3S00P15S	100%	0	0	0	0	0	0	30%	80%	0	0	0	0	0	10%	0	0	100%	0	75%	100%	0	0	0	0	0	0	10%	50%
	3S15P15S	100%	0	0	0	0	0	0	60%	85%	0	0	0	0	0	50%	0	0	100%	0	100%	100%	0	0	0	0	0	0	45%	80%
	3S30P15S	100%	0	0	0	0	0	0	65%	70%	0	0	0	0	0	50%	0	0	95%	0	100%	100%	0	0	0	0	0	0	55%	65%
	3S45P15S	100%	0	0	0	0	0	0	15%	15%	0	0	0	0	0	50%	0	0	0	0	100%	100%	0	0	5%	0	0	0	20%	25%
	3S60P15S	100%	0	0	25%	0	0	0	0	0	0	0	0	0	0	5%	0	0	0	0	95%	85%	0	0	0	0	0	0	0	0
	3S00P40S	100%	0	0	0	10%	0	0	100%	100%	0	0	0	5%	0	60%	0	0	5%	0	20%	100%	0	0	0	5%	0	0	100%	100%
	3S15P40S	100%	0	0	60%	25%	0	0	95%	100%	0	0	0	5%	0	80%	0	0	5%	0	80%	100%	0	0	5%	15%	0	0	100%	100%
	3S30P40S	100%	0	0	95%	65%	0	0	45%	90%	0	0	0	35%	0	75%	0	0	40%	0	80%	100%	0	0	25%	30%	0	0	80%	80%
	3S45P40S	100%	0	0	100%	70%	0	0	10%	45%	0	0	0	5%	0	75%	0	0	10%	0	100%	100%	0	0	35%	35%	0	0	35%	65%
	3S60P40S	100%	0	0	100%	80%	0	0	30%	75%	0	0	0	0	0	70%	0	0	10%	0	95%	100%	0	0	35%	35%	0	0	5%	20%
Preferred limit states:		0	20%	40%	60%	80%	100%																							
Acceptable limit states:		0	20%	40%	60%	80%	100%																							
Unacceptable limit states:		0	20%	40%	60%	80%	100%																							

Abutments of 3S bridges

The occurrences of several critical component limit states at the abutments of 3S bridges were statistically studied and the results are summarized in Table 6.5. For each limit state, the number of analyses with its occurrences and the percentage of these analyses out of all the 1,600 3S bridge analyses are listed in the second column of the table. Additionally, the parameter space, including the five skew angles, two foundation soil conditions, two pier column heights, and four ground motion incident directions, was studied for its effect on the limit state occurrence, by comparing the relative contribution of each parametric variation to the total occurrences. For example, the first limit state in Table 6.5, closure of the expansion joint at Abutment 1, was observed in 1,480 out of all the 1,600 analyses, which resulted in an occurrence percentage of 93%. 240 out of these 1,480 analyses were performed on non-skew 3S bridges and, thus, the contribution of non-skew 3S bridges to the total occurrences of this limit state is 16% $(240/1,480)$.

Closure of the expansion joints at Abutments 1 and 2 of 3S bridges (CEJ@A1 and A2) was observed in most of the analyses, except those of non-skew or lightly skewed bridges subjected to pure transverse ground motions, as shown in Tables 6.4 and 6.5. For highly skewed 3S bridges, even if the ground motions were applied transversely, the bi-axial superstructure displacements caused expansion joint closures in most of the analyses.

Mobilization of ultimate backfill passive resistance (MBU@A1 and A2) was rarely observed in the 3S bridge analyses. The very limited (11) analyses with occurrences of this limit state were of non-skew and lightly skewed, tall-pier 3S bridges in the soft foundation soil, and most of the occurrences were excited by the pure longitudinal ground motions. Bridges under these conditions tend to experience large deck displacements and significant superstructure-abutment interactions normal to the abutment backwall and backfill, when subjected to longitudinal ground motions. Failure of the backwall-to-pile-cap connections (FBP@A1 and A2) was not observed in any 3S bridge analysis.

Rupture of the retainer anchors at Abutments 1 and 2 (RAR@A1 and A2) occurred in 41% and 24% of the 1,600 3S bridge analyses, respectively. As expected, the pure transverse ground motions caused the most occurrences of all the incident directions, because the retainers are configured to restrain the transverse deformation and sliding of elastomeric bearings. Additionally, it can be found in Table 6.5 that the bridges with large skews, tall pier columns, and hard founda-

Table 6.5: Occurrences of limit states at abutments (A1 and A2) of 3S bridge variants

Limit state	No. of analyses with occurrence [1]	Skew angle [2] (°)					Foundation soil [2]		Column height [2] (m)		Ground motion incident angle [2] (°)			
		0	15	30	45	60	Hard	Soft	4.57	12.19	0	45	90	135
Closure of expansion joint (CEJ@A1)	1480 (93%)	240 (16%)	293 (20%)	311 (21%)	318 (21%)	318 (21%)	747 (50%)	733 (50%)	721 (49%)	759 (51%)	400 (27%)	400 (27%)	284 (19%)	396 (27%)
Mobilization of backfill ultimate capacity (MBU@A1)	11 (1%)	5 (45%)	5 (45%)	1 (9%)	0 (0%)	0 (0%)	0 (0%)	11 (100%)	0 (0%)	11 (100%)	10 (91%)	1 (9%)	0 (0%)	0 (0%)
Failure of backwall-to-pile-cap connection (FBP@A1)	0 (0%)	0	0	0	0	0	0	0	0	0	0	0	0	0
Rupture of retainer anchor (RRA@A1)	662 (41%)	61 (9%)	103 (16%)	155 (23%)	176 (27%)	167 (25%)	378 (57%)	284 (43%)	144 (22%)	518 (78%)	59 (9%)	114 (17%)	306 (46%)	183 (28%)
Slidng of elastomeric bearing (SEB@A1)	528 (33%)	56 (11%)	88 (17%)	119 (23%)	136 (26%)	129 (24%)	259 (49%)	269 (51%)	25 (5%)	503 (95%)	124 (23%)	91 (17%)	197 (37%)	116 (22%)
Unseating of bearing at obtuse corner of deck (UBA@A1)	0 (0%)	0	0	0	0	0	0	0	0	0	0	0	0	0
Unseating of bearing at acute corner of deck (UBO@A1)	0 (0%)	0	0	0	0	0	0	0	0	0	0	0	0	0
Yielding of pile supporting wingwall (YPW@A1)	983 (61%)	202 (21%)	223 (23%)	227 (23%)	187 (19%)	144 (15%)	566 (58%)	417 (42%)	364 (37%)	619 (63%)	349 (36%)	318 (32%)	128 (13%)	188 (19%)
Yielding of pile supporting backwall (YPB@A1)	1020 (64%)	223 (22%)	242 (24%)	236 (23%)	185 (18%)	134 (13%)	460 (45%)	560 (55%)	356 (35%)	664 (65%)	323 (32%)	307 (30%)	182 (18%)	208 (20%)
Closure of expansion joint (CEJ@A2)	1428 (89%)	240 (17%)	280 (20%)	287 (20%)	306 (21%)	315 (22%)	723 (51%)	705 (49%)	670 (47%)	758 (53%)	400 (28%)	400 (28%)	231 (16%)	397 (28%)
Mobilization of backfill ultimate capacity (MBU@A2)	8 (1%)	3 (38%)	4 (50%)	1 (13%)	0 (0%)	0 (0%)	0 (0%)	8 (100%)	0 (0%)	8 (100%)	7 (88%)	1 (13%)	0 (0%)	0 (0%)
Failure of backwall-to-pile-cap connection (FBP@A2)	0 (0%)	0	0	0	0	0	0	0	0	0	0	0	0	0
Rupture of retainer anchor (RRA@A2)	391 (24%)	17 (4%)	32 (8%)	107 (27%)	132 (34%)	103 (26%)	236 (60%)	155 (40%)	15 (4%)	376 (96%)	65 (17%)	111 (28%)	144 (37%)	71 (18%)
Slidng of elastomeric bearing (SEB@A2)	352 (22%)	28 (8%)	43 (12%)	83 (24%)	92 (26%)	106 (30%)	151 (43%)	201 (57%)	2 (1%)	350 (99%)	140 (40%)	95 (27%)	73 (21%)	44 (13%)
Unseating of bearing at obtuse corner of deck (UBO@A2)	0 (0%)	0	0	0	0	0	0	0	0	0	0	0	0	0
Unseating of bearing at acute corner of deck (UBA@A2)	0 (0%)	0	0	0	0	0	0	0	0	0	0	0	0	0
Yielding of pile supporting wingwall (YPW@A2)	961 (60%)	201 (21%)	214 (22%)	222 (23%)	192 (20%)	132 (14%)	552 (57%)	409 (43%)	357 (37%)	604 (63%)	359 (37%)	323 (34%)	68 (7%)	211 (22%)
Yielding of pile supporting backwall (YPB@A2)	927 (58%)	192 (21%)	217 (23%)	223 (24%)	185 (20%)	110 (12%)	424 (46%)	503 (54%)	311 (34%)	616 (66%)	341 (37%)	294 (32%)	96 (10%)	196 (21%)

1 The number above the parentheses indicates the number of analyses with occurrences of a limit state.
The percentage inside the parentheses indicates the ratio of the number above the parentheses to all the 1,600 analyses.

2 The number above the parentheses indicates the number of analyses with occurrences of a limit state contributed by a parametric variation.
The percentage inside the parentheses indicates the relative contribution of a parametric variation to the total occurrences of a limit state.

tion soil contributed experienced more occurrences of this limit state than those with small skews, short columns, and soft soil. This trend is consistent with the pushover response characteristics discussed in Chapter 5.

Sliding of the elastomeric bearings at the abutments (SEB@A1 and A2) was observed in many analyses (33% for A1 and 22% for A2), most of which involved tall-pier bridges that generally experienced larger deck displacements than their short-pier equivalents. This naming convention of deck corners is illustrated in Figure 6.6 and will be consistently used in later sections. The "Upper-left corner" and "Lower-left corner" in the figure refer to the acute and obtuse corners of the left-skewed deck end supported by Abutment 1, respectively. The “Upper-right corner” and “Lower-right corner” refer to the obtuse and acute corners of the other deck end supported by Abutment 2. The “abutment-parallel” and “abutment-normal” sliding directions of the elastomeric bearings at deck corners are also illustrated in Figure 6.6. The bearings at these corners are more prone to unseating than those placed further away from the corners.

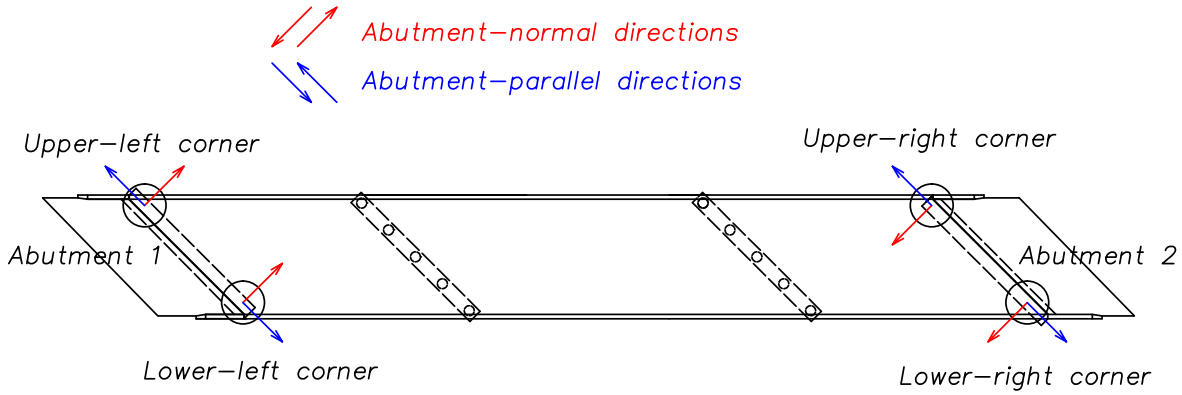

Figure 6.6: Naming convention of deck corners and bearing sliding directions at abutments

In conjunction with Table 6.5 and Figure 6.6, Figure 6.7 illustrates the peak bearing sliding at the four abutment corners. For each of the 1,600 3S bridge analyses, the peak abutment-parallel and abutment-normal sliding distances of elastomeric bearings at the four deck corners were normalized to the corresponding minimum seat width in either direction and are designated as “Abutment-parallel sliding ratio” and “Abutment-normal sliding ratio” in Figure 6.7. The sliding ratio is an indicator of bearing unseating (a sliding ratio greater than one means that unseating occurred in the analysis). The bridge variants with different skews are represented by the dots with different

colors in the figure. As can be seen, bearing unseating at abutments did not occur in any 3S bridge analyses (all sliding ratios are smaller than unity). As illustrated in Figure 6.7(a) and 6.7(b), at the upper-left and lower-right deck corners, highly skewed (45°-skew and 60°-skew) 3S bridges sustained the largest abutment-normal sliding of all the variants, which exceeded one half of the seat width in this direction. At the lower-left deck corner supported by Abutment 1, non-skew 3S bridges sustained the largest abutment-parallel bearing sliding, but it did not exceed one half of the seat width in this direction.

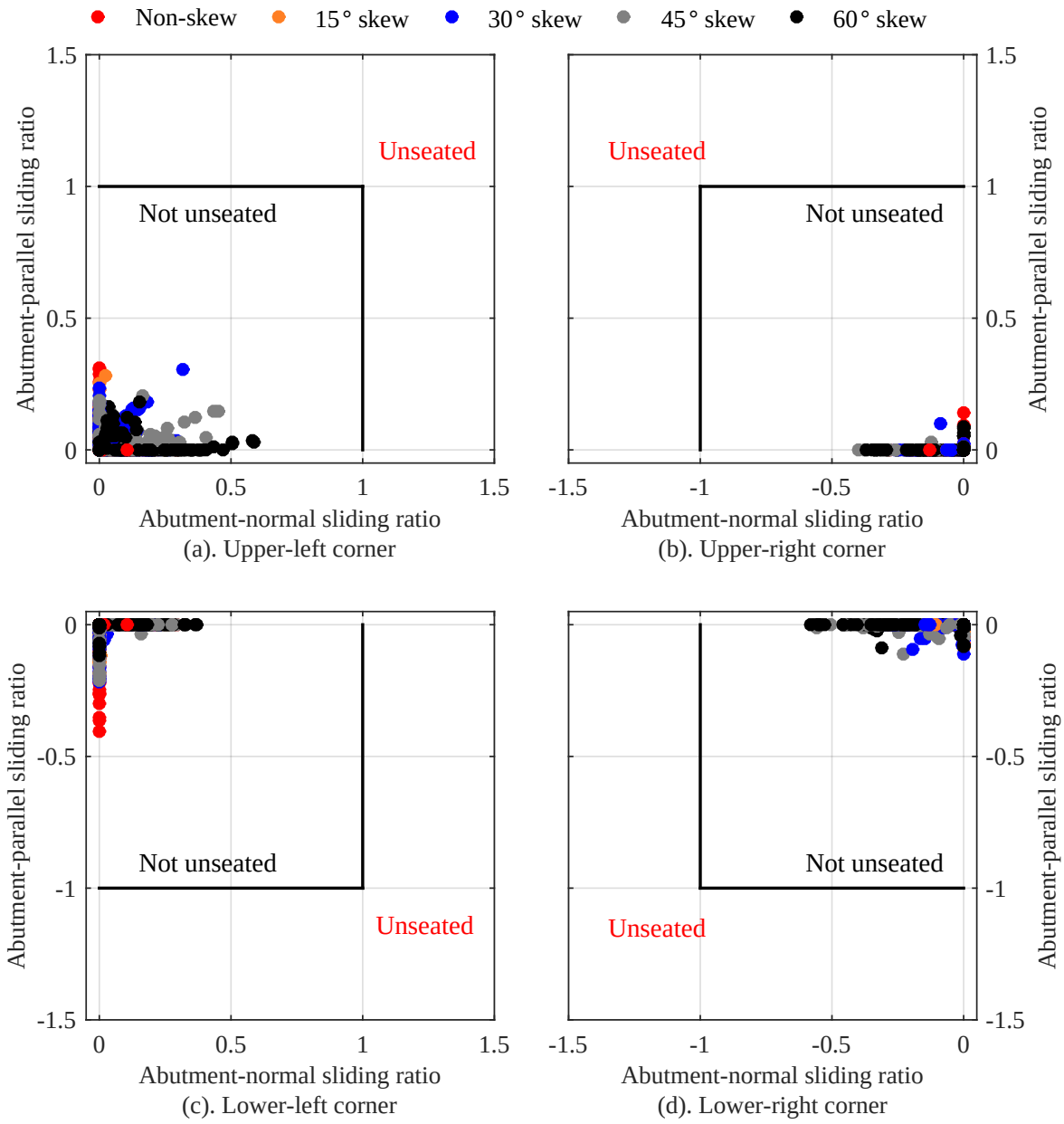

Figure 6.7: Peak sliding ratios of elastomeric bearings at deck corners of 3S bridges

Yielding of the steel H piles supporting abutment wingwalls (YPW@A1 and A2) and backwalls (YPB@A1 and A2) was observed in around 60% of the 3S bridge analyses. As can bee seen in Table 6.5, the occurrences of pile yielding under the pure transverse ground motions were the least of all the incident directions. This can be further confirmed by comparing the median peak pile strains listed in Table 6.6, which indicates that the abutment piles were also strained the least under the pure transverse ground motions. This trend is consistent with the pushover response characteristics. As observed in the longitudinal pushover analyses of 3S bridges, abutment piles typically yielded shortly after closure of the expansion joint. But in the transverse pushover analyses, yielding of abutment piles was either not observed in the entire analysis or until the superstructure was pushed by a large displacement. As shown in the Tables 6.5 and 6.6, tall-pier bridges sustained larger abutment pile strains than the short-pier ones. The median peak pile strains of highly skewed 3S bridges were commonly smaller than those with smaller skews.

Table 6.6: Normalized peak strains of steel H piles supporting abutments of 3S bridges (peak strains are normalized to the yield strain of steel piles, 0.0017; numbers outside and inside the parentheses are medians and median absolute deviations, respectively; data for piles supporting backwalls and wingwalls are placed on the left and right sides of the commas, respectively)

Foundation soil condition			Hard				Soft			
Pier column height (m)			4.57		12.19		4.57		12.19	
Longitudinal (0º) ground motions	Bridge skew (º)	0	1.1 (0.2) , 2.0 (0.3)		4.4 (1.9) , 6.0 (2.1)		1.2 (0.3) , 1.1 (0.2)		6.4 (1.9) , 5.6 (2.4)	
		15	1.7 (0.3) , 2.4 (0.6)		7.3 (2.4) , 8.1 (2.3)		2.2 (0.6) , 1.7 (0.4)		7.9 (1.8) , 7.1 (1.8)	
		30	1.8 (0.6) , 2.2 (0.7)		6.4 (2.2) , 7.8 (2.3)		3.0 (0.9) , 2.5 (0.7)		7.6 (2.7) , 6.7 (2.5)	
		45	1.1 (0.3) , 1.4 (0.4)		1.7 (0.4) , 2.9 (0.7)		1.5 (0.4) , 1.4 (0.4)		5.3 (1.9) , 5.2 (1.8)	
		60	0.6 (0.1) , 0.7 (0.1)		1.0 (0.2) , 1.3 (0.2)		0.9 (0.2) , 0.9 (0.2)		2.8 (1.2) , 2.7 (1.2)	
45º ground motions	Bridge skew (º)	0	1.0 (0.2) , 1.3 (0.3)		2.3 (0.9) , 3.2 (1.0)		1.1 (0.2) , 0.9 (0.1)		4.1 (0.9) , 3.0 (0.9)	
		15	1.2 (0.2) , 1.6 (0.3)		3.9 (1.6) , 4.9 (1.5)		1.0 (0.1) , 1.0 (0.1)		4.4 (1.5) , 3.4 (1.3)	
		30	1.4 (0.3) , 1.8 (0.5)		5.6 (2.9) , 7.1 (2.5)		1.6 (0.6) , 1.3 (0.3)		5.9 (2.2) , 5.1 (2.0)	
		45	1.1 (0.2) , 1.5 (0.3)		2.4 (0.9) , 4.5 (1.2)		1.0 (0.2) , 0.9 (0.1)		5.7 (2.3) , 4.9 (2.3)	
		60	0.8 (0.1) , 1.0 (0.2)		1.3 (0.4) , 2.2 (1.0)		0.8 (0.1) , 0.7 (0.1)		3.0 (1.6) , 2.5 (1.3)	
Transverse (90º) ground motions	Bridge skew (º)	0	0.8 (0.1) , 0.4 (0.1)		0.9 (0.1) , 0.5 (0.0)		0.8 (0.1) , 0.5 (0.1)		1.2 (0.3) , 0.8 (0.2)	
		15	0.8 (0.1) , 0.5 (0.1)		0.9 (0.1) , 0.9 (0.2)		0.7 (0.1) , 0.5 (0.1)		1.2 (0.3) , 0.8 (0.1)	
		30	0.8 (0.1) , 0.5 (0.2)		1.3 (0.3) , 1.5 (0.5)		0.7 (0.1) , 0.6 (0.1)		1.5 (0.4) , 1.1 (0.2)	
		45	0.6 (0.1) , 0.6 (0.2)		1.1 (0.3) , 1.9 (0.6)		0.7 (0.1) , 0.6 (0.1)		1.6 (0.4) , 1.3 (0.3)	
		60	0.5 (0.1) , 0.6 (0.2)		1.1 (0.3) , 1.8 (0.6)		0.6 (0.1) , 0.5 (0.1)		1.6 (0.6) , 1.3 (0.5)	
135º ground motions	Bridge skew (º)	0	1.0 (0.2) , 1.2 (0.3)		2.1 (0.5) , 3.1 (0.8)		1.1 (0.1) , 0.9 (0.1)		4.0 (0.8) , 3.1 (0.7)	
		15	0.9 (0.1) , 1.0 (0.2)		2.5 (0.8) , 3.2 (1.1)		1.7 (0.4) , 1.3 (0.3)		3.4 (1.1) , 2.5 (0.8)	
		30	0.8 (0.1) , 0.8 (0.1)		1.1 (0.2) , 1.2 (0.2)		1.4 (0.4) , 1.2 (0.3)		1.6 (0.6) , 1.3 (0.4)	
		45	0.6 (0.1) , 0.6 (0.1)		0.8 (0.2) , 0.9 (0.2)		0.8 (0.1) , 0.8 (0.1)		1.0 (0.2) , 0.9 (0.1)	
		60	0.4 (0.1) , 0.4 (0.1)		0.7 (0.2) , 0.8 (0.2)		0.7 (0.1) , 0.7 (0.1)		0.9 (0.2) , 0.8 (0.2)	

Unyielded: normalized strain < 1 (unnormalized strain < 0.0017)

Yielded without signficniant strain hardening: 1 ≤ normalized strain < 10 (0.0017 ≤ unnormalized strain < 0.017)

Yielded and significantly strain hardened: 10 ≤ normalized strain (0.017 ≤ unnormalized strain)

Expansion piers (Pier 1) of 3S bridges

Table 6.7 statistically summarizes the occurrences of a few component limit states at Pier 1 of the 3S bridges. As introduced in Section 3.5, the bearing retainer anchors were proportioned based on the superstructure dead load imposed on the bearings (IDOT 2012a). Because the intermediate piers withstand much higher dead load than the abutments, the retainer anchors at the expansion piers are larger in diameter (38.1 mm, 1.5 in.) than those at the abutments (25.4 mm, 1.0 in.). Moreover, due to the lateral flexibility of pier columns, the intermediate piers are laterally more flexible than the abutments that directly seat on their pile foundations. As a result, the piers may not be able to provide the required stiffness and reaction to rupture the retainer anchors but tend to deflect laterally without rupture of the retainer anchors under the seismic forces of bridge superstructures. These are the primary reasons why retainer anchor ruptures at Pier 1 (RRA@P1) did not occur in any 3S bridge analysis while those at the abutments were observed in many analyses.

Table 6.7: Occurrences of limit states at expansion piers (Pier 1) of 3S bridge variants

Limit state	No. of analyses with occurrence [1]	Skew angle [2] (°)					Foundation soil [2]		Column height [2] (m)		Ground motion incident angle [2] (°)			
		0	15	30	45	60	Hard	Soft	4.57	12.19	0	45	90	135
Rupture of retainer anchor (RRA@P1)	0 (0%)	0	0	0	0	0	0	0	0	0	0	0	0	0
Sliding of elastomeric bearing (SEB@P1)	0 (0%)	0	0	0	0	0	0	0	0	0	0	0	0	0
Unseating of elastomeric bearing (UEB@P1)	0 (0%)	0	0	0	0	0	0	0	0	0	0	0	0	0
Yielding of vertical reinforcing steel at column end (YRS@P1)	177 (11%)	28 (16%)	33 (19%)	47 (27%)	24 (14%)	45 (25%)	100 (56%)	77 (44%)	4 (2%)	173 (98%)	12 (7%)	33 (19%)	100 (56%)	32 (18%)
Crushing of concrete cover at column end (CCC@P1)	0 (0%)	0	0	0	0	0	0	0	0	0	0	0	0	0
Yielding of pile at pier (YPP@P1)	267 (17%)	79 (30%)	62 (23%)	64 (24%)	41 (15%)	21 (8%)	38 (14%)	229 (86%)	71 (27%)	196 (73%)	6 (2%)	17 (6%)	129 (48%)	115 (43%)

1 The number above the parentheses indicates the number of analyses with occurrences of a limit state.
The percentage inside the parentheses indicates the ratio of the number above the parentheses to all the 1,600 analyses.
2 The number above the parentheses indicates the number of analyses with occurrences of a limit state contributed by a parametric variation.
The percentage inside the parentheses indicates the relative contribution of a parametric variation to the total occurrences of a limit state.

Yielding of the vertical reinforcing steel at the column bases of Pier 1 (YRS@P1) was observed only in a small percentage of the 3S bridge analyses (11%). In addition to Table 6.7, Table 6.8 lists the normalized peak strains of vertical reinforcing steel at the pier column bases of 3S bridges. The

data on the left and right sides of the commas are for the expansion and fixed piers, respectively. Kowalsky (2001) adopted a serviceability steel tension strain of 0.015 and a damage control strain of 0.06 for circular RC bridge columns. The serviceability strain was defined as the strain at which repair is likely to be required due to residual crack widths larger than 1 mm, while the damage control strain is the strain at which repair may become infeasible. On the basis of these two strain limits, four performance levels were defined by Revell (2013) and were adopted in this study. As shown in Table 6.8, the reinforcing steel at the column bases of Pier 1 was undamaged in most of the analyses, except a few lightly damaged cases. As indicated in Table 6.7, 98% of the yieldings occurred at the tall expansion piers. This trend can be confirmed by comparing the median peak strains in Table 6.8 between tall- and short-pier bridges. Table 6.9 lists the normalized median peak strain of unconfined concrete cover at the column bases. In all the tabulated cases, the concrete cover at the bases of expansion pier columns was undamaged.

Yielding of the steel H piles supporting Pier 1 (YSP@P1) was also observed in 17% of the analyses, as indicated in Table 6.7. Table 6.10 indicates the peak strains of steel H piles supporting the piers of 3S bridges. The data on the left and right sides of the commas are for the expansion and fixed piers, respectively. In most cases, the piles supporting Pier 1 were unyielded or only lightly strained beyond yielding. It can be found in Table 6.7 that the tall pier and soft foundation soil account for more pile yielding than the short pier and hard soil. Additionally, 91% of the yielding were caused by the pure transverse and 135° ground motions. These observations can be confirmed by comparing the median peak strains listed in Table 6.10 among different cases. Consistently, yielding of pier piles was only observed in transverse pushover analyses of 3S bridges but not in the longitudinal ones.

Overall, although the preferred limit states for quasi-isolation, such as rupture of retainer anchors (RRA@P1) and sliding of elastomeric bearings (SEB@P1), did not occur, the expansion piers did not sustain excessive seismic damage. Yielding of column reinforcing steel and foundation piles, only occurred in a limited number of analyses with small strains. Neither crushing of concrete cover (CCC@P1) nor unseating of elastomeric bearings (UEB@P1) occurred at Pier 1 in any 3S bridge analysis.

Table 6.8: Normalized peak strain of vertical reinforcing steel at pier column base of 3S bridges (peak strains are normalized to the yield strain, 0.0021; numbers outside the parentheses are medians, while those inside are median absolute deviations; data of reinforcing steel at column base of expansion and fixed piers are placed on the left and right sides of the commas, respectively; performance levels in the footnote are defined per Kowalsky (2001) and Revell (2013))

Foundation soil condition			Hard				Soft			
Pier column height (m)			4.57		12.19		4.57		12.19	
Longitudinal (0º) ground motions	Bridge skew (º)	0	0.2 (0.0) ,	2.0 (0.2)	0.6 (0.1) ,	0.6 (0.1)	0.4 (0.0) ,	2.4 (0.4)	0.7 (0.2) ,	0.9 (0.2)
		15	0.2 (0.0) ,	2.3 (0.3)	0.6 (0.1) ,	0.7 (0.1)	0.4 (0.1) ,	3.1 (0.7)	0.7 (0.2) ,	0.9 (0.3)
		30	0.3 (0.0) ,	2.8 (0.9)	0.7 (0.1) ,	0.8 (0.1)	0.4 (0.0) ,	4.2 (1.2)	0.7 (0.1) ,	1.0 (0.2)
		45	0.2 (0.0) ,	1.4 (0.2)	0.5 (0.2) ,	0.9 (0.2)	0.2 (0.0) ,	1.1 (0.1)	0.5 (0.1) ,	1.0 (0.2)
		60	0.2 (0.0) ,	0.8 (0.0)	0.6 (0.1) ,	1.1 (0.4)	0.1 (0.0) ,	0.7 (0.1)	0.4 (0.1) ,	0.8 (0.1)
45º ground motions	Bridge skew (º)	0	0.2 (0.0) ,	1.5 (0.2)	0.6 (0.1) ,	0.5 (0.0)	0.2 (0.0) ,	1.4 (0.1)	0.6 (0.1) ,	0.7 (0.0)
		15	0.3 (0.0) ,	1.8 (0.3)	0.6 (0.1) ,	0.6 (0.1)	0.4 (0.0) ,	1.8 (0.3)	0.6 (0.1) ,	0.7 (0.1)
		30	0.5 (0.1) ,	2.4 (0.7)	0.8 (0.1) ,	0.8 (0.1)	0.6 (0.1) ,	3.0 (1.1)	0.9 (0.1) ,	0.9 (0.2)
		45	0.5 (0.1) ,	1.4 (0.2)	0.9 (0.2) ,	1.0 (0.2)	0.5 (0.1) ,	1.2 (0.1)	0.9 (0.2) ,	1.2 (0.4)
		60	0.6 (0.1) ,	1.1 (0.2)	0.9 (0.2) ,	1.3 (0.7)	0.6 (0.1) ,	0.9 (0.1)	0.9 (0.2) ,	1.5 (0.9)
Transverse (90º) ground motions	Bridge skew (º)	0	0.3 (0.1) ,	0.4 (0.0)	1.2 (0.5) ,	0.8 (0.1)	0.2 (0.0) ,	0.2 (0.0)	0.9 (0.2) ,	0.6 (0.2)
		15	0.4 (0.1) ,	0.4 (0.0)	1.2 (0.2) ,	0.9 (0.1)	0.2 (0.0) ,	0.3 (0.0)	0.9 (0.1) ,	0.7 (0.2)
		30	0.6 (0.1) ,	0.7 (0.1)	1.2 (0.2) ,	1.0 (0.2)	0.5 (0.1) ,	0.5 (0.1)	1.0 (0.1) ,	0.8 (0.2)
		45	0.6 (0.1) ,	0.8 (0.1)	0.9 (0.2) ,	0.9 (0.2)	0.6 (0.1) ,	0.6 (0.1)	0.8 (0.1) ,	0.6 (0.2)
		60	0.7 (0.1) ,	0.7 (0.1)	1.1 (0.3) ,	0.9 (0.3)	0.7 (0.1) ,	0.7 (0.1)	1.0 (0.2) ,	0.9 (0.4)
135º ground motions	Bridge skew (º)	0	0.2 (0.0) ,	1.5 (0.1)	0.6 (0.0) ,	0.6 (0.0)	0.2 (0.0) ,	1.5 (0.1)	0.6 (0.1) ,	0.7 (0.0)
		15	0.3 (0.1) ,	1.3 (0.1)	0.7 (0.1) ,	0.7 (0.2)	0.3 (0.0) ,	1.6 (0.2)	0.6 (0.2) ,	0.7 (0.1)
		30	0.4 (0.1) ,	1.2 (0.1)	1.1 (0.2) ,	1.2 (0.2)	0.3 (0.0) ,	1.5 (0.2)	0.9 (0.2) ,	0.9 (0.2)
		45	0.5 (0.1) ,	0.7 (0.1)	0.9 (0.1) ,	1.2 (0.2)	0.3 (0.1) ,	0.8 (0.1)	0.7 (0.2) ,	0.8 (0.1)
		60	0.5 (0.0) ,	0.5 (0.0)	0.7 (0.1) ,	1.3 (0.2)	0.4 (0.1) ,	0.5 (0.1)	0.6 (0.2) ,	0.7 (0.1)

Undamaged (unyielded):	normalized strain < 1 (unnormalized strain < 0.0021)
Lightly damaged (unlikely requiring repair):	1 ≤ normalized strain < 7.1 (0.0021 ≤ unnormalized strain < 0.015)
Moderately damaged (repairable):	7.1 ≤ normalized strain < 28.6 (0.015 ≤ unnormalized strain < 0.06)
Severely damaged (not easily repairable):	28.6 ≤ normalized strain (0.06 ≤ unnormalized strain)

Table 6.9: Normalized peak strain of concrete cover at pier column base of 3S bridges (peak strains are normalized to the crushing strain, 0.005; numbers outside the parentheses are medians, while those inside are median absolute deviations; data of concrete cover at column base of expansion and fixed piers are placed on the left and right sides of the commas, respectively; performance levels in the footnote are defined per Kowalsky (2001) and Revell (2013))

Foundation soil condition			Hard				Soft			
Pier column height (m)			4.57		12.19		4.57		12.19	
Longitudinal (0º) ground motions	Bridge skew (º)	0	0.1 (0.0) ,	0.4 (0.0)	0.2 (0.0) ,	0.2 (0.0)	0.1 (0.0) ,	0.5 (0.0)	0.2 (0.0) ,	0.2 (0.0)
		15	0.1 (0.0) ,	0.5 (0.0)	0.2 (0.0) ,	0.2 (0.0)	0.2 (0.0) ,	0.6 (0.1)	0.2 (0.0) ,	0.3 (0.0)
		30	0.1 (0.0) ,	0.5 (0.1)	0.2 (0.0) ,	0.2 (0.0)	0.2 (0.0) ,	0.7 (0.2)	0.2 (0.0) ,	0.3 (0.0)
		45	0.1 (0.0) ,	0.4 (0.0)	0.2 (0.0) ,	0.3 (0.0)	0.1 (0.0) ,	0.3 (0.0)	0.2 (0.0) ,	0.3 (0.0)
		60	0.1 (0.0) ,	0.2 (0.0)	0.2 (0.0) ,	0.3 (0.1)	0.1 (0.0) ,	0.2 (0.0)	0.1 (0.0) ,	0.2 (0.0)
45º ground motions	Bridge skew (º)	0	0.1 (0.0) ,	0.3 (0.0)	0.2 (0.0) ,	0.2 (0.0)	0.1 (0.0) ,	0.3 (0.0)	0.2 (0.0) ,	0.2 (0.0)
		15	0.1 (0.0) ,	0.4 (0.0)	0.2 (0.0) ,	0.2 (0.0)	0.1 (0.0) ,	0.4 (0.0)	0.2 (0.0) ,	0.2 (0.0)
		30	0.2 (0.0) ,	0.5 (0.1)	0.2 (0.0) ,	0.2 (0.0)	0.2 (0.0) ,	0.6 (0.1)	0.2 (0.0) ,	0.2 (0.0)
		45	0.2 (0.0) ,	0.3 (0.0)	0.2 (0.0) ,	0.2 (0.0)	0.2 (0.0) ,	0.3 (0.0)	0.2 (0.0) ,	0.3 (0.1)
		60	0.2 (0.0) ,	0.3 (0.0)	0.2 (0.0) ,	0.3 (0.1)	0.2 (0.0) ,	0.3 (0.0)	0.2 (0.0) ,	0.3 (0.1)
Transverse (90º) ground motions	Bridge skew (º)	0	0.1 (0.0) ,	0.2 (0.0)	0.3 (0.1) ,	0.2 (0.0)	0.1 (0.0) ,	0.1 (0.0)	0.3 (0.0) ,	0.2 (0.0)
		15	0.2 (0.0) ,	0.2 (0.0)	0.3 (0.0) ,	0.3 (0.0)	0.1 (0.0) ,	0.1 (0.0)	0.3 (0.0) ,	0.2 (0.0)
		30	0.2 (0.0) ,	0.2 (0.0)	0.3 (0.0) ,	0.3 (0.0)	0.1 (0.0) ,	0.2 (0.0)	0.3 (0.0) ,	0.2 (0.0)
		45	0.2 (0.0) ,	0.2 (0.0)	0.2 (0.0) ,	0.2 (0.0)	0.2 (0.0) ,	0.2 (0.0)	0.2 (0.0) ,	0.2 (0.0)
		60	0.2 (0.0) ,	0.2 (0.0)	0.3 (0.1) ,	0.2 (0.1)	0.2 (0.0) ,	0.2 (0.0)	0.3 (0.0) ,	0.2 (0.1)
135º ground motions	Bridge skew (º)	0	0.1 (0.0) ,	0.4 (0.0)	0.2 (0.0) ,	0.2 (0.0)	0.1 (0.0) ,	0.4 (0.0)	0.2 (0.0) ,	0.2 (0.0)
		15	0.1 (0.0) ,	0.3 (0.0)	0.2 (0.0) ,	0.2 (0.0)	0.1 (0.0) ,	0.4 (0.0)	0.2 (0.0) ,	0.2 (0.0)
		30	0.1 (0.0) ,	0.3 (0.0)	0.3 (0.0) ,	0.3 (0.0)	0.1 (0.0) ,	0.4 (0.0)	0.2 (0.0) ,	0.2 (0.0)
		45	0.1 (0.0) ,	0.2 (0.0)	0.3 (0.0) ,	0.3 (0.0)	0.1 (0.0) ,	0.2 (0.0)	0.2 (0.0) ,	0.2 (0.0)
		60	0.2 (0.0) ,	0.2 (0.0)	0.2 (0.0) ,	0.3 (0.0)	0.1 (0.0) ,	0.2 (0.0)	0.2 (0.0) ,	0.2 (0.0)

Undamaged (ultimate strength not mobillized):	normalized strain < 0.4 (unnormalized strain < 0.002)
Lightly damaged (ultimate strength mobilized but uncrushed):	0.4 ≤ normalized strain < 1 (0.002 ≤ unnormalized strain < 0.005)
Moderately damaged (crushed but repairable):	1 ≤ normalized strain < 3.6 (0.005 ≤ unnormalized strain < 0.018)
Severely damaged (not easily repairable):	3.6 ≤ normalized strain (0.018 ≤ unnormalized strain)

Table 6.10: Normalized peak strains of steel H piles at piers of 3S bridges (peak strains are normalized to the yield strain, 0.0017; numbers outside the parentheses are medians, while those inside are median absolute deviations; data for piles supporting expansion and fixed piers are placed on the left and right sides of the commas, respectively)

Foundation soil condition			Hard		Soft	
Pier column height (m)			4.57	12.19	4.57	12.19
Longitudinal (0º) ground motions	Bridge skew (º)	0	0.2 (0.0) , 0.4 (0.0)	0.3 (0.0) , 0.3 (0.0)	0.2 (0.0) , 0.6 (0.0)	0.3 (0.0) , 0.4 (0.0)
		15	0.3 (0.0) , 0.6 (0.0)	0.4 (0.0) , 0.4 (0.0)	0.3 (0.0) , 0.9 (0.1)	0.5 (0.0) , 0.6 (0.0)
		30	0.3 (0.0) , 0.8 (0.0)	0.4 (0.1) , 0.5 (0.1)	0.5 (0.1) , 1.4 (0.1)	0.6 (0.0) , 0.8 (0.1)
		45	0.3 (0.0) , 1.0 (0.1)	0.5 (0.1) , 0.7 (0.1)	0.6 (0.0) , 2.1 (0.5)	0.7 (0.1) , 1.4 (0.3)
		60	0.3 (0.0) , 1.0 (0.1)	0.5 (0.1) , 0.9 (0.2)	0.7 (0.1) , 4.4 (1.1)	0.8 (0.2) , 2.9 (1.2)
45º ground motions	Bridge skew (º)	0	0.6 (0.1) , 0.7 (0.0)	0.6 (0.0) , 0.6 (0.0)	0.8 (0.1) , 1.0 (0.1)	1.1 (0.1) , 0.9 (0.0)
		15	0.5 (0.1) , 0.6 (0.1)	0.6 (0.0) , 0.5 (0.0)	0.8 (0.0) , 0.8 (0.0)	0.9 (0.1) , 0.7 (0.1)
		30	0.4 (0.0) , 0.6 (0.0)	0.5 (0.0) , 0.5 (0.0)	0.6 (0.0) , 0.8 (0.0)	0.6 (0.0) , 0.6 (0.1)
		45	0.4 (0.0) , 0.7 (0.0)	0.4 (0.0) , 0.5 (0.0)	0.5 (0.0) , 0.9 (0.0)	0.5 (0.0) , 0.6 (0.1)
		60	0.3 (0.0) , 0.7 (0.0)	0.3 (0.1) , 0.4 (0.0)	0.4 (0.0) , 0.9 (0.0)	0.4 (0.0) , 0.6 (0.1)
Transverse (90º) ground motions	Bridge skew (º)	0	0.8 (0.1) , 0.9 (0.1)	1.1 (0.3) , 0.8 (0.0)	1.2 (0.1) , 1.3 (0.2)	4.0 (2.8) , 1.7 (0.4)
		15	0.8 (0.1) , 0.9 (0.1)	1.1 (0.2) , 0.8 (0.0)	1.2 (0.1) , 1.2 (0.1)	2.9 (1.6) , 1.6 (0.4)
		30	0.7 (0.1) , 0.8 (0.1)	0.8 (0.1) , 0.7 (0.0)	1.0 (0.1) , 1.0 (0.1)	1.6 (0.5) , 1.4 (0.3)
		45	0.5 (0.1) , 0.8 (0.1)	0.6 (0.0) , 0.7 (0.1)	0.8 (0.0) , 0.9 (0.1)	1.0 (0.2) , 1.3 (0.4)
		60	0.4 (0.0) , 0.6 (0.1)	0.4 (0.0) , 0.6 (0.0)	0.5 (0.0) , 0.7 (0.1)	0.6 (0.1) , 0.9 (0.1)
135º ground motions	Bridge skew (º)	0	0.6 (0.1) , 0.7 (0.1)	0.6 (0.0) , 0.6 (0.0)	0.8 (0.1) , 1.0 (0.1)	1.1 (0.1) , 0.9 (0.1)
		15	0.7 (0.1) , 0.9 (0.0)	0.8 (0.1) , 0.7 (0.1)	1.0 (0.1) , 1.6 (0.1)	1.4 (0.5) , 1.3 (0.2)
		30	0.6 (0.1) , 0.9 (0.1)	0.9 (0.1) , 0.8 (0.1)	1.0 (0.1) , 2.3 (0.4)	1.7 (0.7) , 1.6 (0.5)
		45	0.5 (0.0) , 1.0 (0.1)	0.9 (0.1) , 1.0 (0.1)	1.0 (0.1) , 3.1 (1.0)	1.5 (0.6) , 3.7 (2.2)
		60	0.4 (0.0) , 0.9 (0.1)	0.7 (0.1) , 1.0 (0.1)	0.8 (0.1) , 1.8 (0.5)	1.2 (0.4) , 2.8 (1.7)

Unyielded: normalized strain < 1 (unnormalized strain < 0.0017)

Yielded without signficniant strain hardening: 1 ≤ normalized strain < 10 (0.0017 ≤ unnormalized strain < 0.017)

Yielded and significantly strain hardened: 10 ≤ normalized strain (0.017 ≤ unnormalized strain)

Fixed piers (Pier 2) of 3S bridges

Table 6.11 statistically summarizes the occurrences of component limit states at the fixed piers (Pier 2). Rupture of the steel fixed bearing anchors at Pier 2 (RFA@P2) was observed in only 71 out of the 1,600 analyses. It can be found that the large skews, hard foundation soil, and short pier columns account for more occurrences of this limit state than the small skews, soft soil, and tall pier columns. These tendencies are consistent with the pushover response characteristics. The short pier columns and hard foundation soil result in high lateral stiffness of the fixed pier, which is favorable to fusing of the fixed bearing anchors. Highly skewed 3S bridges have more columns at the piers than those with smaller skews, which also increases the lateral stiffness of the piers. Moreover, the superstructures of highly skewed bridges displaced in both longitudinal and transverse bridge axes, and the deformation components in these two axes may result in a large resultant anchor deformation. It can also be found that the pure longitudinal and 135° ground motions accounted for much more occurrences than the pure transverse and 45° motions.

Yielding of the reinforcing steel at the column bases of Pier 2 (YRS@P2) was observed in more analyses than that of Pier 1 (YRS@P1). This is expected as the fixed pier typically incur larger seismic forces than the expansion pier when subjected to non-transverse ground motions, due to the much higher lateral stiffness. The pure transverse ground motions caused the fewest occurrences of reinforcing steel yielding at Pier 2 among all the incident directions. This directional effect can be further confirmed by examining the median peak strains listed in Table 6.8. Short-pier 3S bridges experienced this limit state more than tall-pier ones.

Yielding of the steel H piles supporting Pier 2 (YSP@P2) was observed in 32% of the 3S bridge analyses. Similar to Pier 1, the 90° and 135° ground motions accounted for more occurrences of this limit state than those in the other two directions. 3S bridges in the soft foundation soil experienced pile yielding at Pier 2 more than their equivalents in the hard soil, which is similar to the situation at Pier 1. This tendency was also observed in the pushover analyses. The soft foundation soil provided lower lateral resistance to the pile deflection and resulted in more pile yielding. Short-pier 3S bridges sustained larger pile strains and more yielding than their tall-pier equivalents. As indicated in Table 6.8, the piles supporting Pier 2 were either unyielded or only lightly strained beyond yielding in all the tabulated cases. As indicated in Tables 6.11 and 6.9, crushing of the concrete cover at the column bases of Pier 2 (CCC@P2) occurred in only a few

analyses. Unseating of the steel bearings after anchorage failure (USB@P2) was not observed in any analysis.

By comparing the same limit states in Tables 6.7 and 6.11, it can be found that the fixed piers (Pier 2) of 3S bridges generally sustained more seismic damage (yielding of vertical reinforcing steel and steel piles, as well as crushing of concrete cover) than the expansion piers (Pier 1), when the bridges were subjected to non-transverse ground motions. This difference is expected as the steel fixed bearings possess much higher stiffness and can incur larger seismic forces to the pier supporting them than the elastomeric bearings when the ground motion has a significant longitudinal component. However, the transverse bearing retainers on top of the expansion piers possess high stiffness that is comparable to that of the steel fixed bearings, which may result in similar seismic forces between the expansion and fixed piers under pure transverse ground motions.

Table 6.11: Occurrences of limit states at fixed piers (Pier 2) of 3S bridge variants

Limit state	No. of analyses with occurrence [1]	Skew angle [2] (°)					Foundation soil [2]		Column height [2] (m)		Ground motion incident angle [2] (°)			
		0	15	30	45	60	Hard	Soft	4.57	12.19	0	45	90	135
Rupture of steel fixed bearing anchors (RFA@P2)	71	0	0	0	16	55	65	6	57	14	40	6	0	25
	(4%)	(0%)	(0%)	(0%)	(23%)	(77%)	(92%)	(8%)	(80%)	(20%)	(56%)	(8%)	(0%)	(35%)
Unseating of steel fixed bearing (USB@P2)	0	0	0	0	0	0	0	0	0	0	0	0	0	0
	(0%)													
Yielding of vertical reinforcing steel at column end (YRS@P2)	692	134	138	180	133	107	361	331	462	230	220	245	50	177
	(43%)	(19%)	(20%)	(26%)	(19%)	(15%)	(52%)	(48%)	(67%)	(33%)	(32%)	(35%)	(7%)	(26%)
Crushing of concrete cover at column end (CCC@P2)	4	0	0	4	0	0	1	3	4	0	4	0	0	0
	(0%)	(0%)	(0%)	(100%)	(0%)	(0%)	(25%)	(75%)	(100%)	(0%)	(100%)	(0%)	(0%)	(0%)
Yielding of pile at pier (YPP@P2)	517	79	86	94	132	126	101	416	289	228	130	21	144	222
	(32%)	(15%)	(17%)	(18%)	(26%)	(24%)	(20%)	(80%)	(56%)	(44%)	(25%)	(4%)	(28%)	(43%)

1 The number above the parentheses indicates the number of analyses with occurrences of a limit state.
The percentage inside the parentheses indicates the ratio of the number above the parentheses to all the 1,600 analyses.
2 The number above the parentheses indicates the number of analyses with occurrences of a limit state contributed by a parametric variation.
The percentage inside the parentheses indicates the relative contribution of a parametric variation to the total occurrences of a limit state.

Summary of 3S bridge analyses

1,600 nonlinear dynamic analyses were performed on the 20 three-span steel-plate-girder (3S) bridge variants that were subjected to the suite of 20 seismic ground motions applied in four incident directions. The 20 bridge variants possess five skew angles (0°, 15°, 30°, 45°, and 60°),

two pier column clear heights (4.57 m and 12.19 m), and two foundation soil conditions (hard and soft). The four ground motion incident directions are 0° (pure longitudinal), 45°, 90° (pure transverse), and 135°.

The 3S bridges have the lightest superstructures, which resulted in the smallest seismic force demands of all the four major types of bridges. Largely due to the smallest seismic demands and the quasi-isolation strategy, the 3S bridges only sustained very limited seismic damage that is acceptable to the ERS bridge design philosophy. The preferred limit states for the quasi-isolation strategy, such as rupture of superstructure-substructure connections and sliding of elastomeric bearings, were observed in many analyses. The acceptable limit states, such as yielding of column reinforcing steel and steel piles, crushing of column concrete cover, and mobilization of ultimate backfill capacity, occurred in some analyses but with only small material strains. The short fixed piers sustained more damage than the short expansion piers under non-transverse ground motions. The high fixed and expansion piers sustained similar strains of reinforcing steel and concrete cover. Most importantly, the unacceptable limit states, namely bearing unseating at abutments and piers, were not observed in any 3S bridge analysis. This is consistent with the observation of a similar three-span steel-plate-girder bridge studied in a previous phase of the research that unseating of IDOT Type I elastomer bearings (the only type of bearings in this study) was not recorded at design-level earthquake hazard (LaFave et al. 2013b).

A number of important observations on the seismic performance of 3S bridge variants are briefly summarized as follows:

1. The uni-axial ground motions were more critical for causing large deck displacements along the two bridge axes than the bi-axial (45° and 135°) ones, which is consistent with the observation of bi-axial excitation made in the previous phase of the research (LaFave et al. 2013b). The superstructures of skew 3S bridges were always bi-axially displaced, regardless of the ground motion direction. In general, the tall pier columns and soft foundation soil caused larger deck displacements than the short columns and hard soil, which is also consistent with the findings of previous research (LaFave et al. 2013b).

2. The peak in-plane deck rotations in all the analyses were smaller than 1°. For left-skewed 3S bridges (only left skew is considered in this study), the clockwise peak deck rotations were

always larger than the counterclockwise. The peak clockwise rotations of highly skewed bridges were generally larger than those of the bridges with smaller skews. Tall-pier bridges rotated more than their short-pier equivalents in both directions.

3. Closure of expansion joints occurred in most 3S bridge analyses, except those of non-skew or lightly skewed bridges subjected to the pure transverse ground motions.

4. Mobilization of ultimate backfill passive resistance was observed in less than 1% of the analyses. The limited occurrences involved non-skew or lightly skewed, tall-pier bridges in the soft soil, most of which were caused by the pure longitudinal ground motions. Failure of the backwall-pile cap connections was not observed in any analysis.

5. Rupture of the retainer anchors at the abutments occurred in at least 41% of the analyses. 78% and 96% of the ruptures at Abutments 1 and 2 involved tall-pier bridges, respectively. The pure transverse ground motions caused the most ruptures of all the incident directions. The tall pier columns, large skews, and hard foundation soil account for more occurrences than the short columns, small skews, and soft soil, respectively. In contrast, rupture of the retainer anchors at the expansion piers was not observed at all.

6. Rupture of the steel fixed bearing anchors at Pier 2 occurred in only 4% of the analyses. Most of these ruptures occurred in bridges with the short columns, large skews, and hard foundation soil, when subjected to the pure longitudinal and 135° ground motions.

7. Sliding of the elastomeric bearings at Abutments 1 and 2 was observed in 33% and 22% of the analyses, respectively. Over 95% of the sliding occurred in tall-pier bridges. In contrast, bearing sliding at Pier 1 did not occur in any analysis. This observation on the sliding behavior is consistent with the findings of the prior research (Revell 2013). Neither unseating of the elastomeric bearings at the abutments or expansion piers, nor unseating of the steel fixed bearings at the fixed piers was observed in any analysis.

8. Reinforcing steel at the column bases of the expansion piers yielded in 10% of the analyses, but it rose up to 42% for the fixed piers. The short fixed piers sustained larger reinforcing steel strains than the tall ones, when subjected to non-transverse ground motions. The short

expansion piers experienced larger reinforcing steel strain than the tall ones, regardless of the ground motion direction. For both types of piers, the reinforcing steel and concrete cover was either undamaged or only lightly damaged.

9. Yielding of the abutment piles occurred in over 60% of the analyses. The piles were either unyielded or only lightly strained beyond yielding. Tall-pier bridges experienced larger strains and more yielding of abutment piles than short-pier ones. The pure transverse ground motions caused the fewest occurrences of abutment pile yielding of all the incident directions.

10. Yielding of the piles supporting the expansion and fixed piers was observed in 17% and 32% of the analyses, respectively. The pier piles were also either unyielded or lightly strained beyond yielding. Tall-pier bridges experienced larger strains and more yielding of the expansion-pier piles than their short-pier equivalents, but this tendency was reversed for the fixed-pier piles. The pier piles in the soft foundation soil were more prone to yielding than those in the hard soil. Much more yielding of the pier piles was caused by the pure transverse and 135° ground motions than those in the other two directions.

6.3.2 Four-span steel-plate-girder (4S) bridges

Superstructures of 4S bridges

Table 6.12 indicates the medians and median absolute deviations of the peak deck center displacements of 4S bridge variants caused by the 20 seismic ground motions applied in different incident directions. By comparing Tables 6.2 and 6.12, it can be found that the overall magnitude of the 4S bridge displacements is much larger than that of the 3S bridges.

As can be seen in Table 6.12, the superstructures of skew 4S bridges bi-axially displaced, even though the ground motions were uni-axially applied. Additionally, the tabulated peak displacement components perpendicular to the uni-axial ground motion direction generally increased with the skew. The uni-axial ground motions were generally more critical than the bi-axial ones for causing large deck displacements. These behaviors are similar to those of 3S bridges.

Overall, tall-pier 4S bridges experienced larger deck displacements in both bridge axes than

their short-pier equivalents. The effect of foundation soil condition on the deck displacements varied from case to case in Table 6.12.

Table 6.12: Peak deck center displacements (units: mm) of 4S bridges (longitudinal and transverse displacement components are placed on the left and right sides of the commas, respectively; numbers outside the parentheses are medians while those inside are median absolute deviations; for each bridge, the largest median peak displacement caused by the ground motions in the four incident directions is highlighted by bold numbers)

Foundation soil condition			Hard				Soft			
Pier column height (m)			4.57		12.19		4.57		12.19	
Longitudinal (0°) ground motions	Bridge skew (°)	0	**162** (23) ,	0 (0)	**244** (42) ,	0 (0)	**187** (28) ,	0 (0)	**300** (70) ,	0 (0)
		15	**170** (19) ,	42 (5)	**250** (33) ,	87 (8)	**192** (30) ,	41 (5)	**283** (58) ,	91 (19)
		30	**162** (18) ,	**80** (11)	**229** (32) ,	162 (17)	**188** (23) ,	63 (10)	**266** (80) ,	152 (50)
		45	**157** (18) ,	**97** (16)	**195** (48) ,	197 (27)	**189** (33) ,	35 (4)	**269** (62) ,	194 (48)
		60	**178** (30) ,	57 (8)	**200** (50) ,	207 (22)	**194** (34) ,	52 (8)	**240** (68) ,	179 (22)
45° ground motions	Bridge skew (°)	0	124 (11) ,	36 (7)	164 (27) ,	145 (21)	129 (9) ,	63 (6)	210 (36) ,	145 (20)
		15	136 (13) ,	**51** (7)	202 (24) ,	155 (32)	142 (13) ,	71 (8)	227 (72) ,	152 (30)
		30	146 (18) ,	79 (13)	195 (43) ,	194 (23)	149 (16) ,	84 (11)	265 (67) ,	184 (50)
		45	144 (18) ,	96 (12)	187 (29) ,	**248** (43)	145 (10) ,	94 (9)	238 (58) ,	240 (58)
		60	146 (17) ,	88 (17)	184 (20) ,	**300** (57)	136 (13) ,	92 (12)	199 (44) ,	**290** (64)
Transverse (90°) ground motions	Bridge skew (°)	0	0 (0) ,	**45** (9)	0 (0) ,	**232** (46)	0 (0) ,	**114** (25)	0 (0) ,	**219** (52)
		15	38 (8) ,	48 (9)	83 (7) ,	**237** (37)	42 (12) ,	**115** (21)	76 (7) ,	**231** (54)
		30	69 (4) ,	69 (8)	108 (12) ,	**259** (45)	54 (14) ,	**121** (21)	102 (19) ,	**263** (65)
		45	72 (6) ,	78 (10)	142 (21) ,	233 (50)	40 (3) ,	**101** (12)	119 (35) ,	**272** (56)
		60	65 (3) ,	**97** (14)	159 (31) ,	257 (66)	40 (4) ,	**110** (14)	148 (42) ,	278 (87)
135° ground motions	Bridge skew (°)	0	124 (11) ,	36 (6)	164 (28) ,	146 (23)	130 (10) ,	63 (6)	209 (35) ,	145 (20)
		15	118 (10) ,	50 (5)	152 (22) ,	180 (36)	138 (12) ,	72 (10)	195 (40) ,	150 (21)
		30	115 (9) ,	68 (8)	158 (39) ,	203 (27)	149 (18) ,	88 (15)	203 (58) ,	175 (27)
		45	105 (9) ,	77 (5)	153 (36) ,	209 (14)	155 (20) ,	87 (14)	200 (58) ,	171 (25)
		60	110 (23) ,	80 (7)	181 (23) ,	219 (23)	157 (29) ,	79 (9)	179 (35) ,	193 (33)

Table 6.13 indicates the medians and median absolute deviations of the peak deck rotations of 4S bridges. All the tabulated median peak rotations were smaller than 1°, and the overall magnitude was much smaller than that of the 3S bridges. In many of the tabulated cases, the rotations of the highly skewed decks were larger than those of the decks with smaller skews. In most cases, tall-pier bridges sustained much larger rotations than their short-pier equivalents in either direction. The effect of foundation soil condition on the deck rotations was insignificant. These observations

are similar to those of 3S bridges.

Table 6.13: Peak deck rotations (units: 0.01°) of 4S bridges (data for clockwise and counterclockwise rotations are placed on the left and right sides of the commas, respectively; numbers outside the parentheses are medians while those inside are median absolute deviations; for each bridge, the largest median peak rotation caused by the ground motions in the four incident directions is highlighted by bold numbers)

Foundation soil condition			Hard				Soft			
Pier column height (m)			4.57		12.19		4.57		12.19	
Longitudinal (0º) ground motions	Bridge skew (º)	0	0 (0) , 0 (0)		0 (0) , 0 (0)		0 (0) , 0 (0)		0 (0) , 0 (0)	
		15	**4** (1) , **2** (0)		7 (1) , 4 (0)		**4** (1) , 2 (0)		7 (2) , 4 (1)	
		30	**8** (2) , **4** (0)		11 (2) , 7 (1)		**7** (1) , 3 (0)		12 (2) , 7 (1)	
		45	**9** (2) , 5 (1)		14 (3) , 8 (1)		5 (1) , 2 (0)		14 (2) , 7 (1)	
		60	4 (1) , 2 (0)		15 (2) , 7 (1)		4 (1) , 2 (0)		13 (1) , 7 (1)	
45º ground motions	Bridge skew (º)	0	1 (0) , 1 (0)		6 (1) , 6 (1)		2 (0) , 2 (0)		6 (1) , 6 (1)	
		15	**4** (1) , **2** (0)		8 (1) , 7 (1)		**4** (1) , 3 (0)		**9** (1) , 7 (0)	
		30	7 (1) , **4** (0)		**13** (1) , 8 (1)		6 (1) , 3 (0)		**13** (2) , 8 (1)	
		45	9 (1) , **5** (0)		**18** (2) , **10** (1)		**6** (1) , **4** (0)		**16** (3) , **10** (1)	
		60	**7** (1) , **4** (1)		**19** (5) , **11** (1)		**5** (1) , **3** (0)		**20** (4) , **11** (1)	
Transverse (90º) ground motions	Bridge skew (º)	0	**2** (1) , **2** (1)		**8** (2) , **8** (1)		4 (1) , **4** (1)		**8** (2) , **8** (2)	
		15	3 (1) , 2 (1)		**9** (1) , **8** (1)		**4** (1) , **4** (1)		8 (2) , **8** (2)	
		30	3 (1) , 3 (1)		10 (4) , **9** (1)		4 (1) , **4** (0)		11 (2) , **9** (2)	
		45	3 (0) , 3 (0)		12 (5) , 8 (1)		4 (1) , 3 (0)		12 (4) , **10** (1)	
		60	5 (1) , 3 (1)		15 (6) , 9 (1)		4 (1) , **3** (0)		14 (6) , 9 (1)	
135º ground motions	Bridge skew (º)	0	1 (0) , 1 (0)		6 (1) , 6 (1)		2 (0) , 2 (0)		6 (1) , 6 (1)	
		15	3 (0) , **2** (0)		8 (1) , 6 (1)		3 (0) , 2 (0)		6 (1) , 5 (0)	
		30	5 (1) , 3 (0)		8 (1) , 7 (1)		4 (0) , 3 (1)		8 (1) , 6 (0)	
		45	5 (0) , 4 (0)		8 (2) , 7 (1)		4 (0) , 3 (0)		7 (1) , 6 (1)	
		60	4 (0) , 3 (1)		8 (2) , 7 (1)		4 (0) , **3** (0)		7 (1) , 6 (1)	

Full data of limit state occurrences for 4S bridges

Table 6.14 lists the full data of component limit state occurrences for each of the 20 4S bridge variants, when subjected to the suite of 20 seismic ground motions applied in the four different incident directions. Each percentage in the table indicates the number of analyses with occurrences of a limit state out of the 20 analyses with the 20 ground motions applied to a bridge variant in one incident direction. Three gradient color scales, blue, yellow, and red, were used in conjunction with the percentages in Table 6.14 to highlight the occurrences of the preferred, acceptable, and

unacceptable limit states defined in Table 5.1.

The data listed in Table 6.14 were subsequently grouped by bridge substructures, including the two abutments, two expansion piers, and one fixed pier. For the substructure groups, the data in Table 6.14 were further analyzed and their statistical summaries are presented in Tables 6.15, 6.19, and 6.21.

Table 6.14: Limit state occurrences of each 4S bridge variant under 0° and 45° ground motions (each percentage indicates the number of analyses with occurrences of a limit state out of the 20 analyses with ground motions applied to a bridge variant in an incident direction)

Ground motion direction	Bridge variant	Critical limit states: Abutment 1 (A1)									Pier 1 (P1, expansion pier)						Pier 2 (P2, fixed pier)					Pier 3 (P3, expansion pier)						Abutment 2 (A2)								
		CEJ	MBU	FBP	RRA	SEB	UBA	UBO	YPW	YPB	RRA	SEB	UEB	YRS	CCC	YPP	RFA	USB	YRS	CCC	YPP	RRA	SEB	UEB	YRS	CCC	YPP	CEJ	MBU	FBP	RRA	SEB	UBO	UBA	YPW	YPB
0°	4S00P15H	100%	0	0	0	50%	0	0	100%	100%	0	0	0	50%	5%	0	0	0	100%	90%	0	0	0	0	55%	5%	0	100%	0	0	0	40%	0	0	100%	100%
	4S15P15H	100%	0	0	0	55%	0	0	100%	100%	0	0	0	65%	5%	0	0	0	100%	100%	0	0	0	0	65%	5%	0	100%	0	0	0	40%	0	0	100%	100%
	4S30P15H	100%	0	0	0	20%	0	0	100%	100%	0	0	0	80%	15%	0	0	0	100%	100%	5%	0	0	0	85%	25%	0	100%	0	0	0	35%	0	0	100%	100%
	4S45P15H	100%	0	0	0	5%	0	0	100%	100%	0	0	0	80%	5%	0	45%	0	100%	100%	100%	0	0	0	75%	20%	0	100%	0	0	0	20%	0	0	100%	100%
	4S60P15H	100%	0	0	0	60%	0	0	100%	65%	0	0	0	0	0	0	100%	0	100%	0	100%	0	0	0	0	0	0	100%	0	0	0	50%	0	0	90%	75%
	4S00P40H	100%	25%	0	0	75%	0	0	100%	100%	0	0	0	65%	0	0	0	0	80%	0	0	0	0	0	65%	0	0	100%	20%	0	0	75%	0	0	100%	100%
	4S15P40H	100%	20%	0	0	75%	0	0	100%	100%	0	0	0	75%	0	0	0	0	80%	0	0	0	0	0	75%	0	0	100%	0	0	0	80%	0	0	100%	100%
	4S30P40H	100%	0	0	25%	75%	0	0	100%	100%	0	0	0	75%	0	0	0	0	80%	0	0	0	0	0	80%	0	0	100%	0	0	10%	80%	0	0	100%	100%
	4S45P40H	100%	0	0	65%	55%	0	0	100%	80%	0	0	0	80%	0	0	0	0	80%	0	55%	0	0	0	75%	0	5%	100%	0	0	70%	70%	0	0	100%	80%
	4S60P40H	100%	0	0	70%	75%	0	0	85%	80%	0	0	0	80%	0	0	65%	0	95%	0	75%	0	0	0	75%	0	0	100%	0	0	70%	65%	0	0	85%	75%
	4S00P15S	100%	0	0	0	50%	0	0	100%	100%	0	0	0	75%	5%	0	0	0	100%	100%	0	0	0	0	75%	5%	0	100%	0	0	0	55%	0	0	100%	100%
	4S15P15S	100%	0	0	0	50%	0	0	100%	100%	0	0	0	75%	0	0	0	0	100%	100%	0	0	0	0	75%	0	0	100%	0	0	0	50%	0	0	100%	100%
	4S30P15S	100%	0	0	0	45%	0	0	100%	100%	0	0	0	80%	10%	0	0	0	100%	100%	100%	0	0	0	85%	5%	5%	100%	0	0	0	45%	0	0	100%	100%
	4S45P15S	100%	0	0	0	35%	0	0	100%	100%	0	0	0	10%	0	45%	0	0	100%	80%	100%	0	0	0	20%	0	40%	100%	0	0	0	40%	0	0	100%	100%
	4S60P15S	100%	0	0	0	45%	0	0	90%	90%	0	0	0	0	0	70%	80%	0	100%	0	100%	0	0	0	0	0	75%	100%	0	0	0	30%	0	0	80%	90%
	4S00P40S	100%	60%	5%	0	75%	0	0	100%	100%	0	0	0	75%	0	0	0	0	80%	5%	0	0	0	0	80%	0	0	100%	70%	5%	0	80%	0	0	100%	100%
	4S15P40S	100%	35%	0	0	80%	0	0	100%	100%	0	0	0	80%	15%	0	0	0	80%	20%	0	0	0	0	80%	15%	0	100%	55%	0	0	80%	0	0	100%	100%
	4S30P40S	100%	25%	0	20%	75%	0	0	100%	100%	0	0	0	75%	15%	25%	0	0	80%	20%	65%	0	0	0	75%	20%	15%	100%	35%	0	20%	80%	0	0	100%	100%
	4S45P40S	100%	0	0	50%	70%	0	0	100%	100%	0	0	0	75%	0	50%	0	0	80%	10%	90%	0	0	0	70%	0	60%	100%	0	0	30%	75%	0	0	100%	100%
	4S60P40S	100%	0	0	55%	80%	0	0	80%	85%	0	0	0	75%	0	60%	0	0	80%	0	100%	0	0	0	65%	0	60%	100%	0	0	25%	65%	0	0	80%	85%
45°	4S00P15H	100%	0	0	0	5%	0	0	100%	100%	0	0	0	5%	0	5%	0	0	100%	75%	50%	0	0	0	5%	0	0	100%	0	0	0	5%	0	0	100%	100%
	4S15P15H	100%	0	0	0	5%	0	0	100%	100%	0	0	0	70%	0	0	0	0	100%	90%	40%	0	0	0	65%	0	0	100%	0	0	0	5%	0	0	100%	100%
	4S30P15H	100%	0	0	0	5%	0	0	100%	100%	0	0	0	90%	15%	0	0	0	100%	100%	50%	0	0	0	90%	5%	0	100%	0	0	0	10%	0	0	100%	100%
	4S45P15H	100%	0	0	0	5%	0	0	100%	95%	0	0	0	80%	5%	0	0	0	100%	95%	100%	0	0	0	85%	10%	0	100%	0	0	0	5%	0	0	100%	95%
	4S60P15H	100%	0	0	0	30%	0	0	95%	75%	0	0	0	80%	0	0	100%	0	100%	65%	100%	0	0	0	65%	0	0	100%	0	0	0	0	0	0	85%	65%
	4S00P40H	100%	0	0	5%	45%	0	0	100%	100%	0	0	0	70%	0	40%	0	0	80%	5%	55%	0	0	0	70%	0	25%	100%	0	0	0	50%	0	0	100%	95%
	4S15P40H	100%	0	0	0	75%	0	0	100%	100%	0	0	0	75%	0	5%	0	0	80%	0	5%	0	0	0	75%	0	5%	100%	0	0	5%	75%	0	0	100%	100%
	4S30P40H	100%	0	0	25%	75%	0	0	100%	100%	0	0	0	80%	0	0	0	0	80%	0	0	0	0	0	80%	0	0	100%	0	0	0	75%	0	0	100%	100%
	4S45P40H	100%	0	0	60%	75%	0	0	100%	90%	0	0	0	80%	0	0	0	0	80%	0	0	0	0	0	80%	0	0	100%	0	0	35%	60%	0	0	100%	90%
	4S60P40H	100%	0	0	75%	75%	0	0	100%	80%	0	0	0	80%	5%	0	0	0	85%	5%	0	0	0	0	80%	20%	0	100%	0	0	75%	70%	0	0	100%	80%
	4S00P15S	100%	0	0	0	5%	0	0	100%	100%	0	0	0	15%	0	80%	0	0	100%	100%	100%	0	0	0	20%	0	80%	100%	0	0	0	5%	0	0	100%	100%
	4S15P15S	100%	0	0	0	10%	0	0	100%	100%	0	0	0	55%	0	55%	0	0	100%	100%	100%	0	0	0	45%	0	70%	100%	0	0	0	5%	0	0	100%	100%
	4S30P15S	100%	0	0	0	10%	0	0	100%	100%	0	0	0	80%	0	40%	0	0	100%	100%	100%	0	0	0	80%	0	70%	100%	0	0	0	15%	0	0	100%	100%
	4S45P15S	100%	0	0	0	10%	0	0	100%	100%	0	0	0	70%	0	45%	0	0	100%	90%	100%	0	0	0	65%	0	55%	100%	0	0	0	5%	0	0	100%	100%
	4S60P15S	100%	0	0	0	0	0	0	65%	80%	0	0	0	65%	0	10%	15%	0	100%	45%	100%	0	0	0	35%	0	5%	100%	0	0	0	0	0	0	70%	80%
	4S00P40S	100%	0	0	0	75%	0	0	95%	90%	0	0	0	55%	0	80%	0	0	80%	0	100%	0	0	0	40%	0	80%	100%	0	0	0	75%	0	0	95%	95%
	4S15P40S	100%	30%	0	0	75%	0	0	100%	100%	0	0	0	75%	0	75%	0	0	80%	0	95%	0	0	0	75%	0	75%	100%	35%	0	0	75%	0	0	100%	100%
	4S30P40S	100%	25%	0	20%	80%	0	0	100%	100%	0	0	0	75%	10%	20%	0	0	80%	20%	75%	0	0	0	75%	20%	15%	100%	35%	0	20%	80%	0	0	100%	100%
	4S45P40S	100%	15%	0	55%	80%	0	0	100%	100%	0	0	0	80%	10%	0	0	0	80%	25%	5%	0	0	0	80%	15%	0	100%	20%	0	20%	80%	0	0	100%	100%
	4S60P40S	100%	0	0	75%	75%	0	0	90%	90%	0	0	0	80%	15%	0	0	0	80%	20%	0	0	0	0	80%	15%	0	100%	0	0	50%	65%	0	0	90%	95%
Preferred limit states:		0	20%	40%	60%	80%	100%																											
Acceptable limit states:		0	20%	40%	60%	80%	100%																											
Unacceptable limit states:		0	20%	40%	60%	80%	100%																											

Table 6.14 Continued: limit state occurrences of each 4S bridge variant under 90° and 135° ground motions

Ground motion direction	Bridge variant	Critical limit states																														
		Abutment 1 (A1)									Pier 1 (P1, expansion pier)						Pier 2 (P2, fixed pier)					Pier 3 (P3, expansion pier)						Abutment 2 (A2)							
		CEJ	MBU	FBP	RRA	SEB	UBA	UBO	YPW	YPB	RRA	SEB	UEB	YRS	CCC	YPP	RFA	USB	YRS	CCC	YPP	RRA	SEB	UEB	YRS	CCC	YPP	CEJ	MBU	FBP	RRA	SEB	UBO	UBA	YPW	YPB
90°	4S00P15H	0	0	0	0	0	0	0	0	75%	0	0	0	0	0	45%	0	0	30%	0	90%	0	0	0	0	0	45%	0	0	0	0	0	0	0	0	70%
	4S15P15H	5%	0	0	0	0	0	0	5%	85%	0	0	0	0	0	45%	0	0	70%	0	100%	0	0	0	0	0	40%	5%	0	0	0	0	0	0	5%	75%
	4S30P15H	90%	0	0	0	0	0	0	40%	85%	0	0	0	25%	0	25%	25%	0	100%	0	100%	0	0	0	20%	0	40%	95%	0	0	0	0	0	0	50%	80%
	4S45P15H	100%	0	0	0	0	0	0	80%	40%	0	0	0	65%	0	0	70%	0	100%	5%	100%	0	0	0	65%	0	0	100%	0	0	0	0	0	0	55%	25%
	4S60P15H	100%	0	0	5%	0	0	0	70%	0	0	0	0	100%	0	0	95%	0	100%	0	100%	0	0	0	100%	0	0	100%	0	0	0	0	0	0	25%	0
	4S00P40H	0	0	0	60%	40%	0	0	0	100%	0	0	0	100%	20%	75%	0	0	100%	50%	90%	0	0	0	100%	15%	75%	0	0	0	60%	25%	0	0	0	100%
	4S15P40H	75%	0	0	55%	20%	0	0	65%	100%	0	0	0	95%	10%	75%	0	0	100%	45%	85%	0	0	0	100%	20%	75%	75%	0	0	65%	35%	0	0	65%	100%
	4S30P40H	100%	0	0	70%	40%	0	0	95%	100%	0	0	0	85%	10%	75%	0	0	100%	70%	85%	0	0	0	80%	25%	75%	100%	0	0	65%	40%	0	0	95%	100%
	4S45P40H	100%	0	0	70%	70%	0	0	80%	85%	0	0	0	75%	0	35%	0	0	100%	35%	95%	0	0	0	70%	20%	50%	100%	0	0	65%	40%	0	0	80%	80%
	4S60P40H	100%	0	0	75%	75%	0	0	85%	80%	0	0	0	75%	0	0	30%	0	100%	20%	75%	0	0	0	75%	20%	0	100%	0	0	70%	45%	0	0	85%	80%
	4S00P15S	0	0	0	0	0	0	0	0	70%	0	0	0	0	0	100%	0	0	0	0	100%	0	0	0	0	0	100%	0	0	0	0	0	0	0	0	60%
	4S15P15S	35%	0	0	0	0	0	0	5%	80%	0	0	0	0	0	100%	0	0	55%	5%	100%	0	0	0	0	0	100%	35%	0	0	0	0	0	0	5%	70%
	4S30P15S	75%	0	0	0	0	0	0	15%	80%	0	0	0	0	0	100%	0	0	85%	5%	100%	0	0	0	15%	0	100%	75%	0	0	0	0	0	0	15%	80%
	4S45P15S	80%	0	0	0	0	0	0	5%	80%	0	0	0	35%	0	95%	0	0	95%	5%	100%	0	0	0	20%	0	90%	55%	0	0	0	0	0	0	0	50%
	4S60P15S	100%	0	0	0	0	0	0	0	70%	0	0	0	100%	0	65%	0	0	100%	0	100%	0	0	0	90%	0	45%	100%	0	0	0	0	0	0	0	45%
	4S00P40S	0	0	0	10%	5%	0	0	0	85%	0	0	0	80%	0	100%	0	0	90%	0	100%	0	0	0	80%	0	100%	0	0	0	10%	0	0	0	0	85%
	4S15P40S	70%	0	0	20%	15%	0	0	40%	85%	0	0	0	80%	0	100%	0	0	100%	0	100%	0	0	0	80%	0	100%	70%	0	0	10%	0	0	0	35%	85%
	4S30P40S	100%	0	0	15%	10%	0	0	80%	100%	0	0	0	80%	0	100%	0	0	100%	5%	100%	0	0	0	80%	15%	100%	100%	0	0	30%	25%	0	0	75%	95%
	4S45P40S	100%	0	0	45%	30%	0	0	80%	85%	0	0	0	75%	0	90%	0	0	80%	0	100%	0	0	0	75%	15%	90%	100%	0	0	35%	35%	0	0	80%	80%
	4S60P40S	100%	0	0	65%	60%	0	0	80%	80%	0	0	0	80%	10%	45%	0	0	80%	20%	100%	0	0	0	80%	20%	40%	100%	0	0	50%	45%	0	5%	80%	80%
135°	4S00P15H	100%	0	0	0	5%	0	0	100%	100%	0	0	0	0	0	5%	0	0	100%	80%	50%	0	0	0	5%	0	0	100%	0	0	0	5%	0	0	100%	100%
	4S15P15H	100%	0	0	0	0	0	0	100%	100%	0	0	0	0	0	5%	5%	0	100%	85%	90%	0	0	0	5%	0	5%	100%	0	0	0	0	0	0	100%	100%
	4S30P15H	100%	0	0	0	0	0	0	100%	100%	0	0	0	55%	0	10%	25%	0	100%	85%	100%	0	0	0	55%	0	0	100%	0	0	0	0	0	0	100%	100%
	4S45P15H	100%	0	0	0	0	0	0	90%	70%	0	0	0	60%	0	0	100%	0	100%	20%	100%	0	0	0	30%	0	0	100%	0	0	0	0	0	0	90%	70%
	4S60P15H	100%	0	0	0	10%	0	0	25%	0	0	0	0	35%	0	0	100%	0	70%	0	100%	0	0	0	25%	0	0	100%	0	0	0	0	0	0	50%	25%
	4S00P40H	100%	0	0	0	50%	0	0	100%	95%	0	0	0	70%	0	35%	0	0	85%	5%	55%	0	0	0	70%	0	30%	100%	0	0	0	45%	0	0	100%	100%
	4S15P40H	100%	0	0	25%	20%	0	0	100%	100%	0	0	0	75%	0	60%	0	0	100%	25%	75%	0	0	0	80%	0	60%	100%	0	0	20%	15%	0	0	100%	95%
	4S30P40H	100%	0	0	50%	40%	0	0	95%	100%	0	0	0	85%	5%	75%	0	0	100%	35%	80%	0	0	0	85%	5%	75%	100%	0	0	60%	40%	0	0	100%	100%
	4S45P40H	80%	0	0	60%	70%	0	0	45%	80%	0	0	0	75%	5%	75%	0	0	100%	50%	100%	0	0	0	75%	0	75%	80%	0	0	75%	50%	0	0	45%	75%
	4S60P40H	75%	0	0	75%	75%	0	0	5%	25%	0	0	0	75%	0	25%	85%	0	100%	25%	100%	0	0	0	75%	0	15%	65%	0	0	65%	40%	0	0	0	30%
	4S00P15S	100%	0	0	0	5%	0	0	100%	100%	0	0	0	20%	0	80%	0	0	100%	100%	100%	0	0	0	15%	0	80%	100%	0	0	0	5%	0	0	100%	100%
	4S15P15S	100%	0	0	0	5%	0	0	100%	100%	0	0	0	0	0	80%	0	0	100%	100%	100%	0	0	0	5%	0	80%	100%	0	0	0	5%	0	0	100%	100%
	4S30P15S	100%	0	0	0	5%	0	0	100%	100%	0	0	0	0	0	85%	0	0	100%	85%	100%	0	0	0	5%	0	80%	100%	0	0	0	0	0	0	100%	100%
	4S45P15S	100%	0	0	0	5%	0	0	85%	90%	0	0	0	0	0	80%	0	0	100%	25%	100%	0	0	0	0	0	80%	100%	0	0	0	0	0	0	100%	100%
	4S60P15S	100%	0	0	0	5%	0	0	75%	75%	0	0	0	0	0	80%	0	0	100%	0	100%	0	0	0	0	0	80%	100%	0	0	0	0	0	0	75%	75%
	4S00P40S	100%	0	0	0	75%	0	0	95%	95%	0	0	0	55%	0	80%	0	0	80%	0	100%	0	0	0	60%	0	80%	100%	0	0	0	75%	0	0	95%	90%
	4S15P40S	100%	0	0	0	55%	0	0	100%	100%	0	0	0	45%	0	100%	0	0	85%	0	100%	0	0	0	45%	0	100%	100%	0	0	0	45%	0	0	95%	100%
	4S30P40S	100%	0	0	10%	40%	0	0	100%	100%	0	0	0	75%	0	100%	0	0	100%	0	100%	0	0	0	80%	0	100%	100%	0	0	0	50%	0	0	95%	100%
	4S45P40S	80%	0	0	10%	35%	0	0	75%	90%	0	0	0	30%	0	100%	0	0	85%	0	100%	0	0	0	45%	0	100%	80%	0	0	0	50%	0	0	80%	80%
	4S60P40S	85%	0	0	25%	45%	0	0	80%	85%	0	0	0	35%	0	85%	0	0	85%	0	100%	0	0	0	35%	0	85%	80%	0	0	15%	15%	0	0	75%	85%
Preferred limit states:		0	20%	40%	60%	80%	100%																											
Acceptable limit states:		0	20%	40%	60%	80%	100%																											
Unacceptable limit states:		0	20%	40%	60%	80%	100%																											

Abutments of 4S bridges

Table 6.15 statistically summarizes the occurrences of component limit states at the abutments of 4S bridges. Similar to the 3S bridges, closure of the expansion joints at Abutments 1 and 2 (CEJ@A1 and A2) occurred in most 4S bridge analyses, except those of non-skew or lightly skewed bridge subjected to the pure transverse ground motions.

Mobilization of ultimate backfill passive resistance (MBU@A1 and A2) occurred in only 3% of the analyses, all of which involved non-skew and lightly skewed, tall-pier bridges subjected to the pure longitudinal and 45° ground motions. The small skews, tall pier columns and these two ground motion directions are necessary conditions for large longitudinal superstructure displacements and significant superstructure-abutment interactions normal to the abutment backwall and backfill, which is required to mobilize ultimate backfill resistance. Failure of the backwall-pile cap connections (FBP@A1 and A2) occurred in only one analysis of a non-skew and tall-pier bridge in the soft soil (4S00P40H), when subjected to a longitudinal ground motion.

Rupture of the retainer anchors at Abutments 1 and 2 (RRA@A1 and A2) was observed in 17% and 14% of the 4S bridge analyses, respectively. These percentages are lower than those of 3S bridges (41% and 24%). The ruptures occurred almost exclusively in the analyses of tall-pier 4S bridges that experienced much larger deck displacements than their short-pier equivalents. It can also be observed in Table 6.5 that the ruptures increased with the bridge skew. The pure transverse ground motions caused the most occurrences among all the incident directions, similar to the 3S bridges. Bridges in the hard soil sustained much more ruptures than those in the soft soil. These tendencies are similar to those of 3S bridges.

Sliding of the elastomeric bearings at Abutments 1 and 2 (SEB@A1 and A2) was observed in 36% and 33% of the analyses, respectively. Similar to the observation of 3S bridges, tall-pier 4S bridges accounted for over 80% of the occurrences. Figure 6.8 illustrates the peak bearing sliding at the four deck corners. In only one of the 1,600 4S bridge analyses, bearing unseating at the abutment was observed, which occurred in the analysis of a 60°-skew tall-pier bridge with the hard foundation soil subjected to a pure transverse ground motion, as shown in Figure 6.8(d) and Table 6.15. Besides this occurrence of unseating, the peak bearing sliding distance in several other analyses of highly skewed (30°-, 45°-, and 60°-skew) bridges is quite close to the minimum seat width in the abutment-normal direction. At all the four deck corners, the abutment-normal

direction is more critical for bearing unseating than the abutment-parallel direction. By comparing Figures 6.7 and 6.8, it can be found that the overall abutment-normal bearing sliding ratio of 4S bridges is larger than that of 3S bridges.

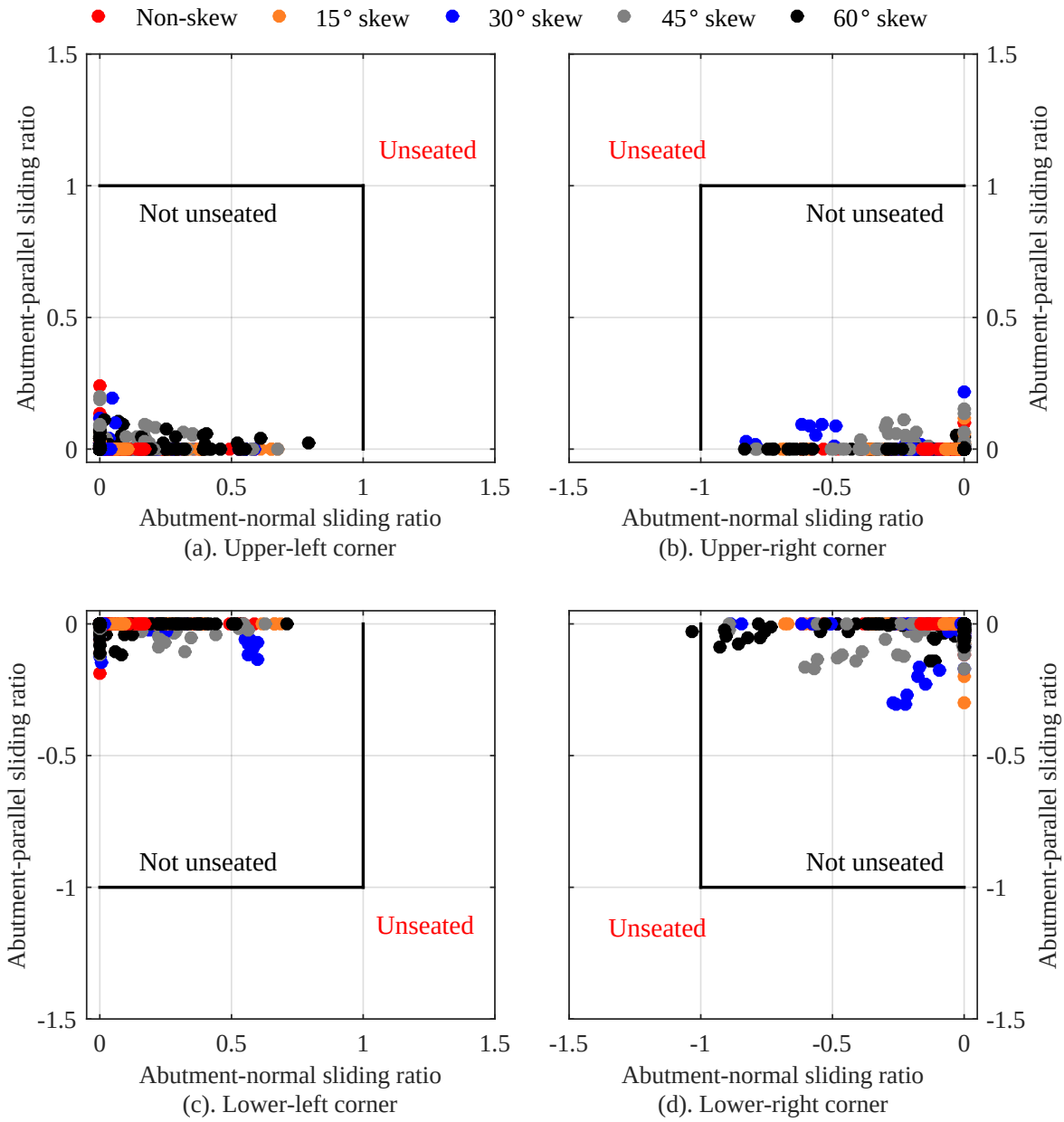

Figure 6.8: Peak sliding ratios of elastomeric bearings at deck corners of 4S bridges

Yielding of the steel H piles supporting the abutments of 4S bridges (YPW & YPB @A1 and A2) was observed in over 80% of the analyses, as indicated in Table 6.15. Additionally, Table 6.16 lists the median peak strains of the abutment piles. It can be found that the piles were yielded in most

of the tabulated cases. Consistent with the observation of 3S bridges, the abutment piles were the least strained under the pure transverse ground motions and the piles of tall-pier 4S bridges experienced larger strains than their short-pier equivalents. By comparing Tables 6.15 and 6.16 with Tables 6.5 and 6.6, it can be found that yielding of the abutment piles occurred in more 4S bridge analyses than in 3S bridge analyses and the overall peak pile strain of 4S bridges is also larger.

Expansion piers (Piers 1 and 3) of 4S bridges

Table 6.19 statistically summarizes the occurrences of several component limit states at the expansion piers (Piers 1 and 3) of 4S bridges. Similar to the response of 3S bridges, the anchors of bearing side retainers at the expansion piers of 4S bridges were not ruptured in any analysis (RRA@P1 and P3).

Yielding of the vertical reinforcing steel at the column base of Piers 1 and 3 (YRS@P1 and P3) was observed in more than 50% of the 4S bridge analyses. Table 6.17 lists the median peak strains of vertical reinforcing steel at the pier column base of 4S bridges. The data on the left and right sides of the commas are for the expansion and fixed piers, respectively. It can be seen that in most of the tabulated cases, the reinforcing steel was lightly or moderately damaged, while in only a few cases it elastically deformed without yielding. By comparing the median peak strains in Table 6.17 with those in Table 6.8, it can be clearly observed that the column reinforcing steel of 4S bridges was strained more than that of 3S bridges. This can be further confirmed by comparing the occurrence percentage of reinforcing steel yielding indicated in Tables 6.7 and 6.19. The occurrence percentage of 4S bridges (around 50%) is much higher than that of 3S bridges (7%). A potential reason for this difference is the superstructure mass and induced seismic force. 4S bridges have more massive superstructures than 3S bridges, which induces almost twice the seismic force of 3S bridges under the same ground motion. The other potential reason for the difference in reinforcing steel yielding is that the steel fixed bearings of 4S bridges are larger in diameter than those of 3S bridges, which is also a result of the larger superstructure mass as the anchors were sized using the superstructure dead load imposed on the bearings. 65% of the analyses with reinforcing steel yielding involved tall-pier 4S bridge variants, while only 35% involved short-pier variants, which is similar to the tendency of 3S bridges.

Yielding of the steel piles supporting the expansion piers (YSP@P1 and P3) of 4S bridges oc-

Table 6.15: Occurrences of limit states at abutments (A1 and A2) of 4S bridge variants

Limit state	No. of analyses with occurrence [1]	Skew angle [2] (°)					Foundation soil [2]		Column height [2] (m)		Ground motion incident angle [2] (°)			
		0	15	30	45	60	Hard	Soft	4.57	12.19	0	45	90	135
Closure of expansion joint (CEJ@A1)	1450 (91%)	240 (17%)	277 (19%)	313 (22%)	308 (21%)	312 (22%)	725 (50%)	725 (50%)	717 (49%)	733 (51%)	400 (28%)	400 (28%)	266 (18%)	384 (26%)
Mobilization of backfill ultimate capacity (MBU@A1)	47 (3%)	17 (36%)	17 (36%)	10 (21%)	3 (6%)	0 (0%)	9 (19%)	38 (81%)	0 (0%)	47 (100%)	33 (70%)	14 (30%)	0 (0%)	0 (0%)
Failure of backwall-to-pile-cap connection (FBP@A1)	1 (0%)	1 (100%)	0 (0%)	0 (0%)	0 (0%)	0 (0%)	0 (0%)	1 (100%)	0 (0%)	1 (100%)	1 (100%)	0 (0%)	0 (0%)	0 (0%)
Rupture of retainer anchor (RRA@A1)	269 (17%)	15 (6%)	20 (7%)	47 (17%)	83 (31%)	104 (39%)	174 (65%)	95 (35%)	1 (0%)	268 (100%)	57 (21%)	63 (23%)	98 (36%)	51 (19%)
Sliding of elastomeric bearing (SEB@A1)	575 (36%)	112 (19%)	108 (19%)	104 (18%)	109 (19%)	142 (25%)	291 (51%)	284 (49%)	108 (19%)	467 (81%)	230 (40%)	163 (28%)	73 (13%)	109 (19%)
Unseating of bearing at obtuse corner of deck (UBA@A1)	0 (0%)	0	0	0	0	0	0	0	0	0	0	0	0	0
Unseating of bearing at acute corner of deck (UBO@A1)	0 (0%)	0	0	0	0	0	0	0	0	0	0	0	0	0
Yielding of pile supporting wingwall (YPW@A1)	1279 (80%)	238 (19%)	263 (21%)	285 (22%)	268 (21%)	225 (18%)	652 (51%)	627 (49%)	609 (48%)	670 (52%)	391 (31%)	389 (30%)	165 (13%)	334 (26%)
Yielding of pile supporting backwall (YPB@A1)	1414 (88%)	302 (21%)	310 (22%)	313 (22%)	277 (20%)	212 (15%)	677 (48%)	737 (52%)	681 (48%)	733 (52%)	380 (27%)	380 (27%)	313 (22%)	341 (24%)
Closure of expansion joint (CEJ@A2)	1443 (90%)	240 (17%)	277 (19%)	314 (22%)	303 (21%)	309 (21%)	724 (50%)	719 (50%)	713 (49%)	730 (51%)	400 (28%)	400 (28%)	262 (18%)	381 (26%)
Mobilization of backfill ultimate capacity (MBU@A2)	54 (3%)	18 (33%)	18 (33%)	14 (26%)	4 (7%)	0 (0%)	4 (7%)	50 (93%)	0 (0%)	54 (100%)	36 (67%)	18 (33%)	0 (0%)	0 (0%)
Failure of backwall-to-pile-cap connection (FBP@A2)	1 (0%)	1 (100%)	0 (0%)	0 (0%)	0 (0%)	0 (0%)	0 (0%)	1 (100%)	0 (0%)	1 (100%)	1 (100%)	0 (0%)	0 (0%)	0 (0%)
Rupture of retainer anchor (RRA@A2)	225 (14%)	14 (6%)	20 (9%)	41 (18%)	66 (29%)	84 (37%)	162 (72%)	63 (28%)	0 (0%)	225 (100%)	45 (20%)	41 (18%)	92 (41%)	47 (21%)
Sliding of elastomeric bearing (SEB@A2)	529 (33%)	108 (20%)	102 (19%)	115 (22%)	106 (20%)	98 (19%)	258 (49%)	271 (51%)	95 (18%)	434 (82%)	231 (44%)	152 (29%)	58 (11%)	88 (17%)
Unseating of bearing at obtuse corner of deck (UBO@A2)	0 (0%)	0	0	0	0	0	0	0	0	0	0	0	0	0
Unseating of bearing at acute corner of deck (UBA@A2)	1 (0%)	0 (0%)	0 (0%)	0 (0%)	0 (0%)	1 (100%)	0 (0%)	1 (100%)	0 (0%)	1 (100%)	0 (0%)	0 (0%)	1 (100%)	0 (0%)
Yielding of pile supporting wingwall (YPW@A2)	1265 (79%)	238 (19%)	261 (21%)	286 (23%)	266 (21%)	214 (17%)	641 (51%)	624 (49%)	599 (47%)	666 (53%)	387 (31%)	388 (31%)	150 (12%)	340 (27%)
Yielding of pile supporting backwall (YPB@A2)	1393 (87%)	299 (21%)	305 (22%)	311 (22%)	265 (19%)	213 (15%)	672 (48%)	721 (52%)	666 (48%)	727 (52%)	381 (27%)	379 (27%)	288 (21%)	345 (25%)

1 The number above the parentheses indicates the number of analyses with occurrences of a limit state.
The percentage inside the parentheses indicates the ratio of the number above the parentheses to all the 1,600 analyses.

2 The number above the parentheses indicates the number of analyses with occurrences of a limit state contributed by a parametric variation.
The percentage inside the parentheses indicates the relative contribution of a parametric variation to the total occurrences of a limit state.

Table 6.16: Normalized peak strains of steel H piles at abutments of 4S bridges (peak strains are normalized to the yield strain, 0.0017; numbers outside the parentheses are medians, while those inside are median absolute deviations; data for piles supporting backwalls and wingwalls are placed on the left and right sides of the commas, respectively)

Foundation soil condition			Hard								Soft							
Pier column height (m)			4.57				12.19				4.57				12.19			
Longitudinal (0º) ground motions	Bridge skew (º)	0	7.2	(2.2) ,	9.8	(2.5)	16.4	(4.4) ,	20.5	(4.8)	7.3	(2.0) ,	7.3	(2.3)	13.5	(3.3) ,	14.9	(3.7)
		15	12.3	(2.7) ,	13.3	(2.5)	25.7	(4.3) ,	26.6	(4.3)	9.6	(3.0) ,	9.0	(3.1)	17.3	(4.8) ,	17.1	(4.7)
		30	11.3	(3.3) ,	12.0	(3.1)	22.7	(6.6) ,	22.8	(6.2)	10.2	(3.4) ,	9.5	(2.9)	17.5	(8.1) ,	16.4	(7.1)
		45	4.8	(2.1) ,	6.4	(2.4)	6.8	(3.1) ,	8.9	(3.4)	7.8	(3.8) ,	7.9	(3.7)	16.1	(7.2) ,	15.5	(6.5)
		60	1.2	(0.4) ,	1.8	(0.7)	1.3	(0.4) ,	2.3	(1.3)	3.0	(1.6) ,	3.0	(1.7)	6.5	(4.3) ,	7.4	(4.9)
45º ground motions	Bridge skew (º)	0	3.7	(1.2) ,	5.6	(1.2)	8.9	(3.2) ,	11.1	(3.3)	3.3	(0.9) ,	2.5	(0.7)	9.9	(1.7) ,	9.8	(2.0)
		15	6.9	(2.0) ,	8.2	(1.8)	16.7	(4.3) ,	19.2	(3.6)	4.6	(1.3) ,	4.0	(1.2)	12.4	(5.7) ,	12.5	(5.4)
		30	9.1	(3.0) ,	9.7	(2.7)	19.0	(10.1) ,	20.3	(8.6)	5.4	(1.9) ,	4.9	(1.7)	18.4	(6.8) ,	17.3	(6.1)
		45	4.3	(1.7) ,	6.2	(1.7)	12.2	(4.2) ,	15.2	(4.1)	4.1	(1.3) ,	4.1	(1.2)	17.1	(6.2) ,	16.7	(5.2)
		60	1.0	(0.2) ,	1.7	(0.5)	2.4	(0.8) ,	5.9	(1.5)	1.5	(0.5) ,	1.4	(0.4)	9.2	(4.3) ,	9.2	(3.6)
Transverse (90º) ground motions	Bridge skew (º)	0	1.1	(0.1) ,	0.6	(0.0)	2.1	(0.4) ,	1.1	(0.2)	1.1	(0.2) ,	0.7	(0.1)	1.8	(0.8) ,	1.1	(0.4)
		15	1.1	(0.1) ,	0.7	(0.1)	2.0	(0.6) ,	2.1	(0.9)	1.2	(0.2) ,	0.9	(0.2)	2.2	(1.1) ,	1.5	(0.6)
		30	1.1	(0.1) ,	1.0	(0.1)	3.2	(1.3) ,	4.6	(2.3)	1.3	(0.2) ,	1.0	(0.2)	3.6	(2.0) ,	2.3	(1.4)
		45	0.8	(0.1) ,	1.0	(0.3)	2.2	(1.3) ,	4.6	(2.6)	1.0	(0.2) ,	0.9	(0.1)	3.2	(2.3) ,	3.2	(2.4)
		60	0.7	(0.1) ,	0.8	(0.1)	1.7	(0.5) ,	4.4	(1.0)	1.1	(0.2) ,	0.7	(0.2)	4.7	(3.2) ,	5.4	(2.7)
135º ground motions	Bridge skew (º)	0	3.5	(1.1) ,	5.5	(1.1)	8.8	(3.5) ,	11.0	(3.2)	3.3	(1.0) ,	2.5	(0.7)	9.8	(1.8) ,	9.7	(2.1)
		15	4.5	(1.8) ,	5.7	(1.7)	8.2	(3.4) ,	9.0	(3.1)	4.7	(1.7) ,	3.8	(1.3)	11.8	(4.1) ,	10.1	(3.9)
		30	2.8	(1.2) ,	3.9	(1.3)	4.1	(2.5) ,	5.2	(3.4)	5.0	(2.1) ,	4.3	(1.8)	10.0	(6.0) ,	9.0	(5.3)
		45	1.0	(0.2) ,	1.5	(0.3)	1.2	(0.2) ,	1.2	(0.3)	3.3	(1.5) ,	3.2	(1.7)	3.3	(2.4) ,	3.2	(2.3)
		60	0.7	(0.1) ,	0.8	(0.2)	0.9	(0.1) ,	0.8	(0.1)	1.5	(0.5) ,	1.3	(0.5)	1.9	(0.7) ,	1.8	(0.6)

Unyielded: normalized strain < 1 (unnormalized strain < 0.0017)

Yielded without signficniant strain hardening: 1 ≤ normalized strain < 10 (0.0017 ≤ unnormalized strain < 0.017)

Yielded and significantly strain hardened: 10 ≤ normalized strain (0.017 ≤ unnormalized strain)

curred in 39% of the analyses. Similar to the yielding of column reinforcing steel, this percentage is also higher than that of 3S bridges (17%). Table 6.20 indicates the median peak strains of steel H piles supporting the piers of 4S bridges. It can be found in Tables 6.19 and 6.20 that the piles in the soft soil were strained more than those in the hard soil, because the soft soil provides relatively low lateral resistance to the deflection of the piles. Meanwhile, over 75% of the pile yieldings occurred under the pure transverse and 135° ground motions. These observations are consistent with those of 3S bridges.

Table 6.17: Normalized peak strain of vertical reinforcing steel at pier column bases of 4S bridges (peak strain values are normalized to the yield strain, 0.0021; numbers outside the parentheses are medians, while those inside are median absolute deviations; data of reinforcing steel at column bases of expansion and fixed piers are placed on the left and right sides of the commas, respectively; performance levels in the footnote are defined per Kowalsky (2001) and Revell (2013))

Foundation soil condition			Hard				Soft			
Pier column height (m)			4.57		12.19		4.57		12.19	
Longitudinal (0º) ground motions	Bridge skew (º)	0	1.0 (0.4) ,	14.6 (3.1)	1.2 (0.3) ,	1.8 (0.6)	1.2 (0.3) ,	15.2 (3.3)	1.4 (0.8) ,	2.7 (1.5)
		15	1.2 (0.4) ,	16.0 (3.0)	1.3 (0.3) ,	1.9 (0.8)	1.3 (0.4) ,	16.2 (2.8)	1.3 (0.7) ,	2.4 (1.3)
		30	1.7 (0.6) ,	16.7 (2.7)	1.3 (0.3) ,	2.1 (0.8)	1.4 (0.4) ,	16.6 (2.9)	1.6 (0.8) ,	2.9 (1.4)
		45	1.6 (0.6) ,	15.3 (3.6)	1.3 (0.5) ,	2.3 (1.2)	0.7 (0.2) ,	10.1 (3.1)	1.4 (0.8) ,	2.7 (1.6)
		60	0.6 (0.1) ,	3.5 (1.1)	1.3 (0.3) ,	3.6 (0.6)	0.3 (0.1) ,	1.8 (0.2)	1.1 (0.2) ,	2.0 (0.9)
45º ground motions	Bridge skew (º)	0	0.6 (0.1) ,	9.6 (2.3)	1.4 (0.6) ,	2.5 (0.9)	0.7 (0.1) ,	9.7 (1.7)	1.0 (0.1) ,	1.6 (0.4)
		15	1.1 (0.2) ,	12.4 (2.7)	1.5 (0.5) ,	2.5 (0.8)	1.0 (0.1) ,	11.9 (1.4)	1.3 (0.3) ,	2.1 (1.2)
		30	1.9 (0.6) ,	15.1 (2.1)	1.6 (0.5) ,	2.6 (0.6)	1.4 (0.4) ,	12.8 (1.9)	1.5 (1.0) ,	3.1 (1.6)
		45	1.7 (0.5) ,	14.2 (3.0)	1.7 (1.0) ,	3.1 (1.0)	1.1 (0.2) ,	9.8 (1.8)	1.8 (1.2) ,	3.7 (1.8)
		60	1.2 (0.3) ,	9.7 (3.7)	2.7 (1.3) ,	4.1 (1.8)	1.0 (0.2) ,	5.9 (2.4)	2.1 (1.6) ,	4.5 (1.8)
Transverse (90º) ground motions	Bridge skew (º)	0	0.5 (0.1) ,	0.8 (0.2)	2.9 (1.4) ,	5.2 (2.7)	0.4 (0.0) ,	0.5 (0.0)	1.2 (0.2) ,	1.6 (0.3)
		15	0.6 (0.1) ,	1.1 (0.1)	2.9 (1.2) ,	5.3 (1.7)	0.6 (0.1) ,	1.1 (0.4)	1.2 (0.3) ,	1.8 (0.4)
		30	0.9 (0.1) ,	1.7 (0.4)	2.6 (0.8) ,	5.4 (0.9)	0.9 (0.1) ,	3.0 (1.2)	1.4 (0.5) ,	2.2 (1.0)
		45	1.1 (0.1) ,	2.5 (0.5)	1.8 (1.0) ,	4.6 (1.5)	0.9 (0.1) ,	2.1 (0.3)	1.3 (0.8) ,	1.9 (1.0)
		60	1.2 (0.1) ,	2.8 (0.9)	1.6 (1.0) ,	3.1 (1.6)	1.3 (0.2) ,	3.2 (1.2)	1.5 (1.0) ,	2.2 (1.3)
135º ground motions	Bridge skew (º)	0	0.7 (0.1) ,	9.6 (2.4)	1.2 (0.6) ,	2.4 (1.0)	0.7 (0.1) ,	9.9 (1.7)	1.0 (0.1) ,	1.7 (0.4)
		15	0.7 (0.1) ,	9.3 (1.5)	2.0 (0.9) ,	3.9 (1.8)	0.7 (0.1) ,	8.8 (1.0)	1.0 (0.3) ,	1.6 (0.4)
		30	1.0 (0.2) ,	8.3 (0.5)	2.3 (0.7) ,	5.2 (1.3)	0.8 (0.1) ,	7.3 (1.6)	1.1 (0.2) ,	1.6 (0.3)
		45	1.0 (0.1) ,	4.3 (2.2)	1.9 (0.5) ,	5.4 (0.7)	0.7 (0.1) ,	4.4 (1.8)	1.0 (0.1) ,	1.2 (0.1)
		60	0.9 (0.1) ,	1.1 (0.1)	1.3 (0.3) ,	3.4 (0.9)	0.7 (0.1) ,	1.5 (0.2)	0.9 (0.2) ,	1.4 (0.1)
Undamaged (unyielded):			normalized strain < 1 (unnormalized strain < 0.0021)							
Lightly damaged (unlikely requiring repair):			1 ≤ normalized strain < 7.1 (0.0021 ≤ unnormalized strain < 0.015)							
Moderately damaged (repairable):			7.1 ≤ normalized strain < 28.6 (0.015 ≤ unnormalized strain < 0.06)							
Severely damaged (not easily repairable):			28.6 ≤ normalized strain (0.06 ≤ unnormalized strain)							

Crushing of the concrete cover at the column bases of Piers 1 and 3 (CCC@P1 and P3) occurred in only a smaller percentage (< 5%) of the 4S bridge analyses.

Similar to the response of 3S bridges, sliding or unseating of the elastomeric bearings on Piers

Table 6.18: Normalized peak strain of concrete cover at pier column base of 4S bridges (peak strains are normalized to the crushing strain, 0.005; numbers outside the parentheses are medians, while those inside are median absolute deviations; data of concrete cover at column base of expansion and fixed piers are placed on the left and right sides of the commas, respectively; performance levels in the footnote are defined per Kowalsky (2001) and Revell (2013))

Foundation soil condition			Hard				Soft			
Pier column height (m)			4.57		12.19		4.57		12.19	
Longitudinal (0º) ground motions	Bridge skew (º)	0	0.3 (0.1) , 2.5 (0.7)		0.3 (0.0) , 0.4 (0.1)		0.3 (0.1) , 2.6 (0.7)		0.4 (0.1) , 0.5 (0.2)	
		15	0.3 (0.1) , 2.9 (0.6)		0.3 (0.0) , 0.4 (0.0)		0.4 (0.1) , 3.0 (0.6)		0.4 (0.1) , 0.5 (0.1)	
		30	0.4 (0.1) , 3.1 (0.7)		0.4 (0.0) , 0.5 (0.1)		0.4 (0.1) , 3.1 (0.7)		0.4 (0.1) , 0.5 (0.3)	
		45	0.4 (0.1) , 2.7 (0.8)		0.3 (0.1) , 0.4 (0.1)		0.2 (0.0) , 1.8 (0.6)		0.3 (0.1) , 0.5 (0.2)	
		60	0.2 (0.0) , 0.6 (0.2)		0.3 (0.0) , 0.6 (0.1)		0.1 (0.0) , 0.4 (0.0)		0.3 (0.0) , 0.4 (0.1)	
45º ground motions	Bridge skew (º)	0	0.2 (0.0) , 1.5 (0.4)		0.4 (0.1) , 0.5 (0.2)		0.2 (0.0) , 1.5 (0.3)		0.3 (0.0) , 0.4 (0.1)	
		15	0.3 (0.0) , 2.1 (0.6)		0.3 (0.1) , 0.5 (0.1)		0.3 (0.0) , 2.0 (0.3)		0.3 (0.1) , 0.4 (0.2)	
		30	0.4 (0.1) , 2.7 (0.4)		0.3 (0.0) , 0.4 (0.1)		0.4 (0.0) , 2.4 (0.4)		0.4 (0.1) , 0.5 (0.2)	
		45	0.4 (0.1) , 2.5 (0.6)		0.4 (0.1) , 0.5 (0.1)		0.3 (0.0) , 1.6 (0.2)		0.4 (0.2) , 0.6 (0.2)	
		60	0.3 (0.1) , 1.8 (0.6)		0.5 (0.2) , 0.7 (0.2)		0.3 (0.0) , 0.9 (0.4)		0.4 (0.3) , 0.7 (0.2)	
Transverse (90º) ground motions	Bridge skew (º)	0	0.2 (0.0) , 0.3 (0.0)		0.6 (0.2) , 1.0 (0.5)		0.2 (0.0) , 0.2 (0.0)		0.3 (0.0) , 0.4 (0.0)	
		15	0.2 (0.0) , 0.3 (0.0)		0.6 (0.2) , 0.9 (0.4)		0.2 (0.0) , 0.3 (0.0)		0.4 (0.0) , 0.4 (0.1)	
		30	0.2 (0.0) , 0.4 (0.0)		0.6 (0.2) , 1.1 (0.2)		0.2 (0.0) , 0.5 (0.2)		0.4 (0.1) , 0.5 (0.1)	
		45	0.3 (0.0) , 0.5 (0.1)		0.4 (0.1) , 0.9 (0.3)		0.2 (0.0) , 0.4 (0.0)		0.3 (0.1) , 0.4 (0.1)	
		60	0.3 (0.0) , 0.5 (0.1)		0.3 (0.1) , 0.6 (0.2)		0.3 (0.0) , 0.5 (0.1)		0.3 (0.2) , 0.4 (0.1)	
135º ground motions	Bridge skew (º)	0	0.2 (0.0) , 1.8 (0.4)		0.3 (0.1) , 0.4 (0.1)		0.3 (0.0) , 1.8 (0.4)		0.3 (0.0) , 0.4 (0.0)	
		15	0.2 (0.0) , 1.7 (0.2)		0.5 (0.1) , 0.7 (0.3)		0.2 (0.0) , 1.7 (0.2)		0.3 (0.0) , 0.4 (0.0)	
		30	0.3 (0.0) , 1.6 (0.1)		0.5 (0.1) , 0.9 (0.3)		0.2 (0.0) , 1.3 (0.3)		0.3 (0.0) , 0.4 (0.0)	
		45	0.3 (0.0) , 0.7 (0.3)		0.4 (0.1) , 1.0 (0.2)		0.2 (0.0) , 0.8 (0.3)		0.3 (0.0) , 0.3 (0.0)	
		60	0.2 (0.0) , 0.3 (0.0)		0.3 (0.0) , 0.6 (0.1)		0.2 (0.0) , 0.4 (0.0)		0.3 (0.0) , 0.4 (0.0)	

Undamaged (ultimate strength not mobillized):	normalized strain < 0.4 (unnormalized strain < 0.002)
Lightly damaged (ultimate strength mobilized but uncrushed):	0.4 ≤ normalized strain < 1 (0.002 ≤ unnormalized strain < 0.005)
Moderately damaged (crushed but repairable):	1 ≤ normalized strain < 3.6 (0.005 ≤ unnormalized strain < 0.018)
Severely damaged (not easily repairable):	3.6 ≤ normalized strain (0.018 ≤ unnormalized strain)

1 and 3 (SEB@P1 and P3, UEB@P1 and P3) was not observed in any 4S bridge analysis.

Table 6.19: Occurrence of limit states at expansion piers (P1 and P3) of 4S bridge variants when subjected to seismic ground motions

Limit state	No. of analyses with occurrence [1]	Skew angle [2] (°)					Foundation soil [2]		Column height [2] (m)		Ground motion incident angle [2] (°)			
		0	15	30	45	60	Hard	Soft	4.57	12.19	0	45	90	135
Rupture of retainer anchor (RRA@P1)	0 (0%)	0	0	0	0	0	0	0	0	0	0	0	0	0
Sliding of elastomeric bearing (SEB@P1)	0 (0%)	0	0	0	0	0	0	0	0	0	0	0	0	0
Unseating of elastomeric bearing (UEB@P1)	0 (0%)	0	0	0	0	0	0	0	0	0	0	0	0	0
Yielding of vertical reinforcing steel at column end (YRS@P1)	918 (57%)	148 (16%)	175 (19%)	209 (23%)	194 (21%)	192 (21%)	504 (55%)	414 (45%)	328 (36%)	590 (64%)	254 (28%)	272 (30%)	231 (25%)	161 (18%)
Crushing of concrete cover at column end (CCC@P1)	39 (2%)	6 (15%)	6 (15%)	16 (41%)	5 (13%)	6 (15%)	21 (54%)	18 (46%)	13 (33%)	26 (67%)	15 (38%)	12 (31%)	10 (26%)	2 (5%)
Yielding of pile at pier (YPP@P1)	627 (39%)	145 (23%)	140 (22%)	131 (21%)	123 (20%)	88 (14%)	143 (23%)	484 (77%)	270 (43%)	357 (57%)	50 (8%)	91 (15%)	254 (41%)	232 (37%)
Rupture of retainer anchor (RRA@P3)	0 (0%)	0	0	0	0	0	0	0	0	0	0	0	0	0
Sliding of elastomeric bearing (SEB@P3)	0 (0%)	0	0	0	0	0	0	0	0	0	0	0	0	0
Unseating of elastomeric bearing (UEB@P3)	0 (0%)	0	0	0	0	0	0	0	0	0	0	0	0	0
Yielding of vertical reinforcing steel at column end (YRS@P3)	898 (56%)	148 (16%)	174 (19%)	214 (24%)	186 (21%)	176 (20%)	269 (30%)	629 (70%)	309 (34%)	589 (66%)	255 (28%)	258 (29%)	226 (25%)	159 (18%)
Crushing of concrete cover at column end (CCC@P3)	68 (4%)	5 (7%)	8 (12%)	24 (35%)	16 (24%)	15 (22%)	39 (57%)	29 (43%)	16 (24%)	52 (76%)	20 (29%)	17 (25%)	30 (44%)	1 (1%)
Yielding of pile at pier (YPP@P3)	626 (39%)	139 (22%)	142 (23%)	135 (22%)	129 (21%)	81 (13%)	139 (22%)	487 (78%)	273 (44%)	353 (56%)	52 (8%)	96 (15%)	253 (40%)	225 (36%)

1 The number above the parentheses indicates the number of analyses with occurrences of a limit state.
The percentage inside the parentheses indicates the ratio of the number above the parentheses to all the 1,600 analyses.
2 The number above the parentheses indicates the number of analyses with occurrences of a limit state contributed by a parametric variation.
The percentage inside the parentheses indicates the relative contribution of a parametric variation to the total occurrences of a limit state.

Fixed piers (Pier 2) of 4S bridges

Table 6.21 statistically summarizes the occurrences of component limit states at the fixed piers (Pier 2) of 4S bridges. Rupture of the steel fixed bearing anchors at Pier 2 (RFA@P2) was observed in 12% of the 4S bridge analyses, which is higher than the occurrence percentage of 3S bridges (4%). It can be found in Table 6.21 that among these analyses, the large skews, hard foundation

Table 6.20: Normalized peak strains of steel H piles at piers of 4S bridges (peak strains are normalized to the yield strain, 0.0017; numbers outside the parentheses are medians, while those inside are median absolute deviations; data for piles supporting expansion and fixed piers are placed on the left and right sides of the commas, respectively)

Foundation soil condition			Hard				Soft			
Pier column height (m)			4.57		12.19		4.57		12.19	
Longitudinal (0º) ground motions	Bridge skew (º)	0	0.3 (0.0) , 0.4 (0.0)		0.4 (0.0) , 0.4 (0.0)		0.4 (0.0) , 0.5 (0.0)		0.4 (0.0) , 0.4 (0.0)	
		15	0.4 (0.0) , 0.6 (0.0)		0.5 (0.0) , 0.5 (0.0)		0.6 (0.1) , 0.8 (0.0)		0.7 (0.1) , 0.7 (0.0)	
		30	0.5 (0.0) , 0.9 (0.0)		0.7 (0.1) , 0.8 (0.1)		0.7 (0.1) , 1.5 (0.1)		0.8 (0.1) , 1.1 (0.1)	
		45	0.6 (0.0) , 1.4 (0.1)		0.7 (0.1) , 1.0 (0.1)		0.9 (0.2) , 6.1 (1.4)		1.0 (0.2) , 2.2 (0.7)	
		60	0.6 (0.1) , 1.5 (0.1)		0.7 (0.1) , 1.2 (0.1)		1.3 (0.4) , 10.8 (3.2)		1.1 (0.2) , 4.6 (2.5)	
45º ground motions	Bridge skew (º)	0	0.7 (0.1) , 1.0 (0.1)		0.9 (0.1) , 1.0 (0.1)		1.1 (0.1) , 1.7 (0.2)		1.4 (0.3) , 2.3 (0.6)	
		15	0.7 (0.1) , 0.9 (0.1)		0.8 (0.1) , 0.9 (0.1)		1.0 (0.1) , 1.4 (0.2)		1.1 (0.1) , 1.4 (0.1)	
		30	0.7 (0.1) , 1.0 (0.1)		0.6 (0.0) , 0.7 (0.1)		1.0 (0.1) , 1.5 (0.2)		0.8 (0.1) , 1.1 (0.0)	
		45	0.6 (0.0) , 1.2 (0.1)		0.5 (0.0) , 0.6 (0.0)		1.0 (0.2) , 3.1 (0.5)		0.6 (0.1) , 0.7 (0.0)	
		60	0.5 (0.0) , 1.5 (0.1)		0.5 (0.0) , 0.6 (0.0)		0.8 (0.1) , 5.0 (1.8)		0.6 (0.1) , 0.7 (0.1)	
Transverse (90º) ground motions	Bridge skew (º)	0	1.0 (0.1) , 1.3 (0.3)		1.2 (0.1) , 1.2 (0.1)		3.3 (1.4) , 6.7 (2.4)		4.3 (2.4) , 6.9 (3.9)	
		15	0.9 (0.1) , 1.4 (0.3)		1.2 (0.1) , 1.2 (0.0)		3.1 (1.3) , 5.8 (1.5)		3.8 (2.0) , 6.8 (3.4)	
		30	0.9 (0.1) , 1.9 (0.5)		1.1 (0.1) , 1.2 (0.0)		3.0 (1.2) , 4.5 (1.9)		3.0 (1.6) , 5.6 (2.7)	
		45	0.8 (0.1) , 2.2 (0.5)		1.0 (0.1) , 1.3 (0.1)		1.6 (0.3) , 2.4 (0.6)		1.6 (0.5) , 3.7 (1.4)	
		60	0.6 (0.0) , 1.5 (0.2)		0.7 (0.1) , 1.1 (0.1)		1.1 (0.2) , 1.6 (0.2)		0.9 (0.1) , 2.5 (0.4)	
135º ground motions	Bridge skew (º)	0	0.8 (0.1) , 1.0 (0.1)		0.9 (0.2) , 1.0 (0.1)		1.1 (0.1) , 1.7 (0.2)		1.4 (0.3) , 2.3 (0.6)	
		15	0.8 (0.1) , 1.2 (0.1)		1.0 (0.1) , 1.1 (0.1)		1.4 (0.1) , 3.5 (0.8)		1.9 (0.8) , 3.5 (1.9)	
		30	0.9 (0.1) , 1.9 (0.5)		1.1 (0.1) , 1.2 (0.1)		2.0 (0.6) , 7.7 (1.7)		2.9 (1.6) , 7.3 (2.4)	
		45	0.8 (0.0) , 3.0 (0.7)		1.1 (0.1) , 1.5 (0.1)		1.9 (0.4) , 8.4 (2.7)		2.9 (1.3) , 11.4 (3.1)	
		60	0.6 (0.0) , 2.0 (0.3)		0.9 (0.1) , 1.3 (0.1)		1.1 (0.2) , 8.8 (1.9)		1.8 (0.7) , 11.0 (2.0)	

Unyielded: normalized strain < 1 (unnormalized strain < 0.0017)

Yielded without signficniant strain hardening: 1 ≤ normalized strain < 10 (0.0017 ≤ unnormalized strain < 0.017)

Yielded and significantly strain hardened: 10 ≤ normalized strain (0.017 ≤ unnormalized strain)

soil, and short pier columns were more prone to this limit state than the small skews, soft soil, and tall pier columns, respectively. Meanwhile, the pure longitudinal and 135° ground motions contributed much more of the total occurrences than the pure transverse and 45° motions. These observations are consistent with those of 3S bridges.

Yielding of the vertical reinforcing steel at the column bases of Pier 2 (YRS@P2) was very common to 4S bridges, which was observed in 89% of the analyses. In most of the cases in Table 6.20, the reinforcing steel was lightly or moderately damaged. By comparing the median peak strains in Table 6.20 with those in Table 6.10, it can be found that the Pier 2 reinforcing steel of 4S bridges was strained more than that of 3S bridges. The peak reinforcing steel strains of the fixed piers are much larger than those of the expansion piers listed in Table 6.20, due to the high lateral stiffness of the steel fixed bearings and the large seismic forces incurred by the high bearing stiffness.

Although rarer than yielding of reinforcing steel, crushing of the concrete cover at the column bases of Pier 2 (CCC@P2) was observed in 34% of the 4S bridge analyses, which basically did not occur in any 3S bridge analysis. As can be seen in Table 6.21, 81% of these occurrences were observed in short-pier 4S bridges and the non-transverse ground motions caused 90% of the occurrences. This tendency is expected as the short pier typically attracts more seismic force than the tall pier due to its much higher lateral stiffness. Additionally, when subjected to the pure transverse ground motions, the bearing retainers at the expansion piers and abutments collaborate with the fixed bearings to resist the superstructure seismic force and the frame action of multi-column piers results in very limited flexural deformation of pier columns in the transverse direction.

Yielding of the steel piles supporting Pier 2 (YSP@P2) was observed in 73% of the 4S bridge analyses and this percentage is much higher than that of 3S bridges (32%). 57% of the occurrences were observed in the bridges with the soft foundation soil and 65% were observed in the analyses with the pure transverse and 135° ground motions. These observations were consistent with those of 3S bridges. In most of the cases in Table 6.20, the piles supporting Pier 2 were yielded and only lightly strained beyond yielding, although they were generally strained more than the piles supporting Piers 1 and 3.

Unseating of the steel fixed bearings at Pier 2 (USB@P2) after rupture of their anchors was not observed in any 4S bridge analysis.

Table 6.21: Occurrence of limit states at fixed piers (Pier 2) of 4S bridge variants when subjected to seismic ground motions

Limit state	No. of analyses with occurrence [1]	Skew angle [2] (°)					Foundation soil [2]		Column height [2] (m)		Ground motion incident angle [2] (°)			
		0	15	30	45	60	Hard	Soft	4.57	12.19	0	45	90	135
Rupture of fixed bearing anchor (RFA@P2)	188 (12%)	0 (0%)	1 (1%)	10 (5%)	43 (23%)	134 (71%)	169 (90%)	19 (10%)	152 (81%)	36 (19%)	58 (31%)	23 (12%)	44 (23%)	63 (34%)
Unseating of steel fixed bearing (USB@P2)	0 (0%)	0	0	0	0	0	0	0	0	0	0	0	0	0
Yielding of vertical reinforcing steel at column end (YRS@P2)	1439 (90%)	261 (18%)	286 (20%)	301 (21%)	296 (21%)	295 (21%)	735 (51%)	704 (49%)	735 (51%)	704 (49%)	363 (25%)	361 (25%)	337 (23%)	378 (26%)
Crushing of concrete cover at column end (CCC@P2)	549 (34%)	122 (22%)	134 (24%)	145 (26%)	108 (20%)	40 (7%)	292 (53%)	257 (47%)	446 (81%)	103 (19%)	165 (30%)	187 (34%)	53 (10%)	144 (26%)
Yielding of pile at pier (YPP@P2)	1167 (73%)	198 (17%)	198 (17%)	232 (20%)	269 (23%)	270 (23%)	501 (43%)	666 (57%)	655 (56%)	512 (44%)	178 (15%)	235 (20%)	384 (33%)	370 (32%)

1 The number above the parentheses indicates the number of analyses with occurrences of a limit state.
The percentage inside the parentheses indicates the ratio of the number above the parentheses to all the 1,600 analyses.
2 The number above the parentheses indicates the number of analyses with occurrences of a limit state contributed by a parametric variation.
The percentage inside the parentheses indicates the relative contribution of a parametric variation to the total occurrences of a limit state.

Summary of 4S bridges

1,600 nonlinear dynamic analyses were performed on the 20 four-span steel-plate-girder (4S) bridge variants using the suite of 20 seismic ground motions applied in four incident directions. The analysis results were statistically studied with emphasis on the occurrence of component limit states.

Most importantly, unseating of the elastomeric bearings at acute deck corners occurred in one 4S bridge analysis and almost occurred in several other analyses, all of which involved highly skewed bridges supported by the tall piers. However, the bearings at the expansion piers did not even slide in any analysis.

The overall magnitude of the superstructure displacements of 4S bridges is larger than that of 3S bridges, but the rotations of 4S bridges are generally smaller.

Rupture of the retainer anchors at the abutments occurred in less than 20% of the 4S bridge analyses. Rupture of the steel fixed bearing anchors occurred in only 12% of the analyses. Similar to 3S bridges, rupture of the retainer anchors at the expansion piers did not occur in any analysis.

Yielding of the abutment piles occurred in around 80% of the analyses, but mobilization of ultimate backfill passive resistance occurred in only a few percent of the analyses.

Yielding of the reinforcing steel at pier column bases was quite common to both the expansion and fixed piers of 4S bridges, and the median peak steel strains were always in the range of light to moderate damage. The fixed piers sustained much larger damage than the expansion ones, especially when the piers were short. Most of the concrete cover crushing occurred at the fixed piers. Yielding of the fixed-pier piles occurred in around 80% of the analyses, which is twice of the occurrence percentage of yielding of the expansion-pier piles. Therefore, although the expansion piers of 4S bridge were effectively isolated against excessive seismic damage, the fixed piers sustained much more seismic damage.

On the whole, 4S bridges sustained more seismic damage than 3S bridges. This general performance is consistent with the fact that the superstructure mass of 4S bridges is more than twice that of 3S bridges. The more massive superstructures incurred larger seismic forces to 4S bridges and caused more damage to critical bridge components. Specifically, the following limit states occurred in more 4S bridge analyses than 3S bridge analyses

- Mobilization of ultimate backfill passive resistance (CEJ@A1 and A2)
- Sliding of elastomeric bearings at abutments (SEB@A1 and A2)
- Yielding of abutment piles (YPW@A1 and A2, YPB@A1 and A2)
- Unseating of bearings at acute deck corners (UBA@A2)
- Yielding of vertical reinforcing steel at column bases of expansion and fixed piers (YRS@P1, P2, and P3)
- Crushing of concrete cover at column bases of expansion and fixed piers (CCC@P1, P2, and P3)
- Yielding of pier piles (YSP@P1, P2, and P3)
- Rupture of steel fixed bearing anchors (RFA@P2)

Most of the observations of 3S bridges, regarding the tendencies of bridge variants with different skews, pier column heights, foundation soil conditions, and ground motion directions to the occurrence of a limit state, are still valid for 4S bridges.

6.3.3 Three-span precast-prestressed-concrete-girder (3C) bridges

Superstructures of 3C bridges

Table 6.22 indicates the medians and median absolute deviations of the peak deck center displacements of 3C bridge variants excited by the 20 seismic ground motions applied in different incident directions. The overall magnitude of the displacements is in between that of 3S and 4S bridges. The superstructure mass of 3C bridges is also in between that of the two types of steel-plate-girder bridges, as shown in Table 3.3.

The superstructures of skew 3C bridges bi-axially displaced, even though the ground motions were uni-axially applied, which is similar to the behavior of 3S and 4S bridges. For each 3C bridge variant, the median peak longitudinal and transverse deck displacement components excited by the uni-axial (0° and 90°) ground motions were larger than those excited by the bi-axial (45° and 135°) motions, which is also similar to the behavior of 3S and 4S bridges. The effect of bridge skew on the deck displacements varied from case to case. A relatively clear trend is that under the uni-axial ground motions, the displacement component in the ground motion direction always increased with bridge skew. Tall-pier 3C bridges typically experienced larger deck displacements in both axes than their short-pier equivalents. In general, 3C bridges in the soft foundation soil experienced larger deck displacements than those of the equivalent bridges in the hard soil.

Table 6.23 indicates the medians and median absolute deviations of the peak deck rotations of 3C bridges. The overall magnitude is close to that of 3S bridges but larger than that of 4S bridges. Similar to 3S and 4S bridges, the clockwise rotations of left-skewed 3C bridges were always larger than the counterclockwise. While the clockwise rotations of highly skewed 3C bridges were generally larger than those of the equivalent bridges with smaller skews, the counterclockwise rotations might stay the same or decrease as the skew increased, which is similar to the behavior of 3S bridges. Tall-pier 3C bridges sustained larger rotations than their short-pier equivalents. The deck rotations were insensitive to the foundation soil condition. These two findings are consistent with those of the 3S and 4S bridges.

Full data of limit state occurrences for 3C bridges

Table 6.24 lists the full data of component limit state occurrences for each of the 20 3C bridge variants, when subjected to the suite of 20 seismic ground motions applied in the four incident directions. Each percentage in the table indicates the number of analyses with occurrences of a limit state out of the 20 analyses with the 20 ground motions applied to a bridge variant in an incident direction. Three gradient color scales, blue, yellow, and red, were used in conjunction

Table 6.22: Peak deck center displacements (units: mm) of 3C bridges (longitudinal and transverse components are placed on the left and right sides of the commas, respectively; numbers outside the parentheses are medians while those inside are median absolute deviations; for each bridge, the largest median peak displacement caused by the ground motions in the four incident directions is highlighted by bold numbers)

Foundation soil condition			Hard				Soft			
Pier column height (m)			4.57		12.19		4.57		12.19	
Longitudinal (0º) ground motions	Bridge skew (º)	0	**96** (11) , 0 (0)		**149** (28) , 0 (0)		**125** (16) , 0 (0)		**189** (31) , 0 (0)	
		15	**106** (8) , 20 (1)		**147** (18) , 33 (5)		**144** (25) , 17 (2)		**201** (49) , 37 (11)	
		30	**109** (12) , 34 (4)		**155** (27) , 70 (19)		**147** (25) , 21 (2)		**224** (42) , 69 (18)	
		45	**125** (19) , 29 (2)		**144** (21) , 90 (21)		**153** (26) , 40 (10)		**198** (36) , 59 (11)	
		60	**138** (18) , 23 (2)		**182** (26) , 73 (21)		**176** (35) , 36 (10)		**219** (29) , 45 (7)	
45º ground motions	Bridge skew (º)	0	79 (4) , 30 (3)		110 (12) , 61 (5)		96 (9) , 47 (5)		127 (16) , 88 (14)	
		15	86 (6) , 35 (3)		116 (13) , 70 (7)		107 (9) , 50 (6)		138 (25) , 99 (16)	
		30	92 (9) , 46 (4)		127 (24) , 89 (15)		111 (15) , 59 (5)		155 (45) , 112 (24)	
		45	76 (7) , 51 (5)		109 (26) , 115 (36)		94 (12) , 63 (6)		148 (29) , 138 (48)	
		60	99 (11) , 58 (6)		108 (29) , 150 (52)		88 (17) , 63 (7)		138 (25) , 145 (49)	
Transverse (90º) ground motions	Bridge skew (º)	0	1 (0) , **41** (5)		1 (0) , **134** (23)		1 (0) , **81** (14)		0 (1) , **178** (42)	
		15	28 (5) , **47** (7)		58 (5) , **144** (23)		35 (4) , **83** (14)		52 (7) , **192** (53)	
		30	47 (5) , **56** (5)		85 (16) , **161** (39)		37 (4) , **75** (9)		74 (13) , **207** (50)	
		45	42 (4) , **60** (5)		94 (25) , **159** (44)		28 (2) , **74** (7)		83 (20) , **189** (40)	
		60	35 (3) , **74** (8)		90 (24) , **186** (40)		22 (3) , **82** (7)		93 (32) , **211** (63)	
135º ground motions	Bridge skew (º)	0	80 (5) , 30 (3)		106 (14) , 59 (5)		96 (9) , 48 (5)		128 (15) , 87 (14)	
		15	84 (6) , 38 (4)		113 (11) , 88 (14)		118 (12) , 58 (9)		138 (24) , 111 (24)	
		30	86 (12) , 47 (8)		143 (22) , 143 (23)		128 (19) , 69 (11)		180 (34) , 127 (34)	
		45	103 (9) , 55 (8)		142 (36) , 149 (32)		137 (34) , 66 (17)		193 (39) , 136 (35)	
		60	110 (9) , 59 (7)		156 (33) , 145 (33)		154 (33) , 64 (13)		181 (34) , 144 (30)	

Table 6.23: Peak deck rotations (units: 0.01°) of 3C bridges (data for clockwise and counterclockwise rotations are placed on the left and right sides of the commas, respectively; numbers outside the parentheses are medians, while those inside are median absolute deviations; for each bridge, the largest median peak rotation caused by the ground motions in the four incident directions is highlighted by bold numbers)

Foundation soil condition			Hard				Soft			
Pier column height (m)			4.57		12.19		4.57		12.19	
Longitudinal (0º) ground motions	Bridge skew (º)	0	0 (0) , 0 (0)		0 (0) , 0 (0)		0 (0) , 0 (0)		0 (0) , 0 (0)	
		15	5 (1) , 4 (0)		8 (1) , 4 (1)		6 (1) , 3 (1)		11 (3) , 6 (2)	
		30	11 (2) , 5 (1)		20 (8) , 8 (1)		10 (2) , 4 (0)		18 (5) , 7 (1)	
		45	12 (2) , 6 (0)		32 (14) , 8 (1)		**11** (4) , 4 (1)		20 (2) , 6 (1)	
		60	10 (1) , 5 (0)		21 (5) , 6 (1)		9 (2) , 4 (1)		17 (2) , 5 (1)	
45º ground motions	Bridge skew (º)	0	6 (1) , 6 (1)		10 (1) , 11 (1)		5 (1) , 5 (1)		10 (3) , 10 (2)	
		15	7 (1) , 6 (1)		12 (1) , 10 (1)		7 (1) , 6 (1)		12 (3) , 10 (3)	
		30	10 (1) , 7 (1)		20 (7) , 9 (2)		9 (1) , 7 (1)		29 (10) , 8 (2)	
		45	11 (2) , 8 (1)		34 (11) , 6 (1)		9 (1) , 6 (0)		**38** (11) , 7 (2)	
		60	12 (1) , 8 (1)		39 (13) , 6 (2)		9 (1) , 7 (1)		34 (13) , 6 (3)	
Transverse (90º) ground motions	Bridge skew (º)	0	**11** (2) , **11** (2)		**36** (6) , **39** (7)		**11** (2) , **11** (1)		**33** (14) , **34** (21)	
		15	**12** (2) , **12** (2)		**41** (10) , **33** (3)		**12** (2) , **12** (2)		**40** (9) , **26** (5)	
		30	**15** (2) , **14** (2)		**44** (10) , **27** (2)		**11** (2) , **10** (1)		**42** (11) , **14** (4)	
		45	**15** (2) , **13** (1)		**40** (17) , **17** (3)		**11** (1) , **10** (1)		37 (17) , **12** (3)	
		60	**14** (1) , **10** (1)		**47** (14) , 11 (1)		**14** (1) , **10** (1)		**43** (14) , 8 (2)	
135º ground motions	Bridge skew (º)	0	6 (1) , 6 (0)		10 (1) , 10 (1)		6 (1) , 5 (0)		10 (2) , 10 (2)	
		15	8 (2) , 7 (1)		16 (3) , 14 (2)		6 (1) , 4 (1)		13 (4) , 10 (3)	
		30	11 (2) , 9 (2)		33 (8) , 19 (5)		7 (1) , 6 (1)		19 (5) , 11 (3)	
		45	12 (2) , 10 (2)		28 (3) , 15 (1)		8 (1) , 7 (0)		23 (5) , 10 (2)	
		60	12 (1) , 9 (1)		26 (4) , **12** (2)		9 (1) , 8 (1)		26 (5) , **11** (3)	

with the percentages in Table 6.24 to highlight the occurrences of the preferred, acceptable, and unacceptable limit states defined in Table 5.1.

The data listed in Table 6.24 were subsequently grouped by the substructures of 3C bridges, namely the two abutments, one expansion pier, and one fixed pier. For the substructure groups, the data in Table 6.24 were further analyzed and their statistical summaries are presented in Tables 6.25, 6.27, and 6.31. Later in this section, the statistical summary of each substructure group will be discussed.

Table 6.24: Limit state occurrences of each 3C bridge variant under 0° and 45° ground motions (each percentage indicates the number of analyses with occurrences of a limit state out of the 20 analyses with ground motions applied to a bridge variant in an incident direction)

Ground motion direction	Bridge variant	Critical limit states																										
		Abutment 1 (A1)									Pier 1 (P1, expansion pier)						Pier 2 (P2, fixed pier)					Abutment 2 (A2)								
		CEJ	MBU	FBP	RRA	SEB	UBA	UBO	YPW	YPB	RRA	SEB	UEB	YRS	CCC	YPP	RRA	RSD	YRS	CCC	YPP	CEJ	MBU	FBP	RRA	SEB	UBO	UBA	YPW	YPB
0°	3C00P15H	100%	0	0	0	0	0	0	100%	95%	0	0	0	0	0	0	0	0	100%	25%	0	100%	0	0	0	0	0	0	100%	100%
	3C15P15H	100%	0	0	0	0	0	0	100%	100%	0	0	0	0	0	0	0	0	100%	65%	0	100%	0	0	0	0	0	0	100%	100%
	3C30P15H	100%	0	0	0	0	0	0	100%	100%	0	0	0	0	0	0	0	5%	100%	80%	25%	100%	0	0	0	0	0	0	100%	100%
	3C45P15H	100%	0	0	0	0	0	0	100%	100%	0	0	0	0	0	0	0	100%	100%	0	25%	100%	0	0	0	0	0	0	100%	100%
	3C60P15H	100%	0	0	0	0	0	0	100%	80%	0	0	0	0	0	0	0	100%	0	0	10%	100%	0	0	0	0	0	0	100%	75%
	3C00P40H	100%	0	0	0	35%	0	0	100%	100%	0	0	0	40%	0	0	0	0	35%	0	0	100%	10%	5%	0	35%	0	0	100%	100%
	3C15P40H	100%	0	0	0	10%	0	0	100%	100%	0	0	0	35%	0	0	0	0	45%	0	0	100%	5%	0	0	10%	0	0	100%	100%
	3C30P40H	100%	0	0	20%	20%	0	0	100%	100%	0	10%	0	45%	0	0	0	0	65%	0	5%	100%	0	0	65%	20%	0	0	100%	100%
	3C45P40H	100%	0	0	70%	5%	0	0	100%	100%	0	5%	0	20%	0	0	0	5%	70%	0	40%	100%	0	0	80%	35%	0	0	100%	100%
	3C60P40H	100%	0	0	30%	0	0	0	100%	100%	0	0	0	0	0	0	0	95%	85%	0	35%	100%	0	0	65%	5%	0	0	100%	100%
	3C00P15S	100%	0	0	0	5%	0	0	100%	95%	0	5%	0	10%	0	0	0	0	100%	55%	0	100%	5%	0	0	0	0	0	100%	95%
	3C15P15S	100%	0	0	0	5%	0	0	100%	100%	0	15%	0	30%	15%	5%	0	0	100%	75%	70%	100%	0	0	0	5%	0	0	100%	100%
	3C30P15S	100%	0	0	0	5%	0	0	100%	100%	0	5%	0	5%	0	25%	0	5%	100%	80%	100%	100%	0	0	0	0	0	0	100%	100%
	3C45P15S	100%	0	0	0	0	0	0	100%	100%	0	0	0	0	0	70%	0	90%	100%	0	100%	100%	0	0	0	0	0	0	100%	100%
	3C60P15S	100%	0	0	0	0	0	0	80%	85%	0	0	0	0	0	75%	0	100%	5%	0	100%	100%	0	0	0	0	0	0	75%	80%
	3C00P40S	100%	30%	0	0	55%	0	0	100%	100%	0	15%	0	55%	0	0	0	0	65%	0	0	100%	20%	5%	0	55%	0	0	100%	100%
	3C15P40S	100%	35%	5%	0	55%	0	0	100%	100%	0	5%	0	75%	0	0	0	0	80%	0	0	100%	50%	0	0	60%	0	0	100%	100%
	3C30P40S	100%	35%	0	0	55%	0	0	100%	100%	0	40%	0	75%	0	55%	0	0	80%	0	75%	100%	40%	0	20%	60%	0	0	100%	100%
	3C45P40S	100%	0	0	0	25%	0	0	100%	100%	0	10%	0	20%	0	65%	0	0	75%	0	100%	100%	0	0	20%	35%	0	0	100%	100%
	3C60P40S	100%	0	0	0	5%	0	0	100%	100%	0	0	0	0	0	70%	0	40%	60%	0	100%	100%	0	0	0	0	0	0	100%	100%
45°	3C00P15H	100%	0	0	0	0	0	0	100%	100%	0	0	0	0	0	0	0	0	100%	0	15%	100%	0	0	0	0	0	0	100%	95%
	3C15P15H	100%	0	0	0	0	0	0	100%	100%	0	0	0	0	0	0	0	0	100%	5%	10%	100%	0	0	0	0	0	0	100%	100%
	3C30P15H	100%	0	0	0	0	0	0	100%	100%	0	0	0	0	0	0	0	0	100%	65%	5%	100%	0	0	0	0	0	0	100%	100%
	3C45P15H	100%	0	0	0	0	0	0	100%	90%	0	0	0	5%	0	0	0	30%	100%	5%	5%	100%	0	0	5%	0	0	0	100%	100%
	3C60P15H	100%	0	0	0	0	0	0	100%	85%	0	0	0	0	0	0	0	100%	75%	0	0	100%	0	0	15%	0	0	0	100%	100%
	3C00P40H	100%	0	0	5%	0	0	0	100%	100%	0	0	0	5%	0	0	0	0	5%	0	0	100%	0	0	0	0	0	0	100%	100%
	3C15P40H	100%	0	0	5%	5%	0	0	100%	100%	0	0	0	15%	0	0	0	0	10%	0	0	100%	0	0	0	5%	0	0	100%	100%
	3C30P40H	100%	0	0	30%	5%	0	0	100%	100%	0	0	0	30%	0	0	0	0	35%	0	0	100%	0	0	45%	5%	0	0	100%	100%
	3C45P40H	100%	0	0	75%	35%	0	0	100%	100%	0	5%	0	40%	0	0	0	0	60%	0	0	100%	0	0	95%	35%	0	0	100%	100%
	3C60P40H	100%	10%	10%	80%	40%	0	0	100%	100%	0	0	0	75%	0	0	0	0	80%	10%	0	100%	0	0	100%	40%	0	0	100%	100%
	3C00P15S	100%	0	0	0	0	0	0	75%	90%	0	0	0	0	0	60%	0	0	100%	0	100%	100%	0	0	0	0	0	0	85%	95%
	3C15P15S	100%	0	0	0	0	0	0	95%	95%	0	0	0	0	0	60%	0	0	100%	45%	75%	100%	0	0	0	0	0	0	95%	95%
	3C30P15S	100%	0	0	0	0	0	0	100%	100%	0	0	0	35%	5%	20%	0	0	100%	75%	75%	100%	0	0	0	0	0	0	100%	100%
	3C45P15S	100%	0	0	0	0	0	0	80%	85%	0	0	0	5%	0	0	0	0	100%	10%	95%	100%	0	0	0	0	0	0	90%	90%
	3C60P15S	100%	0	0	0	0	0	0	80%	80%	0	0	0	10%	0	0	0	55%	85%	0	90%	100%	0	0	0	0	0	0	80%	80%
	3C00P40S	100%	0	0	5%	15%	0	0	95%	100%	0	0	0	30%	0	75%	0	0	20%	0	75%	100%	0	0	0	15%	0	0	95%	95%
	3C15P40S	100%	10%	0	25%	25%	0	0	100%	100%	0	0	0	35%	0	70%	0	0	30%	0	55%	100%	10%	0	0	20%	0	0	95%	100%
	3C30P40S	100%	30%	0	70%	50%	0	0	100%	100%	0	0	0	65%	0	10%	0	0	60%	0	5%	100%	20%	0	35%	35%	0	0	100%	100%
	3C45P40S	100%	30%	0	75%	50%	0	0	100%	100%	0	0	0	65%	0	0	0	0	70%	0	0	100%	25%	0	80%	35%	0	0	100%	100%
	3C60P40S	100%	15%	10%	80%	40%	0	0	100%	100%	0	5%	0	75%	5%	0	0	0	85%	20%	5%	100%	10%	5%	100%	35%	0	10%	100%	100%

Preferred limit states:	0	20%	40%	60%	80%	100%
Acceptable limit states:	0	20%	40%	60%	80%	100%
Unacceptable limit states:	0	20%	40%	60%	80%	100%

Table 6.24 Continued: limit state occurrences of each 3C bridge variant under 90° and 135° ground motions

Ground motion direction	Bridge variant	Critical limit states																												
		Abutment 1 (A1)									Pier 1 (P1, expansion pier)						Pier 2 (P2, fixed pier)					Abutment 2 (A2)								
		CEJ	MBU	FBP	RRA	SEB	UBA	UBO	YPW	YPB	RRA	SEB	UEB	YRS	CCC	YPP	RRA	RSD	YRS	CCC	YPP	CEJ	MBU	FBP	RRA	SEB	UBO	UBA	YPW	YPB
90°	3C00P15H	0	0	0	0	0	0	0	0	60%	0	0	0	0	0	45%	0	0	0	0	60%	0	0	0	0	0	0	0	0	10%
	3C15P15H	50%	0	0	0	0	0	0	0	80%	0	0	0	0	0	70%	0	0	0	0	90%	5%	0	0	0	0	0	0	0	20%
	3C30P15H	100%	0	0	5%	0	0	0	65%	95%	0	0	0	5%	0	10%	0	10%	75%	0	75%	100%	0	0	0	0	0	0	0	35%
	3C45P15H	100%	0	0	20%	0	0	0	100%	55%	0	0	0	15%	0	0	0	35%	50%	0	70%	100%	0	0	5%	0	0	0	35%	15%
	3C60P15H	100%	0	0	30%	0	0	0	75%	50%	0	0	0	35%	0	0	0	65%	75%	0	35%	100%	0	0	5%	0	0	0	25%	10%
	3C00P40H	0	0	0	95%	80%	0	0	0	100%	0	0	0	95%	0	95%	0	0	75%	0	40%	0	0	0	45%	10%	0	0	0	100%
	3C15P40H	95%	0	0	100%	75%	0	0	75%	100%	0	0	0	95%	0	95%	0	0	70%	0	55%	100%	0	0	55%	5%	0	0	65%	95%
	3C30P40H	100%	0	0	100%	70%	0	0	95%	100%	0	0	0	100%	10%	75%	0	0	80%	0	40%	100%	0	0	70%	10%	0	0	95%	100%
	3C45P40H	100%	0	0	90%	55%	0	0	100%	100%	0	0	0	75%	0	50%	5%	40%	75%	0	55%	100%	0	0	80%	25%	0	0	100%	85%
	3C60P40H	100%	5%	10%	100%	55%	0	0	100%	95%	0	0	0	75%	0	0	0	30%	70%	0	5%	100%	5%	5%	90%	25%	0	0	100%	85%
	3C00P15S	0	0	0	5%	5%	0	0	0	80%	0	0	0	0	0	100%	0	0	0	0	100%	0	0	0	0	0	0	0	0	15%
	3C15P15S	40%	0	0	5%	5%	0	0	5%	80%	0	0	0	0	0	100%	0	0	0	0	100%	35%	0	0	0	0	0	0	0	25%
	3C30P15S	95%	0	0	5%	0	0	0	5%	80%	0	0	0	0	0	100%	0	0	55%	0	100%	65%	0	0	0	0	0	0	0	40%
	3C45P15S	100%	0	0	5%	0	0	0	0	75%	0	0	0	0	0	85%	0	0	50%	0	95%	95%	0	0	0	0	0	0	0	10%
	3C60P15S	100%	0	0	25%	0	0	0	0	70%	0	0	0	30%	0	15%	0	0	90%	0	55%	100%	0	0	0	0	0	0	0	10%
	3C00P40S	15%	0	0	75%	70%	0	0	0	100%	0	0	0	60%	0	100%	0	0	20%	0	100%	0	0	0	15%	0	0	0	0	85%
	3C15P40S	90%	0	0	80%	70%	0	0	35%	100%	0	0	0	70%	0	100%	0	0	50%	0	100%	80%	0	0	25%	10%	0	0	5%	85%
	3C30P40S	100%	0	0	80%	75%	0	0	75%	100%	0	0	0	75%	0	100%	0	0	65%	0	100%	100%	0	0	65%	25%	0	0	60%	90%
	3C45P40S	100%	0	0	90%	65%	0	0	90%	100%	0	0	0	65%	0	90%	0	0	45%	0	100%	100%	0	0	85%	20%	0	0	80%	100%
	3C60P40S	100%	0	0	100%	65%	0	0	100%	100%	0	0	0	75%	0	35%	0	0	65%	15%	75%	100%	0	0	95%	25%	0	0	95%	100%
135°	3C00P15H	100%	0	0	0	0	0	0	100%	100%	0	0	0	0	0	0	0	0	100%	0	15%	100%	0	0	0	0	0	0	100%	85%
	3C15P15H	100%	0	0	0	0	0	0	100%	100%	0	0	0	0	0	20%	0	5%	100%	0	100%	100%	0	0	0	0	0	0	100%	100%
	3C30P15H	100%	0	0	0	0	0	0	85%	75%	0	0	0	0	0	5%	0	70%	100%	0	100%	100%	0	0	0	0	0	0	100%	100%
	3C45P15H	100%	0	0	0	0	0	0	100%	60%	0	0	0	0	0	5%	0	100%	0	0	100%	100%	0	0	0	0	0	0	100%	55%
	3C60P15H	100%	0	0	10%	0	0	0	40%	10%	0	0	0	5%	0	0	0	100%	0	0	45%	100%	0	0	0	0	0	0	15%	10%
	3C00P40H	100%	0	0	0	0	0	0	100%	100%	0	0	0	5%	0	0	0	0	5%	0	0	100%	0	0	0	0	0	0	100%	100%
	3C15P40H	100%	0	0	45%	0	0	0	100%	100%	0	0	0	50%	0	40%	0	0	55%	0	25%	100%	0	0	10%	5%	0	0	100%	100%
	3C30P40H	100%	0	0	100%	40%	0	0	100%	100%	0	0	0	90%	0	55%	0	0	80%	5%	75%	100%	0	0	75%	10%	0	0	100%	100%
	3C45P40H	100%	0	0	95%	30%	0	0	60%	90%	0	0	0	75%	0	70%	10%	75%	85%	0	80%	100%	0	0	65%	5%	0	0	75%	55%
	3C60P40H	100%	0	0	100%	20%	0	0	60%	90%	0	5%	0	60%	0	25%	5%	100%	100%	0	35%	100%	0	0	55%	0	0	0	5%	15%
	3C00P15S	100%	0	0	0	0	0	0	90%	95%	0	0	0	0	0	70%	0	0	100%	0	100%	100%	0	0	0	0	0	0	75%	80%
	3C15P15S	100%	0	0	0	0	0	0	80%	100%	0	0	0	0	0	90%	0	0	100%	25%	100%	100%	0	0	0	0	0	0	90%	100%
	3C30P15S	100%	0	0	0	0	0	0	75%	80%	0	0	0	0	0	85%	0	10%	100%	20%	100%	100%	0	0	5%	0	0	0	90%	100%
	3C45P15S	100%	0	0	5%	0	0	0	75%	75%	0	0	0	0	0	80%	0	80%	75%	0	100%	100%	0	0	10%	0	0	0	75%	75%
	3C60P15S	100%	0	0	0	0	0	0	45%	50%	0	0	0	0	0	80%	0	95%	0	0	100%	100%	0	0	5%	0	0	0	50%	60%
	3C00P40S	100%	0	0	10%	10%	0	0	95%	100%	0	0	0	25%	0	80%	0	0	25%	0	70%	100%	0	0	0	10%	0	0	95%	100%
	3C15P40S	100%	0	0	45%	0	0	0	95%	100%	0	0	0	20%	0	80%	0	0	30%	0	80%	100%	0	0	5%	0	0	0	95%	100%
	3C30P40S	100%	0	0	70%	15%	0	0	80%	100%	0	0	0	70%	0	85%	0	0	75%	0	80%	100%	0	0	0	0	0	0	80%	85%
	3C45P40S	100%	0	0	80%	15%	0	0	85%	100%	0	0	0	55%	0	85%	0	0	75%	0	100%	100%	0	0	15%	0	0	0	80%	85%
	3C60P40S	100%	0	0	85%	15%	0	0	75%	100%	0	0	0	40%	0	75%	0	5%	35%	0	100%	100%	0	0	40%	0	0	0	50%	80%

Preferred limit states:	0	20%	40%	60%	80%	100%
Acceptable limit states:	0	20%	40%	60%	80%	100%
Unacceptable limit states:	0	20%	40%	60%	80%	100%

Abutments of 3C bridges

Table 6.25 statistically summarizes the occurrences of several component limit states at Abutments 1 and 2 of 3C bridges. Similar to 3S and 4S bridges, closure of expansion joints (CEJ@A1 and A2) occurred in most 3C bridge analyses, except those of non-skew variants subjected to the pure transverse ground motions.

Mobilization of ultimate backfill passive resistance (MBU@A1 and A2) occurred in only 3% of the analyses, which is close to the percentage of 4S bridges but larger than that of 3S bridges. The majority of these occurrences in 3C bridges involved the tall pier, soft foundation soil, and pure longitudinal or 45° ground motions. The combination of these conditions can result in large superstructure displacements normal to the abutments, significant superstructure-abutment interactions, and mobilization of high passive resistance of the backfill. Failure of the backwall-pile cap connections (FBP@A1 and A2) was only observed in a few analyses, which exclusively involved tall-pier 3C bridges.

Rupture of the retainer anchors at Abutments 1 and 2 (RRA@A1 and A2) was observed in 28% and 21% of the 3C bridge analyses, respectively. These percentages are higher than those of 4S bridges but lower than those of 3S bridges. 95% of these ruptures were observed in the analyses of tall-pier 3C bridges. The occurrences increased with bridge skew. The ground motions applied in the transverse direction caused the most occurrences among all the incident directions. These tendencies are consistent with those of 3S and 4S bridges.

Sliding of the elastomeric bearings at Abutments 1 and 2 (SEB@A1 and A2) occurred in some 3C bridge analyses (17% for A1 and 9% for A2). Similar to the behavior of 3S and 4S bridges, 80% of the bearing sliding occurred in tall-pier 3C bridges. Figure 6.9 illustrates the peak abutment bearing sliding at the four deck corners. In only one of the 1,600 3C bridge analyses, bearing unseating at the abutment was observed, which occurred in a 60°-skew bridge with the tall-pier columns and soft foundation soil, excited by a 45° ground motion, as illustrated in Figure 6.9 and Table 6.25. In general, the peak bearing sliding distance in the majority of the 1,600 analyses did not exceed one half of the seat width in either the abutment-normal or abutment-parallel direction. As the four deck corners, the overall bearing sliding ratio in the abutment-normal direction is larger than that in the abutment-parallel direction, except in a few cases of non-skew bridges excited by the transverse ground motions, the bearing at the lower-left deck corner slided for a large distance

Table 6.25: Occurrences of limit states at abutments (A1 and A2) of 3C bridge variants

Limit state	No. of analyses with occurrence [1]	Skew angle[2] (°)					Foundation soil [2]		Column height [2] (m)		Ground motion incident angle [2] (°)			
		0	15	30	45	60	Hard	Soft	4.57	12.19	0	45	90	135
Closure of expansion joint (CEJ@A1)	1497 (94%)	243 (16%)	295 (20%)	319 (21%)	320 (21%)	320 (21%)	749 (50%)	748 (50%)	737 (49%)	760 (51%)	400 (27%)	400 (27%)	297 (20%)	400 (27%)
Mobilization of backfill ultimate capacity (MBU@A1)	41 (3%)	6 (15%)	10 (24%)	13 (32%)	6 (15%)	6 (15%)	3 (7%)	38 (93%)	1 (2%)	40 (98%)	21 (51%)	19 (46%)	1 (2%)	0 (0%)
Failure of backwall-to-pile-cap connection (FBP@A1)	7 (0%)	0 (0%)	1 (14%)	0 (0%)	0 (0%)	6 (86%)	4 (57%)	3 (43%)	0 (0%)	7 (100%)	1 (14%)	4 (57%)	2 (29%)	0 (0%)
Rupture of retainer anchor (RRA@A1)	446 (28%)	39 (9%)	61 (14%)	96 (22%)	122 (27%)	128 (29%)	241 (54%)	205 (46%)	23 (5%)	423 (95%)	25 (6%)	90 (20%)	202 (45%)	129 (29%)
Sliding of elastomeric bearing (SEB@A1)	276 (17%)	55 (20%)	50 (18%)	67 (24%)	56 (20%)	48 (17%)	116 (42%)	160 (58%)	5 (2%)	271 (98%)	56 (20%)	53 (19%)	138 (50%)	29 (11%)
Unseating of bearing at obtuse corner of deck (UBA@A1)	0 (0%)	0	0	0	0	0	0	0	0	0	0	0	0	0
Unseating of bearing at acute corner of deck (UBO@A1)	0 (0%)	0	0	0	0	0	0	0	0	0	0	0	0	0
Yielding of pile supporting wingwall (YPW@A1)	1293 (81%)	231 (18%)	257 (20%)	276 (21%)	278 (22%)	251 (19%)	691 (53%)	602 (47%)	590 (46%)	703 (54%)	396 (31%)	385 (30%)	184 (14%)	328 (25%)
Yielding of pile supporting backwall (YPB@A1)	1465 (92%)	303 (21%)	311 (21%)	306 (21%)	286 (20%)	259 (18%)	722 (49%)	743 (51%)	670 (46%)	795 (54%)	391 (27%)	385 (26%)	344 (23%)	345 (24%)
Closure of expansion joint (CEJ@A2)	1479 (92%)	243 (16%)	284 (19%)	313 (21%)	319 (22%)	320 (22%)	741 (50%)	738 (50%)	720 (49%)	759 (51%)	400 (27%)	400 (27%)	279 (19%)	400 (27%)
Mobilization of backfill ultimate capacity (MBU@A2)	40 (3%)	7 (18%)	13 (33%)	12 (30%)	5 (13%)	3 (8%)	4 (10%)	36 (90%)	1 (3%)	39 (97%)	26 (65%)	13 (33%)	1 (3%)	0 (0%)
Failure of backwall-to-pile-cap connection (FBP@A2)	4 (0%)	2 (50%)	0 (0%)	0 (0%)	0 (0%)	2 (50%)	2 (50%)	2 (50%)	0 (0%)	4 (100%)	2 (50%)	1 (25%)	1 (25%)	0 (0%)
Rupture of retainer anchor (RRA@A2)	329 (21%)	12 (4%)	19 (6%)	76 (23%)	108 (33%)	114 (35%)	205 (62%)	124 (38%)	10 (3%)	319 (97%)	50 (15%)	95 (29%)	127 (39%)	57 (17%)
Sliding of elastomeric bearing (SEB@A2)	146 (9%)	25 (17%)	24 (16%)	33 (23%)	38 (26%)	26 (18%)	57 (39%)	89 (61%)	1 (1%)	145 (99%)	64 (44%)	45 (31%)	31 (21%)	6 (4%)
Unseating of bearing at obtuse corner of deck (UBO@A2)	0 (0%)	0	0	0	0	0	0	0	0	0	0	0	0	0
Unseating of bearing at acute corner of deck (UBA@A2)	2 (0%)	0 (0%)	0 (0%)	0 (0%)	0 (0%)	2 (100%)	0 (0%)	2 (100%)	0 (0%)	2 (100%)	0 (0%)	2 (100%)	0 (0%)	0 (0%)
Yielding of pile supporting wingwall (YPW@A2)	1230 (77%)	230 (19%)	249 (20%)	265 (22%)	267 (22%)	219 (18%)	643 (52%)	587 (48%)	556 (45%)	674 (55%)	395 (32%)	388 (32%)	132 (11%)	315 (26%)
Yielding of pile supporting backwall (YPB@A2)	1320 (83%)	271 (21%)	284 (22%)	290 (22%)	254 (19%)	221 (17%)	649 (49%)	671 (51%)	572 (43%)	748 (57%)	390 (30%)	390 (30%)	223 (17%)	317 (24%)

1 The number above the parentheses indicates the number of analyses with occurrences of a limit state.
The percentage inside the parentheses indicates the ratio of the number above the parentheses to all the 1,600 analyses.

2 The number above the parentheses indicates the number of analyses with occurrences of a limit state contributed by a parametric variation.
The percentage inside the parentheses indicates the relative contribution of a parametric variation to the total occurrences of a limit state.

parallel to the abutment. At all the four deck corners, 60°-skew 3C bridges experienced the largest abutment-normal bearing sliding of all the 3C bridge analyses.

Yielding of the abutment piles of 3C bridges (YPW@A1 and A2, YPB@A1 and A2) was observed in over 80% of the analyses, as can be seen in Table 6.25. This percentage is in between that of 3S and 4S bridges. Additionally, Table 6.26 lists the median peak strains. It can be seen that the piles yielded in most of the tabulated cases. The piles were strained the least when 3C bridges were subjected to the pure transverse ground motions. The piles of tall-pier 3C bridge variants were strained more than those of the short-pier equivalents. These tendencies are consistent with those of 3S and 4S bridges.

Table 6.26: Normalized peak strains of steel H piles at abutments of 3C bridges (peak strains are normalized to the yield strain, 0.0017; numbers outside the parentheses are medians, while those inside are median absolute deviations; data for piles supporting backwalls and wingwalls are placed on the left and right sides of the commas, respectively)

Foundation soil condition			Hard								Soft							
Pier column height (m)			4.57				12.19				4.57				12.19			
Longitudinal (0º) ground motions	Bridge skew (º)	0	2.3	(0.9) ,	3.8	(1.2)	8.9	(3.4) ,	11.3	(3.9)	3.8	(1.5) ,	3.0	(1.3)	8.3	(1.9) ,	8.2	(2.6)
		15	5.7	(1.4) ,	6.9	(1.4)	12.5	(3.0) ,	13.4	(2.9)	6.3	(2.5) ,	5.5	(2.5)	11.5	(4.0) ,	10.9	(3.8)
		30	5.9	(2.4) ,	7.0	(2.1)	13.4	(3.7) ,	14.0	(4.9)	6.1	(2.8) ,	5.2	(2.7)	14.8	(3.1) ,	13.8	(3.0)
		45	3.8	(2.0) ,	5.3	(2.5)	5.6	(2.7) ,	7.8	(2.9)	3.7	(2.1) ,	3.5	(2.1)	10.9	(2.8) ,	10.7	(2.8)
		60	1.2	(0.2) ,	1.5	(0.4)	2.9	(1.2) ,	4.4	(1.5)	2.5	(1.5) ,	2.5	(1.5)	7.2	(2.5) ,	7.5	(2.2)
45º ground motions	Bridge skew (º)	0	1.5	(0.3) ,	2.3	(0.5)	4.7	(1.8) ,	6.3	(1.9)	2.1	(0.6) ,	1.6	(0.4)	4.7	(2.2) ,	3.6	(1.8)
		15	2.5	(0.5) ,	3.8	(0.8)	8.2	(2.7) ,	9.3	(2.6)	2.9	(0.9) ,	2.1	(0.8)	6.2	(2.1) ,	5.7	(2.4)
		30	4.1	(1.8) ,	5.2	(1.7)	11.2	(4.4) ,	12.1	(4.1)	3.8	(1.5) ,	2.9	(1.4)	9.7	(3.9) ,	9.1	(4.2)
		45	2.0	(0.5) ,	3.0	(0.8)	7.9	(3.6) ,	9.9	(4.2)	2.7	(0.8) ,	2.6	(0.9)	9.1	(3.9) ,	8.5	(3.9)
		60	1.3	(0.2) ,	1.9	(0.3)	2.7	(1.3) ,	4.5	(2.1)	1.8	(0.7) ,	1.7	(0.7)	6.6	(3.0) ,	6.0	(2.6)
Transverse (90º) ground motions	Bridge skew (º)	0	0.9	(0.1) ,	0.5	(0.0)	1.6	(0.2) ,	0.9	(0.1)	1.0	(0.2) ,	0.6	(0.1)	1.8	(0.7) ,	1.1	(0.4)
		15	1.0	(0.1) ,	0.6	(0.1)	1.7	(0.4) ,	1.4	(0.4)	1.0	(0.2) ,	0.7	(0.1)	2.3	(0.9) ,	1.5	(0.3)
		30	1.1	(0.1) ,	1.0	(0.3)	2.6	(1.5) ,	3.1	(1.4)	1.0	(0.2) ,	0.8	(0.1)	4.3	(2.1) ,	2.1	(1.0)
		45	0.9	(0.1) ,	1.1	(0.2)	2.2	(0.8) ,	4.0	(1.6)	1.0	(0.1) ,	0.8	(0.1)	4.0	(2.1) ,	2.7	(1.2)
		60	0.8	(0.2) ,	0.9	(0.2)	2.1	(1.0) ,	4.2	(1.8)	0.9	(0.1) ,	0.7	(0.2)	4.8	(2.8) ,	3.6	(1.8)
135º ground motions	Bridge skew (º)	0	1.6	(0.3) ,	2.4	(0.4)	4.8	(1.8) ,	6.2	(2.0)	2.0	(0.5) ,	1.7	(0.4)	5.7	(2.0) ,	4.5	(1.6)
		15	1.9	(0.6) ,	2.7	(0.8)	3.9	(1.2) ,	5.1	(1.4)	3.7	(1.8) ,	3.0	(1.3)	6.9	(3.2) ,	5.5	(2.7)
		30	1.7	(0.7) ,	2.3	(0.9)	3.5	(1.8) ,	4.4	(2.4)	3.4	(1.5) ,	2.8	(1.3)	6.3	(3.3) ,	5.6	(2.7)
		45	1.1	(0.2) ,	1.5	(0.4)	1.1	(0.2) ,	1.2	(0.2)	1.9	(1.1) ,	1.8	(1.0)	2.2	(0.9) ,	1.9	(0.9)
		60	0.8	(0.1) ,	0.8	(0.1)	1.1	(0.4) ,	1.0	(0.4)	1.1	(0.3) ,	1.0	(0.2)	1.5	(0.5) ,	1.3	(0.4)

Unyielded: normalized strain < 1 (unnormalized strain < 0.0017)

Yielded without signficniant strain hardening: 1 ≤ normalized strain < 10 (0.0017 ≤ unnormalized strain < 0.017)

Yielded and significantly strain hardened: 10 ≤ normalized strain (0.017 ≤ unnormalized strain)

Expansion piers (Pier 1) of 3C bridges

Table 6.27 statistically summarizes the occurrences of several component limit states at the expansion piers (Pier 1) of 3C bridges. Similar to the behavior of the 3S and 4S bridges, rupture of

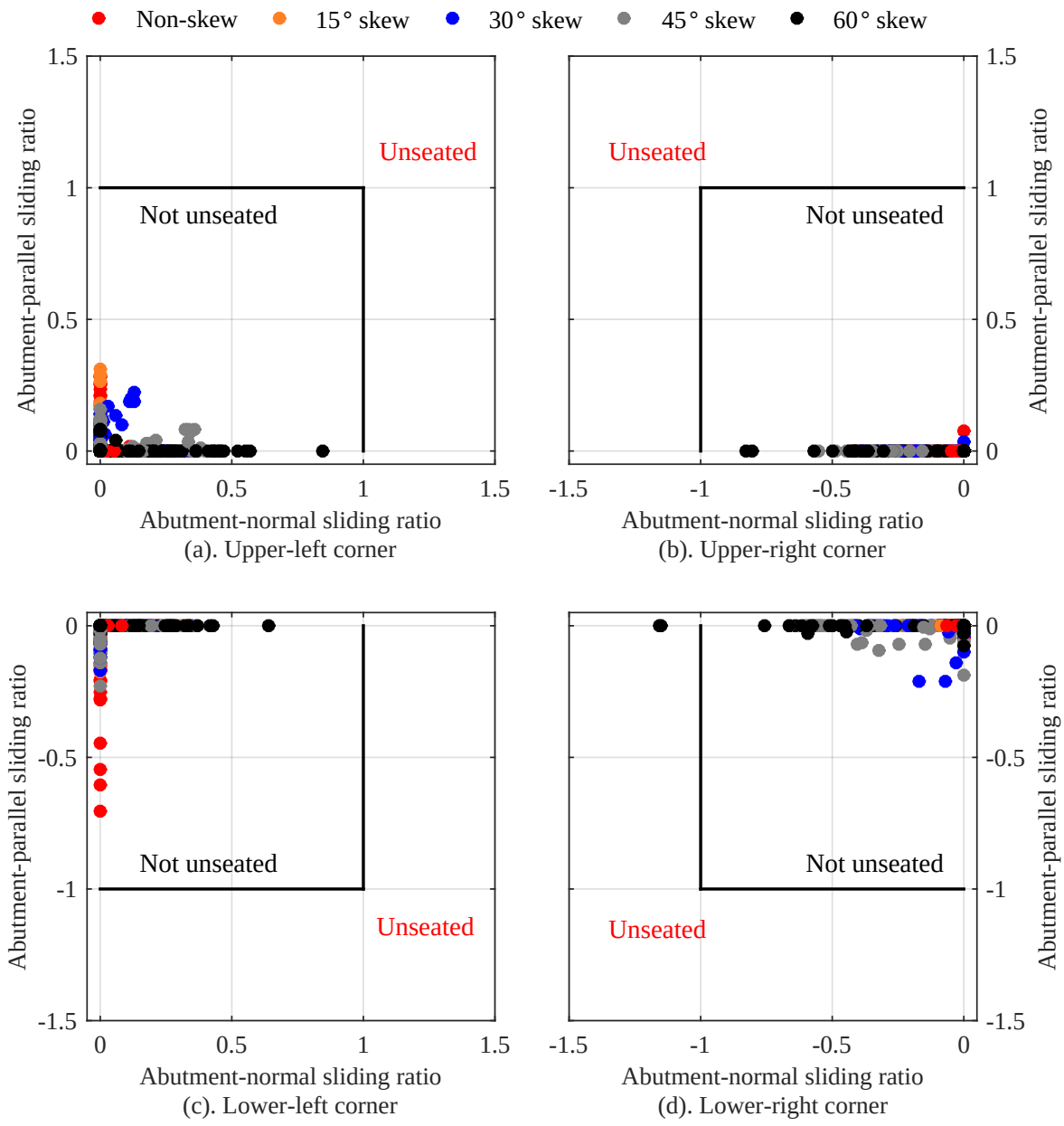

Figure 6.9: Peak sliding ratios of elastomeric bearings at deck corners of 3C bridges

the elastomeric bearing retainers at Pier 1 (RRA@P1) was not observed in any 3C bridge analysis.

Table 6.27: Occurrences of limit states at expansion piers (Pier 1) of 3C bridge variants

Limit state	No. of analyses with occurrence [1]	Skew angle[2] (°)					Foundation soil [2]		Column height [2] (m)		Ground motion incident angle [2] (°)			
		0	15	30	45	60	Hard	Soft	4.57	12.19	0	45	90	135
Rupture of retainer anchor (RRA@P1)	0 (0%)	0	0	0	0	0	0	0	0	0	0	0	0	0
Sliding of elastomeric bearing (SEB@P1)	25 (2%)	4 (16%)	4 (16%)	11 (44%)	4 (16%)	2 (8%)	5 (20%)	20 (80%)	5 (20%)	20 (80%)	22 (88%)	2 (8%)	0 (0%)	1 (4%)
Unseating of elastomeric bearing (UEB@P1)	0 (0%)	0	0	0	0	0	0	0	0	0	0	0	0	0
Yielding of vertical reinforcing steel at column end (YRS@P1)	453 (28%)	65 (14%)	85 (19%)	119 (26%)	88 (19%)	96 (21%)	218 (48%)	235 (52%)	38 (8%)	415 (92%)	82 (18%)	98 (22%)	174 (38%)	99 (22%)
Crushing of concrete cover at column end (CCC@P1)	7 (0%)	0 (0%)	3 (43%)	3 (43%)	0 (0%)	1 (14%)	7 (100%)	0 (0%)	4 (57%)	3 (43%)	3 (43%)	2 (29%)	2 (29%)	0 (0%)
Yielding of pile at pier (YPP@P1)	591 (37%)	125 (21%)	146 (25%)	125 (21%)	120 (20%)	75 (13%)	132 (22%)	459 (78%)	255 (43%)	336 (57%)	73 (12%)	59 (10%)	253 (43%)	206 (35%)

1 The number above the parentheses indicates the number of analyses with occurrences of a limit state.
The percentage inside the parentheses indicates the ratio of the number above the parentheses to all the 1,600 analyses.
2 The number above the parentheses indicates the number of analyses with occurrences of a limit state contributed by a parametric variation.
The percentage inside the parentheses indicates the relative contribution of a parametric variation to the total occurrences of a limit state.

Sliding of the elastomeric bearings at Pier 1 (SEB@P1) was observed in 25 3C bridge analyses, but was not observed in any 3S or 4S bridge analysis. Unseating of the bearings at Pier 1 (UEB@P1) was not observed at all, which is the same as the behavior of 3S and 4S bridges.

Yielding of the vertical reinforcing steel at the column bases of Pier 1 (YRS@P1) was observed in 27% of the 3C bridge analyses. This percentage is in between that of 3S and 4S bridges. Table 6.30 lists the median peak strains of vertical reinforcing steel at the pier column bases of 3C bridges. The data on the left and right sides of the commas are for the expansion and fixed piers, respectively. Similar to the damage level of 3S and 4S bridges, the reinforcing steel was undamaged or only lightly damaged in the 3C bridge analyses. 92% of the yieldings occurred in tall-pier 3C bridges, which is similar to the tendency of 3S and 4S bridges. Among all the incident directions, the transverse ground motions caused the most yieldings (43%), which is similar to the behavior of 3S bridges.

Crushing of the concrete cover at the column bases of Pier 1 (CCC@P1) occurred in only several analyses that exclusively involved the hard foundation soil.

Yielding of the steel H piles supporting Pier 1 (YSP@P1) occurred in 37% of the 3C bridge

Table 6.28: Normalized median peak strain of vertical reinforcing steel at pier column bases of 3C bridges (peak strains are normalized to the yield strain, 0.0021; numbers outside the parentheses are medians, while those inside are median absolute deviations; data for expansion and fixed piers are placed on the left and right sides of the commas, respectively; performance levels in the footnote are defined per Kowalsky (2001) and Revell (2013))

Foundation soil condition			Hard				Soft			
Pier column height (m)			4.57		12.19		4.57		12.19	
Longitudinal (0º) ground motions	Bridge skew (º)	0	0.5 (0.1) ,	5.2 (1.3)	0.9 (0.2) ,	0.9 (0.2)	0.6 (0.1) ,	6.8 (2.4)	1.2 (0.5) ,	1.1 (0.3)
		15	0.6 (0.1) ,	7.0 (1.0)	0.9 (0.2) ,	1.0 (0.1)	0.8 (0.3) ,	10.3 (3.2)	1.4 (0.5) ,	1.4 (0.5)
		30	0.6 (0.1) ,	7.8 (1.2)	0.9 (0.3) ,	1.1 (0.3)	0.8 (0.1) ,	10.0 (3.4)	1.5 (0.6) ,	1.7 (0.7)
		45	0.4 (0.1) ,	1.5 (0.1)	0.7 (0.2) ,	1.3 (0.5)	0.5 (0.1) ,	1.4 (0.1)	0.7 (0.2) ,	1.1 (0.2)
		60	0.3 (0.0) ,	0.7 (0.1)	0.6 (0.2) ,	1.1 (0.1)	0.3 (0.1) ,	0.8 (0.1)	0.6 (0.1) ,	1.0 (0.1)
45º ground motions	Bridge skew (º)	0	0.3 (0.0) ,	2.6 (0.4)	0.7 (0.1) ,	0.7 (0.1)	0.5 (0.1) ,	2.8 (0.7)	0.8 (0.3) ,	0.8 (0.1)
		15	0.6 (0.1) ,	4.3 (0.6)	0.6 (0.1) ,	0.7 (0.1)	0.7 (0.1) ,	6.2 (1.4)	0.9 (0.3) ,	0.9 (0.2)
		30	0.8 (0.1) ,	6.6 (1.1)	0.8 (0.3) ,	0.9 (0.3)	0.9 (0.2) ,	8.6 (1.5)	1.3 (0.7) ,	1.3 (0.6)
		45	0.8 (0.1) ,	3.2 (1.2)	0.9 (0.4) ,	1.0 (0.3)	0.8 (0.1) ,	3.4 (0.9)	1.4 (0.7) ,	1.2 (0.4)
		60	0.7 (0.1) ,	1.2 (0.2)	1.2 (0.6) ,	1.3 (0.5)	0.8 (0.1) ,	1.5 (0.5)	1.2 (0.7) ,	1.2 (0.3)
Transverse (90º) ground motions	Bridge skew (º)	0	0.4 (0.1) ,	0.5 (0.1)	1.9 (0.6) ,	1.1 (0.2)	0.3 (0.0) ,	0.3 (0.0)	1.1 (0.2) ,	0.9 (0.1)
		15	0.5 (0.1) ,	0.6 (0.1)	2.3 (0.7) ,	1.3 (0.4)	0.4 (0.0) ,	0.7 (0.1)	1.2 (0.2) ,	1.0 (0.1)
		30	0.7 (0.1) ,	1.1 (0.1)	3.2 (0.5) ,	1.6 (0.9)	0.6 (0.1) ,	1.0 (0.1)	1.7 (0.5) ,	1.1 (0.3)
		45	0.9 (0.1) ,	1.0 (0.1)	1.3 (0.6) ,	1.6 (0.5)	0.7 (0.1) ,	1.0 (0.1)	1.1 (0.4) ,	0.9 (0.3)
		60	1.0 (0.1) ,	1.3 (0.2)	1.5 (0.5) ,	1.2 (0.4)	1.0 (0.1) ,	1.2 (0.1)	1.8 (0.9) ,	1.2 (0.4)
135º ground motions	Bridge skew (º)	0	0.3 (0.0) ,	2.6 (0.4)	0.7 (0.1) ,	0.7 (0.1)	0.5 (0.1) ,	2.8 (0.8)	0.8 (0.2) ,	0.8 (0.1)
		15	0.4 (0.1) ,	2.8 (0.5)	1.0 (0.2) ,	1.0 (0.2)	0.5 (0.1) ,	3.7 (1.7)	0.8 (0.2) ,	0.9 (0.1)
		30	0.7 (0.1) ,	2.2 (0.3)	1.5 (0.5) ,	2.5 (1.0)	0.5 (0.1) ,	3.4 (0.8)	1.1 (0.2) ,	1.3 (0.2)
		45	0.6 (0.1) ,	0.8 (0.0)	1.8 (0.9) ,	2.0 (0.6)	0.5 (0.0) ,	1.1 (0.2)	1.0 (0.1) ,	1.0 (0.1)
		60	0.7 (0.1) ,	0.6 (0.1)	1.0 (0.3) ,	1.2 (0.1)	0.6 (0.1) ,	0.8 (0.0)	0.9 (0.2) ,	0.9 (0.1)

Undamaged (unyielded):	normalized strain < 1 (unnormalized strain < 0.0021)
Lightly damaged (unlikely requiring repair):	1 ≤ normalized strain < 7.1 (0.0021 ≤ unnormalized strain < 0.015)
Moderately damaged (repairable):	7.1 ≤ normalized strain < 28.6 (0.015 ≤ unnormalized strain < 0.06)
Severely damaged (not easily repairable):	28.6 ≤ normalized strain (0.06 ≤ unnormalized strain)

Table 6.29: Normalized peak strain of concrete cover at pier column base of 3C bridges (peak strains are normalized to the crushing strain, 0.005; numbers outside the parentheses are medians, while those inside are median absolute deviations; data of concrete cover at column base of expansion and fixed piers are placed on the left and right sides of the commas, respectively; performance levels in the footnote are defined per Kowalsky (2001) and Revell (2013))

Foundation soil condition			Hard				Soft			
Pier column height (m)			4.57		12.19		4.57		12.19	
Longitudinal (0º) ground motions	Bridge skew (º)	0	0.2 (0.0) , 0.8 (0.2)		0.3 (0.0) , 0.3 (0.0)		0.2 (0.0) , 1.1 (0.4)		0.3 (0.1) , 0.3 (0.1)	
		15	0.2 (0.0) , 1.2 (0.2)		0.3 (0.0) , 0.3 (0.0)		0.3 (0.1) , 1.8 (0.6)		0.4 (0.1) , 0.4 (0.1)	
		30	0.2 (0.0) , 1.4 (0.2)		0.3 (0.1) , 0.3 (0.1)		0.3 (0.0) , 1.8 (0.6)		0.4 (0.1) , 0.4 (0.1)	
		45	0.2 (0.0) , 0.4 (0.0)		0.2 (0.0) , 0.3 (0.1)		0.2 (0.0) , 0.4 (0.0)		0.2 (0.1) , 0.3 (0.0)	
		60	0.1 (0.0) , 0.2 (0.0)		0.2 (0.0) , 0.3 (0.0)		0.1 (0.0) , 0.2 (0.0)		0.2 (0.0) , 0.2 (0.0)	
45º ground motions	Bridge skew (º)	0	0.2 (0.0) , 0.5 (0.0)		0.2 (0.0) , 0.2 (0.0)		0.2 (0.0) , 0.5 (0.1)		0.2 (0.0) , 0.2 (0.0)	
		15	0.2 (0.0) , 0.7 (0.1)		0.2 (0.0) , 0.2 (0.0)		0.2 (0.0) , 0.9 (0.2)		0.2 (0.0) , 0.2 (0.0)	
		30	0.2 (0.0) , 1.1 (0.2)		0.2 (0.0) , 0.2 (0.1)		0.2 (0.0) , 1.4 (0.3)		0.3 (0.1) , 0.3 (0.1)	
		45	0.2 (0.0) , 0.6 (0.2)		0.2 (0.1) , 0.3 (0.1)		0.2 (0.0) , 0.6 (0.1)		0.3 (0.1) , 0.3 (0.1)	
		60	0.2 (0.0) , 0.3 (0.0)		0.3 (0.1) , 0.3 (0.1)		0.2 (0.0) , 0.4 (0.1)		0.3 (0.1) , 0.3 (0.0)	
Transverse (90º) ground motions	Bridge skew (º)	0	0.2 (0.0) , 0.2 (0.0)		0.4 (0.1) , 0.3 (0.0)		0.1 (0.0) , 0.1 (0.0)		0.3 (0.0) , 0.3 (0.0)	
		15	0.2 (0.0) , 0.2 (0.0)		0.5 (0.1) , 0.4 (0.1)		0.2 (0.0) , 0.2 (0.0)		0.3 (0.0) , 0.3 (0.0)	
		30	0.2 (0.0) , 0.3 (0.0)		0.6 (0.1) , 0.4 (0.2)		0.2 (0.0) , 0.3 (0.0)		0.4 (0.1) , 0.3 (0.1)	
		45	0.2 (0.0) , 0.3 (0.0)		0.3 (0.1) , 0.4 (0.1)		0.2 (0.0) , 0.3 (0.0)		0.3 (0.0) , 0.2 (0.0)	
		60	0.3 (0.0) , 0.3 (0.0)		0.3 (0.1) , 0.3 (0.1)		0.3 (0.0) , 0.3 (0.0)		0.4 (0.1) , 0.3 (0.1)	
135º ground motions	Bridge skew (º)	0	0.2 (0.0) , 0.5 (0.1)		0.2 (0.0) , 0.2 (0.0)		0.2 (0.0) , 0.6 (0.1)		0.3 (0.0) , 0.3 (0.0)	
		15	0.2 (0.0) , 0.6 (0.1)		0.3 (0.0) , 0.3 (0.0)		0.2 (0.0) , 0.7 (0.2)		0.2 (0.0) , 0.2 (0.0)	
		30	0.2 (0.0) , 0.5 (0.0)		0.4 (0.1) , 0.5 (0.1)		0.2 (0.0) , 0.6 (0.1)		0.3 (0.0) , 0.3 (0.0)	
		45	0.2 (0.0) , 0.3 (0.0)		0.4 (0.1) , 0.4 (0.1)		0.2 (0.0) , 0.3 (0.0)		0.3 (0.0) , 0.2 (0.0)	
		60	0.2 (0.0) , 0.2 (0.0)		0.3 (0.1) , 0.3 (0.0)		0.2 (0.0) , 0.2 (0.0)		0.3 (0.0) , 0.3 (0.0)	

Undamaged (ultimate strength not mobillized):	normalized strain < 0.4 (unnormalized strain < 0.002)
Lightly damaged (ultimate strength mobilized but uncrushed):	0.4 ≤ normalized strain < 1 (0.002 ≤ unnormalized strain < 0.005)
Moderately damaged (crushed but repairable):	1 ≤ normalized strain < 3.6 (0.005 ≤ unnormalized strain < 0.018)
Severely damaged (not easily repairable):	3.6 ≤ normalized strain (0.018 ≤ unnormalized strain)

analyses. This percentage is close to that of 4S bridges (39%) but much higher than that of the bridges (17%). Table 6.30 indicates the median peak strains of the steel H piles supporting the piers of 3C bridges. The data on the left and right sides of the commas are for the expansion and fixed piers, respectively. It can be found in Tables 6.27 and 6.30 that the piles in the soft soil were generally strained more than those in the hard soil and contributed a larger percentage of the yieldings. The pure transverse and 135° ground motions caused 78% of the yieldings. These observations are consistent with those of 3S and 4S bridges.

Table 6.30: Normalized median peak strains of steel H piles at piers of 3C bridges (peak strains are normalized to the yield strain, 0.0017; numbers outside the parentheses are medians, while those inside are median absolute deviations; data for piles supporting expansion and fixed piers are placed on the left and right sides of the commas, respectively)

Foundation soil condition		Hard				Soft			
Pier column height (m)		4.57		12.19		4.57		12.19	
Longitudinal (0º) ground motions	Bridge skew (º) 0	0.3 (0.0) , 0.5 (0.0)		0.4 (0.0) , 0.4 (0.0)		0.4 (0.0) , 0.7 (0.1)		0.4 (0.1) , 0.4 (0.0)	
	15	0.4 (0.0) , 0.8 (0.0)		0.4 (0.0) , 0.5 (0.0)		0.5 (0.1) , 1.1 (0.1)		0.7 (0.1) , 0.7 (0.1)	
	30	0.4 (0.0) , 1.0 (0.1)		0.5 (0.1) , 0.6 (0.1)		0.9 (0.2) , 1.9 (0.5)		1.0 (0.2) , 1.2 (0.1)	
	45	0.6 (0.1) , 0.9 (0.1)		0.6 (0.1) , 1.0 (0.1)		1.4 (0.6) , 2.5 (0.4)		1.1 (0.3) , 2.3 (0.8)	
	60	0.6 (0.1) , 0.8 (0.1)		0.7 (0.1) , 0.9 (0.1)		1.3 (0.5) , 4.7 (1.2)		1.4 (0.2) , 6.9 (2.2)	
45º ground motions	Bridge skew (º) 0	0.8 (0.1) , 0.9 (0.1)		0.8 (0.0) , 0.7 (0.0)		1.0 (0.1) , 1.3 (0.1)		1.4 (0.5) , 1.1 (0.1)	
	15	0.7 (0.1) , 0.8 (0.1)		0.7 (0.0) , 0.6 (0.0)		1.0 (0.1) , 1.0 (0.1)		1.1 (0.2) , 1.0 (0.1)	
	30	0.6 (0.0) , 0.7 (0.0)		0.5 (0.0) , 0.5 (0.1)		0.9 (0.1) , 1.1 (0.0)		0.8 (0.1) , 0.9 (0.1)	
	45	0.5 (0.0) , 0.9 (0.0)		0.5 (0.0) , 0.6 (0.0)		0.8 (0.1) , 1.3 (0.1)		0.7 (0.1) , 0.8 (0.1)	
	60	0.5 (0.0) , 0.8 (0.0)		0.4 (0.1) , 0.5 (0.0)		0.7 (0.1) , 1.3 (0.1)		0.6 (0.1) , 0.9 (0.1)	
Transverse (90º) ground motions	Bridge skew (º) 0	1.0 (0.1) , 1.1 (0.1)		1.4 (0.3) , 1.0 (0.1)		2.7 (1.0) , 2.5 (0.8)		8.9 (3.6) , 4.0 (2.2)	
	15	1.0 (0.1) , 1.1 (0.1)		1.4 (0.3) , 1.0 (0.1)		3.1 (1.3) , 2.0 (0.5)		9.1 (3.6) , 4.7 (2.1)	
	30	0.9 (0.1) , 1.2 (0.1)		1.2 (0.1) , 0.9 (0.1)		1.7 (0.3) , 1.4 (0.1)		4.2 (1.8) , 2.4 (0.8)	
	45	0.7 (0.1) , 1.2 (0.2)		1.0 (0.2) , 1.1 (0.1)		1.3 (0.1) , 1.1 (0.1)		2.0 (0.8) , 1.8 (0.7)	
	60	0.5 (0.0) , 0.9 (0.1)		0.6 (0.1) , 0.8 (0.1)		0.9 (0.0) , 1.0 (0.1)		0.9 (0.2) , 1.3 (0.3)	
135º ground motions	Bridge skew (º) 0	0.8 (0.1) , 0.9 (0.1)		0.7 (0.0) , 0.6 (0.0)		1.0 (0.1) , 1.3 (0.1)		1.5 (0.5) , 1.1 (0.2)	
	15	0.8 (0.1) , 1.2 (0.1)		1.0 (0.1) , 0.9 (0.1)		1.4 (0.3) , 2.6 (0.8)		2.9 (1.8) , 2.1 (1.2)	
	30	0.8 (0.0) , 1.3 (0.1)		1.0 (0.2) , 1.1 (0.1)		1.8 (0.5) , 5.2 (1.8)		3.0 (2.1) , 4.1 (3.0)	
	45	0.7 (0.0) , 1.5 (0.2)		1.1 (0.2) , 1.2 (0.1)		1.7 (0.8) , 7.2 (2.0)		3.9 (2.8) , 7.6 (3.6)	
	60	0.6 (0.0) , 1.0 (0.1)		0.9 (0.1) , 0.9 (0.0)		1.3 (0.3) , 5.7 (2.4)		1.9 (1.1) , 7.3 (3.2)	

Unyielded: normalized strain < 1 (unnormalized strain < 0.0017)

Yielded without signficniant strain hardening: 1 ≤ normalized strain < 10 (0.0017 ≤ unnormalized strain < 0.017)

Yielded and significantly strain hardened: 10 ≤ normalized strain (0.017 ≤ unnormalized strain)

Fixed piers (Pier 2) of 3C bridges

Table 6.31 statistically summarizes the occurrences of several limit states at the fixed piers (Pier 2) of 3C bridges. As introduced in Chapter 2, a pair of retainers are typically installed on the fixed piers of recent precast-prestressed-concrete-girder bridges in Illinois to help secure the

diaphragm-pier-cap connections. Each retainer is secured to the pier cap through two anchor bolts with a diameter of 38.1 mm (1.5 in.). Rupture of these anchors (RRA@P2) was observed in only four analyses, all of which involved tall-pier and highly skewed 3C bridges in the hard foundation soil, when subjected to the pure transverse or 135° ground motions. The hard foundation soil leads to a relatively high pier stiffness that may incur large seismic force and deformation demands on the retainers.

Table 6.31: Occurrences of limit states at fixed piers (Pier 2) of 3C bridge variants

Limit state	No. of analyses with occurrence [1]	Skew angle [2] (°)					Foundation soil [2]		Column height [2] (m)		Ground motion incident angle [2] (°)			
		0	15	30	45	60	Hard	Soft	4.57	12.19	0	45	90	135
Rupture of retainer anchor (RRA@P2)	4 (0%)	0 (0%)	0 (0%)	0 (0%)	3 (75%)	1 (25%)	4 (100%)	0 (0%)	0 (0%)	4 (100%)	0 (0%)	0 (0%)	1 (25%)	3 (75%)
Rupture of steel dowel connection (RSD@P2)	309 (19%)	0 (0%)	1 (0%)	20 (6%)	111 (36%)	177 (57%)	213 (69%)	96 (31%)	231 (75%)	78 (25%)	108 (35%)	37 (12%)	36 (12%)	128 (41%)
Yielding of vertical reinforcing steel at column end (YRS@P2)	1026 (64%)	170 (17%)	194 (19%)	254 (25%)	226 (22%)	182 (18%)	512 (50%)	514 (50%)	567 (55%)	459 (45%)	293 (29%)	283 (28%)	202 (20%)	248 (24%)
Crushing of concrete cover at column end (CCC@P2)	136 (9%)	16 (12%)	43 (32%)	65 (48%)	3 (2%)	9 (7%)	52 (38%)	84 (62%)	126 (93%)	10 (7%)	76 (56%)	47 (35%)	3 (2%)	10 (7%)
Yielding of pile at pier (YPP@P2)	870 (54%)	135 (16%)	172 (20%)	192 (22%)	213 (24%)	158 (18%)	255 (29%)	615 (71%)	508 (58%)	362 (42%)	157 (18%)	122 (14%)	290 (33%)	301 (35%)

1 The number above the parentheses indicates the number of analyses with occurrences of a limit state.
The percentage inside the parentheses indicates the ratio of the number above the parentheses to all the 1,600 analyses.
2 The number above the parentheses indicates the number of analyses with occurrences of a limit state contributed by a parametric variation.
The percentage inside the parentheses indicates the relative contribution of a parametric variation to the total occurrences of a limit state.

Rupture of the steel dowel connections at Pier 2 (RSD@P2) was observed in 19% of the 3C bridge analyses. It can be found in Table 6.31 that the large skews, hard foundation soil, and short pier made up more occurrences than the small skews, soft soil, and tall pier, respectively. The pure longitudinal and 135° ground motions caused this limit state much more than the pure transverse and 45° ones. These observations are consistent with those of the rupture of steel fixed bearing anchors (RFA@P2) in 3S and 4S bridges.

Yielding of the vertical reinforcing steel at the column bases of Pier 2 (YRS@P2) occurred in 63% of the 3C bridge analyses. This percentage is in between that of 3S and 4S bridges. As shown in Table 6.28, the reinforcing steel was undamaged, lightly, or moderately damaged in different cases and the median peak strains of vertical reinforcing steel in Pier 2 were generally much higher than those of Pier 1, when subjected to the non-transverse ground motions. Tall-pier

3C bridges sustained more occurrences that their short-pier equivalents. These observations are consistent with those of 3S bridges.

Crushing of the concrete cover at the column bases of Pier 2 (CCC@P2) occurred in only 9% of the 3C bridge analyses, but this limit state did not occur to Pier 1. The majority of these occurrences involved short-pier bridge variants excited by the non-transverse ground motions. These tendencies are similar to those of the aforementioned limit state of reinforcing steel yielding at Pier 2 (YRS@P2), as expected.

Yielding of the steel piles supporting Pier 2 (YSP@P2) was observed in 54% of the 3C bridge analyses. This percentage is in between that of 3S and 4S bridges. Similar to the behavior of 3S and 4S bridges, the piles that are in the soft soil were more susceptible to this limit state than those in the hard soil and more occurrences of the yielding were caused by the pure transverse and 135° ground motions than those in the other two directions. These observations can be confirmed by examining the median peak strains listed in Table 6.30.

Summary of 3C bridges

1,600 nonlinear dynamic analyses were performed on the 20 three-span precast-prestressed-concrete-girder (3C) bridge variants using the suite of 20 seismic ground motions applied in four incident directions. The analysis results were statistically studied with emphasis on the occurrence of component limit states.

As an unacceptable limit state that usually causes losses of bridge spans and transportation disruption, unseating of elastomeric bearings occurred in two of the 1,600 3C bridge analyses. In these two analyses, the elastomeric bearing at the acute deck corner supported by Abutment 2 experienced large abutment-normal sliding that exceeded the seat width in the corresponding direction. These two analyses were performed on a 60°-skew 3C bridge with the tall pier columns and soft foundation soil, excited by two 45° ground motions. The only one bearing unseating case of 4S bridges occurred in the 4S equivalent of such a bridge.

The overall magnitude of the deck displacements of 3C bridges is in between that of 3S and 4S bridges. The overall deck rotation magnitude is close to that of 3S bridges but larger than that of 4S bridges.

The occurrence percentage of retainer anchor rupture at the abutments of 3C bridges is smaller than that of 3S bridges but larger than that of 4S bridges. Similar to 3S and 4S bridges, the retainer anchors at the expansion piers were not ruptured in any 3C bridge analysis. In 19% of the 3C bridge analyses, the steel dowel connections between the superstructure and fixed pier were ruptured.

While the expansion piers of 3C bridges were effectively protected by the elastomeric bearings, the fixed piers sustained much more seismic damage, in terms of yielding of column reinforcing steel and steel piles, as well as crushing of column concrete cover.

Overall, the seismic damage to 3C bridges is in between that of 3S and 4S bridges, which is consistent with the fact that the superstructure mass of 3C bridges is also in between the two types of steel-plate-girder bridges. Specifically, the occurrence percentage of each of the following limit states in 3C bridges is in between the equivalents in 3S and 4S bridges

- Mobilization of ultimate backfill passive resistance (MBU@A1 and A2)
- Yielding of abutment piles (YPW@A1 and A2, YPB@A1 and A2)
- Yielding of vertical reinforcing steel at column bases of expansion and fixed piers (YRS@P1, P2, and P3)

- Crushing of concrete cover at column bases of expansion and fixed piers (CCC@P1, P2, and P3)
- Yielding of pier piles (YSP@P1, P2, and P3)

6.3.4 Four-span precast-prestressed-concrete-girder (4C) bridges

Superstructures of 4C bridges

Table 6.32 indicates the medians and median absolute deviations of the deck center displacements of 4C bridge variants excited by the 20 seismic ground motions applied in different incident directions. By comparing the displacements in Tables 6.2, 6.12, 6.22, and 6.32, it can be found that 4C bridge variants experienced the largest displacements of all the four types of bridges. This finding seems reasonable because 4C bridges have the largest superstructure mass and, thus, experienced the largest seismic force among all the four types of bridges.

The aforementioned bi-axial deck displacement behavior is observed again in 4C bridges. Additionally, for most of the cases in Table 6.32, the uni-axially applied ground motions were more critical for exciting large deck displacements along the two bridge axes than the bi-axial motions, except for the 4C60P40H and 4C60P40S variants, of which the largest median peak transverse displacement among all the four incident directions was excited by a 45° ground motion, rather than a transverse one.

It can be found in Table 6.32 that the effect of bridge skew on the deck displacements of 4C bridges varied from case to case. For the cases with the uni-axial ground motions, the deck displacement component perpendicular to the ground motion direction always increased with the bridge skew, but the component in the motion direction did not always increase. For the cases with the bi-axial ground motions, the displacement components in both axes generally increased with the bridge skew. The tall pier and soft foundation soil caused larger deck displacements than the short pier and hard soil, respectively.

Table 6.33 indicates the medians and median absolute deviations of the peak deck rotations of 4C bridges. By comparing Table 6.33 to Tables 6.3, 6.13, 6.23, it can be found that the overall magnitude of the rotations in Table 6.33 is close to that of the 4S bridges, but much smaller than that of the two types of three-span bridges. Once again, the clockwise rotations of left-skewed 4C bridges were larger than the counterclockwise. Highly skewed 4C bridges typically sustained larger peak deck rotations in the clockwise direction than their less skewed equivalents. Tall-pier 4C bridges experienced larger rotations than their short-pier equivalents. Foundation soil condition had little effect on the deck rotations. These findings are generally consistent with those of the other

Table 6.32: Peak deck center displacements (units: mm) of 4C bridges (longitudinal and transverse displacement components are placed on the left and right sides of the commas, respectively; numbers outside the parentheses are medians while those inside are median absolute deviations; for each bridge, the largest median peak displacement caused by the ground motions in the four incident directions is highlighted by bold numbers)

Foundation soil condition			Hard				Soft			
Pier column height (m)			4.57		12.19		4.57		12.19	
Longitudinal (0º) ground motions	Bridge skew (º)	0	**169** (27)	0 (0)	**290** (70)	0 (0)	**229** (59)	0 (0)	**315** (85)	0 (0)
		15	**175** (28)	46 (8)	**279** (81)	96 (25)	**249** (73)	62 (15)	**312** (86)	90 (16)
		30	**183** (38)	83 (15)	**267** (73)	159 (52)	**248** (68)	82 (17)	**286** (71)	161 (37)
		45	**193** (33)	60 (6)	**263** (102)	235 (43)	**247** (39)	36 (5)	**310** (105)	205 (56)
		60	**228** (35)	46 (3)	**281** (81)	208 (51)	**253** (64)	52 (18)	**301** (105)	212 (36)
45º ground motions	Bridge skew (º)	0	125 (10)	43 (7)	182 (26)	162 (33)	147 (14)	77 (7)	231 (80)	156 (34)
		15	145 (17)	57 (8)	207 (53)	170 (43)	163 (29)	84 (14)	264 (87)	160 (32)
		30	144 (16)	88 (17)	226 (72)	208 (55)	189 (40)	111 (22)	270 (88)	186 (49)
		45	155 (17)	96 (14)	228 (54)	259 (72)	181 (39)	123 (23)	269 (84)	234 (88)
		60	168 (26)	124 (25)	189 (60)	335 (92)	182 (40)	143 (34)	226 (60)	**321** (114)
Transverse (90º) ground motions	Bridge skew (º)	0	0 (0)	**73** (20)	0 (0)	**249** (52)	0 (0)	**134** (40)	0 (0)	**278** (73)
		15	47 (11)	**84** (29)	78 (9)	**291** (63)	49 (25)	**135** (46)	70 (8)	**289** (70)
		30	67 (6)	**106** (25)	112 (13)	**290** (78)	58 (17)	**136** (37)	95 (10)	**312** (64)
		45	69 (14)	**155** (26)	154 (25)	**274** (63)	47 (9)	**151** (39)	147 (45)	**317** (70)
		60	76 (13)	**179** (35)	179 (37)	**312** (74)	47 (10)	**175** (39)	163 (49)	315 (72)
135º ground motions	Bridge skew (º)	0	129 (15)	43 (6)	185 (35)	163 (36)	152 (13)	78 (8)	230 (68)	154 (33)
		15	136 (14)	64 (11)	190 (54)	172 (26)	172 (19)	88 (14)	251 (80)	186 (42)
		30	138 (16)	93 (10)	200 (58)	204 (32)	188 (24)	112 (21)	238 (71)	204 (53)
		45	147 (28)	118 (27)	200 (40)	239 (37)	207 (34)	122 (39)	199 (66)	232 (44)
		60	159 (34)	133 (26)	214 (48)	233 (48)	218 (51)	138 (33)	190 (81)	236 (34)

types of bridges.

Table 6.33: Peak deck rotations (units: 0.01°) of 4C bridge superstructures (data for clockwise and counterclockwise rotations are placed on the left and right sides of the commas, respectively; numbers outside the parentheses are medians, while those inside are median absolute deviations; for each bridge, the largest median peak rotation caused by the ground motions in the four incident directions is highlighted by bold numbers)

Foundation soil condition			Hard				Soft			
Pier column height (m)			4.57		12.19		4.57		12.19	
Longitudinal (0º) ground motions	Bridge skew (º)	0	0 (0) , 0 (0)		0 (0) , 0 (0)		0 (0) , 0 (0)		0 (0) , 0 (0)	
		15	**4** (1) , 3 (1)		7 (1) , 4 (1)		**6** (1) , 4 (0)		7 (1) , 4 (0)	
		30	**7** (1) , 5 (1)		12 (5) , 6 (1)		**9** (2) , 5 (1)		**12** (3) , 6 (1)	
		45	6 (1) , 3 (0)		**19** (7) , 7 (1)		5 (1) , 2 (0)		**14** (5) , 7 (1)	
		60	5 (1) , 3 (0)		13 (4) , 6 (1)		3 (1) , 2 (0)		12 (4) , 7 (3)	
45º ground motions	Bridge skew (º)	0	1 (0) , 2 (0)		5 (1) , 6 (1)		2 (0) , 2 (0)		5 (0) , 5 (1)	
		15	**4** (0) , 3 (1)		**8** (2) , 6 (1)		4 (1) , **3** (1)		7 (2) , 6 (1)	
		30	6 (2) , 4 (1)		**12** (2) , **8** (1)		8 (2) , **5** (1)		10 (3) , **8** (2)	
		45	**7** (1) , 4 (0)		15 (4) , **9** (1)		**8** (2) , **5** (1)		**14** (5) , **9** (3)	
		60	7 (1) , **5** (1)		**19** (4) , **11** (1)		6 (3) , 4 (1)		**18** (8) , **14** (3)	
Transverse (90º) ground motions	Bridge skew (º)	0	**3** (1) , **3** (1)		**7** (1) , **7** (1)		3 (1) , **3** (1)		**7** (1) , **7** (1)	
		15	**4** (1) , **4** (1)		**8** (2) , **8** (1)		3 (1) , **3** (1)		7 (1) , **7** (1)	
		30	5 (1) , **5** (0)		11 (3) , **8** (1)		3 (1) , 3 (1)		9 (1) , 8 (1)	
		45	6 (2) , **5** (1)		11 (3) , 9 (2)		5 (2) , 4 (1)		11 (4) , 9 (1)	
		60	**8** (2) , **5** (1)		14 (2) , 9 (1)		**7** (3) , **6** (2)		14 (5) , 9 (2)	
135º ground motions	Bridge skew (º)	0	2 (0) , 2 (0)		6 (1) , 5 (1)		2 (0) , 2 (0)		5 (1) , 4 (1)	
		15	**4** (1) , 3 (1)		8 (1) , 5 (0)		4 (1) , 3 (0)		**8** (1) , 4 (0)	
		30	6 (1) , 4 (0)		9 (1) , 6 (1)		5 (1) , 3 (0)		10 (2) , 5 (1)	
		45	**7** (1) , **5** (1)		9 (1) , 7 (2)		5 (1) , 4 (1)		8 (1) , 6 (1)	
		60	5 (1) , **5** (1)		8 (1) , 7 (1)		6 (1) , 4 (1)		8 (2) , 7 (1)	

Full data of limit state occurrences for 4C bridges

Table 6.34 lists the full data of limit state occurrences for each of the 20 4C bridge variants, when subjected to the suite of 20 seismic ground motions applied in the four incident directions. Each percentage in the table indicates the number of analyses with occurrences of a limit state out of the 20 analyses with the 20 ground motions applied to a bridge variant in an incident direction. Three gradient color scales, blue, yellow, and red, were used in conjunction with the percentages in Table 6.34 to highlight the occurrences of the preferred, acceptable, and unacceptable limit states defined in Table 5.1.

The data listed in Table 6.34 were subsequently grouped by the substructures of 4C bridges, namely the two abutments, two expansion piers, and one fixed pier. For the substructure groups, the data in Table 6.34 were further analyzed and their statistical summaries are presented in Ta-

bles 6.35, 6.37, and 6.41. Later in this section, the statistical summary of each substructure group will be discussed.

Table 6.34: Limit state occurrences of each 4C bridge variant under 0° and 45° ground motions (each percentage indicates the number of analyses with occurrences of a limit s3tate out of the 20 analyses with ground motions applied to a bridge variant in an incident direction)

Ground motion direction	Bridge variant	Critical limit states																														
		Abutment 1 (A1)									Pier 1 (P1, expansion pier)						Pier 2 (P2, fixed pier)					Pier 3 (P3, expansion pier)						Abutment 2 (A2)							
		CEJ	MBU	FBP	RRA	SEB	UBA	UBO	YPW	YPB	RRA	SEB	UEB	YRS	CCC	YPP	RRA	RSD	YRS	CCC	YPP	RRA	SEB	UEB	YRS	CCC	YPP	CEJ	MBU	FBP	RRA	SEB	UBO	UBA	YPW	YPB
0°	4C00P15H	100%	15%	0	0	10%	0	0	100%	100%	0	45%	0	90%	50%	0	0	0	100%	100%	0	0	30%	0	95%	65%	0	100%	0	0	0	20%	0	0	100%	100%
	4C15P15H	100%	5%	0	0	15%	0	0	100%	100%	0	50%	0	100%	75%	0	0	0	100%	100%	0	0	50%	0	100%	65%	0	100%	5%	0	0	10%	0	0	100%	100%
	4C30P15H	100%	10%	0	0	0	0	0	100%	100%	0	45%	0	100%	80%	25%	0	25%	100%	100%	10%	0	40%	0	100%	90%	20%	100%	0	0	0	15%	0	0	100%	100%
	4C45P15H	100%	0	0	0	0	0	0	100%	100%	0	5%	0	75%	10%	40%	0	100%	100%	20%	30%	0	5%	0	75%	15%	25%	100%	0	0	0	0	0	0	100%	100%
	4C60P15H	100%	0	0	0	0	0	0	100%	100%	0	0	0	25%	0	55%	0	100%	50%	0	60%	0	0	0	25%	0	70%	100%	0	0	0	0	0	0	100%	100%
	4C00P40H	100%	45%	0	0	75%	0	0	100%	100%	0	20%	0	80%	20%	0	0	0	80%	15%	0	0	25%	0	80%	25%	0	100%	50%	0	0	65%	0	0	100%	100%
	4C15P40H	100%	40%	0	0	60%	0	0	100%	100%	0	25%	0	80%	25%	0	0	0	80%	20%	0	0	30%	0	80%	30%	0	100%	35%	0	0	55%	0	0	100%	100%
	4C30P40H	100%	20%	0	40%	50%	0	0	100%	100%	0	25%	0	80%	25%	0	0	0	80%	20%	0	0	25%	0	80%	25%	0	100%	25%	0	35%	40%	0	0	100%	100%
	4C45P40H	100%	0	0	60%	30%	0	0	100%	100%	0	25%	0	80%	25%	25%	0	0	95%	25%	45%	0	30%	0	80%	40%	25%	100%	0	0	65%	55%	0	0	100%	100%
	4C60P40H	100%	0	0	45%	25%	0	0	100%	80%	0	20%	0	75%	25%	55%	0	100%	100%	15%	90%	0	25%	0	75%	25%	60%	100%	0	0	60%	30%	0	0	100%	90%
	4C00P15S	100%	30%	0	0	30%	0	0	100%	100%	0	65%	0	95%	75%	0	0	0	100%	100%	0	0	65%	0	90%	75%	0	100%	15%	0	0	30%	0	0	100%	100%
	4C15P15S	100%	45%	0	0	40%	0	0	100%	100%	0	60%	0	90%	80%	60%	0	0	100%	100%	15%	0	70%	0	90%	80%	50%	100%	15%	0	0	45%	0	0	100%	100%
	4C30P15S	100%	25%	0	0	25%	0	0	100%	100%	0	65%	0	100%	80%	80%	0	40%	100%	100%	85%	0	70%	0	95%	80%	75%	100%	15%	0	0	25%	0	0	100%	100%
	4C45P15S	100%	0	0	0	0	0	0	100%	100%	0	0	0	70%	0	80%	0	100%	100%	70%	100%	0	5%	0	75%	0	80%	100%	0	0	0	0	0	0	100%	100%
	4C60P15S	100%	0	0	0	0	0	0	95%	100%	0	0	0	0	0	90%	0	100%	90%	0	100%	0	10%	0	0	0	90%	100%	0	0	0	0	0	0	100%	95%
	4C00P40S	100%	65%	5%	0	70%	0	0	100%	100%	0	30%	0	80%	30%	0	0	0	80%	20%	0	0	35%	0	80%	30%	0	100%	50%	0	0	70%	0	0	100%	100%
	4C15P40S	100%	55%	0	0	65%	0	0	100%	100%	0	25%	0	75%	30%	0	0	0	80%	25%	0	0	15%	0	80%	30%	0	100%	50%	0	0	65%	0	0	100%	100%
	4C30P40S	100%	30%	0	20%	60%	0	0	100%	100%	0	20%	0	75%	25%	25%	0	0	85%	25%	35%	0	15%	0	75%	25%	25%	100%	40%	0	20%	45%	0	0	100%	100%
	4C45P40S	100%	20%	0	30%	35%	0	0	100%	100%	0	20%	0	75%	25%	70%	0	0	80%	30%	100%	0	25%	0	70%	30%	75%	100%	20%	0	55%	30%	0	0	100%	100%
	4C60P40S	100%	20%	0	0	20%	0	0	90%	95%	0	20%	0	60%	10%	80%	0	20%	80%	20%	100%	0	25%	0	60%	30%	80%	100%	10%	0	45%	20%	0	0	100%	100%
45°	4C00P15H	100%	0	0	0	0	0	0	100%	100%	0	0	0	20%	15%	5%	0	25%	100%	100%	50%	0	5%	0	30%	15%	5%	100%	0	0	0	0	0	0	100%	100%
	4C15P15H	100%	0	0	0	0	0	0	100%	100%	0	25%	0	90%	30%	5%	0	15%	100%	100%	35%	0	15%	0	75%	30%	0	100%	0	0	0	0	0	0	100%	100%
	4C30P15H	100%	0	0	0	0	0	0	100%	100%	0	5%	0	100%	65%	0	0	50%	100%	100%	55%	0	25%	0	100%	70%	0	100%	0	0	0	0	0	0	100%	100%
	4C45P15H	100%	0	0	0	0	0	0	100%	100%	0	0	0	100%	45%	20%	0	100%	100%	70%	85%	0	0	0	100%	55%	25%	100%	0	0	0	0	0	0	100%	100%
	4C60P15H	100%	0	0	0	0	0	0	100%	85%	0	0	0	95%	30%	10%	0	100%	100%	40%	5%	0	0	0	90%	45%	5%	100%	0	0	5%	0	0	0	100%	75%
	4C00P40H	100%	0	0	10%	15%	0	0	100%	100%	0	0	0	75%	0	5%	0	0	100%	35%	0	0	0	0	75%	0	0	100%	0	0	0	10%	0	0	100%	100%
	4C15P40H	100%	30%	0	0	30%	0	0	100%	100%	0	15%	0	80%	20%	0	0	0	85%	10%	0	0	10%	0	75%	15%	0	100%	15%	0	5%	30%	0	0	100%	100%
	4C30P40H	100%	20%	0	20%	40%	0	0	100%	100%	0	10%	0	80%	25%	0	0	0	80%	25%	0	0	20%	0	80%	20%	0	100%	25%	0	20%	40%	0	0	100%	100%
	4C45P40H	100%	10%	0	55%	20%	0	0	100%	100%	0	20%	0	80%	20%	0	0	0	80%	20%	0	0	5%	0	80%	25%	0	100%	15%	0	25%	25%	0	5%	100%	100%
	4C60P40H	100%	20%	20%	60%	20%	0	0	100%	80%	0	0	0	80%	20%	0	0	0	80%	50%	0	0	0	0	80%	45%	0	100%	5%	0	70%	55%	0	10%	100%	85%
	4C00P15S	100%	0	0	0	0	0	0	100%	100%	0	10%	0	55%	15%	80%	0	5%	100%	100%	100%	0	10%	0	45%	15%	80%	100%	0	0	0	0	0	0	100%	100%
	4C15P15S	100%	0	0	0	0	0	0	100%	100%	0	45%	0	80%	75%	85%	0	0	100%	100%	100%	0	30%	0	80%	70%	80%	100%	0	0	0	0	0	0	100%	100%
	4C30P15S	100%	0	0	0	0	0	0	100%	100%	0	30%	0	85%	75%	85%	0	0	100%	100%	100%	0	40%	0	80%	75%	80%	100%	0	0	0	0	0	0	100%	100%
	4C45P15S	100%	0	0	0	0	0	0	100%	100%	0	40%	0	85%	65%	95%	0	65%	100%	90%	100%	0	20%	0	85%	50%	90%	100%	0	0	0	0	0	0	100%	100%
	4C60P15S	100%	0	0	0	0	0	0	90%	95%	0	0	0	85%	20%	100%	0	100%	100%	45%	100%	0	5%	0	90%	35%	100%	100%	0	0	10%	0	0	0	95%	95%
	4C00P40S	100%	35%	0	0	35%	0	0	100%	100%	0	25%	0	80%	25%	90%	0	0	80%	20%	100%	0	15%	0	80%	20%	85%	100%	25%	0	0	35%	0	0	100%	100%
	4C15P40S	100%	45%	0	0	55%	0	0	100%	100%	0	20%	0	75%	20%	80%	0	0	80%	20%	90%	0	20%	0	75%	20%	70%	100%	30%	0	0	55%	0	0	100%	100%
	4C30P40S	100%	25%	0	0	50%	0	0	100%	100%	0	5%	0	75%	20%	50%	0	0	80%	25%	45%	0	10%	0	75%	25%	35%	100%	40%	0	20%	35%	0	0	100%	100%
	4C45P40S	100%	25%	0	20%	40%	0	0	100%	100%	0	15%	0	75%	25%	10%	0	0	85%	40%	15%	0	15%	0	75%	25%	0	100%	30%	0	25%	30%	0	0	100%	100%
	4C60P40S	100%	0	0	40%	20%	0	0	100%	100%	0	15%	0	75%	35%	35%	0	0	100%	45%	45%	0	10%	0	75%	45%	30%	100%	30%	0	60%	40%	0	10%	100%	100%
Preferred limit states:		0	20%	40%	60%	80%	100%																											
Acceptable limit states:		0	20%	40%	60%	80%	100%																											
Unacceptable limit states:		0	20%	40%	60%	80%	100%																											

Table 6.34 Continued: limit state occurrences of each 4C bridge variant under 90° and 135° ground motions

Ground motion direction	Bridge variant	Critical limit states																														
		Abutment 1 (A1)									Pier 1 (P1, expansion pier)						Pier 2 (P2, fixed pier)					Pier 3 (P3, expansion pier)						Abutment 2 (A2)							
		CEJ	MBU	FBP	RRA	SEB	UBA	UBO	YPW	YPB	RRA	SEB	UEB	YRS	CCC	YPP	RRA	RSD	YRS	CCC	YPP	RRA	SEB	UEB	YRS	CCC	YPP	CEJ	MBU	FBP	RRA	SEB	UBO	UBA	YPW	YPB
90°	4C00P15H	0	0	0	0	0	0	0	0	100%	0	0	0	20%	0	75%	0	75%	70%	0	100%	0	0	0	10%	0	70%	0	0	0	0	0	0	0	0	100%
	4C15P15H	25%	0	0	0	0	0	0	10%	95%	0	0	0	40%	0	75%	5%	75%	80%	0	90%	0	0	0	35%	0	65%	25%	0	0	0	0	0	0	10%	85%
	4C30P15H	95%	0	0	0	0	0	0	70%	100%	0	0	0	90%	5%	90%	30%	100%	100%	5%	100%	0	0	0	90%	5%	85%	90%	0	0	5%	0	0	0	70%	100%
	4C45P15H	100%	0	0	20%	0	0	0	80%	100%	0	0	0	100%	40%	95%	50%	100%	100%	10%	100%	0	0	0	100%	30%	95%	95%	0	0	25%	0	0	0	90%	100%
	4C60P15H	100%	0	0	50%	0	0	0	95%	100%	0	0	0	100%	65%	45%	60%	100%	100%	35%	85%	0	0	0	100%	70%	70%	100%	0	0	45%	10%	0	0	100%	95%
	4C00P40H	0	0	0	65%	20%	0	0	0	100%	0	0	0	100%	35%	25%	0	0	100%	65%	15%	0	0	0	100%	45%	15%	0	0	0	65%	25%	0	0	0	100%
	4C15P40H	85%	0	0	70%	20%	0	0	55%	100%	0	0	0	100%	70%	0	0	0	100%	70%	0	0	0	0	100%	70%	0	90%	0	0	70%	10%	0	0	60%	100%
	4C30P40H	100%	0	0	70%	15%	0	0	100%	100%	0	0	0	100%	65%	0	0	0	100%	80%	0	0	0	0	100%	60%	0	100%	0	0	75%	35%	0	0	100%	100%
	4C45P40H	100%	0	0	70%	30%	0	0	100%	100%	0	0	0	95%	30%	65%	0	40%	100%	50%	95%	0	0	0	95%	20%	60%	100%	0	0	70%	20%	0	0	100%	100%
	4C60P40H	100%	5%	5%	75%	20%	0	0	90%	85%	0	0	0	80%	15%	60%	0	100%	100%	20%	80%	0	0	0	80%	25%	35%	100%	0	0	75%	25%	0	10%	100%	85%
	4C00P15S	0	0	0	0	0	0	0	0	80%	0	0	0	0	0	100%	0	0	0	0	100%	0	0	0	0	0	100%	0	0	0	0	0	0	0	0	85%
	4C15P15S	65%	0	0	0	0	0	0	20%	80%	0	0	0	10%	0	100%	0	5%	75%	0	100%	0	0	0	5%	0	100%	70%	0	0	0	0	0	0	20%	85%
	4C30P15S	80%	0	0	0	0	0	0	60%	90%	0	0	0	60%	0	100%	0	15%	95%	40%	100%	0	0	0	70%	0	100%	75%	0	0	0	0	0	0	55%	90%
	4C45P15S	100%	0	0	0	0	0	0	60%	100%	0	0	0	80%	0	100%	0	65%	100%	60%	100%	0	0	0	85%	10%	100%	100%	0	0	20%	0	0	0	70%	100%
	4C60P15S	100%	0	0	15%	0	0	0	45%	100%	0	0	0	95%	25%	100%	25%	60%	100%	80%	100%	0	0	0	100%	65%	100%	100%	0	0	50%	15%	0	0	90%	100%
	4C00P40S	0	0	0	30%	0	0	0	20%	100%	0	0	0	85%	5%	100%	0	0	95%	15%	100%	0	0	0	85%	15%	100%	0	0	0	25%	0	0	0	20%	100%
	4C15P40S	65%	0	0	30%	10%	0	0	75%	100%	0	0	0	85%	15%	100%	0	0	100%	30%	100%	0	0	0	85%	20%	100%	65%	0	0	25%	10%	0	0	75%	100%
	4C30P40S	100%	0	0	35%	10%	0	0	80%	100%	0	0	0	85%	20%	100%	0	0	100%	55%	100%	0	0	0	85%	25%	95%	100%	0	0	35%	20%	0	0	85%	100%
	4C45P40S	100%	0	0	50%	20%	0	0	90%	100%	0	0	0	80%	15%	95%	0	0	95%	20%	100%	0	0	0	80%	20%	100%	100%	5%	0	55%	35%	0	0	100%	100%
	4C60P40S	100%	0	0	65%	25%	0	0	85%	100%	0	0	0	80%	20%	80%	0	0	85%	20%	100%	0	0	0	80%	25%	80%	100%	20%	0	75%	30%	5%	15%	100%	95%
135°	4C00P15H	100%	0	0	0	0	0	0	100%	100%	0	5%	0	40%	15%	10%	0	20%	100%	95%	45%	0	0	0	35%	15%	5%	100%	0	0	0	0	0	0	100%	100%
	4C15P15H	100%	0	0	0	0	0	0	100%	100%	0	5%	0	60%	10%	15%	0	75%	100%	75%	90%	0	0	0	45%	15%	15%	100%	0	0	0	0	0	0	100%	100%
	4C30P15H	100%	0	0	5%	0	0	0	100%	100%	0	10%	0	100%	40%	75%	0	100%	100%	60%	100%	0	5%	0	100%	40%	85%	100%	0	0	0	0	0	0	100%	100%
	4C45P15H	100%	0	0	0	0	0	0	100%	100%	0	0	0	100%	10%	80%	20%	100%	100%	0	95%	0	0	0	100%	20%	80%	100%	0	0	0	0	0	0	100%	100%
	4C60P15H	100%	0	0	0	0	0	0	100%	85%	0	0	0	100%	5%	75%	45%	100%	100%	0	100%	0	0	0	100%	10%	75%	100%	0	0	5%	0	0	0	100%	70%
	4C00P40H	100%	0	0	5%	10%	0	0	100%	100%	0	0	0	80%	0	0	0	0	100%	0	0	0	0	0	75%	0	5%	100%	0	0	15%	10%	0	0	100%	100%
	4C15P40H	100%	0	0	25%	10%	0	0	100%	100%	0	0	0	100%	15%	5%	0	0	100%	15%	0	0	0	0	100%	0	0	100%	0	0	5%	0	0	0	100%	100%
	4C30P40H	100%	0	0	55%	10%	0	0	100%	100%	0	0	0	100%	25%	0	0	0	100%	70%	0	0	0	0	100%	30%	5%	100%	0	0	55%	5%	0	0	100%	100%
	4C45P40H	100%	0	0	65%	10%	0	0	85%	100%	0	0	0	100%	25%	75%	35%	65%	100%	50%	100%	0	0	0	100%	50%	80%	95%	0	0	75%	10%	0	0	100%	100%
	4C60P40H	100%	0	0	75%	0	0	0	65%	90%	0	0	0	80%	20%	75%	70%	100%	100%	0	100%	0	0	0	85%	20%	75%	100%	0	0	55%	0	0	0	55%	80%
	4C00P15S	100%	0	0	0	0	0	0	100%	100%	0	10%	0	65%	15%	80%	0	5%	100%	100%	100%	0	10%	0	60%	15%	85%	100%	0	0	0	0	0	0	100%	100%
	4C15P15S	100%	0	0	0	0	0	0	100%	100%	0	10%	0	75%	25%	90%	0	15%	100%	100%	100%	0	10%	0	70%	30%	85%	100%	0	0	0	0	0	0	100%	95%
	4C30P15S	100%	0	0	0	0	0	0	100%	100%	0	0	0	65%	20%	90%	0	45%	100%	100%	100%	0	0	0	80%	30%	90%	100%	0	0	0	0	0	0	100%	90%
	4C45P15S	100%	0	0	0	0	0	0	95%	95%	0	0	0	55%	5%	100%	0	80%	100%	40%	100%	0	0	0	65%	5%	95%	100%	0	0	0	0	0	0	100%	95%
	4C60P15S	100%	0	0	0	0	0	0	80%	85%	0	0	0	85%	0	100%	0	100%	100%	0	100%	0	0	0	85%	5%	100%	100%	0	0	5%	0	0	0	100%	90%
	4C00P40S	100%	35%	0	0	40%	0	0	100%	100%	0	20%	0	80%	25%	90%	0	0	85%	25%	100%	0	20%	0	80%	30%	90%	100%	30%	0	0	35%	0	0	100%	100%
	4C15P40S	100%	25%	0	0	40%	0	0	100%	100%	0	20%	0	80%	20%	95%	0	0	95%	20%	100%	0	20%	0	80%	25%	100%	100%	15%	0	5%	30%	0	0	100%	100%
	4C30P40S	100%	0	0	5%	20%	0	0	100%	100%	0	10%	0	80%	20%	95%	0	0	100%	25%	100%	0	20%	0	80%	20%	95%	100%	20%	0	25%	10%	0	0	100%	100%
	4C45P40S	100%	0	0	0	20%	0	0	85%	100%	0	20%	0	80%	0	95%	0	0	100%	0	100%	0	0	0	80%	0	100%	100%	0	0	10%	0	0	0	100%	100%
	4C60P40S	80%	0	0	15%	10%	0	0	80%	90%	0	0	0	80%	0	95%	0	30%	85%	0	100%	0	0	0	80%	0	95%	80%	0	0	30%	5%	0	0	80%	85%

Preferred limit states:	0	20%	40%	60%	80%	100%	
Acceptable limit states:	0	20%	40%	60%	80%	100%	
Unacceptable limit states:	0	20%	40%	60%	80%	100%	

Abutments of 4C bridges

Table 6.35 statistically summarizes the occurrences of component limit states at the abutments of 4C bridges. Similar to the other bridge types, closure of expansion joints (CEJ@A1 and A2) occurred in most of the 4C bridge analyses except those of non-skew or small skew bridge variants subjected to the pure transverse ground motions.

Mobilization of ultimate backfill passive resistance (MBU@A1 and A2) occurred in around 9% of the 4C bridge analyses. This percentage is the largest of all the four types of bridges. Similar to the observation of the other three types of bridges, 4C bridges with the small skews, tall pier, and soft foundation soil sustained more occurrences than those with the large skews, short pier, and hard soil, respectively. Around 90% of the occurrences were caused by the pure longitudinal and 45° ground motions. Failure of the backwall-pile cap connections (FBP@A1 and A2) occurred in only 6 analyses that exclusively involved tall-pier 4C bridges.

Rupture of the retainer anchors at Abutments 1 and 2 occurred in around 19% of the 4C bridge analyses. This percentage is less than that of 3S and 3C bridges, but close to that of 4S bridges. Similar to the other types of bridges, 4C bridges with the large skews, tall pier, and hard foundation soil experienced much more occurrences than those with the small skews, short pier, and soft soil. The pure transverse ground motions caused nearly 50% of the occurrences.

Sliding of the elastomeric bearings at Abutments 1 and 2 (SEB@A1 and A2) occurred in 16% of the 4C bridge analyses. Similar to the other three types of bridges, around 90% of the occurrences involved tall-pier 4C bridges. Figure 6.10 illustrates the peak abutment bearing sliding at the four deck corners. In 11 out of the 1,600 analyses, bearing unseating at the abutments of 4C bridges was observed, which occurred in 45°- and 60°-skew bridges with the tall piers, when subjected to the pure transverse or 45° ground motions. The tendency of highly skewed bridges with tall piers to bearing unseating at abutments is similar to that of 4S and 3C bridges. In 10 analyses, abutment-normal unseating occurred at the acute deck corner supported by Abutment 2. In the other one analyses, abutment-normal unseating occurred at the obtuse deck corner supported by Abutment 2. Besides these 11 analyses, the peak bearing sliding distance in many other analyses of highly skewed bridges is quite close to the seat width in the abutment-normal direction, which indicating a high-risk of bearing unseating. It was also observed that the bearing unseating at abutments typically occurred after anchorage failure of the accompanying bearing retainer. Figure 6.11a

Table 6.35: Occurrences of limit states at abutments (A1 and A2) of 4C bridge variants

Limit state	No. of analyses with occurrence [1]	Skew angle[2] (°)					Foundation soil [2]		Column height [2] (m)		Ground motion incident angle [2] (°)			
		0	15	30	45	60	Hard	Soft	4.57	12.19	0	45	90	135
Closure of expansion joint (CEJ@A1)	1479 (92%)	240 (16%)	288 (19%)	315 (21%)	320 (22%)	316 (21%)	741 (50%)	738 (50%)	733 (50%)	746 (50%)	400 (27%)	400 (27%)	283 (19%)	396 (27%)
Mobilization of backfill ultimate capacity (MBU@A1)	140 (9%)	45 (32%)	49 (35%)	26 (19%)	11 (8%)	9 (6%)	44 (31%)	96 (69%)	26 (19%)	114 (81%)	85 (61%)	42 (30%)	1 (1%)	12 (9%)
Failure of backwall-to-pile-cap connection (FBP@A1)	6 (0%)	1 (100%)	0 (0%)	0 (0%)	0 (0%)	5 (83%)	5 (83%)	1 (17%)	0 (0%)	6 (100%)	1 (17%)	4 (67%)	1 (17%)	0 (0%)
Rupture of retainer anchor (RRA@A1)	259 (16%)	22 (8%)	25 (10%)	50 (19%)	74 (29%)	88 (34%)	188 (73%)	71 (27%)	18 (7%)	241 (93%)	39 (15%)	41 (16%)	129 (50%)	50 (19%)
Sliding of elastomeric bearing (SEB@A1)	255 (16%)	61 (24%)	69 (27%)	56 (22%)	41 (16%)	28 (11%)	107 (42%)	148 (58%)	24 (9%)	231 (91%)	122 (48%)	65 (25%)	34 (13%)	34 (13%)
Unseating of bearing at obtuse corner of deck (UBA@A1)	0 (0%)	0	0	0	0	0	0	0	0	0	0	0	0	0
Unseating of bearing at acute corner of deck (UBO@A1)	0 (0%)	0	0	0	0	0	0	0	0	0	0	0	0	0
Yielding of pile supporting wingwall (YPW@A1)	1400 (88%)	244 (17%)	272 (19%)	302 (22%)	299 (21%)	283 (20%)	710 (51%)	690 (49%)	680 (49%)	720 (51%)	397 (28%)	398 (28%)	227 (16%)	378 (27%)
Yielding of pile supporting backwall (YPB@A1)	1562 (98%)	316 (20%)	315 (20%)	318 (20%)	319 (20%)	294 (19%)	780 (50%)	782 (50%)	778 (50%)	784 (50%)	395 (25%)	392 (25%)	386 (25%)	389 (25%)
Closure of expansion joint (CEJ@A2)	1477 (92%)	240 (16%)	290 (20%)	313 (21%)	318 (22%)	316 (21%)	739 (50%)	738 (50%)	731 (49%)	746 (51%)	400 (27%)	400 (27%)	282 (19%)	395 (27%)
Mobilization of backfill ultimate capacity (MBU@A2)	127 (8%)	34 (27%)	33 (26%)	33 (26%)	14 (11%)	13 (10%)	35 (28%)	92 (72%)	10 (8%)	117 (92%)	66 (52%)	43 (34%)	5 (4%)	13 (10%)
Failure of backwall-to-pile-cap connection (FBP@A2)	0 (0%)	0	0	0	0	0	0	0	0	0	0	0	0	0
Rupture of retainer anchor (RRA@A2)	304 (19%)	21 (7%)	22 (7%)	58 (19%)	85 (28%)	118 (39%)	185 (61%)	119 (39%)	34 (11%)	270 (89%)	56 (18%)	48 (16%)	143 (47%)	57 (19%)
Sliding of elastomeric bearing (SEB@A2)	263 (16%)	60 (23%)	62 (24%)	54 (21%)	41 (16%)	46 (17%)	120 (46%)	143 (54%)	34 (13%)	229 (87%)	124 (47%)	71 (27%)	47 (18%)	21 (8%)
Unseating of bearing at obtuse corner of deck (UBO@A2)	1 (0%)	0 (0%)	0 (0%)	0 (0%)	0 (0%)	1 (100%)	0 (0%)	1 (100%)	0 (0%)	1 (100%)	0 (0%)	0 (0%)	1 (100%)	0 (0%)
Unseating of bearing acute corner of deck (UBA@A2)	10 (0%)	0 (0%)	0 (0%)	0 (0%)	1 (10%)	9 (90%)	5 (50%)	5 (50%)	0 (0%)	10 (100%)	0 (0%)	5 (50%)	5 (50%)	0 (0%)
Yielding of pile supporting wingwall (YPW@A2)	1435 (90%)	244 (17%)	273 (19%)	302 (21%)	312 (22%)	304 (21%)	717 (50%)	718 (50%)	700 (49%)	735 (51%)	400 (28%)	399 (28%)	249 (17%)	387 (27%)
Yielding of pile supporting backwall (YPB@A2)	1553 (97%)	317 (20%)	313 (20%)	316 (20%)	319 (21%)	288 (19%)	773 (50%)	780 (50%)	769 (50%)	784 (50%)	397 (26%)	391 (25%)	384 (25%)	381 (25%)

1 The number above the parentheses indicates the number of analyses with occurrences of a limit state.
The percentage inside the parentheses indicates the ratio of the number above the parentheses to all the 1,600 analyses.

2 The number above the parentheses indicates the number of analyses with occurrences of a limit state contributed by a parametric variation.
The percentage inside the parentheses indicates the relative contribution of a parametric variation to the total occurrences of a limit state.

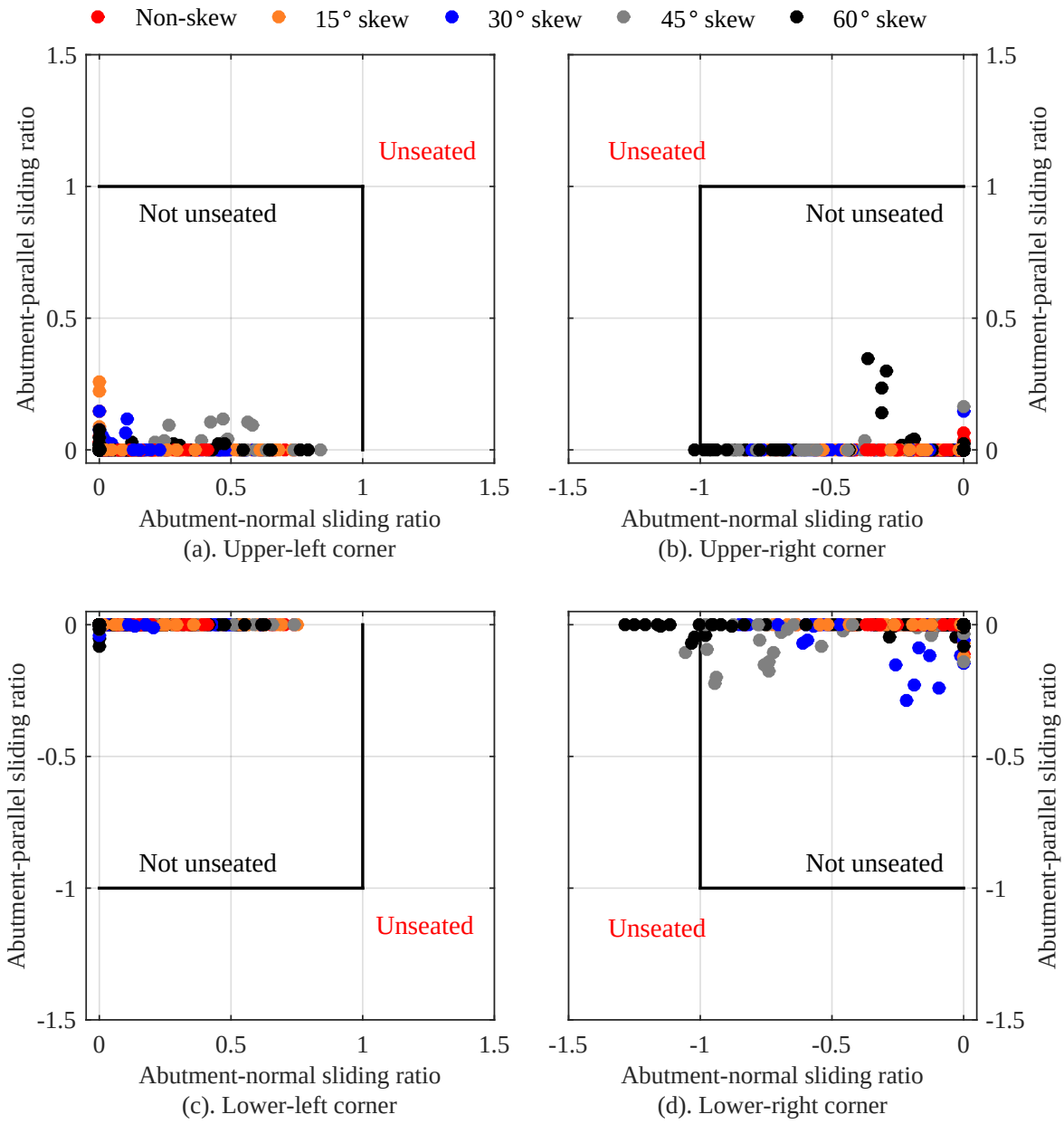

Figure 6.10: Peak sliding ratios of elastomeric bearings at deck corners of 4C bridges

shows the force-deformation response of bearing retainer anchors at the lower-right corner (acute deck corner supported by Abutment 2) of 4C60P40S bridge when subjected to a transverse ground motion. As a result, large bearing sliding and unseating occurred in the abutment-normal direction, as shown in 6.11b.

Yielding of abutment piles (YPW and YPB@A1 and A2) was observed in most of the 4C bridge analyses. Table 6.36 lists the median peak strains of abutment piles recorded in the 4C bridge analyses. It can be seen that the piles were strained the least under the pure transverse ground motions. Additionally, the piles of tall-pier 4C bridges experienced larger strains than their short-pier equivalents. These findings are generally consistent with those of the other three types of bridges.

Table 6.36: Normalized peak strains of steel H piles at abutments of 4C bridges (peak strains are normalized to the yield strain, 0.0017; numbers outside the parentheses are medians, while those inside are median absolute deviations; data for piles supporting backwalls and wingwalls are placed on the left and right sides of the commas, respectively)

Foundation soil condition			Hard								Soft							
Pier column height (m)			4.57				12.19				4.57				12.19			
Longitudinal (0°) ground motions	Bridge skew (°)	0	6.9	(3.2) ,	12.3	(3.7)	17.0	(7.8) ,	25.5	(6.6)	7.5	(3.4) ,	10.3	(3.8)	13.3	(5.7) ,	16.5	(5.3)
		15	9.2	(3.2) ,	14.4	(4.8)	24.0	(11.3) ,	28.1	(9.5)	13.5	(5.8) ,	14.0	(6.3)	18.4	(8.4) ,	19.6	(6.4)
		30	13.5	(5.2) ,	17.2	(6.4)	22.4	(12.3) ,	24.5	(11.2)	14.7	(6.4) ,	15.8	(6.3)	18.0	(7.7) ,	19.0	(7.2)
		45	13.5	(5.1) ,	15.1	(4.7)	9.0	(5.5) ,	14.0	(6.1)	11.6	(4.1) ,	12.4	(4.4)	12.9	(7.7) ,	13.8	(8.5)
		60	3.4	(1.8) ,	5.5	(2.4)	3.2	(2.3) ,	6.1	(4.9)	8.3	(4.5) ,	8.6	(4.6)	8.7	(6.9) ,	9.9	(7.5)
45° ground motions	Bridge skew (°)	0	3.9	(2.2) ,	6.6	(1.7)	9.2	(4.3) ,	14.2	(4.1)	4.2	(1.7) ,	4.6	(1.3)	11.9	(5.9) ,	12.7	(5.3)
		15	7.1	(3.2) ,	10.0	(3.1)	14.1	(8.0) ,	19.3	(7.8)	5.8	(3.4) ,	6.5	(3.2)	12.2	(8.4) ,	14.9	(6.8)
		30	8.3	(3.3) ,	10.6	(3.4)	23.6	(12.2) ,	26.2	(11.7)	8.5	(5.0) ,	9.9	(3.8)	18.1	(7.6) ,	18.4	(7.7)
		45	7.7	(4.3) ,	9.8	(3.9)	19.7	(7.4) ,	24.4	(7.7)	7.6	(2.4) ,	9.1	(3.3)	16.9	(8.2) ,	20.0	(6.7)
		60	2.3	(0.7) ,	4.7	(1.8)	5.0	(2.7) ,	10.2	(6.0)	5.2	(2.8) ,	6.8	(3.3)	6.4	(3.9) ,	10.3	(4.0)
Transverse (90°) ground motions	Bridge skew (°)	0	1.2	(0.1) ,	0.7	(0.1)	4.0	(1.5) ,	2.3	(0.8)	1.5	(0.5) ,	1.0	(0.4)	4.8	(3.1) ,	2.9	(1.7)
		15	1.3	(0.2) ,	0.9	(0.2)	4.3	(1.4) ,	2.9	(1.4)	1.7	(0.8) ,	1.2	(0.5)	5.9	(3.3) ,	3.8	(1.9)
		30	1.6	(0.3) ,	1.6	(0.4)	4.2	(1.7) ,	5.8	(2.6)	2.0	(0.9) ,	1.5	(0.6)	6.0	(3.6) ,	4.5	(2.3)
		45	2.1	(0.7) ,	2.4	(0.8)	5.9	(4.0) ,	10.4	(6.1)	2.1	(0.8) ,	1.5	(0.5)	7.4	(3.9) ,	7.2	(4.4)
		60	1.6	(0.4) ,	2.6	(0.7)	2.9	(1.6) ,	6.8	(4.4)	1.8	(0.5) ,	1.9	(0.6)	5.5	(3.0) ,	8.4	(4.0)
135° ground motions	Bridge skew (°)	0	3.3	(1.0) ,	6.8	(1.5)	10.3	(4.7) ,	15.1	(4.1)	2.9	(1.3) ,	4.4	(1.2)	10.5	(6.0) ,	11.9	(5.7)
		15	4.4	(1.2) ,	8.2	(2.2)	10.1	(7.9) ,	14.1	(7.9)	5.3	(2.9) ,	6.5	(2.5)	11.8	(8.6) ,	14.1	(6.7)
		30	6.0	(3.6) ,	7.3	(3.0)	5.0	(3.1) ,	8.4	(5.2)	6.3	(4.4) ,	6.8	(4.0)	8.4	(6.0) ,	9.6	(6.7)
		45	2.3	(1.0) ,	3.4	(1.0)	2.9	(1.1) ,	2.5	(0.9)	8.1	(3.9) ,	7.9	(3.5)	6.7	(3.5) ,	5.9	(3.8)
		60	1.3	(0.3) ,	1.8	(0.3)	1.7	(0.3) ,	1.4	(0.4)	3.2	(1.9) ,	3.9	(2.2)	4.3	(3.0) ,	3.1	(2.1)

Unyielded: normalized strain < 1 (unnormalized strain < 0.0017)

Yielded without signficniant strain hardening: 1 ≤ normalized strain < 10 (0.0017 ≤ unnormalized strain < 0.017)

Yielded and significantly strain hardened: 10 ≤ normalized strain (0.017 ≤ unnormalized strain)

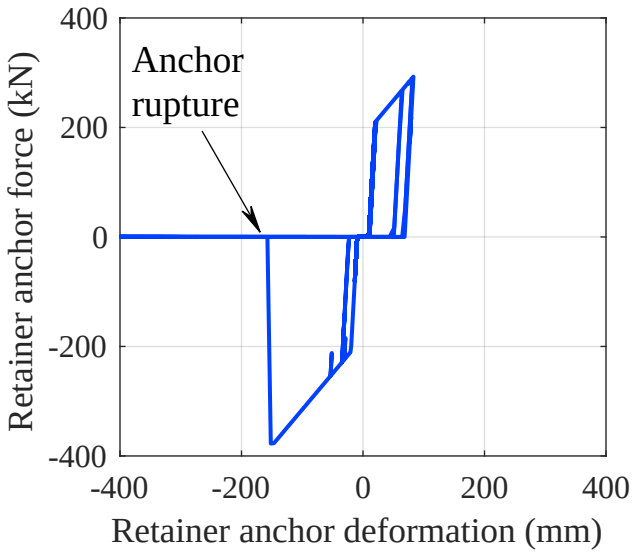

(a) Retainer anchor response

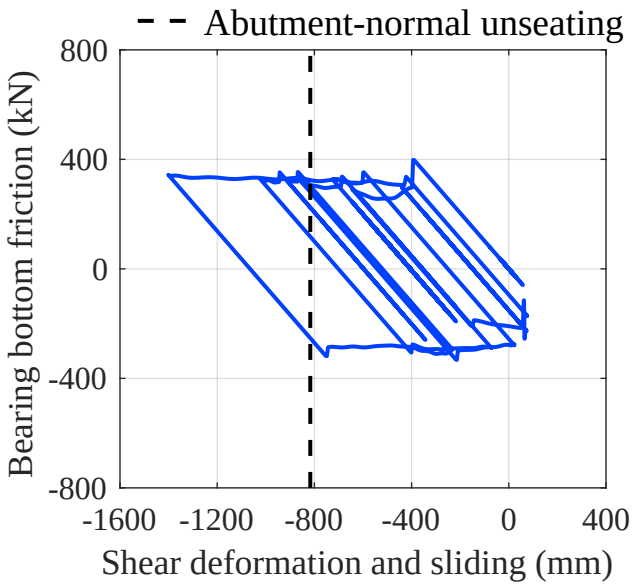

(b) Elastomeric bearing response in the abutment-normal direction

Figure 6.11: Retainer anchor and elastomeric bearing response at the lower-right corner (acute deck corner supported by Abutment 2) of 4C60P40S bridge when subjected to a transverse ground motion (bearing unseating occurred in abutment-normal direction after retainer anchor rupture)

Expansion piers (Piers 1 and 3) of 4C bridges

Table 6.37 statistically summarizes the occurrences of several component limit states at the expansion piers (Piers 1 and 3) of 4C bridges. Similar to the other types of bridges, rupture of the bearing retainer anchors at Piers 1 and 3 was not observed in any 4C bridge analyses.

Table 6.37: Occurrences of limit states at expansion piers (Piers 1 and 3) of 4C bridge variants

Limit state	No. of analyses with occurrence [1]	Skew angle[2] (°)					Foundation soil [2]		Column height [2] (m)		Ground motion incident angle [2] (°)			
		0	15	30	45	60	Hard	Soft	4.57	12.19	0	45	90	135
Rupture of retainer anchor (RRA@P1)	0 (0%)	0	0	0	0	0	0	0	0	0	0	0	0	0
Sliding of elastomeric bearing (SEB@P1)	169 (11%)	46 (27%)	60 (36%)	45 (27%)	29 (17%)	11 (7%)	71 (42%)	98 (58%)	106 (63%)	63 (37%)	113 (67%)	56 (33%)	0 (0%)	22 (13%)
Unseating of elastomeric bearing (UEB@P1)	0 (0%)	0	0	0	0	0	0	0	0	0	0	0	0	0
Yielding of vertical reinforcing steel at column end (YRS@P1)	1227 (77%)	209 (17%)	244 (20%)	275 (22%)	266 (22%)	239 (19%)	654 (53%)	579 (47%)	576 (47%)	657 (53%)	301 (25%)	314 (26%)	297 (24%)	321 (26%)
Crushing of concrete cover at column end (CCC@P1)	411 (26%)	65 (16%)	102 (25%)	118 (29%)	68 (17%)	58 (14%)	219 (53%)	192 (47%)	233 (57%)	178 (43%)	138 (34%)	129 (31%)	85 (21%)	59 (14%)
Yielding of pile at pier (YPP@P1)	857 (54%)	132 (15%)	142 (17%)	163 (19%)	209 (24%)	211 (25%)	237 (28%)	620 (72%)	502 (59%)	355 (41%)	137 (16%)	151 (18%)	301 (35%)	268 (31%)
Rupture of retainer anchor (RRA@P3)	0 (0%)	0	0	0	0	0	0	0	0	0	0	0	0	0
Sliding of elastomeric bearing (SEB@P3)	187 (12%)	43 (23%)	54 (29%)	54 (29%)	21 (11%)	15 (8%)	69 (37%)	118 (63%)	104 (56%)	83 (44%)	119 (64%)	51 (27%)	0 (0%)	17 (9%)
Unseating of elastomeric bearing (USB@P3)	0 (0%)	0	0	0	0	0	0	0	0	0	0	0	0	0
Yielding of vertical reinforcing steel at column end (YRS@P3)	1227 (77%)	204 (17%)	235 (19%)	278 (23%)	269 (22%)	241 (20%)	315 (26%)	912 (74%)	571 (47%)	656 (53%)	301 (25%)	309 (25%)	297 (24%)	320 (26%)
Crushing of concrete cover at column end (CCC@P3)	465 (29%)	73 (16%)	100 (22%)	124 (27%)	79 (17%)	89 (19%)	245 (53%)	220 (47%)	259 (56%)	206 (44%)	152 (33%)	140 (30%)	101 (22%)	72 (15%)
Yielding of pile at pier (YPP@P3)	838 (52%)	128 (15%)	133 (16%)	158 (19%)	206 (25%)	213 (25%)	231 (28%)	607 (72%)	495 (59%)	343 (41%)	135 (16%)	137 (16%)	294 (35%)	272 (32%)

1 The number above the parentheses indicates the number of analyses with occurrences of a limit state.
The percentage inside the parentheses indicates the ratio of the number above the parentheses to all the 1,600 analyses.
2 The number above the parentheses indicates the number of analyses with occurrences of a limit state contributed by a parametric variation.
The percentage inside the parentheses indicates the relative contribution of a parametric variation to the total occurrences of a limit state.

Sliding of the elastomeric bearings at Piers 1 and 3 (SEB@P1 and P3) was observed in around 11% of the analyses, which is the highest occurrence percentage of all the four types of bridges. It can be found in Table 6.37 that the bearings on the top of Piers 1 and 3 did not slide in any

4C bridge analysis when subjected to the pure transverse ground motions, because the unfused retainers prevented the transverse bearing sliding. This is similar to the response of 3C bridges shown in Table 6.27. Same as the other three types of bridges, unseating of the bearings at Piers 1 and 3 (UEB@P1 and P3) was not observed in any 4C bridge analysis.

Yielding of the vertical reinforcing steel at the column bases of Piers 1 and 3 (YRS@P1 and P3) occurred in 76% of the 4C bridge analyses. This percentage is the largest of all the four types of bridges. Table 6.38 lists the median peak strains of vertical reinforcing steel at the pier column bases of 4C bridges. The data on the left and right sides of the commas are for the expansion and fixed piers, respectively. In most of the tabulated cases, the reinforcing steel was lightly or moderately damaged. By comparing the median peak strains in Tables 6.8, 6.17, 6.28, and 6.38, it can be found that the column reinforcing steel of 4C bridges was the most strained of the four types of bridges. The yielding occurred in more analyses of high-pier bridge variants than those of short-pier ones, which is consistent with the tendency of the other types of bridges.

Crushing of the concrete cover at the column bases of Piers 1 and 3 (CCC@P1 and P3) occurred in more than 25% of the 4C bridge analyses. In contrast, the occurrence percentage of this limit state in all the other types of bridges is less than 5%. Table 6.39 lists the normalized median peak strain of concrete cover at pier column bases of 4C bridges. A number of short-pier bridges with 0° to 30° skews sustained severe damage to the pier column concrete cover, which may not be easily repairable Kowalsky (2001). The damage to the short piers is generally much severer than that to the tall piers.

Yielding of the steel piles supporting Piers 1 and 3 (YSP@P1 and P3) was observed in over 50% of the 4C bridge analyses. Again, this percentage is the largest of all the four types of bridges. Table 6.40 indicates the median peak strains of steel H piles supporting Piers 1 and 3 of 4C bridges. The data on the left and right sides of the commas are for the expansion (Piers 1 and 3) and fixed piers (Pier 2), respectively. In most of the tabulated cases, the piles were yielded. It can be found in Table 6.37 that the piles yielded in more analyses in the presence of the soft soil than the hard soil. Also, the pure transverse and 135° ground motions caused more occurrences than those in the other two directions. These response characteristics are similar to those of the other three types of bridges.

Table 6.38: Normalized median peak strain of vertical reinforcing steel at pier column bases of 4C bridges (peak strains are normalized to the steel yield strain, 0.0021; numbers outside the parentheses are medians, while those inside are median absolute deviations; data of reinforcing steel at column bases of expansion and fixed piers are placed on the left and right sides of the commas, respectively; performance levels in the footnote are defined per Kowalsky (2001) and Revell (2013))

Foundation soil condition			Hard								Soft							
Pier column height (m)			4.57				12.19				4.57				12.19			
Longitudinal (0º) ground motions	Bridge skew (º)	0	8.9	(7.9) ,	16.0	(3.0)	2.8	(1.4) ,	3.0	(1.3)	22.2	(5.0) ,	22.0	(3.9)	3.1	(2.2) ,	3.4	(1.9)
		15	18.5	(7.8) ,	16.4	(3.5)	2.9	(1.8) ,	2.7	(1.8)	24.2	(4.2) ,	23.5	(2.9)	3.7	(2.6) ,	3.6	(2.1)
		30	20.0	(5.4) ,	19.4	(3.9)	2.8	(1.8) ,	3.0	(1.7)	21.1	(3.9) ,	24.3	(0.9)	3.0	(1.8) ,	3.5	(2.1)
		45	1.3	(0.4) ,	2.4	(0.5)	3.6	(2.5) ,	3.7	(2.2)	1.2	(0.3) ,	5.5	(1.1)	3.0	(2.2) ,	4.0	(2.4)
		60	0.9	(0.1) ,	1.0	(0.1)	1.5	(0.8) ,	2.2	(0.4)	0.6	(0.1) ,	1.2	(0.1)	1.9	(1.4) ,	3.4	(2.1)
45º ground motions	Bridge skew (º)	0	0.9	(0.1) ,	9.8	(1.8)	2.1	(1.2) ,	3.0	(1.7)	1.0	(0.1) ,	11.0	(1.4)	2.0	(1.4) ,	2.1	(1.1)
		15	1.4	(0.4) ,	12.3	(2.7)	2.0	(1.2) ,	2.6	(1.5)	14.5	(7.7) ,	18.3	(3.6)	2.6	(1.6) ,	2.8	(1.8)
		30	13.4	(7.8) ,	14.6	(3.4)	2.8	(2.0) ,	3.3	(1.7)	18.0	(6.2) ,	20.5	(2.1)	2.7	(1.7) ,	3.7	(2.2)
		45	4.9	(3.5) ,	6.9	(1.9)	3.5	(2.0) ,	4.3	(1.9)	8.5	(6.7) ,	17.3	(4.0)	3.1	(2.2) ,	4.7	(3.0)
		60	4.4	(2.4) ,	4.1	(1.3)	4.0	(2.6) ,	5.9	(2.9)	2.6	(1.5) ,	5.3	(1.7)	4.2	(3.3) ,	5.8	(3.2)
Transverse (90º) ground motions	Bridge skew (º)	0	0.8	(0.1) ,	1.1	(0.2)	4.2	(1.6) ,	5.8	(2.1)	0.6	(0.1) ,	0.7	(0.1)	2.5	(0.5) ,	3.4	(0.6)
		15	0.9	(0.2) ,	1.3	(0.2)	5.2	(1.9) ,	7.0	(2.3)	0.8	(0.1) ,	1.9	(0.7)	2.9	(0.7) ,	3.9	(0.9)
		30	1.6	(0.6) ,	1.6	(0.4)	5.2	(2.3) ,	6.8	(2.3)	1.1	(0.3) ,	4.2	(2.3)	3.2	(1.1) ,	4.5	(1.3)
		45	3.4	(2.0) ,	1.7	(0.5)	3.3	(1.3) ,	5.0	(1.7)	1.7	(0.8) ,	7.2	(2.7)	2.7	(1.2) ,	3.3	(1.0)
		60	7.6	(4.2) ,	4.1	(1.4)	2.9	(1.6) ,	3.3	(1.7)	4.8	(3.2) ,	10.5	(3.2)	3.2	(1.8) ,	4.0	(2.2)
135º ground motions	Bridge skew (º)	0	0.9	(0.1) ,	9.8	(2.0)	2.2	(1.1) ,	2.8	(1.6)	1.1	(0.2) ,	11.3	(1.5)	1.8	(1.2) ,	2.1	(1.1)
		15	1.0	(0.1) ,	7.3	(2.7)	2.7	(1.0) ,	3.6	(1.3)	1.1	(0.2) ,	11.7	(1.6)	2.1	(1.2) ,	3.0	(1.4)
		30	1.8	(0.7) ,	5.1	(2.1)	4.1	(1.1) ,	6.4	(1.4)	1.4	(0.5) ,	9.1	(2.7)	2.5	(0.8) ,	3.8	(1.1)
		45	1.6	(0.4) ,	1.6	(0.1)	4.3	(1.8) ,	4.9	(1.9)	1.0	(0.2) ,	5.0	(0.7)	1.7	(0.4) ,	2.2	(0.4)
		60	2.1	(0.5) ,	1.6	(0.1)	3.0	(1.4) ,	1.9	(0.3)	1.7	(0.4) ,	2.6	(0.6)	1.4	(0.2) ,	1.6	(0.2)

Undamaged (unyielded):	normalized strain < 1 (unnormalized strain < 0.0021)
Lightly damaged (unlikely requiring repair):	1 ≤ normalized strain < 7.1 (0.0021 ≤ unnormalized strain < 0.015)
Moderately damaged (repairable):	7.1 ≤ normalized strain < 28.6 (0.015 ≤ unnormalized strain < 0.06)
Severely damaged (not easily repairable):	28.6 ≤ normalized strain (0.06 ≤ unnormalized strain)

Table 6.39: Normalized median peak strain of concrete cover at pier column bases of 4C bridges (peak strains are normalized to the steel yield strain, 0.005; numbers outside the parentheses are medians, while those inside are median absolute deviations; data of concrete cover at column bases of expansion and fixed piers are placed on the left and right sides of the commas, respectively; performance levels in the footnote are defined per Kowalsky (2001) and Revell (2013))

Foundation soil condition			Hard								Soft							
Pier column height (m)			4.57				12.19				4.57				12.19			
Longitudinal (0º) ground motions	Bridge skew (º)	0	2.0	(1.7) ,	3.1	(0.6)	0.6	(0.2) ,	0.6	(0.2)	5.1	(1.4) ,	4.4	(0.9)	0.6	(0.4) ,	0.6	(0.2)
		15	4.3	(2.0) ,	3.4	(0.8)	0.6	(0.3) ,	0.5	(0.2)	5.8	(1.3) ,	5.1	(0.9)	0.7	(0.4) ,	0.7	(0.3)
		30	4.5	(1.4) ,	4.2	(0.9)	0.5	(0.3) ,	0.6	(0.3)	4.9	(1.0) ,	5.5	(0.4)	0.6	(0.3) ,	0.7	(0.3)
		45	0.4	(0.1) ,	0.5	(0.1)	0.6	(0.4) ,	0.7	(0.3)	0.4	(0.1) ,	1.2	(0.3)	0.6	(0.4) ,	0.8	(0.4)
		60	0.3	(0.0) ,	0.3	(0.0)	0.4	(0.1) ,	0.4	(0.1)	0.2	(0.0) ,	0.3	(0.0)	0.4	(0.3) ,	0.6	(0.3)
45º ground motions	Bridge skew (º)	0	0.3	(0.0) ,	1.9	(0.3)	0.5	(0.2) ,	0.7	(0.3)	0.3	(0.0) ,	2.0	(0.3)	0.4	(0.2) ,	0.5	(0.2)
		15	0.4	(0.1) ,	2.5	(0.6)	0.4	(0.2) ,	0.5	(0.2)	3.1	(1.8) ,	3.9	(1.0)	0.5	(0.3) ,	0.6	(0.2)
		30	2.9	(1.8) ,	2.9	(0.7)	0.6	(0.3) ,	0.5	(0.2)	4.1	(1.6) ,	4.4	(0.6)	0.6	(0.3) ,	0.7	(0.3)
		45	1.0	(0.6) ,	1.3	(0.3)	0.6	(0.3) ,	0.7	(0.3)	1.6	(1.3) ,	3.4	(0.9)	0.6	(0.4) ,	0.8	(0.4)
		60	0.8	(0.4) ,	0.8	(0.3)	0.7	(0.4) ,	1.0	(0.4)	0.5	(0.2) ,	1.0	(0.3)	0.8	(0.5) ,	0.9	(0.4)
Transverse (90º) ground motions	Bridge skew (º)	0	0.3	(0.0) ,	0.4	(0.0)	0.9	(0.3) ,	1.2	(0.5)	0.2	(0.0) ,	0.3	(0.0)	0.6	(0.1) ,	0.7	(0.1)
		15	0.3	(0.0) ,	0.4	(0.0)	1.2	(0.5) ,	1.5	(0.5)	0.3	(0.0) ,	0.4	(0.1)	0.7	(0.1) ,	0.9	(0.2)
		30	0.4	(0.1) ,	0.4	(0.0)	1.2	(0.5) ,	1.6	(0.5)	0.3	(0.0) ,	0.7	(0.4)	0.7	(0.2) ,	1.0	(0.2)
		45	0.6	(0.3) ,	0.4	(0.1)	0.6	(0.2) ,	1.0	(0.4)	0.4	(0.1) ,	1.2	(0.6)	0.5	(0.1) ,	0.6	(0.2)
		60	1.4	(0.8) ,	0.8	(0.3)	0.5	(0.2) ,	0.6	(0.2)	0.9	(0.5) ,	1.9	(0.7)	0.5	(0.3) ,	0.6	(0.3)
135º ground motions	Bridge skew (º)	0	0.3	(0.0) ,	2.0	(0.5)	0.5	(0.2) ,	0.6	(0.2)	0.4	(0.0) ,	2.4	(0.3)	0.5	(0.2) ,	0.5	(0.2)
		15	0.3	(0.0) ,	1.5	(0.7)	0.6	(0.2) ,	0.7	(0.2)	0.4	(0.1) ,	2.5	(0.4)	0.5	(0.2) ,	0.6	(0.2)
		30	0.5	(0.1) ,	1.1	(0.5)	0.9	(0.2) ,	1.3	(0.2)	0.4	(0.1) ,	2.0	(0.7)	0.6	(0.1) ,	0.8	(0.2)
		45	0.4	(0.0) ,	0.4	(0.0)	0.9	(0.3) ,	1.0	(0.3)	0.3	(0.0) ,	0.9	(0.2)	0.4	(0.0) ,	0.5	(0.1)
		60	0.4	(0.0) ,	0.4	(0.0)	0.6	(0.2) ,	0.5	(0.0)	0.4	(0.1) ,	0.5	(0.1)	0.4	(0.0) ,	0.4	(0.0)

Undamaged (ultimate strength not mobillized):	normalized strain < 0.4 (unnormalized strain < 0.002)
Lightly damaged (ultimate strength mobilized but uncrushed):	0.4 ≤ normalized strain < 1 (0.002 ≤ unnormalized strain < 0.005)
Moderately damaged (crushed but repairable):	1 ≤ normalized strain < 3.6 (0.005 ≤ unnormalized strain < 0.018)
Severely damaged (not easily repairable):	3.6 ≤ normalized strain (0.018 ≤ unnormalized strain)

Table 6.40: Normalized peak strains of steel H piles at piers of 4C bridges (peak strains are normalized to the steel yield strain, 0.0017; numbers outside the parentheses are medians, while those inside are median absolute deviations; data for piles supporting expansion and fixed piers are placed on the left and right sides of the commas, respectively)

Foundation soil condition			Hard				Soft			
Pier column height (m)			4.57		12.19		4.57		12.19	
Longitudinal (0º) ground motions	Bridge skew (º)	0	0.4 (0.0) , 0.4 (0.0)		0.4 (0.0) , 0.4 (0.0)		0.6 (0.0) , 0.5 (0.0)		0.4 (0.0) , 0.4 (0.0)	
		15	0.6 (0.1) , 0.6 (0.0)		0.5 (0.0) , 0.5 (0.0)		1.0 (0.2) , 0.9 (0.1)		0.6 (0.1) , 0.6 (0.0)	
		30	0.9 (0.1) , 0.9 (0.0)		0.6 (0.1) , 0.7 (0.0)		1.9 (0.6) , 1.7 (0.6)		0.9 (0.1) , 0.9 (0.1)	
		45	0.9 (0.2) , 0.9 (0.0)		0.9 (0.1) , 1.0 (0.1)		3.6 (2.3) , 2.2 (0.2)		1.5 (0.7) , 1.9 (0.5)	
		60	1.1 (0.2) , 1.1 (0.1)		1.0 (0.2) , 1.2 (0.1)		6.0 (3.9) , 6.3 (1.7)		2.6 (1.7) , 8.2 (4.3)	
45º ground motions	Bridge skew (º)	0	0.9 (0.0) , 1.0 (0.1)		0.9 (0.1) , 0.9 (0.0)		1.5 (0.2) , 1.9 (0.4)		1.4 (0.2) , 1.5 (0.3)	
		15	0.8 (0.1) , 0.9 (0.1)		0.7 (0.0) , 0.8 (0.0)		1.4 (0.2) , 1.4 (0.2)		1.1 (0.2) , 1.2 (0.1)	
		30	0.8 (0.0) , 1.0 (0.0)		0.6 (0.0) , 0.6 (0.0)		1.6 (0.2) , 1.6 (0.2)		1.0 (0.1) , 1.0 (0.1)	
		45	0.9 (0.1) , 1.1 (0.0)		0.5 (0.1) , 0.6 (0.0)		1.9 (0.6) , 2.7 (0.6)		0.8 (0.1) , 0.9 (0.1)	
		60	0.9 (0.1) , 0.8 (0.1)		0.6 (0.1) , 0.7 (0.1)		1.8 (0.3) , 3.1 (0.3)		0.9 (0.2) , 0.9 (0.2)	
Transverse (90º) ground motions	Bridge skew (º)	0	1.1 (0.2) , 1.4 (0.2)		0.9 (0.0) , 0.9 (0.0)		5.2 (3.2) , 7.7 (3.8)		4.9 (2.9) , 6.9 (1.9)	
		15	1.1 (0.1) , 1.3 (0.2)		0.9 (0.0) , 0.9 (0.0)		5.2 (3.4) , 7.2 (4.5)		4.7 (2.7) , 6.4 (1.9)	
		30	1.2 (0.2) , 1.4 (0.1)		0.9 (0.0) , 0.9 (0.0)		4.8 (2.7) , 6.7 (3.7)		3.0 (1.0) , 4.5 (0.5)	
		45	1.5 (0.4) , 1.3 (0.1)		1.1 (0.1) , 1.1 (0.0)		4.4 (2.4) , 3.8 (2.1)		3.2 (1.9) , 6.6 (2.3)	
		60	1.0 (0.1) , 1.1 (0.1)		1.0 (0.1) , 1.1 (0.0)		2.0 (0.7) , 2.1 (0.5)		1.8 (0.7) , 3.6 (1.8)	
135º ground motions	Bridge skew (º)	0	0.9 (0.1) , 1.0 (0.1)		0.9 (0.1) , 0.9 (0.0)		1.5 (0.2) , 1.9 (0.4)		1.4 (0.2) , 1.5 (0.3)	
		15	0.9 (0.1) , 1.2 (0.1)		0.9 (0.1) , 0.9 (0.0)		2.6 (0.8) , 4.5 (1.3)		2.3 (0.9) , 2.6 (1.1)	
		30	1.1 (0.1) , 1.1 (0.1)		0.9 (0.0) , 0.9 (0.0)		4.4 (2.9) , 7.4 (4.1)		3.1 (1.2) , 4.8 (0.9)	
		45	1.4 (0.2) , 1.3 (0.1)		1.2 (0.1) , 1.2 (0.0)		7.4 (4.9) , 10.1 (3.8)		6.5 (3.2) , 12.8 (2.7)	
		60	1.3 (0.2) , 1.2 (0.0)		1.3 (0.2) , 1.3 (0.1)		7.8 (5.0) , 10.4 (2.7)		6.0 (3.7) , 15.3 (5.2)	

Unyielded: normalized strain < 1 (unnormalized strain < 0.0017)

Yielded without signficiant strain hardening: 1 ≤ normalized strain < 10 (0.0017 ≤ unnormalized strain < 0.017)

Yielded and significantly strain hardened: 10 ≤ normalized strain (0.017 ≤ unnormalized strain)

Fixed piers (Pier 2) of 4C bridges

Table 6.41 statistically summarizes the occurrences of several limit states at the fixed piers (Pier 2) of 4C bridges. Rupture of the anchors securing side retainers at Pier 2 (RRA@P2) occurred in 68 out of the 1,600 4C bridge analyses, which is much more than that of the 3C bridges. All of these ruptures were caused by the pure transverse and 135° ground motions. 93% of these ruptures occurred in the presence of the hard foundation soil. These two observations are consistent with those of the 3C bridges.

Table 6.41: Occurrences of limit states at fixed piers (Pier 2) of 4C bridge variants

Limit state	No. of analyses with occurrence [1]	Skew angle [2] (°)					Foundation soil [2]		Column height [2] (m)		Ground motion incident angle [2] (°)			
		0	15	30	45	60	Hard	Soft	4.57	12.19	0	45	90	135
Rupture of retainer anchor (RRA@P2)	68 (4%)	0 (0%)	1 (1%)	6 (9%)	21 (31%)	40 (59%)	63 (93%)	5 (7%)	47 (69%)	21 (31%)	0 (0%)	0 (0%)	34 (50%)	34 (50%)
Rupture of steel dowel connection (RSD@P2)	523 (33%)	26 (5%)	37 (7%)	75 (14%)	163 (31%)	222 (42%)	353 (67%)	170 (33%)	432 (83%)	91 (17%)	117 (22%)	92 (18%)	147 (28%)	167 (32%)
Yielding of vertical reinforcing steel at column end (YRS@P2)	1478 (92%)	278 (19%)	295 (20%)	304 (21%)	307 (21%)	294 (20%)	752 (51%)	726 (49%)	752 (51%)	726 (49%)	356 (24%)	370 (25%)	359 (24%)	393 (27%)
Crushing of concrete cover at column end (CCC@P2)	694 (43%)	158 (23%)	157 (23%)	186 (27%)	119 (17%)	74 (11%)	333 (48%)	361 (52%)	467 (67%)	227 (33%)	181 (26%)	227 (33%)	131 (19%)	155 (22%)
Yielding of pile at pier (YPP@P2)	1018 (64%)	162 (16%)	164 (16%)	186 (18%)	253 (25%)	253 (25%)	352 (35%)	666 (65%)	607 (60%)	411 (40%)	154 (15%)	205 (20%)	333 (33%)	326 (32%)

1 The number above the parentheses indicates the number of analyses with occurrences of a limit state.
The percentage inside the parentheses indicates the ratio of the number above the parentheses to all the 1,600 analyses.
2 The number above the parentheses indicates the number of analyses with occurrences of a limit state contributed by a parametric variation.
The percentage inside the parentheses indicates the relative contribution of a parametric variation to the total occurrences of a limit state.

Rupture of the steel dowel connections at Pier 2 (RSD@P2) was observed in 33% of the 4C bridge analyses. This percentage is larger than that of the 3C bridges (19%). Similar to the response characteristics of 3C bridges, the large skews, hard soil, and short pier contributed much more ruptures than the small skews, soft soil, and tall pier. Of all the incident directions, the 45° ground motions caused the fewest ruptures, which is consistent with the behavior of 3C bridges. This is expected because for highly skewed bridges, the 45° ground motions can induce significant superstructure-abutment interactions and the abutments tend to provide large resistance to the superstructure; consequently, the deformation and force demands on the fixed piers are reduced.

Yielding of the vertical reinforcing steel at the column bases of Pier 2 (YRS@P2) occurred in 92% of the 4C bridge analyses. This percentage is also the largest among all the four types

of bridges. In most of the cases included in Table 6.38, the reinforcing steel sustained light or moderate damage and the overall magnitude of the peak strains is larger than that of the other three types of bridges.

Crushing of the concrete cover at the column bases of Pier 2 (CCC@P2) occurred in 43% of the 4C bridge analyses. This percentage is the largest of all the four types of bridges.

Yielding of the steel piles supporting Pier 2 (YSP@P2) was observed in 64% of the 4C bridge analyses. This percentage is in between that of the 3C and 4S bridge analyses. Table 6.40 indicates the median peak strains of these piles.

Summary of 4C bridges

1,600 nonlinear dynamic analyses were performed on the 20 four-span precast-prestressed-concrete-girder (4C) bridge variants using the suite of 20 seismic ground motions applied in four incident directions. The analysis results were statistically studied with emphasis on the occurrence of component limit states.

Most importantly, bearing unseating at both the acute and obtuse deck corners was observed in some highly skewed 4C bridge variants supported by the tall pier columns. The number of analyses with bearing unseating, 16, is the largest of all the four types of bridges. Similar to the other types of bridges, bearing unseating at the expansion piers was not observed.

The overall magnitude of the superstructure displacements of 4C bridges is the largest of all the four types of bridges. The overall rotation magnitude is close to that of 4S bridges but smaller than that of the three-span bridges.

The occurrence percentage of retainer anchor rupture at the abutments of 4C bridges is close to that of 4S bridges but smaller than that of the three-span bridges. Similar to the other bridges, retainer anchor rupture at the expansion piers was not observed. The occurrence percentage of steel dowel connection rupture at the fixed piers of 4C bridges is higher than that of 3C bridges.

The seismic damage to the expansion and fixed piers of 4C bridges is the largest of all the four types of bridges, in terms of yielding of column reinforcing steel and steel piles, as well as crushing of column concrete cover. For instance, even the expansion piers, which were effectively protected in the other types of bridges, sustained crushing of column concrete cover in over 25% of the 4C bridge analyses. The fixed piers of 4C bridges sustained even more damaging limit states than the expansion piers.

Overall, 4C bridges sustained the largest seismic damage of all the four types of bridges. This overall performance is consistent with the fact that 4C bridges possess the largest superstructure mass of all the prototype bridges. The occurrence percentage of the following limit states in 4C bridge analyses is the largest of all the prototype bridges

- Unseating of elastomeric bearings at abutments (UBO@A2 and UBA@A2)
- Mobilization of ultimate backfill passive resistance (CEJ@A1 and A2)
- Yielding of abutment piles (YPW@A1 and A2, YPB@A1 and A2)

- Yielding of vertical reinforcing steel at column bases of expansion and fixed piers (YRS@P1, P2, and P3)
- Crushing of concrete cover at column bases of expansion and fixed piers (CCC@P1, P2, and P3)
- Yielding of pier piles (YSP@P1, P2, and P3)

6.4 Effects of Bridge Properties and Ground Motion Incident Direction on Bridge Seismic Performance

6.4.1 The effect of basic bridge type

The superstructure mass of the four different types of bridges played an important role in their seismic response and limit state occurrences, because the bridge seismic force, mainly coming from the superstructure, is in direction proportion to the superstructure mass. Table 6.42 lists the superstructure mass of the non-skew and skew prototype bridges. As can be seen, the four types of bridges differ significantly in the superstructure mass. The superstructures of 3C and 4C bridges are approximately 40% to 60% heavier than those of 3S and 4S bridges, respectively. The superstructures of 4S and 4C bridges are more than twice as heavy as those of the 3S and 3C bridges, respectively, which is consistent with the difference between their span lengths. As the bridge skew increases, the superstructure diaphragms at deck ends and intermediate pier locations are elongated, which is the reason for the increasing of superstructure mass with the skew shown in Table 6.42. Table 6.43 compares the occurrence percentage of a few damaging limit states of abutments and intermediate piers among the four bridge types. In this table, the four basic bridge types are sorted in ascending order, based on their superstructure mass. It can be found that for most of the tabulated limit states, the occurrence percentage monotonically increases from 3S bridges to 4C bridges, whose superstructure mass also monotonically increases. These observations indicate that the superstructure mass has a positive correlation with various seismic damage of bridge substructures.

Table 6.42: Superstructure mass of non-skew and skew prototype bridges (units: ton)

Skew (°)	3S bridges	4S bridges	3C bridges	4C bridges
0	1197	2758	1680	3949
15	1197	2766	1726	4024
30	1198	2766	1767	4091
45	1198	2772	1823	4180
60	1199	2773	1948	4390

In addition to the damaging limit states, Table 6.44 compares the occurrence percentage of fusing limit states among the four basic bridge types. It can be found that fusing of elastomeric

Table 6.43: Comparison of damaging limit state occurrences among different bridge types (each percentage indicates the number of analyses with occurrences of a limit state out of the 1,600 analyses for a basic bridge type; data in the table are obtained from Section 6.3)

Substructure	Damaging limit state	3S bridges	3C bridges	4S bridges	4C bridges
Abutment 1	Mobilization of backfill ultimate capacity (MBU@A1)	1%	3%	3%	9%
	Yielding of pile supporting wingwall (YPW@A1)	61%	81%	80%	88%
	Yielding of pile supporting backwall (YPB@A1)	64%	92%	88%	98%
Abutment 2	Mobilization of backfill ultimate capacity (MBU@A2)	1%	3%	3%	8%
	Yielding of pile supporting wingwall (YPW@A2)	60%	77%	79%	90%
	Yielding of pile supporting backwall (YPB@A2)	58%	83%	87%	97%
Pier 1 (expansion pier)	Yielding of vertical reinforcing steel at column ends (YRS@P1)	10%	27%	57%	76%
	Crushing of concrete cover at column ends (CCC@P1)	0%	0%	2%	26%
	Yielding of piles (YSP@P1)	17%	37%	39%	54%
Pier 3 (expansion pier)	Yielding of vertical reinforcing steel at column ends (YRS@P3)	N/A	N/A	55%	76%
	Crushing of concrete cover at column ends (CCC@P3)	N/A	N/A	4%	29%
	Yielding of piles (YSP@P3)	N/A	N/A	39%	52%
Pier 2 (fixed pier)	Yielding of vertical reinforcing steel at column ends (YRS@P2)	42%	63%	89%	92%
	Crushing of concrete cover at column ends (CCC@P2)	0%	9%	34%	43%
	Yielding of piles (YSP@P2)	32%	54%	73%	64%

bearing retainers rarely occurred at the expansion piers, regardless of the bridge type. Sliding of the elastomeric bearings at the expansion piers basically only occurred in 4C bridge analyses. At the fixed piers of the steel-plate-girder bridges, rupture of the steel fixed bearing anchors occurred only in around 10% of the analyses. At the fixed piers of the PPC-girder bridges, rupture of the steel dowel connections occurred in 19% and 33% of the 3C and 4C bridge analyses, respectively. Hence, the steel dowel connections of the PPC-girder bridges ruptured more than the steel fixed bearings of the steel-plate-girder bridges. Rupture of the bearing retainer anchors at the abutments occurred more in the two types of three-span bridges than in the four-span bridges.

Unseating of elastomeric bearings at abutments occurred in only a few analyses of 4S, 3C, and 4C bridges. For all these three bridge types, the variants that sustained bearing unseating are highly skewed and supported by the tall pier columns. Unseating of bearings at intermediate piers was not observed in any type of bridges.

The peak superstructure displacement and rotation also exhibit clear differences among the basic types of bridges, as shown in Table 6.45. It can be found that the ranges of longitudinal and transverse deck displacements increase with the superstructure mass. The superstructure rotations of the two types of four-span bridges are much smaller than those of the three-span bridges.

Table 6.44: Comparison of fusing limit state occurrences among different bridge types (each percentage indicates the number of analyses with occurrences of a limit state out of the 1,600 analyses for a basic bridge type; data in the table are obtained from Section 6.3)

Substructure	Fusing limit state	3S bridges	3C bridges	4S bridges	4C bridges
Abutment 1	Rupture of retainer anchor (RRA@A1)	41%	28%	17%	16%
Abutment 2	Rupture of retainer anchor (RRA@A2)	24%	21%	14%	19%
Pier 1 (expansion pier)	Rupture of retainer anchor (RRA@P1)	0%	0%	0%	0%
	Sliding of elastomeric bearing (SEB@P1)	0%	0%	2%	11%
Pier 3 (expansion pier)	Rupture of retainer anchor (RRA@P3)	N/A	N/A	0%	0%
	Sliding of elastomeric bearing (SEB@P3)	N/A	N/A	0%	12%
Pier 2 (fixed pier)	Rupture of steel fixed bearing anchors (RFA@P2)	4%	N/A	12%	N/A
	Rupture of steel dowel connection (RSD@P2)	N/A	19%	N/A	33%
	Rupture of retainer anchor (RRA@P2)	N/A	0%	N/A	4%

Table 6.45: Median peak superstructure displacements and rotations (data in the table are obtained from Section 6.3)

Superstructure response	3S bridges	3C bridges	4S bridges	4C bridges
Median peak longitudinal disp.[1] (mm)	79 ~164	96 ~ 219	162 ~ 300	169 ~ 315
Median peak transverse disp.[2] (mm)	46 ~ 148	41~211	45 ~ 278	73 ~ 315
Median peak clockwise rotation[2] (0.01°)	13 ~ 40	11 ~ 47	2 ~ 15	3 ~ 14
Median peak counterclockwise rotation[2] (0.01°)	9 ~ 33	10 ~ 39	2 ~ 10	3 ~ 9

1. Response exicted by pure longitudinal ground motions
2. Response excited by pure transverse ground motions

6.4.2 The effect of bridge skew

For the skew variants of all the four bridge types, the superstructures displaced in both the longitudinal and transverse bridge directions, and also rotated in both the clockwise and counterclockwise directions, regardless of the ground motion incident direction. For the bridges supported by tall piers, large bridge skew typically resulted in larger deck rotations as compared to the bridge with smaller skews. For short-pier bridges, the influence of bridge skew on deck rotation is insignificant.

When subjected to the uni-axial ground motions, the deck center displacements of highly skewed (45°- and 60°-skew) bridges perpendicular to the ground motion direction are generally larger than those of the bridges with smaller skews.

The highly skewed variants of all the four types of bridges typically sustained more retainer anchor ruptures at their abutments than the bridges with smaller skews. For instance, as shown in Table 6.15, 4S bridge variants with 45° and 60° skews accounted for 70% of all the ruptures of retainer anchors at Abutment 1 of 4S bridges, while those with 0°, 15°, and 30° skews only made up 30% of the total ruptures. This is largely due to the bi-axial and rotational response of skew bridge superstructures. In addition to transverse deck displacements, the in-plane rotations of highly skewed superstructures resulted in higher deformation demands on and more fusing of the abutment bearing retainers than the bridges with small skews. Similar to the fusing of abutment retainers, the ruptures of the superstructure-substructure connections (steel fixed bearings and steel dowel bars) at the fixed piers significantly increased with the bridge skew for all the four types of

bridges. For example, as shown in Table 6.31, 94% of the ruptures of steel fixed bearing anchors at Pier 2 of 3C bridges occurred in 3C bridge variants with 45° and 60° skews, while the non-skew, 15°-, and 30°-skew variants only sustained 6% of the ruptures; as shown in Table 6.11, for 3S bridges, all of the 71 analyses in which rupture of steel fixed bearing anchors was observed involved bridge variants with 45° and 60° skews.

Directly impacted by the larger superstructure displacements and more ruptures of retainer anchors at abutments, the highly skewed bridge variants appeared to be much more susceptible to bearings unseating at abutments than the bridges with small skews. As discussed in Section 6.3, the observed bearing unseating at abutments of all the bridges exclusively occurred in the 45°-, and 60°-skew variants supported by the tall piers. Additionally, the peak bearing sliding distance of many highly skewed bridge variants was quite close to the seat width at the abutments.

For all the four types of highly skewed bridges, closure of expansion joints occurred in almost all the analyses regardless of the ground motion incident direction, because these bridges always bi-axially displaced. The joints of non-skew or lightly skewed bridges did not close in some analyses with the pure transverse ground motions, but closed in all the analyses with non-transverse ground motions. Mobilization of ultimate backfill passive resistance was more susceptible to non-skew and lightly-skewed bridges than highly skewed bridges. The bridges with the small skews and tall piers tend to induce significant superstructure-abutment interactions and transfer large seismic forces from the deck end to the abutment backwall and backfill, when subjected to the longitudinal and 45° ground motions. For instance, as shown in Table 6.35, the non-skew, 15°-, and 30°-skew 4C bridge variants accounted for 86% of the total mobilizations of ultimate backfill resistance in 4C bridges.

6.4.3 The effect of pier column height

As discussed in Section 6.3, for all the four types of bridges, the tall (12.19 m) pier columns generally resulted in significantly larger peak deck displacements and rotations than the short (4.57 m) pier columns, regardless of the ground motion direction. This tendency is expected as the tall pier columns are much more laterally flexible than the short ones and it is consistent with the finding of prior research (LaFave et al. 2013b).

The most undesirable consequence of the large deck displacements and rotations is the unseating of elastomeric bearings, which occurred exclusively at the abutments of the tall-pier bridge variants in this study. Besides the bearing unseating, the tall-pier variants of all four basic bridge types appeared to be significantly more susceptible to a number of component limit states than their short-pier equivalents, as shown in Table 6.46. The large response of these components in the tall-pier bridges is essentially a direct result of the large deck displacements and rotations, as well as the associated significant superstructure-abutment interactions.

Table 6.46: Component limit states that occurred more in tall-pier bridge variants than in short-pier equivalents (percentages indicate the contribution to the total occurrences of a limit state by tall- or short-pier bridge variants; data in the table are obtained from Section 6.3)

Substructure	Limit state	3S bridges		4Sbridges		3C bridges		4C bridges	
		Short pier	Tall pier	Short pier	Tall pier	Short pier	Tall pier	Short pier	Tall pier
Abutment 1	Rupture of retainer anchor (RRA@A1)	22%	78%	0%	100%	5%	95%	7%	93%
	Mobilization of backfill ultimate capacity (MBU@A1)	0%	100%	0%	100%	2%	98%	19%	81%
	Slidng of elastomeric bearing (SEB@A1)	5%	95%	19%	81%	2%	98%	9%	91%
Abutment 2	Rupture of retainer anchor (RRA@A2)	4%	96%	0%	100%	3%	97%	11%	89%
	Mobilization of backfill ultimate capacity (MBU@A2)	0%	100%	0%	100%	3%	97%	8%	92%
	Slidng of elastomeric bearing (SEB@A2)	1%	99%	17%	83%	1%	99%	13%	87%
	Unseating of bearing at obtuse corner of deck (UBO@A2)	N/A	N/A	N/A	N/A	N/A	N/A	0%	100%
	Unseating of bearing at acute corner of deck (UBA@A2)	N/A	N/A	0%	100%	0%	100%	0%	100%
Pier 1 (expansion pier)	Yielding of vertical reinforcing steel at column base (YRS@P1)	2%	98%	35%	65%	8%	92%	47%	53%
Pier 3 (expansion pier)	Yielding of vertical reinforcing steel at column end (YRS@P3)	N/A	N/A	34%	66%	N/A	N/A	46%	54%

In contrast, the occurrence of some other limit states favors short-pier bridge variants rather than tall-pier ones. These limit states are all associated with the fixed pier (Pier 2), as shown in Table 6.47. In short-pier bridges, the fixed pier has much larger lateral stiffness than the expansion piers. The large lateral stiffness incurred considerable seismic forces and resulted in significant seismic damage to the fixed pier.

Table 6.47: Component limit states that occurred more in short-pier bridge variants than in tall-pier equivalents (percentages indicate the contribution to the total occurrences of a limit state by tall- or short-pier bridge variants; data in the table are obtained from Section 6.3)

Substructure	Limit state	3S bridges		4Sbridges		3C bridges		4C bridges	
		Short pier	Tall pier	Short pier	Tall pier	Short pier	Tall pier	Short pier	Tall pier
Pier 2 (fixed pier)	Rupture of steel fixed bearing anchors (RFA@P2)	80%	20%	81%	19%	N/A	N/A	N/A	N/A
	Rupture of steel dowel connection (RSD@P2)	N/A	N/A	N/A	N/A	75%	25%	83%	17%
	Yielding of vertical reinforcing steel at column end (YRS@P2)	67%	33%	51%	49%	56%	44%	51%	49%
	Crushing of concrete cover at column end (CCC@P2)	100%	0%	81%	19%	93%	7%	67%	33%
	Yielding of pile (YSP@P2)	56%	44%	56%	44%	58%	42%	60%	40%

6.4.4 The effect of foundation soil condition

As discussed in Section 6.3, for all the four types of bridges, the peak deck displacements were generally higher in the presence of the soft soil. However, the deck rotations appeared to be insensitive to the foundation soil condition.

Table 6.48 summarizes the limit states that occurred more in the presence of the hard foundation soil than the soft soil. The ruptures of the retainer anchors at abutments, the steel fixed bearings at the fixed piers of 3S and 4S bridges, as well as the retainer anchors and steel dowel connections at the fixed piers of 3C and 4C bridges were found to occur more in the presence of the hard foundation soil than the soft soil. The hard soil increases the lateral stiffness of substructure foundations, provides the necessary base reactions to fail the anchors, and eventually facilitates the fusing action of these sacrificial components.

On the contrary, Table 6.48 summarizes the limit states that occurred more in the presence of the soft foundation soil. At the abutments, mobilization of the ultimate backfill resistance was more susceptible to the bridges in the soft foundation soil than those in the hard soil. The reason is twofold: the soft foundation soil typically causes larger deck displacements and more superstructure-abutment interactions, which imposes higher deformation and force demands on the abutment backfill; secondly, the soft foundation soil provides less resistance to the displaced abutment and superstructure, and, thus, more passive resistance of the backfill soil needs to be mobilized. Larger peak strains and more yieldings of the pier piles were clearly observed in the presence of the soft foundation soil than the hard soil. This is expected as the soft soil provides less

lateral resistance to the pile deflection than the hard soil and caused larger flexural deformation of the piles.

Table 6.48: Component limit states that occurred more in the presence of hard foundation soil than soft soil (percentages indicate the contribution to the total occurrences of a limit state by hard-soil or soft-soil bridge variants; data in the table are obtained from Section 6.3)

Substructure	Limit state	3S bridges		4Sbridges		3C bridges		4C bridges	
		Hard soil	Soft soil	Hard soil	Soft soil	Hard soil	Soft soil	Hard soil	Soft soil
Abutment 1	Rupture of retainer anchor (RRA@A1)	57%	43%	65%	35%	54%	46%	73%	27%
Abutment 2	Rupture of retainer anchor (RRA@A2)	60%	40%	72%	28%	62%	38%	61%	39%
Pier 2 (fixed pier)	Rupture of steel fixed bearing anchors (RFA@P2)	92%	8%	90%	10%	N/A	N/A	N/A	N/A
	Rupture of steel dowel connection (RSD@P2)	N/A	N/A	N/A	N/A	69%	31%	67%	33%
	Rupture of retainer anchor (RRA@P2)	N/A	N/A	N/A	N/A	100%	0%	93%	7%

Table 6.49: Component limit states that occurred more in the presence of soft foundation soil than hard soil (percentages indicate the contribution to the total occurrences of a limit state by hard-soil or soft-soil bridge variants; data in the table are obtained from Section 6.3)

Substructure	Limit state	3S bridges		4Sbridges		3C bridges		4C bridges	
		Hard soil	Soft soil	Hard soil	Soft soil	Hard soil	Soft soil	Hard soil	Soft soil
Abutment 1	Mobilization of backfill ultimate capacity (MBU@A1)	0%	100%	19%	81%	7%	93%	31%	69%
Abutment 2	Mobilization of backfill ultimate capacity (MBU@A2)	0%	100%	7%	93%	10%	90%	28%	72%
Pier 1 (expansion pier)	Yielding of pile (YSP@P1)	14%	86%	23%	77%	22%	78%	28%	72%
Pier 3 (expansion pier)	Yielding of pile (YSP@P3)	N/A	N/A	22%	78%	N/A	N/A	28%	72%
Pier 2 (fixed pier)	Yielding of pile (YSP@P2)	20%	80%	43%	57%	29%	71%	35%	65%

6.4.5 The effect of ground motion incident direction

The limited occurrences of bearing unseating at the abutments of different types of bridges were all excited by the 45° and pure transverse ground motions. Bearing unseating caused by the motions from the other two directions was not observed in any analysis.

For all the four types of bridges, the uni-axial ground motions were more critical than the bi-axial ones for exciting large displacements along the longitudinal and transverse bridge axes.

Closure of the expansion joints occurred in all the analyses with the non-transverse ground motions. For skew bridges, even if the ground motions were transversely applied, the joints were

closed in most of the analyses. Most of the mobilization of ultimate backfill passive resistance was caused by the pure longitudinal and 45° ground motions. When applied in these two directions, the ground motions typically cause large superstructure-abutment interactions normal to the abutment backwall and impose large deformation and force demands to the backfill behind the backwall.

Ruptures of the superstructure-substructure connections at the fixed piers (steel fixed bearings for steel-plate-girder bridges and steel dowel bars for PPC-girder bridges) were found to be much more susceptible to the pure longitudinal and 135° ground motions than those in the other two directions. In contrast, the pure transverse ground motions caused the most ruptures of retainer anchors at abutments of the four incident directions.

Yielding of the piles supporting abutment wingwalls was the least susceptible to pure transverse ground motions, as these piles were subjected to strong-axis bending when the ground motions were transversely applied. The piles supporting the expansion and fixed piers appeared to be more prone to yielding under the pure transverse and 135° ground motions.

6.5 Preliminary Recommendations for Improving Bridge Seismic Performance

An overview of the bridge seismic performance discussed in Section 6.3 reveals that the bridges exhibited two primary performance deficiencies that can potentially result in extensive seismic damage and even losses of bridge spans during a major earthquake. One is the unseating of elastomeric bearings at the deck corners of highly skewed bridges supported by tall pier columns. The other is the damage to the short pier columns of non-skew or lightly skewed bridges, especially the heavy 4C bridges. Table 6.50 summarizes the pier column damage of each major type of bridges. Except these two deficiencies, the other observed structural responses and limit states are less likely to cause global bridge failure and are generally accepted by the quasi-isolation design.

Table 6.50: Summary of pier column damage

Pier column type		Major bridge type			
		3S	3C	4S	4C
Short columns (3.5 ft dia., 2% reinforcing ratio)	Expansion pier	Undamaged	Undamged	Undamaged to light	Moderate to severe
	Fixed pier	Undamaged to light	Light to moderate	Moderate	Moderate to severe
Tall columns (4 ft dia., 2% reinforcing ratio)	Expansion pier	Undamaged	Undamaged to light	Light	Light
	Fixed pier	Undamaged	Undamaged to light	Light	Light

To improve the bridge seismic performance in these two aspects, two preliminary recommendations are proposed. Specifically, the bearing unseating at abutments could be prevented by strengthening the bearing retainer anchorage, while the damage to the pier columns could be mitigated by weakening the connections between the superstructure and fixed piers. Compared with increasing member sizes or installing specially designed seismic protection devices, these two strategies are economical and easy to be implemented.

6.5.1 Strengthening bearing retainer anchorage to prevent bearing unseating at abutments

As indicated in Table 6.51, the anchorage of bearing retainers at the abutments of a few highly skewed tall-pier bridges that sustained bearing unseating at their abutments was strengthened to

prevent retainer anchor rupture and subsequent bearing unseating. As introduced in Chapter 3, the specified shear capacity of retainer anchors is 20% of the superstructure dead load at the given bearing (IDOT 2012a). As the anchors are typically over-designed in many existing bridges, the anchor shear capacity of the five tabulated prototype bridges was originally designed to be around 30% of the superstructure dead load on the bearing. Through a number of trial analyses, it was found that in order to completely prevent bearing unseating at the abutments of these bridges, this percentage needs to be increased to around 90% by using more anchors with larger diameters, as shown in Table 6.51.

Table 6.51: Original and strengthened bearing retainer anchorage at abutments of selected bridges

Bridge variant	No. of anchor per retainer		Anchor diameter [mm (in.)]		Shear capacity / bearing dead load	
	Original	Strengthened	Original	Strengthened	Original	Strengthened
4S60P40S	1	2	31.8 (1.25)	38.1 (1.5)	30%	88%
3C60P40S	1	2	31.8 (1.25)	38.1 (1.5)	30%	88%
4C45P40H	1	2	38.1 (1.50)	50.8 (2.00)	27%	96%
4C60P40H	1	2	38.1 (1.50)	50.8 (2.00)	27%	96%
4C60P40S	1	2	38.1 (1.50)	50.8 (2.00)	27%	96%

To evaluate the efficacy of this strengthening strategy, 400 additional nonlinear dynamic analyses were performed on the five selected bridge variants using the same suite of 20 earthquake ground motions applied in the four incident directions. The only difference between these additional analyses and those discussed in Section 6.3 is the strengthened retainer anchorage at abutments. Table 6.52 compares the occurrence of retainer anchor rupture and bearing unseating at the abutments of the five bridge variants. As seen in the table, the strengthened retainer anchorage basically did not rupture in the additional analyses. As a result, the bearing unseating observed in the original bridge analyses are completely prevented by the strengthened retainer anchorage.

Figure 6.12 compares the peak sliding distance and unseating of the elastomeric bearings at the deck corners of 4C60P40S bridge between the cases with original and strengthened retainer anchorage. This bridge variant sustained the most occurrences of bearing unseating at abutments among all the bridges and, thus, it is selected as an example to show the efficacy of the strengthening strategy. It can be seen that at all the four deck corners, the peak bearing sliding in the abutment-normal direction was effectively reduced and bearing unseating was completely pre-

Table 6.52: Comparison of retainer anchor rupture and bearing unseating in bridges with original and strengthened retainer anchorage

Bridge	Rupture of retainer anchor at Abut. 1 (RRA@A1)		Rupture of retainer anchor at Abut. 2 (RRA@A2)		Unseating of elastimeric bearing at Abut. 1 (UBA and UBO@A1)		Unseating of elastimeric bearing at Abut. 2 (UBA and UBO@A2)	
	Original[1, 2]	Strengthened[1, 2]	Original[1, 2]	Strengthened[1, 2]	Original[1]	Strengthened[1]	Original[1]	Strengthened[1]
4S60P40S	44 (55%)	0 (0%)	28 (35%)	0 (0%)	0	0	1	0
3C60P40S	53 (66%)	0 (0%)	47 (59%)	0 (0%)	0	0	2	0
4C45P40H	50 (63%)	0 (0%)	47 (59%)	0 (0%)	0	0	1	0
4C60P40H	51 (64%)	0 (0%)	52 (65%)	0 (0%)	0	0	4	0
4C60P40S	24 (30%)	0 (0%)	42 (53%)	1 (1%)	0	0	6	0

1 The number outside (without) the parentheses indicates the number of analyses with occurrences of a limit state.
2 The percentage inside the parentheses indicates the ratio of the number outside the parentheses to the 80 analyses of one bridge.

vented by the strengthened retainer anchors. The same result that bearing unseating is effectively prevented is also observed in the other four bridge variants, as illustrated in Figures C.1, C.4, C.7, and C.10 in Appendix C.

Figure 6.13 compares the bearing and retainer anchor responses at the lower-right corner (acute deck corner supported by Abutment 2) of 4C60P40S bridge when subjected to a transverse ground motion. As shown in Figure 6.13(a), the strengthened anchor did not rupture in the analysis but the original one did. In consequence, shear deformation and sliding of the bearing was significantly suppressed and unseating was prevented, as shown in Figure 6.13b.

A major concern of strengthening the retainer anchorage is that the force demands on the abutment pile foundation may be increased due to the unfused bearing retainers. Figure 6.14 compares the peak pile strain in 4C60P40S bridge with the original and strengthened retainer anchorage. The comparison for the other four bridge variants are illustrated in Figures C.2, C.5, C.8, and C.11 in Appendix C. As seen in these figures, the influence of the strengthened retainer anchorage on pile strains varies with the ground motion incident direction. An undesired effect observed in all the five bridge variants is that when subjected to the pure longitudinal ground motions, the peak strain of abutment piles was typically increased, which is shown in Figures 6.14(a), C.2(a), C.5(a), C.8(a), and C.11(a). For the other incident directions, the pile strain at the abutments may increase or decrease. Article 5.2.4 of the AASHTO Guide Specifications for LRFD Seismic Bridge Design (AASHTO 2011) indicates that for earthquake-resisting system (ERS) with abutment contribution, "pile-supported foundations shall be designed to sustain the design earthquake displacements; inelastic behavior of piles at the abutment shall be considered acceptable." So in general, the poten-

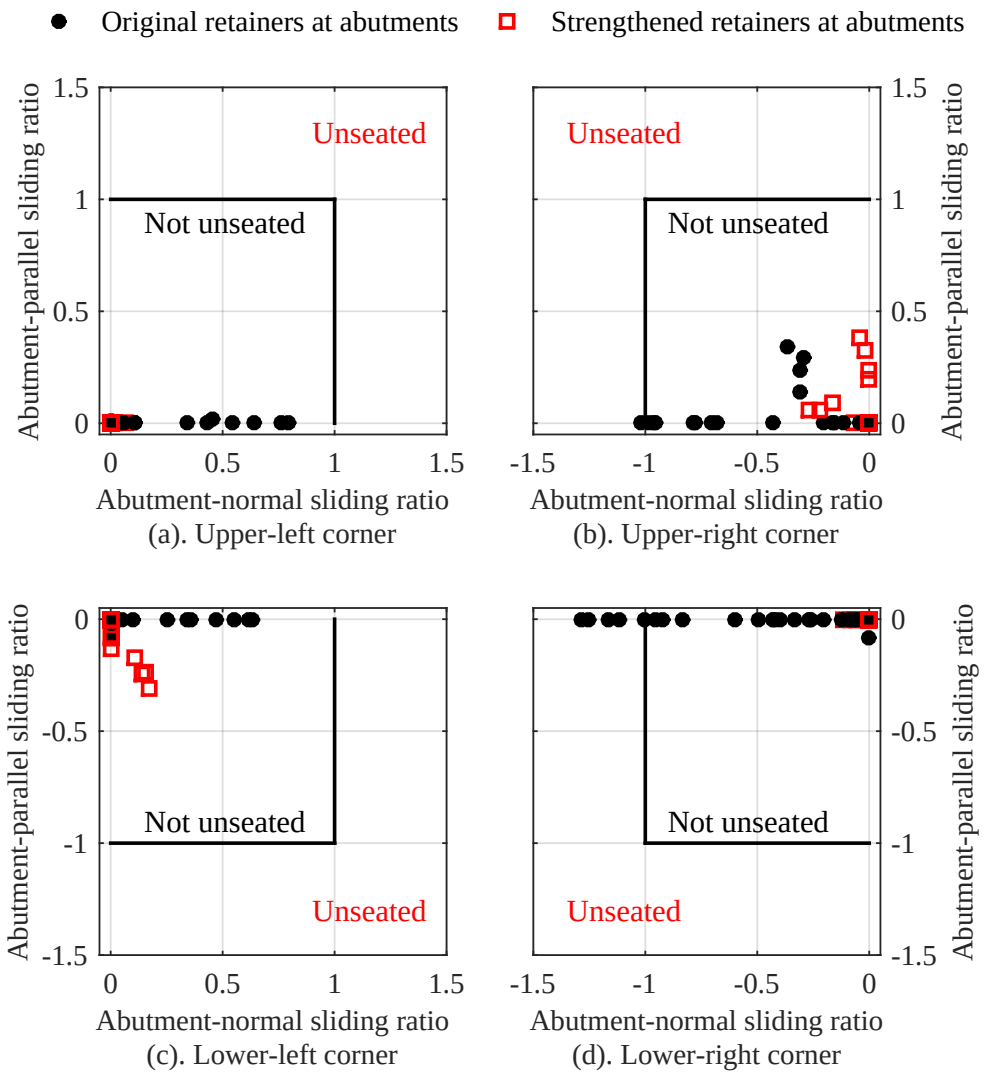

Figure 6.12: Comparison of peak sliding ratios of elastomeric bearings at deck corners of 4C60P40S bridge variant with original and strengthened retainer anchorage at abutments

tially increased inelastic pile response is preferred to superstructure unseating at the abutments. No significantly negative effect was observed in other aspects of the seismic response of the bridges with strengthened bearing retainers at the abutments.

Figures 6.15, C.3, C.6, C.9, and C.12 compare the peak strain of column reinforcing steel between the original and strengthened cases, which is an indicator of seismic damage to the pier columns. As seen in these figures, the peak strain of pier column reinforcing steel is not largely increased in any selected bridge. This is expected as strengthening the retainer anchorage at abutments is a local modification to the entire bridge.

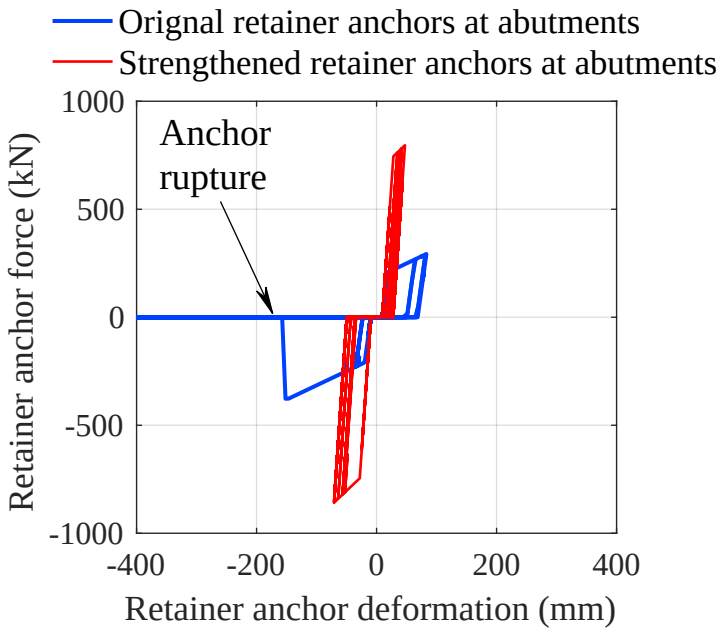

(a) Retainer anchor response

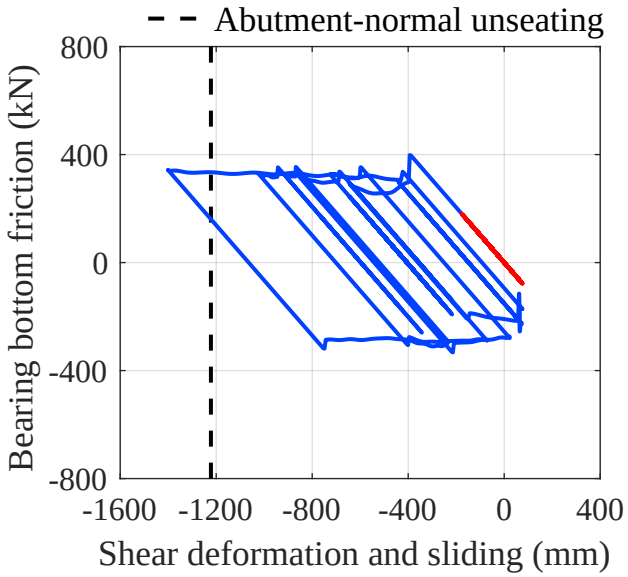

(b) Elastomeric bearing response in the abutment-normal direction

Figure 6.13: Comparison of retainer anchor and elastomeric bearing response at the lower-right corner (acute deck corner supported by Abutment 2) of 4C60P40S bridge when subjected to a transverse ground motion (anchor rupture and bearing unseating were prevented by strengthening retainer anchors)

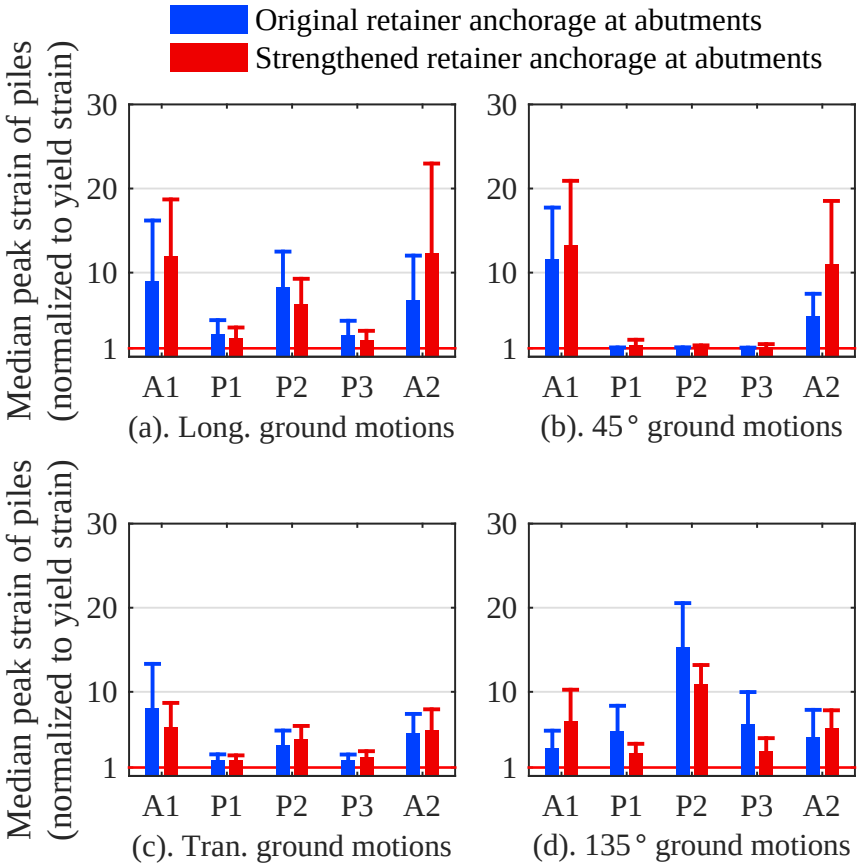

Figure 6.14: Comparison of peak pile strain (median + median absolute deviation) of 4C60P40S bridge variant with original and strengthened retainer anchorage at abutments: (a). response under longitudinal ground motions; (b). response under 45° ground motions; (c). response under transverse ground motions; (d). response under 135° ground motions

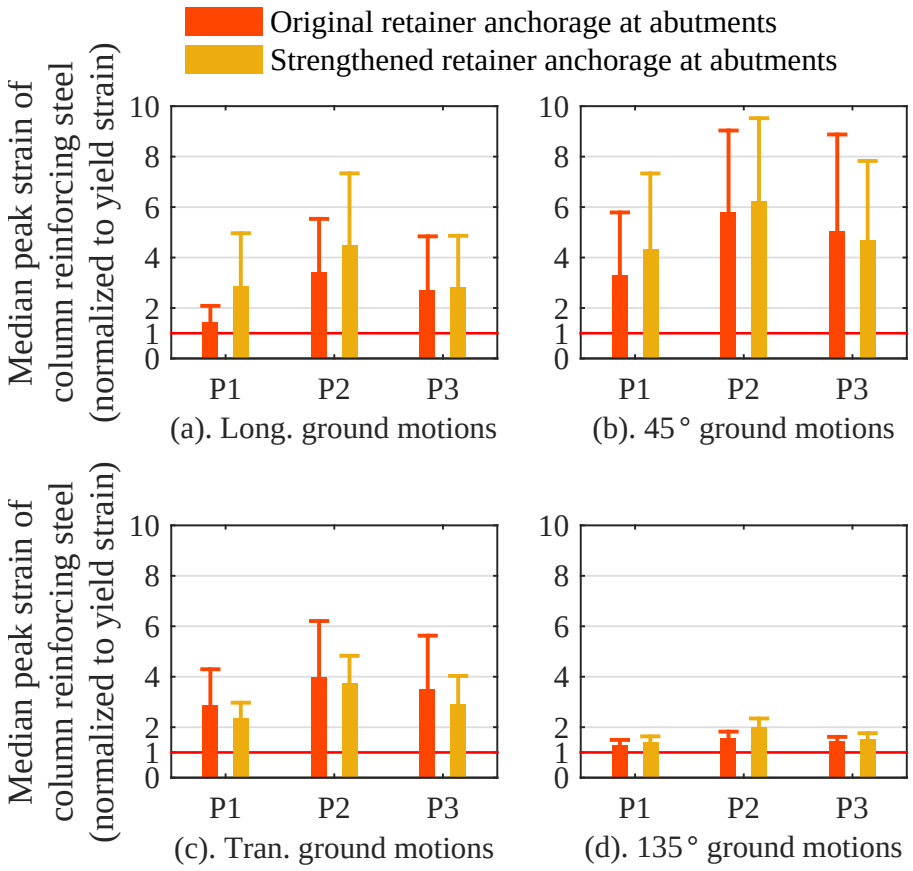

Figure 6.15: Comparison of peak strain (median + median absolute deviation) of reinforcing steel at pier column bases of 4C60P40S bridge variant with original and strengthened retainer anchorage at abutments: (a). response under longitudinal ground motions; (b). response under 45° ground motions; (c). response under transverse ground motions; (d). response under 135° ground motions

6.5.2 Weakening connections between superstructures and fixed piers to mitigate pier column damage

Installed on top of the fixed piers, the anchors of low-profile steel fixed bearings (in steel-plate-girder bridges) and the steel dowels (in PPC-girder bridges) are intended to act as structural fuses that should be ruptured during major earthquake events. Before rupture of these components, the superstructure seismic force is transferred to the fixed pier columns through not only the anchors or dowels but also the interface friction between the leveling pad (in steel-plate-girder bridges) or performed joint filler (in PPC-girder bridges) and the concrete surface of the pier cap. After these fuses are ruptured, the superstructure seismic force can only be transferred to the fixed pier through the interface friction and the total force transfer capacity is substantially reduced, thereby the pier columns are protected.

As introduced in Section 3.5, the IDOT Bridge Manual (IDOT 2012a) provides a simple method for nominally designing the anchor bolts of steel fixed bearings. In this method, the nominal fusing capacity of the steel fixed bearing is specified as 20% of the superstructure dead load on the bearing. By inspection of the plans of many recently constructed highway bridges in Illinois, it was found that the specified nominal fusing capacity of low-profile steel fixed bearing anchors, namely 20% of the superstructure dead load on the bearing, is heavily over-designed in many of these bridges. A primary potential reason for this design trend in practice may be that bridge engineers tend to regard the specified fusing capacity as a minimum requirement and use larger or more anchor bolts for conservatism. However, because the anchor bolts are intended to act as structural fuses during earthquake events, this "conservatism" may prevent the anchor bolts from rupture, and incur more seismic damage to the pier columns. A secondary potential reason may be that a fusing capacity in the close vicinity of 20% of the dead load on the bearing is not always available in actual design due to the limited options for anchor diameters. In this situation, bridge designers may round the anchor diameter up to the nearest available size and result in over-designed fusing capacity.

For the PPC-girder bridges, connection details at the fixed pier are shown in Figures 3.34a and 3.35b (IDOT 2015a). The minimum required number of #8 (U.S.) steel dowels on each face of the pier between two adjacent girders, denoted by N in Figure 3.35b, is given by Equation (6.3)

$$N = \frac{1}{2}\left[\frac{0.2DL}{28.3(S)} - 2\right] \geq 2 \tag{6.3}$$

where DL is the sum of all superstructure dead loads at the given pier under consideration (kips); S is the number of beam spaces. The 28.3, in kips, is the nominal shear capacity of a #8 (U.S.) steel dowel with an ultimate tensile material strength of 60 ksi. As seen in Figure 3.35b, except these dowels between adjacent girders, additional dowels are used at each girder line to connect the bottom girder flange to the pier cap (one dowel for each exterior girder and two dowels for each interior girder). Although Equation (6.3) aims to provide a total fusing capacity of the dowels between girders equal to 20% of the superstructure dead load imposed on the fixed pier, there are two potential sources that lead to over-designed fusing capacity at this fixed pier connection. First, as seen in Figure 3.35b, a minimum value of 2 is specified for N, which can be much larger than the N value calculated by Equation (6.3). Second, the dowels at girder lines provide extra shear capacity to the global fixed pier connection.

As indicated in Table 6.53, the steel fixed bearing anchors of a few steel-plate-girder bridges and the steel dowel connections of a few PPC-girder bridges were weakened in an attempt to improve the fusing performance of these components and mitigate the damage to pier columns. As seen in the table, besides the over-designed connections, two additional design cases are considered, namely specified and weakened designs. The connection in the specified design possesses a fusing capacity that is around 20% of the superstructure dead load at the given bearing, while the weakened design possesses a fusing capacity around 10% to 15% of the superstructure dead load on the bearing.

Figures 6.16 to 6.21 comparatively demonstrate the effect of weakening the superstructure-to-fixed-pier connections on mitigating seismic damage to pier columns, indicated by the peak strain of reinforcing steel and concrete cover at the column bases of the fixed pier (P2). Additional comparative results are illustrated in Figures C.13 to C.28 in Appendix C. It can be seen that this strategy is generally effective for all the nine 3S, 4C and 3C bridges listed in Table 6.53. For these bridges, reducing the connection fusing capacity leads to mitigated pier column

seismic damage. Although the specific amount of mitigation varies in different bridge variants and ground motion incident directions, reducing the connection fusing capacity to the "further

Table 6.53: Different designs of connections between superstructure and fixed pier

Bridge	Design cases	No. of anchor per girder	Anchor diameter [mm (in.)]	Shear capacity / bearing dead load
[3S00P15S,	Over-designed	2	38.1 (1.5)	44%
3S15P15S,	Specified	2	25.4 (1.0)	20%
3S30P15S]	Further weakened	2	19.1 (0.75)	11%
[4S00P15S,	Over-designed	4	31.8 (1.25)	46%
4S15P15S,	Specified	2	31.8 (1.25)	23%
4S30P15S]	Further weakened	2	25.4 (1.0)	15%
[3C00P15S,	Over-designed	3 (exterior), 6 (interior)	25.4 (1.0)	64%
3C15P15S,	Specified	2 (exterior), 3 (interior)	19.1 (0.75)	19%
3C30P15S]	Further weakened	2 (exterior), 3 (interior)	15.9 (0.625)	13%
[4C00P15S,	Over-designed	3 (exterior), 6 (interior)	25.4 (1.0)	45%
4C15P15S, 4C30P15S]	Weakened	2 (exterior), 3 (interior)	19.1 (0.75)	13%

weakened" level defined in Table 6.53 (a fusing capacity equal to 10% $\sim$ 15% of the superstructure dead load on the considered bearing), significant reduction of the seismic damage to pier columns were achieved for all the nine 3S, 4C and 3C bridges.

As an example of the pier column response, Figure 6.22 compares force-deflection response of Pier 2 columns between the three design cases of fixed bearing anchorage strength. In the cases of over-designed and specified cases, the pier columns exhibited clear inelastic and large-deflection response. In contrast, the column response was essentially elastic and the deflection was the smallest in the case with the further weakened fixed bearing anchorage strength.

Although weakening the fixed bearing anchors is effective for the selected 3S, 4S, and 3C bridge variants, merely using this strategy appeared to be ineffective for some of the selected 4C bridges, as illustrated in Figures 6.23 and 6.24. An inspection of the peak steel strain at the expansion piers (P1 and P3) shown in Figures 6.23(a) and 6.24(a) reveals that even the elastomer friction can cause large steel and concrete strain at the expansion pier, as the heavy superstructure of 4C bridges directly results in large elastomer friction on top of the pier columns. For the fixed piers, even if the connections can be fused, the post-fusing friction between the elastomeric leveling pad or performed joint filler and the concrete surface can result in considerable damage to the pier columns, due to the large superstructure dead load. Therefore, merely weakening the connections at the fixed pier may not be an effective strategy for long-span massive concrete bridges. In this situa-

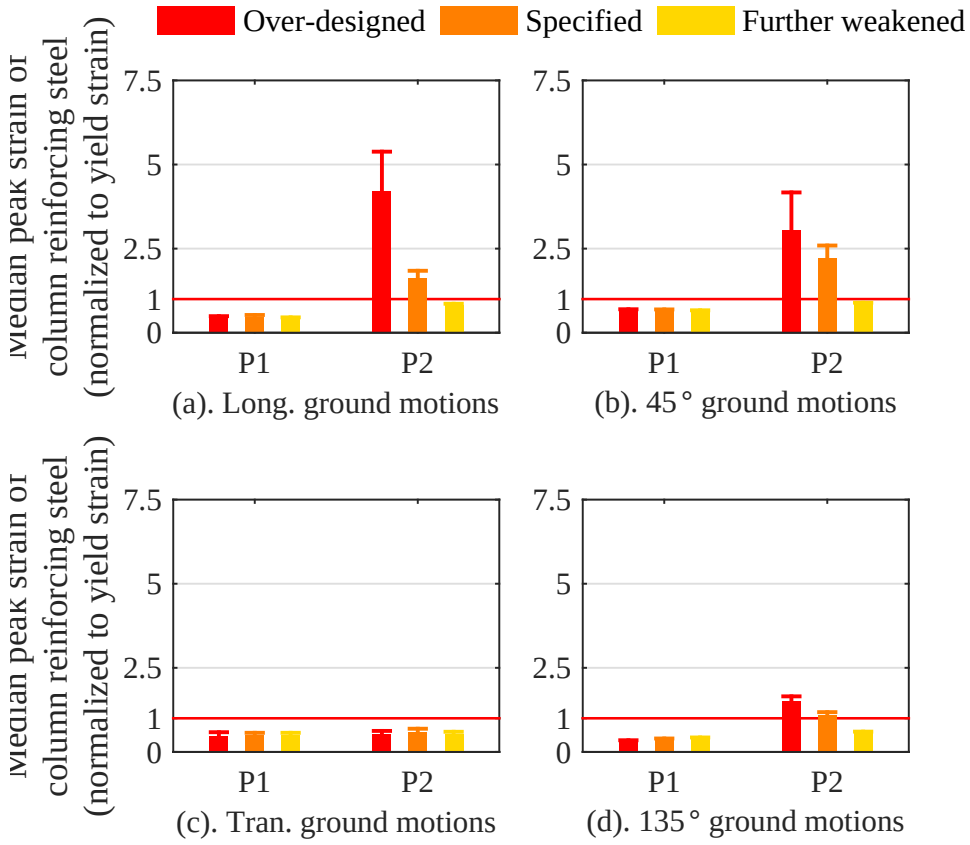

Figure 6.16: Comparison of peak strain (median + median absolute deviation) of reinforcing steel at pier column bases of 3S30P15S bridge variant with different designs of steel fixed bearing anchorage: (a). response under longitudinal ground motions; (b). response under 45° ground motions; (c). response under transverse ground motions; (d). response under 135° ground motions

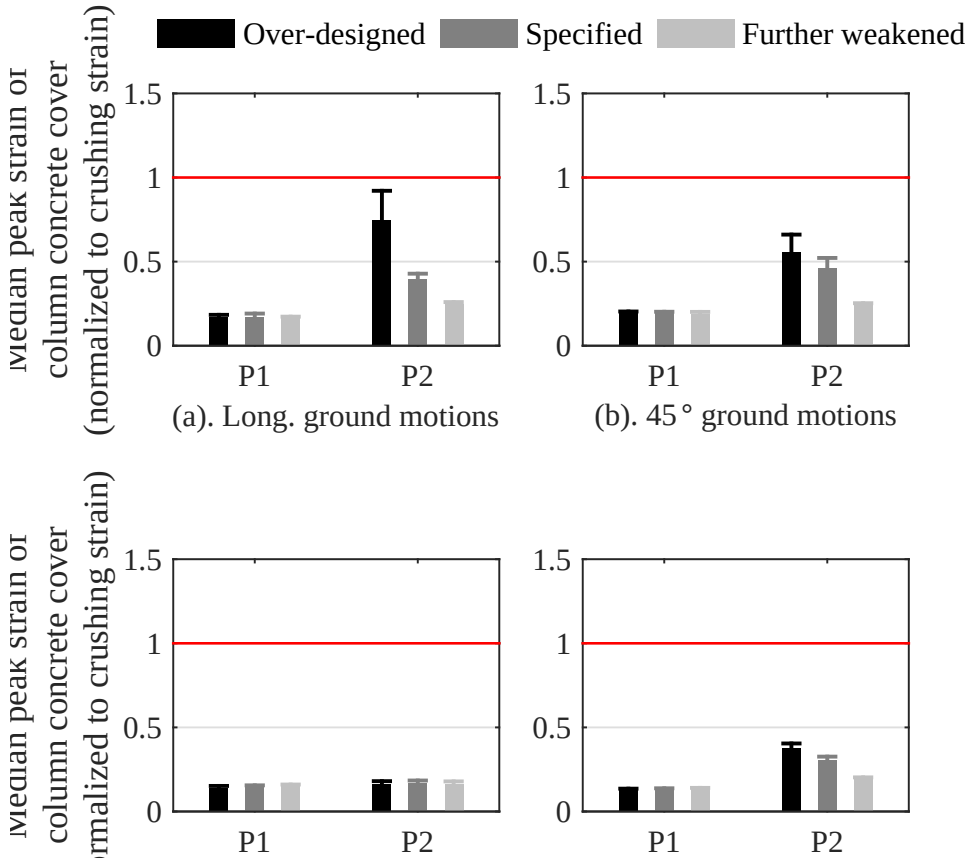

Figure 6.17: Comparison of peak strain (median + median absolute deviation) of concrete cover at pier column bases of 3S30P15S bridge variant with different designs of steel fixed bearing anchorage: (a). response under longitudinal ground motions; (b). response under 45° ground motions; (c). response under transverse ground motions; (d). response under 135° ground motions

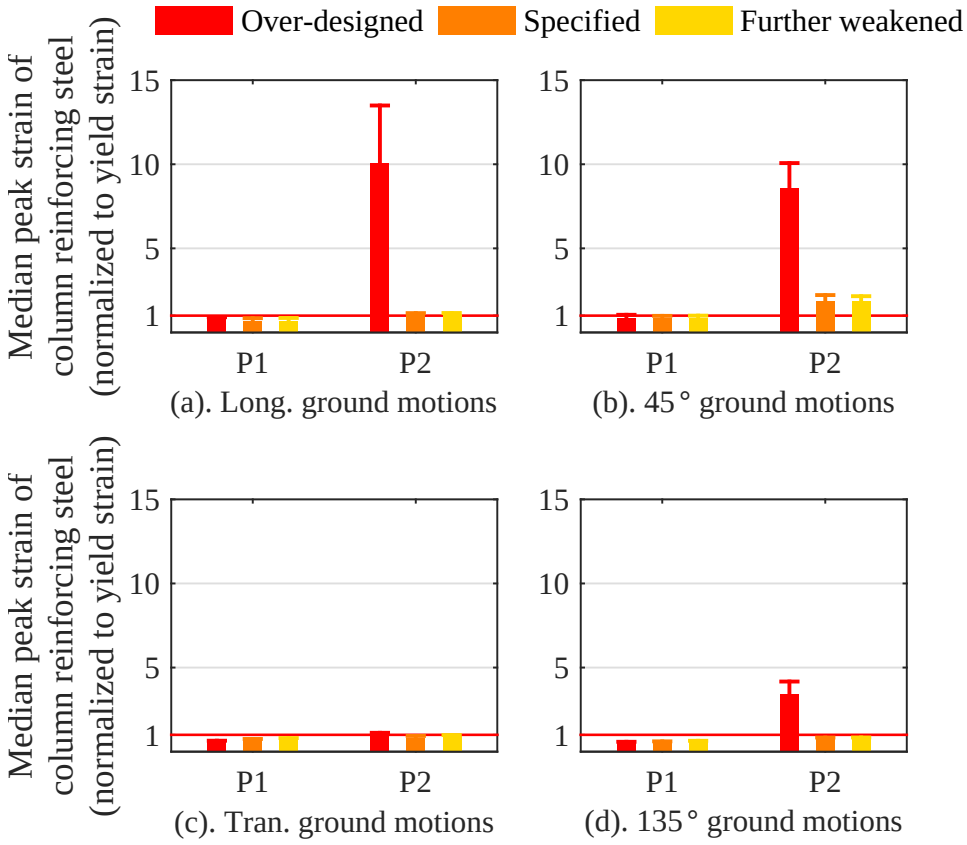

Figure 6.18: Comparison of peak strain (median + median absolute deviation) of reinforcing steel at pier column bases of 3C30P15S bridge variant with different designs of steel dowel connections at fixed pier: (a). response under longitudinal ground motions; (b). response under 45° ground motions; (c). response under transverse ground motions; (d). response under 135° ground motions

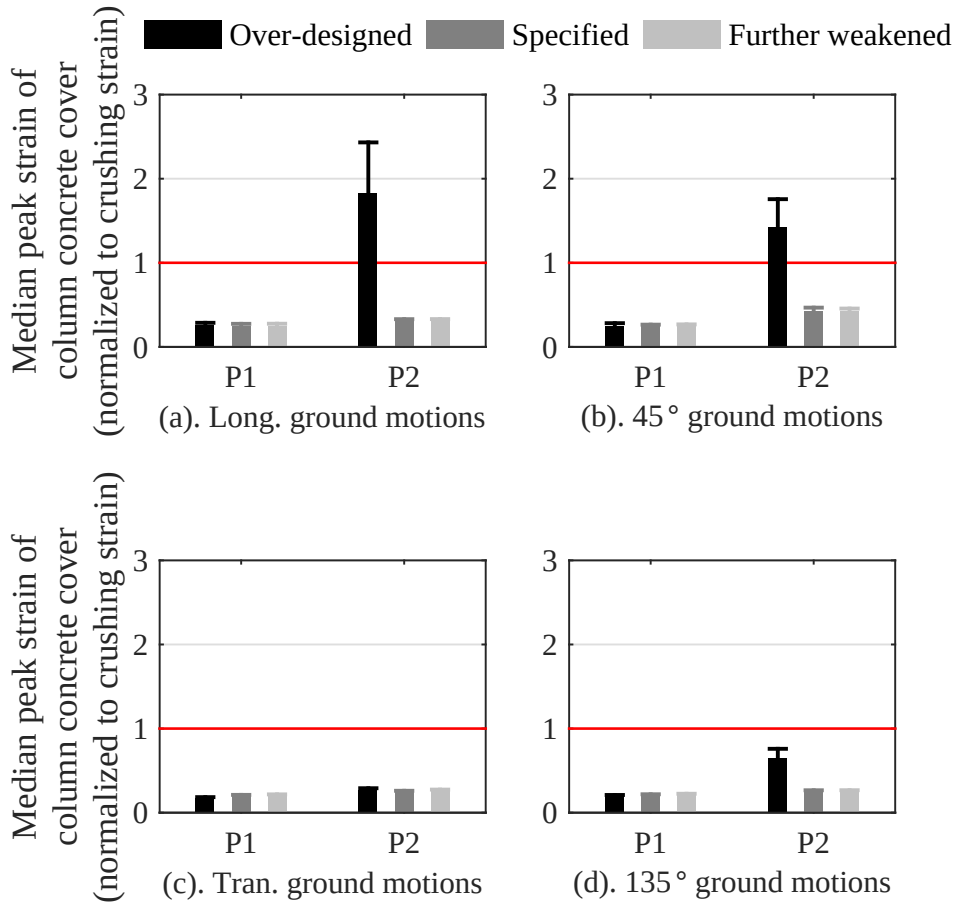

Figure 6.19: Comparison of peak strain (median + median absolute deviation) of concrete cover at pier column bases of 3C30P15S bridge variant with different designs of steel dowel connections at fixed pier: (a). response under longitudinal ground motions; (b). response under 45° ground motions; (c). response under transverse ground motions; (d). response under 135° ground motions

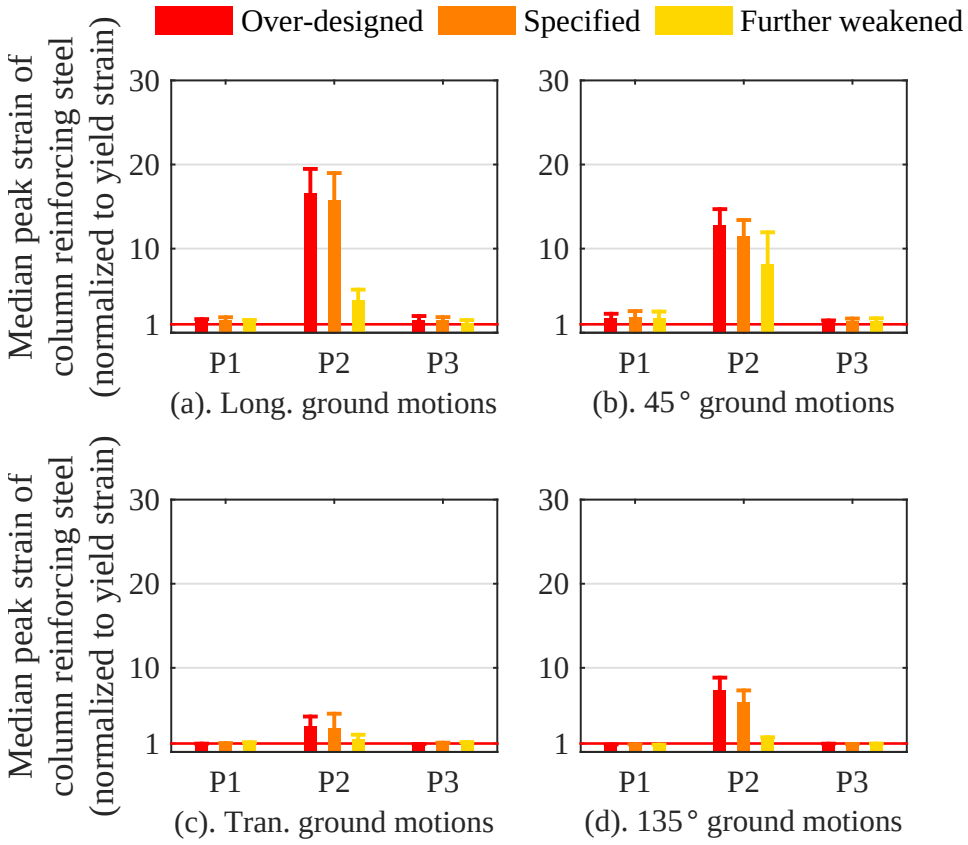

Figure 6.20: Comparison of peak strain (median + median absolute deviation) of reinforcing steel at pier column bases of 4S30P15S bridge variant with different designs of steel fixed bearing anchorage: (a). response under longitudinal ground motions; (b). response under 45° ground motions; (c). response under transverse ground motions; (d). response under 135° ground motions

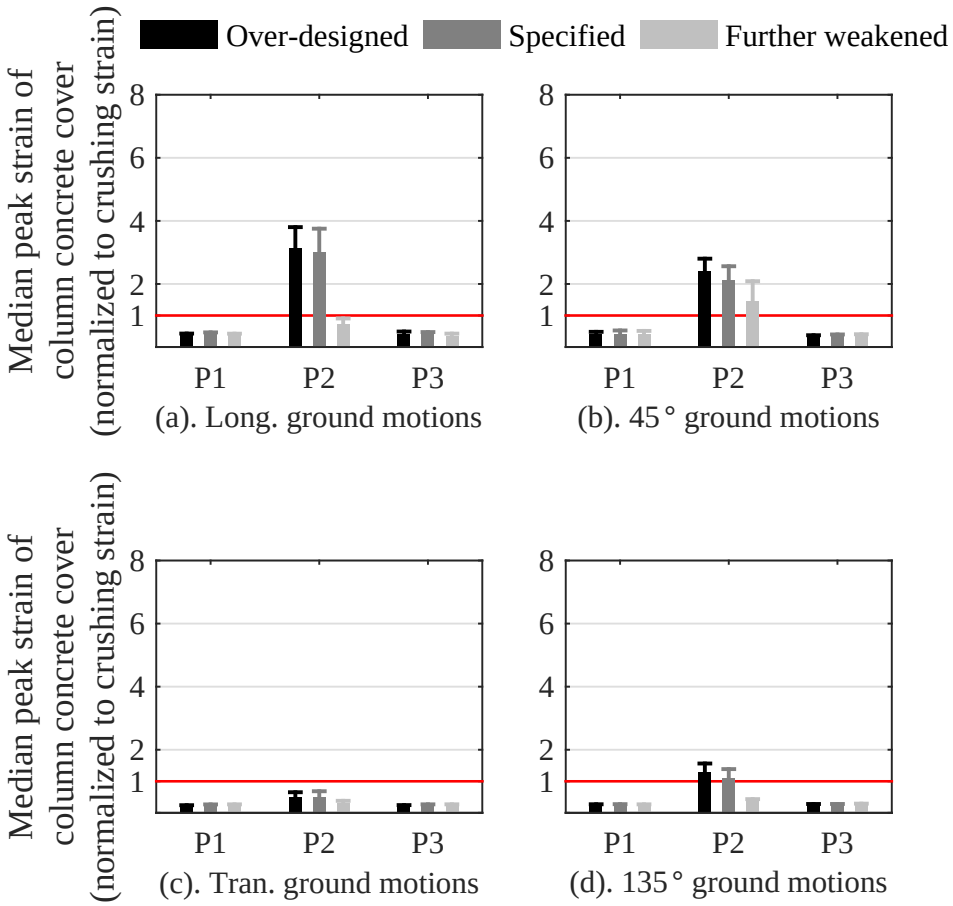

Figure 6.21: Comparison of peak strain (median + median absolute deviation) of concrete cover at pier column bases of 4S30P15S bridge variant with different designs of steel fixed bearing anchorage: (a). response under longitudinal ground motions; (b). response under 45° ground motions; (c). response under transverse ground motions; (d). response under 135° ground motions

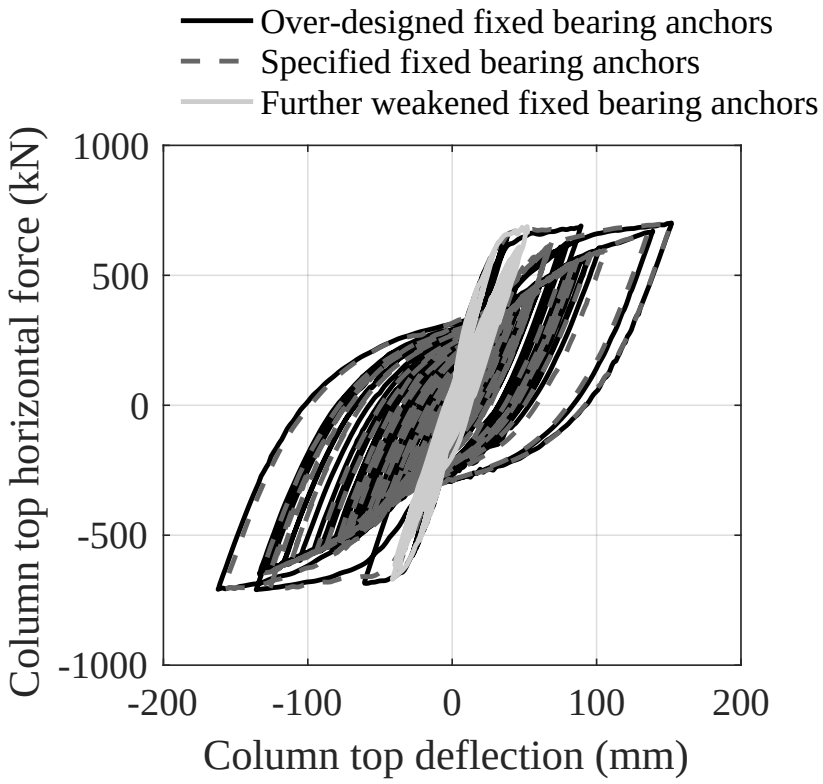

Figure 6.22: Comparison of column response at Pier 2 of 4S30P15S bridge when subjected to a longitudinal ground motion (pier-normal response averaged over four columns at Pier 2)

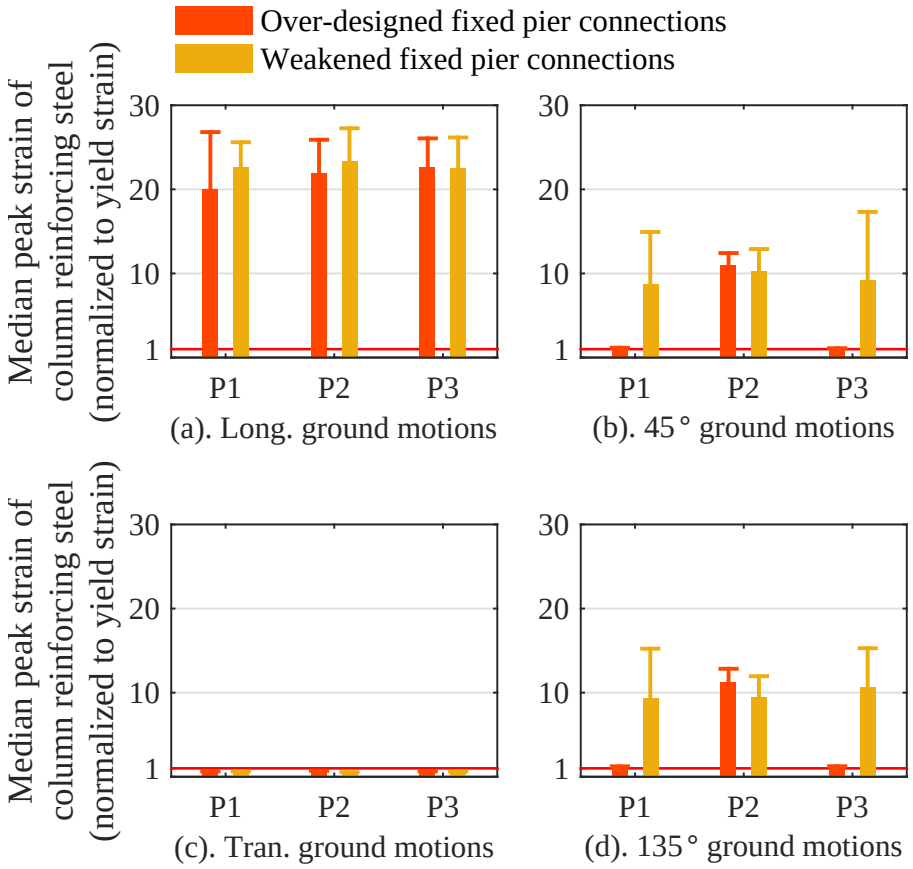

Figure 6.23: Comparison of peak strain (median + median absolute deviation) of reinforcing steel at pier column bases of 4C00P15S bridge variant with different designs of steel fixed bearing anchorage: (a). response under longitudinal ground motions; (b). response under 45° ground motions; (c). response under transverse ground motions; (d). response under 135° ground motions

tion, using larger pier columns in conjunction with weakening the connections might be necessary to reduce the seismic damage to the pier columns.

Table 6.54 lists three cases with different configurations of the pier columns and connections between the superstructure and fixed pier. The bridges in Case 1 are the original ones studied in Section 6.3 without any modification of the components. In Case 2, the columns of both the expansion and fixed piers are enlarged but the steel dowel connection on top of the fixed pier is not weakened. In Case 3, enlarged pier columns are used in conjunction with the weakened connections. In Cases 2 and 3, except the larger column diameter, the reinforcing ratio, 2%, and grade of the steel and concrete material of the pier column remain the same.

Figures 6.25 and 6.26 compare the mitigation effect between Cases 1 and 2. It can be seen

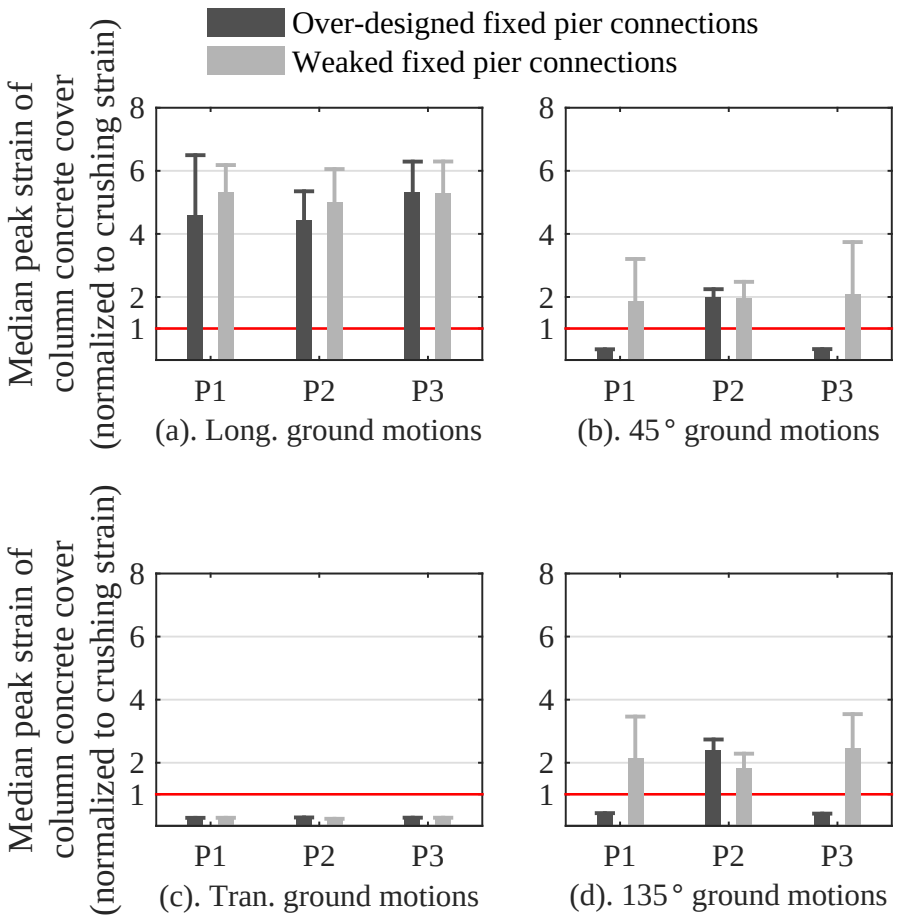

Figure 6.24: Comparison of peak strain (median + median absolute deviation) of concrete cover at pier column bases of 4C00P15S bridge variant with different designs of steel fixed bearing anchorage: (a). response under longitudinal ground motions; (b). response under 45° ground motions; (c). response under transverse ground motions; (d). response under 135° ground motions

that enlarging the pier column diameter significantly reduces the peak steel and concrete strain at both the expansion and fixed piers. As seen in Figures 6.25 and 6.26 , when the enlarged pier columns were used in conjunction with the weakened connections, additional reduction of peak steel and concrete strain at the fixed pier was achieved. The comparative results of the 4C15P15S and 4C30P15S bridges listed in Table 6.54 are shown in Figures C.29 to C.36 in Appendix C.

For weakening the fixed bearing anchors, the only observed negative effect is that the bridges with weakened fixed bearing anchors sustained slightly larger peak deck displacements. For example, when the fixed bearing anchor diameter of the 3S00P15S bridge was reduced from 38.1 mm to 25.4 mm, the averaged deck center peak displacement caused by longitudinal ground motions was increased from 95 mm to 100 mm. No significantly negative effect was observed in other aspects of the bridge seismic response.

Table 6.54: Enlarged pier columns in conjunction with weakened connection for mitigation of seismic damage to pier columns

Case	Bridge variant	No. of dowels per girder	Dowel diameter [mm (in.)]	Pier column diameter [m (ft)]
1	4C00P15S 4C15P15S 4C30P15S	3 (exterior) 6 (interior) over-designed (45% dead load)	25.4 (1.0)	1.07 (3.5) original
2	4C00P15S 4C15P15S 4C30P15S	3 (exterior) 6 (interior) over-designed (45% dead load)	25.4 (1.0)	1.37 (4.5) enlarged
3	4C00P15S 4C15P15S 4C30P15S	2 (exterior) 3 (interior) weakened (13% dead load)	19.1 (0.75)	1.37 (4.5) enlarged

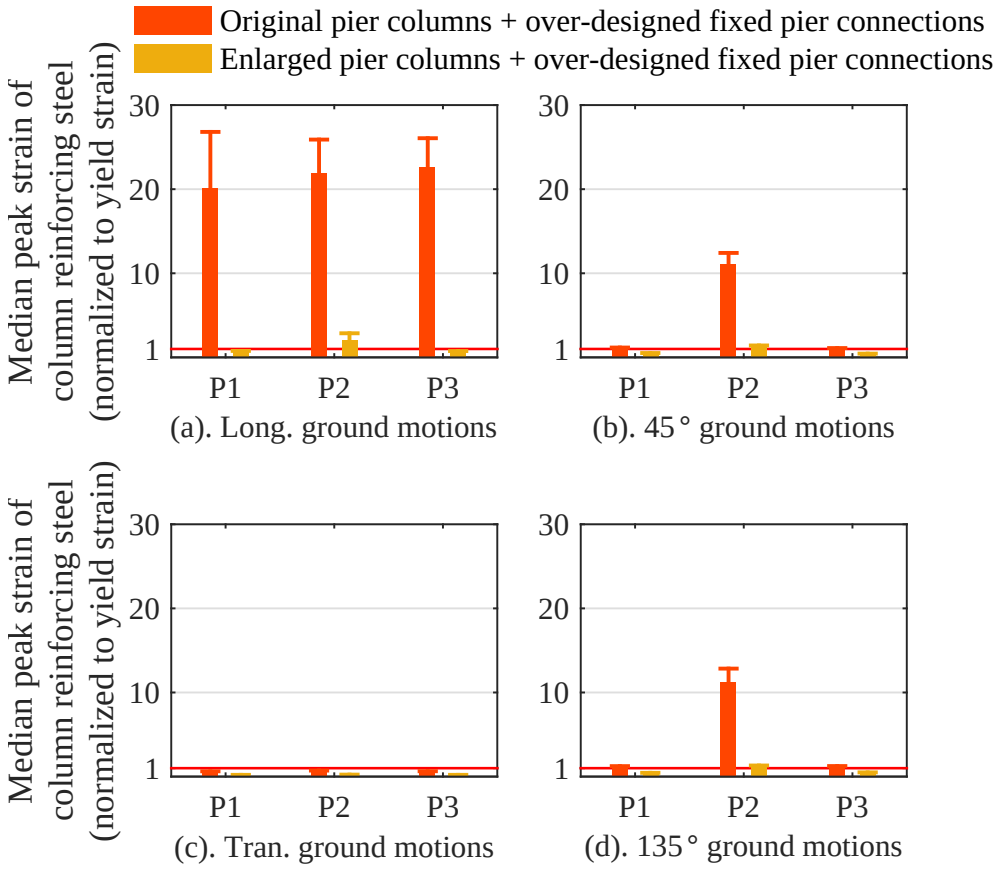

Figure 6.25: Comparison of peak strain (median + median absolute deviation) of reinforcing steel at pier column bases of 4C00P15S bridge between Cases 1 and 2 of Table 6.54: (a). response under longitudinal ground motions; (b). response under 45° ground motions; (c). response under transverse ground motions; (d). response under 135° ground motions

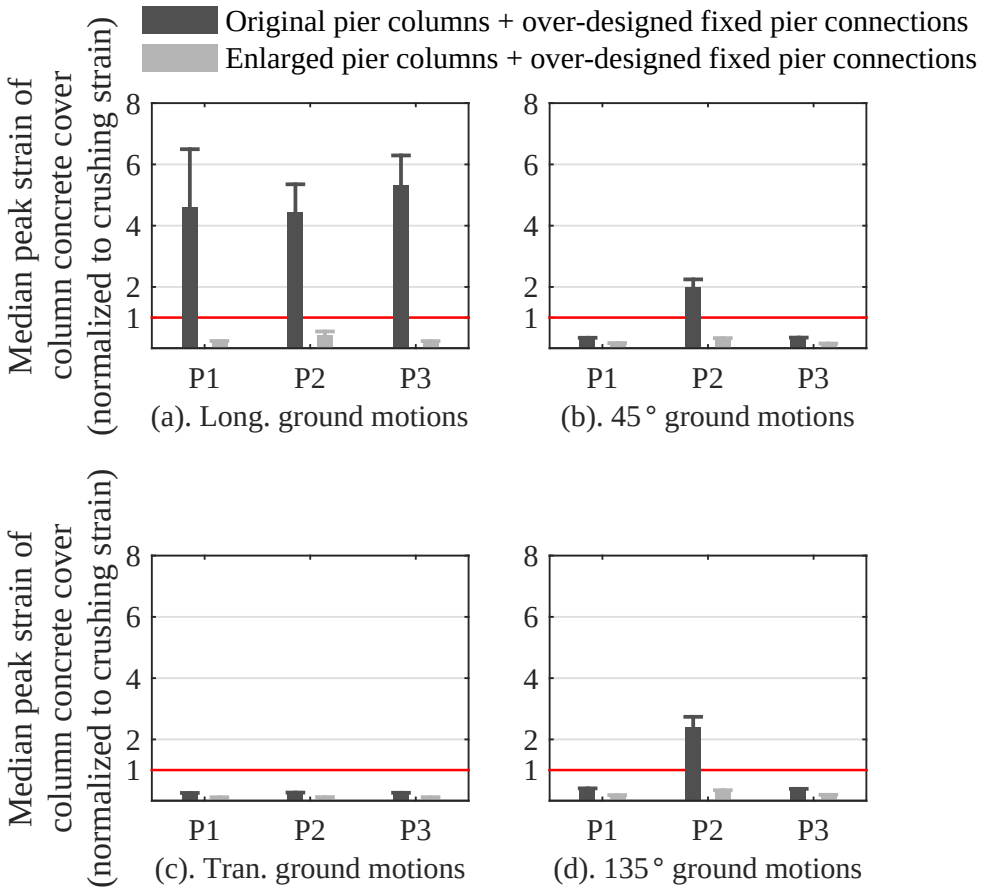

Figure 6.26: Comparison of peak strain (median + median absolute deviation) of concrete cover at pier column bases of 4C00P15S bridge between Cases 1 and 2 of Table 6.54: (a). response under longitudinal ground motions; (b). response under 45° ground motions; (c). response under transverse ground motions; (d). response under 135° ground motions

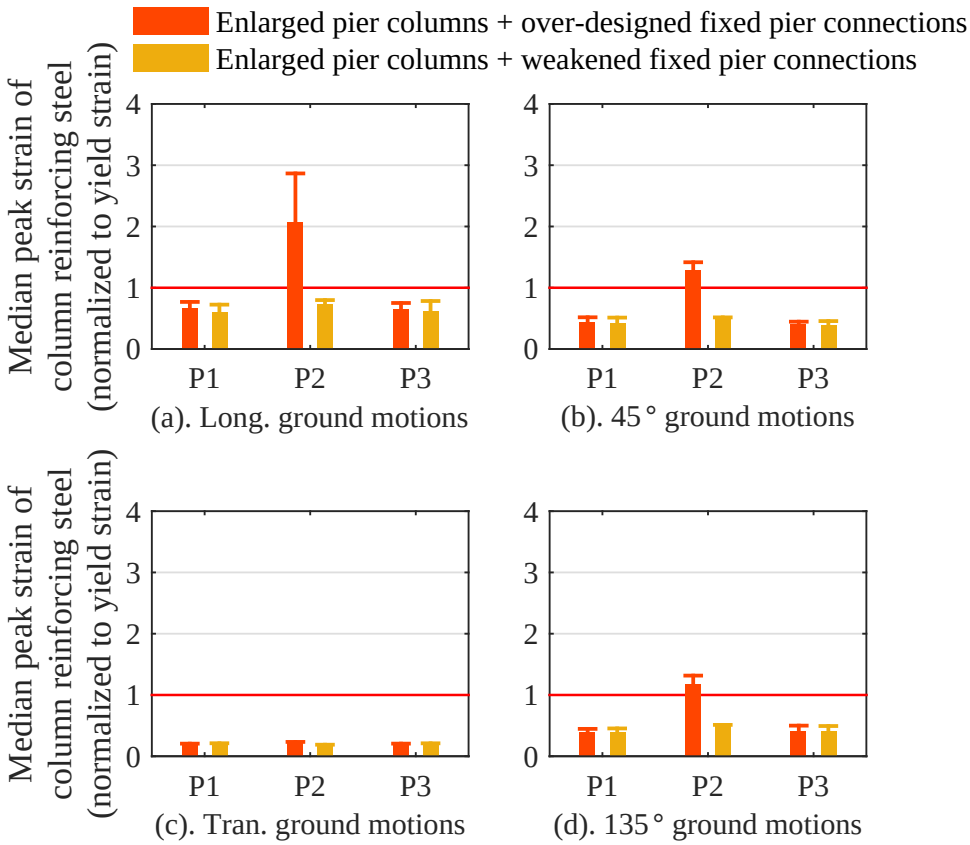

Figure 6.27: Comparison of peak strain (median + median absolute deviation) of reinforcing steel at pier column bases of 4C00P15S bridge between Cases 2 and 3 of Table 6.54: (a). response under longitudinal ground motions; (b). response under 45° ground motions; (c). response under transverse ground motions; (d). response under 135° ground motions

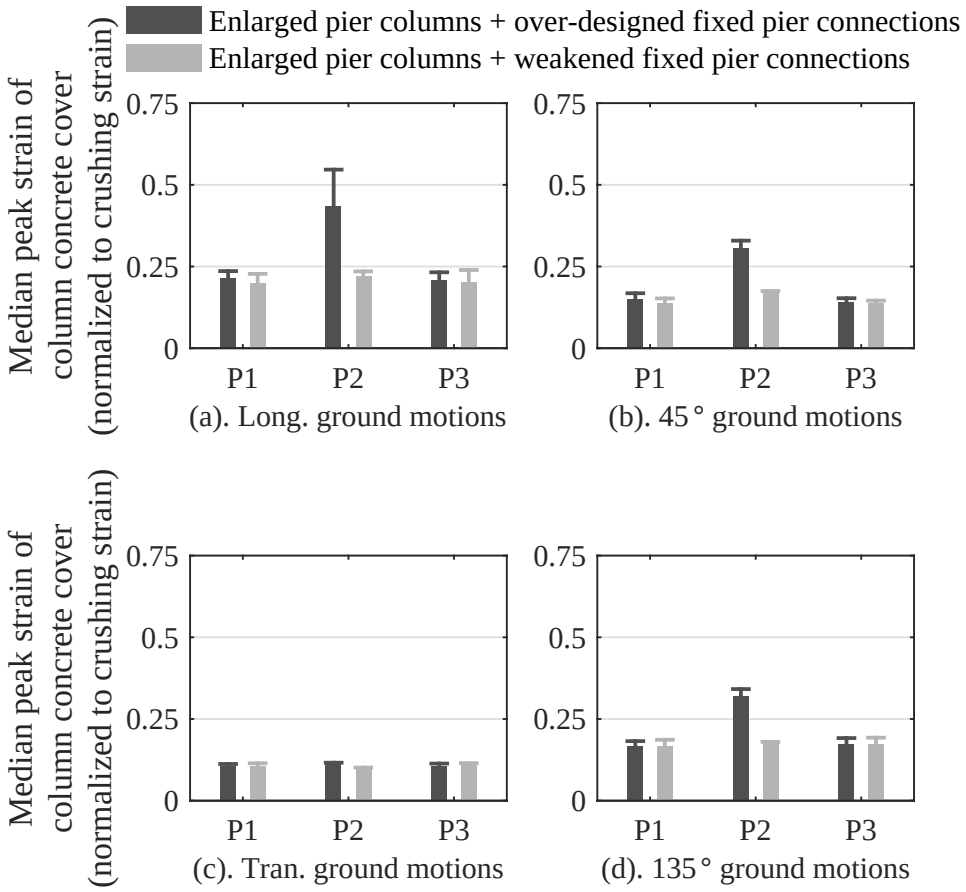

Figure 6.28: Comparison of peak strain (median + median absolute deviation) of concrete cover at pier column bases of 4C00P15S bridge between Cases 2 and 3 of Table 6.54: (a). response under longitudinal ground motions; (b). response under 45° ground motions; (c). response under transverse ground motions; (d). response under 135° ground motions

6.5.3 Summary of recommendations for the ERS bridge design on the basis of dynamic analysis results

Two preliminary recommendations for calibrating the current ERS bridge design are proposed on the basis of the dynamic bridge analysis results, aiming to prevent unseating of elastomeric bearings at the abutments and mitigate excessive damage to the pier columns.

As discussed in Section 6.3, highly skewed bridge variants supported by tall pier columns are most susceptible to bearing unseating at their abutments as compared to other bridge variants. As presented in Section 6.5.1, a number of bridges sustained bearing unseating at abutments were selected and the fusing capacity of their retainer anchorage at the abutments were strengthened from the original 30% of the superstructure dead load on the bearing to around 90%, which is much higher than the specified 20% (IDOT 2012a). Comparative nonlinear dynamic analyses were then performed to evaluate the proposed strengthening strategy. It was found that this strategy effectively prevented bearing unseating at the abutments of these highly-skewed and tall-pier bridges.

As presented in Section 6.3, the fixed pier columns typically sustained much severer damage than the expansion pier columns due to the high lateral stiffness of the connections between the superstructure and fixed pier. These connections are found to be commonly over-designed in many existing bridges. Comparative studies were performed on a few bridge variants sustained considerable seismic damage to their pier columns. The fusing capacity of the superstructure-fixed-pier connections in these bridges were reduced. The comparative analysis results demonstrated that when the connection fusing capacity is reduced to around 10% $\sim$ 15% of the superstructure dead load on the bearing, effective mitigation of the seismic damage to pier columns can be achieved in a number of 3S, 4S, and 3C bridge variants. Due to the large superstructure dead load of 4C bridges, the interface friction on top of the pier columns is large enough to damage the pier columns and, thus, merely weakening the superstructure to fixed pier connection is insufficient to protect the pier columns. For the selected 4C bridge variants, larger pier columns are necessary to avoid severe seismic damage. When the larger pier columns are used in conjunction with the weakened fixed pier connections, additional mitigation effect was achieved.

CHAPTER 7

SUMMARY AND CONCLUSIONS

7.1 Objectives and Scope of Research

The research presented in this dissertation focused on the seismic performance of quasi-isolated highway bridges with seat-type abutments, when subjected to a suite of earthquake ground motions with a 1,000-year return period, considering the site condition and regional seismicity of Cairo, Illinois. It is a major part of the research project, "Calibration and Refinement of Illinois' Earthquake Resisting System Bridge Design Methodology: Phase II", sponsored by the Illinois Department of Transportation (IDOT) and Illinois Center for Transportation (ICT). A quasi-isolated earthquake-resistant bridge is primarily realized by strategically employing sacrificial connections between superstructures and substructures. These connections include non-seismically designed elastomeric expansion bearings, steel fixed bearings, bearing side retainers, and steel dowel bars. When the bridge is subjected to high seismic demands, fusing actions of these sacrificial connections as well as subsequent bearing deformation and sliding are expected to reduce the seismic forces transferred from superstructures down to substructures and foundations. In conjunction with the sacrificial connections, conservatively designed seat width at substructures are relied upon to accommodate displacement demands of superstructures and prevent span loss. The overall goal of the quasi-isolation strategy is to ensure that the bridges will not collapse during moderate to extreme seismic events.

A suite of prototype earthquake-resistant quasi-isolated highway bridges were computationally modeled, in order to assess the bridge seismic performance and provide insight into their response characteristics. The suite included three-span and four-span bridges with steel-plate and prestressed-precast-concrete (PPC) girders, as well as non-skew and skew seat-type abutments. In conjunction with the seat-type abutments, the bridge superstructures were supported by interme-

diate piers with multiple reinforced-concrete (RC) pier columns. The bridge substructures were supported by steel pile foundations. In order to represent typical quasi-isolated seat-type abutment bridges in Illinois, 80 prototype bridge variants in total were included in the suite. These bridge variants encompassed two span arrangements, two girder types, five skew angles, two pier heights, and two foundation soil conditions. All of the bridges were proportioned in accordance with the IDOT and AASHTO bridge design specifications (IDOT 2012a; AASHTO 2011).

Detailed yet efficient three-dimensional nonlinear finite-element models were developed for all of the 80 bridge variants. The finite-element model incorporated various critical structural components and geotechnical mechanisms that are necessary to capture important bridge seismic response characteristics. Multi-mode adaptive pushover analyses were performed on a number of representative bridge variants. Various pushover responses, in terms of force distribution among substructures, sequence of limit state occurrences, fusing performance of sacrificial superstructure-substructure connections, and vulnerability of critical bridge components were investigated. Multiple eigenvalue modal analyses were performed at different bridge deformation states in each pushover analysis. Through studying the bridge periods and mode shapes, important modal response characteristics were revealed.

The research culminated in a comprehensive and extensive assessment of bridge seismic performance, for which 6,400 nonlinear dynamic time-history analyses were carried out using a supercomputer. A suite of 20 earthquake ground motions with a 1,000-year return period, considering the site condition and regional seismicity of Cairo, Illinois, which possess the highest seismicity in the state, was applied to each bridge variant in four horizontal directions. The occurrences of various fusing and damaging limit states of critical bridge components were statistically summarized. Bridge seismic response characteristics including bearing unseating, fusing of sacrificial superstructure-substructure connections, and critical component damaging at substructures and foundations were revealed. The assessment results validate that the current quasi-isolation earthquake-resistant bridge design strategy is effective and most of the studied prototype bridges are unlikely to fail in global collapse when subjected to earthquake ground motions with a 1,000-year return period in the Midwestern United States. Although the majority of the prototype bridges exhibited satisfactory seismic performance, the response of a small number of bridge variants demonstrated a high risk of bearing unseating and severe pier column damage. Aiming

at improving bridge seismic performance in these two aspects, two preliminary recommendations for calibrating the current bridge design were proposed and their efficacy was demonstrated by comparative studies. In addition to the 6,400 nonlinear dynamic analyses in the primary study, additional 2,320 nonlinear dynamic analyses were performed for the comparative studies.

7.2 General Observations and Recommendations

The comprehensive and extensive seismic performance assessment presented in this dissertation demonstrated that the majority of the prototype quasi-isolated highway bridges only sustained limited local damage and were unlikely to collapse when subjected to horizontal earthquake ground motions with a 1,000-year return period in the Midwestern United States.

Despite of the overall satisfactory performance, the primary unacceptable damaging limit state, bearing unseating, occurred in the analyses of several highly skewed bridges supported by tall intermediate piers. All of the bearing unseating occurred after fusing of the bearing retainers at the abutments of these bridges. In addition to the bearing unseating, a small number of non-skew or lightly skewed bridges supported by short pier columns sustained severe damage to the pier columns. In some cases, the severe column damage might not be easily repairable. The post-earthquake reconnaissance of several major earthquakes has indicated various seismic damage and failure modes of seat-type abutments. The observed abutment damage and failure modes include large displacement and tilting of foundations (Jennings 1971; Sardo et al. 2006), local pounding damage and global failure of concrete backwall (Lee and Loh 2000; Sardo et al. 2006), excessive residual deformation of embankment soil (Lee and Loh 2000), displacement of approach slabs (Lee and Loh 2000), as well as shear key failure and superstructure unseating (Shamsabadi et al. 2007; Kawashima et al. 2011). As observed from the static and dynamic analysis results, similar limit states are expected to occur at the seat-type abutments of quasi-isolated bridges, which include closure of expansion joints and pounding between abutments and superstructures, rupture of bearing retainer anchors, sliding of elastomeric bearings, and inelastic deflection of steel H-piles. While these limit states are common to the majority of the prototype bridges, bearing unseating at abutments due to excessive sliding distance was only observed in a number of highly skew bridges

supported by tall piers.

In an attempt to improve bridge seismic performance in these two aspects, two preliminary recommendations for calibrating the current design strategy were proposed. The first one was to strengthen the bearing side retainers at the abutments of highly skewed bridges supported by tall piers. In the several bridge variants that experienced bearing unseating at their abutments, the fusing capacity of the retainer anchors was improved from the original 30% of the superstructure dead load on the bearing to around 90%. Comparative nonlinear dynamic analyses were performed to evaluate the proposed strengthening strategy and the results demonstrated that bearing unseating at the abutments of these bridges were prevented by strengthening the retainer anchorage. The other recommendation was to weaken the commonly over-designed superstructure-to-fixed-pier connections of non-skew or lightly-skewed bridges with short pier columns, in order to mitigate the column damage. Comparative dynamic analysis results demonstrated that when the connection fusing capacity was reduced from more than 40% to around 10% to 15% of the superstructure dead load on the connection, effective mitigation of the column damage was achieved in many bridge variants. For the heaviest four-span PPC-girder bridges, enlarged pier columns in conjunction with the weakened connections were found to significantly mitigate the column damage. For these long-span massive bridges, merely weakening the sacrificial connections seemed to be ineffective in mitigating the column damage.

7.3 Observations from Nonlinear Static Analyses

A series of multi-mode adaptive static pushover analyses were carried out on a number of prototype quasi-isolated bridges in the longitudinal and transverse directions. Bridge response characteristics including force distribution among substructures, sequence of component limit states, fusing performance of sacrificial superstructure-substructure connections, and vulnerability of critical bridge components were investigated.

7.3.1 Longitudinal pushover analyses

The following representative bridge responses were observed in the longitudinal pushover analyses:

- After closure of the expansion joint, the abutment that was pushed by the superstructure provided much larger resisting forces than the intermediate piers. Yielding of the piles supporting this abutment occurred shortly after the joint closure.

- For non-skew bridges, fusing of the sacrificial connections at the fixed pier was not observed in any longitudinal pushover analysis. This undesired fusing performance typically resulted in global yielding of the short fixed-pier columns. For highly skewed bridges, fusing of the sacrificial connections at the fixed pier was observed, but typically occurred after global yielding of the short fixed pier columns. This fusing and damaging sequence is undesired by the quasi-isolation strategy.

- For highly skewed bridges, the deck end that engaged with the skew abutment sustained coupled longitudinal and transverse displacements due to the oblique contact with the abutment. The displaced acute deck corner tended to drop off the abutment.

- The overall longitudinal stiffness of the four-span bridge is much larger than that of the counterpart three-span bridge. When pushed to a same superstructure displacement, larger forces were generally needed for a four-span bridge than for its equivalent three-span bridge. The overall longitudinal stiffness of the PPC-girder bridge is slightly larger than that of the counterpart steel-plate-girder bridge.

7.3.2 Transverse pushover analyses

The following representative bridge responses were observed in the transverse pushover analyses:

- Fusing of the bearing retainers at the abutments was commonly observed. After this fusing limit state, the acute deck corner of highly skewed bridges experienced large abutment-normal displacements and tended to drop off the abutment. In consistent with these re-

sponses, bearing unseating at abutments occurred exclusively in highly skewed bridges and in the abutment-normal direction, as observed in the dynamic bridge analyses.

- The intermediate piers typically withstood larger forces than the abutments, which was opposite to the force distribution among substructures observed in the longitudinal pushover analyses.

- The soft foundation soil was unfavorable to the fusing action of sacrificial superstructure-substructure connections at both the piers and abutments. The tall pier columns were unfavorable to the fusing of sacrificial connections at the piers. These trends were also clearly observed in the dynamic bridge analyses.

- For the asymmetric three-span bridges, the retainer anchors at abutments typically occurred first due to rotation of the bridge superstructure. In contrast, the first fusing limit state of the symmetric four-span bridges typically occurred at the connections between the superstructure and central fixed pier.

- Yielding of the substructure piles was commonly observed in the transverse pushover analyses. The substructure piles in the soft foundation soil typically yielded at a smaller superstructure pushover displacement than those in the hard soil. Consistent with this observation, it was noted in the dynamic analyses that the pier piles in the soft foundation soil were more susceptible to yielding than those in the hard soil.

- Similar to the observation from longitudinal pushover analyses, the overall transverse stiffness of the four-span bridge is much larger than that of the counterpart three-span bridge. The overall transverse stiffness of the PPC-girder bridge is slightly larger than that of the counterpart steel-plate-girder bridge.

7.4 Observations from Eigenvalue Modal Analyses

During each pushover analysis, multiple eigenvalue analyses were performed to capture the instantaneous modal response characteristics at both the elastic and inelastic bridge deformation states. The following modal response characteristics were observed:

- The predominant mode (the mode with the largest effective modal mass) in the longitudinal or transverse direction was typically the first or second mode, regardless of the bridge deformation state. Consistently, the earthquake-resisting system design strategy is generally intended for common bridge types whose first mode of vibration dominates the seismic response (Tobias et al. 2008; IDOT 2012a).

- In the longitudinal direction, the effective modal mass of only the predominant mode was typically sufficient to incorporate the superstructure mass. In the transverse direction, the effective modal mass of the predominant one or two modes were sufficient to incorporate the superstructure mass.

- The period of the predominant mode was globally elongated as the bridge deformation increased, although there can be some local shortening effect along the way.

- For many bridge variants, the median periods of the longitudinal and transverse predominant modes were close to each other, which means that the bridges tend to be subjected to similar seismic force demands in the two horizontal directions.

7.5 Observations from Nonlinear Dynamic Analyses

7.5.1 Displacement and rotation of superstructures

In general, the peak superstructure center displacements increased with the superstructure mass among the four major bridge types. The peak superstructure rotations of the four-span bridges were much smaller than those of the three-span bridges. Tall-pier bridges sustained much larger superstructure displacements and rotations than their short-pier equivalent bridges. Bridges in the soft foundation soil generally experienced larger superstructure displacements than those in the hard soil, but the influence of foundation soil on the superstructure rotation appeared to be insignificant. For the left-skewed bridges considered in this study, the peak deck rotations in the clockwise direction were typically larger than those in the counterclockwise direction. For tall-pier bridges, a positive correlation between the bridge skew and peak deck rotation was observed in all

the four types of bridges. However, for short-pier bridges, the effect of bridge skew on peak deck rotations was insignificant.

7.5.2 Fusing of sacrificial connections

Except the four-span PPC-girder bridges, fusing of the bearing retainers at the abutments occurred much more than fusing of the sacrificial connections at the intermediate piers. For the four-span PPC-girder bridges, fusing of steel dowel connections at the fixed piers occurred in more analyses than fusing of the abutment bearing retainers. Bearing retainer fusing at the expansion piers was not observed in any dynamic analysis.

Fusing of the steel fixed bearings at the fixed piers of steel-plate-girder bridges was not common, which occurred in only 4% and 12% of the three-span and four-span steel-plate-girder bridge analyses, respectively. By contrast, fusing of the steel dowel connections at the fixed piers of PPC-girder bridges was more common, which occurred in 19% and 33% of the three-span and four-span PPC-girder bridge analyses, respectively.

It was also noted that all the fusing limit states occurred more in the presence of the hard foundation soil than the soft soil. A similar trend was also observed in the transverse pushover analyses. The tall pier columns were unfavorable to the fusing of sacrificial connections at the piers, which was also observed in the transverse pushover analyses. Highly skewed bridges were more prone to bearing retainer fusing at the abutments than the equivalent bridges with smaller skews. Similarly, fusing of the sacrificial connections at the fixed piers occurred more in highly skewed bridges than in bridges with smaller skews.

7.5.3 Unseating of elastomeric bearings

Overall, unseating of bearings at substructures occurred very rarely in the dynamic bridge analyses. Bearing unseating at the piers was not observed in any analysis, while that at the abutments was observed in only 14 out of the 6,400 analyses. All of these 14 analyses were performed on highly skewed bridges supported by tall pier columns. The elastomeric bearing at their acute deck corner unseated in the abutment-normal direction, when subjected to transverse or 45° ground motions.

This tendency was consistent with the transverse pushover response of highly skewed bridges.

7.5.4 Damaging to pier columns

For both the fixed and expansion piers, statistical results clearly demonstrated a positive correlation between the superstructure mass and pier column damage. As the superstructure mass increased from the three-span steel-plate-girder to four-span PPC-girder bridges, severer damage to the columns of both the expansion and fixed piers was observed.

The other general observation is that the fixed pier columns sustained severer seismic damage than the expansion pier columns, in terms of yielding of reinforcing steel and crushing of concrete cover at pier column bases. The expansion pier columns were generally well isolated and basically did not experience concrete cover crushing, except those of some four-span PPC-girder bridges. In contrast, concrete cover crushing at the fixed pier columns was observed in many three-span PPC-girder, four-span steel-plate-girder, and four-span PPC-girder bridges. For a number of non-skew or lightly skewed four-span PPC-girder bridges supported by short pier columns, severe damage to the concrete cover at column bases was observed, which might not be easily repairable.

The short pier columns generally sustained much severer damage than the tall columns. It was also noted that the columns of tall expansion piers were typically damaged more than those of short expansion piers. In contrast, the columns of short fixed piers sustained severer damage than those of tall fixed piers.

7.5.5 Yielding of foundation piles

Yielding of the abutment piles was quite commonly observed in all the four types of bridges. Yielding of the expansion-pier piles occurred less than that of the fixed-pier piles. The piles supporting the intermediate piers in the soft foundation soil were more susceptible to yielding than those in the hard soil. This trend was also observed in the transverse pushover analyses.

7.6 Future Research Needs

On the basis of the presented research, a number of future research needs are proposed for further investigation and improvement of the current quasi-isolation earthquake-resistant bridge design strategy.

- In the prototype configuration of quasi-isolated bridges, bearing retainers are employed at the substructures to prevent bearing unseating, while concrete shear keys are not used as motion-limiting devices for the bearings and girders. Since the highly skewed and tall-pier bridges are susceptible to bearing unseating at their abutments, concrete shear keys could be employed as a second line of defense against excessive bearing sliding and unseating.

- The current grillage superstructure model consisting of many elastic beam elements that may take considerable computational resource in the bridge analysis. Since the superstructure of quasi-isolated bridges is typically intended to stay essentially elastic during earthquake events, a more simplified and economical superstructure model, such as the so-called "spine model" that uses only one line of beam elements to represent the entire superstructure, could be studied and implemented into the global bridge model if it would not lose important aspects of interested bridge response.

- The detailed nonlinear finite-element full bridge model presented in the dissertation was developed for high-fidelity assessment of bridge seismic response. However, a much simplified bridge model would be more helpful for the design work of practicing bridge engineers with limited computational resource. Development of such a simplified bridge model from the detailed model could be investigated in the future research.

- The main purpose of the quasi-isolation design strategy is to achieve, at least, some of the desired isolation effects of conventionally isolated bridges that are typically designed for high seismic regions. Unlike the conventionally isolated bridges that typically employ specially designed isolation bearing and damper devices, the quasi-isolated bridges employ economical and non-seismically designed bearing components. A direct and comprehensive comparison between the isolation performance and construction cost of quasi-isolated and

conventionally isolated bridges would provide insight into the efficiency of the quasi-isolated bridges.

- Although the study considers prototype bridges with a wide variety of configurations, some common bridge configurations are not included in the study, such as curved bridges and bridges with unequal pier column heights. These bridges may possess unique seismic response characteristics and could be investigated in future research.

- It was claimed that the ratio of deck width to length can affect the in-plane rotational response of skew bridges (Kawashima et al. 2011). The effect of deck width on the seismic response of quasi-isolated bridges, especially skew ones, needs to be investigated in the future research.

- The ground motions used in this study are site-specific motions that are developed for the unique seismicity and geotechnical conditions of southern Illinois area. The ground motions in the west coastal regions may possess different spectral characteristics and intensities, which can result in some different bridge responses. The general efficacy and applicability of the quasi-isolation strategy for protecting bridges that are subjected to site-specific ground motions in the west coastal regions can be investigated in the future.

- The water table of bridge foundation soil may vary in different seasons and weather conditions. The water table affects the effective weight and strength of the foundation soil and may further affect bridge seismic response. In future research, seismic response of bridges with different foundation soil water table can be studied.

APPENDIX A

PROTOTYPE BRIDGE PARAMETERS

Table A.1: Component mass of prototype bridges (units: 10^3 kg)

Bridge	3S00P15H	4S00P15H	3C00P15H	4C00P15H
Superstructure	1197	2758	1680	3949
Abutments				
Backwall	48	72	58	76
Pile cap	128	128	128	128
Wingwall	54	78	62	81
Approach slab	206	206	206	206
Pile body (6.1 m)	12	14	14	18
Piers				
Pier cap	117	176	117	176
Pier column	79	117	79	117
Pile cap	240	360	240	386
Pile body (6.1 m)	19	38	21	48
Soil around piles	189	280	193	347
Total mass	2289	4227	2798	5532
Total mass in computer model	2288	4231	2797	5535

Table A.2: Girder reaction and sizing of bearing components of 3S bridges

	Abutment	Expansion pier	Fixed pier
$R_{DC1} + R_{DC2}$ (kips)	31	130	130
R_{DW} (kips)	15	43	43
R_{LL} (kips)	62	130	130
Expansion length (ft)	200	120	N.A.
Bearing size	11-d	18-a	N.A.
No. of anchor per retainer	1	1	N.A.
Dia. of retainer anchor (in.)	1	1.5	N.A.
No. of anchor per fixed bearing	N.A.	N.A.	2
Dia. of fixed bearing anchor (in.)	N.A.	N.A.	1.5

Table A.3: Girder reaction and sizing of bearing components of 4S bridges

	Abutment	Expansion pier	Fixed pier
$R_{DC1} + R_{DC2}$ (kips)	70	180	180
R_{DW} (kips)	17	53	48
R_{LL} (kips)	74	152	175
Expansion length (ft)	305	160	N.A.
Bearing size	15-e	20-a	N.A.
No. of anchor per retainer	1	1	N.A.
Dia. of retainer anchor (in.)	1.25	2	N.A.
No. of anchor per fixed bearing	N.A.	N.A.	4
Dia. of fixed bearing anchor (in.)	N.A.	N.A.	1.25

Table A.4: Girder reaction and sizing of bearing components of 3C bridges

	Abutment	Expansion pier (Abut. side)	Expansion pier (Pier side)	Fixed pier
R_{DC1} (kips)	65.5	65.5	98	164
R_{DC2} (kips)	6	7.5	7.5	15
R_{DW} (kips)	15	21.5	21.5	43
R_{LL} (kips)	62	65	65	130
Expansion length (ft)	200	120	120	N.A.
Bearing size	12-e	13-b	13-b	N.A.
No. of anchor per retainer	1	1	1	2
Dia. of retainer anchor (in.)	1.25	1.25	1.25	1.5
No. of anchor per fixed bearing	N.A.	N.A.	N.A.	
Dia. of fixed bearing anchor (in.)	N.A.	N.A.	N.A.	

Table A.5: Girder reaction and sizing of bearing components of 4C bridges

	Abutment	Expansion pier (Abut. side)	Expansion pier (Pier side)	Fixed pier
R_{DC1} (kips)	122.5	122.5	135.4	271.5
R_{DC2} (kips)	2.3	3.6	3.6	6.5
R_{DW} (kips)	17	26	26	48
R_{LL} (kips)	74	76	76	175
Expansion length (ft)	305	160	160	N.A.
Bearing size	15-e	15-b	15-b	N.A.
No. of anchor per retainer	1	1	1	2
Dia. of retainer anchor (in.)	1.5	1.5	1.5	1.5
No. of anchor per fixed bearing	N.A.	N.A.	N.A.	
Dia. of fixed bearing anchor (in.)	N.A.	N.A.	N.A.	

APPENDIX B

TIME HISTORIES AND RESPONSE SPECTRA OF EARTHQUAKE GROUND MOTIONS

As introduced in Section 6.1, a suite of 20 site-specific earthquake ground motion time histories with a 1,000-year return period for Cairo, Illinois was developed by Kozak et al. (2016). The time history, 5%-damping elastic pseudo-acceleration spectrum, pseudo-velocity spectrum, and displacement spectrum of each ground motion are illustrated in this appendix.

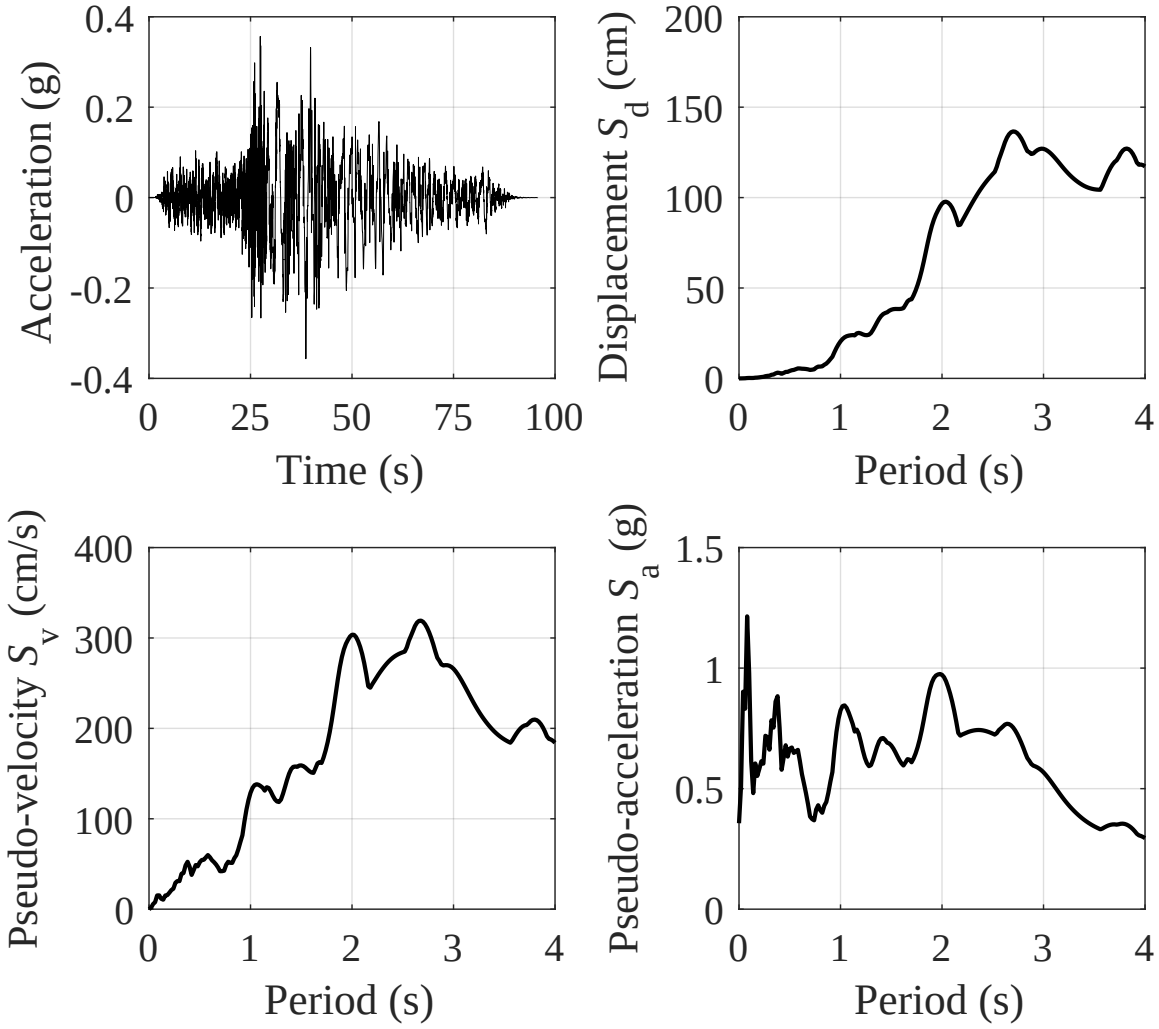

Figure B.1: Time history, 5%-damped pseudo-acceleration spectrum, pseudo-velocity spectrum, and displacement spectrum of earthquake ground motion Cro01

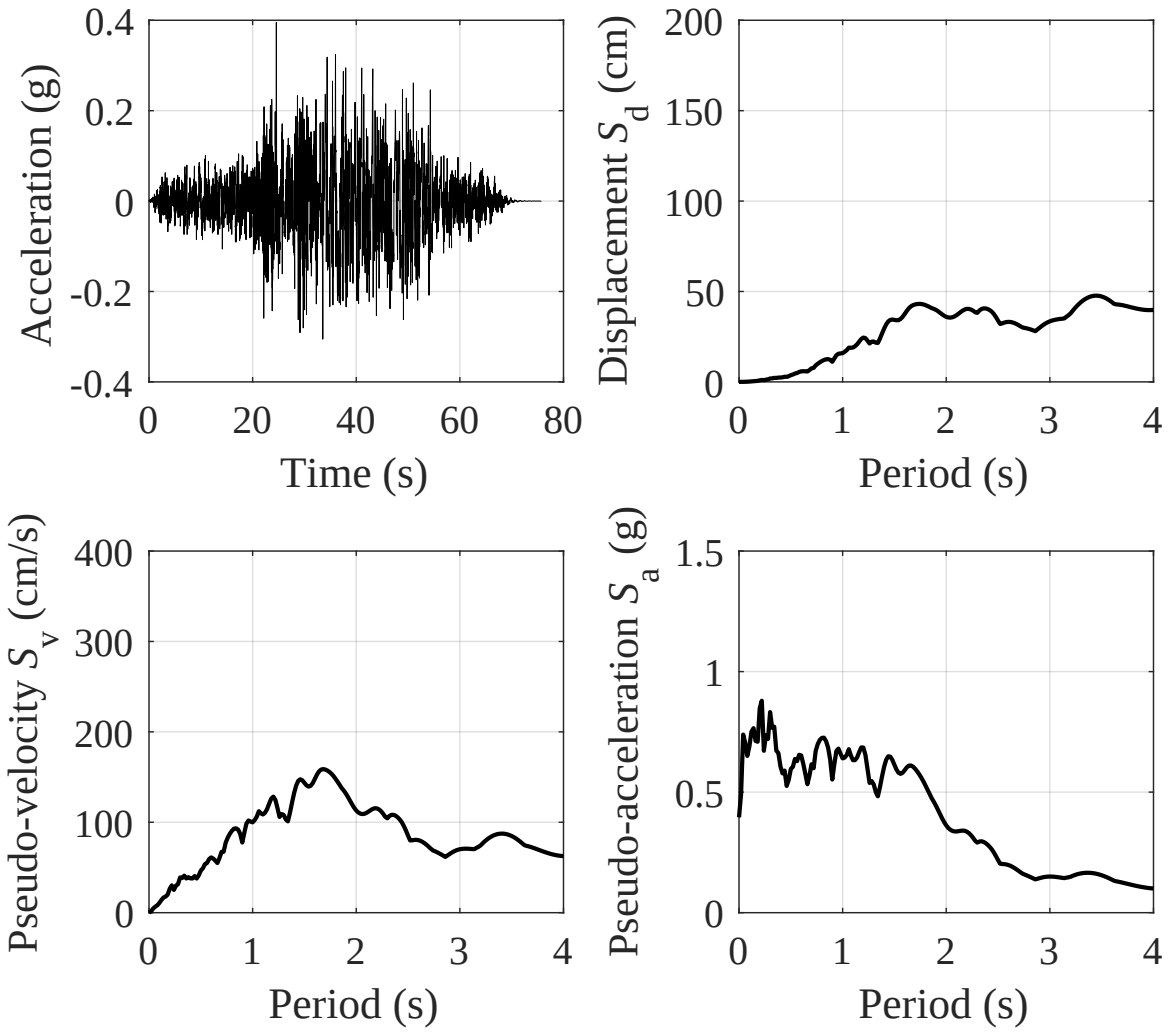

Figure B.2: Time history, 5%-damped pseudo-acceleration spectrum, pseudo-velocity spectrum, and displacement spectrum of earthquake ground motion Cro02

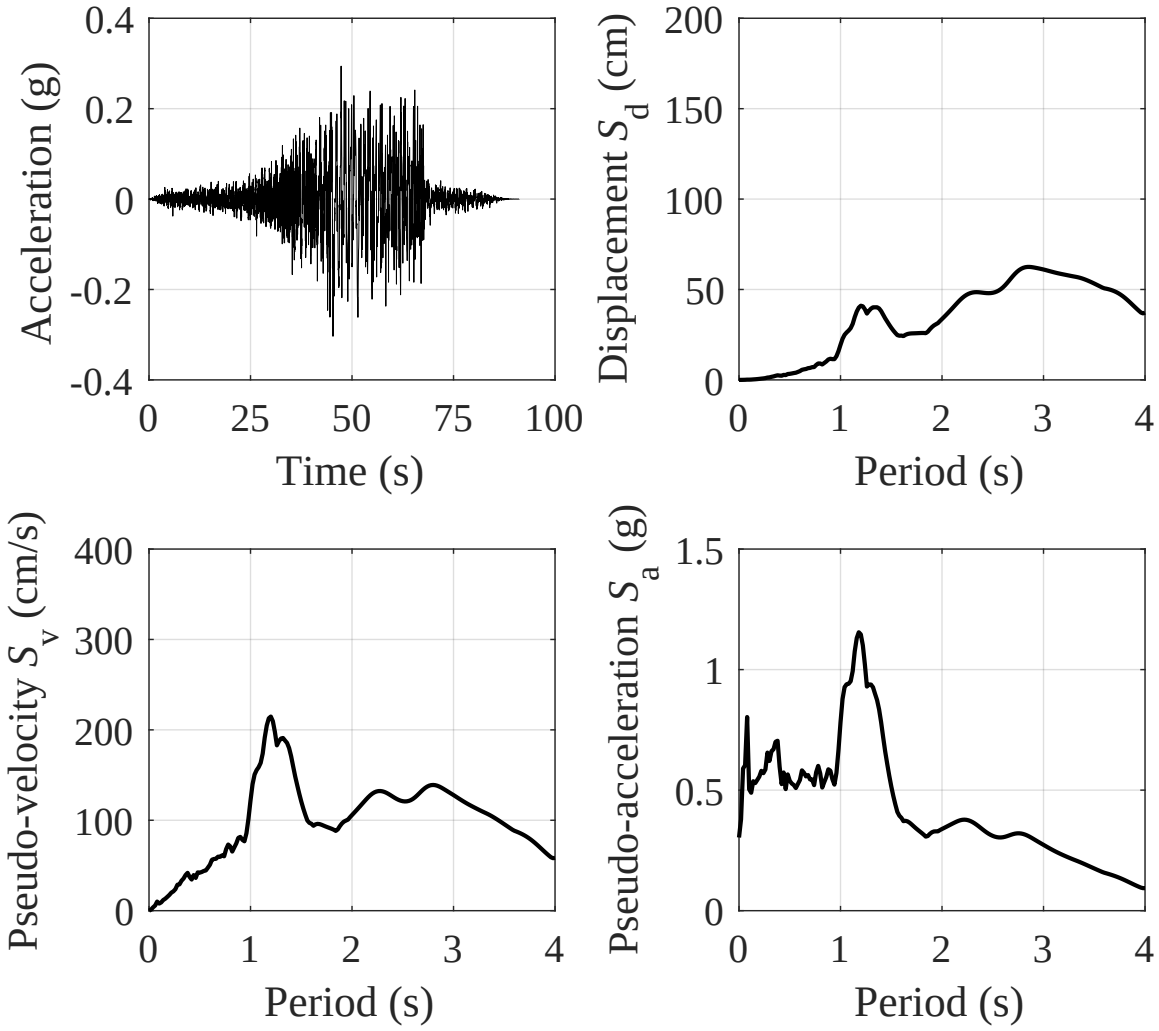

Figure B.3: Time history, 5%-damped pseudo-acceleration spectrum, pseudo-velocity spectrum, and displacement spectrum of earthquake ground motion Cro03

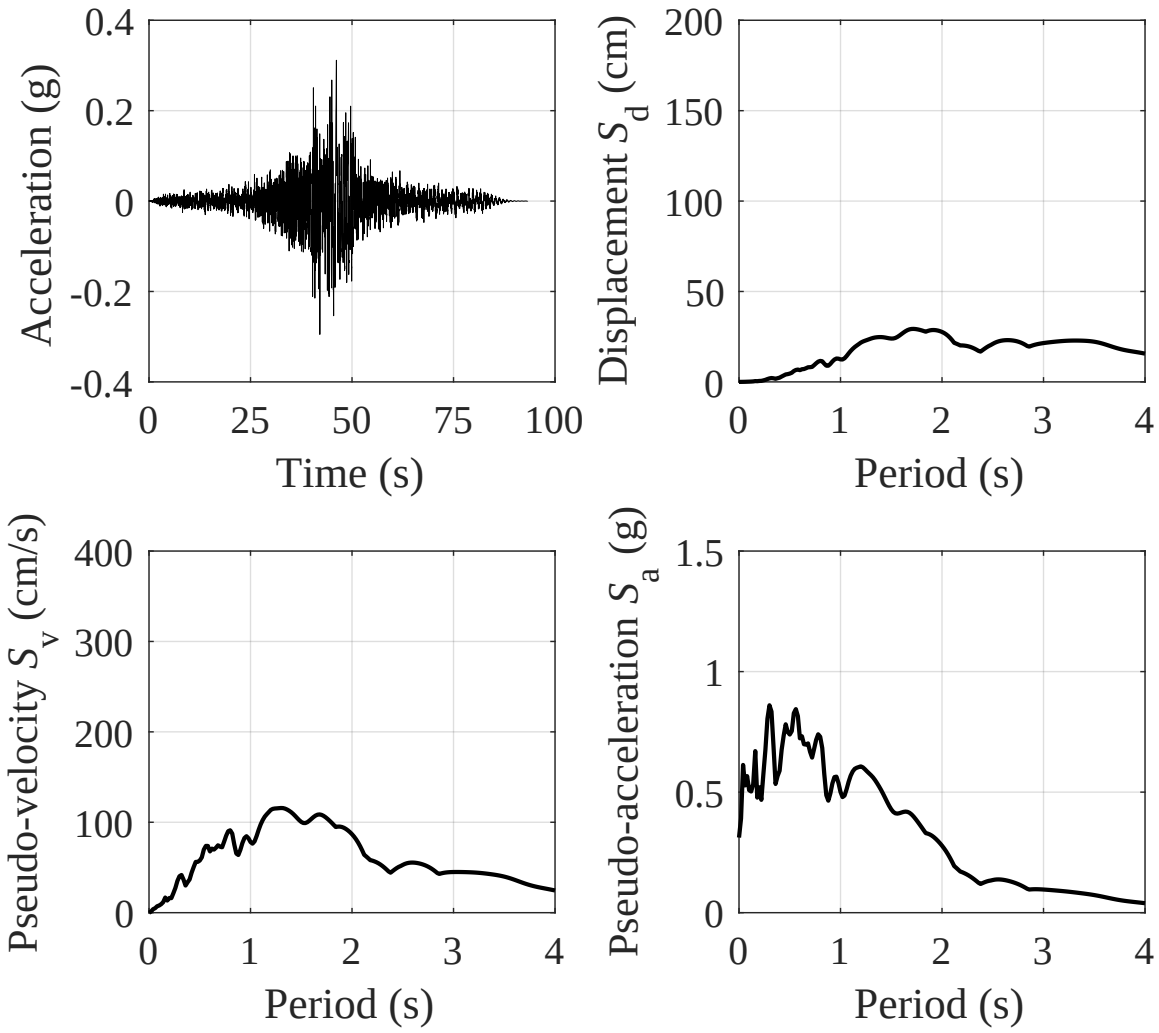

Figure B.4: Time history, 5%-damped pseudo-acceleration spectrum, pseudo-velocity spectrum, and displacement spectrum of earthquake ground motion Cro04

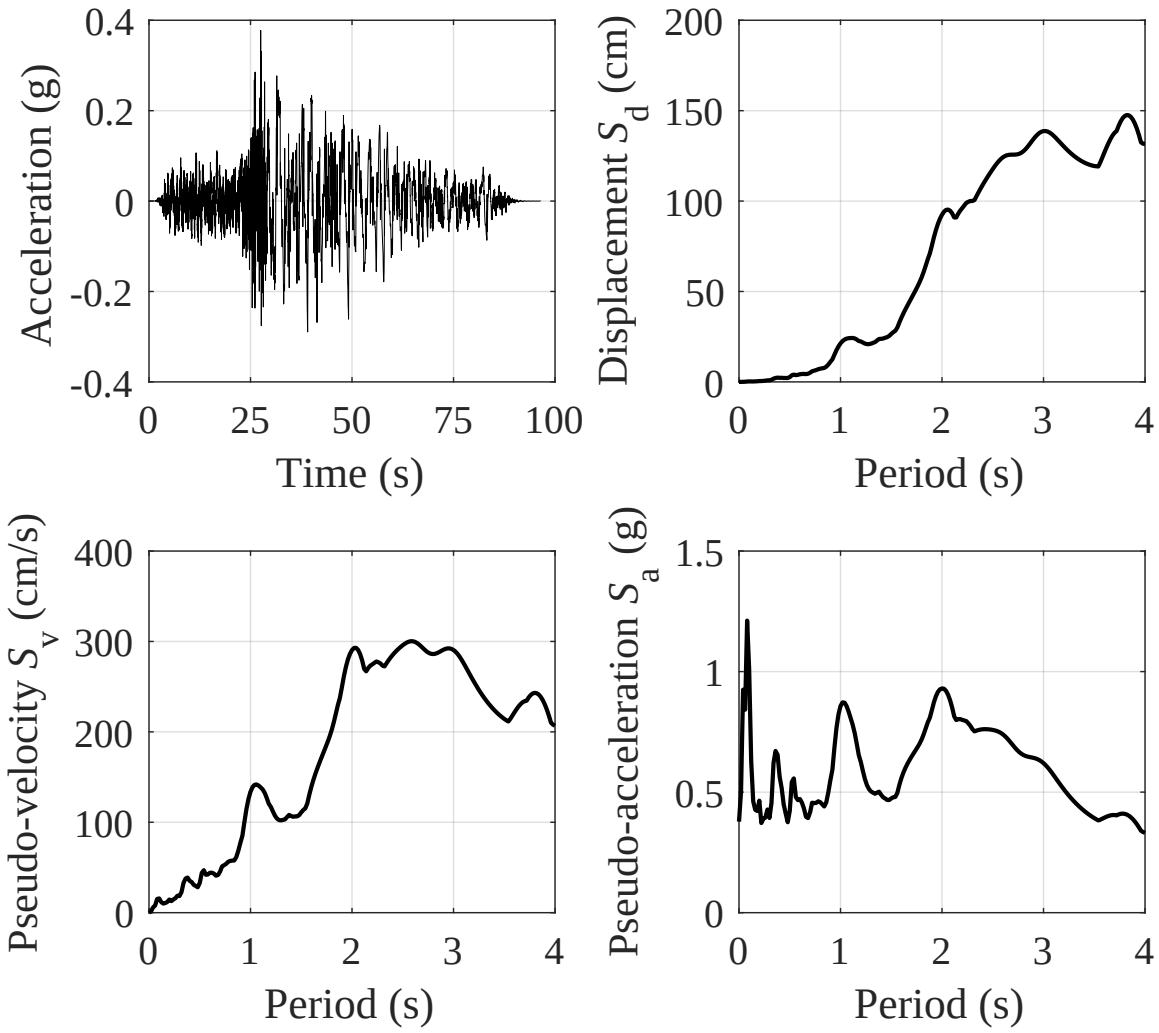

Figure B.5: Time history, 5%-damped pseudo-acceleration spectrum, pseudo-velocity spectrum, and displacement spectrum of earthquake ground motion Cro05

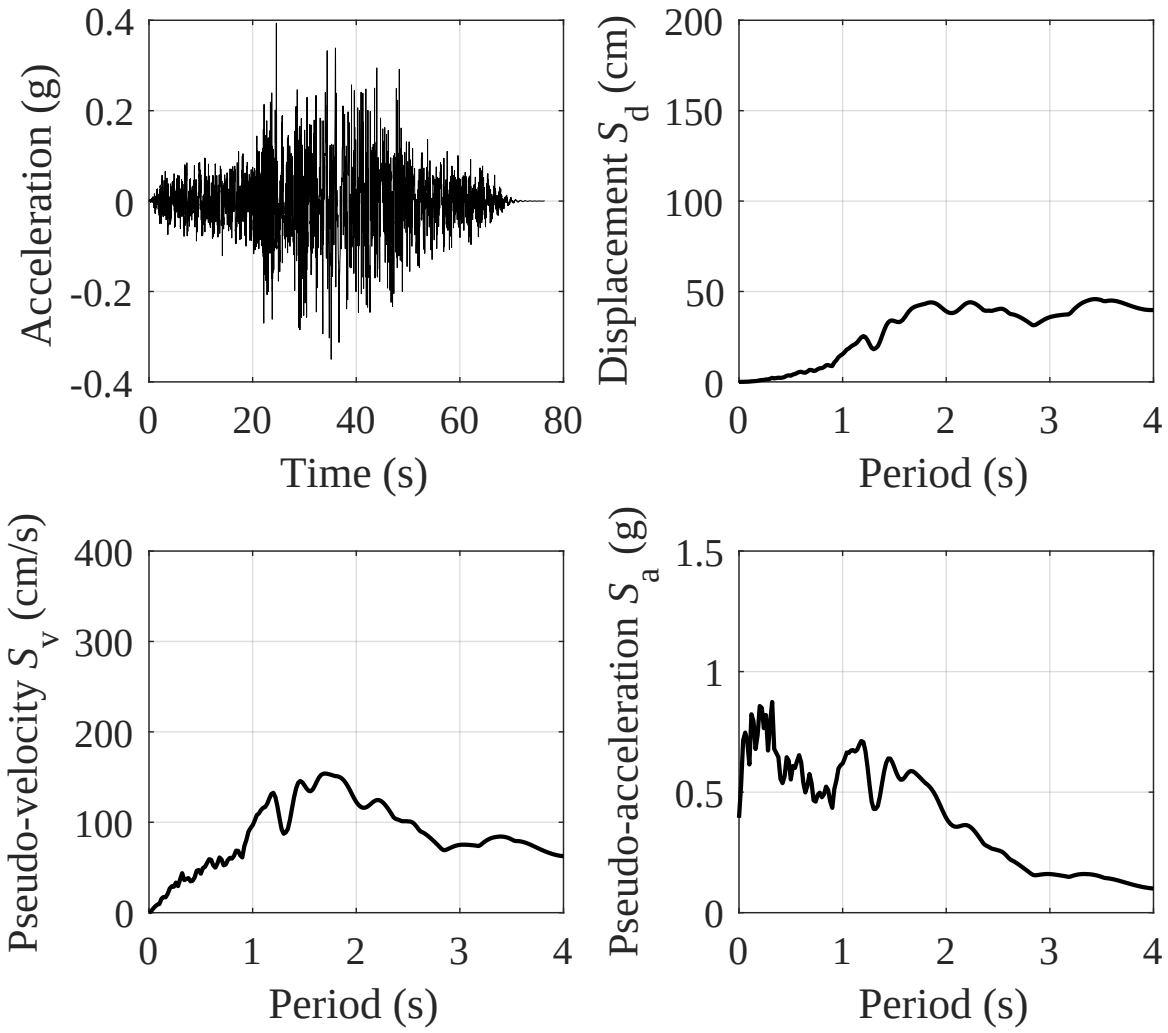

Figure B.6: Time history, 5%-damped pseudo-acceleration spectrum, pseudo-velocity spectrum, and displacement spectrum of earthquake ground motion Cro06

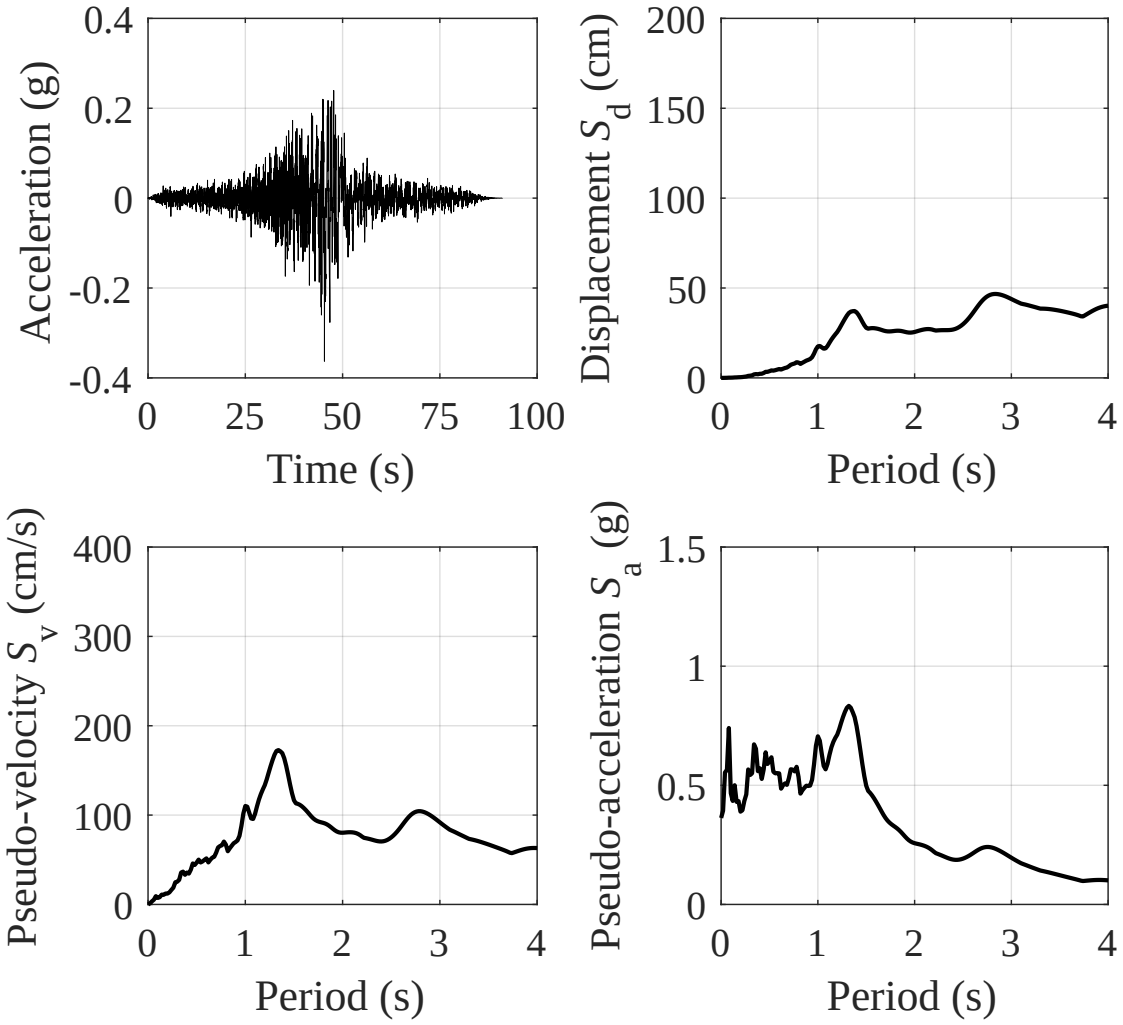

Figure B.7: Time history, 5%-damped pseudo-acceleration spectrum, pseudo-velocity spectrum, and displacement spectrum of earthquake ground motion Cro07

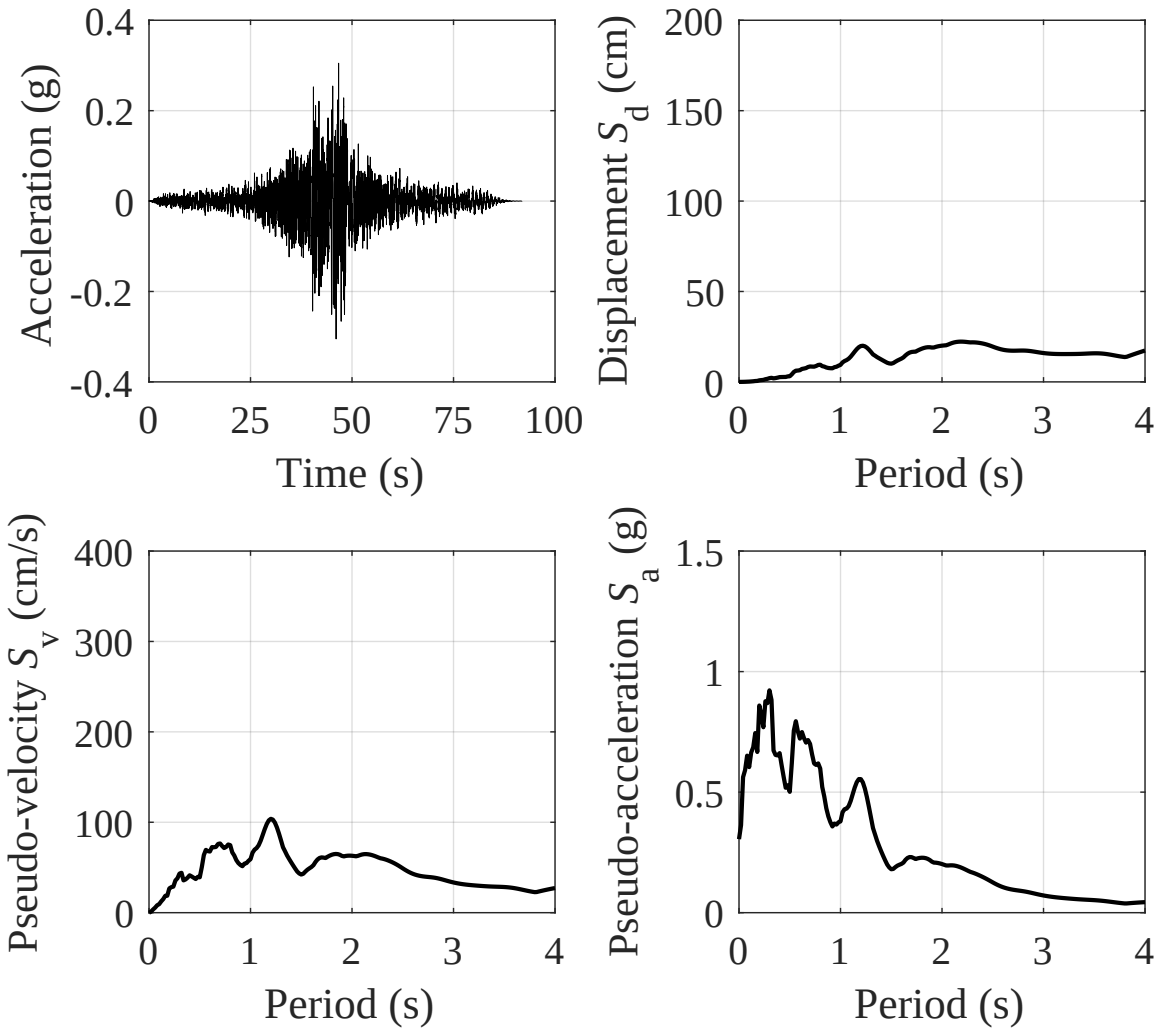

Figure B.8: Time history, 5%-damped pseudo-acceleration spectrum, pseudo-velocity spectrum, and displacement spectrum of earthquake ground motion Cro08

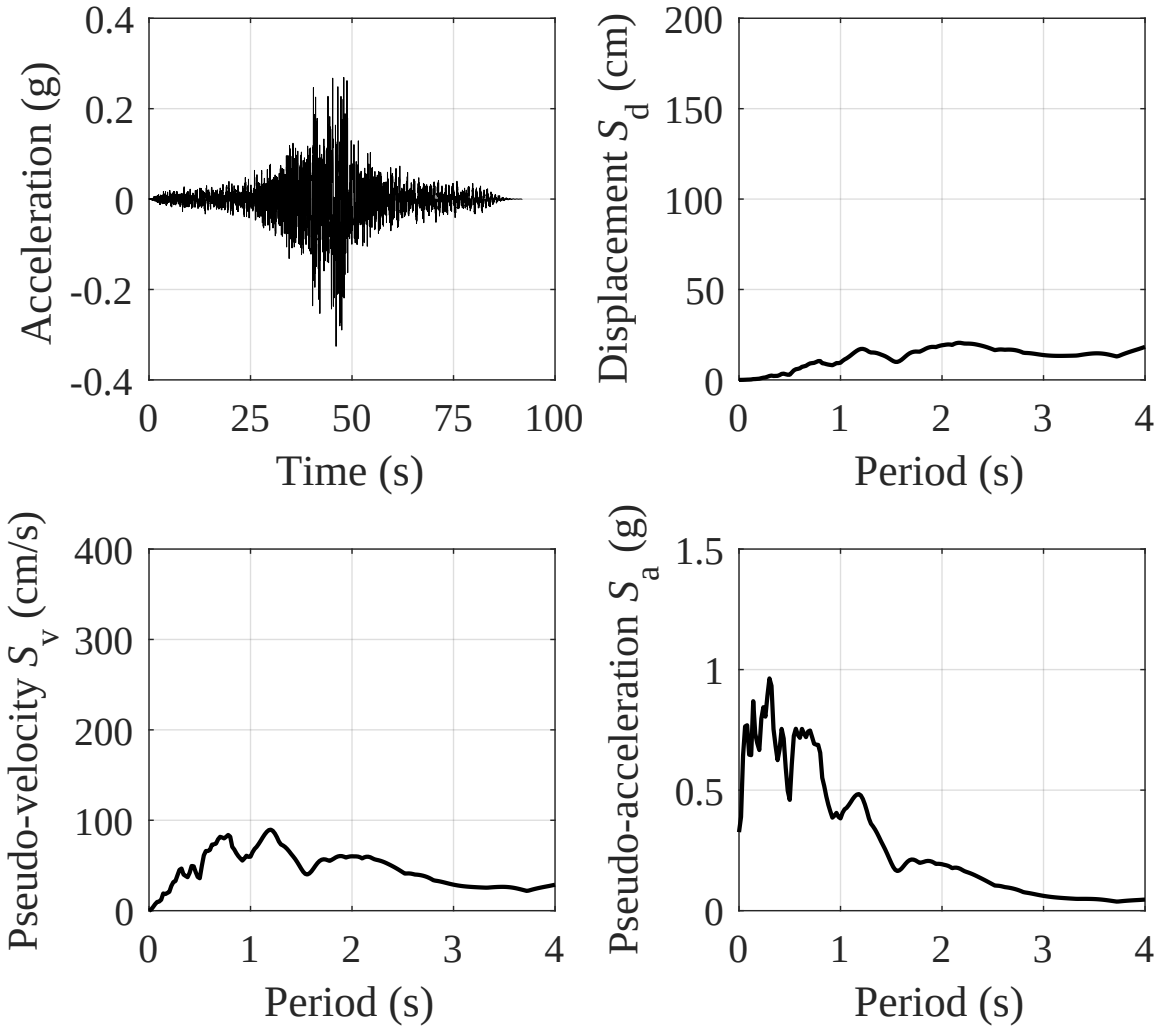

Figure B.9: Time history, 5%-damped pseudo-acceleration spectrum, pseudo-velocity spectrum, and displacement spectrum of earthquake ground motion Cro09

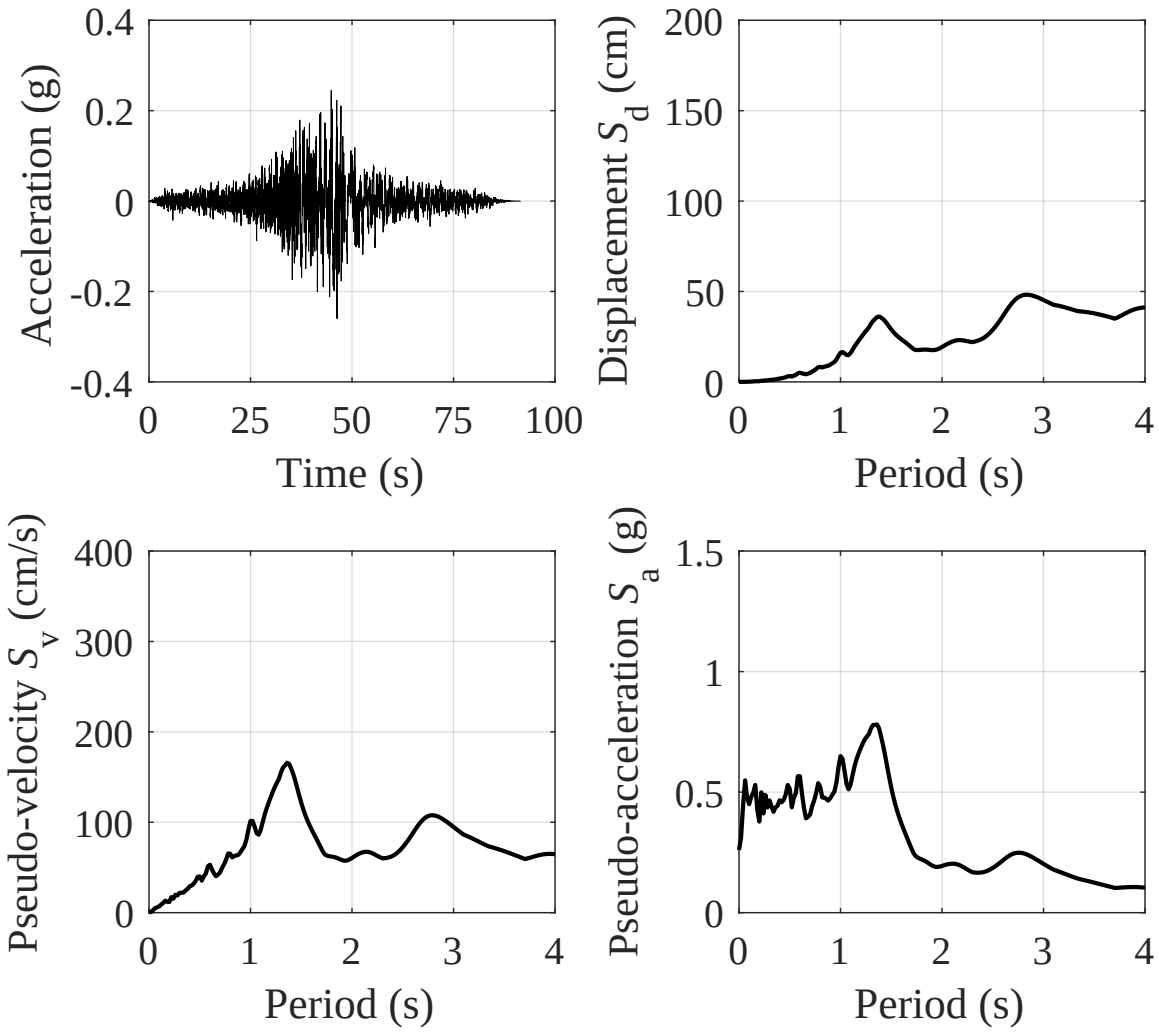

Figure B.10: Time history, 5%-damped pseudo-acceleration spectrum, pseudo-velocity spectrum, and displacement spectrum of earthquake ground motion Cro10

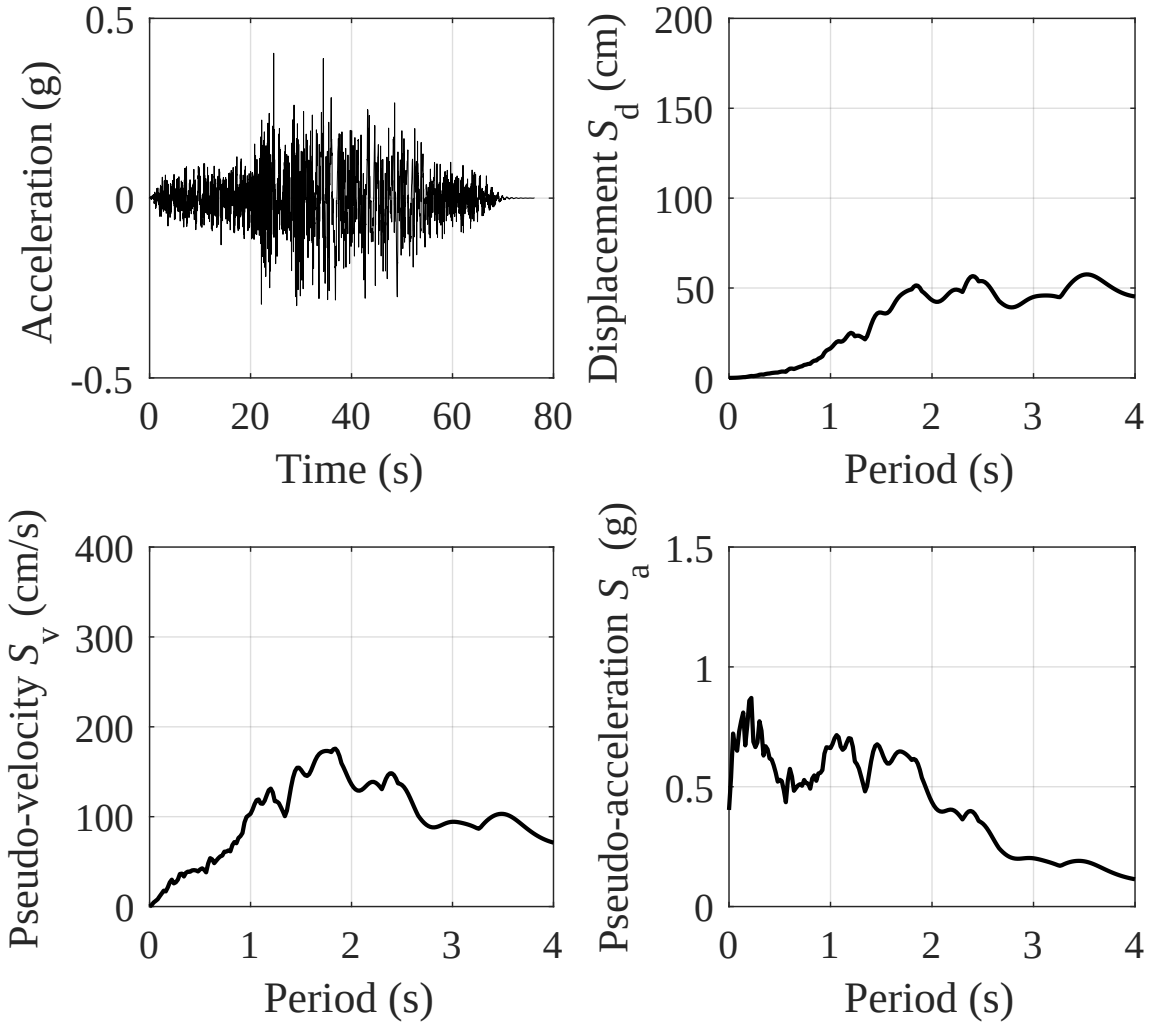

Figure B.11: Time history, 5%-damped pseudo-acceleration spectrum, pseudo-velocity spectrum, and displacement spectrum of earthquake ground motion Cro11

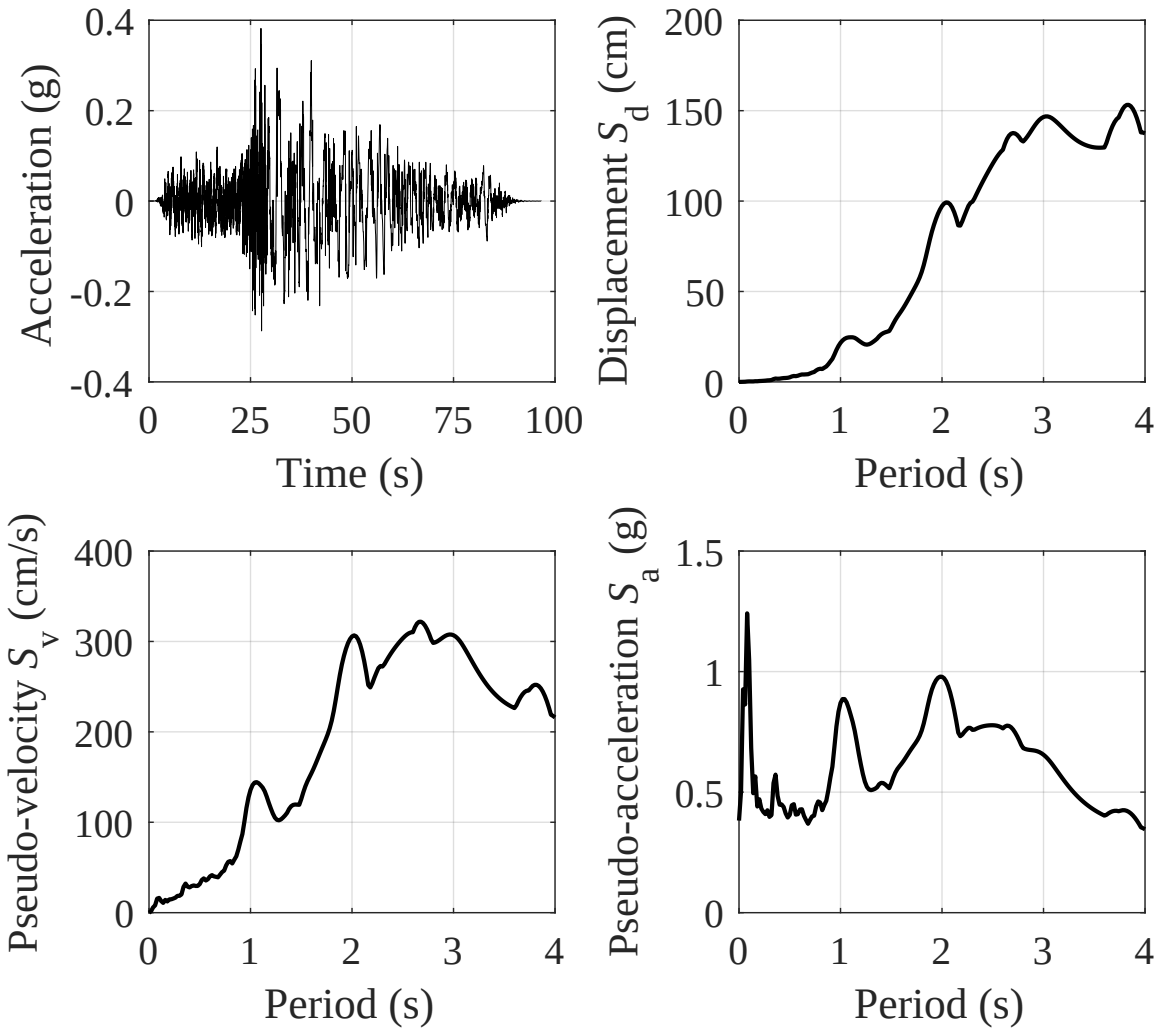

Figure B.12: Time history, 5%-damped pseudo-acceleration spectrum, pseudo-velocity spectrum, and displacement spectrum of earthquake ground motion Cro12

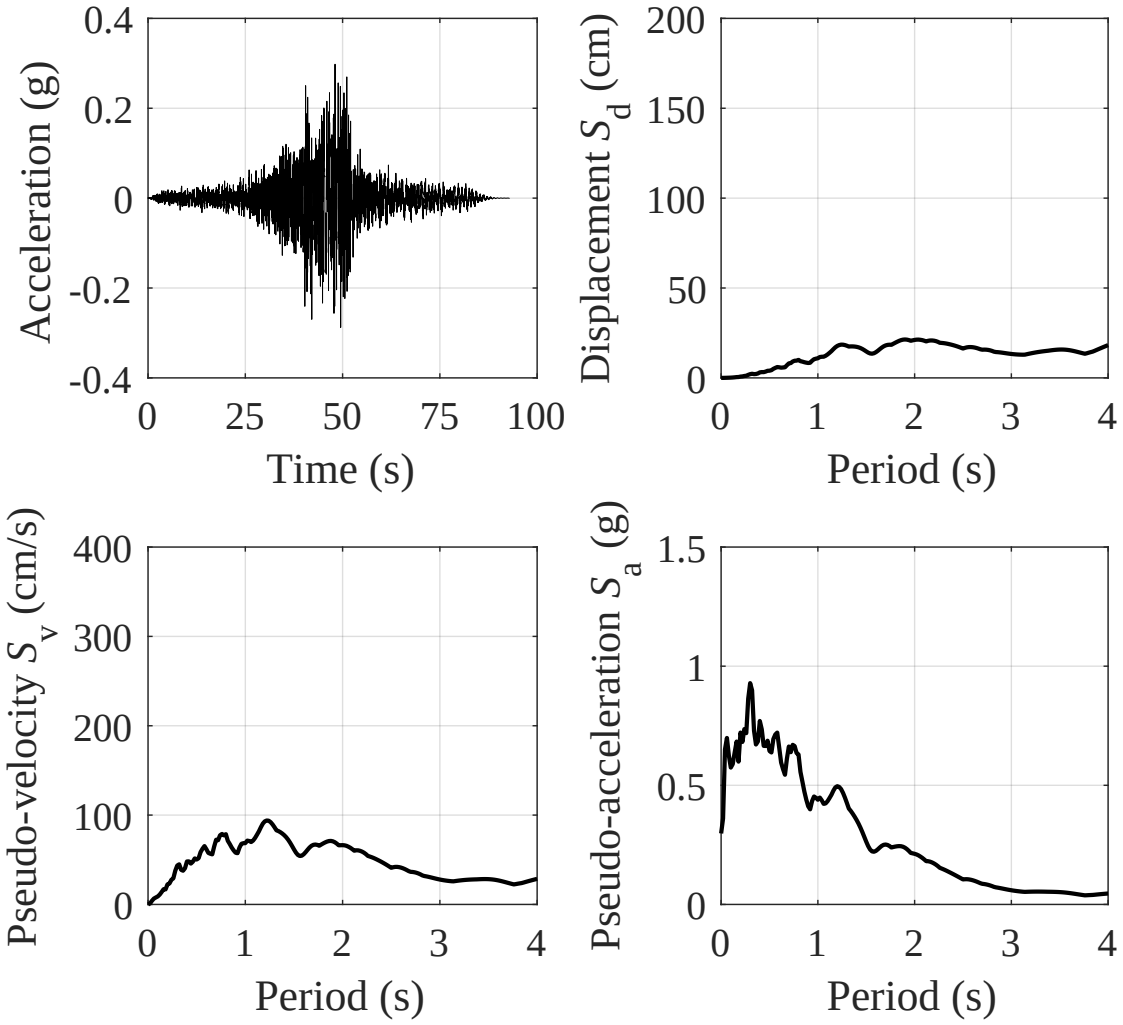

Figure B.13: Time history, 5%-damped pseudo-acceleration spectrum, pseudo-velocity spectrum, and displacement spectrum of earthquake ground motion Cro13

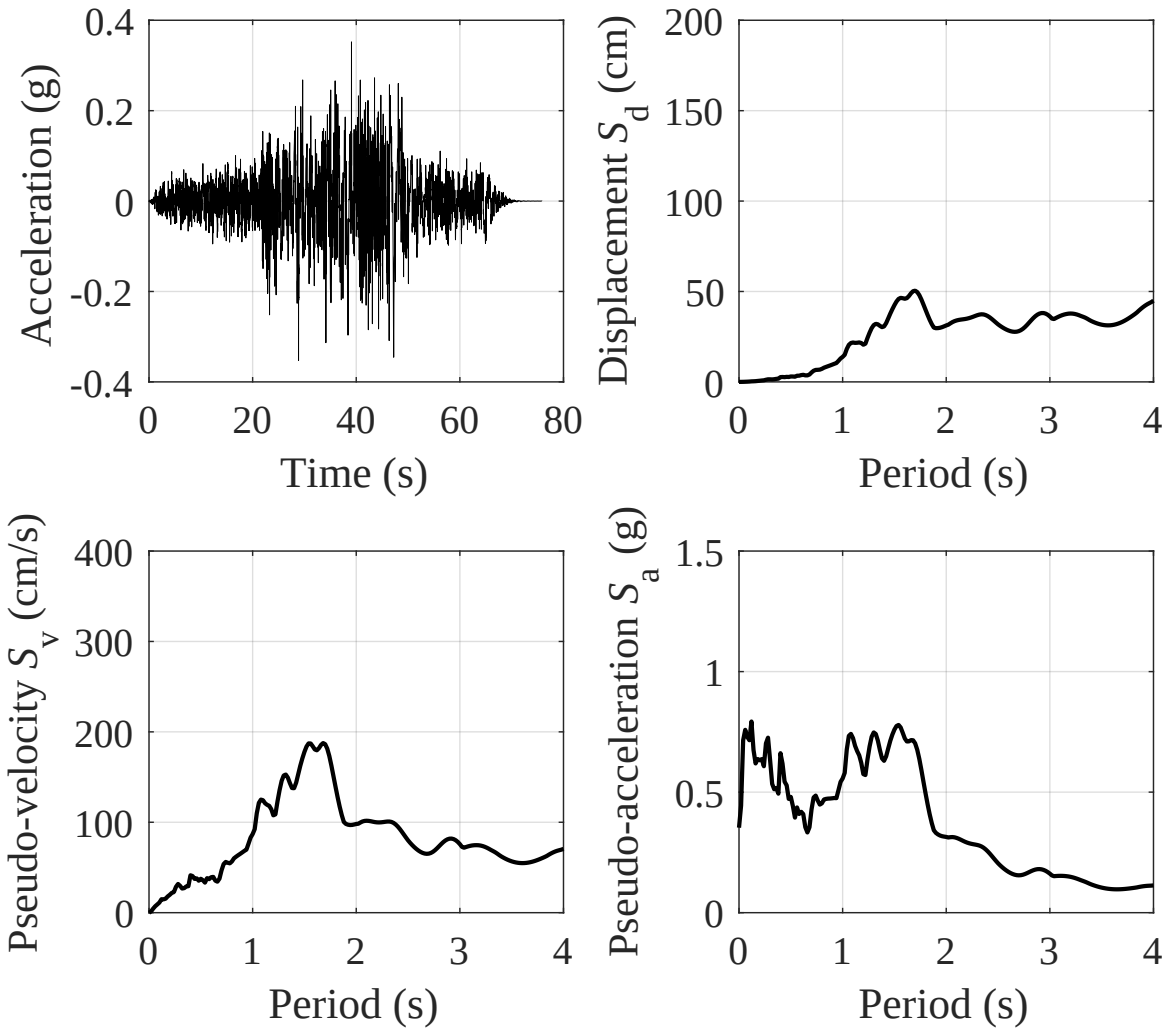

Figure B.14: Time history, 5%-damped pseudo-acceleration spectrum, pseudo-velocity spectrum, and displacement spectrum of earthquake ground motion Cro14

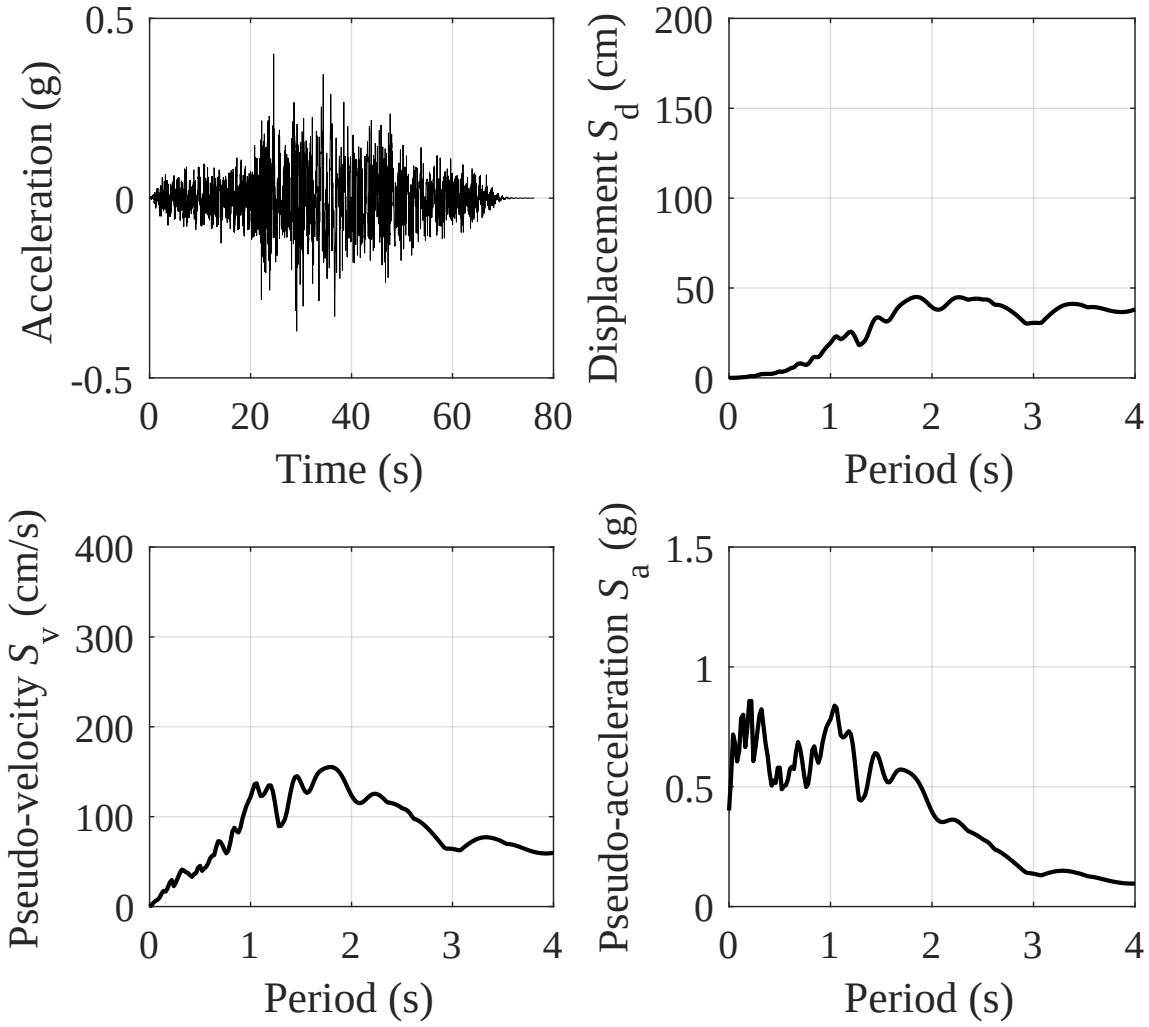

Figure B.15: Time history, 5%-damped pseudo-acceleration spectrum, pseudo-velocity spectrum, and displacement spectrum of earthquake ground motion Cro15

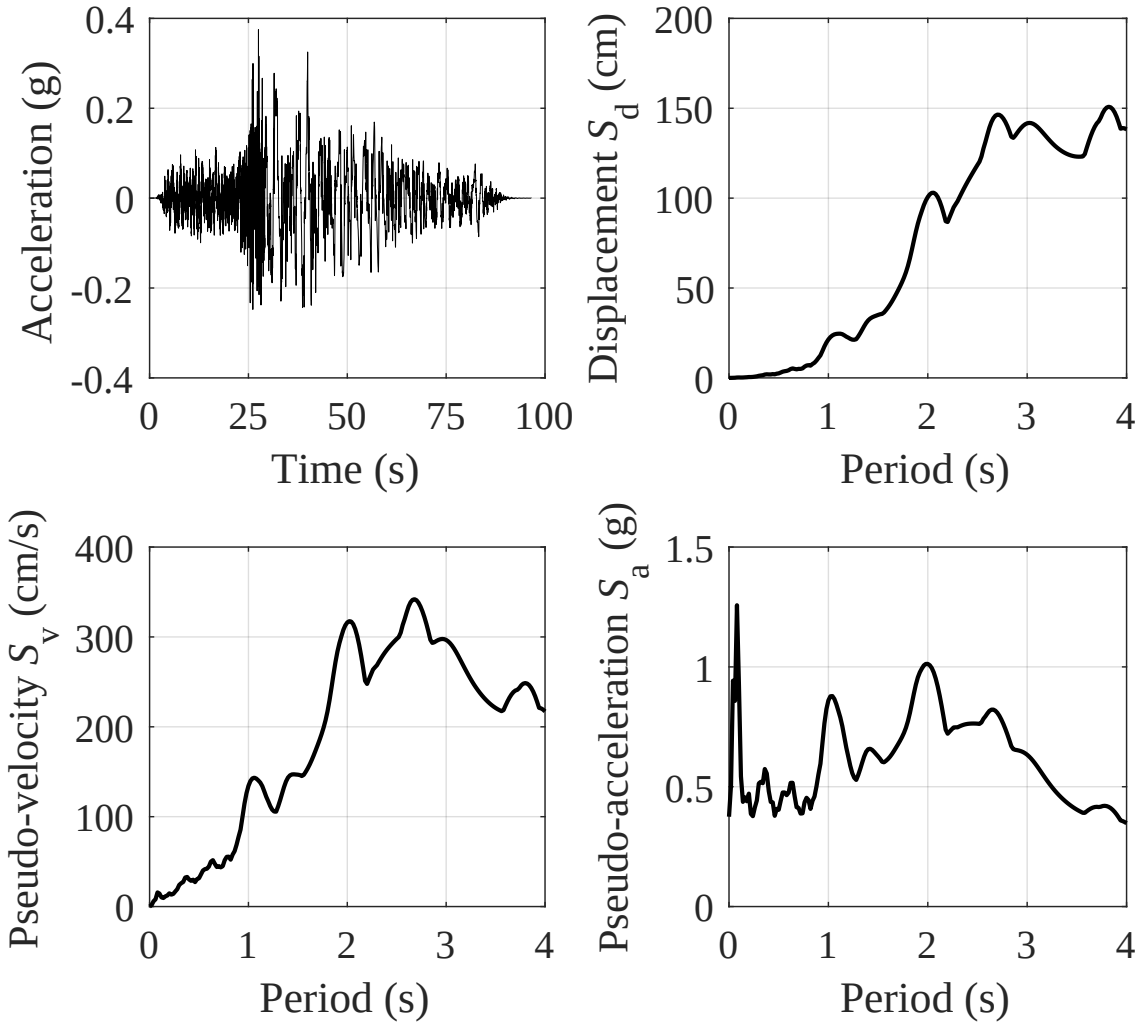

Figure B.16: Time history, 5%-damped pseudo-acceleration spectrum, pseudo-velocity spectrum, and displacement spectrum of earthquake ground motion Cro16

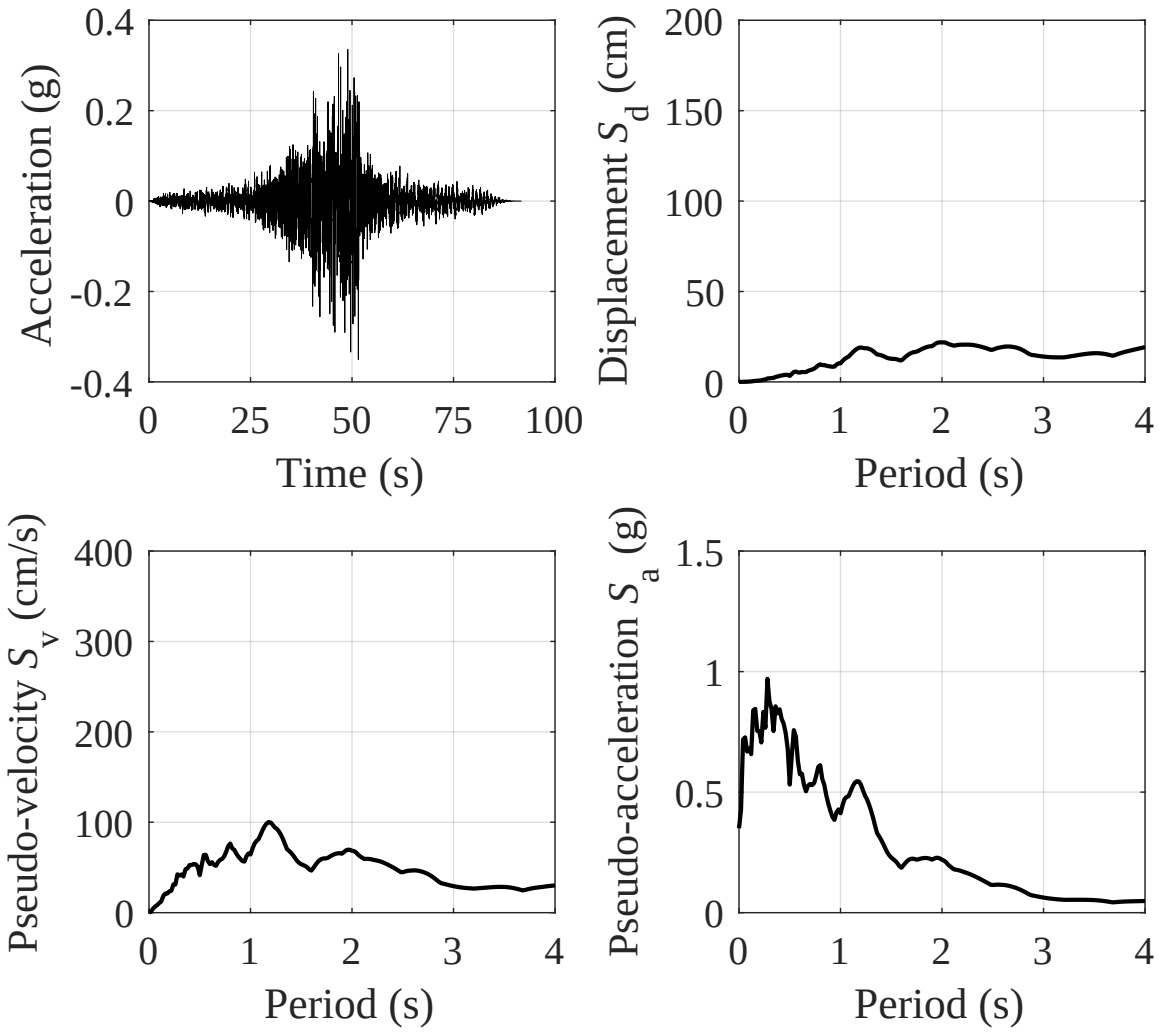

Figure B.17: Time history, 5%-damped pseudo-acceleration spectrum, pseudo-velocity spectrum, and displacement spectrum of earthquake ground motion Cro17

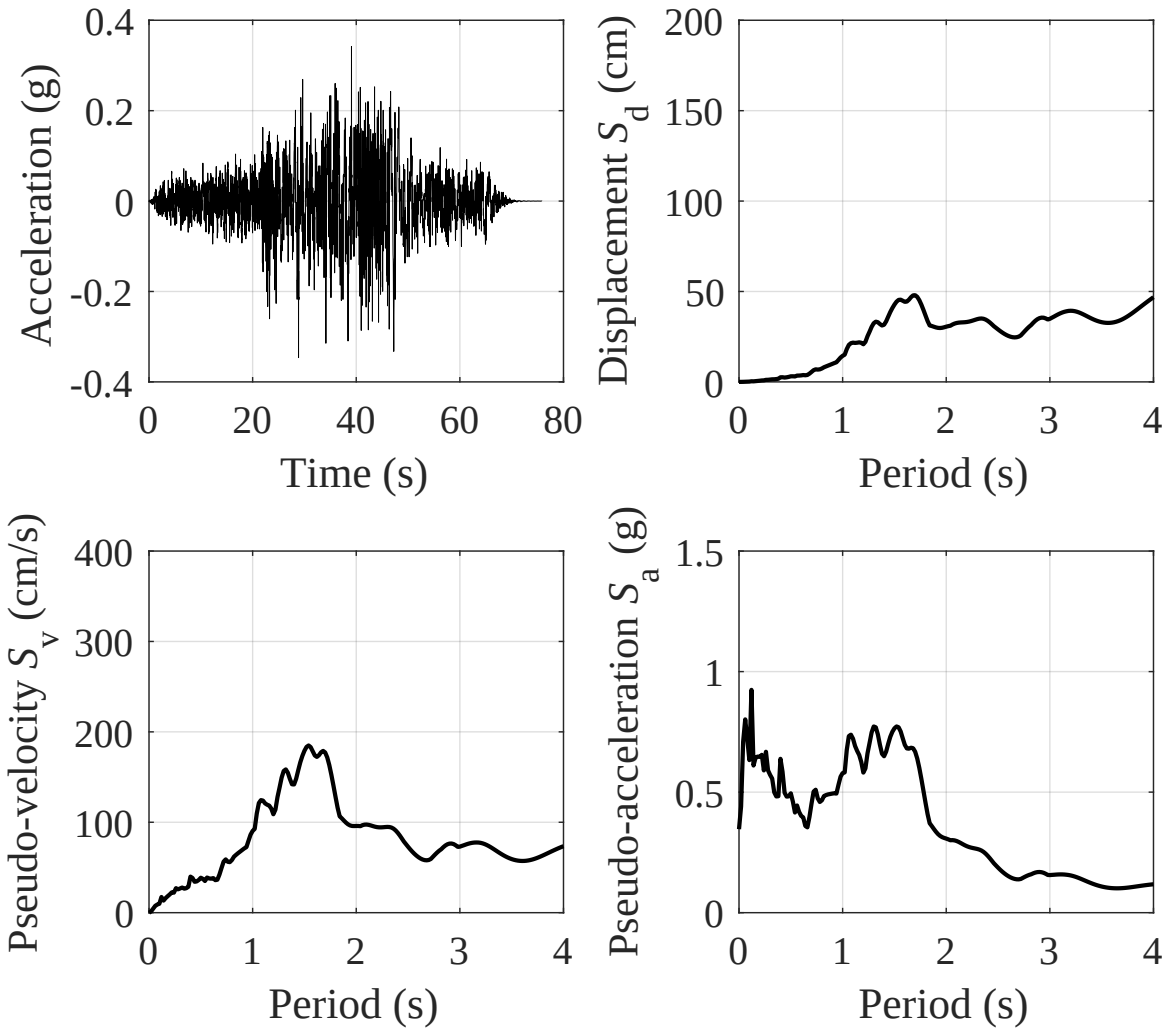

Figure B.18: Time history, 5%-damped pseudo-acceleration spectrum, pseudo-velocity spectrum, and displacement spectrum of earthquake ground motion Cro18

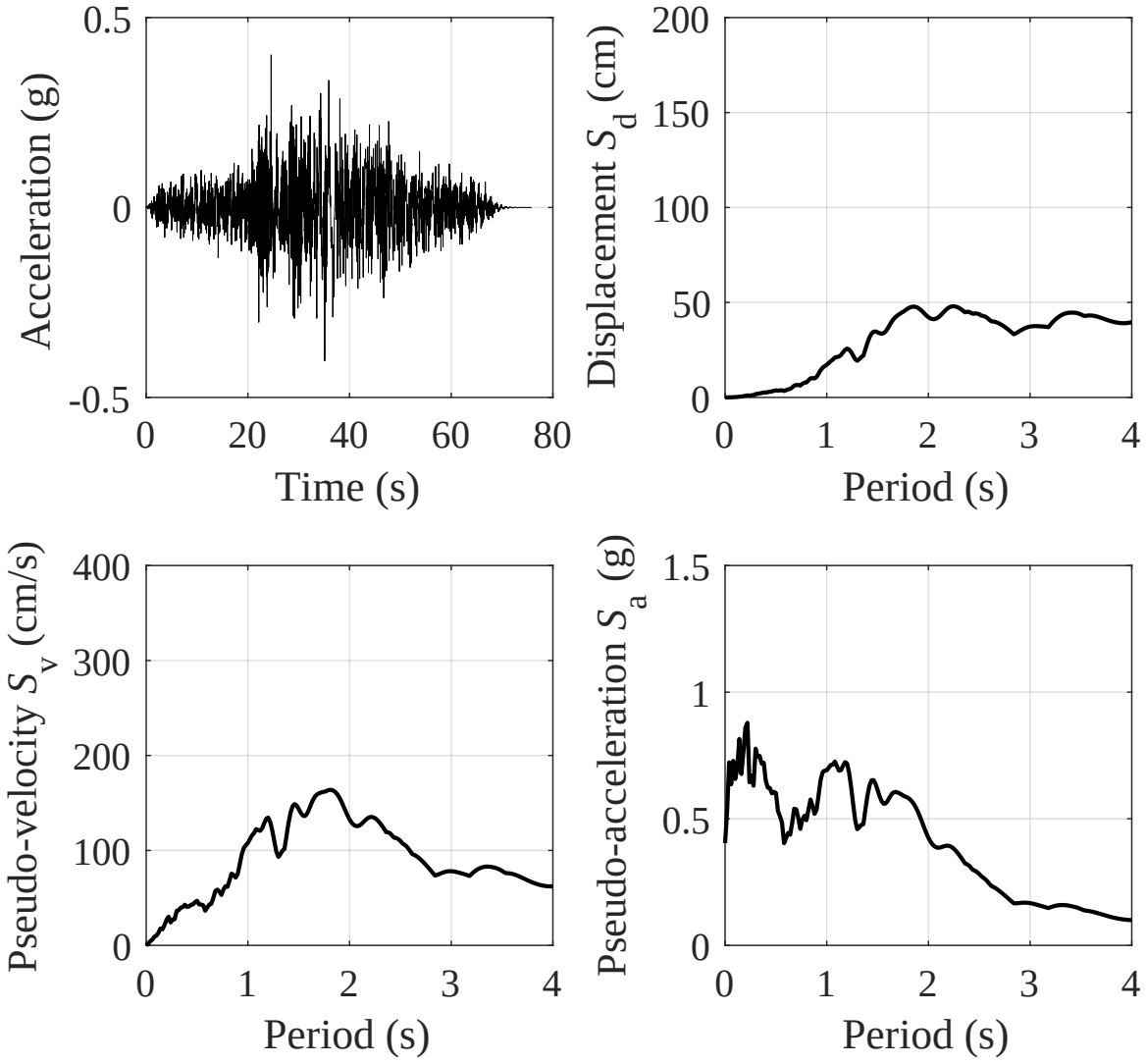

Figure B.19: Time history, 5%-damped pseudo-acceleration spectrum, pseudo-velocity spectrum, and displacement spectrum of earthquake ground motion Cro19

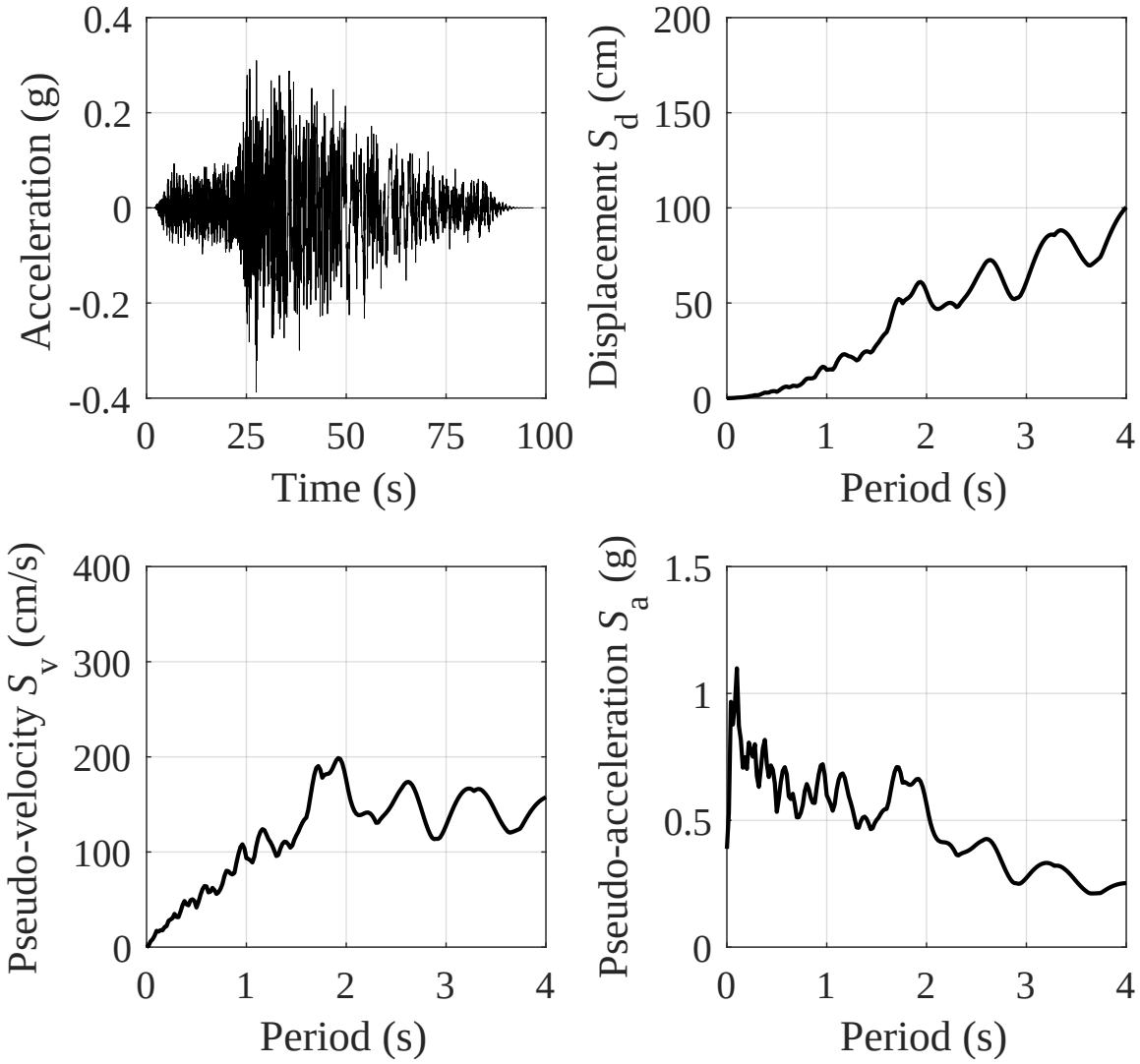

Figure B.20: Time history, 5%-damped pseudo-acceleration spectrum, pseudo-velocity spectrum, and displacement spectrum of earthquake ground motion Cro20

APPENDIX C

ADDITIONAL ANALYSIS RESULTS FOR CHAPTER 6

C.1 Additional analysis results for Section 6.5.1

4S60P40S bridge variant

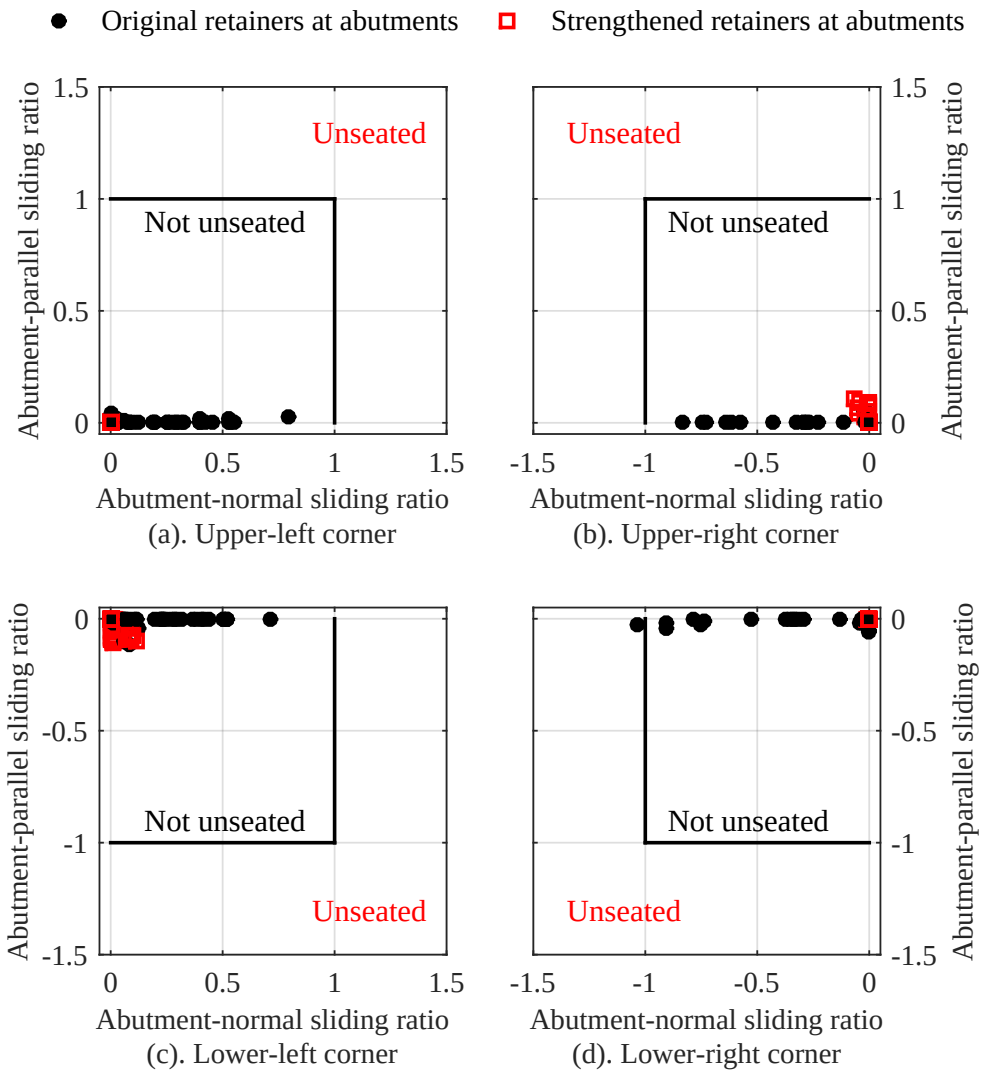

Figure C.1: Comparison of peak sliding distance of elastomeric bearings at deck corners of 4S60P40S bridge variant with original and strengthened retainer anchorage at abutments

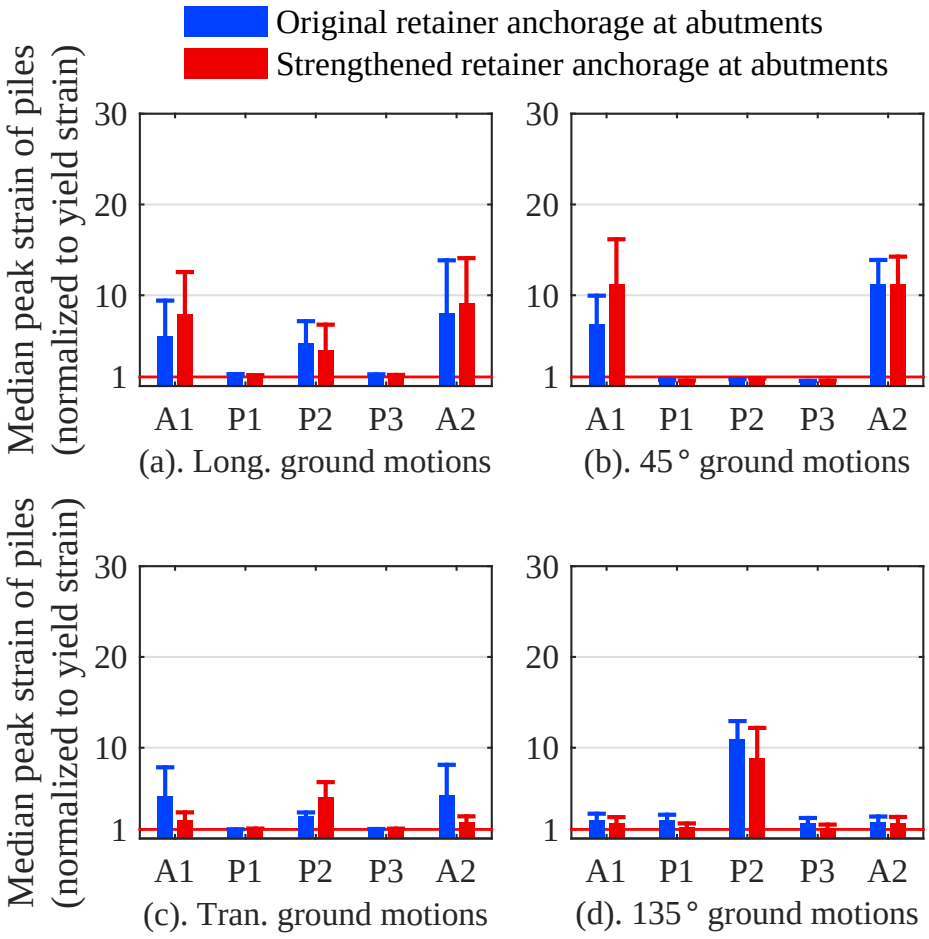

Figure C.2: Comparison of peak pile strain (median + median absolute deviation) of 4S60P40S bridge variant with original and strengthened retainer anchorage at abutments: (a). response under longitudinal ground motions; (b). response under 45° ground motions; (c). response under transverse ground motions; (d). response under 135° ground motions

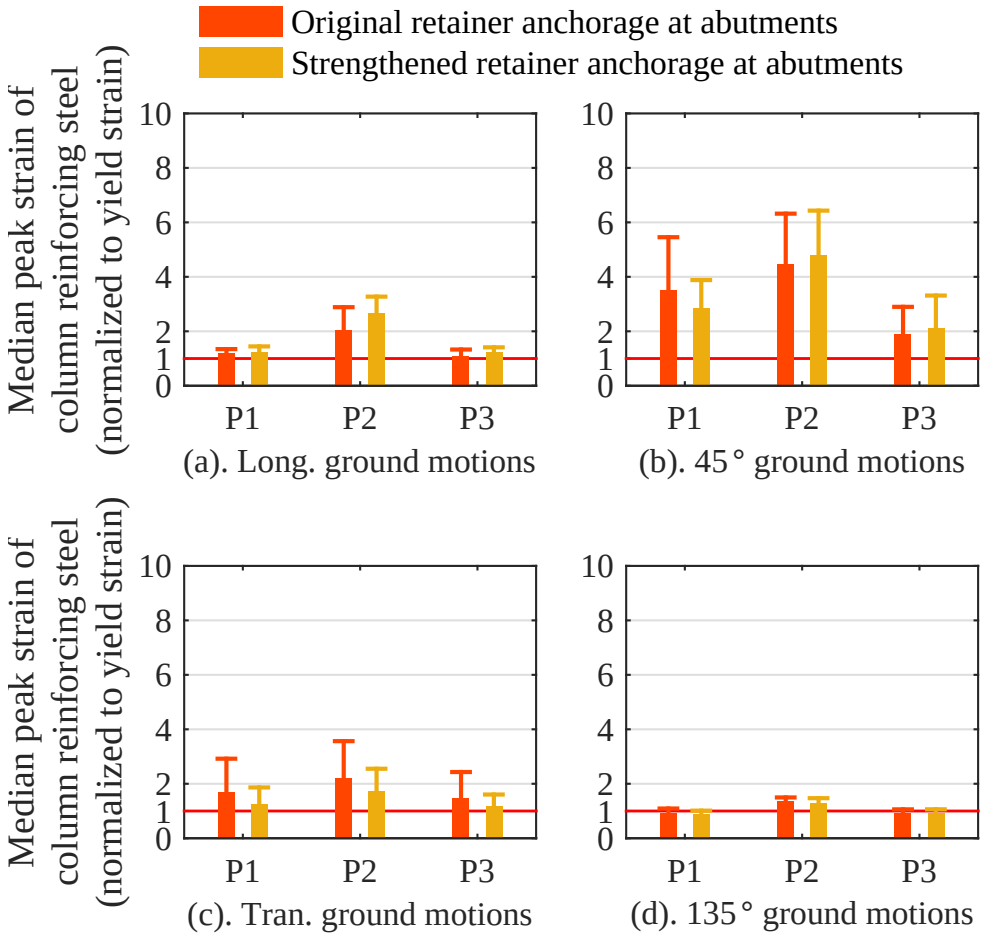

Figure C.3: Comparison of peak strain (median + median absolute deviation) of reinforcing steel at pier column bases of 4S60P40S bridge variant with original and strengthened retainer anchorage at abutments: (a). response under longitudinal ground motions; (b). response under 45° ground motions; (c). response under transverse ground motions; (d). response under 135° ground motions

3C60P40S bridge variant

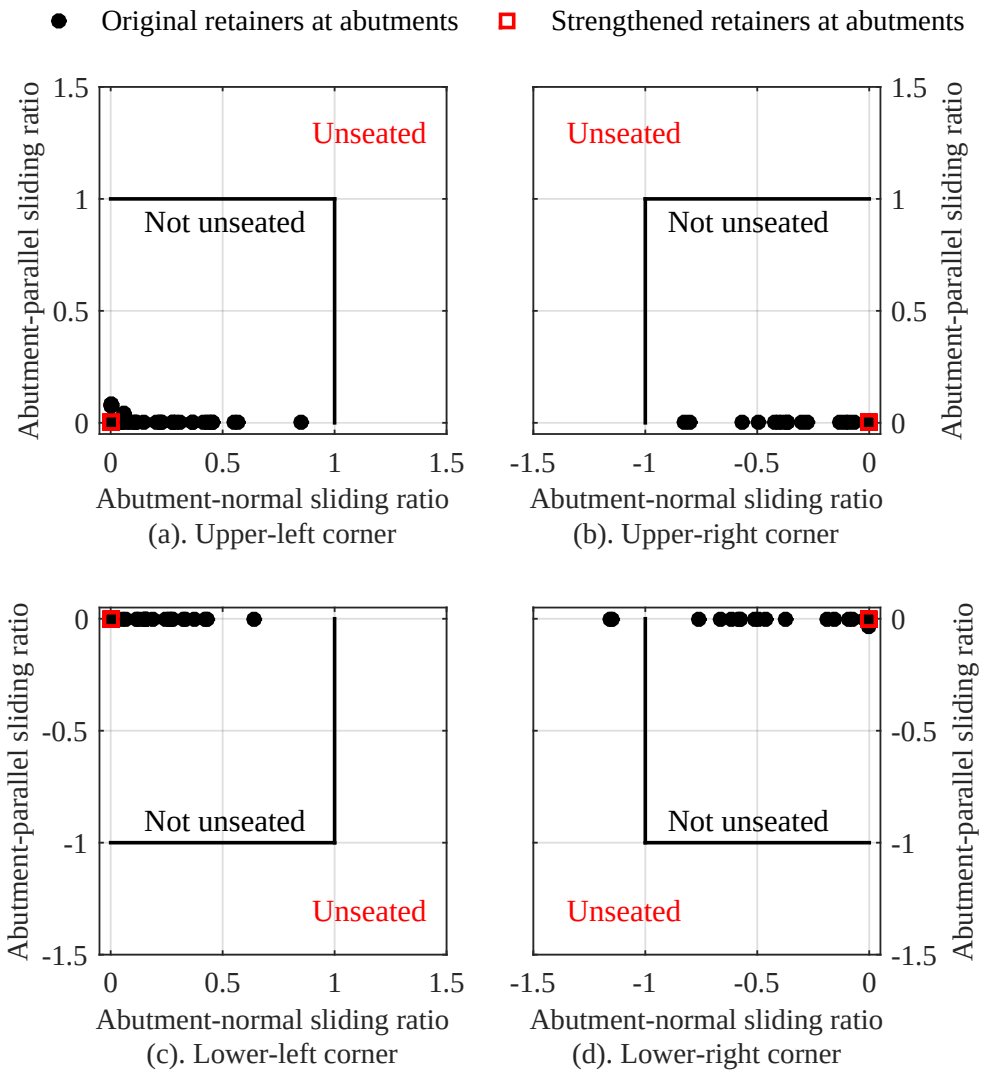

Figure C.4: Comparison of peak sliding distance of elastomeric bearings at deck corners of 3C60P40S bridge variant with original and strengthened retainer anchorage at abutments

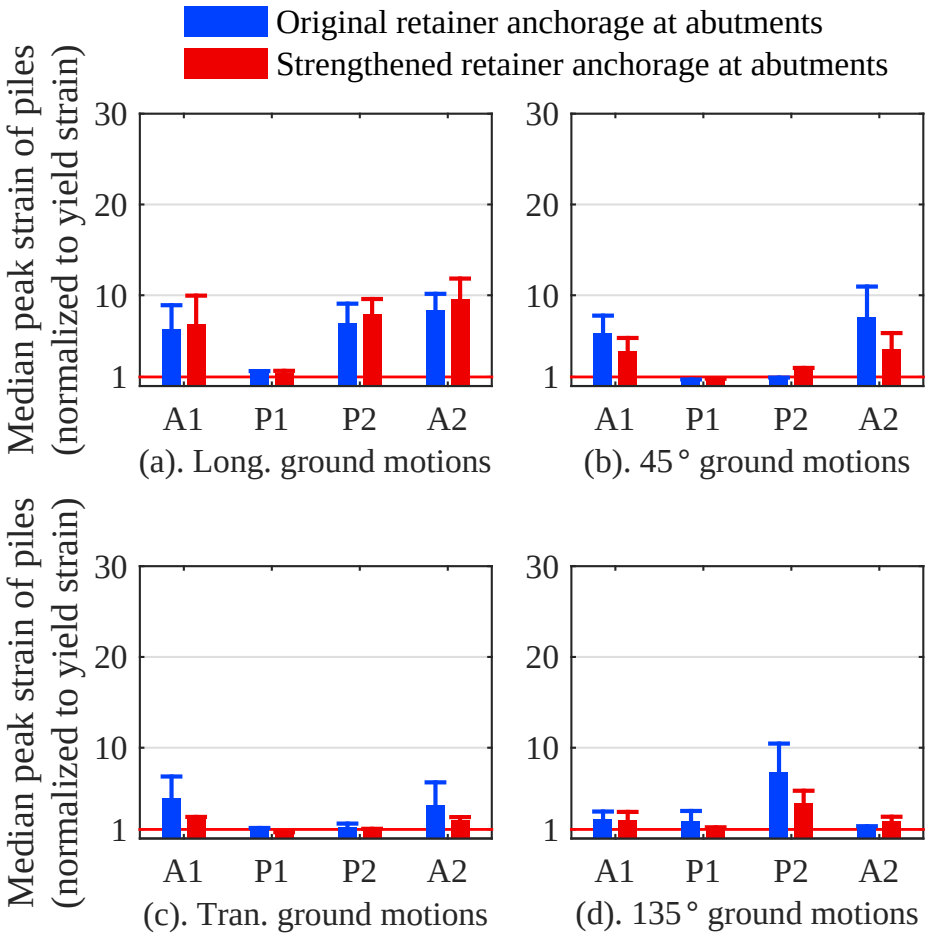

Figure C.5: Comparison of peak pile strain (median + median absolute deviation) of 3C60P40S bridge variant with original and strengthened retainer anchorage at abutments: (a). response under longitudinal ground motions; (b). response under 45° ground motions; (c). response under transverse ground motions; (d). response under 135° ground motions

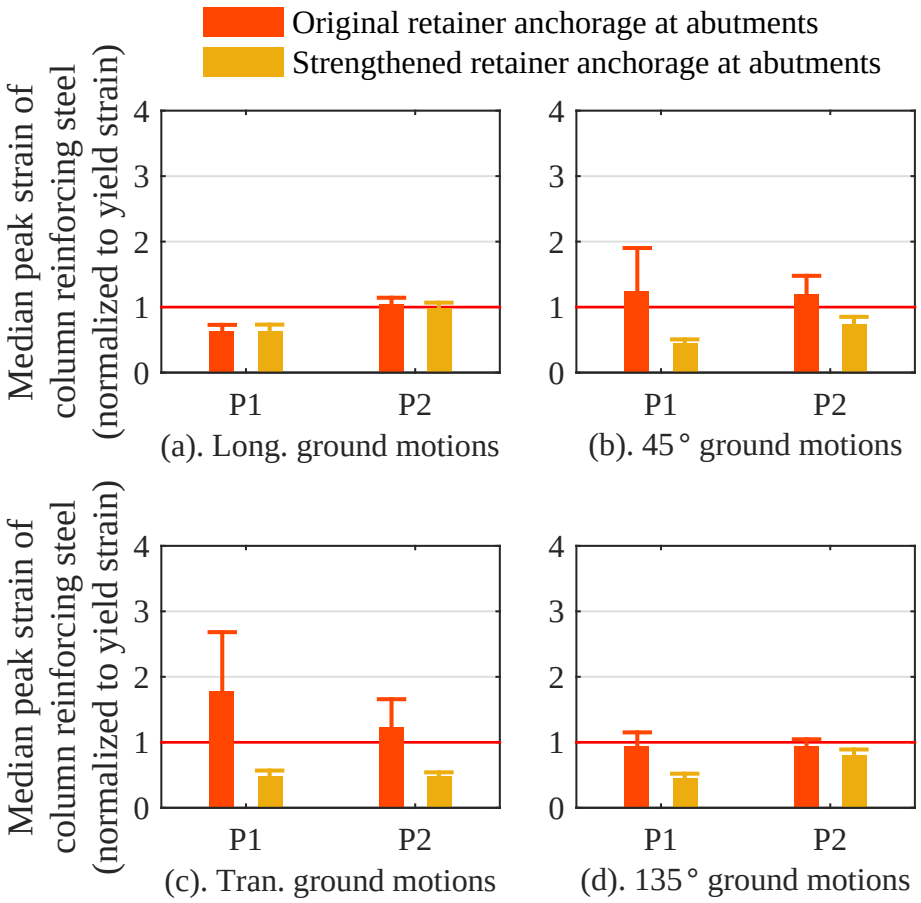

Figure C.6: Comparison of peak strain (median + median absolute deviation) of reinforcing steel at pier column bases of 3C60P40S bridge variant with original and strengthened retainer anchorage at abutments: (a). response under longitudinal ground motions; (b). response under 45° ground motions; (c). response under transverse ground motions; (d). response under 135° ground motions

4C45P40H bridge variant

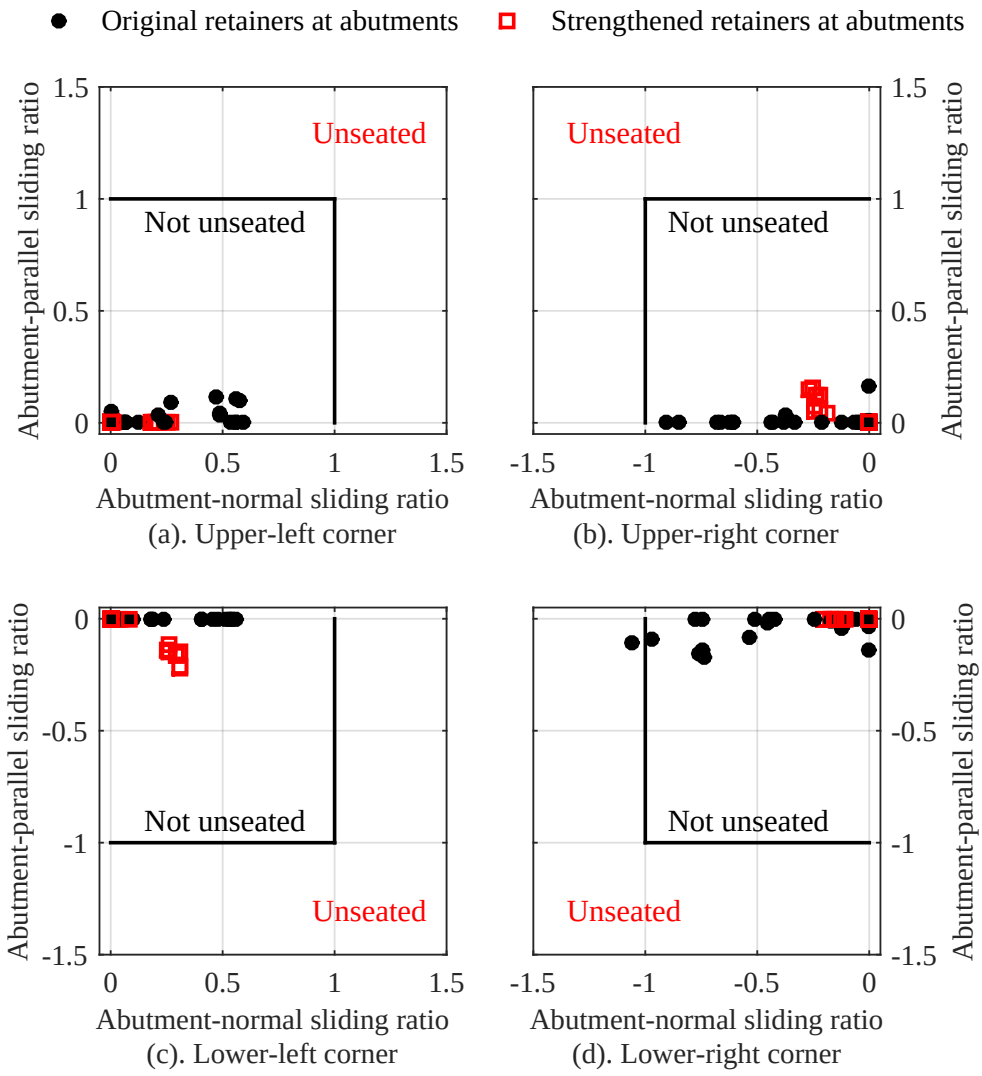

Figure C.7: Comparison of peak sliding distance of elastomeric bearings at deck corners of 4C45P40H bridge variant with original and strengthened retainer anchorage at abutments

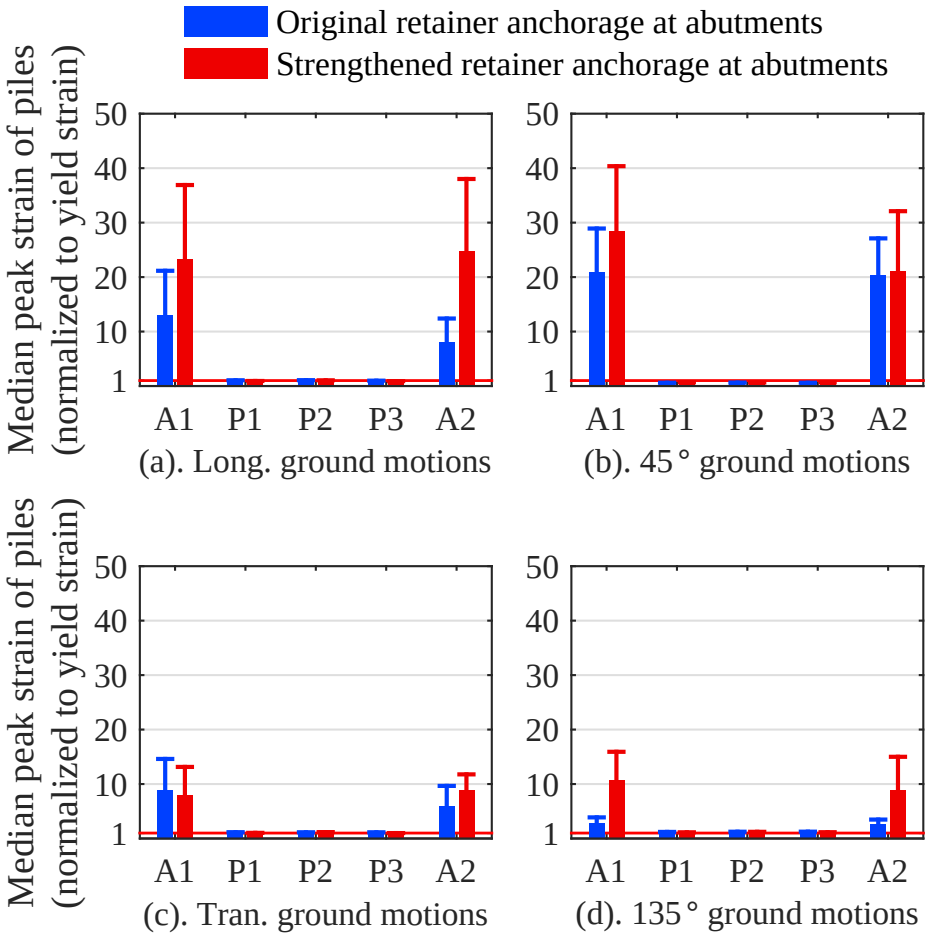

Figure C.8: Comparison of peak pile strain (median + median absolute deviation) of 4C45P40H bridge variant with original and strengthened retainer anchorage at abutments: (a). response under longitudinal ground motions; (b). response under 45° ground motions; (c). response under transverse ground motions; (d). response under 135° ground motions

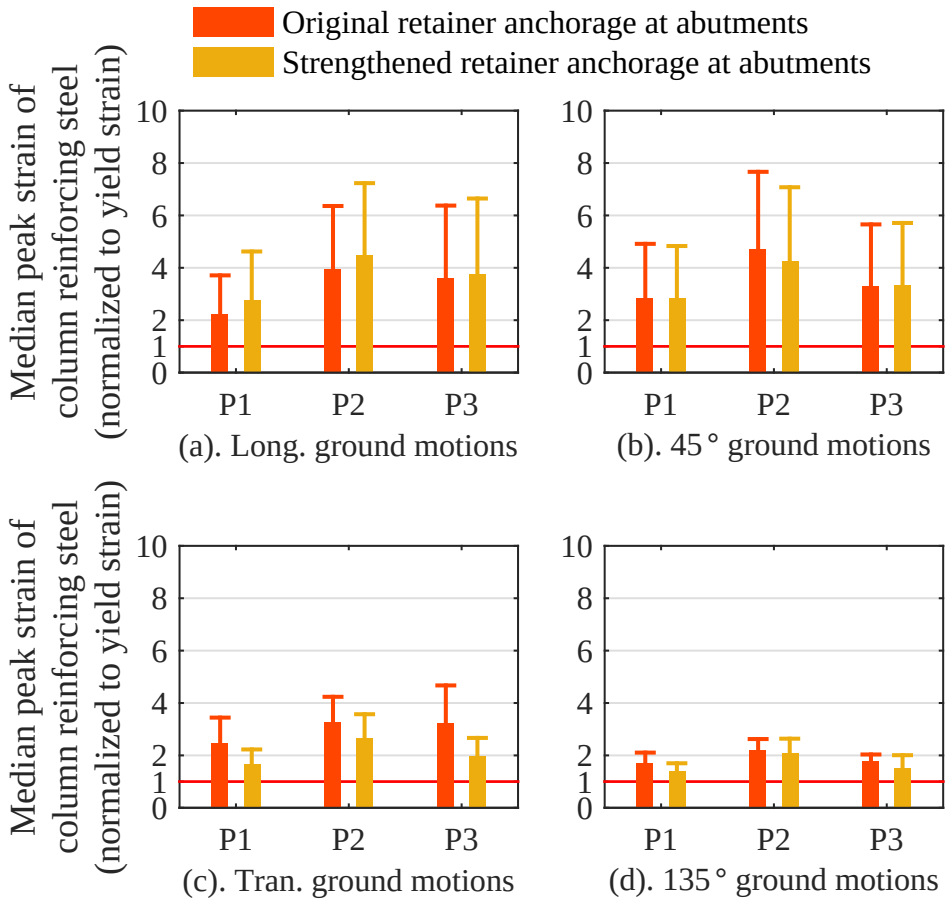

Figure C.9: Comparison of peak strain (median + median absolute deviation) of reinforcing steel at pier column bases of 4C45P40H bridge variant with original and strengthened retainer anchorage at abutments: (a). response under longitudinal ground motions; (b). response under 45° ground motions; (c). response under transverse ground motions; (d). response under 135° ground motions

4C60P40H bridge variant

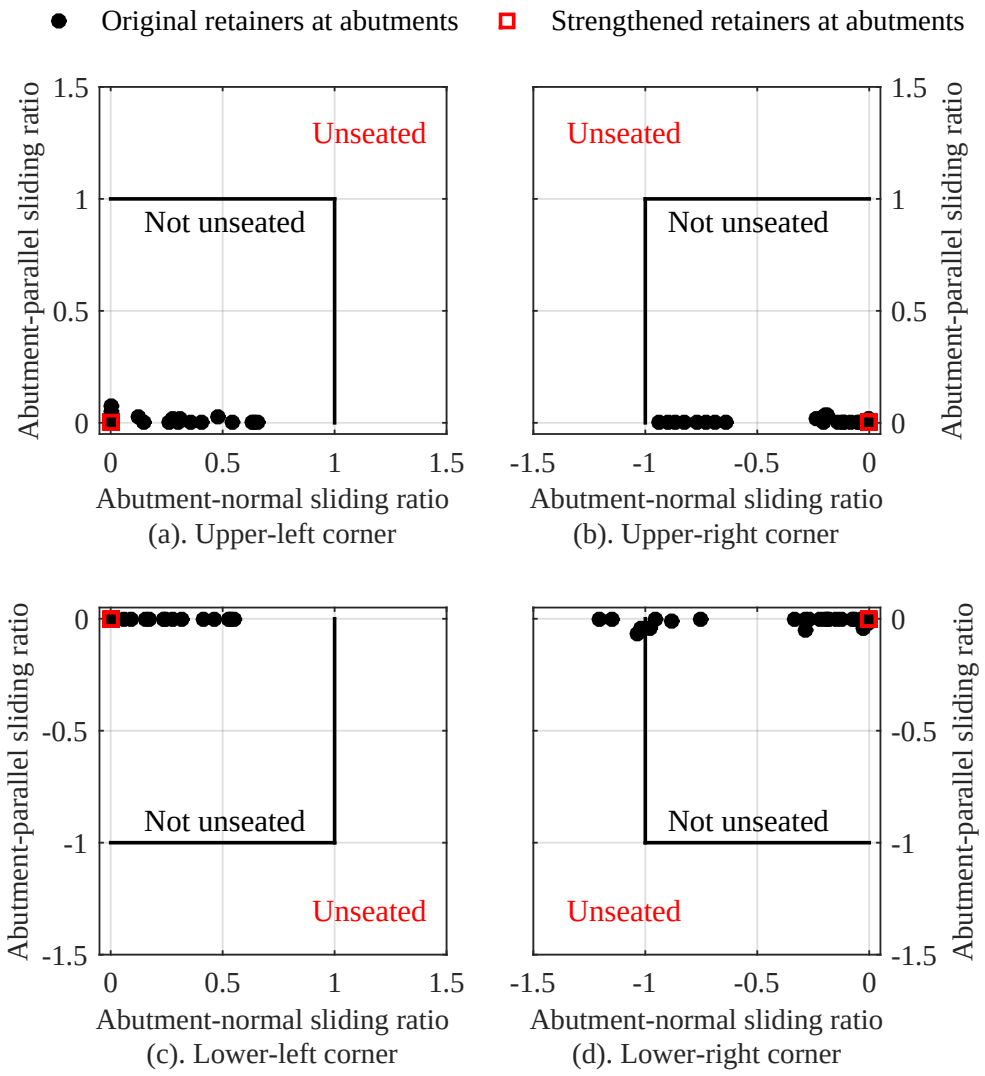

Figure C.10: Comparison of peak sliding distance of elastomeric bearings at deck corners of 4C60P40H bridge variant with original and strengthened retainer anchorage at abutments

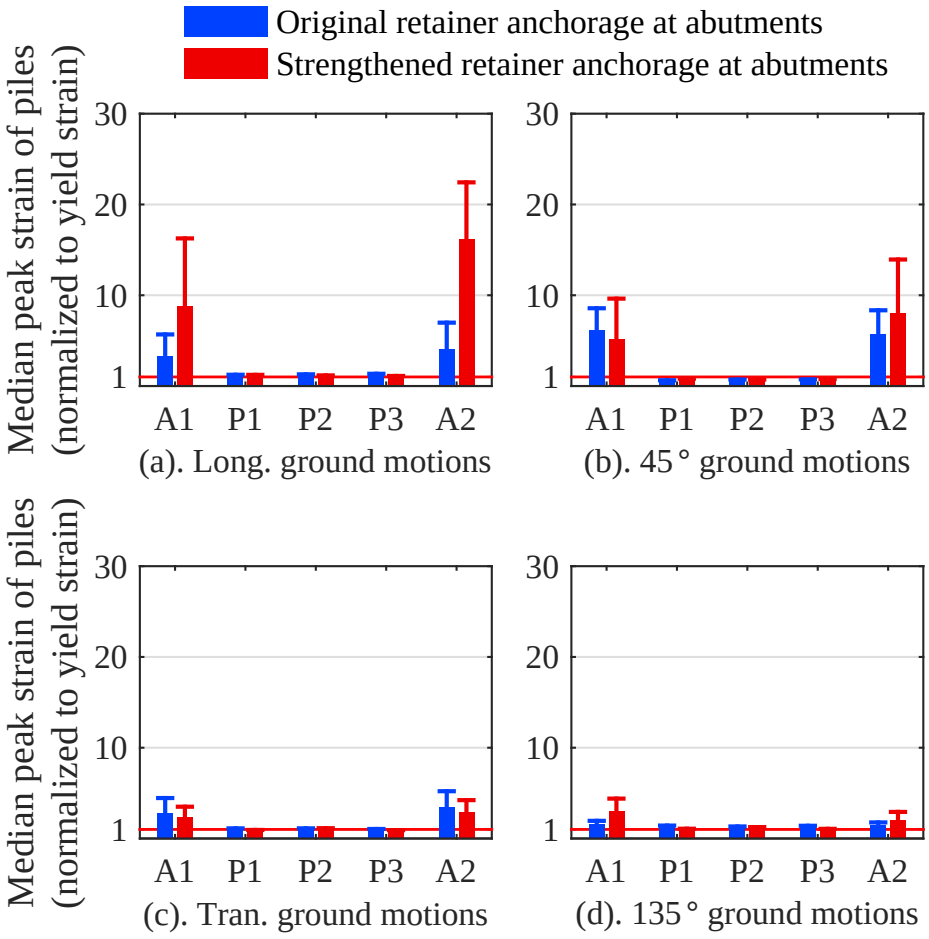

Figure C.11: Comparison of peak pile strain (median + median absolute deviation) of 4C60P40H bridge variant with original and strengthened retainer anchorage at abutments: (a). response under longitudinal ground motions; (b). response under 45° ground motions; (c). response under transverse ground motions; (d). response under 135° ground motions

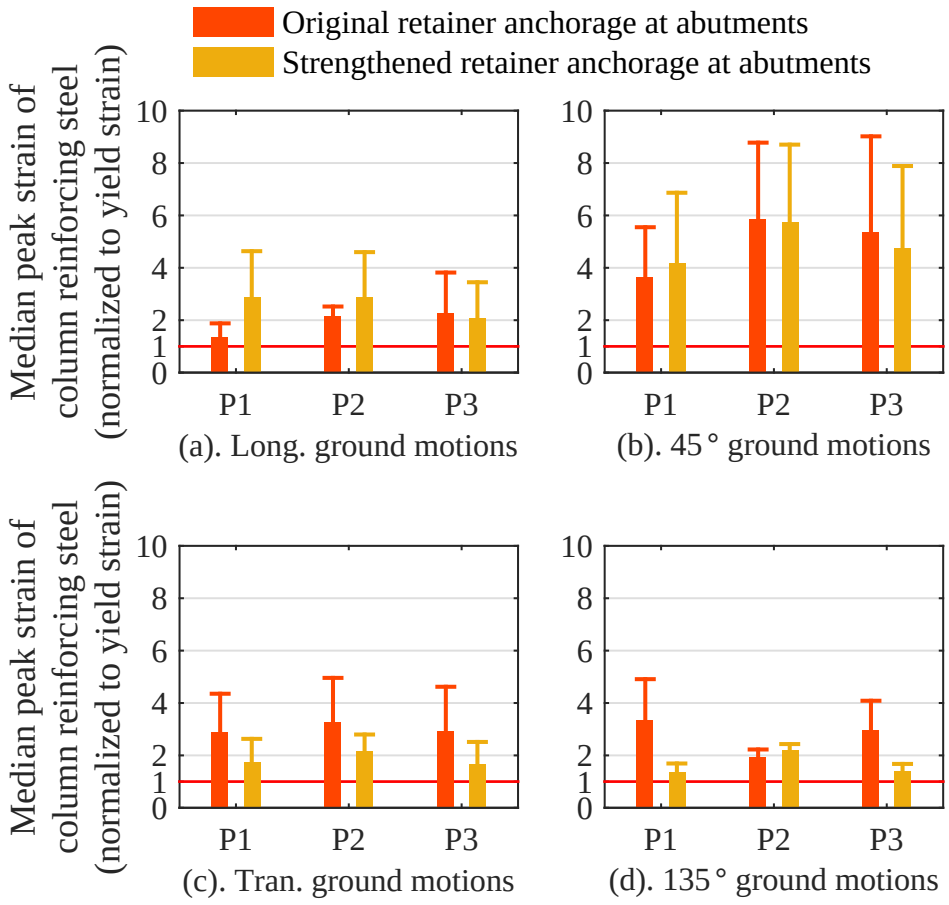

Figure C.12: Comparison of peak strain (median + median absolute deviation) of reinforcing steel at pier column bases of 4C60P40H bridge variant with original and strengthened retainer anchorage at abutments: (a). response under longitudinal ground motions; (b). response under 45° ground motions; (c). response under transverse ground motions; (d). response under 135° ground motions

C.2 Additional analysis results for Section 6.5.2

3S00P15S bridge variant

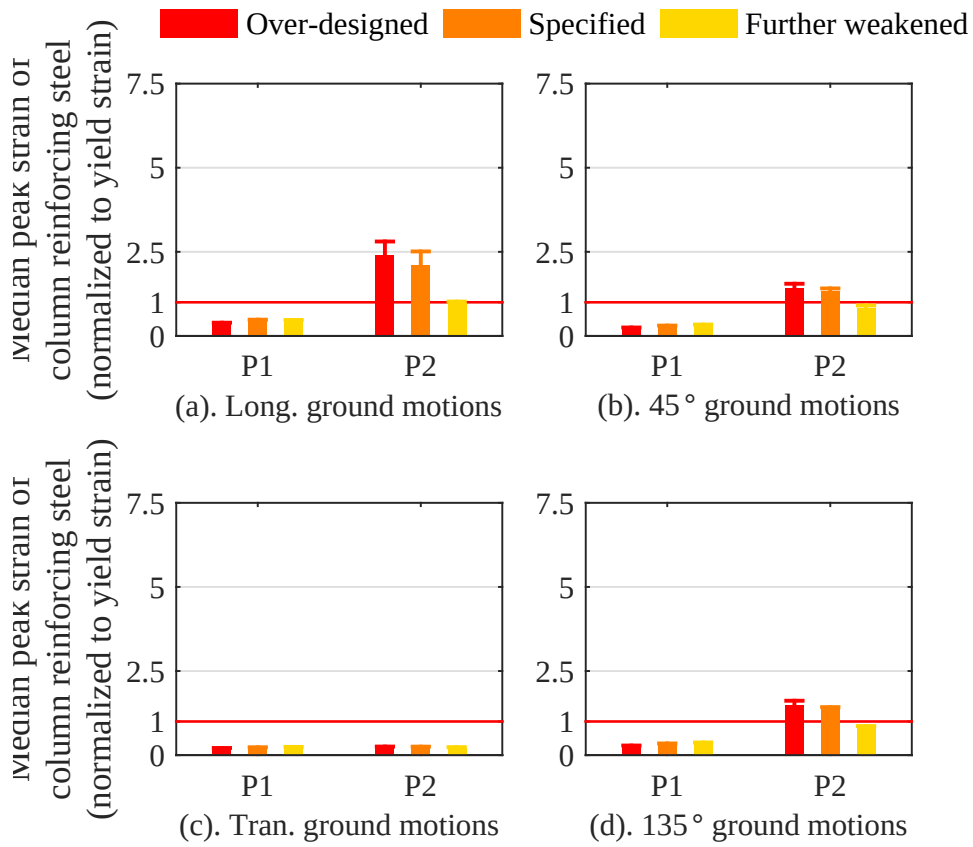

Figure C.13: Comparison of peak strain (median + median absolute deviation) of reinforcing steel at pier column bases of 3S00P15S bridge variant with different designs of steel fixed bearing anchorage: (a). response under longitudinal ground motions; (b). response under 45° ground motions; (c). response under transverse ground motions; (d). response under 135° ground motions

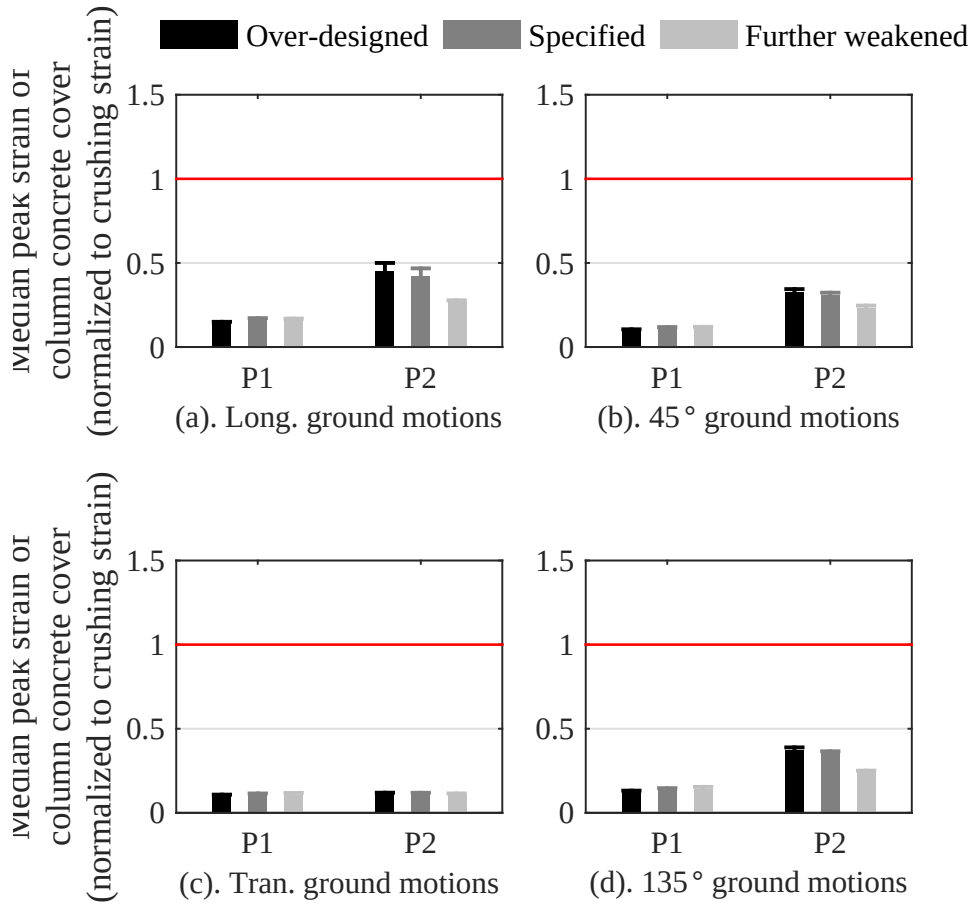

Figure C.14: Comparison of peak strain (median + median absolute deviation) of concrete cover at pier column bases of 3S00P15S bridge variant with different designs of steel fixed bearing anchorage: (a). response under longitudinal ground motions; (b). response under 45° ground motions; (c). response under transverse ground motions; (d). response under 135° ground motions

3S15P15S bridge variant

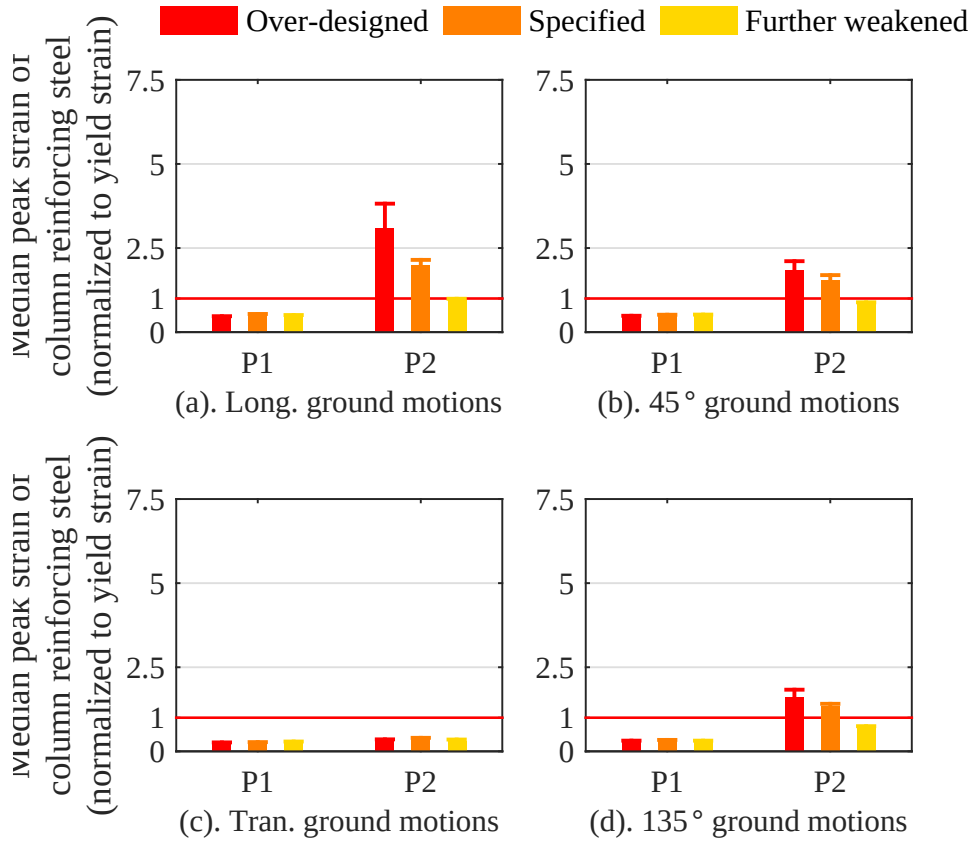

Figure C.15: Comparison of peak strain (median + median absolute deviation) of reinforcing steel at pier column bases of 3S15P15S bridge variant with different designs of steel fixed bearing anchorage: (a). response under longitudinal ground motions; (b). response under 45° ground motions; (c). response under transverse ground motions; (d). response under 135° ground motions

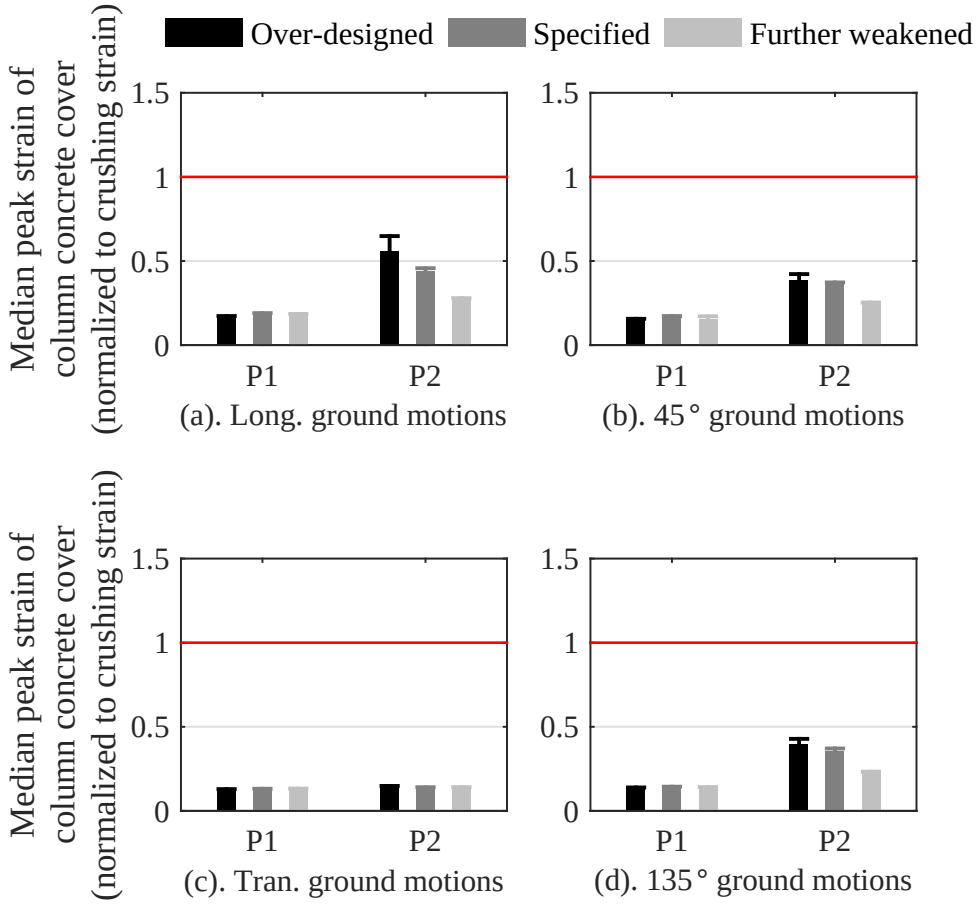

Figure C.16: Comparison of peak strain (median + median absolute deviation) of concrete cover at pier column bases of 3S15P15S bridge variant with different designs of steel fixed bearing anchorage: (a). response under longitudinal ground motions; (b). response under 45° ground motions; (c). response under transverse ground motions; (d). response under 135° ground motions

3C00P15S bridge variant

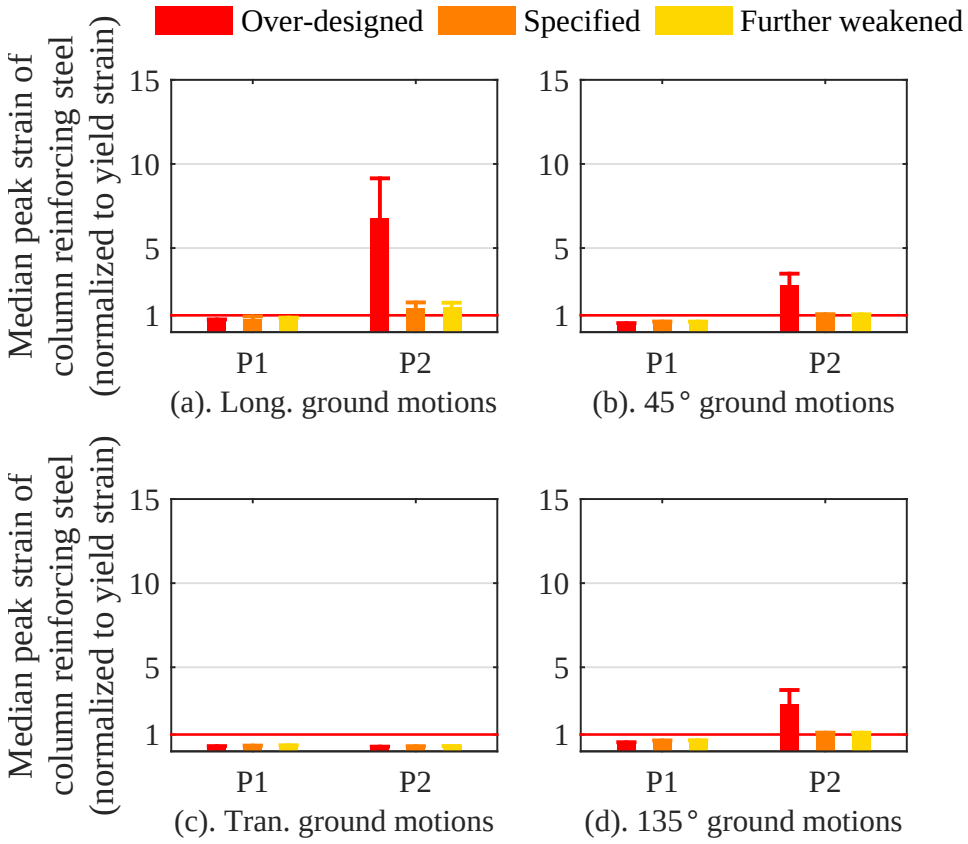

Figure C.17: Comparison of peak strain (median + median absolute deviation) of reinforcing steel at pier column bases of 3C00P15S bridge variant with different designs of steel dowel connections at fixed pier: (a). response under longitudinal ground motions; (b). response under 45° ground motions; (c). response under transverse ground motions; (d). response under 135° ground motions

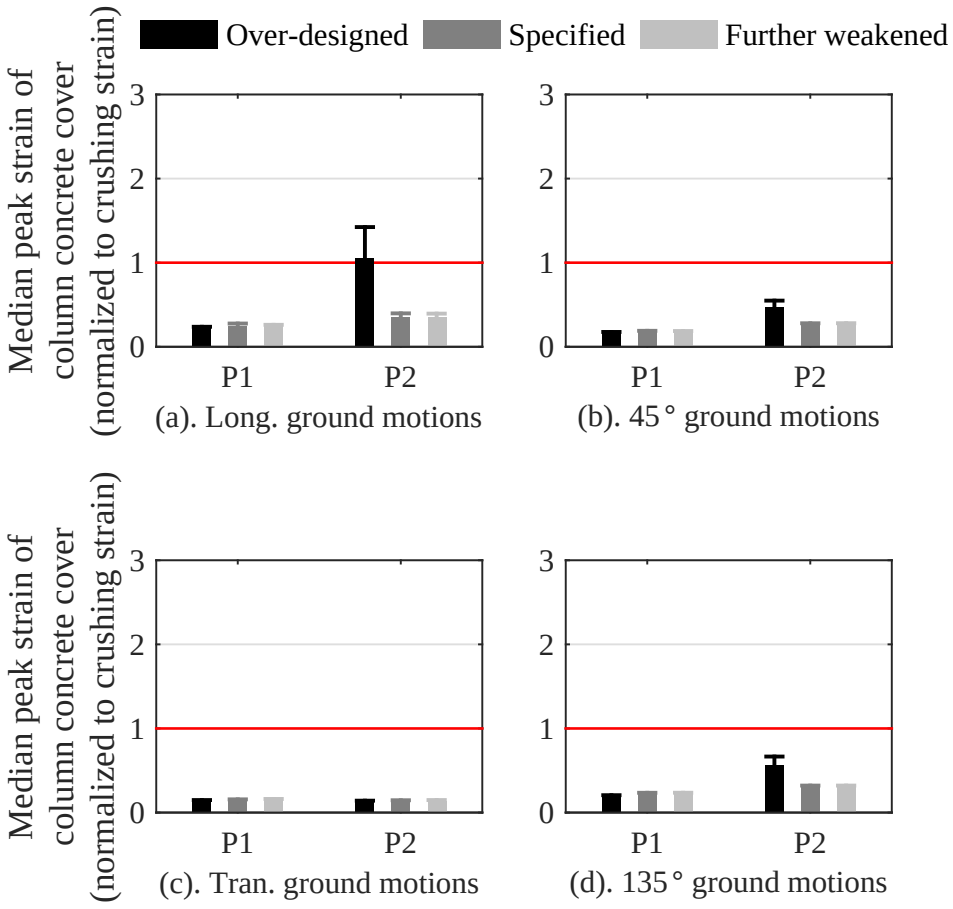

Figure C.18: Comparison of peak strain (median + median absolute deviation) of concrete cover at pier column bases of 3C00P15S bridge variant with different designs of steel dowel connections at fixed pier: (a). response under longitudinal ground motions; (b). response under 45° ground motions; (c). response under transverse ground motions; (d). response under 135° ground motions

3C15P15S bridge variant

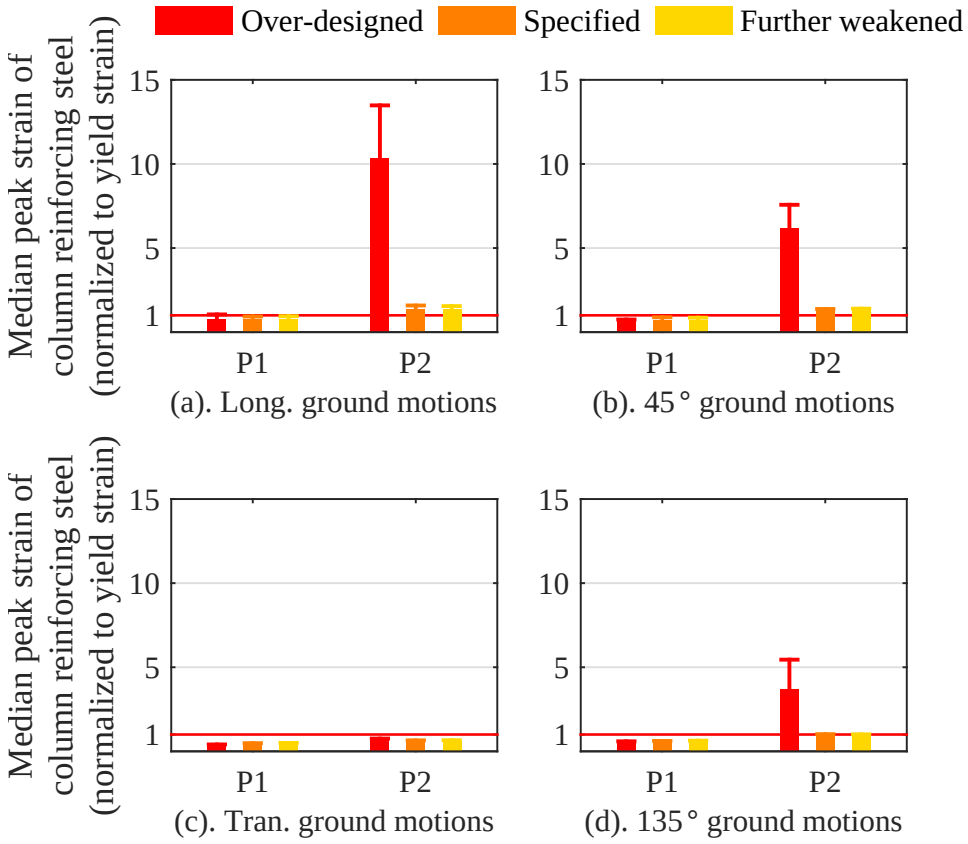

Figure C.19: Comparison of peak strain (median + median absolute deviation) of reinforcing steel at pier column bases of 3C15P15S bridge variant with different designs of steel dowel connections at fixed pier: (a). response under longitudinal ground motions; (b). response under 45° ground motions; (c). response under transverse ground motions; (d). response under 135° ground motions

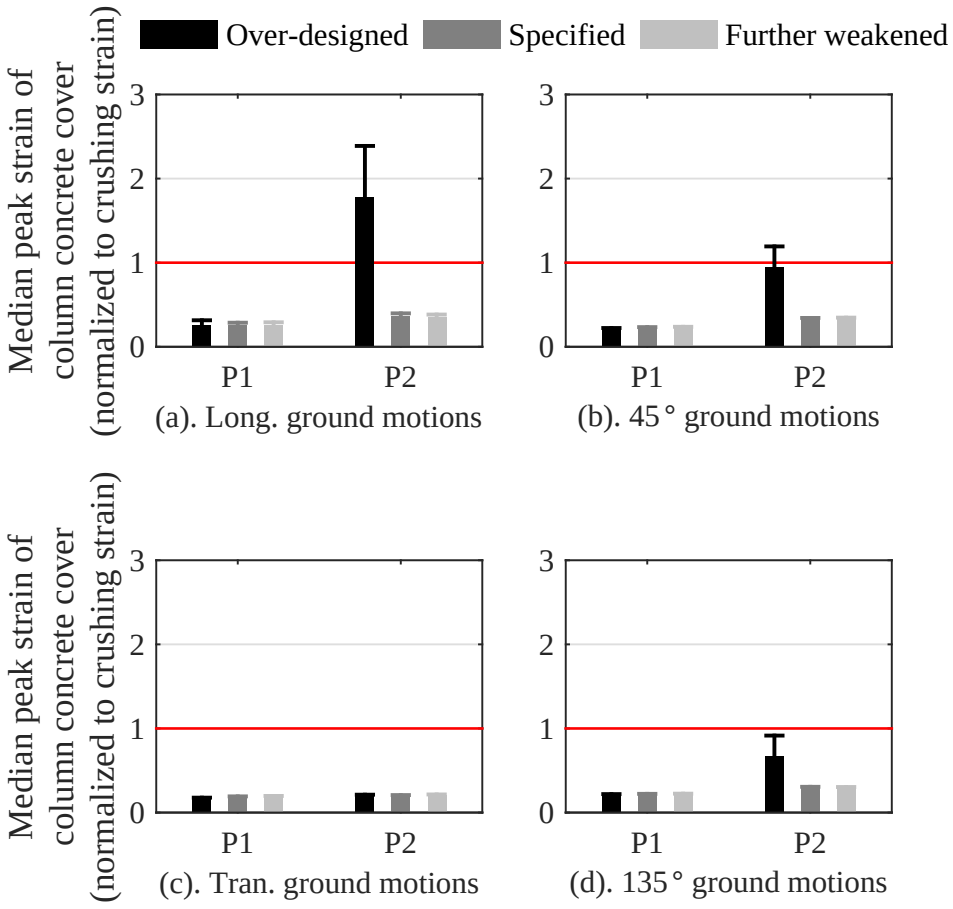

Figure C.20: Comparison of peak strain (median + median absolute deviation) of concrete cover at pier column bases of 3C15P15S bridge variant with different designs of steel dowel connections at fixed pier: (a). response under longitudinal ground motions; (b). response under 45° ground motions; (c). response under transverse ground motions; (d). response under 135° ground motions

4S00P15S bridge variant

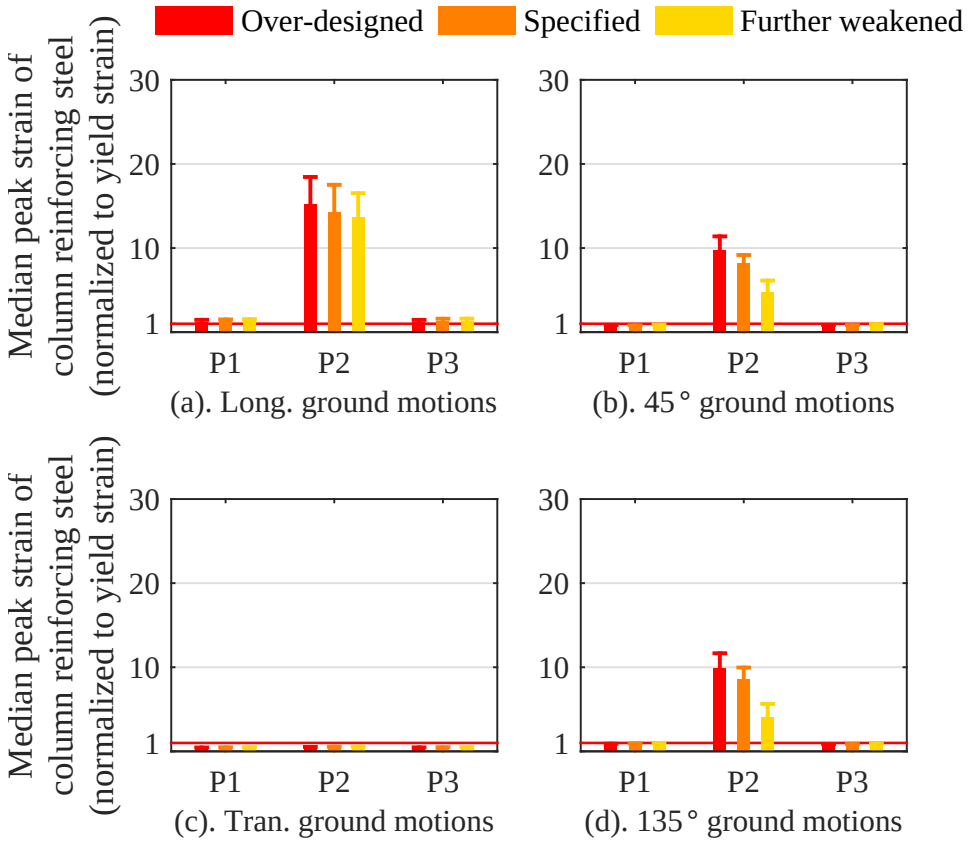

Figure C.21: Comparison of peak strain (median + median absolute deviation) of reinforcing steel at pier column bases of 4S00P15S bridge variant with different designs of steel fixed bearing anchorage: (a). response under longitudinal ground motions; (b). response under 45° ground motions; (c). response under transverse ground motions; (d). response under 135° ground motions

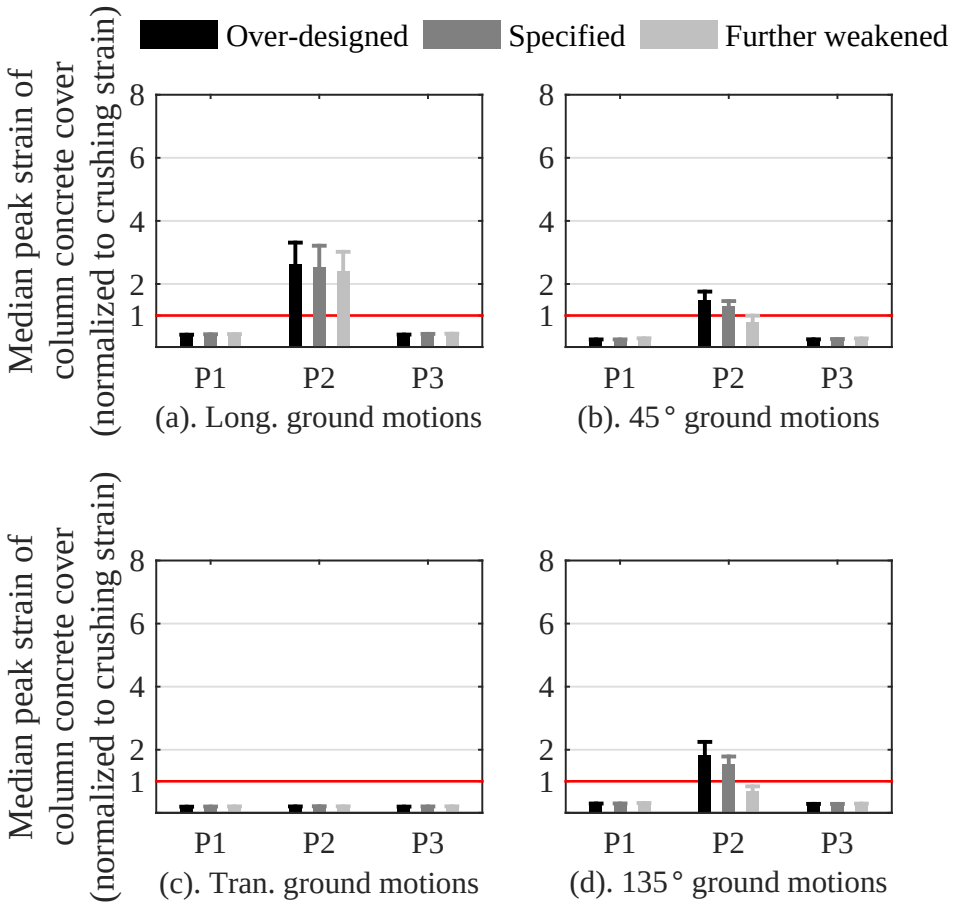

Figure C.22: Comparison of peak strain (median + median absolute deviation) of concrete cover at pier column bases of 4S00P15S bridge variant with different designs of steel fixed bearing anchorage: (a). response under longitudinal ground motions; (b). response under 45° ground motions; (c). response under transverse ground motions; (d). response under 135° ground motions

4S15P15S bridge variant

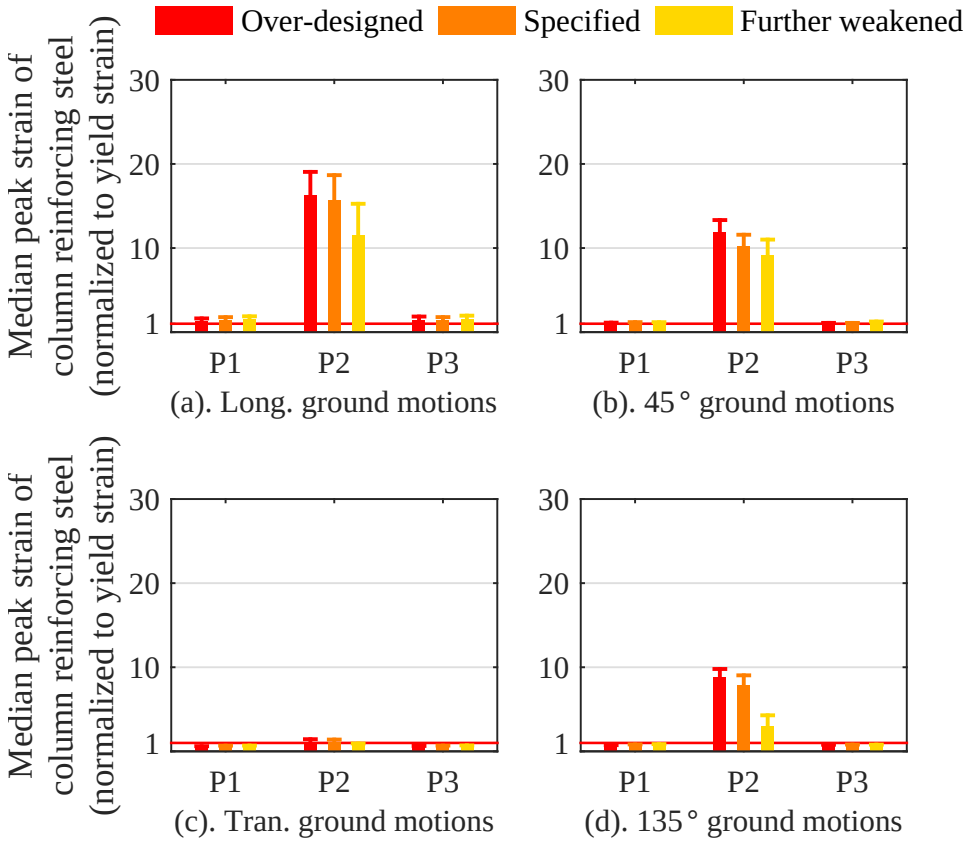

Figure C.23: Comparison of peak strain (median + median absolute deviation) of reinforcing steel at pier column bases of 4S15P15S bridge variant with different designs of steel fixed bearing anchorage: (a). response under longitudinal ground motions; (b). response under 45° ground motions; (c). response under transverse ground motions; (d). response under 135° ground motions

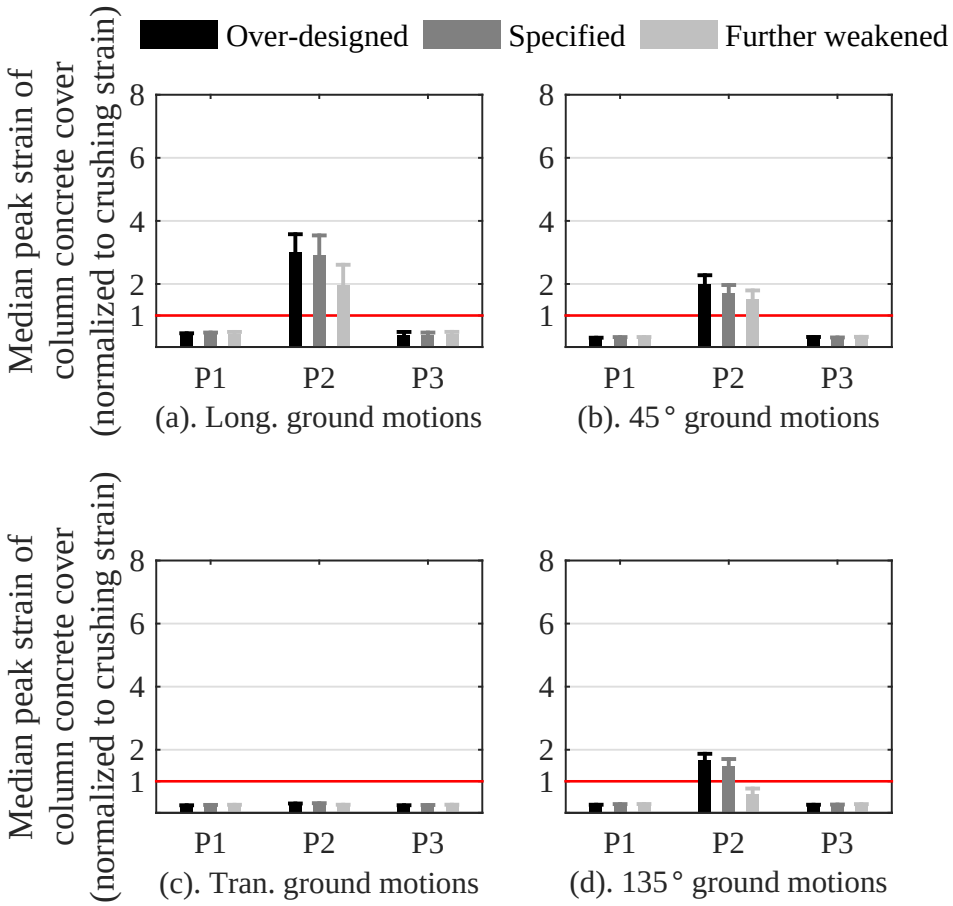

Figure C.24: Comparison of peak strain (median + median absolute deviation) of concrete cover at pier column bases of 4S15P15S bridge variant with different designs of steel fixed bearing anchorage: (a). response under longitudinal ground motions; (b). response under 45° ground motions; (c). response under transverse ground motions; (d). response under 135° ground motions

4C15P15S bridge variant

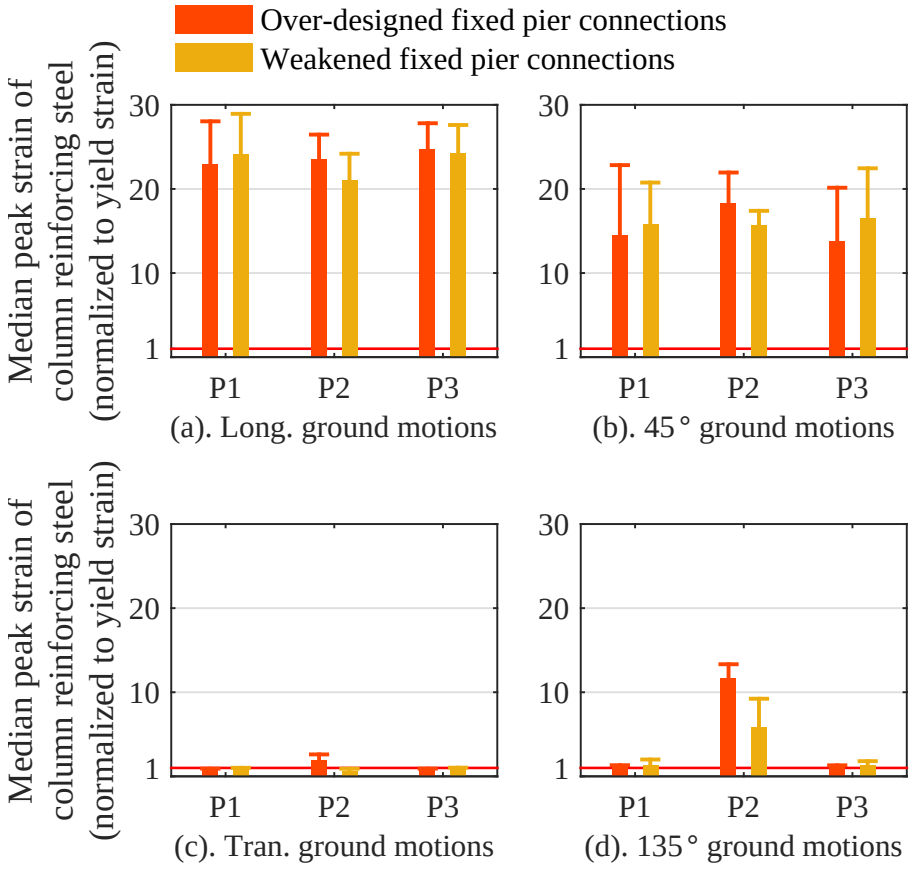

Figure C.25: Comparison of peak strain (median + median absolute deviation) of reinforcing steel at pier column bases of 4C15P15S bridge variant with different designs of steel dowel connections at fixed pier: (a). response under longitudinal ground motions; (b). response under 45° ground motions; (c). response under transverse ground motions; (d). response under 135° ground motions

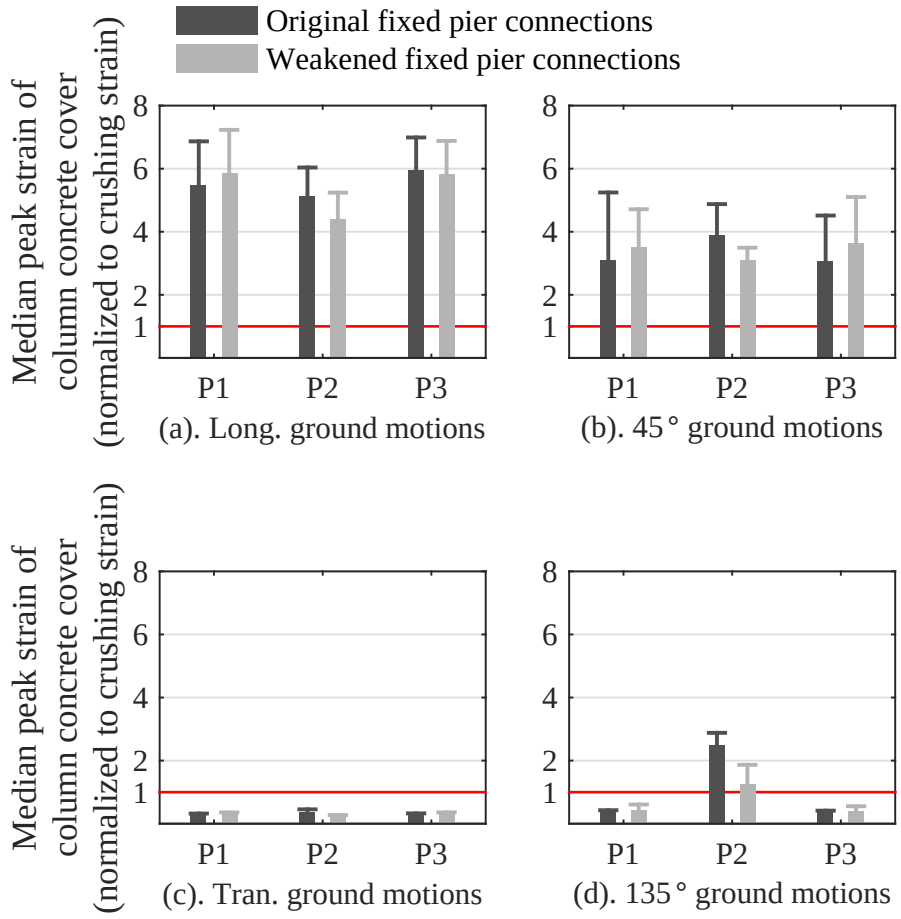

Figure C.26: Comparison of peak strain (median + median absolute deviation) of concrete cover at pier column bases of 4C15P15S bridge variant with different designs of steel dowel connections at fixed pier: (a). response under longitudinal ground motions; (b). response under 45° ground motions; (c). response under transverse ground motions; (d). response under 135° ground motions

4C30P15S bridge variant

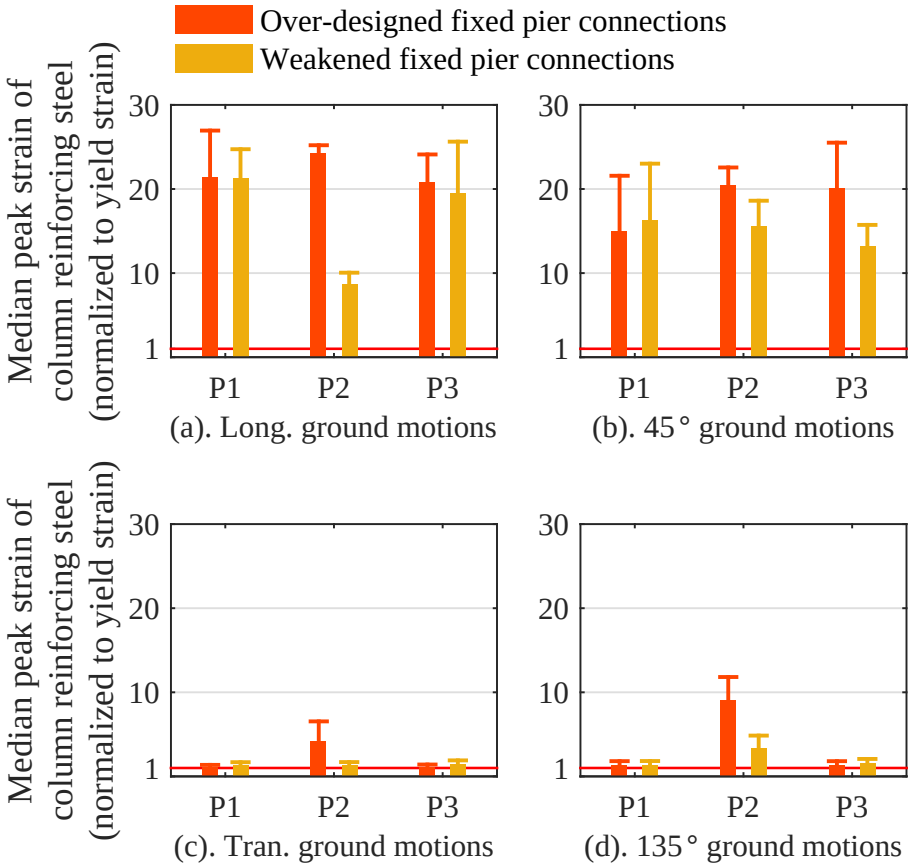

Figure C.27: Comparison of peak strain (median + median absolute deviation) of reinforcing steel at pier column bases of 4C30P15S bridge variant with original and weakened connections between fixed pier and superstructure: (a). response under longitudinal ground motions; (b). response under 45° ground motions; (c). response under transverse ground motions; (d). response under 135° ground motions

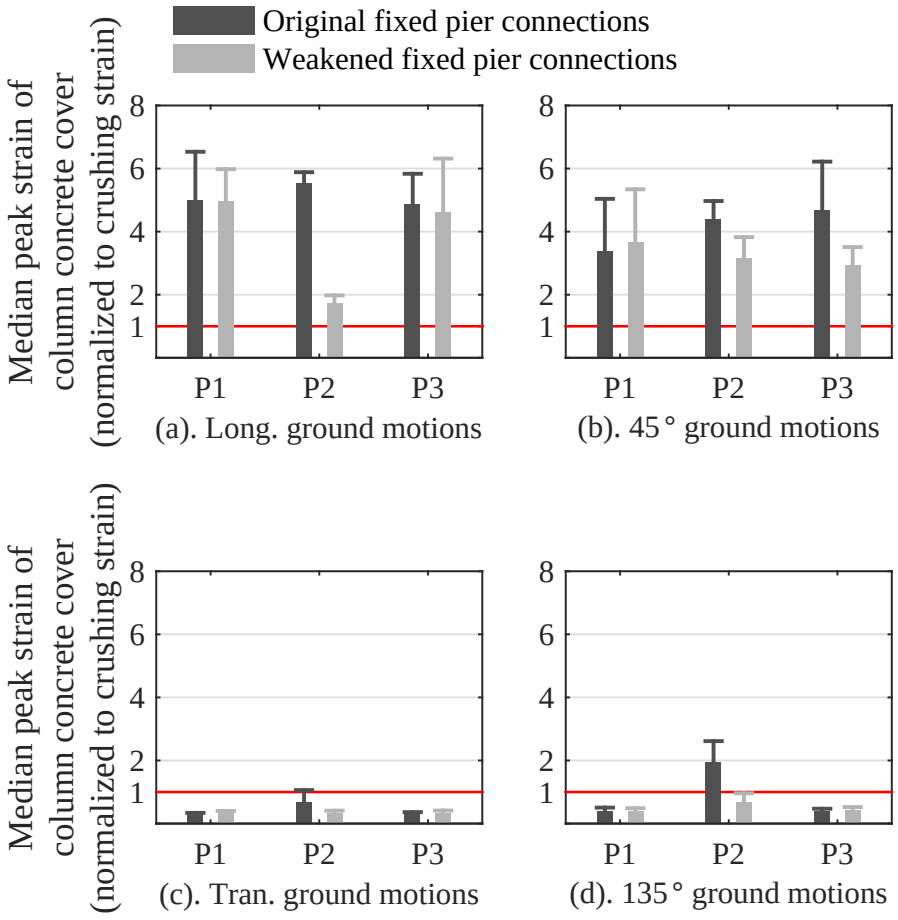

Figure C.28: Comparison of peak strain (median + median absolute deviation) of concrete cover at pier column bases of 4C30P15S bridge variant with original and weakened connections between fixed pier and superstructure: (a). response under longitudinal ground motions; (b). response under 45° ground motions; (c). response under transverse ground motions; (d). response under 135° ground motions

4C15P15S bridge variant

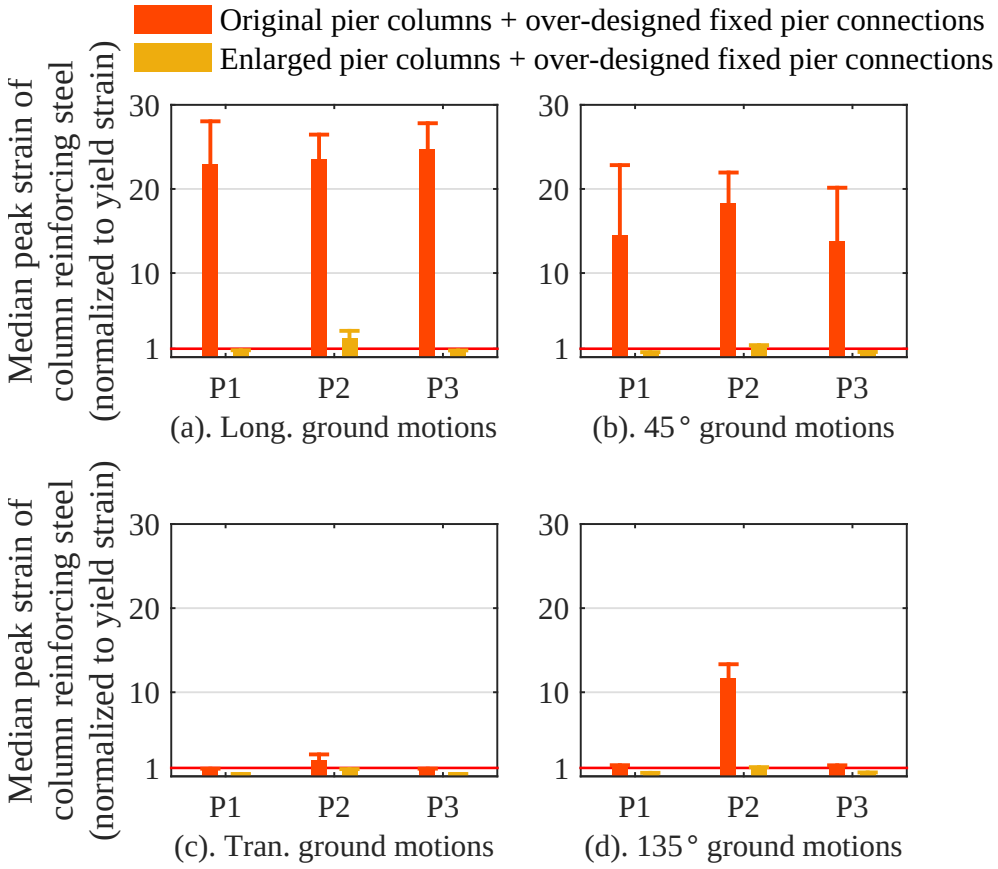

Figure C.29: Comparison of peak strain (median + median absolute deviation) of reinforcing steel at pier column bases of 4C15P15S bridge between Cases 1 and 2 of Table 6.54: (a). response under longitudinal ground motions; (b). response under 45° ground motions; (c). response under transverse ground motions; (d). response under 135° ground motions

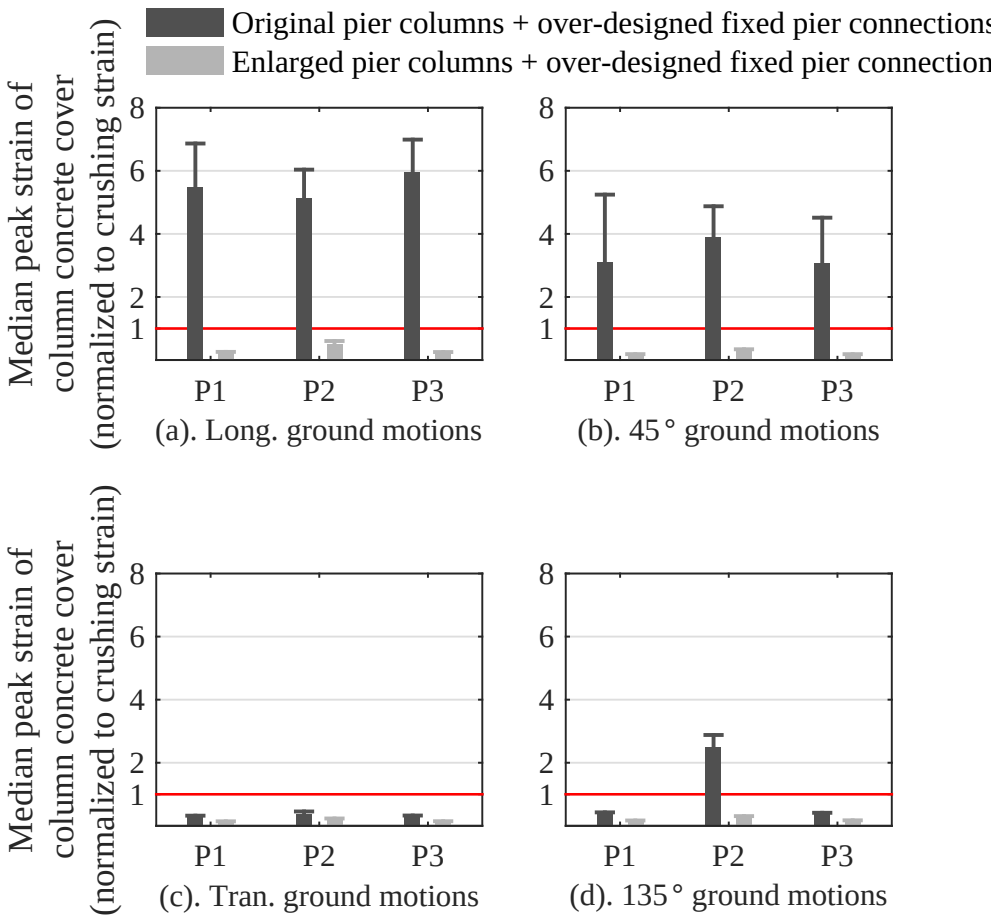

Figure C.30: Comparison of peak strain (median + median absolute deviation) of concrete cover at pier column bases of 4C15P15S bridge between Cases 1 and 2 of Table 6.54: (a). response under longitudinal ground motions; (b). response under 45° ground motions; (c). response under transverse ground motions; (d). response under 135° ground motions

4C30P15S bridge variant

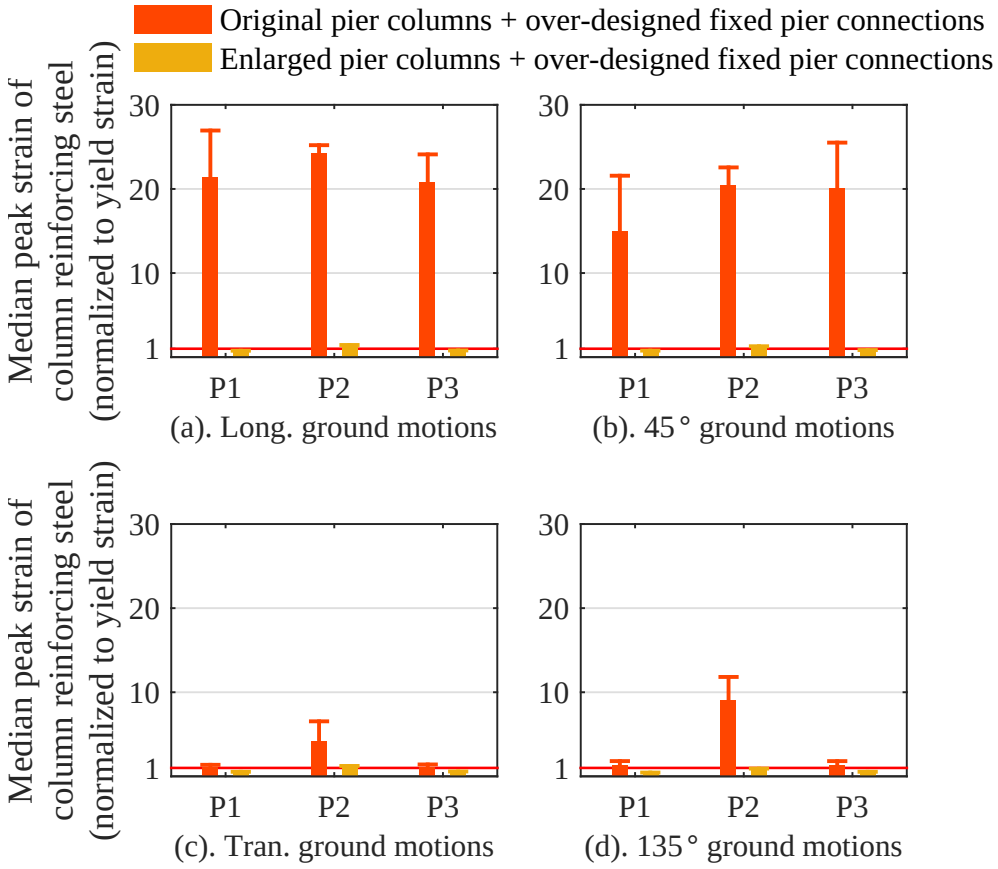

Figure C.31: Comparison of peak strain (median + median absolute deviation) of reinforcing steel at pier column bases of 4C30P15S bridge between Cases 1 and 2 of Table 6.54: (a). response under longitudinal ground motions; (b). response under 45° ground motions; (c). response under transverse ground motions; (d). response under 135° ground motions

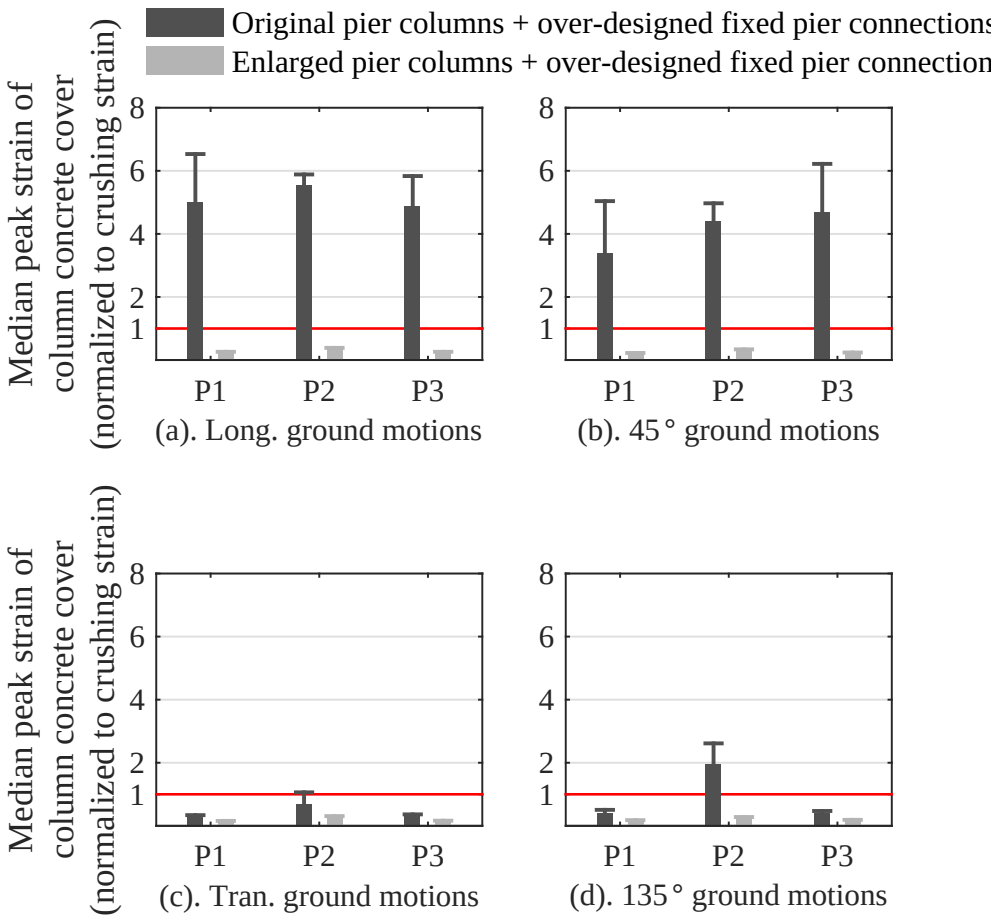

Figure C.32: Comparison of peak strain (median + median absolute deviation) of concrete cover at pier column bases of 4C30P15S bridge between Cases 1 and 2 of Table 6.54: (a). response under longitudinal ground motions; (b). response under 45° ground motions; (c). response under transverse ground motions; (d). response under 135° ground motions

4C15P15S bridge variant

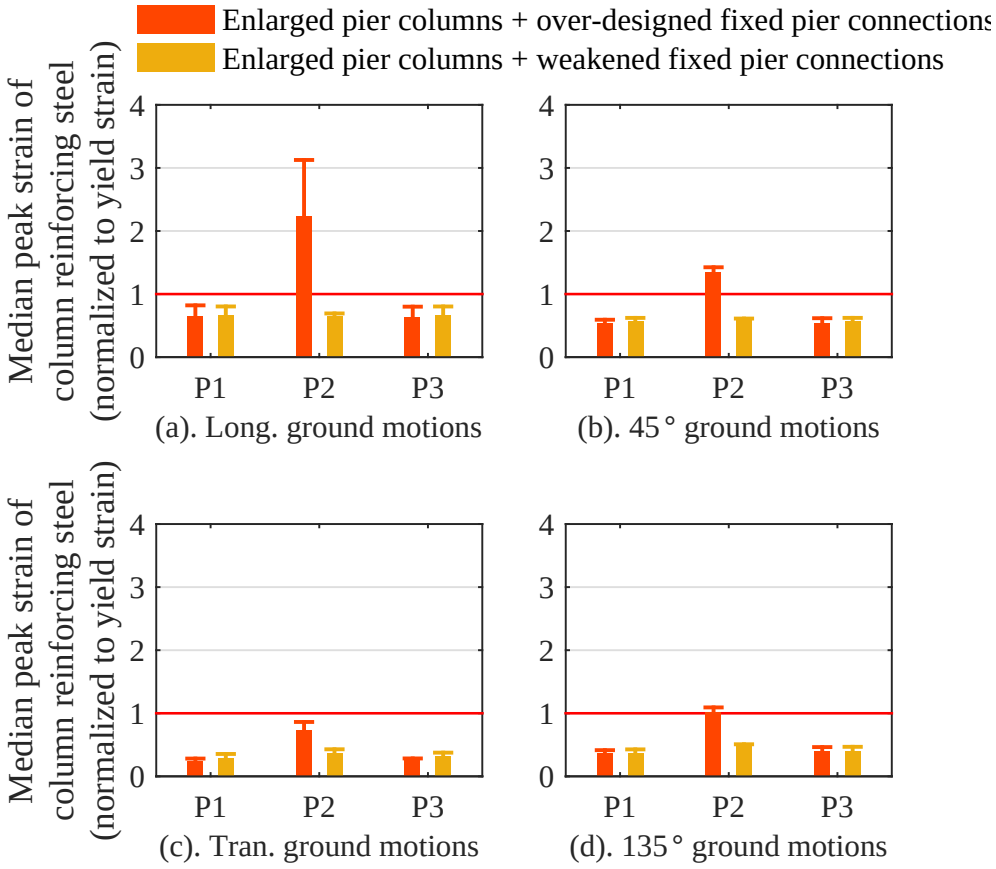

Figure C.33: Comparison of peak strain (median + median absolute deviation) of reinforcing steel at pier column bases of 4C15P15S bridge between Cases 2 and 3 of Table 6.54: (a). response under longitudinal ground motions; (b). response under 45° ground motions; (c). response under transverse ground motions; (d). response under 135° ground motions

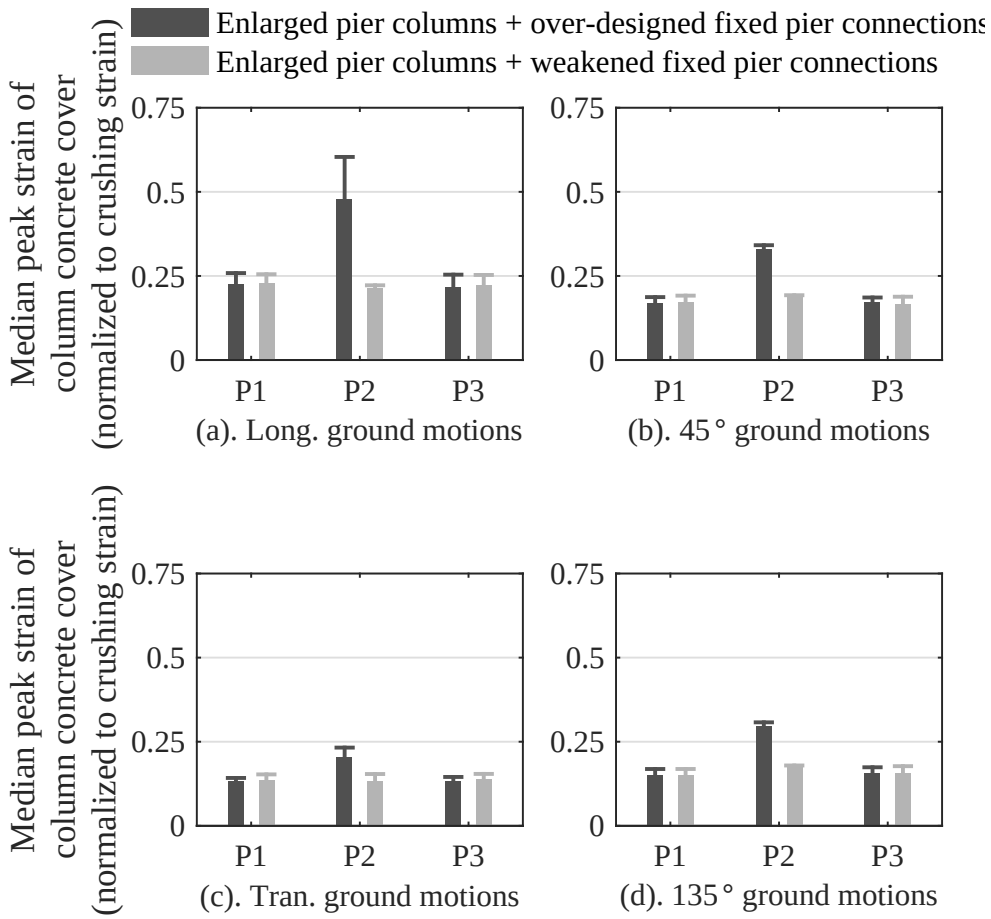

Figure C.34: Comparison of peak strain (median + median absolute deviation) of concrete cover at pier column bases of 4C15P15S bridge between Cases 2 and 3 of Table 6.54: (a). response under longitudinal ground motions; (b). response under 45° ground motions; (c). response under transverse ground motions; (d). response under 135° ground motions

4C30P15S bridge variant

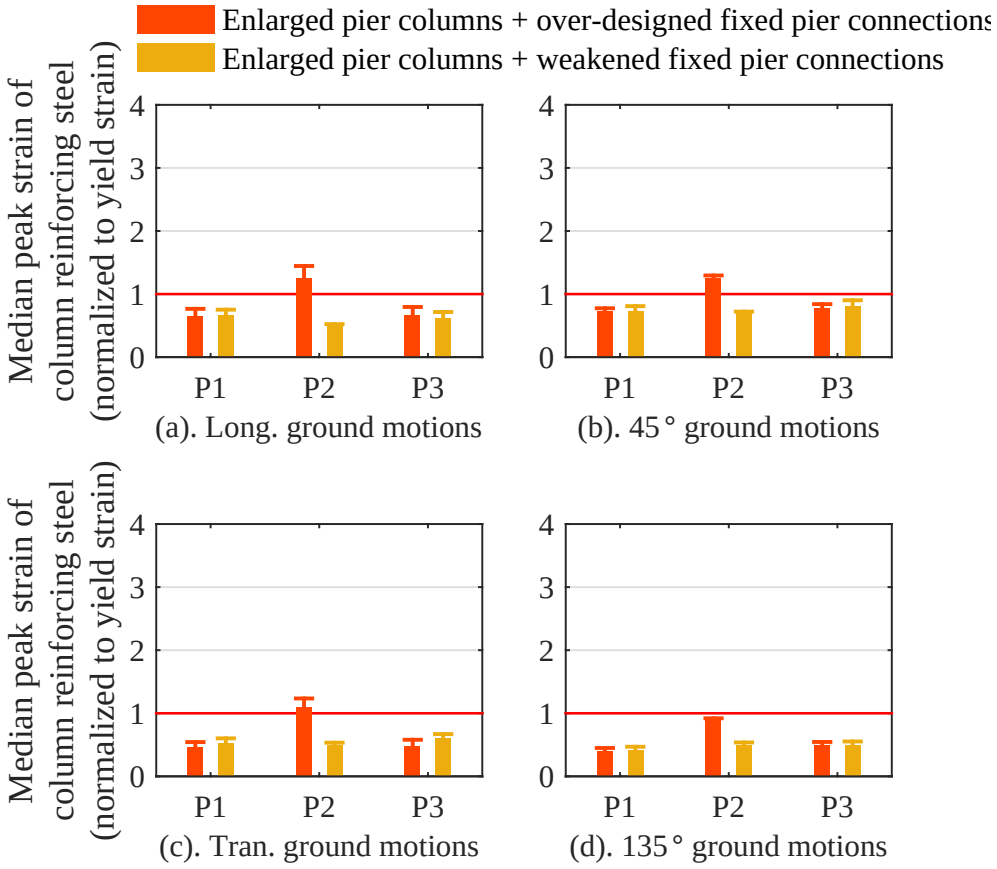

Figure C.35: Comparison of peak strain (median + median absolute deviation) of reinforcing steel at pier column bases of 4C30P15S bridge between Cases 2 and 3 of Table 6.54: (a). response under longitudinal ground motions; (b). response under 45° ground motions; (c). response under transverse ground motions; (d). response under 135° ground motions

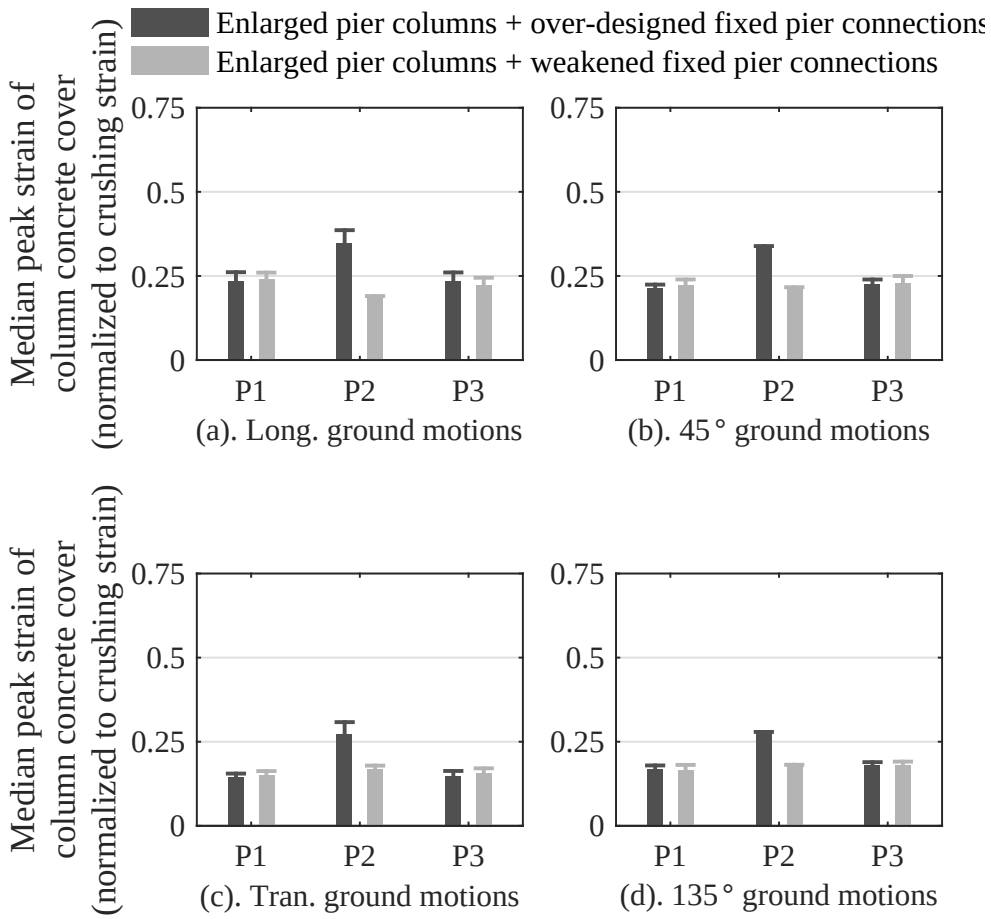

Figure C.36: Comparison of peak strain (median + median absolute deviation) of concrete cover at pier column bases of 4C30P15S bridge between Cases 2 and 3 of Table 6.54: (a). response under longitudinal ground motions; (b). response under 45° ground motions; (c). response under transverse ground motions; (d). response under 135° ground motions

REFERENCES

AASHTO. (2008a). *LRFD bridge design specifications and interim specifications*, Washington, D.C.

AASHTO. (2008b). *Guide specifications for LRFD seismic bridge design*, Washington, D.C.

AASHTO. (2010). *LRFD bridge design specifications*, Washington, D.C.

AASHTO. (2011). *Guide specification for LRFD seismic bridge design*, Washington, D.C.

AASHTO/NSBA Steel Bridge Collaboration. (2014). "Guidelines for Steel Girder Bridge Analysis.", *G13.1*, 2nd Ed., Washington, D.C.

Abbasnia, R., Davoudi, A. T., and Maddah, M. M. (2013). "An adaptive pushover procedure based on effective modal mass combination rule." *Eng. Struct.*, 52, 654–666.

Abdel-Mohti, A., and Pekcan, G. (2008). "Seismic response of skewed RC box-girder bridges." *Earthq. Eng. Eng. Vib.*, 7(4), 415–426.

Abo-Shadi, N., Saiidi, M., and Sanders, D. (2000). "Seismic response of reinforced concrete bridge pier walls in the weak direction." *Rep. No. MCEER-00-0006*, Univ. of Nevada, Reno, NV.

ACI. (2009). "Building code requirements for structural concrete and commentary." *ACI 318-08*, Farmington Hills, MI.

Al Atik, L., and Abrahamson, N. (2010). "An improved method for nonstationary spectral matching." *Earthq. Spectra*, 26(3), 601–617.

Antoniou, S. and Pinho, R. (2004). "Advantages and limitations of adaptive and non-adaptive force-based pushover procedures." *J. Earthq. Eng.*, 8(4), 497–522.

API. (1987). "Recommended practice for planning, designing and constructing fixed offshore platforms." *API Recommended practice 2A (RP 2A)*, 17th Ed., Washington, D.C.

API. (2000). "Recommended practice for planning, designing and constructing fixed offshore platforms–working stress design." *API Recommended practice 2A-WSD (RP 2A-WSD)*, 31st Ed., Washington, D.C.

ATC. "Seismic evaluation and retrofit of concrete buildings." *ATC-40 Rep., Volumes 1 & 2*, Redwood City, CA.

Awoshika, K. and Reese, L. C. "Analysis of foundation with widely spaced batter piles." *Rep. No. 117-3F*, Center for Highway Research, Univ. of Texas at Austin, Texas.

Baker, J. (2011). "Conditional mean spectrum: Tool for ground-motion selection." *J. Struct. Eng.*, 10.1061/(ASCE)ST.1943-541X.0000215, 322-331.

Bathe, K. (2007). "Conserving energy and momentum in nonlinear dynamics: A simple implicit time integration scheme." *Comput. Struct.*, 85(7-8), 437–445.

Bignell, J. L., LaFave, J. M., and Hawkins, N. M. (2005). "Seismic vulnerability assessment of wall pier supported highway bridges using nonlinear pushover analyses." *Eng. Struct.*, 27(14), 2044–2063.

Bignell, J. L. and LaFave, J. M. (2010). "Analytical fragility analysis of southern Illinois wall pier supported highway bridges." *Earthq. Eng. Struct. D.*, 39(7), 709–729.

Boulanger, R., Curras, C., Kutter, B., Wilson, D., and Abghari, A. (1999). "Seismic soil-pile-structure interaction experiments and analyses." *J. Geotech. Geoenviron. Eng.*, 10.1061/(ASCE)1090-0241(1999)125:9(750), 750-759.

Bozorgzadeh, A., Ashford, S. A., Restrepo, J. I., and Nimityongskul, N. "Experimental and analytical investigation on stiffness and ultimate capacity of bridge abutments." *Rep. No. UCSD/SSRP-07/12*, Univ. of California, San Diego, La Jolla, CA.

Bracci, J. M., Kunnath, S. K., and Reinhorn, A. M. (1997). "Seismic performance and retrofit evaluation of reinforced concrete structures." *J. Struct. Eng.*, 10.1061/(ASCE)0733-9445(1997)123:1(3), 3–10.

Buckle, I. G. (1994). "The Northridge, California earthquake of January 17, 1994: performance of highway bridges." *Rep. No. NCEER-94-0008*, State Univ. of New York at Buffalo, NY.

Caltrans. (1992). *Bridge memo to designers (5-1)*. Sacramento, CA.

Caltrans. (2013). *Caltrans Seismic Design Criteria (Version 1.7)*, Sacramento, CA.

Castilla, F., Martin, P., and Link, J. (1984). "Fixity of members embedded in concrete." *Rep. No. CERL M-339*, U.S. Army Corps of Engineers, Champaign, IL.

Charney, F. A. (2008). "Unintended consequences of modeling damping in structures." *J. Struct. Eng.*, 10.1061/(ASCE)0733-9445(2008)134:4(581), 581-592.

Chopra, A. K., and Goel, R. K. (2002). "A modal pushover analysis procedure for estimating seismic demands for buildings." *Earthq. Eng. Struct. D.*, 31(3), 561–582.

Clough, R. W. and Penzien, J. (1975). *Dynamics of structures*, McGraw-Hill, New York.

Crouse, C. B., Hushmand, B., and Martin, G. R. (1987). "Dynamic soil-structure interaction of a single-span bridge." *Earthq. Eng. Struct. D.*, 15(6), 711–729.

Cruz-Noguez, C. and Saiidi, M (2010). "Experimental and Analytical Seismic Studies of a Four-Span Bridge System with Innovative Materials." *Rep. No. CCEER-10-4*, Univ. of Nevada, Reno, NV.

Dao, N. D., Ryan, K. L., Sato, E., and Sasaki, T. (2013). "Predicting the displacement of triple pendulum^{TM} bearings in a full-scale shaking experiment using a three-dimensional element." *Earthq. Eng. Struct. D.*, 42(11), 1677–1695.

Dimitrakopoulos, E. G. (2011). "Seismic response analysis of skew bridges with pounding deck-abutment joints." *Eng. Struct.*, 3(3), 813–826.

Elnashai, A. S. (2001). "Advanced inelastic static (pushover) analysis for earthquake applications." *Struct. Eng. Mech.*, 12(1), 51–69.

Elnashai, A. S., Gencturk, B., Kwon, O., Al-Qadi, I. L., Hashash, Y., Roesler, J. R., and Valdivia, A. (2010). "The Maule (Chile) earthquake of February 27, 2010: consequence assessment and case studies." *Rep. No. 10-04*, MAE Center, Univ. of Illinois at Urbana-Champaign, Champaign, IL.

Fernandez, J., and Rix, G. (2008). Seismic Hazard Analysis and Probabilistic Ground Motions in the Upper Mississippi Embayment. Geotechnical Earthquake Engineering and Soil Dynamics IV:pp. 1-10. doi: 10.1061/40975(318)8

Filipov, E. T. (2012). "Nonlinear seismic analysis of quasi-isolation systems for earthquake protection of bridges." M.S. Thesis, Univ. of Illinois at Urbana-Champaign, Champaign, IL.

Filipov, E. T., Fahnestock, L. A., Steelman, J. S., Hajjar, J. F., and LaFave, J. M. (2013). "Evaluation of quasi-isolated seismic bridge behavior using nonlinear bearing models." *Eng. Struct.*, 49(0), 168–181.

Filipov, E. T., Revell, J. R., Fahnestock, L. A., LaFave, J. M., Hajjar, J. F., Foutch, D. A., and Steelman, J. S. (2013). "Seismic performance of highway bridges with fusing bearing components for quasi-isolation." *Earthq. Eng. Struct. D.*, 42(9), 1375–1394.

Freeman, S. A. (1978). "Prediction of response of concrete buildings to severe earthquake motion." *Special publication of American Concrete Institute*, 55, 589–605.

Gencturk, B. and Elnashai, A. S. (2008). "Development and application of an advanced capacity spectrum method." *Eng. Struct.*, 30(11), 3345–3354.

Goel, R. K. and Chopra, A. K. (2002). "Evaluation of bridge abutment capacity and stiffness during earthquakes." *Earthq. Spectra*, 13(1), 1–23.

Gupta, B. and Kunnath, S. K. (2000). "Adaptive spectra-based pushover procedure for seismic evaluation of structures." *Eathq. Spectra*, 16(2), 367–392.

Hashash, Y. M. A., Musgrove, M. I., Harmon, J. A., Groholski, D. R., Phillips, C. A., and Park, D. (2015). *DEEPSOIL 6.1, User Manual*. Urbana, IL: Board of Trustees of Univ. of Illinois at Urbana-Champaign.

IDOT (Illinois Dept. of Transportation). (2012). *Bridge manual*, Springfield, IL.

IDOT (Illinois Dept. of Transportation). (2012). *Strandard specifications for road and bridge construction*, Springfield, IL.

IDOT (Illinois Dept. of Transportation). (2015). "ABD 15.2: New Precast Prestressed Concrete IL-Beam Sections and Revisions to the I-Beams and Bulb T-Beams." Retrieved from http://www.idot.illinois.gov/Assets/uploads/files/Doing-Business/Memorandums-&-Letters/Highways/Bridges/ABD-Memos/ABD152.pdf.

IDOT (Illinois Dept. of Transportation). (n.d.). *Illinois Department of Transportation Bridge Information website*. Retrieved from http://apps.dot.illinois.gov/bridgesinfosystem/main.aspx.

Jennings, P. C. (2012). "Engineering features of the San Fernando earthquake of February 9, 1971." *Rep. No. EERL-71-02*. California Institute of Technology, Pasadena, CA.

Kalantari, A., and Amjadian, M. (2010). "An approximate method for dynamic analysis of skewed highway bridges with continuous rigid deck." *Eng. Struct.*, 32(9), 2850–2860.

Kawashima, K., Unjoh, S., Hoshikuma, J., and Kosa, K. (2011). "Damage of Bridges due to the 2010 Maule, Chile, earthquake." *J. Earthq. Eng.*, 15(7), 1036–1068.

Kaviani, P., Zareian, F. and Ertugrul, T. (2012). "Seismic behavior of reinforced concrete bridges with skew-angled seat-type abutments." *Eng. Struct.*, 45, 137–150.

Kornkasem, W., Foutch, D. A., and Long, J. H. (2001). "Seismic behavior of pile-supported bridges." *Rep. No. 03-05*. Mid-America Earthquake Center, Univ. of Illinois at Urbana-Champaign, Champaign, IL.

Kowalsky, J. (2001). "Deformation limit states for circular reinforced concrete bridge columns." *J. Struct. Eng.*, 10.1061/(ASCE)0733-9445(2000)126:8(869), 869-878.

Kozak, D. L., Luo, J., Olson, S. M., LaFave, J. M., and Fahnestock, L. A. (2016). "Modification of ground motions for use with dynamic structural analyses in Central North America." *J. Earthq. Eng.*, under review.

Krawinkler, H. and Seneviratna, G. D. P. K. (1998). "Pros and cons of a pushover analysis of seismic performance evaluation." *Eng. Struct.*, 20(4), 452–464.

Kubo, K. (1964). "Experimental study of the behavior of laterally loaded piles." *Rep. No. 12(2)*. Transportation Technology Research Institute, Japan.

Kulhawy, F. H., and Mayne, P. W. (1990). "Manual on estimating soil properties for foundation design." *Research Project No. 1493-6, EL-6800*, Electric Power Research Institute, Palo Alto, CA.

Kunnath, S. K., El-Bahy, A., Taylor, A., and Stone, W. (1997). "Cumulative seismic damage of reinforced concrete bridge piers." *Rep. No. NCEER-97-0006*. National Center for Earthquake Engineering Research, State Univ. of New York at Buffalo, Buffalo, NY.

Kwon, O., and Jeong, S. (2013). "Seismic displacement demands on skewed bridge decks supported on elastomeric bearings." *J. Earthq. Eng.*, 17(7), 998–1022.

LaFave, J., Fahnestock, L., Foutch, D., Steelman, J., Revell, J., Filipov, E., and Hajjar, J. (2013). "Experimental investigation of the seismic response of bridge bearings." *Rep. No. FHWA-ICT-13-002*. Illinois Center for Transportation, Springfield, IL.

LaFave, J., Fahnestock, L., Foutch, D., Steelman, J., Revell, J., Filipov, E., and Hajjar, J. (2013). "Seismic performance of quasi-isolated highway bridges in Illinois." *Rep. No. FHWA-ICT-13-015*. Illinois Center for Transportation, Springfield, IL.

Lawson, R. S., Vance, V., and Krawinkler, H. (1994). "Nonlinear static pushover analysis, why, when, and how?" *Proceedings of 5th U.S. National Conference on Earthquake Engineering*. Chicago, IL.

Lee, G. C. and Loh, C. (2000). "The Chi-chi, Taiwan earthquake of September 21, 1999: reconnaissance report." *Rep. No. MCEER-00-0003*. State Univ. of New York at Buffalo, Buffalo, NY.

Lehman, D. E. and Moehle, J. P. (1998). "Seismic performance of well-confined concrete bridge columns." *PEER Rep. No. 1998/01*. Pacific Earthquake Engineering Research Center, Univ. of California, Berkeley, CA.

Lemnitzer, A., Ahlberg, E. R., Nigbor, R. L, Shamsabadi, A., Wallace, J. W., and Stewart, J. P. (2009). "Lateral performance of full-scale bridge abutment wall with granular backfill." *J. Geotech. Geoenviron. Eng.*, 10.1061/(ASCE)1090-0241(2009)135:4(506), 506-514.

Luo, J., Fahnestock, L. A., Kozak, D. L., and LaFave, J. M. (2016). "Seismic analysis incorporating detailed structure-abutment-foundation interaction for quasi-isolated highway bridges." *Struct. Infrastructure E.*, in press.

Makris, N. and Zhang, J. (2004). "Seismic response analysis of a highway overcrossing equipped with elastomeric bearings and fluid dampers." *J. Struct. Eng.*, 130(6), 830-845.

Mander, J., Priestley, M., and Park, R. (1988). "Theoretical stress-strain model for confined concrete." *J. Struct. Eng.*, 10.1061/(ASCE)0733-9445(1988)114:8(1804), 1804-1826.

Maragakis, E. and Jennings, P. C. (1987). "Analytical models for the rigid body motions of skew bridges." *Earthq. Eng. Struct. D.*, 15(8), 923–944.

Marsh, A. (2013). "Evaluation of passive force on skewed bridge abutments with large-scale tests," M.S. Thesis, Brigham Young Univ., Provo, UT.

Martin, G. R., Yan, L., and Lam, I. P. (1997). "Development and implementation of improved seismic design and retrofit procedures for bridge abutments." Univ. of Southern California, Los Angeles, CA.

MATLAB [Computer software]. MathWorks, Natick, MA.

Matlock, H. (1970). "Correlations for design of laterally loaded piles in soft clay." *Proc., 2nd Annu. Offshore Technol. Conf.*, Vol. 1, 577-594.

Matlock, H., Foo, S. H., and Bryant, L. L. (1978). "Simulation of lateral pile behavior." *Proc., Earthq. Eng. and Soil Dyn.*, ASCE, New York, 600-619.

McCallen, D. B. and Romstad, K. M. (1994). "Dynamic analysis of a skewed short-span, box-girder overpass." *Earthq. Spectra*, 10(4), 729–756.

McGuire, R. K., Silva, W. J., and Costantino, C. J. (2001). "Technical basis for revision of regulatory guidance on design ground motions: Hazard- and risk-consistent ground motion spectra guidelines." *Rep. No. NUREG/CR-6728*. U.S. Nuclear Regulatory Commission, Washington, D.C.

McKenna, F., and Fenves, G. (2008, April 17). *Using the OpenSees Interpreter on Parallel Computers*. Retrieved from http://opensees.berkeley.edu/OpenSees/parallel/TNParallelProcessing.pdf

Menegotto, M., and Pinto, P. E. (1973). "Method of analysis for cyclically loaded reinforced concrete plane frames including changes in geometry and non-elastic behavior of elements under combined normal force and bending." *Proc., IABSE Symp. of Resistance and Ultimate Deformability of Structures Acted on by Well-Defined Repeated Loads, Vol. 13, Libson, Portugal, 15-22*

Meng, J. Y., Lui, E. M., and Liu, Y. (2001). "Dynamic response of skew highway bridges." *J. Earthq. Eng.*, *5* (2), 205–223.

Mitchell, D., Huffman, S., Tremblay, R., Saatcioglu, M., Palermo, D., Rinawi, R., & Lau, D. (2013). Damage to bridges due to the 27 February 2010 Chile earthquake. *Canadian Journal of Civil Engineering*, *40* (8), 675–692.

Mitoulis, S. A. (2012). "Seismic design of bridges with the participation of seat-type abutments." *Eng. Struct.*, *42* (0), 222–233.

Mohd Yassin, M. (1994). "Nonlinear analysis of prestressed concrete structures under monotonic and cyclic loading," Ph.D. Dissertation, Univ. of California, Berkeley, CA.

Mosher, R. L. (1984). "Load transfer criteria for numerical analysis of axially loaded piles in sand." U.S. Army Engineering Waterways Experimental Station, Automatic Data Processing Center, Vicksburg, MS.

Muthukumar, S. (2003). *A contact element approach with hysteresis damping for the analysis and design of pounding in bridges*. Ph.D. Dissertation, Georgia Institute of Technology, Atlanta, GA.

Mwafy, A. M. and Elnashai, S. A. (2000). "Static pushover versus dynamic-to-collapse analysis of RC buildings." *ESEE Research Rep. No. 00/1*. London, United Kingdom: Imperial College London.

Neuenhofer, A. and Filippou, F. C. (1997). "Evaluation of nonlinear frame finite-element models." *J. Struct. Eng.*, 10.1061/(ASCE)0733-9445(1997)123:7(958), 958-966.

Nielson, B. G. and DesRoches, R. (2007). "Seismic performance assessment of simply supported and continuous multispan concrete girder highway bridges." *J. Bridge Eng.*, 10.1061/(ASCE)1084-0702(2007)12:5(611), 611-620.

Nogami, T., Otani, J., Konagai, K., and Chen, H. (1992). "Nonlinear soil-pile interaction model for dynamic lateral motion." *J. Geotech. Engrg.*, 10.1061/(ASCE)0733-9410(1992)118:1(89), 89-106.

Novak, M., and Sheta, M. (1980). "Approximate approach to contact problems of piles." *Proc., ASCE Nat. Convention, Dyn. Response of Pile Found: Analytical Aspects*, ASCE, New York, 55-79.

O'Brien, E. J., Keogh, D. L., O'Connor, A. J., and Lehane, B. M. (2015). *Bridge deck analysis*, 2nd Ed., CRC Press, Taylor & Francis Group, Boca Raton, FL.

O'Neil, M. W., and Reese, L. C. (1999). "Drilled shafts: Construction procedures and design methods." *Rep. No. FHWA-HI-99-025*, U.S. Department of Transportation, Federal Highway Administration, Office of Infrastructure, Washington, D.C.

OpenSees [Computer software]. Pacific Earthquake Engineering Research Center, Univ. of California, Berkeley, CA.

Pant, D. R., Wijeyewickrema, A. C., and ElGawady, M. A. (2013). "Appropriate viscous damping for nonlinear time-history analysis of base-isolated reinforced concrete buildings." *Earthq. Eng. Struct. D.*, 42(15), 2321–2339.

Petrini, L., Maggi, C., Priestley, M. J. N., and Calvi, G. M. (2008). "Experimental verification of viscous damping modeling for inelastic time history analyzes." *J. Earthq. Eng.*, 12(S1), 125–145.

Priestley, M. J. N., Seible, F., and Calvi, G. M. (1996). *Seismic design and retrofit of bridges*, John Wiley & Sons, New York.

Reese, L. C., and Wang, S. T. (1996). "Technical manual for documentation for program group." Ensoft, Austin, TX.

Reese, L. C., and Van Impe, W. F. (2011). *Single piles and pile groups under lateral loading*, 2nd Ed., CRC Press, Taylor & Francis Group, London, U.K.

Revell, J. (2013). "Quasi-isolated highway bridges: influence of bearing anchorage strength on seismic performance," M.S. Thesis, Univ. of Illinois at Urbana-Champaign, Champaign, IL.

Robinson, W. H. (1982). "Lead-rubber hysteretic bearings suitable for protecting structures during earthquakes." *Earthq. Eng. Struct. D.*, 10(4), 593–604.

Rollins, K. M., Lane, J., and Gerber, T. (2005). "Measured and computed lateral response of a pile group in sand." *J. Geotech. Geoenviron. Eng.*, 10.1061/(ASCE)1090-0241(2005)131:1(103), 103-114.

Rollins, K. M., Gerber, T. M., Cummings, C. R., and Pruett, J. M. (2010). "Dynamic passive pressure on abutments and pile caps." *Rep. No. UT-10.18*. Brigham Young Univ., Provo, UT.

Rollins, K. M., Gerber, and Nasr, M. (2010). "Numerical analysis of dense narrow backfills for increasing lateral passive resistance." *Rep. No. UT-10.19*. Brigham Young Univ. Provo, UT.

Romstad, K., Kutter, B., Maroney,B., Vanderbilt, E., Griggs, M., and Chai, Y. H. (1995). "Experimental measurements of bridge abutment behavior." *Rep. No. UCD-STR-95-1*, Structural Engineering Group, Univ. of California, Davis, CA.

Ryan, T. P. (2006). *Modern engineering statistics*, John Wiley & Sons, Hoboken, NJ.

SAP2000 [Computer software]. Computers and Structures, Walnut Creek, CA.

Sardo, A. G., Sardo, T. E., and Harik, I. E. (2006). "Post earthquake investigation field manual for the state of Kentucky." *Rep. No. KTC-06-30/SPR2234-01-1F*. Kentucky Transportation Center, Univ. of Kentucky, Lexington, KY.

Scott, M. H. and Fenves, G. L. (2010). "Krylov Subspace accelerated Newton algorithm: Application to dynamic progressive collapse simulation of frames." *J. Struct. Eng.*, 10.1061/(ASCE)ST.1943-541X.0000143, 473-480.

Shamsabadi, A., Ashour, M., and Norris, G. (2005). "Bridge abutment nonlinear force-displacement-capacity prediction for seismic design." *J. Geotech. Geoenviron. Eng.*, 10.1061/(ASCE)1090-0241(2005)131:2(151), 151-161.

Shamsabadi, A. (2007). "Three-dimensional nonlinear seismic soil-abutment-foundation-structure interaction analysis of skewed bridges," Ph.D. Dissertation, Univ. of Southern California, Los Angeles, CA.

Shamsabadi, A., Rollins, K., and Kapuskar, M. (2007). "Nonlinear soil-abutment-bridge structure interaction for seismic performance-based design." *J. Geotech. Geoenviron. Eng.*, 10.1061/(ASCE)1090-0241(2007)133:6(707), 707-720..

Sheskin, D. J. (2011). *Handbook of parametric and nonparametric statistical procedures*. Boca Raton, FL: Chapman & Hall/CRC.

Shields, D. H., and Tolunay, A. Z. (1973). "Passive pressure coefficients by method of slices." *J. Soil Mech. Found. Div.*, 99(12), 1043-1053.

Steelman, J. (2013). "Sacrificial bearing components for quasi-isolated response of bridges subjected to high-magnitude, low-probability seismic hazard." Ph.D. Dissertation, Univ. of Illinois at Urbana-Champaign, Champaign, IL.

Steelman, J., Fahnestock, L., Filipov, E., LaFave, J., Hajjar, J., and Foutch, D. (2014). "Shear and friction response of nonseismic laminated elastomeric bridge bearings subject to seismic demands." *J. Bridge Eng.*, 10.1061/(ASCE)BE.1943-5592.0000406, 612-623.

Steelman, J., Filipov, E., Fahnestock, L., Revell, J., LaFave, J., Hajjar, J., and Foutch, D. (2014). "Experimental behavior of steel fixed bearings and implications for seismic bridge response." *J. Bridge Eng.*, *19* (8), A4014007.

Steelman, J., Fahnestock, L., Hajjar, J., and LaFave, J. (2016). "Performance of nonseismic PTFE sliding bearings when subjected to seismic demands." *J. Bridge Eng.*, 10.1061/(ASCE)BE.1943-5592.0000777, 04015028.

Stewart, J. P. et al. (2007). "Full scale cyclic testing of foundation support systems for highway bridges. Part II: Abutment backwalls." *Rep. No. UCLA-SGEL-2007/02*, Structural and Geotechnical Engineering Laboratory, Univ. of California, Los Angeles.

Terzaghi, K., Peck, R. B., and Mesri, G. (1996). *Soil mechanics in engineering practice*, 3rd Ed., Wiley, U.K.

Tobias, D., Anderson, R., Hodel, C., Kramer, W., Wahab, R., and Chaput, R. (2008). "Overview of earthquake resisting system design and retrofit strategy for bridges in Illinois." *Pract. Period. Struct. Des. and Constr.*, 10.1061/(ASCE)1084-0680(2008)13:3(147), 147-158.

USGS (United States Geological Survey) (2015). "U.S. Seismic Design Maps." ⟨http://earthquake.usgs.gov/hazards/designmaps/usdesign.php⟩.

Wang, S. T., and Reese, L. C. (1986). "Study of design method for vertical drilled shaft retaining walls." *Rep. FHWA/TX-87/44+415-2F*, Center for Transportation Research, The Univ. of Texas at Austin, Austin, TX.

Werner, S. D., Beck, J. L., and Levine, M. B. (1987). "Seismic response evaluation of Meloland Road overpass using 1979 Imperial Valley earthquake records." *Earthq. Eng. Struct. D.*, 15(2), 249–274.

Wilson, J. C. (1988). "Stiffness of non-skew monolithic bridge abutments for seismic analysis." *Earthq. Eng. Struct. D.*, 16(6), 867–883.

Wilson, P. and Elgamal, A. (2010). "Large-scale passive earth pressure load-displacement tests and numerical simulation." *J. Geotech. Geoenviron. Eng.*, *136* (12), 1634–1643.

Wilson, P. and Tan, B. (1990). "Bridge abutments: Assessing their influence on earthquake response of Meloland Road Overpass." *J. Eng. Mech.*, 10.1061/(ASCE)0733-9399(1990)116:8(1838), 1838-1856.

Vintzeleou, E. N. and Tassios, T. P. (1986). "Mathematical models for dowel action under monotonic and cyclic conditions." *Mag. Concrete res.*, 38(134), 13–22.

Yen, W. P., Chen, G., Buckle, I., Allen, T., Alzamora, D., Ger, J. and Arias, J. G. (2011). "Postearthquake reconnaissance report on transportation infrastructure impact of the Feburary 27, 2010 offshore Maule Earthquake in Chile." *Rep. No. FHWA-HRT-11-030*, Federal Highway Administration, U. S. Department of Transportation, McLean, VA.

Zandieh A. and Pezeshk S. (2011). "A study of horizontal-to-vertical component spectral ratio in the New Madrid Seismic Zone." *B. Seismol. Soc. Am.*, 101(1), 287–296.

Zhang, J. and Makris, N. (2002). "Seismic response analysis of highway overcrossing including soil-structure interaction." *Earthq. Eng. Struct. D.*, 31(11), 1967–1991.